

IEEE Signal Processing MAGAZINE

[VOLUME 31 NUMBER 3 MAY 2014]



SOURCE SEPARATION AND APPLICATIONS *RECENT ADVANCES*



**PHYSICAL LAYER SERVICE INTEGRATION
IN WIRELESS NETWORKS**

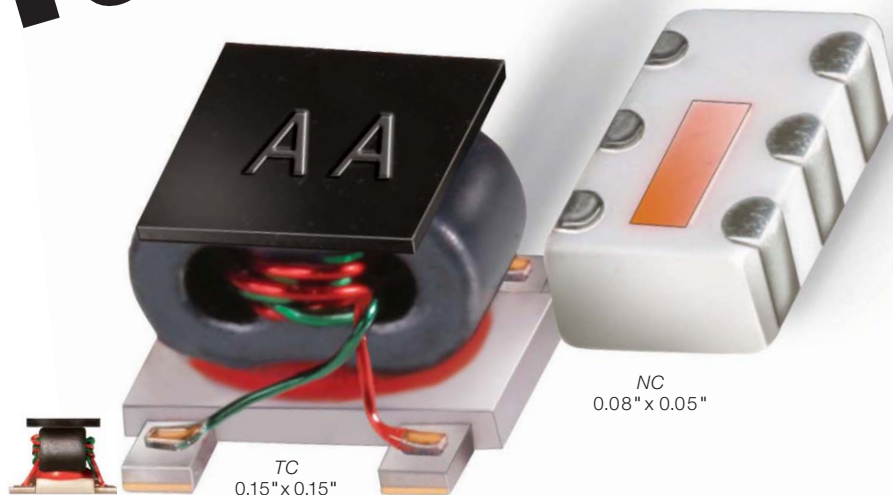
SPECTRALLY CONSTRAINED WAVEFORM DESIGN

UHDTV: THE EVOLUTION OF TELEVISION

THE PHOTOGRAPHIC AND IMAGING REVOLUTION



TINY Wideband Transformers



0.15-8000 MHz as low as **99¢** each (qty. 1000)  RoHS compliant.

Rugged, repeatable performance.

At Mini-Circuits, we're passionate about transformers. We even make our own transmission line wire under tight manufacturing control, and utilize all-welded connections to maximize performance, reliability, and repeatability. And for signals up to 8 GHz, our rugged LTCC ceramic models feature wrap-around terminations for your visual solder inspection, and they are even offered in packages as small as 0805!

Continued innovation: Top Hat.

A Mini-Circuits exclusive, this new feature is now available on every open-core transformer we sell. Top Hat speeds customer pick-and-place throughput in four distinct ways: (1) faster set-up times, (2) fewer missed components,

(3) better placement accuracy and consistency, and (4) high-visibility markings for quicker visual identification and inspection.

More models, to meet more needs

Mini-Circuits has over 250 different SMT models in stock. So for RF or microwave baluns and transformers, with or without center taps or DC isolation, you can probably find what you need at minicircuits.com. Enter your requirements, and Yoni2, our patented search engine, can identify a match in seconds. And new custom designs are just a phone call away, with surprisingly quick turnaround times gained from over 40 years of manufacturing and design experience!



www.minicircuits.com P.O. Box 350166, Brooklyn, NY 11235-0003 (718) 934-4500 sales@minicircuits.com

377 rev AB

CONTENTS

[VOLUME 31 NUMBER 3]

SPECIAL SECTION—SOURCE SEPARATION AND APPLICATIONS

16 FROM THE GUEST EDITORS

Tülay Adalı, Christian Jutten, Arie Yeredor, Andrzej Cichocki, and Eric Moreau

18 DIVERSITY IN INDEPENDENT COMPONENT AND VECTOR ANALYSES

Tülay Adalı, Matthew Anderson, and Geng-Shen Fu

34 JOINT MATRICES DECOMPOSITIONS AND BLIND SOURCE SEPARATION

Gilles Chabriel, Martin Kleinsteuber, Eric Moreau, Hao Shen, Petr Tichavsky, and Arie Yeredor

44 TENSORS

Pierre Comon

54 NONNEGATIVE MATRIX AND TENSOR FACTORIZATIONS

Guoxu Zhou, Andrzej Cichocki, Qibin Zhao, and Shengli Xie

66 STATIC AND DYNAMIC SOURCE SEPARATION USING NONNEGATIVE FACTORIZATIONS

Paris Smaragdis, Cédric Févotte, Gautham J. Mysore, Nasser Mohammadiha, and Matthew Hoffman

76 PUTTING NONNEGATIVE MATRIX FACTORIZATION TO THE TEST

Kejun Huang and Nicholas D. Sidiropoulos

87 CONVEXITY IN SOURCE SEPARATION

Michael B. McCoy, Volkan Cevher, Quoc Tran Dinh, Afsaneh Asaei, and Luca Baldassarre

96 SPARSE REPRESENTATION FOR BRAIN SIGNAL PROCESSING

Yuanqing Li, Zhu Liang Yu, Ning Bi, Yong Xu, Zhenghui Gu, and Shun-ichi Amari

107 FROM BLIND TO GUIDED AUDIO SOURCE SEPARATION

Emmanuel Vincent, Nancy Bertin, Rémi Gribonval, and Frédéric Bimbot

116 SCORE-INFORMED SOURCE SEPARATION FOR MUSICAL AUDIO RECORDINGS

Sebastian Ewert, Bryan Pardo, Meinard Müller, and Mark D. Plumbley

125 AUDIOVISUAL SPEECH SOURCE SEPARATION

Bertrand Rivet, Wenwu Wang, Syed Mohsen Naqvi, and Jonathon A. Chambers

135 SOURCE SEPARATION IN CHEMICAL ANALYSIS

Leonardo Tomazeli Duarte, Saïd Moussaoui, and Christian Jutten

6 PRESIDENT'S MESSAGE

GlobalSIP and ChinaSIP: New Conferences Developed by the IEEE Signal Processing Society
Alex Acero

10 SPECIAL REPORTS

Signal Processing Leads a Photographic and Imaging Revolution
John Edwards

157 SP TIPS & TRICKS

Spectrally Constrained Waveform Design
William Rowe, Petre Stoica, and Jian Li

163 LECTURE NOTES

From the STFT to the Wigner Distribution
Ljubiša Stanković, Srdjan Stanković, and Miloš Daković

170 STANDARDS IN A NUTSHELL

Ultra-High-Definition Television (Rec. ITU-R BT.2020): A Generational Leap in the Evolution of Television
Masayuki Sugawara, Seo-Young Choi, and David Wood

FEATURE

147 PHYSICAL LAYER SERVICE INTEGRATION IN WIRELESS NETWORKS

Rafael F. Schaefer and Holger Boche

COLUMNS

4 FROM THE EDITOR

Journals and Magazine Reviews: A Quality Control Mechanism
Abdelhak Zoubir

DEPARTMENTS

8 SOCIETY NEWS

SPS Members Recognized with Awards

175 DATES AHEAD

IEEE SIGNAL PROCESSING magazine

IEEE SIGNAL PROCESSING MAGAZINE

Abdelhak Zoubir—*Editor-in-Chief*
Technische Universität Darmstadt, Germany

AREA EDITORS

Feature Articles

Marc Moonen—KU Leuven, Belgium

Columns and Forum

Andrea Cavallaro—Queen Mary, University of London, United Kingdom

Andres Kwasinski—Rochester Institute of Technology, United States

Special Issues

Fulvio Gini—University of Pisa, Italy

e-Newsletter

Z. Jane Wang, —University of British Columbia

EDITORIAL BOARD

Moeness G. Amin—Villanova University, United States

Sergio Barbarossa—University of Rome "La Sapienza," Italy

Mauro Barni—Università di Siena, Italy

Helmut Bölcskei—ETH Zürich, Switzerland

A. Enis Cetin—Bilkent University, Turkey

Patrick Flandrin—CNRS chez ENS Lyon, France

Bastiaan Kleijn—Victoria University of Wellington, New Zealand

Visa Koivunen—Aalto University, Finland

Hamid Krim—North Carolina State University, United States

Ying-Chang Liang—Institute for Infocomm Research, Singapore

V. John Mathews—University of Utah, United States

Satoshi Nakamura—Nara Institute of Science and Technology, Japan

Kuldip Paliwal—Griffith University, Australia

Béatrice Pesquet-Popescu—Télécom ParisTech, France

Eli Saber—Rochester Institute of Technology, United States

Ali Sayed—University of California, Los Angeles, United States

Hing Cheung So—City University of Hong Kong, Hong Kong

Victor Solo—University of New South Wales, Australia

Sergios Theodoridis—University of Athens, Greece

Isabel Trancoso—INESC-ID/Instituto Superior Técnico, Portugal

Michael K. Tsatsanis—Entropic Communications

Min Wu—University of Maryland

Pramod K. Varshney—Syracuse University, United States

Z. Jane Wang—The University of British Columbia, Canada

ASSOCIATE EDITORS—

COLUMNS AND FORUM

Rodrigo Capobianco Guido —

University of Sao Paulo, Brazil

Aleksandra Mojsilovic —

IBM T.J. Watson Research Center

Douglas O'Shaughnessy — INRS, Canada

Gene Cheung — National Institute of Informatics

Alessandro Vinciarelli — IDIAP-EPFL

Michael Gormish — Ricoh Innovations, Inc.

Xiaodong He — Microsoft Research

Fatih Porikli — MERL

Stefan Winkler — UIUC/ADSC, Singapore

Saeid Sanei, — University of Surrey, United Kingdom

Azadeh Vosoughi — University of Central Florida

Danilo Mandic — Imperial College, United Kingdom

Roberto Togneri — The University of Western Australia

Gail Rosen — Drexel University

ASSOCIATE EDITORS—

E-NEWSLETTER

Gwenaél Doerr—Technicolor, France

Vitor Nascimento—University of São Paulo, Brazil

Shantanu Rane—MERL

Yan Lindsay Sun—University of Rhode Island

IEEE SIGNAL PROCESSING SOCIETY

Alex Acero—*President*

Rabab Ward—*President-Elect*

Konstantinos (Kostas) N. Plataniotis—*Vice President, Awards and Membership*

Wan-Chi Siu—*Vice President, Conferences*

Alex Kot—*Vice President, Finance*

Mari Ostendorf—*Vice President, Publications*

Charles Bouman —*Vice President, Technical Directions*

COVER

©ISTOCKPHOTO.COM/OLGAYAKOVENKO



IEEE PERIODICALS MAGAZINES DEPARTMENT

Jessica Barragué

Managing Editor

Geraldine Krolin-Taylor

Senior Managing Editor

Susan Schneiderman

Business Development Manager

+1 732 562 3946 Fax: +1 732 981 1855

Felicia Spagnoli

Advertising Production Manager

Janet Dudar

Senior Art Director

Gail A. Schnitzer

Assistant Art Director

Theresa L. Smith

Production Coordinator

Dawn M. Melley

Editorial Director

Peter M. Tuohy

Production Director

Fran Zappulla

Staff Director, Publishing Operations

IEEE prohibits discrimination, harassment, and bullying. For more information, visit <http://www.ieee.org/web/aboutus/whatis/policies/p9-26.html>.

IEEE SIGNAL PROCESSING MAGAZINE (ISSN 1053-5888) (ISPREG) is published bimonthly by the Institute of Electrical and Electronics Engineers, Inc., 3 Park Avenue, 17th Floor, New York, NY 10016-5997 USA (+1 212 419 7900). Responsibility for the contents rests upon the authors and not the IEEE, the Society, or its members. Annual member subscriptions included in Society fee. Nonmember subscriptions available upon request. Individual copies: IEEE Members US\$20.00 (first copy only), nonmembers US\$201.00 per copy. Copyright and Reprint Permissions: Abstracting is permitted with credit to the source. Libraries are permitted to photocopy beyond the limits of U.S. Copyright Law for private use of patrons: 1) those post-1977 articles that carry a code at the bottom of the first page, provided the per-copy fee indicated in the code is paid through the Copyright Clearance Center, 222 Rosewood Drive, Danvers, MA 01923 USA; 2) pre-1978 articles without fee. Instructors are permitted to photocopy isolated articles for noncommercial classroom use without fee. For all other copying, reprint, or republication permission, write to IEEE Service Center, 445 Hoes Lane, Piscataway, NJ 08854 USA. Copyright ©2014 by the Institute of Electrical and Electronics Engineers, Inc. All rights reserved. Periodicals postage paid at New York, NY, and at additional mailing offices. Postmaster: Send address changes to IEEE Signal Processing Magazine, IEEE, 445 Hoes Lane, Piscataway, NJ 08854 USA. Canadian GST #125634188 Printed in the U.S.A.

Digital Object Identifier 10.1109/MSP.2014.2300738



Now...

2 Ways to Access the IEEE Member Digital Library

With **two great options** designed to meet the needs—and budget—of every member, the IEEE Member Digital Library provides full-text access to any IEEE journal article or conference paper in the IEEE *Xplore*® digital library.

Simply choose the subscription that's right for you:

IEEE Member Digital Library

Designed for the power researcher who needs a more robust plan. Access all the IEEE content you need to explore ideas and develop better technology.

- 25 article downloads every month

IEEE Member Digital Library Basic

Created for members who want to stay up-to-date with current research. Access IEEE content and rollover unused downloads for 12 months.

- 3 new article downloads every month

Get the latest technology research.

Try the IEEE Member Digital Library—FREE!

www.ieee.org/go/trymdl



IEEE Member Digital Library is an exclusive subscription available only to active IEEE members.

[from the **EDITOR**]

Abdelhak Zoubir
Editor-in-Chief
zoubir@spg.tu-darmstadt.de
<http://signalprocessingsociety.org/publications/periodicals/spm>

Journals and Magazine Reviews: A Quality Control Mechanism

IEEE Technical Activities (IEEE-TA) is a major component of the IEEE that includes all programs of the 45 Societies of the IEEE and technical councils, as well as programs of the Technical Activities Board (TAB) and the Technical Activities Department. The board, as well as each committee, plays a vital role in the success of IEEE-TA. One of these committees is the TAB Periodicals Review and Advisory Committee (PRAC). Under the “Scope” of the TAB PRAC, it is stated [1]:

The objectives of the Committee are to provide suggestions for improvements; determine how well the IEEE Society/Council (S/C)-sponsored periodicals perform in terms of quality and timeliness, and meet the policies and procedures for IEEE periodicals; conduct a financial “health check,” and make recommendations for changes, if required. In carrying out the above objectives, the TAB Periodicals Review and Advisory Committee, on an ongoing basis, will identify best practices and assist/encourage S/Cs in identification of potential improvements to their publishing programs.

On 13 February, I, as well as my colleagues and fellow editors-in-chief (EiCs) of the IEEE Signal Processing Society (SPS) journals, and IEEE SPS senior leaders, such as the current President Alex Acero, Past-President Ray Liu, and VP Publications Mari Ostendorf, attended the five-year review meeting in Los Angeles. Comprehensive five-year review reports, which were compiled by the EiCs with the assistance of IEEE SPS staff and the oversight of the IEEE SPS VP Publications, were

submitted at an earlier stage to the PRAC. These reports are similar to those submitted for an SPS technical committee five-year review.

Publications volunteers from other IEEE Societies conducted the reviews of *IEEE Signal Processing Magazine (SPM)* and SPS transactions and letters. The meeting was collaborative and collegial and, indeed, it was conducive to improvements in many ways, including best practices used by other IEEE periodicals. During and after the meetings, it was mentioned by the review committee members that SPS is to be commended for its best practices.

Clearly, this is the result of the hard work of the many volunteers in the SPS. Editorial boards play a vital role in maintaining the high quality of journals and the magazine. *SPM* consists of a senior editorial board with members who are academics and industrialists and who tirelessly assist in ensuring the high quality of feature articles and special issues. In addition, the editorial boards for columns and forum as well as the eNewsletter play a crucial role in ensuring timely and high-quality publications. I wish to thank all members of the editorial boards for their support and dedication.

Editorial boards rely on external volunteers who conduct reviews of articles and columns. I take this opportunity to wholeheartedly thank all of the colleagues and friends that are always willing to help with reviews of articles for *SPM*.

I also wish to thank the members of the senior editorial board whose term finished in 2013. Their support was instrumental for ensuring high-quality feature articles and special issues.

It gives me great pleasure to introduce the new 2016 class of editorial board mem-

bers: Patrick Flandrin, Hamid Krim, Hing Cheung So, Isabel Trancoso, Pramod Varshney, and Z. Jane Wang. With these energetic and dedicated professionals, we shall move *SPM* to an even higher level with more innovations to come.

It is one of our main duties as researchers to guide young graduate students and introduce professionals to new areas by providing them with invaluable archival resources. This issue of *SPM* includes a feature article on physical layer service integration in wireless networks, indeed a timely topic for next-generation wireless networks. The authors provide an excellent overview of state-of-the-art solutions and identify signal processing challenges and some promising research directions. Also, this special issue is on a topic that has become extremely important in engineering practice: source separation. Five experts guest edited this issue, which provides an overview on the most important advances, as well as some key areas of development in this area in theory and applications. With the energy, dedication, and enthusiasm of all volunteers, working together with guest editors and authors, we shall move SPS’s flagship magazine to greater heights and serve our research and professional communities par excellence.

REFERENCE

[1] IEEE Technical Activities Board Operations Manual. [Online]. Available: https://www.ieee.org/documents/tab_operations_manual.pdf




Digital Object Identifier 10.1109/MSP.2014.2305766
Date of publication: 7 April 2014

USB & Ethernet SIGNAL GENERATORS

To fit your budget.



from **\$1995** ea.

0.25 to 6400 MHz

Control your test setup via Ethernet or USB with a synthesized signal generator to meet your needs and fit your budget! The SSG-6400HS and the new SSG-6000RC feature both USB and Ethernet connections supporting HTTP and Telnet communication protocols, giving you more choices and more freedom. All our models are supplied with easy-to-install, user-friendly GUI software, DLLs and programming instructions for 32 and 64 bit Windows® and Linux® environments. They all provide power sweep and frequency hopping capabilities and are designed for easy integration with other test equipment using trigger and reference ports. All models have built-in automatic calibration scheduling based on actual usage. Housed in rugged cases small enough to fit in your laptop case, these generators are a space efficient solution for almost any layout! Visit minicircuits.com today to find the right model for your application!

Models Available from Stock at Low Prices!

SSG-6400HS \$4,995

- 0.25 to 6400 MHz
- -75 to +10 dBm P_{Out}
- AM, PM, FM, and pulse modulation
- USB and Ethernet control

New

SSG-6000RC \$2,795

- 25 to 6000 MHz
- -60 to +10 dBm P_{Out}
- Pulse modulation
- USB and Ethernet control

SSG-6000 \$2,695

- 25 to 6000 MHz
- -60 to +10 dBm P_{Out}
- Pulse modulation
- USB control



SSG-4000LH \$2,395

- 250 to 4000 MHz
- -60 to +10 dBm P_{Out}
- Pulse modulation
- Low harmonics (-66 dBc typ.)
- USB control

SSG-4000HP \$1,995

- 250 to 4000 MHz
- High power, -50 to +20 dBm P_{Out}
- Pulse modulation
- USB control

Mini-Circuits®

www.minicircuits.com

P.O. Box 350166, Brooklyn, NY 11235-0003 (718) 934-4500 sales@minicircuits.com

519 rev H

[president's MESSAGE]

Alex Acero
2014–2015 SPS President
a.acero@ieee.org



GlobalSIP and ChinaSIP: New Conferences Developed by the IEEE Signal Processing Society

Through member surveys, we have learned that you value attending conferences and workshops as an opportunity to present your work, learn the latest advances in the field, and have a chance to network with colleagues. As the signal processing field grows, more and more members join our Society, and our conferences and workshops attract more and more attendees. We are always looking for opportunities to serve you better, and that includes offering more technical meetings from which you can choose.

The International Conference on Acoustics, Speech, and Signal Processing (ICASSP) is the largest conference organized by the IEEE Signal Processing Society and the only one that covers all of the Society's fields of interest. Since its founding in 1976, ICASSP has taken place in the spring of every year. To cater to the more specialized needs within the signal processing field, many of our 12 technical committees (TCs) have workshops in the fall. Running a workshop is a time-consuming process for the volunteer organizers, as it involves many nontechnical activities such as setting up contracts with hotels for meeting space and meals, registration, local arrangements, etc. To address these responsibilities, the Society's Board of Governors decided to offer another option to such workshop organizers: the IEEE Global Conference on Signal and Information Processing (GlobalSIP).

GlobalSIP is a collection of symposia proposed by our TCs that all take place at the same venue and the same time during

the fall, so that many of the nontechnical logistics can be shared. TCs are not forced to set up their workshops at GlobalSIP though; they can continue running their workshops independently if they so wish. Our first GlobalSIP took place in Austin, Texas, United States, in December 2013. I want to thank General Chairs Robert Heath and Ahmed Tewfik, as well as the rest of the organizing committee for the enthusiasm and work they put in running a very successful conference. GlobalSIP 2013 was a collection of 18 separate symposia, each run by a separate technical program committee with its own technical theme, format, and acceptance rate. GlobalSIP 2013 attracted 466 attendees, many of whom came from other fields. We received positive feedback from the attendees, especially that GlobalSIP provided them an opportunity to meet people with different expertise.

The IEEE Signal Processing Society is becoming more and more international. The first ICASSP took place in Philadelphia, Pennsylvania, United States, in 1976 and, of the first ten ICASSPs, only one took place outside the United States (Paris, France) in 1982. The situation has changed dramatically in the last 40 years. In fact, of the five upcoming ICASSPs, only one will take place in the United States. ICASSP 2014 will be held in Florence, Italy; ICASSP 2015 in Brisbane, Australia; ICASSP 2016 in Shanghai, China; ICASSP 2017 in New Orleans, Louisiana, United States; and ICASSP 2018 in Seoul, South Korea. At the same time, roughly 50% of the Society's members are coming from the United States (Regions 1–6). So, the Society's Board of Governors decided to hold GlobalSIP in

the United States, at least for the next few years, since many of our Region 1–6 members wanted to have access to a premier signal processing conference closer to their home base. GlobalSIP 2014 will take place in Atlanta, Georgia, United States, on 3–5 December 2014. We look forward to seeing you there.

Also, tremendous growth in China prompted us to create a conference in that country. The first IEEE China Summit and International Conference on Signal and Information Processing (ChinaSIP) took place in Beijing in July 2013, and it attracted over 400 attendees. I want to thank General Chairs Thomas Fang Zheng and Zhi Ding as well as the rest of the organizing committee for their hard work. I encourage you to attend ChinaSIP 2014, which will take place in Xi'an, China, on 9–13 July 2014.

ICASSP 2013 in Vancouver, Canada, had over 2,400 attendees and offered plenty of interesting papers and stimulating discussions. I'm looking forward to seeing you at ICASSP 2014 in the beautiful city of Florence, Italy, on 4–9 May 2014. ICIP 2013 took place in Melbourne, Australia, with over 1,000 attendees. ICIP 2014 will take place in another beautiful city, Paris, France, on 27–30 October 2014. There are many more specialized workshops happening this year. I hope you find time in your busy schedule to attend at least one of these conferences or workshops.

[SP]

Digital Object Identifier 10.1109/MSP.2014.2305774
Date of publication: 7 April 2014



Instant Access to IEEE Publications

Enhance your IEEE print subscription with online access to the IEEE *Xplore*® digital library.

- Download papers the day they are published
- Discover related content in IEEE *Xplore*
- Significant savings over print with an online institutional subscription

Start today to maximize your research potential.

Contact: onlinesupport@ieee.org
www.ieee.org/digitalsubscriptions

"IEEE is the umbrella that allows us all to stay current with technology trends."

Dr. Mathukumalli Vidyasagar
Head, Bioengineering Dept.
University of Texas, Dallas



 **IEEE**
Advancing Technology
for Humanity

SPS Members Recognized with Awards

The IEEE Signal Processing Society (SPS) congratulates the following SPS members who are being recognized with the Society's prestigious awards during the International Conference on Acoustics, Speech, and Signal Processing (ICASSP) 2014 in Florence, Italy, on 4–9 May.

2013 IEEE SPS AWARDS TO BE PRESENTED IN FLORENCE, ITALY

The Society Award honors outstanding technical contributions in a field within the scope of the SPS and outstanding leadership within that field. The Society Award comprises a plaque, a certificate, and a monetary award of US\$2,500. It is the highest-level award bestowed by the IEEE SPS. This year's recipients are Al Bovik, "for fundamental contributions to digital image processing theory, technology, leadership and education" and Alan S. Willsky "for fundamental contributions to probabilistic modeling and for pioneering work in the development and application of multiresolution statistical methods."

Two Technical Achievement Awards are presented this year. Yonina Eldar will receive the award "for fundamental contributions to sub-Nyquist and compressed sampling, convex optimization, and statistical signal processing." Al Hero will be recognized "for information-theoretic advances in statistical signal processing and machine learning." The Technical Achievement Award honors a person who, over a period of years, has made outstanding technical contributions to theory and/or practice in technical areas within the scope of the Society, as demonstrated by publications, patents,

or recognized impact on this field. The prize for the award is US\$1,500, a plaque, and a certificate.

Two Meritorious Service Awards will be presented this year to Ali H. Sayed and Rabab Ward "for exemplary service to and leadership in the IEEE Signal Processing Society." The award comprises a plaque and a certificate; judging is based on dedication, effort, and contributions to the Society.

TWO MERITORIOUS SERVICE AWARDS WILL BE PRESENTED THIS YEAR TO ALI H. SAYED AND RABAB WARD "FOR EXEMPLARY SERVICE TO AND LEADERSHIP IN THE IEEE SIGNAL PROCESSING SOCIETY."

The SPS Education Award honors educators who have made pioneering and significant contributions to signal processing education. Judging is based on a career of meritorious achievement in signal processing education as exemplified by writing scholarly books and texts, course materials, and papers on education; inspirational and innovative teaching; and creativity in the development of new curricula and methodology. The award comprises a plaque, a monetary award of US\$1,500, and a certificate. The recipient of the SPS Education Award is Dimitris Manolakis, "for fundamental contributions to education in signal processing and algorithms for adaptive filtering and hyperspectral target detection."

The IEEE Signal Processing Magazine Best Paper Award honors the author(s) of an article of exceptional merit and broad interest on a subject related to the

Society's technical scope and appearing in the Society's magazine. The prize comprises US\$500 per author (up to a maximum of US\$1,500 per award) and a certificate. In the event that there are more than three authors, the maximum prize shall be divided equally among all authors, and each shall receive a certificate. This year, the IEEE Signal Processing Magazine Best Paper Award recipients are Zhou Wang and Alan C. Bovik for their article "Mean Squared Error: Love it or Leave it? A New Look at Signal Fidelity Measures," published in *IEEE Signal Processing Magazine*, vol. 26, no. 1, Jan. 2009.

Five Best Paper Awards were awarded, honoring the author(s) of a paper of exceptional merit dealing with a subject related to the Society's technical scope and appearing in one of the Society's transactions, irrespective of the author's age. The prize is US\$500 per author (up to a maximum of US\$1,500 per award) and a certificate. Eligibility is based on a five-year window preceding the year of election, and judging is based on general quality, originality, subject matter, and timeliness. Up to six Best Paper Awards may be presented each year. This year, the awardees are:

- Amir Beck, Petre Stoica, and Jian Li, "Exact and Approximate Solutions of Source Localization Problems," *IEEE Transactions on Signal Processing*, vol. 56, no. 5, May 2008
- Matthew A. Herman and Thomas Strohmer, "High-Resolution Radar via Compressed Sensing," *IEEE Transactions on Signal Processing*, vol. 57, no. 6, June 2009
- Chunming Li, Chiu-Yen Kao, John C. Gore, and Zhaohua Ding, "Minimization of Region-Scalable Fitting Energy for Image Segmentation," *IEEE Transactions on Image Processing*, vol. 17, no. 10, Oct. 2008

■ Robert W. Heath, Jr., Tao Wu, Young Hoon Kwon, and Anthony C.K. Soong, “Multiuser MIMO in Distributed Antenna Systems with Out-of-Cell Interference,” *IEEE Transactions on Signal Processing*, vol. 59, no. 10, Oct. 2011

■ George E. Dahl, Dong Yu, Li Deng, and Alex Acero, “Context-Dependent Pre-Trained Deep Neural Networks for Large-Vocabulary Speech Recognition,” *IEEE Transactions on Audio, Speech, and Language Processing*, vol. 20, no. 1, Jan. 2012.

The Young Author Best Paper Award honors the author(s) of an especially meritorious paper dealing with a subject related to the Society’s technical scope and appearing in one of the Society’s transactions and who, upon date of submission of the paper, is under 30 years of age. The prize is US\$500 per author (up to a maximum of US\$1,500 per award) and a certificate. Eligibility is based on a three-year window preceding the year of election, and judging is based on general quality, originality,

subject matter, and timeliness. Three Young Author Best Paper Awards are being presented this year:

■ Yuejie Chi, for the paper coauthored with Louis L. Scharf, Ali Pezeshki, and A. Robert Calderbank, “Sensitivity to Basis Mismatch in Compressed Sensing,” *IEEE Transactions on Signal Processing*, vol. 59, no. 5, May 2011

■ Kalpana Seshadrinathan, for the paper coauthored with Alan Conrad Bovik, “Motion Tuned Spatio-Temporal Quality Assessment of Natural Videos,” *IEEE Transactions on Image Processing*, vol. 19, no. 2, Feb. 2010

■ Lin Li, for the paper coauthored with Anna Scaglione and Jonathan H. Manton, “Distributed Principal Subspace Estimation in Wireless Sensor Networks,” *IEEE Journal of Selected Topics in Signal Processing*, vol. 5, no. 4, Aug. 2011.

One IEEE Signal Processing Letters Best Paper Award was awarded, honoring the author(s) of a letter article of

exceptional merit and broad interest on a subject related to the Society’s technical scope and appearing in *IEEE Signal Processing Letters*. The prize shall consist of US\$500 per author (up to a maximum of US\$1,500 per award) and a certificate. To be eligible for consideration, an article must have appeared in *IEEE Signal Processing Letters* in an issue five years preceding the year of election. Judging shall be on the basis of the technical novelty, the research significance of the work, quality, and effectiveness in presenting subjects in an area of high impact to the Society’s members. The recipient of the IEEE Signal Processing Letters Best Paper Award is

■ Gan Zheng, Kai-Kit Wong, Arogyaswami Paulraj, and Björn Ottersten, “Collaborative-Relay Beamforming with Perfect CSI: Optimum and Distributed Implementation,” *IEEE Signal Processing Letters*, vol. 16, no. 4, Apr. 2009.

[SP]

CAMBRIDGE

JOURNALS

APSIPA

TRANSACTIONS ON SIGNAL AND INFORMATION PROCESSING



In partnership with the Asia-Pacific Signal and Information Processing Association (APSIPA)

Benefits of publishing in the journal

- Average submission to first decision time **less** than 2 months
- Average acceptance to publication time **less** than 1.5 months
- Peer-reviewed by international experts
- Global dissemination of your research

Submit your article
mc.manuscriptcentral.com/apsipa



journals.cambridge.org/sip



CAMBRIDGE
UNIVERSITY PRESS

Signal Processing Leads a Photographic and Imaging Revolution

Photography and imaging have been radically transformed over the past couple of decades in ways that 19th-century pioneers such as Louis-Jacques-Mandé Daguerre (Figure 1) and Henry Fox Talbot could have scarcely imagined. Traditional photography and imaging, rooted in chemical processes, have now largely given way to digital methodologies and technologies. The result has been faster, less expensive, and more convenient ways of acquiring and presenting images, and in many cases the creation of clearer, more detailed, and less distorted pictures on many different types of media.

Signal processing plays an important role in virtually all types of digital photography and imaging. In consumer, professional, industrial, and scientific still cameras, sophisticated integrated algorithms help determine how images are collected, interpreted, and stored. Algorithms, for example, ensure that captured raw sensor data are efficiently translated into color-corrected image data that can then be stored either in raw pixels or as compressed images. Image processing algorithms are also involved in image capture and compression, focus and exposure control, managing white balance, demosaicing, image storage, preview display rendering and scaling, and various post-processing tasks.

FREEZING STREAKS

As researchers work to extend the capabilities of existing imaging systems, as well as blaze new technologies, signal processing provides ways of adding new capabilities and improving the performance of

existing features and functions. Researchers at Laguna Hills, California-based MetroLaser, for instance, used signal processing in the creation of a camera that captures full-color images of projectiles traveling at speeds of up to 3,350 m/s, approximately ten times the speed of sound. The digital galvo mirror streak camera, designed to replace now-obsolete film-based streak cameras, records the motion of a projectile as it passes in front of its lens, creating a long, continuous composite image of the object.

Now that digital technology has completed its sweep across the photography industry, the specialized film required for analog streak photography cameras is no longer being manufactured. In 2007, the U.S. Air Force asked MetroLaser to design a modern digital system that could produce high-quality ballistic images. “The Air Force wanted a highly rugged digital camera system that would allow them to get full-color, high-resolution photos of rocket sleds moving up to Mach 10 with schlieren effects (optical inhomogeneities in transparent material that aren’t necessarily visible to the human eye) included,” says Ben Buckner, MetroLaser’s chief scientist.

The imaging system Buckner developed with coresearcher Drew L’Esperance, utilizes a precisely controlled mirror galvanometer to follow a rapidly moving object and freeze its image. Buckner explains that the mirror tracks the ballistic object as it moves past the camera lens and directs appropriate portions of the image onto specified areas of the image sensor to form a complete, undistorted picture. “It enables full-color 15-plus megapixel photography of objects moving at high speeds with standard photographic flashes, or even strong natural light, with schlieren photography of disturbances in the surrounding air,” Buckner says.

Since the mirror is synchronized to the ballistic object, the biggest challenge the researchers faced when developing the system was finding a way of accurately measuring the object’s speed and calculating the swing of the mirror to precisely match that object’s trajectory. “The main challenge is that the software has to control a galvanometer mirror very precisely and very quickly,” Buckner says. “The rocket sled velocity is variable, so you have to measure [the sled] as it’s coming down the track, and in a few milliseconds, the software has to calculate the required trajectory for the mirror to match the speed and generate the control signals,” he continues. At such high speeds, the mirror response tends to be nonlinear. “So in addition to working out the basic kinematic equations for the motion, you have to put in some corrections and then generate the required control waveform on the fly,” he says.

“I put a fair bit of time into optimizing the code for fast execution, since it’s on a



[FIG1] Photography pioneer Louis-Jacques-Mandé Daguerre. (Photo courtesy of www.wikipedia.com.)

Digital Object Identifier 10.1109/MSP.2014.2301793

Date of publication: 7 April 2014

IEEE GlobalSIP

December 3-5, 2014
Georgia Tech Hotel
and Conference Center
Atlanta, GA USA

General Chairs

Geoffrey Li
Georgia Tech

Fred Juang
Georgia Tech

Technical Program Chairs

Douglas Williams
Georgia Tech

Timothy Davidson
McMaster University

Ghassan AlRegib
Georgia Tech

Finance Chair

David V. Anderson
Georgia Tech

Local Arrangement Chair

Xiaoli Ma
Georgia Tech

Publications/Publicity Chair

Zhengdao Wang
Iowa State University

Industrial Liaison Chairs

Ahsan Aziz
National Instruments

Mashhour Solh
Texas Instruments

The 2nd IEEE Global Conference on Signal and Information Processing (GlobalSIP 2014)

The IEEE Global Conference on Signal and Information Processing (GlobalSIP) is a recently launched flagship conference of the IEEE Signal Processing Society. It is made up of a series of symposia and workshops. GlobalSIP 2014 will focus broadly on signal and information processing with an emphasis on up-and-coming signal processing themes. For details and paper submission, please go to <http://www.ieeeglobalsip.org>.

List of Symposia

1. Information Processing for Big Data
2. Perception Inspired Multimedia Signal Processing Techniques
3. Machine Learning Applications in Speech Processing
4. Data Flow Algorithms and Architecture for Signal Processing Systems
5. Advances in Mixed-Signal and Optical Sensing: Hardware to Algorithms
6. Signal Processing Applications Related to Animal Environments
7. Signal Processing for Next Generation Semiconductor Integrated Circuits
8. Energy Exchange and Intelligent Trading
9. Signal Processing for Cognitive Radios and Networks
10. Energy Efficiency and Energy Harvesting Related Signal Processing and Communications
11. Game Theory for Signal Processing and Communications
12. Signal Processing Challenges and Architectures for High Throughput Satellite Communications
13. Massive MIMO Communications
14. Network Theory

Workshops

1. Workshop on Information Forensics and Security (WIFS)
 - Privacy Preserving Technologies
 - Information Forensics and Watermarking
 - Biometrics, Authentication and Secure Multiparty Computation
 - Secure Communication and Networking
2. Workshop on Genomic Signal Processing and Statistics (GENSIPS)
 - Signal Processing of Genomic Sequencing Data
 - Modeling and Integration of Multi-Modality Omics Data
 - Dynamics and Control of Regulatory and Signaling Networks

Paper Submission

Paper submission instructions are available through the GlobalSIP 2014 website at <http://www.ieeeglobalsip.org>.

Contacts

Zhengdao Wang
Email: zhengdao@iastate.edu
for website and EDAS-related questions

Important Dates

May 16, 2014
June 27, 2014
September 5, 2014

Paper submission deadline (regular and invited)
Review results announced
Camera-ready regular and invited papers due



special REPORTS continued

fairly low-end embedded processor,” Buckner says. Other challenges were optimizing the acceleration curve and deriving the nonlinear response corrections. “We’re pushing the galvo controller to its limits, so the way you accelerate it is important,” Buckner says.

Buckner foresees other potential applications for the galvo mirror streak camera, such as determining the finishing order in high-speed races. “There are other ways of doing high-speed imaging, but this one is particularly effective at doing very high-resolution images, color images, schlieren images, and large-scale subjects where it’s very difficult to get a submillisecond flash of sufficient energy,” he explains.

Most other types of high-speed imaging techniques are hampered by resolution and color reproduction limitations, Buckner says. The galvo mirror streak camera, however, has many of the same benefits as conventional professional-level cameras. “We can work with the same flash rigs that any commercial photographer uses, and

largely [with] the same camera back,” Buckner explains. “Our system really just replaces the camera lens, and all the rest of it is the same equipment you would find being used to take school pictures or magazine glamour shots.” The system’s modular design also allows it to be easily upgraded. “Commercial camera backs are always improving,” Buckner says. “We could easily get [the system] up to 80 megapixels now just by putting one of the newer camera backs on it.”

UPGRADING MICROSCOPES

Researchers at the California Institute of Technology (Caltech) relied on signal processing techniques to help develop a method of converting relatively inexpensive conventional microscopes into high-end billion-pixel imaging systems. The new approach, called Fourier Ptychographic Microscopy (FPM), promises to significantly enhance the efficiency of digital pathology, particularly in situations where specialists need to review large

numbers of tissue samples (Figure 2). The researchers also hope that the technology will bring high-performance microscopy capabilities to medical clinics that can’t currently afford high-density imaging systems.

“A microscope’s pixel count is fundamentally limited by the physical nature of the optical lenses—all physical lenses have aberrations that ultimately degrades the imaging process,” says Changhuei Yang, a Caltech professor of electrical engineering, bioengineering, and medical engineering. A standard digital microscope typically creates images with approximately ten megapixels of resolvable pixels. “You can choose between a large field of view and a poor resolution, or small field of view and a high resolution,” Yang says. “If we are simply examining microscope slides with our eyes, this pixel count is quite sufficient, but this pixel count is woefully low to address digital pathology needs.”

FPM provides a computational-oriented approach that aims to free microscope developers from the physical limitations of optical lenses. The microscopy industry’s current approach for creating high-quality microscopes is to use very complicated—and expensive—stacks of exotic glass lenses to cross-compensate for aberration. FPM makes this type of development model unnecessary. “To FPM, the distortions in optical elements are simply mathematical functions that it can manipulate computationally and zero out of the final processed image,” Yang says. “We can take a [poor] microscope, make some cheap modification to its lighting scheme, and use it to collect a sequence of poor-quality images. “The algorithm will then take the data and render a high-quality and high pixel count image.”

FPM stitches the low-resolution images together to create high-resolution intensity and phase information, providing a more complete picture of a particular clinical sample’s entire light field. To create a complete image of a particular sample, the system acquires approximately 150 low-resolution images with each image corresponding to a single element in the light-emission diode (LED) array.

When their work began several years ago, the researchers struggled to reach

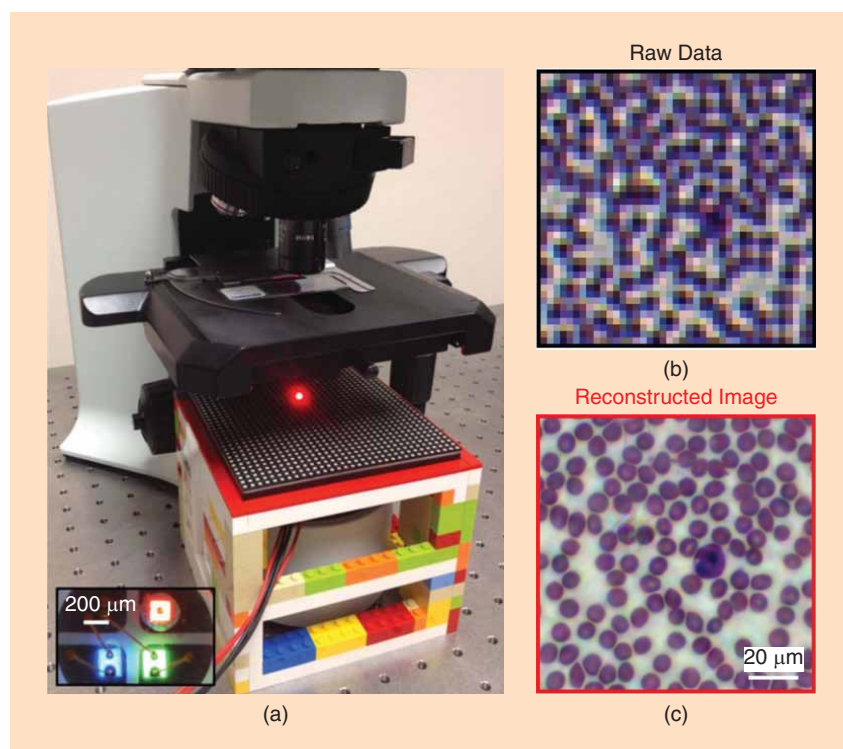


[FIG2] (a) An FPM installation that converts a relatively inexpensive conventional microscope into a billion-pixel imaging system. The inset in (a) shows a magnified image of the LED chip that contains a red-green-blue LED. A raw image of human blood smear taken with a 2X objective lens is shown in (b) along with (c) the reconstructed image produced by the FPM system. (Photo courtesy of the California Institute of Technology.)

their goal by completely eliminating lenses from microscopes. The approach found them trying a variety of chip-scale microscope systems, none of which met their performance or cost targets. "In the past couple of years, we started asking ourselves whether we can tackle optical aberrations head-on rather than side-stepping the problem," Yang says. "If we could, we would not have to throw out the compelling advantages of using lenses in microscopes." Benefits associated with lenses include the ability to concentrate light and easier color handling. By following a computational-oriented approach and developing FPM, the researchers were able to bring the resolution of a conventional 2X objective lens to the level of a 20X objective lens.

FPM's main design strategy is similar to that of interferometric synthetic aperture microscopy: expanding summation

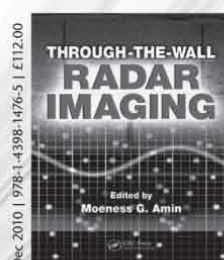
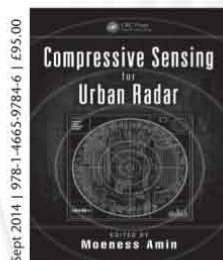
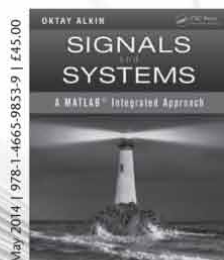
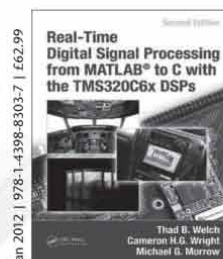
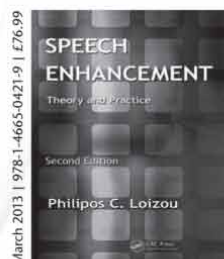
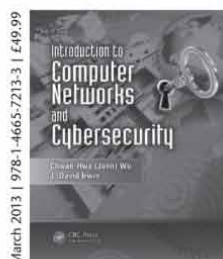
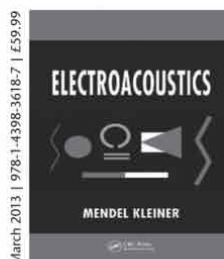
by parts (SBP) in Fourier space through multi-image fusion. However, because no measured phase information is needed for FPM, the researchers' approach eliminates the design challenges associated with interferometric detection. Yet FPM's image recovery procedure follows a strategy common with ptychography scanning diffraction microscopy, iteratively solving for a sample estimate that is consistent with many intensity measurements. Unlike ptychography, however, FPM's object support constraints are imposed in the Fourier domain, offering several unique advantages and opportunities.

FPM's data collection procedure is straightforward, according to Yang. The process involves placing a two-dimensional (2-D) sample at the focal plane of a low-numerical aperture microscope objective and collecting a sequence of images, with the sample successively illuminated

by plane waves at different angles. Unlike other synthetic aperture techniques, the procedure acquires intensity images of the sample, so no interferometric measurements are required. The use of a low-numerical aperture objective lens allows a large field of view to be captured at the expense of a low spatial resolution.

A major advantage of the new approach is relatively pain-free hardware compatibility. Manufacturers only need to add an LED array to an existing microscope—no other hardware modifications are necessary. A computer then handles the rest of the work. The researchers say that their method could have wide applications not only in digital pathology but also in everything from hematology to wafer inspection to forensic photography. "A broad swath of imaging modalities can benefit from this computational approach of tackling imaging," Yang says. Satellite

Engineering from CRC Press



CRC Press will be Exhibiting at this year's ICASSP, please visit our booth!

SAVE 20% when you order online and enter Promo Code EKN02.

FREE standard shipping worldwide!

www.crcpress.com



special **REPORTS** continued

imaging is a particular area of interest. “The features we can resolve in satellite images is tied to the size of the camera you send up to space,” Yang says. “We think FPM can ... allow satellite imaging at unprecedented resolution.” X-ray imaging is another potential application. “X-ray imaging is confounded by the lack of high-quality lenses,” Yang says. FPM makes this a nonissue since it simply treats the distortions as a mathematical function.

Yang is optimistic that FPM microscopy will soon become a scientific mainstay. “Because the hardware is so simple, we hope it will be commercially available in a couple of years,” he says.

FIXING PHOTOS

Sophisticated computational processing also promises to benefit the everyday users of smartphones and various other types of consumer-level cameras. Targeting such individuals, researchers at the Massachusetts Institute of Technology (MIT) have developed a chip-based processor that’s dedicated to helping almost any camera user—amateur or pro—create high-quality photographs.

At MIT’s Microsystems Technology Laboratory, Rahul Rithe, a graduate student in the school’s Department of Electrical Engineering and Computer Science, recently worked on the team that developed the “Maxwell” processor (named after James Clerk Maxwell, who in 1855 first proposed creating color photographs by using red, green, and blue filters to merge together three captured images). The chip (Figure 3) aims to help shutterbugs by

almost instantaneously creating more realistic or enhanced lighting in a shot without destroying the scene’s ambience. “This energy-efficient and scalable implementation is ideal for integration with mobile devices such as smartphones, tablets, digital cameras, and even laptops, to enable live computational photography on these energy-constrained devices,” says Rithe, who was lead author of a paper on the project.

RITHE NOTES THAT SIGNAL PROCESSING TECHNIQUES LIKE NONLINEAR FILTERING ARE ESSENTIAL TO THE PROCESSOR’S OPERATION.

Most current computational photography applications are software based. “Performing [image optimization] tasks on general purpose CPUs and GPUs consumes a significant amount of power and is typically not fast enough to support real-time performance,” Rithe says. He states that the Maxwell processor can perform optimization operations in real-time while consuming dramatically less power. “While software-based systems typically take several seconds to perform an operation like high dynamic range (HDR) imaging, the chip can do it in a few hundred milliseconds on a ten-megapixel image,” says Rithe, who notes that the high-performance chip can also enhance video output.

To create an HDR image, Maxwell tells the camera to take three individual low dynamic range photos: a normally exposed image, an overexposed image capturing details in the dark areas of the scene, and an underexposed image capturing details in the bright areas. The processor then merges the photos to create a single image that captures the scene’s full color and brightness range.

The processor uses bilateral filtering, Rithe says, a nonlinear filtering technique that effectively reduces noise and smooths out an image’s defects without blurring sharp edges, thereby preserving important details. “Nonlinear filtering techniques like bilateral filtering are used in a wide

range of computational photography applications,” he notes. Unfortunately, due to its high computational complexity, bilateral filtering is generally inefficient and slow. “We leveraged the bilateral grid structure ... and developed an optimized hardware implementation that represents a 2-D image using a three-dimensional (3-D) data structure and performs the processing in the 3-D domain,” Rithe says. “This significantly reduces both the computational complexity and the amount of memory required to process large images.”

Rithe notes that signal processing techniques like nonlinear filtering are essential to the processor’s operation. “Signal processing is vital to our research in the form of image processing techniques that enable us to manipulate and create images that could have only come from a handful of prolific artists, like Ansel Adams, in the past,” Rithe says. The algorithms implemented on the chip were inspired by the computational photography work of Fredo Durand and Bill Freeman (an associate professor and professor, respectively), at MIT’s Computer Science and Artificial Intelligence Laboratory.

Multimedia processing applications such as computational photography have very high computational complexity and memory requirements. “The major challenge was to come up with a combination of algorithmic-, architectural-, and circuit-level innovations that significantly brought down the computational complexity, memory requirement, and bandwidth,” Rithe says. “To enable real-time processing while being extremely power efficient, we developed a highly parallel architecture that is able to support real-time processing of high-definition (HD) images while operating at less than 100 MHz frequency, as opposed to CPUs and GPUs that operate at several GHz.” One of the key components in maximizing the processor’s energy-efficiency is voltage/frequency scaling. “Careful circuit design for low-voltage operation ensured reliable performance from 0.9 V down to 0.5 V,” Rithe explains. “This enables voltage/frequency scaling to maximize the energy-efficiency for a required performance level.”

Rithe developed the processor on a team that included Anantha Chandrakasan, MIT’s Joseph F. and Nancy P.



[FIG3] A printed circuit board containing MIT’s “Maxwell” computational photography processor. (Photo courtesy of MIT.)

Keithley Professor of Electrical Engineering. Other members included fellow graduate student Priyanka Raina, research scientist Nathan Ickes, and undergraduate student Srikanth Tenneti.

Work on the processor began in January 2011 when Rithe and his coresearchers started exploring different types of computational photography algorithms. After the team completed algorithmic optimizations, developed a highly parallel architecture to enable real-time processing, and finalized circuit implementations, the chip was sent for fabrication in April 2012 through Taiwan Semiconductor Manufacturing Company's University Shuttle Program.

The researchers presented their work at the IEEE International Solid-State Circuits Conference in February 2013.

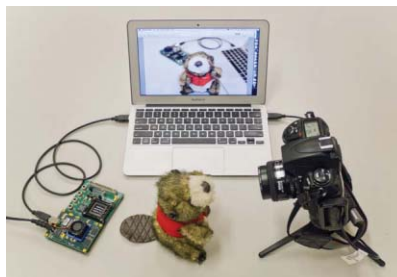


[FIG4] A demonstration system that integrates the processor with DDR2 memory and connects with a camera and a display through the USB interface. The system provides a platform for live computational photography. (Photo courtesy of Nathan Ickes/MIT.)

The live demonstration system prototype combined the processor with external memory, camera, and display (Figure 4). “We received significant interest from

the leading mobile processor and device makers,” Rithe says.

Future processors designed along the lines of Maxwell will permit more complex computational photography applications, Rithe says. He notes that Raina is currently leading an effort to develop a processor capable of sharpening images that are blurred due to camera shake during image capture. “We are also exploring ways of extending computational photography and computer vision techniques to enable portable smartphone-based medical imaging applications,” he says.

AUTHOR

John Edwards (jedwards@johnedwardsmedia.com) is a technology writer based in the Phoenix area.

9

Innovation doesn't just happen.
Read first-person accounts of
IEEE members who were there.

IEEE Global History Network
www.ieeeahn.org

Photo: NASA

IEEE

[from the **GUEST EDITORS**]Tülay Adalı, Christian Jutten,
Arie Yeredor, Andrzej Cichocki,
and Eric Moreau

Source Separation and Applications

Data-driven methods are based on a simple generative model such as matrix or tensor decompositions and hence can minimize the assumptions on the nature of the data and the latent variables. They have emerged as alternatives to the traditional model-based approaches whenever the unknown dynamics are hard to characterize. Source separation has been at the heart of data-driven approaches and has found wide applicability in areas as diverse as biomedicine, communications, finance, geophysics, and remote sensing.

Historically, the source separation problem has been posed with flexible and general assumptions and minimal priors, hence leading to the designation blind source separation (BSS). The first methodology for successful BSS was independent component analysis (ICA), and today, source separation includes a broader range of topics that emphasize incorporation of various priors and different types of decompositions to take the natural dimensionality of the observed data into account. New trends of research include the joint analysis of large-scale heterogeneous multidimensional sets of data, e.g., associated to multimodal data acquisition as in hyperspectral or brain imaging. In addition, underdetermined problems, i.e., those with a weak diversity and a large number of sources, are practically very interesting and can be solved through the use of additional priors such as sparsity. Indeed, many connections between source separation and the fields of sparse representations, compressive sensing, and dictionary learning have emerged, leading to new avenues for research. Hence,

addressing the theory and problems at the junction of these topics, along with other exciting directions such as sparse component analysis and nonnegative matrix factorization (NMF), is of particular interest.

Our aim in this special issue is to provide a comprehensive view of the main advances in the field through a number of overview articles as well as contributions that emphasize the key topics of development in the area, both in terms of theory and applications. The issue contains 12 articles, where the focus of the last five is on applications.

The first two articles are overviews. The first article “Diversity in Independent Component and Vector Analyses” by Adalı et al. provides an overview of ICA and its extension to multiple data sets, independent vector analysis (IVA). Mutual information rate is used as the cost that allows the use of both non-Gaussianity and sample dependence as the form of diversity—statistical property—for achieving the decomposition, which in the case of IVA, adds the use of one more type of diversity, statistical dependence of the sources across the data sets. For this general case, identification conditions are given for both ICA and IVA, underlining the parallels between the two, and noting that both can identify multiple Gaussians under certain conditions when non-Gaussianity is not the only form of diversity that is used. Many existing algorithms and results are discussed as special cases under this broad umbrella along with performances of a few using medical imaging as the motivating example. While the focus in terms of algorithms for the first overview article is on iterative methods that maximize the likelihood, the second article shifts the focus to another important class—source separation through joint diagonalization.

The joint diagonalization of a set of matrices has been a prominent tool in linear ICA and BSS since, in many mixing models, the underlying key features of the mixed sources—such as their mutual statistical independence—can be expressed in terms of diagonal matrices. In fact, exact or approximate joint diagonalization is an important particular case of a broader family of joint matrix decompositions and transformations, which can be useful in a variety of source separation scenarios. The article “Joint Matrices Decompositions and Blind Source Separation” by Chabriel et al. provides a description of some of the theory and practice behind the different signal models and approaches in which advanced techniques for joint matrix decompositions become instrumental.

In recent years, the field of source separation benefited from the gradual assimilation of multilinear algebra into signal processing, in the form of tensors in general and tensor decompositions in particular. In many practical source separation contexts, the observed signals can be arranged in multiway arrays, and much can be gained by considering them as tensors and by applying tensor analysis and decomposition tools—which, in many cases, can produce not only estimates of the mixing parameters but also denoised versions of the underlying source signals. In his article “Tensors,” Comon overviews some of the fundamental properties of tensors, such as their relations with polynomials and different concepts of tensor ranks. Several exact and approximate tensor decomposition approaches are reviewed in a way that can hopefully serve as a solid basis for readers interested in further pursuing these appealing tools.

Nonnegativity is a natural property that one can take into account when achieving source separation, and NMF has indeed

Digital Object Identifier 10.1109/MSP.2014.2300211

Date of publication: 7 April 2014

been an active area. Three articles in the special issue have a focus on nonnegative factorizations. In “Nonnegative Matrix and Tensor Factorizations,” Zhou et al. present an overview of the current and novel efficient algorithms for large-scale NMF and their extensions to nonnegative tensor factorizations and decompositions. The performances of the proposed algorithms are demonstrated by several illustrative examples. In “Static and Dynamic Source Separation Using Nonnegative Factorizations,” Smaragdis et al. discuss models beyond the standard NMF and provide a unifying approach to nonnegative source separation for both static and dynamic models. They show how they can be easily extended to temporal models that are either continuous or discrete. Their approach enables many alternative formulations of dynamic source separation algorithms with nonnegativity constraints. Finally, in “Putting Nonnegative Matrix Factorization to the Test,” Huang and Sidiropoulos give a concise tutorial style derivation for the Cramér–Rao lower bound for standard symmetric and asymmetric NMF. By providing the performance bound, they provide the benchmark against which the performance of the competitive NMF algorithms can be assessed. The proposed approach can be extended to facilitate analogous derivations for related bilinear matrix factorizations problems with constraints other than nonnegativity.

Classical source separation mostly relies on statistical properties of the sources and is usually effective only when the mixing process is invertible, requiring the number of observed mixtures to be equal to (or larger than) the number of sources. Separation of sources from fewer mixtures, and even from a single mixture, is possible when some structural information is available regarding the sources, especially when such information can be expressed using a convex operator—cost function—which promotes the desired structure. The article “Convexity in Source Separation” by McCoy et al. provides an elucidating overview of this emerging field, starting with simple motivating examples and following through with an explanation of underlying theoretical

concepts, separability conditions and algorithmic aspects. Li et al. also addresses the underdetermined problem in “Sparse Representation for Brain Signal Processing” and considers an important application area—brain imaging. The problem that has no solution without extra priors has been addressed in the early 2000s based on sparsity assumption on the sources, and the work has led to a wide class of methods known as sparse component analysis, also related to sparse representation and dictionary learning, two very active areas of research. In their article, the authors provide a review and extension of main results in the area and then demonstrate how sparse representation methods can enhance ill-posed inverse problems in brain signal processing.

Audio processing, the original inspiration to the source separation problem by the “cocktail-party problem,” has been arguably the most active application area for source separation. Today, the area is still a very active one, and three of the articles in this issue have a focus on audio applications. While initially, most of the work in the area considered the convolutive nature of the mixtures and were based on approaches in the time or frequency domain, the current state of the art and recent advances exploit—most often jointly—many priors on signals, such as sparsity, positivity, and sophisticated models of speakers, of instruments or the rooms, leading to informed source separation. The article “From Blind to Guided Audio Source Separation” by Vincent et al. provides an attractive review of this evolution and critical perspectives for the field. The transition from blind, to semiblind, and semi-informed separation is the focus of another article in the issue. In “Score-Informed Source Separation for Musical Audio Recordings,” Ewert et al. address the growing field of music signal processing, which has applications in stereo-to-surround up-mixing, remixing tools, instrument-wise equalizing, karaoke systems, and preprocessing in music analysis tasks. They review recent developments in the field that integrate the prior knowledge encoded by the musical score, a simple prior that is typically available. In

addition to use of different priors that lead to an “informed” solution, one can also make use of complementary information, more specifically, visual information, which can be considered to be insensitive to background noise. The article “Audiovisual Speech Source Separation” by Rivet et al. provides an overview of the key methodologies in audiovisual speech source separation. It focuses on three aspects: modeling the audio-video coherence in a common probabilistic framework for modeling the audiovisual features distribution; use of video as secondary modalities for improving speech detection; and use of video information to regularize/control the audio enhancement based on either ICA or time-frequency masking.

Another application area where the mixing model has been useful is chemical analysis. Data recorded through various chemical sensing procedures can be modeled as linear or nonlinear mixtures of concentrations of spectra. Classical methods of chemometrics can then be enhanced with recent methods of source separation, taking into account special properties of the available data: nonnegativity (of the concentrations, spectra), dependence (due to chemical interactions), and sparsity (mass spectrum) among others. In “Source Separation in Chemical Analysis,” Duarte et al. show how chemical data properties can be exploited through various methods, including ICA, geometrical, and Bayesian methods.

We thank our contributors for their comprehensive and interesting articles and to Fulvio Gini for his support in putting together this special issue. We would like to also extend our thanks to our reviewers for their detailed and insightful comments, to Rebecca Wollman for the great guidance along the way, and to Jessica Barragué for the care in putting together our special issue.

Source separation, we believe, is an exciting area that keeps evolving. We hope that this special issue reflects that sentiment and will help identify some of the new and emerging directions in the area as well as providing critical perspectives on the existing ones.

 SP

[Tülay Adalı, Matthew Anderson, and Geng-Shen Fu]

Diversity in Independent Component and Vector Analyses

[Identifiability, algorithms, and applications in medical imaging]

Starting with a simple generative model and the assumption of statistical independence of the underlying components, independent component analysis (ICA) decomposes a given set of observations by making use of the diversity in the data, typically in terms of statistical properties of the signal. Most of the ICA algorithms introduced to date have considered one of the two types of diversity: non-Gaussianity—i.e., higher-order statistics (HOS)—or, sample dependence. A recent generalization of ICA, independent vector analysis (IVA), generalizes ICA to multiple data sets and adds the use of one more diversity, dependence across multiple data sets for achieving an independent decomposition, jointly across multiple data sets. Finally, both ICA and IVA, when implemented in the complex domain, enjoy the addition of yet another type of diversity, noncircularity of the sources—underlying components. Mutual information rate provides a unifying framework such that all these statistical properties—types of diversity—can be jointly taken into account for achieving the independent decomposition. Most of the ICA methods developed to date can be cast as special cases under this umbrella, as well as

the more recently developed IVA methods. In addition, this formulation allows us to make use of maximum likelihood theory to study large sample properties of the estimator, derive the Cramér–Rao lower bound (CRLB) and determine the conditions for the identifiability of the ICA and IVA models. In this overview article, we first present ICA, and then its generalization to multiple data sets, IVA, both using mutual information rate, present conditions for the identifiability of the given linear mixing model and derive the performance bounds. We address how various methods fall under this umbrella and give examples of performance for a few sample algorithms compared with the performance bound. We then discuss the importance of approaching the performance bound depending on the goal, and use medical image analysis as the motivating example.



Source Separation and Applications

IMAGE LICENSED BY
INGRAM PUBLISHING

INTRODUCTION

Data-driven methods typically start with a simple latent variable model—of which the linear mixing has been the most common—and decompose a given set of V -dimensional P observations, typically arranged as a $P \times V$ observation matrix, into two matrices, a $P \times M$ mixing matrix and an $M \times V$ component/source matrix using a suitable cost. Since in this very general form, this is not a well defined problem, usually additional constraints are imposed

Digital Object Identifier 10.1109/MSP.2014.2300511

Date of publication: 7 April 2014

on the mixing and/or component matrices such as sparsity and nonnegativity. ICA is based on the assumption of statistical independence of the underlying components, and because this is a strong assumption, it enables a solution subject to only scaling and permutation ambiguities. Independence is also a natural assumption in many problems and a set of features that are statistically independent can be easily used for many tasks. This is the reason for the popularity of ICA and its wide use in areas as diverse as biomedicine, communications, finance, geophysics, and remote sensing, see, e.g., [1]–[3]. In this article, we use mutual information rate to provide a common umbrella for ICA such that the two most commonly used types of diversity to achieve ICA, dependence of samples and HOS are both taken into account.

There are numerous applications where not only one set of observations but multiple data sets, which have some dependence among them, need to be jointly analyzed. Examples include the analysis of medical data such as functional magnetic resonance imaging (fMRI) and electroencephalography (EEG) collected from multiple subjects, remote sensing data such as hyperspectral images where each pixel provides spectral information over

multiple frequency bands, analysis of multisensor or multimodality data that provide complementary information, and multisubject biometric data, among many others. In all of these cases, the underlying components within the data sets, and hence the observations themselves, exhibit statistical dependence, which is another form of diversity to exploit. One approach to analyze these multiple data sets is to perform an individual ICA on each data set separately. Since most applications require matching of the corresponding components from each data set, one should then use a permutation algorithm to align the estimated components/sources since the ordering of the sources cannot be determined by ICA. Such an approach becomes computationally prohibitive as the number of data sets and sources increases, but more importantly, it fails to take advantage of the additional diversity, statistical dependence across multiple data sets while performing the analysis. An approach for ICA of multiple data sets, called *group ICA*, which is introduced in the context of fMRI analysis [4], temporally concatenates multiple data sets, and after a dimension reduction step, performs ICA on this concatenated data set and then reconstructs the estimates for each data set separately. As we demonstrate in this article, while practical and useful, using a common subspace for performing ICA is likely to lead to information loss. Multiset canonical correlation analysis (MCCA) [5] alleviates the problem by making full use of all the available data and has found wide application; see, e.g., [6] and [7]. It can be also shown to achieve joint blind source separation [8]. However, MCCA makes use of only second-order statistics (SOS) and constrains the demixing matrix to be orthogonal, hence limiting the search space for the optimal solution.

IVA generalizes the ICA problem to multiple data sets in such a way that it allows making full use of the statistical dependence across multiple data sets, and can take not only SOS but HOS into

account as well, and includes MCCA as a special case. Using the IVA framework, one can exploit the statistical dependence of each source across multiple data sets leading to performance beyond what is achievable with single-set ICA algorithms applied separately to each data set. Additionally, IVA automatically aligns dependent sources across the data sets hence bypassing the need for the use of a second permutation algorithm for the task. The original formulation for IVA [9] assumes that sources across data sets have no second-order dependence, and uses a multivariate Laplacian model for the source component vector (SCV)—which is defined in the section “IVA: Cost Function.” In this overview article, we present a more general formulation for IVA, show that just like ICA, IVA can be cast using mutual information rate and thus all three key statistical properties, sample dependence within a source, source dependence within an SCV, as well as HOS are taken into account [10].

We give the identifiability conditions and present results on large sample properties using maximum likelihood theory for both ICA and IVA, and in the process, discuss the parallels between the two approaches in terms of the role statistical dependence plays. We emphasize the fact that it is the SOS that determine identifiability

for both ICA and IVA, and that the correlation structure defines the diversity needed for establishing an independent decomposition for both, and discuss the parallels for the two. The results for identifiability and large sample properties do consider another important diversity type, which is nonstationarity of the sources. Finally, the application of ICA and IVA to medical image analysis is discussed highlighting the importance of diversity in these studies.

INDEPENDENT COMPONENT ANALYSIS

We consider the basic noiseless ICA problem based on instantaneous mixing where there are as many sources as mixtures—the most common case, the overdetermined one, also the case in fMRI analysis, can be easily reduced to this form using order selection as in [11] and [12]. The linear mixing model is then written as

$$\mathbf{x}(v) = \mathbf{A}\mathbf{s}(v), \quad 1 \leq v \leq V, \quad \mathbf{x}(v), \mathbf{s}(v) \in \mathbb{R}^N, \quad (1)$$

where v is the sample index such as voxel, pixel, or time. The estimates are given by $\mathbf{u}(v) = \mathbf{W}\mathbf{x}(v)$, which can be also written in matrix form as $\mathbf{U} = \mathbf{W}\mathbf{X}$, where $\mathbf{u}_n^T \in \mathbb{R}^V$ is the n th row of $\mathbf{U} = \mathbf{W}\mathbf{X}$, i.e., $\mathbf{U} = [\mathbf{u}_1, \dots, \mathbf{u}_N]^T$, and $\mathbf{X}, \mathbf{U} \in \mathbb{R}^{N \times V}$. Since we consider the more general case that includes sample dependence in the ICA formulation and would like to keep the notation as simple as possible, we make the following definitions. We use $\mathbf{x}(v) \in \mathbb{R}^N$ to refer to the random vector that contains the N mixtures $x_n(v)$, $1 \leq n \leq N$, and $\mathbf{x}_n \in \mathbb{R}^V$ to denote the transpose of the n th row of the observation matrix $\mathbf{X} \in \mathbb{R}^{N \times V}$. When the reference is to a random quantity rather than observation, it will be clear from context.

In ICA, we assume that the sources $s_n(v)$ in $\mathbf{s}(v) = [s_1(v)s_2(v) \dots s_N(v)]^T$ are statistically independent, and make use

ICA CAN HENCE
IDENTIFY TWO OR MORE
GAUSSIAN SOURCES WHEN
NON-GAUSSIANITY IS NOT THE
SOLE TYPE OF DIVERSITY USED.

of different properties of the signal, such as non-Gaussianity, sample dependence, geometric properties, or nonstationarity of the signal, i.e., diversity in some form [1, Ch. 1]. Among those, the most commonly used type of diversity has been non-Gaussianity—HOS—of the sources. Most of the popular ICA algorithms such as Infomax [13], FastICA [14], and joint approximate diagonalization of eigenmatrices (JADE) [15] as well as many of the variants of maximum likelihood (ML) techniques with different approaches for approximating the source density, such as [16] and [17], all fall under this umbrella. Even very recent surveys—such as [18]—primarily consider ICA algorithms within this group. As a result, in the community, most often, fundamental results such as those for identifiability always consider this more limiting view of achieving ICA. It has been hence commonly noted that ICA can identify only a single Gaussian source. As we note next, this is true only when non-Gaussianity is the only form of diversity that is considered.

Besides those making use of non-Gaussianity, another important group is algorithms that make use of linear dependence among the samples, hence SOS. These include the algorithm for multiple unknown signal extraction (AMUSE) [19], second-order blind identification (SOBI) [20], and weights-adjusted SOBI (WASOBI) [21] among others. In this case, we use a random process rather than a random variable model for the sources, and use $s_n(v)$ where v is an index such as time, pixel, or voxel. In this article, we use v for voxel, as medical image analysis, i.e., volume data will be our main motivating example.

Algorithms using only non-Gaussianity form a major portion of the ICA algorithms developed to date, while those using sample dependence come in second. An obvious question one may ask is “Why not make use of both types of diversity, non-Gaussianity and sample dependence together, at the same time?” As one would expect, this approach leads to algorithms with better performance than those using only one type of diversity as demonstrated in [22]–[26]. In addition, use of these two types of diversity jointly allows for more relaxed conditions for the identifiability of the ICA model in (1).

This is our main goal in this section, to show how mutual information rate helps bring most of the ICA algorithms under one umbrella and helps determine identification conditions along with performance bounds so that the performance of various algorithms can be compared against this benchmark.

ICA: COST FUNCTION

Mutual information is a natural cost for ICA since the goal is the maximization of independence among the source estimates $\mathbf{u} = \mathbf{W}\mathbf{x}$, and has been used commonly when providing a general umbrella for approaches based on the use of HOS. Here, using the random process notation as in (1), we write the n th source estimate as $u_n(v) = \mathbf{w}_n^T \mathbf{x}(v)$, where \mathbf{w}_n^T is the n th row of the demixing matrix \mathbf{W} . We can then write the mutual information rate as

$$\begin{aligned} \mathcal{I}_r(\mathbf{W}) &= \sum_{n=1}^N H_r(u_n) - H_r(\mathbf{u}) \\ &= \sum_{n=1}^N H_r(u_n) - \log |\det \mathbf{W}| - H_r(\mathbf{x}) \end{aligned} \quad (2)$$

and take into account both HOS and sample dependence to achieve ICA. In (2), we used the Jacobian expression $p_s(\mathbf{u}) = p_s(\mathbf{W}\mathbf{x}) = p_x(\mathbf{x}) |\det \mathbf{W}|^{-1}$, and hence the last term $H_r(\mathbf{x})$ is a constant with respect to \mathbf{W} , it can be replaced by C resulting in

$$\mathcal{I}_r(\mathbf{W}) = \sum_{n=1}^N H_r(u_n) - \log |\det \mathbf{W}| - C, \quad (3)$$

where $H_r(u_n)$ is the entropy rate, which is $H_r(u_n) = \lim_{v \rightarrow \infty} H[u_n(1), \dots, u_n(v)]/v$ and the entropy is written as $H(u_n) = -E\{\log p_{s_n}(\mathbf{w}_n^T \mathbf{x})\}$. In the rest of the article, we refer to *differential entropy* simply as *entropy* since discrete-valued random variables are not considered in the article. When the process is stationary, we have $H_r(u_n) = \lim_{v \rightarrow \infty} H(u_n(v) | u_n(v-1), \dots, u_n(1))$. Since entropy rate measures the per sample density of the average uncertainty of a random process, minimization of (3)

makes use of both HOS—through the minimization of missing information, entropy—and sample dependence by making samples easier to predict by increasing sample dependence, i.e., decreasing the entropy rate. The term $\log |\det \mathbf{W}|$ acts as a regularization term preserving the volume across the directions

of source estimation. Since entropy is not scale invariant, i.e., $H(x) \neq H(\alpha x)$ for $\alpha \neq 1$, without the regularization term, the cost function could be minimized by simply scaling the source estimates. Mutual information rate hence provides a broad umbrella under which one can study the properties of ICA algorithms by taking into account both HOS and sample dependence, the two types of diversity most commonly used for ICA.

When we constrain the demixing matrix to be orthogonal, i.e., let $\mathbf{W}\mathbf{W}^T = \mathbf{I}$, we have $|\det(\mathbf{W})| = 1$, and the cost in (3) reduces to

$$\mathcal{J}_r(\mathbf{W}) = \sum_{n=1}^N H_r(u_n) - C, \quad (4)$$

which maximizes the negentropy rate, the information-theoretic distance of a random process from that of a Gaussian for each source, under a variance constraint.

For a given set of observations, $\mathbf{X} \in \mathbb{R}^{N \times V}$, we can maximize the likelihood given by

$$\mathcal{L}_{\text{ICA}}(\mathbf{W}) = \sum_{n=1}^N \log p_{s_n}(\mathbf{u}_n) + V \log |\det \mathbf{W}|, \quad (5)$$

where $\mathbf{u}_n \in \mathbb{R}^V$ is the transpose of the n th row of $\mathbf{U} = \mathbf{W}\mathbf{X}$, i.e., $\mathbf{U} = [\mathbf{u}_1, \dots, \mathbf{u}_N]^T$. By the general asymptotic equipartition property [27], as $V \rightarrow \infty$, the maximization of likelihood function $\mathcal{L}_{\text{ICA}}(\mathbf{W})$ becomes equivalent to the minimization of the mutual

IVA GENERALIZES THE ICA PROBLEM TO MULTIPLE DATA SETS IN SUCH A WAY THAT IT ALLOWS USE OF THE STATISTICAL DEPENDENCE ACROSS MULTIPLE DATA SETS.

information rate cost in (3). This is true if the probability density function (pdf) $p_{s_n}(\mathbf{u}_n)$ used in the ML formulation exactly matches the true pdf, which is implied when using mutual information rate as the cost. When there is a mismatch between the estimated pdf through likelihood and the true one, there is a bias that can be represented by the relative entropic—Kullback-Leibler—distance of the true density to the estimated. Using a flexible density model such as those employed by the two algorithms introduced in the section “ICA: Algorithms,” autoregressive mixture of Gaussians (AR-MOG) [24], and entropy rate bound minimization (ERBM) [25], decreases this bias. At this point, and for the performance discussion in the next section, we assume that the source pdf is known. In the section “ICA: Algorithms,” we discuss different ways of estimating the source pdf during adaptation, which lead to a number of different ICA algorithms that can all be studied under the mutual information rate minimization umbrella. In [17], a distinction is made between a true ML scheme that estimates the pdf and one that uses a fixed distribution where the latter is called a *quasi-ML procedure*.

In the rest of the development, to simplify the discussion, we assume that all variables are zero mean so that the definitions of correlation and covariance matrices coincide.

ICA: IDENTIFICATION CONDITIONS AND THE PERFORMANCE BOUND

Given the log likelihood in (5), we can compute the Fisher information matrix (FIM) using the expected value of its Hessian, which tells us how informative the given set of observations are for the estimation of the demixing matrix \mathbf{W} . The FIM also plays a key role in determining the identification conditions of the ICA model as well as the lower bound on the unbiased estimator, the CRLB. We consider the FIM locally around the optimal point, $\mathbf{G} = \mathbf{A}\mathbf{W} = \mathbf{I}$, hence have $\mathbf{u}_n = \mathbf{s}_n$. Due to the invariance of the induced CRLB with respect to \mathbf{G} , the CRLB only depends on the statistics of the sources. Here, we note that since the quantity being estimated is \mathbf{W} rather than \mathbf{G} , the estimated bound is actually the induced CRLB following [28].

By making use of the independence of the sources, one can show that the FIM has a block diagonal structure with N scalars and $N(N-1)/2$ matrices that are 2×2 . The scalar diagonal entries are all positive, and hence, the properties of the FIM are determined by the 2×2 matrices—pairwise interaction of sources—given by

$$\mathbf{J}_{m,n}^{\text{ICA}} = \begin{bmatrix} \kappa_{m,n} & 1 \\ 1 & \kappa_{n,m} \end{bmatrix}, 1 \leq m < n \leq N, \quad (6)$$

where

$$\kappa_{n,m} = \text{trace} (E\{\boldsymbol{\psi}(\mathbf{s}_n)\boldsymbol{\psi}^T(\mathbf{s}_n)\}\mathbf{R}_m),$$

$$\boldsymbol{\psi}(\mathbf{s}_n) = -\frac{\partial \log p_{s_n}(\mathbf{s}_n)}{\partial \mathbf{s}_n} \in \mathbb{R}^V, \text{ and } \mathbf{R}_n = E\{\mathbf{s}_n\mathbf{s}_n^T\} \in \mathbb{R}^{V \times V}.$$

Hence, the FIM is a function of the key source statistics, the two types of diversity the formulation in (5) takes into account—sample dependence and HOS. In addition, source nonstationarity is another type of diversity, and the form in (6) considers the use of this third type of diversity as well since here the definitions are with respect to the complete source vector of dimensionality V , which matches the dimension of the samples in the given observation. The quantity $\boldsymbol{\psi}(\cdot)$ is called the *score function* and is defined as the derivative with respect to the source estimate \mathbf{u}_n . This is a slightly different definition than in traditional ML theory where the score function is defined with respect to the parameter.

Since the blocks $\mathbf{J}_{m,n}^{\text{ICA}}, 1 \leq m < n \leq N$ are the diagonal blocks of a covariance matrix, the FIM, they are positive semidefinite, and since FIM is block diagonal, they determine the condition for positive definiteness of the whole matrix. Evaluating the condition for which $\mathbf{J}_{m,n}^{\text{ICA}}$ becomes singular hence yields the nonidentifiability condition for the ICA model—subject to

the scaling and permutation ambiguities. It can be shown that $\mathbf{J}_{m,n}^{\text{ICA}}$ remains positive definite as long as there are no two sources that are Gaussian with proportional autocovariance matrices, i.e., we do not have two Gaussians, s_m and s_n in the mixture that satisfy $\mathbf{R}_m = \delta^2 \mathbf{R}_n$ [1, Ch. 4]. Hence, in the presence of this simple correlation diversity, i.e., when $\mathbf{R}_m \neq \delta^2 \mathbf{R}_n$, even Gaussian sources are separable using ICA when sample dependence and HOS are both considered. In addition, this result also includes use of nonstationarity as diversity—to keep the notation simple we have not included a time index in the definition of the autocovariance matrices.

For algorithms that only take sample dependence into account however, for algorithms such as AMUSE, SOBI, and WASOBI, any two sources—not only Gaussians—with “similar” covariance matrices cannot be separated [19], [28]. Obviously, using these algorithms, independent and identically distributed (i.i.d.) sources cannot be separated either. When the sources are i.i.d., or when only HOS are taken into account implicitly assuming i.i.d. samples—as is the case in most of the ICA algorithms—then effectively, we have $\mathbf{R}_l = \sigma_l^2 \mathbf{I}$ for $l = n, m$. In this case, we can only identify a single Gaussian source since the correlation diversity is no longer available. This is the commonly known condition for the identifiability of the ICA model since the majority of ICA algorithms only exploit non-Gaussianity. However, as we note here, it is important to remember that this condition is true only for a specific case, and now there are effective algorithms that can take into account multiple types of signal diversity.

Using the expression in (6), we can write the CRLB as

$$\text{var}(w_{m,n}) \geq \frac{1}{V} (\kappa_{m,n} - \kappa_{n,m}^{-1})^{-1}. \quad (7)$$

Assuming that the mixtures are whitened such that $E\{\mathbf{X}\mathbf{X}^T\} = \mathbf{I}$ and $\sigma_{s_n} = 1$, we can calculate the CRLB using the normalized interference-to-signal-ratio (ISR)

$$ISR = \frac{1}{N(N-1)} \sum_{m,n=1, m \neq n}^N E\{g_{m,n}^2\}, \quad (8)$$

where $g_{m,n}$ are the entries of $\mathbf{G} = \mathbf{A}\mathbf{W}$, which we plot in Figure 1 along with performances of two algorithms introduced in the next section against this bound.

ICA: ALGORITHMS

Mutual information rate in (3) can be minimized using relative/natural gradient updates [29], [30] as

$$\mathbf{W}(l+1) = \mathbf{W}(l) + \mu(\mathbf{I} - E\{\Psi(\mathbf{U})\mathbf{U}^T\})\mathbf{W}(l), \quad (9)$$

where $\Psi(\mathbf{U}) = [\psi_1(\mathbf{u}_1), \dots, \psi_N(\mathbf{u}_N)]^T \in \mathbb{R}^{N \times V}$, $\mu > 0$ is the step size, l is the iteration index, and the score function $\psi_n(\cdot)$ is defined in (6). In the update in (9), we include the complete source estimate matrix $\mathbf{U} = \mathbf{W}(l)\mathbf{X}$ as we consider sample correlation, rather than the commonly used random vector notation as in [29] and [30]. The form of this update is the same as the one proposed in [31] based on nonlinear decorrelations, the original approach for achieving ICA [32].

The bound given in (7) assumes that the exact density of each source is known. To approach this bound, a number of density matching methods are proposed, in particular for the i.i.d. case, where the

WITH THE ADDITION OF EACH NEW TYPE OF DIVERSITY, NOT ONLY THE PERFORMANCE IMPROVES, BUT ALSO THE IDENTIFICATION BECOMES EASIER, A BROADER CLASS OF SIGNALS CAN BE SEPARATED USING ICA OR IVA.

problem is simpler as we need to estimate a univariate rather than the multivariate score $\psi_n(\cdot)$ in (9). Solutions for the i.i.d. case include both parametric and nonparametric approaches as in efficient variant of FastICA (EFICA) [33] and nonparametric ICA (NP-ICA) [16], as well as a semiparametric approach, ICA by entropy bound minimization (EBM) [34].

EBM uses an efficient entropy estimator where rather than estimating the entropy directly, an upper bound is estimated among a number of competing candidates determined by the maximum entropy principle and by a finite number of prespecified measuring functions. Available prior information can be used in the selection of measuring functions, and even a simple selection of two odd and two even functions leads to a flexible algorithm that provides robust performance in a number of scenarios [34]. In [25], the flexible EBM density estimation strategy is combined

with an invertible filter model such that both non-Gaussianity and sample dependence are taken into account to derive ERBM—originally introduced as full blind source separation—and hence to directly minimize (3). Other approaches that take both types of diversity into account are Markovian ICA [22] where the Markovian source model is adopted, autoregressive mixture of Gaussians [24], entropy rate minimization

using an AR source model driven by GGD (ERM-ARG) [35], and MULTICOMBI [23] where either non-Gaussianity or sample dependence is taken into account by switching between the EFICA and WASOBI algorithms. All of these solutions assume stationarity of the sources.

The decoupling of the source estimates by assuming an orthogonal \mathbf{W} introduced in the section “ICA: Cost Function” leads to negentropy rate as the cost, and greatly simplifies the score/density matching problem as the estimation for a given source then does not interact—and hence complicates—the estimation of others. This is the approach used in the FastICA algorithm [14], which is noted for its fast convergence. In [33], generalized Gaussian distribution (GGD)

$$p(s) \propto \exp(-|s|^{2\beta}) \quad (10)$$

has been used as the source model to derive EFICA. Besides helping with density estimation, the assumption of orthogonality provides a number of other advantages such as making second-order algorithms such as Newton-variants become more practical and allowing for easier implementation of constrained ICA [36].

However, this decoupling through constraining \mathbf{W} to be orthogonal also limits the search space for the demixing matrices thus also limiting the achievable performance [37]. The decoupling approach given in [38] and [39] transforms the matrix optimization problem to a series of vector optimization problems without having to constrain the matrix to be orthogonal. Here, it is also important to remember that the commonly used whitening

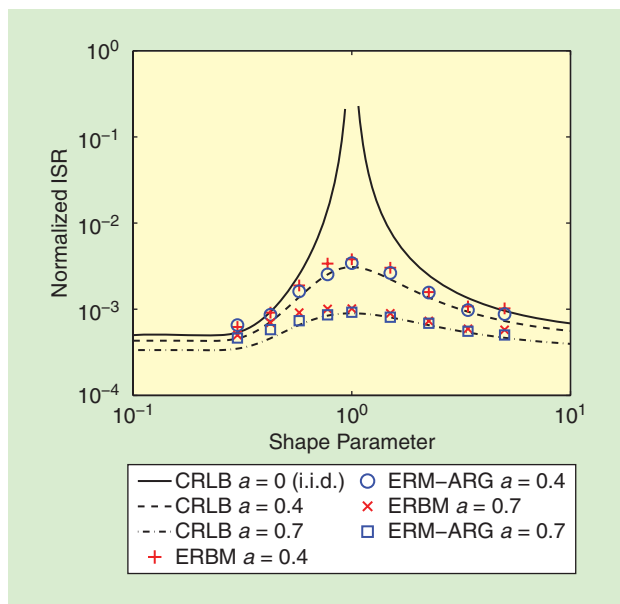


[FIG1] The induced CRLB and performance of two algorithms as a function of shape parameter β (non-Gaussianity) for three levels of sample correlation, for AR coefficient $a = 0, 0.4$, and 0.7 . Note the improvement in performance as the role of HOS (β moves away from 1) and as sample correlation (value of a) increase.

step for the observations implies an orthogonal demixing matrix only when the number of samples $V \rightarrow \infty$, and hence does not guarantee an orthogonal demixing estimate unless it is embedded into the update mechanism. This decoupling approach is used in the EBM and ERBM algorithms that employ flexible density models for each source estimate. Finally, algorithms that only make use of sample dependence, and hence SOS, such as AMUSE, SOBI, and WASOBI jointly diagonalize multiple covariance matrices to determine an estimate for W rather than directly maximizing the likelihood (5). A second-order ICA approach based on ML with a Gaussian density model is given in [40], and it is shown that besides this ML-based algorithm, WASOBI approaches the CRLB as well, when the sources are stationary AR processes.

EXAMPLE: DIVERSITY, CRLB, AND THE PERFORMANCE OF TWO ALGORITHMS

To demonstrate the role of diversity in attaining optimal performance while designing an algorithm, we consider a simple example, the separation of two linearly mixed sources, an i.i.d. source drawn from a GGD (10) and a second source, a first-order AR process generated by a Gaussian process $\nu(v)$ such that $s(v) = as(v-1) + \nu(v)$. GGD assumes the form of a Gaussian for $\beta = 1$, is super-Gaussian when $0 < \beta < 1$ and sub-Gaussian when $\beta > 1$. Hence, as β moves away from 1, the role of HOS increases, and similarly, the role of sample dependence increases as $|a| \rightarrow 1$. In Figure 1, we plot the CRLB given by (7) using the ISR (8). First note that for finite ISR, it suffices for one of the sources to have sample correlation—nonzero a —when both are Gaussian. The widely referenced and repeated condition for the real case that says “with ICA, one can identify only a single Gaussian” hence is true only when sample dependence is not taken into account—or is absent in that the samples are i.i.d., which rarely is the case in practice. In the same figure, we also show the performance of two algorithms that make use of both sample dependence and HOS: one that exactly matches the underlying source models, entropy rate minimization using AR model with a GGD driving process (ERM-ARG) [35] and the more flexible ERBM algorithm [25]. The results are shown for 1,000 samples and 500 independent runs. While we observe that the exact match provides the best performance, the flexible ERBM does a decent job in approaching the bound as well and does not use prior information like the ERM-ARG.

EXAMPLE: PERFORMANCE COMPARISON IN SEPARATION OF NATURAL SOURCES

In Figure 2, we show the ISR of nine different algorithms in separation of ten artificially mixed images from [41] to demonstrate the performance of different algorithms in separation of sources that come from a rich class of distributions. Since, for small sample sizes, there were a number of unstable runs, the results are plotted using the median rather than the mean. The algorithms used in the comparison are JADE; EFICA; Robust, Accurate, Direct ICA algorithm (RADICAL); and ICA-EBM that exploit the HOS, WASOBI that uses sample dependence, AR-MOG, ERM-ARG, and ERBM that use both, and finally MULTICOMBI that uses both but

one at a time. The advantage of making use of both diversity jointly is clear as well as the superior performance of two algorithms that use flexible density models, AR-MOG and ERBM—though the performance of AR-MOG deteriorates with decreasing sample size due to its complexity.

INDEPENDENT VECTOR ANALYSIS

In many applications, not only a single but multiple data sets with dependence among them need to be jointly analyzed. Examples include the analysis of medical data such as fMRI and EEG from multiple subjects or at different conditions, data from multiple frequency bins when solving the convolutive ICA problem in the frequency domain, and the analysis of multisensor or fusion of multimodality data with complementary information. IVA generalizes the ICA problem to multiple data sets so that one can take advantage of this additional type of diversity, the one across multiple data sets when achieving the decomposition.

Next, we show that IVA can be formulated using mutual information rate minimization like ICA but now with the addition of one more diversity, dependence among sources across data sets. Also, as in the case of ICA, we consider the general case that does not constrain the demixing matrices to be orthogonal, and as such, IVA generalizes CCA and MCCA [5] as well, both through incorporation of statistics higher than two and also by allowing a general nonorthogonal demixing matrix. Using this general formulation, we give the general conditions for identifiability of the IVA model as well as the performance bounds. The ICA result, as expected, becomes a special case when the number of data sets is set to one. We then present current algorithms for achieving IVA, and address the challenges in the area.

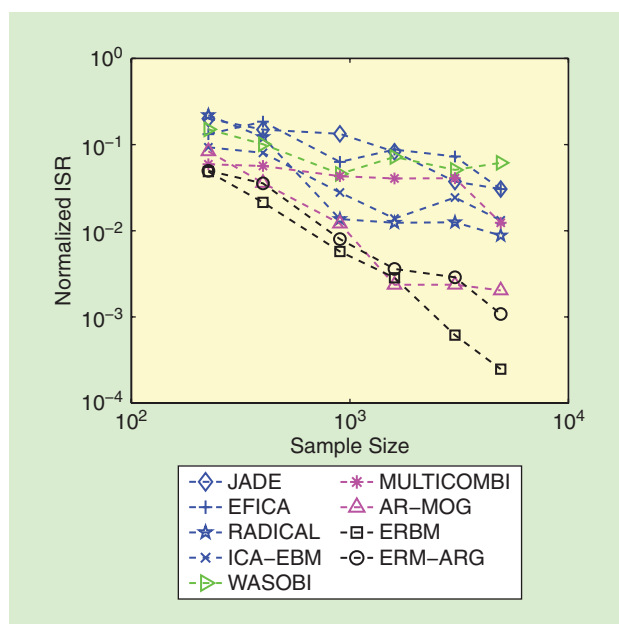


[FIG2] The performance of nine algorithms using different types of diversity—either HOS or sample dependence, or both—in the separation of a mixture of sources that come from a rich density. Note the best performance by algorithms making use of both types of diversity.

IVA: COST FUNCTION

The IVA problem is defined similar to ICA except that we now have K data sets, each containing V samples, and formed from linear mixtures of N independent sources,

$$\mathbf{x}^{[k]}(v) = \mathbf{A}^{[k]} \mathbf{s}^{[k]}(v), 1 \leq k \leq K, 1 \leq v \leq V, \quad (11)$$

where $\mathbf{A}^{[k]} \in \mathbb{R}^{N \times N}$, $k = 1, \dots, K$ are invertible mixing matrices. The problem is finding K demixing matrices $\mathbf{W}^{[k]}$ such that sources for each data set can be estimated through $\mathbf{u}^{[k]}(v) = \mathbf{W}^{[k]} \mathbf{x}^{[k]}(v)$ for $k = 1, \dots, K$ as shown in Figure 3(a).

For K data sets $\mathbf{X}^{[k]} \in \mathbb{R}^{N \times V}$, we can recover the source estimates for each data set using $\mathbf{U}^{[k]} = \mathbf{W}^{[k]} \mathbf{X}^{[k]}$, and by defining augmented matrices \mathbf{X} and \mathbf{S} , write the problem as

$$\begin{bmatrix} \mathbf{X}^{[1]} \\ \vdots \\ \mathbf{X}^{[K]} \end{bmatrix} = \begin{bmatrix} \mathbf{A}^{[1]} & 0 & 0 \\ 0 & \ddots & 0 \\ 0 & 0 & \mathbf{A}^{[K]} \end{bmatrix} \begin{bmatrix} \mathbf{S}^{[1]} \\ \vdots \\ \mathbf{S}^{[K]} \end{bmatrix} \iff \mathbf{X} = \mathbf{A} \mathbf{S} \text{ where } \mathbf{A} = \bigoplus_{k=1}^K \mathbf{A}^{[k]}. \quad (12)$$

The estimates are given by $\mathbf{U} = \mathbf{W} \mathbf{X}$ and the demixing matrix is also block diagonal, $\mathbf{W} = \bigoplus_{k=1}^K \mathbf{W}^{[k]}$. The decomposition is performed on this augmented matrix \mathbf{X} so that the dependence of components of the source matrices $\mathbf{S}^{[k]}$ across data sets can be taken into account. In this model, the components within each $\mathbf{S}^{[k]}$ are assumed to be independent while we allow for dependence across corresponding components of $\mathbf{S}^{[k]}$ in multiple data sets. In fact, it is this additional dependence that IVA takes advantage of, and the following definition helps clarify the idea and is key for the whole development to follow.

We define the SCV for the n th SCV \mathbf{s}_n as

$$\mathbf{s}_n(v) = [s_n^{[1]}(v), s_n^{[2]}(v), \dots, s_n^{[K]}(v)]^T \in \mathbb{R}^K,$$

i.e., by concatenating the n th source from each of the K data sets, or similarly, define the source component matrix (SCM) \mathbf{S}_n shown in Figure 3(a), through concatenation of each row of $\mathbf{S}^{[k]}$ as $\mathbf{S}_n = [s_n^{[1]}, s_n^{[2]}, \dots, s_n^{[K]}]^T$. The SCV takes into account sample dependence through the inclusion of index v in its notation and we use both definitions, SCV and SCM, in the discussion to follow. As an example, in the fMRI analysis we introduce in the section “Application to Medical Image Analysis,” the n th SCM contains the spatial activation maps of the n th source, such as the motor component, for all K subjects in the study. One would expect the activation maps of different subjects to be statistically dependent, as for each subject, voxels at corresponding locations would show comparable levels of activation. This is the additional diversity that the general IVA formulation makes use of when achieving the decomposition. It is, however, important to note that while IVA makes use of this additional diversity, it does not require that it exists, and in its absence, reduces to individual ICAs on each data set. This additional diversity is also what helps with the resolution of permutation ambiguity among the sources estimated across the data sets. The identification condition we introduce in the next section specifies when all the sources in an IVA model can be identified, and is a quite relaxed condition. However, the identification of sources does not imply that the sources will be aligned as well, and sources across data sets—components of each SCV—can be aligned only if the sources across the data sets are statistically dependent [10].

At this point it is also useful to note that the IVA formulation is a special case of the multidimensional ICA (MICA) problem [42], also defined as an independent subspace problem [43]. Though MICA is not necessarily defined for multiple data sets as IVA, we can use the augmented matrix definition in (12) to understand how MICA considers a more general model. For the MICA formulation, the mixing matrix is not assumed to have a block diagonal

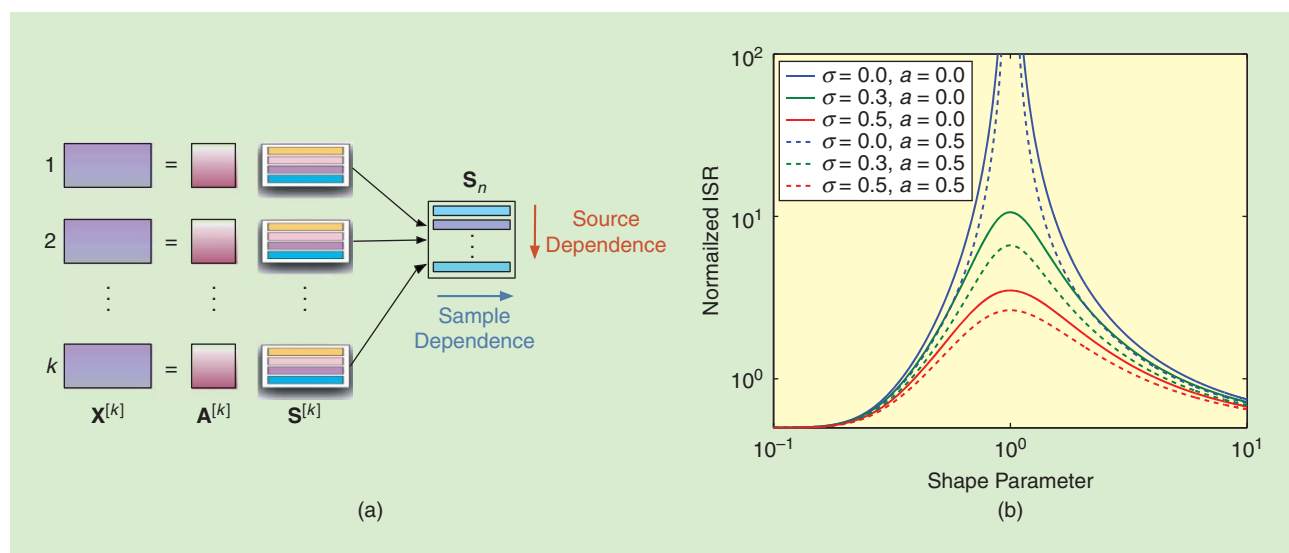


[FIG3] For the IVA problem given in (a), note the improvement in performance shown in (b) as the values of σ (source dependence) and a (sample dependence) increase and shape parameter moves away from 1, i.e., the role of HOS increases. (a) IVA for analysis of multiple data sets and the two key signal properties available in addition to HOS: sample dependence and dependence among sources within an SCM \mathbf{S}_n . (b) The role of three types of diversity on performance in terms of induced CRLB (normalized ISR).

form and the number of components within each SCV can be different. Hence, the problem is one of finding independent subspaces where in each, there might be different number of dependent components. There are many challenges for solving the general MICA problem. A major one among them is determining the number of subspaces and components within each SCV. A recent overview of MICA is given in [44] where an effective solution is offered for the multivariate-Gaussian case. Assuming the correct number of components within each SCV can be determined, MICA then identifies the independent subspaces and does not identify the individual components within each subspace, i.e., the components within an SCV like IVA does. The IVA formulation provides enough additional restrictions to the MICA formulation so as to achieve identifiability of individual components while still creating a more general framework than ICA.

Since \mathbf{W} has far fewer nonzero parameters than its full $KN \times KN$ dimension implies, we define $\mathcal{W} \in \mathbb{R}^{N \times N \times K}$, a three-dimensional array, to denote the set of parameters to be estimated.

Given the definition of an SCV, we formulate the IVA problem similar to that of ICA in (3) as

$$\mathcal{I}_r^{IVA}(\mathcal{W}) = \sum_{n=1}^N H_r(\mathbf{u}_n) - \sum_{k=1}^K \log|\det(\mathbf{W}^{[k]})| - C, \quad (13)$$

where the main difference is that we are now seeking to minimize the mutual information among SCVs rather than individual sources. To provide a clear view of the role of this additional diversity, we rewrite (13) as

$$\mathcal{I}_r^{IVA}(\mathcal{W}) = \sum_{n=1}^N \left(\sum_{k=1}^K H_r(u_n^{[k]}) - \mathcal{I}_r(\mathbf{u}_n) \right) - \sum_{k=1}^K \log|\det(\mathbf{W}^{[k]})| - C. \quad (14)$$

Without the second term $\sum_{n=1}^N \mathcal{I}_r(\mathbf{u}_n)$, the expression in (14) is exactly equivalent to the sum of the cost in (3) across K data sets, hence performing independent ICAs on each data set. It is this second term, sum of mutual information within each SCV, $\sum_{n=1}^N \mathcal{I}_r(\mathbf{u}_n)$ that takes the diversity across data sets into account. The minimization of (14) hence increases mutual information among components of an SCV, thus making use of the natural dependence among data sets.

If we consider no sample dependence—hence the cost is mutual information (\mathcal{I}) rather than mutual information rate (\mathcal{I}_r)—and use the multivariate Gaussian model for the SCV, we have $H(\mathbf{u}_n) = (1/2) \log[(2\pi e)^K \prod_{k=1}^K \lambda_n^{[k]}]$ where $\lambda_n^{[k]}$ is the k th eigenvalue of the covariance matrix of the n th SCV, then (13) reduces to

$$\mathcal{I}^{IVA-G}(\mathcal{W}) = \frac{NK \log(2\pi e)}{2} + \frac{1}{2} \log \left(\prod_{n=1}^N \prod_{k=1}^K \lambda_n^{[k]} \right) - \sum_{k=1}^K \log|\det(\mathbf{W}^{[k]})| - C. \quad (15)$$

This is exactly equivalent to the generalized variance method (GENVAR) cost function proposed for achieving MCCA [5] when we constrain the demixing matrices to be orthogonal

hence eliminating the term $\sum_k \log|\det(\mathbf{W}^{[k]})|$ but imposing a constraint on the sum of estimates, hence the eigenvalues. In [5], five cost functions are introduced for maximizing correlation among linearly transformed multiple data sets, which in our IVA formulation are the SCVs. The cost functions introduced in [5] all have the common objective of estimating $\mathbf{W}^{[k]}$ such that the SCV covariance matrix becomes as ill conditioned as possible, since this maximizes the correlation among the components within an SCV. Obviously the term $\log(\prod_{n=1}^N \prod_{k=1}^K \lambda_n^{[k]})$ achieves this goal when we let the sum of the eigenvalues be constant, i.e., constrain the demixing matrix. In (15), the term $\sum_k \log|\det(\mathbf{W}^{[k]})|$ achieves this purpose and is written using the theoretically well-justified cost of mutual information.

For given $\mathbf{X}^{[k]}, k = 1, \dots, K$, we can write the likelihood as

$$\mathcal{L}_{IVA}(\mathcal{W}) = \sum_{n=1}^N \log(p_n(\mathbf{U}_n)) + V \sum_{k=1}^K \log|\det(\mathbf{W}^{[k]})|,$$

where now the score function for the SCM \mathbf{U}_n is written as

$$\Psi_n^{IVA}(\mathbf{U}_n) = -\frac{\partial \log p_n(\mathbf{U}_n)}{\partial \mathbf{U}_n} \in \mathbb{R}^{K \times V}. \quad (16)$$

Now, we can proceed as in ICA to derive the performance bound and determine the conditions for the identifiability of the IVA model by working within ML theory.

IVA: IDENTIFICATION CONDITIONS AND THE PERFORMANCE BOUND

We evaluate the FIM by the expected value of the Hessian of \mathcal{L}_{IVA} at the optimal point $\mathbf{G} = \bigoplus_{k=1}^K \mathbf{W}_k \mathbf{A}_k = \bigoplus_{k=1}^K \mathbf{G}_k = \mathbf{I}$, which is now $KN^2 \times KN^2$ in dimension, since \mathcal{W} has a total of KN^2 parameters. Since, the IVA formulation replaces the sources with SCMs that are mutually independent, and each SCM includes K components, the FIM is again block diagonal but now with N block matrices that are $K \times K$ and $N(N-1)/2$ matrices of dimension $2K \times 2K$. The properties are again determined by the latter blocks, those that describe the interaction of now the SCMs, the $2K \times 2K$ block matrices

$$\mathbf{J}_{m,n}^{IVA} \triangleq \begin{bmatrix} \mathcal{K}_{m,n} & \mathbf{I}_K \\ \mathbf{I}_K & \mathcal{K}_{n,m} \end{bmatrix} \in \mathbb{R}^{2K \times 2K},$$

where $\{\mathcal{K}_{m,n}\}_{k_1,k_2} = (1/V) E\{(\Psi_m^{IVA,[k_1]})^T \mathbf{S}_n^{[k_1]} (\mathbf{S}_n^{[k_2]})^T \Psi_m^{IVA,[k_2]}\}$ when $m \neq n$, $\Psi_n^{IVA,[k]} = (\Psi_n^{IVA})^T \mathbf{e}_k$, where Ψ_n^{IVA} is given in (16), the subscript for the identity matrix \mathbf{I} denotes its dimension, and \mathbf{e}_k is the k th basis vector. Again, the FIM is a function of the key SCM statistics, and in this case, all three types of diversity—sample dependence, dependence within an SCM, and the HOS—that are considered in this IVA formulation. Since the SCM is written for V samples, i.e., is $K \times V$, nonstationarity is taken into account as well.

The FIM is a block diagonal matrix for this case as well and the identification condition for the IVA model is obtained by evaluating when $\mathbf{J}_{m,n}^{IVA}$ remains positive definite. It is shown that [10], [45] identification of the IVA model in (11) is possible

as long as no two SCMs have α -Gaussian components for which $\mathbf{R}_{m,\alpha} = (\mathbf{I}_V \otimes \mathbf{D})\mathbf{R}_{n,\alpha}(\mathbf{I}_V \otimes \mathbf{D})$, for $1 \leq m \neq n \leq N$, where $\mathbf{D} \in \mathbb{R}^{K_\alpha \times K_\alpha}$ is any full rank diagonal matrix, K_α the number of α -Gaussian components, $\mathbf{R}_n = E\{\mathbf{S}_n \mathbf{S}_n^T\}$, and \otimes is the Kronecker product. An α -Gaussian component is defined as the subset of rows of an SCM that are independent from the others and have multivariate Gaussian distribution, and α refers to the index of this subset within $\{1, \dots, K\}$, and $\mathbf{R}_{n,\alpha}$ refers to the covariance matrix of the matrix formed from the α -Gaussian rows of an SCM. Hence, it is again a second-order condition that determines the identifiability of the model, and the major role played by the source covariance matrix in ICA is now replaced by the SCM covariance matrix. As in the case of ICA, the result holds for the use of nonstationarity as a diversity type.

A useful special case to consider is when the samples are i.i.d., which is equivalent to considering $V = 1$ so that \mathbf{I}_V is a scalar and unity and we now consider SCVs where each entry is a random variable rather than SCMs or an SCV with entries that are random processes. This is the basic assumption in most ICA algorithms where only HOS are taken into account, and it leads to practical and effective solutions that work well for most cases, including many where the samples are actually dependent. However, for ICA, with the i.i.d. assumption, we can only identify a single Gaussian source. For IVA, however, the condition for this case is more general and now we can identify the IVA model as long as there are no two α -Gaussian SCVs for which $\mathbf{R}_{m,\alpha} = \mathbf{D}\mathbf{R}_{n,\alpha}\mathbf{D} \in \mathbb{R}^{K_\alpha \times K_\alpha}$. Hence, the identification of multiple Gaussians is possible with IVA provided that the covariance diversity is available, in the sense that covariance matrices of sources that are Gaussian across data sets are not essentially identical, i.e., satisfy $\mathbf{R}_{m,\alpha} \neq \mathbf{D}\mathbf{R}_{n,\alpha}\mathbf{D} \in \mathbb{R}^{K_\alpha \times K_\alpha}$.

Finally, for $K = 1$, the condition reduces to that for ICA and we cannot identify any two Gaussians that have $\mathbf{R}_m = \delta^2 \mathbf{R}_n$, $\delta \neq 0$ where now the covariance is defined for a single source rather than an SCV. A comparison of these two conditions reveal the dual nature of the role of diversity in these two cases, diversity in the form of source dependence for IVA versus sample dependence in ICA. The diagonal matrix \mathbf{D} for IVA and δ^2 for ICA are present in the conditions simply due to the inherent scaling ambiguity of the problem. The given identification conditions for the i.i.d. case coincide with those derived assuming a multivariate Gaussian model in [46] and [47] since they are determined by second-order statistics.

The CRLB for IVA is given by

$$\text{var}(w_{m,n}^{[k]}) \geq \frac{1}{V} \mathbf{e}_k^T (\mathcal{K}_{m,n} - \mathcal{K}_{m,n}^{-1})^{-1} \mathbf{e}_k, \quad (17)$$

which has a similar form to (7), and, again similarly, can be computed using the sum of ISR values, now defined as $E\{(g_{m,n}^{[k]})^2\}$, $E\{(g_{m,n}^{[k]})^2\}$.

EXAMPLE: ROLE OF THREE TYPES OF DIVERSITY FOR IVA

The simple example shown in Figure 3(b) plots the CRLB in terms of ISR for two sources and two data sets, where the first set of sources—common to both data sets—is drawn from a multivariate GGD, which is Gaussian when the shape parameter $\beta = 1$, and has super-Gaussian marginals for $0 < \beta < 1$ and sub-Gaussian for $\beta > 1$. The second set of sources are an i.i.d. Gaussian and a first-order AR process $s(v) = as(v - 1) + v(v)$, where $v(v)$ is a white Gaussian process. Hence, the AR parameter a characterizes influence of sample correlation and the shape parameter β of non-Gaussianity, i.e., HOS. Finally, we introduce correlation for the first group of sources through a correlation coefficient σ . As observed in Figure 3(b), performance—as measured by the ISR—improves as sample source correlation and dependence across data sets—values of a and σ respectively—increase, and as the sources become more non-Gaussian—i.e., as the value of β moves away from 1. We also note the condition for identifiability of the IVA model in that when the sources are

THE IVA FORMULATION CAN BE CONSIDERED A SPECIAL CASE OF THE MORE GENERAL MICA PROBLEM, WHICH ALLOWS IDENTIFICATION OF NOT ONLY INDEPENDENT SUBSPACES AS IN MICA BUT OF INDIVIDUAL COMPONENTS AS WELL.

all Gaussian ($\beta = 1$) and i.i.d., a finite ISR is still possible as long as there is correlation among the sources, in this example introduced only to the first set of GGD sources through σ .

IVA: ALGORITHMS

In algorithm development, while it is desirable to consider together all types of diversity expressed in the cost (13), current solutions available for the problem only take HOS and source dependence across data sets into account, primarily due to computational and modeling challenges. Hence, they minimize mutual information rather than mutual information rate. A generalization of joint diagonalization proposed in [48] is the only solution we know of that exploits sample dependence for the joint source separation problem in addition to the other two diversity, HOS and source dependence.

We write the relative/natural gradient updates for IVA to minimize the mutual information—hence not accounting for sample dependence—as

$$\mathbf{W}^{[k]}(l + 1) = \mathbf{W}^{[k]}(l) + \mu(\mathbf{I} - E\{\boldsymbol{\psi}^{\text{IVA},[k]}(\mathbf{u}^{[k]})^T\})\mathbf{W}^{[k]}(l), \quad (18)$$

where now the score function has the simpler form $\boldsymbol{\psi}^{\text{IVA},[k]} = -[(\partial \log p_1(\mathbf{u}_1)/\partial \mathbf{u}_1^{[k]}), \dots, (\partial \log p_N(\mathbf{u}_N)/\partial \mathbf{u}_N^{[k]})]^T$. Again, a key problem is the estimation of the score function, i.e., the source pdf, during the adaptation. For IVA, as opposed to ICA, all solutions to date have emphasized parametric methods as non-parametric approaches can easily become prohibitive for the multidimensional case.

IVA is originally formulated for solving the convolutive ICA problem in the frequency domain [9], which is an application where resolution of the permutation ambiguity across frequency bins is critical to the success of the solution.

Hence, the main application domain that is considered has been the separation of acoustic sources resulting in an emphasis on models attractive for this case starting with the multivariate Laplace model [9], [49]. In [50], a mixture of Gaussians is proposed where the noisy IVA problem and an online solution are considered as well. However these solutions fail to consider all-order statistical dependence within an SCV and in certain cases constrain the demixing matrix to be orthogonal/unitary as in [50] and [51]. As discussed earlier, constraining the demixing matrix limits the performance and the decoupling trick introduced in the section “ICA: Algorithms” allows for advantages of orthogonality without having to constrain the matrix, and provides a number of additional advantages such as easier density matching, better convergence properties, and enabling easier derivation of second-order iterative algorithms. In (18), a single step size μ is used to update the entire demixing matrix while each row corresponds to a different source as in the case of ICA. In [47], a number of algorithms—including vector gradient descent and vector Newton algorithms—are derived using the decoupling trick so that the demixing matrices are not constrained to be orthogonal. They are then implemented using a multivariate Gaussian SCV model to derive a class of algorithms called IVA-G, and later using a the Kotz family [52] that includes the GGD, and hence Gaussian and Laplace as special cases. All of these solutions account for all-order statistical dependence for an SCV.

Iterative approaches to optimizing the IVA cost function are subject to similar convergence issues as iterative algorithms for ICA. It is shown that the Hessian matrix for the IVA cost with the multivariate Gaussian model always remains positive definite [47] and thus IVA-G has very desirable convergence properties. Hence, it is a good candidate for initialization of other algorithms, and is used for initializing the

solution of IVA with multivariate Laplace implemented as in [9] for the results we present in the section “Application to Medical Image Analysis.” For non-Gaussian sources, it is known that local minima exist in the cost function. These local minima correspond to demixing solutions that have different permutations across data sets [10]. Thus, even if a local minimum occurs, it is observed that the sources within each data set have been separated but the dependent sources across data sets are not aligned. This issue is addressed in [53] for the special case of spherical and super-Gaussian sources.

EXAMPLE: PERFORMANCE OF TWO IVA SOLUTIONS

In Figure 4, we show the CRLB for separation of sources that are drawn from a multivariate GGD, and the performance of the IVA algorithm of [52] for different sample sizes. We implement two versions of the algorithm, one that estimates the covariance matrix but assumes that the true shape parameter β is known, and a second version that selects one of two $\beta = \{0.5, 2\}$ during the adaptation, which is a practical implementation. As expected, in both cases, the performance improves approaching the CRLB as the number of samples increase. In addition, while the first “clairvoyant” version of the algorithm in Figure 4(a), as expected, provides better performance, the second and practical implementation shown in Figure 4(b) provides quite satisfactory performance as well.

In terms of algorithms that only make use of linear dependence across multiple data sets, MCCA is the oldest, an extension of CCA [54] defined for two data sets. The algorithms given in [5] assume orthogonal demixing and are deflationary in nature such that each row of weights are estimated sequentially. IVA using multivariate Gaussian model also makes use of only linear dependence and can be derived within an ML framework [47], [55]. Since CCA can be achieved using generalized eigenvalue decomposition, it can also be posed as a diagonalization problem, which can be readily extended to achieve IVA using generalized joint

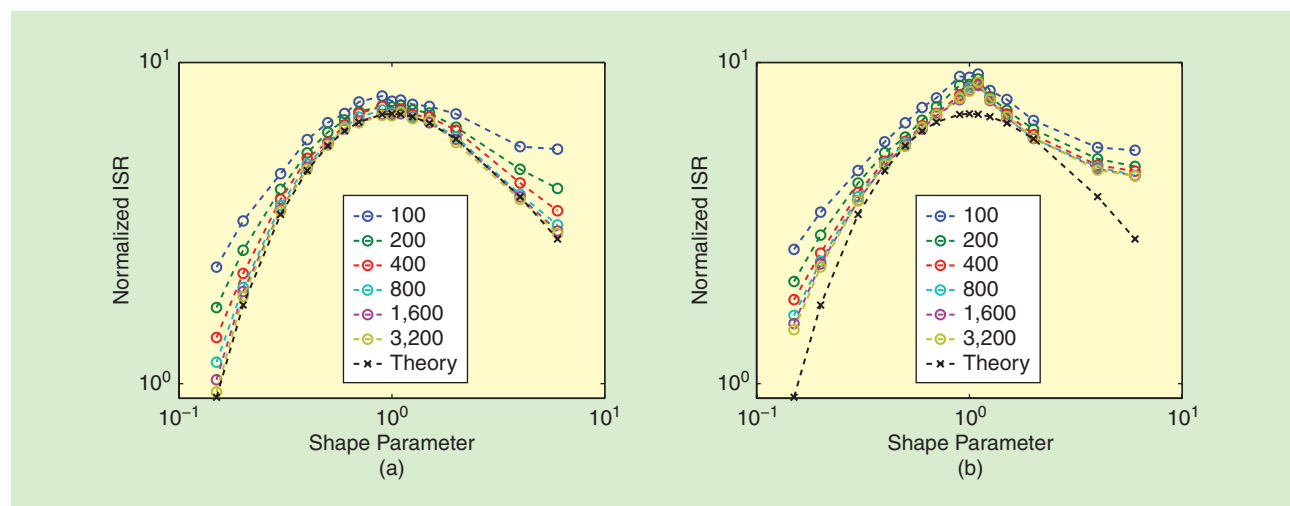


[FIG4] The performance of two IVA algorithms that take source dependence and HOS into account for separation of three GGD sources of dimension $K = 5$ with shape parameter β and a random covariance matrix compared to the induced CRLB (normalized ISR) for different sample sizes. (a) Shape parameter β is assumed to be known. (b) Shape parameter is selected from $\beta = \{0.5, 2\}$.

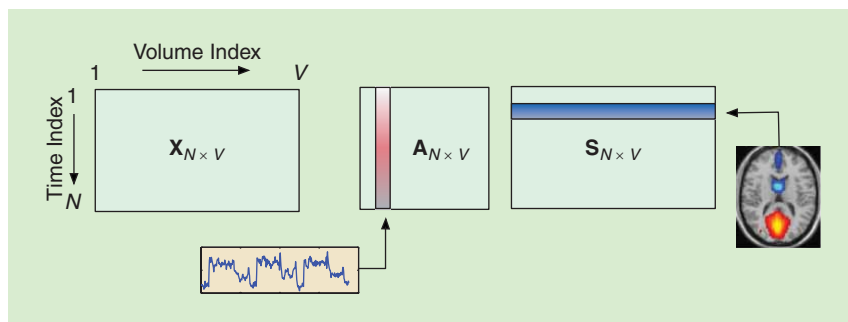


[FIG5] The spatial ICA of fMRI data. Note the presence of both sample dependence and HOS as forms of diversity.

in the study of networks of such intrinsic activity since it naturally takes all the voxels into account when achieving the decomposition and provides a summary statistics for brain activity as well as its modulation across time. Besides, the linear superposition assumption holds for fMRI; see, e.g., [59], and the data-driven nature of ICA helps minimize unrealistic assumptions about the temporal domain and brain hemodynamics.

diagonalization [48]. A review of extensions of CCA to include non-linear dependences is given in [45].

APPLICATION TO MEDICAL IMAGE ANALYSIS

fMRI has enabled us to directly study temporal and spatial changes in both the healthy and the diseased brain as a function of various stimuli, and has contributed greatly to our understanding of the most complex organ of the human body. Relatively low image contrast-to-noise ratio of the blood oxygenation level dependent fMRI signal, head movement, and undesired physiological sources of variability (cardiac, pulmonary) make detection of the activation-related signal changes difficult. The standard approach for the analysis of fMRI data has been correlating the time-series data with an assumed reference signal, i.e., performing a simple linear regression as implemented in the popular statistical parametric mapping (SPM) software [56]. Even though it is robust, use of such a reference time course requires prior information, which most often is not reliable, and more importantly, in most cases it simply is not available. This is the case for data that are acquired when subjects are at rest or performing naturalistic behavior such as watching a movie. Hence, following its first application to fMRI analysis [57], ICA has become an attractive solution and is now widely used for fMRI analysis—for a recent review on ICA of fMRI, see [58].

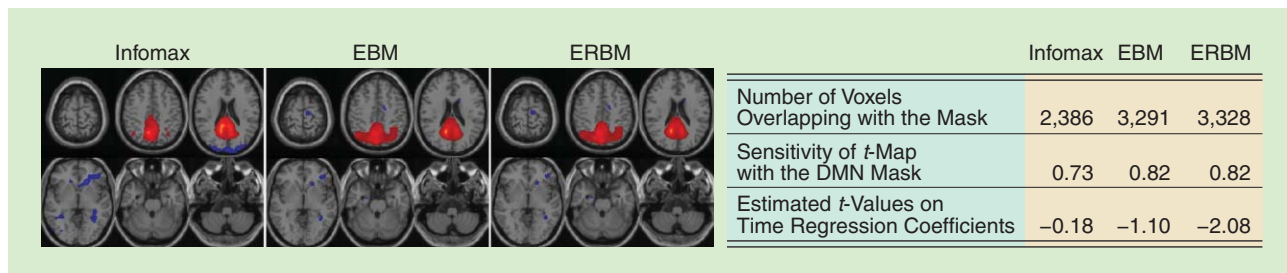
Spatial ICA finds systematically nonoverlapping, temporally coherent brain networks without constraining the temporal domain, hence can effectively recover functional networks. Functional connectivity refers to temporal correlations between spatially distinct regions of the brain, and ICA has been very effective

Figure 5 shows the application of ICA to fMRI analysis for finding spatially independent components, which has been by far

the most common use of ICA for the problem. The observation matrix $X \in \mathbb{R}^{T \times V}$ is formed by flattening the volume image data of V voxels at each time point. The time dimension is typically reduced from T , typically in the hundreds, to N , a value around 30–60 to improve the estimation performance. Information-theoretical criteria (ITC) using principal component analysis (PCA) is most commonly employed for this step [11], i.e., to determine the dimensionality of the signal subspace, usually with a correction for dependence among the samples (voxels) [12] so that a better estimate of ML can be used for the ITC. The spatially independent components—activation maps—form the sources, and the columns of the mixing matrix correspond to the temporal modulation of the corresponding source in the given time frame, $[1, T]$. In Figure 5, we show a sample time course after reconstruction to its original dimension T , and its corresponding Z -thresholded spatial activation map.

EXAMPLE: TAKING SAMPLE DEPENDENCE AND HOS IN ICA OF fMRI DATA

The activation maps, the underlying independent sources, are typically super-Gaussian since they include heavy tails due to active voxels, those with high intensity values, and include sample dependence due to point spread function as well as low pass filtering, a common preprocessing step used for fMRI data. Hence, it would make sense to account for both types of diversity, HOS and sample dependence, when performing ICA of fMRI data. In Figure 6, we show the performance of three ICA algorithms in estimating the default mode network (DMN): 1) Infomax that uses a sigmoidal nonlinearity, a good match to super-Gaussian



[FIG6] Estimated *t*-maps for DMN using Infomax, EBM, and ERBM, and quantitative measures of their performance.

sources; 2) EBM that uses a flexible density model, and 3) ERBM that combines the flexible density estimation of EBM with a filtering approach to account for sample dependence. DMN is part of intrinsic networks, and one that has received much attention lately as it is regarded to be an important biomarker for different disorders. It activates preferentially when individuals focus on internal tasks, when the mind is wandering, and hence it is expected to be negatively correlated with the task time-course, when data are collected during a task. In this example, the data are collected from 20 subjects performing the auditory oddball task [60]. As shown in the figure, all three algorithms have competitive performance, however both EBM and ERBM estimate more voxels than Infomax that correlate with the DMN mask. Also, when we perform a t -test on the multiple regression coefficients of the estimated time courses to determine their task-relatedness, ERBM yields the highest negative value for DMN, hence highest negative correlation with the task, indicating best performance using this metric [60].

Since the need to jointly analyze data from multiple subjects is inherent to most problems in medical data analysis, following the introduction of ICA for fMRI analysis [57] and its success, a simple but effective method, called group ICA [4], is introduced for multisubject fMRI data analysis. Group ICA performs a first-level dimension reduction at the individual subject level, and then temporally concatenates dimension-reduced subject data, to perform a second-level PCA to find a common subspace for data from all subjects. Then a single ICA is performed after which individual subject maps and time-courses are reconstructed as shown in Figure 7(a). There are a number of approaches for reconstructing the subject maps, which are

evaluated and discussed in detail in [61] as well as a number of ways to perform concatenation of data sets [62]. While robust and practical, the projection to a common subspace of data from different subjects can potentially cause loss of information in terms of subject variability. In the application of IVA to fMRI analysis shown in Figure 7(b), individual subject data are directly analyzed following the subject-level dimension reduction. Hence, all individual subject maps are estimated concurrently, and are aligned across subjects when there is dependence among them. This is typically the case for all components of interest, i.e., components corresponding to meaningful functional areas such as DMN and motor areas, since these naturally have statistical dependences across subjects. Components related to artifacts such as the motion artifact, however, might not be aligned for all subjects as these are less likely to have a similar dependence structure across subjects, and are more likely to be subject specific. Next we demonstrate the advantage of IVA over the widely used group ICA approach with two examples, one with simulated fMRI-like data and a second one using real fMRI data.

EXAMPLE: CAPTURING SUBJECT VARIABILITY WITH IVA

To test the ability of IVA in capturing subject variability, we use the fMRI simulation toolbox, SimTB [63], and generate ten components shown in Figure 8(a) for two groups, with 12 subjects in each. For each subject, components are randomly generated with small variations in terms of translation, rotation, and spread. For the first component, however, we introduce significant difference in terms of spread between the two groups of

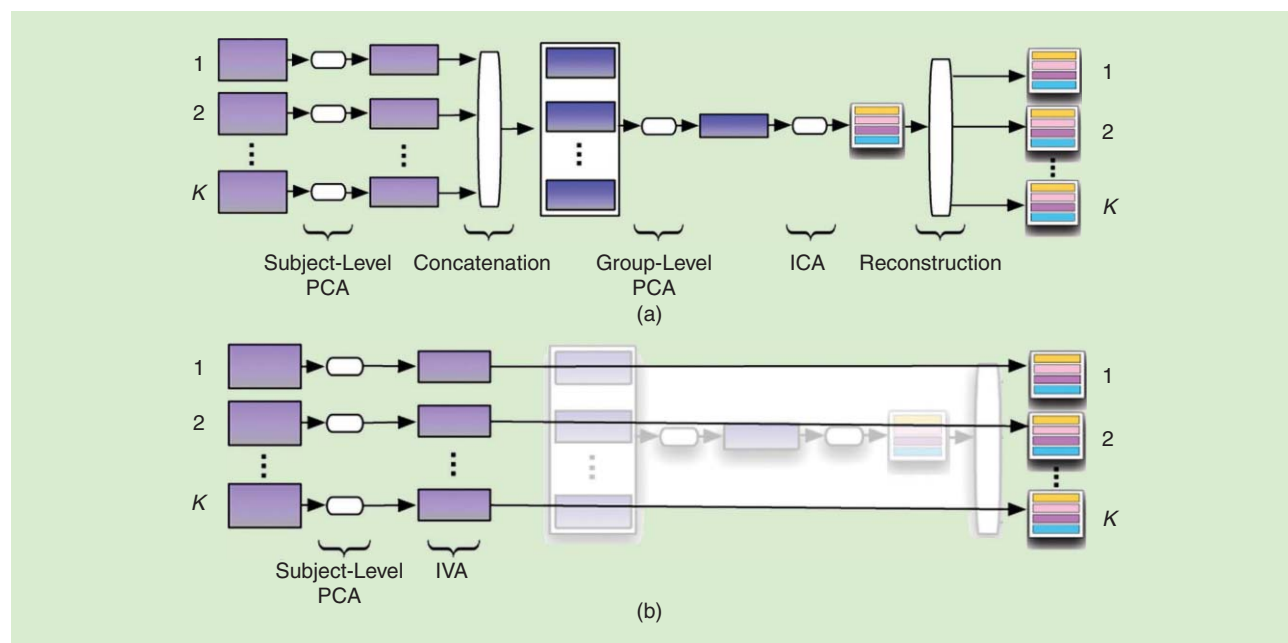


[FIG7] Group ICA and IVA for multisubject fMRI analysis. Note how IVA avoids projecting multisubject data to a common space after subject-level PCA as well as the additional back-reconstruction step of group ICA. (a) Multisubject fMRI analysis with group ICA. (b) Multisubject fMRI analysis with IVA.

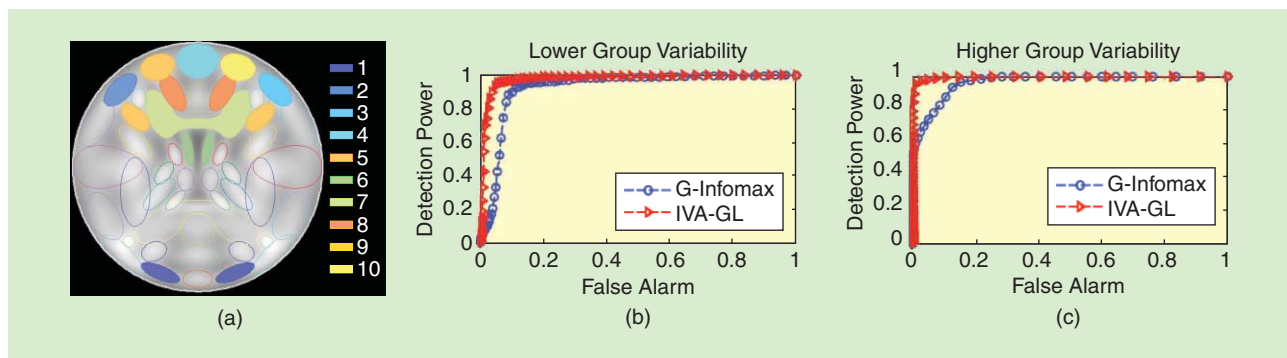


[FIG8] A group analysis study using fMRI-like data. IVA leads to better performance especially with increasing group variability, hence the role of source dependence. (a) SimTB experimental setup. (b) and (c) Receiver operating characteristic curves for IVA and group ICA.

subjects, so as to simulate a typical difference in brain network volume change between the healthy and patient groups found in fMRI studies. The difference in spread is kept at two levels, one indicating a smaller difference between the groups, and a second one with greater difference in spread. Then, the performance is tested between the two approaches: group ICA using Infomax with a nonlinearity matched to Laplacian pdf and IVA using a multivariate Laplacian model following initialization with IVA-G, which we call IVA-GL [64]. In Figure 8(b), we show the receiver operating characteristics curves for the detection of the difference between the two groups at two levels of spread. To obtain the reference map, we perform a two-sample t -test between the two simulated groups, which is thresholded at 0.05 significance. By changing the threshold for t -values, we plot the receiver operating characteristics by counting the number of voxels within (N_{true}) and outside the reference map (N_{false}). The ratios of these values to the total number of voxels within the map and outside, respectively, yields the true positive—detection power—and false alarm values. IVA performs better than the group ICA approach at both lower and higher group variability, and its performance improves when there is higher

group variability. Because with higher group variability, diversity in terms of source dependence has more statistical power, improving the performance of the IVA approach.

EXAMPLE: PERFORMANCE OF IVA AND GROUP ICA WITH REAL fMRI DATA

To test the performance of IVA for the analysis of real fMRI data from subjects that exhibit significant variability, we used data collected from patients who suffered a stroke that primarily affected their motor areas. Data were collected while subjects performed a motor task that had alternating cycles of rest (30 s) and task (24 s), which was squeezing a ball. After standard preprocessing using SPM [56] as in [62], data from ten subjects in two sessions, hence providing a total of 20 data sets, are analyzed using the two approaches for multisubject analysis, group ICA and IVA with the same algorithms as in the previous example, IVA-GL and Infomax with a nonlinearity matched to a Laplace pdf implemented using group ICA of fMRI Toolbox (GIFT) [65]. In Figure 9, we show the t -maps thresholded at a significance level of 0.05.

As clearly observed from the figures, for both components, IVA leads to better estimation of the functional areas as indicated by

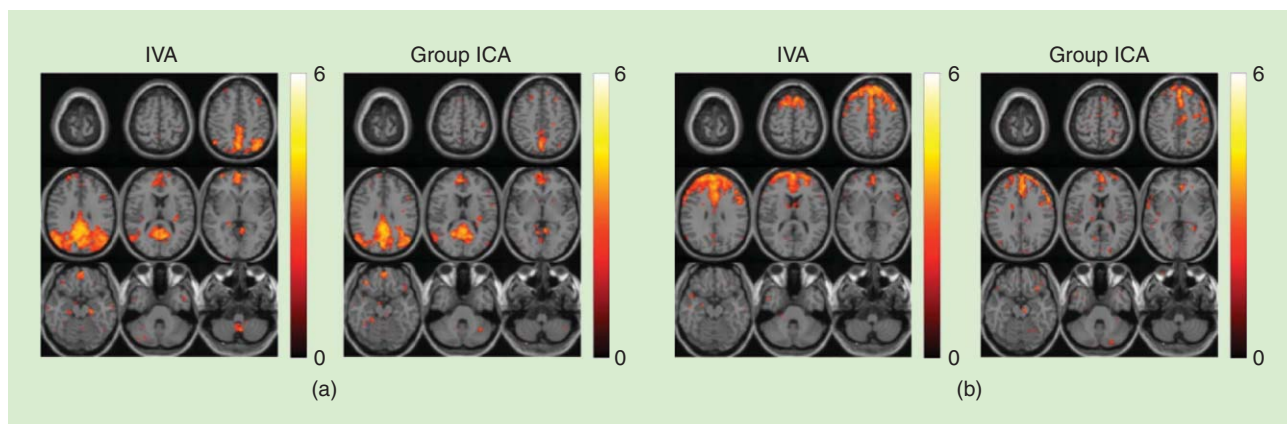


[FIG9] Sample estimated spatial maps for IVA and group ICA for two components: (a) DMN and (b) frontal. Note the higher activation levels and spatial extent of the estimated maps using IVA.

more connected regions and better correlation with the masks generated for these areas as discussed in [66].

DISCUSSION

In this article, we provided an overview of ICA by emphasizing two types of diversity, HOS and sample dependence, which have been the two most typically used for achieving ICA. By using mutual information rate, we showed that a number of ICA approaches can be brought under one umbrella. We then introduced IVA that extends ICA to multiple data sets, and presented a general formulation for IVA that adds a third type of diversity, dependence of sources across data sets to these two. We emphasized the parallels between ICA and IVA in the way diversity plays a role for both and discussed how a number of existing algorithms fit as special cases under this umbrella. Even though this is a rather broad umbrella, this has been a partial survey given the vast activity in the area. For example, algorithms that explicitly compute HOS such as JADE as well as those that make use of other types of diversity such as nonstationarity, noncircularity, and geometrical properties are not considered. Nonstationarity, however, is taken into account in our discussion on identifiability and it has been used with other types of diversity in algorithm development, e.g., along with HOS in [67], and HOS and sample dependence in [68].

Another important diversity type—which we could not discuss here due to space constraints—is noncircularity of the signals when ICA or IVA is implemented in the complex domain, which can be also studied under the mutual information rate umbrella [69]. Since it is the SOS that determine identifiability for ICA and IVA, again in this case, it is the impropriety, second-order noncircularity, that plays a key role. A random vector \mathbf{x} is called second-order circular—or, proper—if its complementary covariance matrix $E\{\mathbf{x}\mathbf{x}^T\}$ vanishes. For improper signals, identification of i.i.d. Gaussians is possible if all circularity coefficients are distinct using strongly uncorrelating transform [70], and in addition, if we make use of HOS and sample dependence, it can be shown that the identification conditions we have given here become more relaxed. Then the ICA problem becomes nonidentifiable only when there are Gaussian sources with both the covariance and complementary covariance matrices that are proportional, and proportional through a complex constant for the latter, as implied by the analyses in [71] and [72]. A conjecture for IVA would be that the condition given here will also include the complementary covariances of SCVs. As one would expect, with the addition of each new type of diversity, identification becomes easier, a broader class of signals can be separated using ICA or IVA. A recent review of complex-valued ICA can be found in [69], and a comprehensive review of the field of blind source separation in [1].

ICA has found a fruitful application in fMRI analysis, and IVA promises to be another attractive solution. ICA has been widely applied to fMRI and EEG analyses, two domains where the linear superposition assumption of ICA holds. A recent review [58] underlined the now wide use of ICA for fMRI

analysis by showing the exponential growth in publications on the topic following its first application in 1998 [57]. An interesting recent claim was that ICA for fMRI has been successful because the widely used algorithms Infomax and FastICA—with kurtosis nonlinearity—select for super-Gaussian sources, hence it is sparsity that determines the final decomposition, and not independence [73]. A response to the article [74] showed that the examples in [73] were flawed and with the correct interpretation of underlying models in ICA, it is indeed independence that achieves a useful decomposition of the fMRI data. Still, it is worth noting that Infomax has been the most widely used algorithm for fMRI analysis, first, due to historical reasons—it was the first algorithm used—and then because its simple fixed score function is a good match for the fMRI sources and provides robustness. However, as the examples we give in this article demonstrate, maximizing independence by using an algorithm with a flexible density matching mechanism can lead to improved performance. In addition, the fact that there is good support for the inherent linear superposition assumption of the basic ICA model of (1) suggests that the spatial maps can be regarded as hidden variables in the model, just like audio sources in a cocktail-party problem. In these cases, maximizing the independence though flexible density matching, and making use of multiple types of diversity to approach the performance bound is meaningful. In applications such as data fusion, however, the approach is mostly exploratory in that the sources do not necessarily have physical meaning, they primarily help explain the data, relationships among modalities. Then, in this case, using a robust algorithm such as Infomax might be sufficient, as discussed in detail in a review on data-driven fusion [75].

The formulation of IVA we present here provides an attractive framework for joint blind source separation with numerous potential applications. These include those where MCCA has been applied such as medical data analysis and fusion, hyperspectral data analysis, blind equalization, and of course the first motivation for the IVA formulation, solution of the convolutive ICA problem. Among many others, multimodality data fusion is an important application area for IVA as it would extend the successful application of MCCA [76] to include HOS without constraining the demixing matrix.

IVA also presents number of challenges and interesting venues for future research. The well-defined structure of IVA might allow a more flexible solution to the MICA—also called subspace ICA—problem where components within each independent subspace are allowed to have dependences. Estimation of the density during adaptation—to truly approach the CRLB and improve performance—is a more difficult task than for ICA. The multivariate nature of the pdf makes the problem more challenging especially when the goal is not only modeling flexible marginals but also taking dependence among the components of an SCV into account. Hence, if successfully extended to the multivariate case, a flexible density model like EBM can achieve this desired

balance, and potentially allow one to also account for sample dependence in the model and estimate an SCM. This is not to say there are not challenges for ICA either. The performance of most ICA algorithms deteriorate when the number of sources increases as well as the noise level. The noisy and the undetermined cases still deserve much attention, and also the problem of nonlinear ICA. Hence, even though the field of blind source separation has now reached a maturity, there are still a good number of important challenges and problems that require our attention.

ACKNOWLEDGMENTS

This work was supported by the National Science Foundation (grants NSF-IIS 1017718 and NSF-CCF 1117056). The authors would like to thank Jonathan Laney for generating the fMRI analysis results using IVA. The MATLAB codes of the ICA and IVA algorithms used in the examples are available at <http://mlsp.umbc.edu/resources.html>.

AUTHORS

Tülay Adalı (adali@umbc.edu) is a professor in the Department of Computer Science and Electrical Engineering at the University of Maryland, Baltimore County. She has actively assisted the IEEE in organizing numerous international conferences and workshops and has chaired and served on various technical committees and editorial boards including the *Proceedings of the IEEE*. She is a Fellow of the IEEE and the AIMBE, an IEEE Distinguished Lecturer, and a recipient of a National Science Foundation CAREER Award, 2010 IEEE Signal Processing Society Best Paper Award, and 2013 University System of Maryland Regents' Award for Research. Her research interests include statistical signal processing, machine learning for signal processing, and medical data analysis.

Matthew Anderson (matt.anderson@umbc.edu) received the B.A. degree in physics from Ithaca College in 2000, the B.S. degree in electrical engineering from Cornell University in 2000, the M.S. degree in electrical engineering from Johns Hopkins University in 2006, and the Ph.D. degree in electrical engineering from the University of Maryland, Baltimore County in 2013. His current research interests include adaptive signal processing, array signal processing, optimization, and blind source separation.

Geng-Shen Fu (fugengs1@umbc.edu) received the B.S. and M.S. degrees, both in electrical engineering, from the Dalian University of Technology, China, in 2002 and 2005, respectively. From 2005 to 2010, he was a software engineer at Panasonic and then at Thomson. He is currently a Ph.D. candidate at the Machine Learning for Signal Processing Lab, University of Maryland, Baltimore County. His research interests include blind source separation and complex-valued signal processing.

REFERENCES

[1] P. Comon and C. Jutten, *Handbook of Blind Source Separation: Independent Component Analysis and Applications*. New York: Academic, 2010.

[2] T. Adalı and S. Haykin, *Adaptive Signal Processing: Next Generation Solutions*. Hoboken, NJ: Wiley Interscience, 2010.

[3] A. Hyvärinen, J. Karhunen, and E. Oja, *Independent Component Analysis*. New York: Wiley, 2001.

[4] V. D. Calhoun, T. Adalı, J. J. Pekar, and G. D. Pearson, "A method for making group inferences from functional MRI data using independent component analysis," *Hum. Brain Mapping*, vol. 14, no. 3, pp. 140–151, Nov. 2001.

[5] J. R. Kettenring, "Canonical analysis of several sets of variables," *Biometrika*, vol. 58, no. 3, pp. 433–451, Dec. 1971.

[6] A. A. Nielsen, "Multiset canonical correlations analysis and multispectral, truly multitemporal remote sensing data," *IEEE Trans. Image Processing*, vol. 11, no. 3, pp. 293–305, Mar. 2002.

[7] J. Via and I. Santamaría, "Adaptive blind equalization of SIMO systems based on canonical correlation analysis," in *Proc. 2005 IEEE 6th Workshop on Signal Processing Advances in Wireless Communications*, June 2005, pp. 318–322.

[8] Y.-O. Li, W. Wang, T. Adalı, and V. D. Calhoun, "Joint blind source separation by multi-set canonical correlation analysis," *IEEE Trans. Signal Processing*, vol. 57, no. 10, pp. 3918–3929, Oct. 2009.

[9] T. Kim, I. Lee, and T.-W. Lee, "Independent vector analysis: Definition and algorithms," in *Proc. 40th Asilomar Conf. Signals, Systems, Computers*, 2006, pp. 1393–1396.

[10] M. Anderson, G.-S. Fu, R. Phlypo, and T. Adalı, "Independent vector analysis: Identification conditions and performance bounds," *IEEE Trans. Signal Processing*, to be published.

[11] M. Wax and T. Kailath, "Detection of signals by information theoretic criteria," *IEEE Trans. Acoust., Speech, Signal Processing*, vol. 33, no. 2, pp. 387–392, Apr. 1985.

[12] Y.-O. Li, T. Adalı, and V. D. Calhoun, "Estimating the number of independent components for fMRI data," *Hum. Brain Mapping*, vol. 28, no. 11, pp. 1251–1266, Nov. 2007.

[13] A. Bell and T. Sejnowski, "An information maximization approach to blind separation and blind deconvolution," *Neural Computat.*, vol. 7, no. 6, pp. 1129–1159, Nov. 1995.

[14] A. Hyvärinen, "Fast and robust fixed-point algorithms for independent component analysis," *IEEE Trans. Neural Networks*, vol. 10, no. 3, pp. 626–634, May 1999.

[15] J.-F. Cardoso and A. Souloumiac, "Blind beamforming for non-Gaussian signals," *IEE Proc. Radar Signal Processing*, vol. 140, no. 6, pp. 362–370, Dec. 1993.

[16] R. Boscolo, H. Pan, and V. Roychowdhury, "Independent component analysis based on nonparametric density estimation," *IEEE Trans. Neural Networks*, vol. 15, no. 1, pp. 55–65, Jan. 2004.

[17] D. Pham and P. Garat, "Blind separation of mixtures of independent sources through a quasi maximum likelihood approach," *IEEE Trans. Signal Processing*, vol. 45, no. 7, pp. 1712–1725, July 1997.

[18] A. Hyvärinen, "Independent component analysis: Recent advances," *Philos. Trans. R. Soc. A*, vol. 1984, pp. 1–19, Feb. 2013.

[19] L. Tong, R.-W. Liu, V. C. Soon, and Y.-F. Huang, "Indeterminacy and identifiability of blind identification," *IEEE Trans. Circuits Syst.*, vol. 38, no. 5, pp. 499–509, May 1991.

[20] A. Belouchrani, K. Abed-Meraim, J.-F. Cardoso, and E. Moulines, "A blind source separation technique using second-order statistics," *IEEE Trans. Signal Processing*, vol. 45, no. 2, pp. 434–444, Feb. 1997.

[21] A. Yeredor, "Blind separation of Gaussian sources via second-order statistics with asymptotically optimal weighting," *IEEE Signal Processing Lett.*, vol. 7, no. 7, pp. 197–200, July 2000.

[22] S. Hosseini, C. Jutten, and D. T. Pham, "Markovian source separation," *IEEE Trans. Signal Processing*, vol. 51, no. 12, pp. 3009–3019, Dec. 2003.

[23] P. Tichavský, Z. Koldovský, and A. Yeredor, "A hybrid technique for blind separation of non-Gaussian and time-correlated sources using a multicomponent approach," *IEEE Trans. Neural Networks*, vol. 19, no. 3, pp. 421–430, Mar. 2008.

[24] K. Hild, H. Attias, and S. Nagarajan, "An expectation-maximization method for spatio-temporal blind source separation using an AR-MoG source model," *IEEE Trans. Neural Networks*, vol. 19, no. 3, pp. 508–519, Mar. 2008.

[25] X.-L. Li and T. Adalı, "Blind spatiotemporal separation of second and/or higher-order correlated sources by entropy rate minimization," in *Proc. IEEE Int. Conf. Acoustics, Speech, Signal Processing (ICASSP)*, Dallas, TX, Mar. 2010, pp. 1934–1937.

[26] G.-S. Fu, R. Phlypo, M. Anderson, X.-L. Li, and T. Adalı, "An efficient entropy rate estimator for complex-valued signal processing: Application to ICA," to appear in *Proc. IEEE Int. Conf. Acoustics, Speech Signal Processing (ICASSP)*, Florence, Italy, May 2014.

[27] T. M. Cover and J. A. Thomas, *Elements of Information Theory*. New York: Wiley, 1991.

[28] A. Yeredor, "Blind separation of Gaussian sources with general covariance structures: Bounds and optimal estimation," *IEEE Trans. Signal Processing*, vol. 58, no. 10, pp. 5057–5068, Oct. 2010.

- [29] S.-I. Amari, A. Cichocki, and H. H. Yang, "A new learning algorithm for blind signal separation," in *Advances in Neural Information Processing Systems, December 1995*, D. S. Touretzky, M. C. Mozer, and M. E. Hasselmo, Eds., vol. 8. Cambridge, MA: MIT, 1996, pp. 757–763.
- [30] J.-F. Cardoso and B. Laheld, "Equivariant adaptive source separation," *IEEE Trans. Signal Processing*, vol. 44, no. 12, pp. 3017–3030, Dec. 1996.
- [31] A. Cichocki, R. Unbehauen, and E. Rummert, "Robust learning algorithm for blind separation of signals," *Electron. Letts.*, vol. 30, no. 17, pp. 1386–1387, Aug. 1994.
- [32] J. Héault and C. Jutten, "Space or time adaptive signal processing by neural networks models," in *Proc. Int. Conf. Neural Networks for Computing*, Snowbird, UT, 1986, pp. 206–211.
- [33] Z. Koldovský, P. Tichavský, and E. Oja, "Efficient variant of algorithm FastICA for independent component analysis attaining the Cramér-Rao lower bound," *IEEE Trans. Neural Networks*, vol. 17, no. 5, pp. 1265–1277, Sept. 2006.
- [34] X.-L. Li and T. Adalı, "Independent component analysis by entropy bound minimization," *IEEE Trans. Signal Processing*, vol. 58, no. 10, pp. 5151–5164, Oct. 2010.
- [35] G.-S. Fu, R. Phlypo, M. Anderson, X.-L. Li, and T. Adalı, "Algorithms for Markovian source separation by entropy rate minimization," in *Proc. IEEE Int. Conf. Acoustics, Speech, Signal Processing (ICASSP)*, Vancouver, BC, Canada, May 2013, pp. 3248–3252.
- [36] W. Lu and J. Rajapakse, "Constrained independent component analysis," in *Proc. Advances in Neural Information Processing Systems*, vol. 13, 2001, pp. 570–576.
- [37] T. Adalı, H. Li, M. Novey, and J.-F. Cardoso, "Complex ICA using nonlinear functions," *IEEE Trans. Signal Processing*, vol. 56, no. 9, pp. 4356–4544, Sept. 2008.
- [38] X.-L. Li and X.-D. Zhang, "Nonorthogonal joint diagonalization free of degenerate solution," *IEEE Trans. Signal Processing*, vol. 55, no. 5, pp. 1803–1814, May 2007.
- [39] M. Anderson, X.-L. Li, P. A. Rodríguez, and T. Adalı, "An effective decoupling method for matrix optimization and its application to the ICA problem," in *Proc. IEEE Int. Conf. Acoustics, Speech, Signal Processing (ICASSP)*, Kyoto, Japan, Mar. 2012, pp. 1885–1888.
- [40] A. Yeredor, "Performance analysis of the strong uncorrelating transformation in blind separation of complex-valued sources," *IEEE Trans. Signal Processing*, vol. 60, no. 1, pp. 478–483, Jan. 2012.
- [41] ICALAB toolboxes. [Online]. Available: <http://www.bsp.brain.riken.jp/ICALAB>
- [42] J.-F. Cardoso, "Multidimensional independent component analysis," in *Proc. IEEE Int. Conf. Acoustics, Speech, Signal Processing (ICASSP)*, Seattle, WA, May 1998, pp. 1941–1944.
- [43] A. Hyvärinen and P. Hoyer, "Emergence of phase- and shift-invariant features by decomposition of emergence of phase- and shift-invariant features by decomposition of natural images into independent feature subspaces," *Neural Computat.*, vol. 12, no. 7, pp. 1705–1720, July 2000.
- [44] D. Lahat, J.-F. Cardoso, and H. Messer, "Second-order multidimensional ICA: Performance analysis," *IEEE Trans. Signal Processing*, vol. 60, no. 9, pp. 4598–4610, Sept. 2012.
- [45] M. Anderson, "Independent vector analysis: Theory, algorithms, and applications," Ph.D. dissertation, University of Maryland Baltimore County, May 2013.
- [46] J. Via, M. Anderson, X.-L. Li, and T. Adalı, "Joint blind source separation from second-order statistics: Necessary and sufficient identifiability conditions," in *Proc. IEEE Int. Conf. Acoustics, Speech Signal Processing (ICASSP)*, Prague, Czech Republic, May 2011, pp. 2520–2523.
- [47] M. Anderson, X.-L. Li, and T. Adalı, "Joint blind source separation with multivariate Gaussian model: Algorithms and performance analysis," *IEEE Trans. Signal Processing*, vol. 60, no. 4, pp. 2049–2055, Apr. 2012.
- [48] X.-L. Li, T. Adalı, and M. Anderson, "Joint blind source separation by generalized joint diagonalization of cumulant matrices," *Signal Process.*, vol. 91, no. 10, pp. 2314–2322, Oct. 2011.
- [49] T. Kim, H. T. Attias, S.-Y. Lee, and T.-W. Lee, "Blind source separation exploiting higher-order frequency dependencies," *IEEE Trans. Audio Speech Lang. Processing*, vol. 15, no. 1, pp. 70–79, Jan. 2007.
- [50] J. Hao, I. Lee, T.-W. Lee, and T. J. Sejnowski, "Independent vector analysis for source separation using a mixture of Gaussians prior," *Neural Computat.*, vol. 22, no. 6, pp. 1646–1673, 2010.
- [51] H. Zhang, L. Li, and W. Li, "Independent vector analysis for convolutive blind non-circular source separation," *Signal Process.*, vol. 92, no. 9, pp. 2275–2283, 2012.
- [52] M. Anderson, G.-S. Fu, R. Phlypo, and T. Adalı, "Independent vector analysis, the Kotz distribution, and performance bounds," in *Proc. IEEE Int. Conf. Acoustics, Speech Signal Processing (ICASSP)*, Vancouver, BC, Canada, May 2013, pp. 3243–3247.
- [53] T. Itahashi and K. Matsuoka, "Stability of independent vector analysis," *Signal Process.*, vol. 92, no. 8, pp. 1809–1820, Aug. 2012.
- [54] H. Hotelling, "Relations between two sets of variates," *Biometrika*, vol. 28, no. 3/4, pp. 321–377, Dec. 1936.
- [55] J. Via, M. Anderson, X.-L. Li, and T. Adalı, "A maximum likelihood approach for independent vector analysis of Gaussian data sets," in *Proc. IEEE Int. Workshop on Machine Learning for Signal Processing (MLSP)*, Beijing, China, 2011, pp. 1–6.
- [56] K. J. Friston, J. T. Ashburner, S. Kiebel, T. Nichols, and W. D. Penny, Eds., *Statistical Parametric Mapping: The Analysis of Functional Brain Images*. New York: Academic, 2006.
- [57] M. J. McKeown, S. Makeig, G. G. Brown, T. P. Jung, S. S. Kindermann, A. J. Bell, and T. J. Sejnowski, "Analysis of fMRI data by blind separation into independent spatial components," *Hum. Brain Mapping*, vol. 6, no. 3, pp. 160–188, 1998.
- [58] V. D. Calhoun and T. Adalı, "Multisubject independent component analysis of fMRI: A decade of intrinsic networks, default mode, and neurodiagnostic discovery," *IEEE Rev. Biomed. Eng.*, vol. 5, pp. 60–73, Aug. 2012.
- [59] A. M. Dale and R. L. Buckner, "Selective averaging of rapidly presented individual trials using fMRI," *Hum. Brain Mapping*, vol. 5, no. 5, pp. 329–340, 1997.
- [60] W. Du, H. Li, X.-L. Li, V. Calhoun, and T. Adalı, "ICA of fMRI data: Performance of three ICA algorithms and the importance of taking correlation information into account," in *Proc. IEEE Int. Symp. Biomedical Imaging*, Chicago, IL, Mar.–Apr. 2011, pp. 1573–1576.
- [61] E. Erhardt, S. Rachakonda, E. Bedrick, T. Adalı, and V. D. Calhoun, "Comparison of multi-subject ICA methods for analysis of fMRI data," *Hum. Brain Mapping*, vol. 12, pp. 2075–2095, Dec. 2011.
- [62] V. D. Calhoun, J. Liu, and T. Adalı, "A review of group ICA for fMRI data and ICA for joint inference of imaging, genetic, and ERP data," *NeuroImage*, vol. 45, no. 1, pp. S163–S172, Mar. 2009.
- [63] E. Erhardt, E. Allen, Y. Wei, T. Eichele, and V. D. Calhoun, "SimTB, a simulation toolbox for fMRI data under a model of spatiotemporal separability," *NeuroImage*, vol. 59, no. 4, pp. 4160–4167, Feb. 2012.
- [64] S. Ma, R. Phlypo, V. D. Calhoun, and T. Adalı, "Capturing group variability using IVA: A simulation study and graph-theoretical analysis," in *Proc. IEEE Int. Conf. Acoustics, Speech Signal Processing (ICASSP)*, Vancouver, BC, Canada, May 2013, pp. 3128–3132.
- [65] Group ICA of fMRI toolbox v3.02. (2013). [Online]. Available: <http://mialab.mrn.org/software/gift/>
- [66] J. Laney, K. Westlake, E. Woytowicz, S. Ma, and T. Adalı, "Capturing subject variability in data-driven fMRI analysis: A graph-theoretical comparison," in *Proc. Conf. Information Sciences and Systems*, Princeton, NJ, Mar. 2014.
- [67] Z. Koldovský, J. Málek, P. Tichavský, Y. Deville, and S. Hosseini, "Blind separation of piecewise stationary non-Gaussian sources," *Signal Process.*, vol. 89, no. 12, pp. 2570–2584, Dec. 2009.
- [68] H. Buchner, R. Aichner, and W. Kellermann, "Blind source separation for convolutive mixtures: A unified treatment," in *Audio Signal Processing*, ser. Editors, Y. Huang and J. Benesty. Boston, MA: Kluwer Academic, pp. 255–293, Feb. 2004.
- [69] E. Moreau and T. Adalı, *Blind Identification and Separation of Complex-valued Signals*. Hoboken, NJ: ISTE and Wiley, 2013.
- [70] J. Eriksson and V. Koivunen, "Complex-valued ICA using second order statistics," in *Proc. IEEE Int. Workshop on Machine Learning for Signal Processing (MLSP)*, São Luis, Brazil, Sept. 2004, pp. 183–192.
- [71] B. Loesch and B. Yang, "Cramér-Rao bound for circular and noncircular complex independent component analysis," *IEEE Trans. Signal Processing*, vol. 61, no. 2, pp. 365–379, Jan. 2013.
- [72] X.-L. Li and T. Adalı, "Blind separation of noncircular correlated sources using Gaussian entropy rate," *IEEE Trans. Signal Processing*, vol. 59, no. 6, pp. 2969–2975, June 2011.
- [73] I. Daubechies, E. Roussos, S. Takerkarta, M. Benharrosha, C. Goldenb, K. D'Ardennea, W. Richtera, J. D. Cohena, and J. Haxyaw, "Independent component analysis for brain fMRI does not select for independence," *Proc. Natl. Acad. Sci.*, vol. 106, no. 26, pp. 10415–10422, June 2009.
- [74] V. D. Calhoun, V. K. Potluru, R. Phlypo, R. F. Silva, B. A. Pearlmuter, A. Caprihan, S. M. Plis, and T. Adalı, "Independent component analysis for brain fMRI does indeed select for maximal independence," *PLoS ONE*, vol. 8, no. 8, 2013.
- [75] V. D. Calhoun and T. Adalı, "Feature-based fusion of medical imaging data," *IEEE Trans. Inform. Technol. Biomed.*, vol. 13, no. 5, pp. 711–720, Sept. 2009.
- [76] N. Correa, T. Adalı, and V. D. Calhoun, "Canonical correlation analysis for data fusion and group inferences," *IEEE Signal Processing Mag.*, vol. 27, no. 4, pp. 39–50, July 2010.

[Gilles Chabriel, Martin Kleinsteuber, Eric Moreau,
Hao Shen, Petr Tichavsky, and Arie Yeredor]

Joint Matrices Decompositions and Blind Source Separation

[A survey of methods, identification, and applications]

Matrix decompositions such as the eigenvalue decomposition (EVD) or the singular value decomposition (SVD) have a long history in signal processing. They have been used in spectral analysis,

signal/noise subspace estimation, principal component analysis (PCA), dimensionality reduction, and whitening in independent component analysis (ICA). Very often, the matrix under consideration is the covariance matrix of some observation signals. However, many other kinds of matrices can be encountered in signal processing problems, such as time-lagged covariance matrices, quadratic spatial time-frequency matrices [21], and matrices of higher-order statistics.

In concert with this diversity, the joint diagonalization (JD) or approximate JD (AJD) of a set of matrices has been recently recognized to be instrumental in signal processing, mainly because of its importance in practical signal processing problems such as source separation, blind beamforming, image denoising, blind channel identification for multiple-input, multiple-output (MIMO) telecommunication system, Doppler-shifted echo

extraction in radar, and ICA. Perhaps one of the first such algorithms is the joint approximate diagonalization of eigenmatrices (JADE) algorithm proposed in [8]. In this algorithm, the matrices under consideration are Hermitian and the considered joint diagonalizer is a unitary matrix. More recently, generalizations and/or new decompositions were found to be of considerable interest. They concern new sets of matrices, a nonunitary joint diagonalizer, and new decompositions.

INTRODUCTION

In the context of noncircular complex-valued signals, complex symmetric (non-Hermitian) matrices provide information that can be useful and even sufficient for blind beamforming or source separation. One example is the complementary covariance matrix, also called the *pseudocovariance matrix*. With such complex symmetric matrices, one ends up with jointly diagonalizing a set of matrices via either the transpose congruence transform or Hermitian congruence transform. For the special two-matrix case with one Hermitian and one complex symmetric matrix, there are particularly fast JD algorithms based on EVD and SVD.

This article provides a comprehensive survey of matrix joint decomposition techniques in the context of source separation. More precisely, we first intend to elaborate upon the signal models leading to different useful sets of matrices and their



Source Separation and Applications

IMAGE LICENSED BY
INGRAM PUBLISHING

Digital Object Identifier 10.1109/MSP.2014.2298045

Date of publication: 7 April 2014

joint decompositions. Second, we present recent identifiability results and algorithms in distinguishing important classes.

SIGNAL MODEL, MATRICES, AND DECOMPOSITIONS

To motivate the JD problem from the perspective of blind source separation (BSS), let us consider the classical linear memoryless source mixing model with additive noise described by

$$\mathbf{x}(t) = \mathbf{A}s(t) + \mathbf{n}(t), \tag{1}$$

where $\mathbf{x}(t) \in \mathbb{C}^M$ is the observation vector, $s(t) \in \mathbb{C}^N$ the source (component) vector, $\mathbf{n}(t) \in \mathbb{C}^M$ the noise vector, and $\mathbf{A} \in \mathbb{C}^{M \times N}$ the mixing matrix assumed full column rank (we shall not address the under-determined case of fewer rows than columns until the section on direct fit methods). Since we suppose that we have more than one source, this leads to $M \geq N \geq 2$. The index t characterizes the variability of the signals. It is very often the time index but it can be the frequency index or the position index for an image, or any physical variables describing the considered signals. For convenience, it is considered in the sequel as the time index.

In BSS, the mixing matrix is assumed unknown and the sources not observable. The problem is then the estimation of the sources given only the observations.

When statistical (or other) information is available regarding the noise, such information can be accounted for in the estimation of the unknown mixing matrix, as well as in the estimation of the sources (even when the mixing matrix is known). However, to capture the essence of the problem and of its links to JD, we shall ignore the noise in here and assume $\mathbf{n}(t) = \mathbf{0}$.

Since the mixing model is not unique, it is well known that estimation of the sources is possible only up to some indeterminacies about the sources' scaling and ordering (see the section "Identifiability Issues for the Symmetric Case"). Among other things, this can be done by estimating a (left) pseudo-inverse (or simply the inverse in the square case) of \mathbf{A} denoted (generically) by \mathbf{B} . Basically there are two ways for that: the first one consists of estimating \mathbf{A} , followed by the calculation of its pseudo-inverse whereas the second one consists of estimating \mathbf{B} directly. Notice that the estimation of \mathbf{A} corresponds to the so-called blind identification problem in signal processing while the direct estimation of \mathbf{B} corresponds to the classical BSS.

The estimation of \mathbf{A} or \mathbf{B} can be formulated as a joint decomposition of a set of well-chosen matrices, to which we shall refer as *target-matrices*. Hence the first step is to choose target-matrices admitting a specific decomposition with respect to (w.r.t.) the matrix for which we are looking. The choice of useful matrices depends on a source model.

Quite commonly, the target-matrices are constructed from statistics of the observation. It is common practice to assume that the sources have zero mean, hence first-order statistics are of no

interest. Thus second-order statistics (SOS) is considered. For a complex-valued random observation vector, one can define two kinds of SOS matrices,

$$\mathbf{R}_x(t, \tau) = \mathbf{E}\{\mathbf{x}(t)\mathbf{x}^H(t - \tau)\}, \quad \bar{\mathbf{R}}_x(t, \tau) = \mathbf{E}\{\mathbf{x}(t)\mathbf{x}^T(t - \tau)\},$$

where $(\cdot)^T$ and $(\cdot)^H$ are the transpose operator and the transpose conjugate operator, respectively, and $\mathbf{E}\{\cdot\}$ denotes the expectation operator. The first matrix $\mathbf{R}_x(t, \tau)$ is the classical correlation matrix, whereas the second one $\bar{\mathbf{R}}_x(t, \tau)$ is the so-called complementary correlation matrix. The usefulness of the complementary correlation matrix is directly related to a noncircularity property of the sources since for circular sources this matrix would be null.

One can also consider higher-order statistics (HOS) described by cumulants. Since third-order statistics are not so useful in practice mainly because the probability density function (PDF) of the sources is often close to symmetric, fourth-

order statistics are often considered. In a very general way, they are defined as

$$C_{x,ijkl}(t, \{\tau\}) = \text{Cum}\{x_i(t), x_j^{(*)_1}(t - \tau_1), x_k(t - \tau_2), x_l^{(*)_2}(t - \tau_3)\},$$

where $(*)_1$ and $(*)_2$ denote optional complex conjugates and $\{\tau\} \equiv \{\tau_1, \tau_2, \tau_3\}$. One way to construct matrices from cumulants consists of considering a linear combination of the above cumulants while keeping free the first two indices that will be used as row and column indices for the constructed matrix. This is written as

$$(\mathbf{C}_x(t, \{\tau\}))_{ij} = \sum_{k,l=1}^M G_{kl} C_{x,ijkl}(t, \{\tau\}),$$

where $\mathbf{G} = (G_{kl})$ is a fixed coefficients matrix. All of the above statistics generally depend on the time index t . In such a case the sources are called *nonstationary*. In the special case where the dependence w.r.t. t is periodic, the sources are called *cyclostationary*. When the statistics do not depend on t , the sources are called *stationary*.

In the noiseless case, using (1), the matrices $\mathbf{R}_x(t, \tau)$ and $\mathbf{C}_x(t, \{\tau\})$ with $(*)_1 \equiv *$, denoted generically as \mathbf{M}_x , all admit the factorization $\mathbf{M}_x = \mathbf{A}\mathbf{M}_s\mathbf{A}^H$, whereas the matrices $\bar{\mathbf{R}}_x(t, \tau)$ and $\mathbf{C}_x(t, \{\tau\})$ with $(*)_1 \equiv 1$, denoted generically as $\bar{\mathbf{M}}_x$, all admit the factorization $\bar{\mathbf{M}}_x = \mathbf{A}\bar{\mathbf{M}}_s\mathbf{A}^T$. With no further assumptions regarding the sources, the matrices \mathbf{M}_s and $\bar{\mathbf{M}}_s$ do not possess any special algebraical structures compared to \mathbf{M}_x and $\bar{\mathbf{M}}_x$, so these decompositions are noninformative. However, quite often some plausible assumptions regarding certain properties of the sources imply a special and "simplified" structure (diagonal or other) of \mathbf{M}_s and $\bar{\mathbf{M}}_s$. This is directly linked to an identifiability property that has to be considered to be able to separate the sources. Basically, for stochastic sources, the classical identifiability assumption is their statistical independence, leading to the ICA problem. For independent

IN CONCERT WITH THIS DIVERSITY, THE JOINT DIAGONALIZATION OR APPROXIMATE JOINT DIAGONALIZATION OF A SET OF MATRICES HAS BEEN RECENTLY RECOGNIZED TO BE INSTRUMENTAL IN SIGNAL PROCESSING.

sources, the matrices M_s and \widetilde{M}_s are always diagonal [5], [8], [15], [20], [29], giving rise to the concept of “JD” of the selected target-matrices, as the result of representing each of these matrices as the corresponding transformation of a respective diagonal matrix.

In practice, however, the set of “true” target-matrices (specifically, the respective true SOS or HOS of the observations) is not available. Only sample-estimates of these matrices may be available, and these estimated matrices may no longer admit an exact JD transformation. In such cases one must resort to AJD, in an attempt to find a transformation being “as close as possible” to JD, with various measures for the quality of the approximation.

Simplifying the notations, we can always consider a set of K complex matrices M_k , to be decomposed as

$$M_k = AD_kA^{\ddagger} + \Pi_k \quad k = 1, \dots, K, \quad (2)$$

where $(\cdot)^{\ddagger}$ corresponds to either the transpose or the conjugate transpose of the matrix argument and matrices D_k all share some prescribed common structure. Depending on the signal model, the matrices D_k can be either all diagonal, all block diagonal, or all zero diagonal, as we shall explain in the sequel. The residual matrices Π_k are perturbation matrices which are linked to estimation errors and/or to modeling errors. This is referred to as the *symmetric case*; see Figure 1. Note that another model $M_k = AD_kA^{-1} + \Pi_k$ has been studied as well [24] but is less popular in applications. A more general formulation, which is sometimes found to be more useful, reads

$$M_k = A_L D_k A_R + \Pi_k, \quad (3)$$

where the matrices A_L and A_R are a priori arbitrary; see, e.g., [12]. This is referred to as the *nonsymmetric case* since A_R is not directly (or explicitly) linked to A_L .

The main problem consists of estimating A (or A_L) or its left inverse up to acceptable indeterminacies. In practice, these

indeterminacies correspond to the estimation of all columns of A up to a scaling factor and up to ordering. This is the concept of essential uniqueness, which will be discussed in the section “Identifiability Issues for the Symmetric Case.”

In all of the following sections, we denote $B = A^\dagger$, $B_R = A_R^\dagger$, and $B_L = A_L^\dagger$ where $(\cdot)^\dagger$ stands for the pseudo-inverse of the matrix argument or directly the inverse in the square case.

IDENTIFIABILITY ISSUES FOR THE SYMMETRIC CASE

One fundamental question in the context of the BSS problem is: “Under what conditions on the sources can the mixing process be uniquely identified up to ordering and scaling?” This is evidently a question of general identifiability conditions, which are independent of a particular separation approach, and have been derived, e.g., in [15], [30], and [41]. However, in the context of JD-based BSS, the identifiability issue is closely related to the uniqueness (up to the trivial ambiguities) of the JD solution, which in turn relies on properties of the target-matrices. An underlying assumption is that under asymptotic conditions the estimated target-matrices can become arbitrarily close to the true target-matrices, and therefore the uniqueness of the joint diagonalizer has to be explored w.r.t. the true target-matrices, in the context of exact, rather than approximate JD. When the mixing matrix is invertible, identifiability of the mixing matrix implies the ability to separate the sources and is therefore often associated with separability. However, even when it is not invertible, the mixing matrix may still be identifiable (even by AJD), but such identifiability would not imply separability of the sources in such cases. Additionally, in some scenarios that are beyond the scope of this article, some sources may be separable from the mixture based on their special key properties (e.g., sparsity) but still without the need for identifiability of the full mixing matrix. In this section, we only focus on the symmetric case with an invertible mixing matrix.

Identifiability conditions for some specific scenarios have been provided, e.g., for the unitary case [5] and for the nonorthogonal real-valued case [2]. In this section, we summarize the necessary and sufficient conditions for the joint diagonalizer to be unique up to permutation and scaling for the noiseless, symmetric JD case (2). While general identifiability conditions for the nonsymmetric case (3) are still an open question, for particular nonsymmetric algorithms [12], [13] a necessary and sufficient condition can be provided (see the sections “Nonunitary Joint Diagonalization” and “Nonunitary Joint Zero Diagonalization,” respectively, for the diagonal and zero-diagonal cases).

In the noiseless case, and under the assumption of full column rank of A , whenever $M > N$ one can easily find N of the M observed mixtures that would be linearly independent and ignore the other observed mixtures without loss of information. Therefore, without loss of generality, we consider the square (or “determined”) BSS problem, i.e., $M = N$. Given $B, B' \in \mathbb{C}^{N \times N}$, B is said to be essentially equivalent to B' , and vice versa, if B is only different from B' by at most a row-wise ordering and scaling. Moreover, we say that the solution of a JD problem is essentially unique, if all solutions are essentially equivalent.

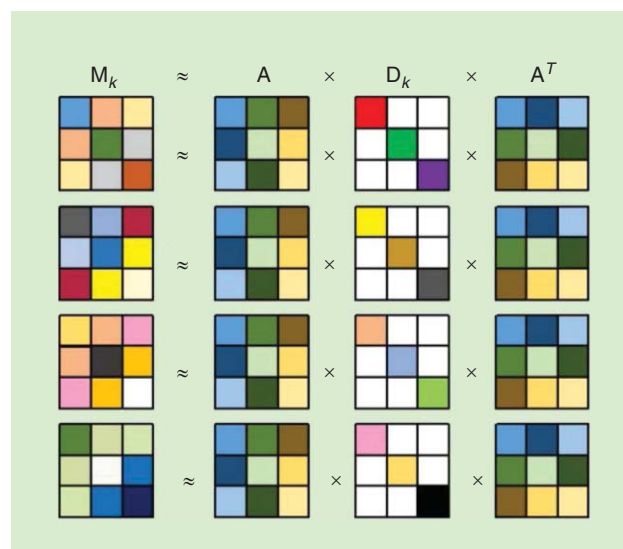


[FIG1] An illustration of AJD of four 3×3 symmetric target-matrices M_1, M_2, M_3, M_4 ($N = 3, K = 4$).

HOMOGENEOUS MODELS AND THEIR UNIQUENESS RESULTS

The uniqueness of JD under transpose congruence transform has been considered for real matrices in [2]. Recently, the extension to complex matrices has been studied in [3] and [25]. We first discuss the case where all matrices are to be diagonalized with the same transformation [i.e., \ddagger is exclusively either T or H in (2)] and refer to this as the *homogeneous case*. For that, we require a measure of collinearity for diagonal matrices, which is obtained by means of the complex angle between the vectors formed by stacking the entries at corresponding positions together. The relation in (4) illustrates an example with (2×2) diagonal matrices. Let $\mathbf{D}_k := \text{diag}(d_{k1}, \dots, d_{kN}) \in \mathbb{C}^{N \times N}$ for $k = 1, \dots, K$. For a fixed diagonal position i , we denote by $\mathbf{d}_i := [d_{1i}, \dots, d_{Ki}]^T \in \mathbb{C}^K$ the vector consisting of the i th diagonal element of each matrix, respectively,

$$\underbrace{\begin{bmatrix} d_{11} & 0 \\ 0 & d_{12} \end{bmatrix}}_{\mathbf{D}_1}, \underbrace{\begin{bmatrix} d_{21} & 0 \\ 0 & d_{22} \end{bmatrix}}_{\mathbf{D}_2}, \dots, \underbrace{\begin{bmatrix} d_{K1} & 0 \\ 0 & d_{K2} \end{bmatrix}}_{\mathbf{D}_K} \Rightarrow \begin{bmatrix} d_{11}, d_{21}, \dots, d_{K1} \\ d_{12}, d_{22}, \dots, d_{K2} \end{bmatrix}^T =: \mathbf{d}_1, \mathbf{d}_2 \quad (4)$$

Recall that the cosine of the complex angle between two nonzero vectors $\mathbf{v}, \mathbf{w} \in \mathbb{C}^K$ computed as $c(\mathbf{v}, \mathbf{w}) := (\mathbf{v}^H \mathbf{w}) / (\|\mathbf{v}\| \|\mathbf{w}\|)$, where $\|\mathbf{v}\|$ denotes the Euclidean norm of a vector \mathbf{v} . (If one of the two vectors is zero, the cosine is defined to be one by convention.) The uniqueness result states that, for a given set of matrices \mathbf{M}_k , the joint diagonalizer \mathbf{B} is essentially unique, if and only if $|c(\mathbf{d}_i, \mathbf{d}_j)| \neq 1$ for all pairs (i, j) with $i \neq j$. In particular, for $K = 2$, this condition allows to uniquely solve the JD problem simply via a generalized EVD approach, i.e., $\mathbf{M}_1 \mathbf{B} = \mathbf{M}_2 \mathbf{B} \mathbf{\Lambda}$, where $\mathbf{\Lambda}$ is diagonal [33].

A HYBRID MODEL AND ITS UNIQUENESS RESULTS

The uniqueness results above state that, when there exists one pair of collinear concatenated vectors $(\mathbf{d}_i, \mathbf{d}_j)$, the solutions under homogeneous transforms are not essentially unique. However, it is known that signals with distinct second-order circularity coefficients are uniquely identifiable via a nonhomogeneous JD of only one covariance matrix (using the conjugate transpose operator $(\cdot)^H$) and one pseudo-covariance matrix (using the transpose operator $(\cdot)^T$). The corresponding method is known as strong uncorrelating transform (SUT) [20].

Recent works in [47] and [39] generalize the SUT approach to jointly diagonalize both Hermitian and complex symmetric matrices. The following statement provides a necessary and sufficient condition for the JD problem with a mixture of Hermitian congruence and transpose congruence. For given matrices $\mathbf{M}_k := \mathbf{A} \mathbf{D}_k \mathbf{A}^H$ with $k = 1, \dots, K$ and $\widetilde{\mathbf{M}}_l := \mathbf{A} \widetilde{\mathbf{D}}_l \mathbf{A}^T$ with $l = 1, \dots, L$, the common joint diagonalizer \mathbf{B} is essentially unique, if and only if there exists no pair (i, j) with $i \neq j$, such that the following two conditions hold:

$$1) |c(\mathbf{d}_i, \mathbf{d}_j)| = |c(\widetilde{\mathbf{d}}_i, \widetilde{\mathbf{d}}_j)| = 1; \quad 2) \|\mathbf{d}_i\| \|\mathbf{d}_j\| = \|\widetilde{\mathbf{d}}_i\| \|\widetilde{\mathbf{d}}_j\|.$$

In other words, when there is at least one pair of collinear concatenated vectors $(\mathbf{d}_i, \mathbf{d}_j)$, then the essential uniqueness implies that the respective norms are not proportional.

In the simplest case, where only one Hermitian and one complex symmetric matrix are considered, $\mathbf{d}_i, \mathbf{d}_j, \widetilde{\mathbf{d}}_i$ and $\widetilde{\mathbf{d}}_j$ are all scalars, so all pairs are trivially collinear. Then the previous result boils down to the following. Given two matrices $\mathbf{M} := \mathbf{A} \mathbf{D} \mathbf{A}^H$ and $\widetilde{\mathbf{M}} := \mathbf{A} \widetilde{\mathbf{D}} \mathbf{A}^T$ with $\mathbf{D} = \text{diag}(d_1, \dots, d_M)$ and $\widetilde{\mathbf{D}} = \text{diag}(\widetilde{d}_1, \dots, \widetilde{d}_M)$, the joint diagonalizer \mathbf{B} is essentially unique if and only if the condition $|d_i| |\widetilde{d}_j| \neq |\widetilde{d}_i| |d_j|$ holds for all pairs (i, j) with $i \neq j$. This result simply recovers the uniqueness condition for SUT, where the matrix \mathbf{M} is Hermitian and positive definite. We refer to [25] for a study of a further generalization of SUT, known as the pseudo-uncorrelating transform (PUT) and to [52] for the separation performance of the SUT for specific signal models.

The identifiability results yield a sufficient theoretical condition on the properties of the sources, such that the BSS problem is uniquely solvable, independent of any JD algorithms. Meanwhile, depending on the properties of the sources, it allows to determine a set of matrices, such that an exact JD solution yields the correct demixing matrix. In the presence of noise, AJD algorithms are used to find a matrix that minimizes some diagonality measures.

MATRIX NORMALIZATION FOR JOINT DIAGONALIZATION

For simplicity, let us only consider the symmetric case. A normalizing linear transformation \mathbf{B}_n can be applied to the observations as $\mathbf{x}_n(t) = \mathbf{B}_n \mathbf{x}(t)$ or directly onto the set of target-matrices as

$$\mathbf{M}_{n,k} = \mathbf{B}_n \mathbf{M}_k \mathbf{B}_n^H \text{ and/or } \widetilde{\mathbf{M}}_{n,k} = \mathbf{B}_n \widetilde{\mathbf{M}}_k \mathbf{B}_n^T, \quad k = 1, \dots, K,$$

(here the subscript $(\cdot)_n$ denotes “normalization”) in such a way that the overall problem is normalized or simplified. The normalizing matrix \mathbf{B}_n is usually determined by selecting a particular Hermitian matrix denoted \mathbf{M}_0 , which would be exactly diagonalized by this transformation, and may (or may not) coincide with one of the target-matrices $\mathbf{M}_1, \dots, \mathbf{M}_K$. It is well known [23] that any such matrix admits diagonalization as $\mathbf{M}_0 = \mathbf{U} \mathbf{\Lambda} \mathbf{U}^H$, where $\mathbf{\Lambda}$ is a real-valued diagonal matrix of eigenvalues and \mathbf{U} is a unitary matrix of orthonormal eigenvectors in its columns, i.e., $\mathbf{U} \mathbf{U}^H = \mathbf{U}^H \mathbf{U} = \mathbf{I}$ where \mathbf{I} is the identity matrix. In the context of BSS, and especially when \mathbf{M}_0 coincides with one of the target-matrices, the matrix \mathbf{U} can often serve as a reasonable initial guess for the approximate joint diagonalizer of the entire set, or can at least serve to “simplify” the matrix set by considering $\mathbf{B}_n = \mathbf{U}^H$.

Now, if the number of sources N is known (or well estimated), then one can do a little more. If N eigenvalues of \mathbf{M}_0 are nonzero and all the $M - N$ others are zero, then we denote $\mathbf{\Lambda}_s$ the diagonal matrix corresponding to these N nonzero eigenvalues and \mathbf{U}_s the matrix of corresponding eigenvectors (spanning the so-called signal subspace). Then we directly have $\mathbf{M}_0 = \mathbf{U}_s \mathbf{\Lambda}_s \mathbf{U}_s^H$. Now we can consider $\mathbf{B}_n = \mathbf{U}_s^H$, which corresponds to a projection of the observations onto the signal subspace. Hence all new matrices

$\mathbf{M}_{n,k}$ and/or $\bar{\mathbf{M}}_{n,k}$ are of size $N \times N$. This is essentially a PCA operation, which corresponds to a useful dimension reduction when $M > N$.

Finally, we point out that \mathbf{M}_0 is often positive semidefinite, that is all nonzero components of Λ (specifically, the diagonal components of Λ_s) are positive. This is usually the case when \mathbf{M}_0 is selected as the (zero lag) sample-covariance matrix of the observations. Then we can set $\mathbf{B}_n = \mathbf{V}\Lambda_s^{-(1/2)}\mathbf{U}_s^H$, where \mathbf{V} is any $N \times N$ unitary matrix. This operation is known as *whitening*, and it can be shown (as evident from the above definition using a nondetermined unitary matrix \mathbf{V}) that following such a whitening step, any unitary diagonalizer of the normalized (“whitened”) set $\mathbf{M}_{n,1}, \dots, \mathbf{M}_{n,K}$ would maintain the whiteness of the transformed \mathbf{M}_0 . Therefore, when a whitening stage is used, the diagonalizer of the whitened set is usually constrained to be unitary, which simplifies the search.

NONUNITARY JOINT DIAGONALIZATION

In this section, we address the nonunitary AJD problem as the most important and common case. Following the alternating columns, diagonal centers (ACDC) algorithm [50], many AJD algorithms have been proposed over the last decade; see, e.g., [13], [21], [38], [43], and [49]. These papers only consider the symmetric version with $\mathbf{B}_L = \mathbf{B}_R^T = \mathbf{B}$. Since, however, an extension to the nonsymmetric version is possible (straightforward for some of these algorithms), we present the problem in the latter form. In the existing literature, we can distinguish four groups of nonunitary AJD algorithms.

- 1) Minimizing the so-called indirect least-squares criterion, which may be a possibly weighted square norm of off-diagonal elements of the transformed matrices $\mathbf{B}_L \mathbf{M}_k \mathbf{B}_R$. To use this criterion the matrices \mathbf{B}_L and \mathbf{B}_R must be properly constrained so as to avoid the trivial zero solution and/or degenerate solutions.
- 2) Minimizing the direct least-square criterion (which can also be weighted), measuring the squared difference between the matrices and their representations, specifically the norms of the residual matrices Π_k in (2) or (3).
- 3) A combination of these two criteria. Here, one seeks matrices \mathbf{B}_L and \mathbf{B}_R that transform the given set of matrices into a set of nearly diagonal matrices, which cannot be diagonalized any further in the direct-fit sense, specifically such that the best direct-fit diagonalizer of the transformed set is the identity matrix.
- 4) Minimizers of an approximate log-likelihood criterion. So far the log-likelihood criterion was derived only for the case where the given matrices reflect second-order statistics of a mixture of Gaussian vector processes.

In many applications, performance of the nonunitary AJD algorithms can be significantly enhanced by appropriate weighting, introduced in the optimization criterion. When a statistical model

**IN MANY APPLICATIONS,
PERFORMANCE OF THE
NONUNITARY AJD ALGORITHMS
CAN BE SIGNIFICANTLY ENHANCED
BY APPROPRIATE WEIGHTING,
INTRODUCED IN THE
OPTIMIZATION CRITERION.**

for the sources is fully known, the optimal weighting may be deduced in advance (e.g., [51]). Usually, however, the proper weights are not known in advance but may be estimated from the observed data, e.g., when a statistical model for the sources is only known up to some parameters, which nonetheless can be estimated as a by-product of the diagonalization process

(e.g., [42]), or when multiple snapshots of the data are available for nonparametric estimation of the weights [53].

MINIMIZING THE INDIRECT-FIT CRITERION

Historically, the first, natural choice of an indirect-fit criterion is

$$C_{J1}(\mathbf{B}_L, \mathbf{B}_R) = \sum_{k=1}^K \|\text{Zdiag}\{\mathbf{B}_L \mathbf{M}_k \mathbf{B}_R\}\|_F^2, \quad (5)$$

where $\text{Zdiag}\{\cdot\}$ sets the diagonal entries of the matrix argument to zero. Since, however, trivial minimization by down-scaling towards $\mathbf{B}_L = \mathbf{B}_R = \mathbf{0}$ is clearly not interesting, one has to consider some constraint or barrier function to evade this. The following options have been proposed in the literature, together with appropriate minimization procedures, derived for the symmetric case where $\mathbf{B}_L = \mathbf{B}$ and $\mathbf{B}_R = \mathbf{B}^T$:

- 1) \mathbf{B} is unitary. This choice has already been discussed in the previous section.
- 2) The rows of \mathbf{B} have unit norm. This constraint is weaker than the former one and was used in [19].
- 3) $\mathbf{B}\mathbf{M}_0\mathbf{B}^T$ must have an all-ones main diagonal [48], where \mathbf{M}_0 may or may not be included among $\{\mathbf{M}_k\}$. In the BSS context, if \mathbf{M}_0 is the zero-lag covariance matrix of the observations, this constraint corresponds to the constraint on the separated sources, that they should have equal (unit) power. The proposed method of optimization uses iterative generalized matrix eigenvector computation.
- 4) \mathbf{B} has a unit determinant. The optimization can be attained through Givens and hyperbolic rotations [40].
- 5) In [28], a penalty term (proportional to $\log|\det \mathbf{B}|$) is added to (5). The optimization proceeds by alternating between optimization w.r.t. individual rows of matrix \mathbf{B} .
- 6) Another suitable AJD criterion, which is scale-invariant in \mathbf{B} , was proposed in [1] and [2],

$$C_{J2}(\mathbf{B}) = \sum_{k=1}^K \|\mathbf{M}_k - \mathbf{B}^{-1} \text{Diag}\{\mathbf{B}\mathbf{M}_k\mathbf{B}^T\}\mathbf{B}^{-T}\|_F^2. \quad (6)$$

The scale invariance means that the criterion is not affected by changing scale of any rows of \mathbf{B} . The optimization was achieved by combination of triangular Jacobi matrices and Givens rotations.

MINIMIZING THE DIRECT-FIT CRITERION

The direct-fit criterion is a measure of difference between the given matrices \mathbf{M}_k and their assumed model in terms of the

estimating the left and right mixing matrix A_L and A_R and diagonal matrices D_k , $k = 1, \dots, K$,

$$C_{J3}(A_L, A_R, \{D_k\}) = \sum_{k=1}^K \|M_k - A_L D_k A_R\|_F^2. \quad (7)$$

Minimization of this criterion is directly linked to tensor decompositions, as we explain shortly. The noiseless part $A_L D_k A_R$ of the target-matrices M_k together represents a third-order tensor \mathcal{T} of dimensions $M \times M \times K$, with elements \mathcal{T}_{ijk} , $i, j = 1, \dots, M$ and $k = 1, \dots, K$ such that its k th slice $\mathcal{T}_{:, :, k}$ equals $A_L D_k A_R$, i.e.,

$$\mathcal{T}_{ijk} = \sum_{r=1}^M (A_L)_{ir} (A_R)_{rj} (D_k)_{rr}. \quad (8)$$

In the tensor terminology, \mathcal{T} is a tensor of rank at most M , because it can be written as a sum of M rank-1 tensors, each of them being an outer product of three vectors, specifically the r th column of A_L , r th row of A_R , and a vector composed of the (r, r) th elements of D_k , $k = 1, \dots, K$. The decomposition of this kind is called *canonical polyadic* or *CANDECOMP-PARAFAC* (CP) decomposition [9], [22]. The special case when two or more factor matrices coincide (in our case, the coinciding factor matrices might be A_L and A_R^T) is called *individual differences in scaling* (*INDSCAL*) [10] (see Figure 2 for an illustration).

The direct-fit criterion, or the CP decomposition, offers more flexibility than the indirect fit: it allows for treating situations where the number of separated sources is not necessarily equal to the dimension of the mixture. If the number of sources is smaller than M , it is still possible to use an indirect-fit criterion and identify the sources among spurious (noisy) ones. A less trivial task is to separate underdetermined mixtures, where the number of sources exceeds the number of mixtures. CP decomposition allows such a separation [16], [45].

The area of CP tensor decompositions is a rapidly growing field, and many techniques have been proposed. A traditional and still the most popular technique is the alternating least squares. Other methods include enhanced line search, damped Gauss–Newton method (also called Levenberg–Marquardt), and others; see, e.g., references in [36]. A link between the CP decomposition and AJD (even in the underdetermined case, rank greater than the dimension) was shown in [17], and more recently was exploited in [37]. It was shown that CP decomposition can be attained through approximate JD of certain sets of matrices.

Beside the CP decomposition approach, a suboptimum direct-fit optimization of (7) was proposed in [13] (called DIEM for “diagonalization using equivalent matrices”), offering a closed-form (noniterative) solution. Moreover, DIEM can deal with the non-symmetric case since the matrices A_L and A_R are not constrained or linked in the derivations. A necessary and sufficient condition for the uniqueness of the DIEM solution is that the set of K underlying diagonal matrices D_1, \dots, D_K spans the N -dimensional subspace of diagonal matrices in $\mathbb{C}^{N \times N}$. New BSS applications using nonsymmetric JD are discussed in the last section.

COMBINATION OF THE DIRECT AND INDIRECT-FIT CRITERIA

Combining the indirect and direct fit of JD is conceptually simple and computationally efficient. A generic algorithm of this type works with a partially diagonalized set of matrices $B_L^{[i]} M_k B_R^{[i]}$, $k = 1, \dots, K$, i is the iteration index. Initially, one can start with $B_L^{[0]} = B_R^{[0]} = I$. Each step consists of one iteration of a direct-fit procedure, which may or may not use weighting. In the unweighted (or uniformly weighted) version, we have

$$\{A_L^{[i]}, A_R^{[i]}\} = \underset{A_L, A_R}{\operatorname{argmin}} \sum_{k=1}^K \|B_L^{[i]} M_k B_R^{[i]} - A_L D_{k,B} A_R\|_F^2, \quad (9)$$

where $D_{k,B} \triangleq \operatorname{Diag}\{B_L^{[i]} M_k B_R^{[i]}\}$. The direct-fit procedure can be of Gauss–Newton type, for fast convergence in a neighborhood of the true local minimum and is sought close to $A_L = A_R = I$. Only one iteration of the Gauss–Newton procedure is applied in each step because, at the initial point $A_L = A_R = I$, the Hessian matrix has an attractive decoupled form that enables its inversion through solving distinct sets of 2×2 linear equations.

Once an approximation of the best fitting mixing matrices $A_L^{[i]}$ and $A_R^{[i]}$ is found, the estimated demixing matrices are updated as $B_L^{[i+1]} = (A_L^{[i]})^{-1} B_L^{[i]}$ and $B_R^{[i+1]} = B_R^{[i]} (A_R^{[i]})^{-1}$. This algorithm was named WEDGE (for “weighted exhaustive diagonalization with Gauss iteration”), or U-WEDGE in its uniformly weighted version, in [43].

MAXIMIZATION OF A LOG-LIKELIHOOD CRITERION

The last principle of AJD is a maximum likelihood (ML) approach. It was developed by Pham [35] for JD of a set of sample covariance matrices taken from distinct signal-blocks, where the statistical model assumes independent Gaussian distributed sources with variances that are constant within each block but varying between blocks. For real-valued signals and mixtures, the ML method with $B = B_L = B_R^T$ leads to the criterion

$$C_{LL}(B) = \sum_{k=1}^K \log \frac{\det \operatorname{Diag}\{B M_k B^T\}}{\det(B M_k B^T)}, \quad (10)$$

which is scale-invariant in B and does not require any constraints. This criterion may also be used as a generic AJD criterion (outside the ML framework), however it is meaningful only for positive definite target-matrices $\{M_k\}$.

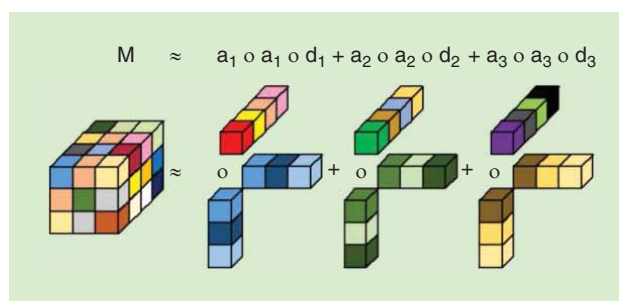


[FIG2] The AJD of the target-matrices of Figure 1 viewed as a partially symmetric CP decomposition (INDSCAL).

COMPUTATIONAL COMPLEXITY

The fastest nonorthogonal AJD algorithms such as U-WEDGE/WEDGE [43], fast AJD (FAJD) [28], and Pham’s [35] have asymptotic computational complexity of $O(KM^2)$ operations per iteration. This is the lower bound for any algorithm that should have access to all elements of the target-matrices. Some other algorithms have slightly higher complexity, $O(KM^3)$ operations per iteration, such as quadratic AJD (QAJD) [48], Souloumiac’s [40] or Afsari’s [1]. The number of iterations is varying. Among the algorithms, U-WEDGE/WEDGE, Pham’s, Souloumiac’s, and Afsari’s algorithm exhibit a quadratic convergence, as inherited from the approximate Gauss–Newton methods, and usually only need a few dozens of iterations to converge; FAJD and QAJD are based on alternating minimization, exhibit only linear convergence, and usually require hundreds of iterations.

For fixed and moderate K and M , a very fast AJD algorithm is the noniterative DIEM algorithm of Chabriel and Barrère [13] that, however, only attains an approximate optimum of the direct fit, and works with matrices of the size $M^2 \times M^2$, so that its complexity is at least $O(KM^6)$.

All direct-fit algorithms have complexity of at least $O(KM^3)$ per iteration because this is the complexity of one least-squares solution step (fixing two factor matrices and minimizing w.r.t. the third one). Indeed, more complex algorithms require a higher number of operations per iteration. For example, the fastest available implementation of the Levenberg–Marquardt algorithm has complexity $O(KM^3 + M^6)$ operations per iteration.

APPROXIMATE JOINT BLOCK DIAGONALIZATION

In this subsection, we briefly mention the concept of approximate joint block diagonalization that was first introduced in [54]. Indeed it might happen that for some given sets of target-matrices it is not possible to find mixing or demixing matrices such that the indirect or direct-fit error is satisfactorily small, but it is

possible to fit them well by a block diagonal model. The latter model resembles (3), but the matrices D_k are block diagonal, with diagonal blocks of appropriate size; see Figure 3(a). Such a model is usually relevant in cases where not all sources are independent, but several groups of sources exist, with intragroup dependence but with intergroup independence. As in the ordinary diagonalization task, the block diagonalization can be either unitary or nonunitary. The first block-diagonalization algorithms were unitary, [7]. Later, nonunitary algorithms were proposed as well: direct-fit methods by Nion [31], indirect methods by Tichavsky et al. [44], and ML methods by Lahat et al. [27].

NONUNITARY JOINT ZERO DIAGONALIZATION

In this section, we consider the case where, in (2) or (3), the matrices D_k are zero diagonal for all k and where the searched matrix is a priori nonunitary; see Figure 3(b). This problem is termed *approximate zero diagonalization (AZD)*. The matrices D_k for all k are denoted Z_k here for a direct interpretation. We consider both the symmetric and the nonsymmetric cases when all matrices are square $N \times N$. This can always be considered in using a first-dimension reduction operation.

In the symmetric case, the problem can be addressed by considering the indirect least squares criterion [21] $C(\mathbf{B}) = \sum_{k=1}^K \|\text{Diag}\{\mathbf{B}\mathbf{M}_k\mathbf{B}^H\}\|^2$ that has to be minimized. As initially proposed in [21], the optimization of $C(\mathbf{B})$ can be performed row by row in searching iteratively for eigenvectors associated to matrices built from the target-matrices. Even if the optimization scheme is rather simple, it can lead to nonuseful solutions (certainly corresponding to local minima). However since JD algorithms are more robust, very interestingly, it can be shown that the above problem can be cast as an ordinary nonunitary JD problem [11]. This is possible when the set of K underlying zero-diagonal matrices Z_1, \dots, Z_K spans the $N^2 - N$ dimensional subspace of zero-diagonal matrices in $\mathbb{C}^{N \times N}$. In fact, this

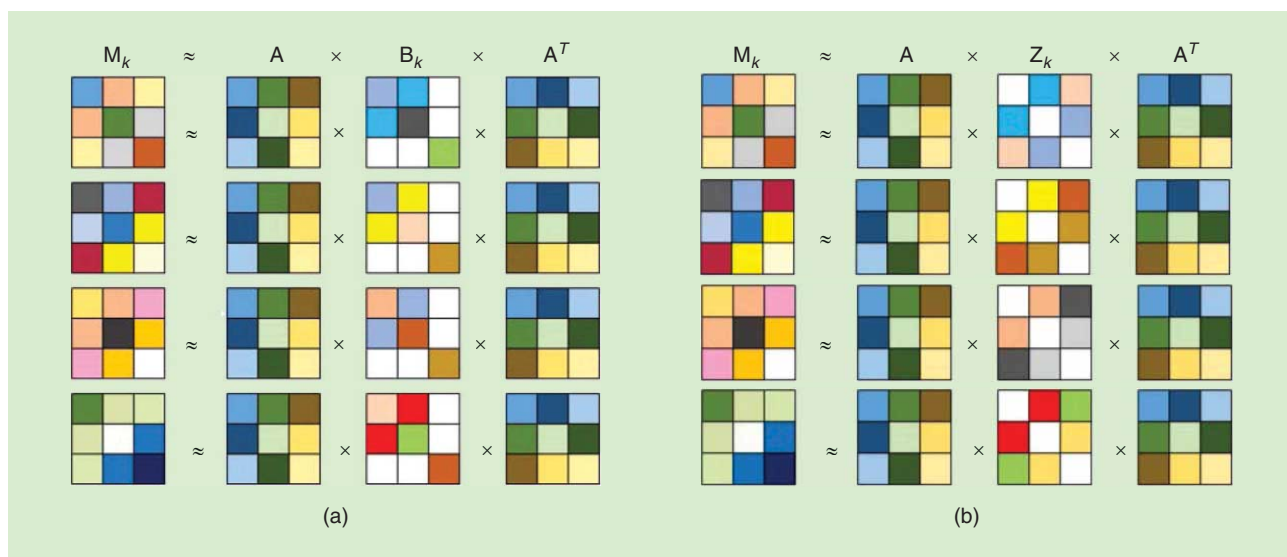


[FIG3] (a) The approximate joint block diagonalization of four 3×3 symmetric target-matrices M_1, M_2, M_3, M_4 , with one 2×2 block and one 1×1 “block.” (b) The approximate joint zero diagonalization of four 3×3 symmetric target-matrices M_1, M_2, M_3, M_4 .

condition is also a sufficient for essential uniqueness of the joint zero diagonalizer. Note that the number of target-matrices has to be relatively large, $K \geq N^2 - N$ for this condition to hold.

In the nonsymmetric case, matrices A_R and A_L are a priori not linked. Following [11], a nonsymmetric algorithm [12] can be derived in turning the problem into a nonsymmetric JD one that can be solved using, e.g., the nonsymmetric version of DIEM mentioned earlier.

EXAMPLES OF BSS APPLICATIONS

In this section, we mention examples of two applications of AJD-based BSS techniques, one for symmetric AJD and the other one for symmetric or nonsymmetric AJD. As an application of joint zero diagonalization, we can mention the zero-division multiple access wireless telecommunications system [12] where all the signals to be sent use the same bandwidth.

BLIND AUDIO SOURCE SEPARATION

Since modern AJD algorithms allow the JD of sets of large matrices with dimensions such as 100×100 or 500×500 within time of order fraction of seconds or few seconds, they enable us to solve blind audio source separation (BASS), also known as the “cocktail-party problem”; see Figure 4(a), in the time domain [26].

Most of the existing BASS algorithms work in the frequency domain by transforming the convolutive mixture model into an instantaneous mixture model using the short-time Fourier transform. The individual sources were separated in each frequency bin independently. Since, however, the order of sources obtained in each bin is arbitrary, it is necessary to resolve the permutation ambiguity simultaneously in all the bins. Random errors in the estimated order of the components in different bins, which are inevitable in practice, lead to nonlinear distortion of the estimated signals.

Time-domain BSS methods do not produce nonlinear distortions in the data but estimate linear MIMO filters that separate the sources. In short, the input signals measured by the microphones are augmented by their time-shifted replicas to become a multidimensional input of an BSS algorithm. The number of the time-shifted replicas should be large enough to cover mutual time delays of arrival of the individual source signals at the microphones and their reflections. An insufficient number of the time replicas would lead to poor performance of the whole system.

In principle, it is possible to use any ICA algorithm to transform the input data set (microphone outputs with their time-shifted replicas), in “pseudo-independent” components; the “pseudo-independent” components are further grouped and used to reconstruct the source images (contributions of all sources at all microphones) [26]. A successful ICA algorithm in this application was the block Gaussian separation algorithm, which consists in applying a nonunitary AJD algorithm UWEDGE/WEDGE to the set of covariance matrices of the input signals at nonoverlapping time windows.

In [14], the cocktail-party problem is addressed differently, using a compact array of microphones. It is shown that if the

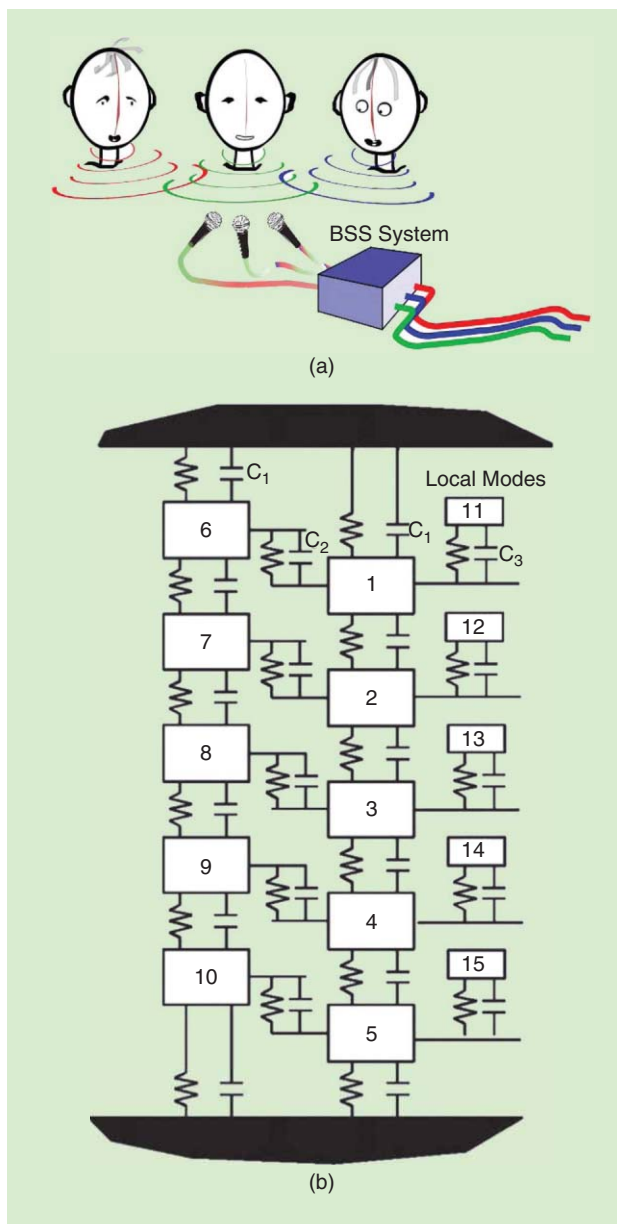


[FIG4] (a) An illustration of the cocktail-party problem with three speakers and three microphones. (b) An analytical 15 degrees-of-freedom system. (Figure reprinted from [4], with permission from Elsevier.)

distance between any pair of microphones is sufficiently small (relatively to the coherence time of each source), a linear instantaneous mixing model, as the one in (1), holds, but w.r.t. an extended mixture model, where the temporal derivatives of the sources are added as “additional” (pseudo-independent) sources.

OPERATIONAL MODAL ANALYSIS

Operational modal analysis (OMA) is concerned with the analysis of a mechanical or electrical vibration system in terms of individual vibration modes; see Figure 4(b). The analysis is based on the system output, assuming white input noise. It was shown in [4] that SOS-based BSS methods are able to separate a

set of system responses into modal coordinates from which the system poles can be extracted by single-degree-of-freedom techniques. In addition, these methods return a mixing matrix whose columns are the estimates of the system mode shapes.

The method is based on JD of the set of time-lagged covariance matrices of the observations. The authors of [4] considered the algorithm for multiple unknown signals extraction (AMUSE) (based on generalized eigendecomposition of a pair of the covariance matrices with lags 0 and $\tau \neq 0$) [46] and second-order blind identification [5] algorithms in forming the AJD problem. Next, they proposed their own nonsymmetric AJD algorithm, which was shown to be more adequate for this problem.

CONCLUSIONS

We presented a survey of AJD methods and related joint matrix decomposition methods that can be used in various BSS applications, together with conditions for uniqueness of the solutions. In addition, we pointed out the option of weighted AJD methods, which might yield optimized performance through proper selection of the weights. The selection of the most suitable AJD/AZD method will always depend on the target application because criteria of success might be quite different. Finally, we mentioned joint nonsymmetric matrix decompositions that should lead to new (promising) BSS or array processing applications.

ACKNOWLEDGMENT

The work of Martin Kleinstüber and Hao Shen has been supported by the German DFG-funded Cluster of Excellence CoTeSys—Cognition for Technical Systems. The work of Petr Tichavsky was supported by the Czech Science Foundation through project 102/09/1278.

AUTHORS

Gilles Chabriel (gilles.chabriel@im2np.fr) received the microelectronic and automatic engineer diploma from the Institut des Sciences de l'Ingénieur de Montpellier (currently Polytech Montpellier), Montpellier, France, in 1992 and the Ph.D. degree in physics from the Université de Toulon (UTLN), La Garde, France, in 1997. He is currently an assistant professor in the Sciences and Applied Sciences Department of UTLN, where he teaches courses in electronics and signal processing. In the Signals and Systems Team of the Institut Matériaux, Microélectronique, Nanosciences de Provence (IM2NP, UMR CNRS 7334), his research is in the areas of signal processing, telecommunications, and electronic systems.

Martin Kleinstüber (kleinstueber@tum.de) received the Ph.D. degree in mathematics from the University of Würzburg, Germany, in 2006. After postdoctoral positions at National ICT Australia Ltd, the Australian National University, Canberra, and the University of Würzburg, he was appointed assistant professor for geometric optimization and machine learning with the Department of Electrical Engineering and Information Technology, Technische Universität München, Germany, in 2009. He won the SIAM Student Paper Prize in 2004 and the Robert-Sauer-Award of the Bavarian Academy of Science in 2008 for his works on Jacobi-type

methods on Lie algebras. His research focuses on latent variable analysis, pattern recognition, and feature extraction in signals together with their applications to audio and image processing.

Eric Moreau (moreau@univ-tln.fr) received the Ph.D. degree in signal processing from Université Paris 11 Orsay, France, in 1995 and the habilitation degree from the Université de Toulon, France, in 2000. He is currently a full professor with the Engineering School ISITV at Université de Toulon and head of the Telecommunications Department. He is also head of the research group SIIM (Signal and Images) with LSIS UMR CNRS 7296. His main research interests are in statistical signal processing and matrix/tensor decompositions with an emphasis on source separation.

Hao Shen (hao.shen@tum.de) received the bachelor's degree in mechanical engineering and applied mathematics from Xi'an Jiaotong University, China, in 2000, the master's degrees in computer studies and computer science from the University of Wollongong, Australia, in 2002 and 2004, respectively, and the Ph.D. degree in engineering from the Australian National University in 2008. He is a postdoctoral researcher at the Institute for Data Processing, Technische Universität München, Germany. His research interests focus on machine learning for signal processing, in particular, BSS, sparse representation, geometric optimization, and reinforcement learning.

Petr Tichavsky (tichavsk@utia.cas.cz) received the Ph.D. degree in theoretical cybernetics from the Czechoslovak Academy of Sciences in 1992. Since then, he has been with the Institute of Information Theory and Automation, Academy of Sciences of the Czech Republic in Prague. He was an associate editor of *IEEE Signal Processing Letters* from 2002 to 2004 and an associate editor of *IEEE Transactions on Signal Processing* from 2005 to 2009 and from 2011–present. He has also served as a general cochair of the 2011 36th IEEE International Conference on Acoustics, Speech, and Signal Processing in Prague, Czech Republic. He is a Senior Member of the IEEE.

Arie Yeredor (arie@eng.tau.ac.il) received the B.Sc. (summa cum laude) and Ph.D. degrees in electrical engineering from Tel-Aviv University (TAU), Tel-Aviv, Israel, in 1984 and 1997, respectively. He is currently an associate professor with the School of Electrical Engineering at TAU, where his research and teaching areas are in statistical and digital signal processing. He was previously an associate editor of *IEEE Signal Processing Letters*, *IEEE Transactions on Circuits and Systems-Part II*, and *IEEE Transactions on Signal Processing*. He recently served as general cochair of the 2012 10th International Conference on Latent Variables Analysis and Signal Separation. He is a Senior Member of the IEEE.

REFERENCES

- [1] B. Afsari, "Simple LU and QR based non-orthogonal matrix joint diagonalization," in *Proc. 6th Int. Conf. Independent Component Analysis and Blind Source Separation*, ICA 2006, LNCS 3889, Charleston, J. P. Rosca, D. Erdogmus, J. C. Principe, and S. Haykin, Eds. Springer Verlag: Berlin, Heidelberg, 2006, pp. 17–24.
- [2] B. Afsari, "Sensitivity analysis for the problem of matrix joint diagonalization," *SIAM J. Matrix Anal. Applicat.*, vol. 30, no. 3, pp. 1148–1171, 2008.
- [3] A. Aïssa-El-Bey, K. Abed-Meraim, Y. Grenier, and Y. Hua, "A general framework for second-order blind separation of stationary colored sources," *Signal Process.*, vol. 88, no. 9, pp. 2123–2137, Sept. 2008.

- [4] J. Antoni and S. Chauhan, "A study and extension of second-order blind source separation to operational modal analysis," *J. Sound Vib.*, vol. 332, no. 4, pp. 1079–1106, Feb. 2013.
- [5] A. Belouchrani, K. Abed-Meraim, J.-F. Cardoso, and E. Moulines, "A blind source separation technique using second-order statistics," *IEEE Trans. Signal Processing*, vol. 45, no. 2, pp. 434–444, Feb. 1997.
- [6] A. Belouchrani, K. Abed-Meraim, M. G. Amin, and A. M. Zoubir, "Blind separation of non-stationary sources," *IEEE Signal Processing Lett.*, vol. 11, no. 7, pp. 605–608, July 2004.
- [7] H. Bousbia-Salah, A. Belouchrani, and K. Abed-Meraim, "Jacobi-like algorithm for blind signal separation of convolutive mixtures," *IEE Electron. Lett.*, vol. 37, no. 16, pp. 1049–1050, Aug. 2001.
- [8] J.-F. Cardoso and A. Souloumiac, "Blind beamforming for non-Gaussian signals," *IEE Proc. Radar and Signal Processing F*, vol. 140, no. 6, pp. 362–370, Dec. 1993.
- [9] J. D. Carroll, "Generalization of canonical correlation analysis to three or more sets of variables," in *Proc. 76th Annu. Conf. American Psychological Association*, vol. 3, pp. 227–228, 1968.
- [10] J. D. Carroll and J.-J. Chang, "Analysis of individual differences in multidimensional scaling via an N-way generalization of Eckart-Young decomposition," *Psychometrika*, vol. 35, no. 3, pp. 283–319, Sept. 1970.
- [11] G. Chabriel, J. Barrère, N. Thirion-Moreau, and E. Moreau, "Algebraic joint zero-diagonalization and blind sources separation," *IEEE Trans. Signal Processing*, vol. 56, no. 3, pp. 980–989, Mar. 2008.
- [12] G. Chabriel and J. Barrère, "Non-symmetrical joint zero-diagonalization and MIMO zero division multiple access," *IEEE Trans. Signal Processing*, vol. 59, no. 5, pp. 2296–2307, May 2011.
- [13] G. Chabriel and J. Barrère, "A direct algorithm for nonorthogonal approximate joint diagonalization," *IEEE Trans. Signal Processing*, vol. 60, no. 1, pp. 39–47, Jan. 2012.
- [14] G. Chabriel and J. Barrère, "An instantaneous formulation of mixtures for blind separation of propagating waves," *IEEE Trans. Signal Processing*, vol. 54, no. 1, pp. 49–58, 2006.
- [15] P. Comon, "Independent component analysis, a new concept?," *Signal Process.*, vol. 36, no. 3, pp. 287–314, 1994.
- [16] L. De Lathauwer and J. Castaing, "Blind identification of underdetermined mixtures by simultaneous matrix diagonalization," *IEEE Trans. Signal Processing*, vol. 56, no. 3, pp. 1096–1105, 2008.
- [17] L. De Lathauwer, "A link between the canonical decomposition in multilinear algebra and simultaneous matrix diagonalization," *SIAM J. Matrix Anal. Appl.*, vol. 28, no. 3, pp. 642–666, July 2006.
- [18] L. De Lathauwer, B. De Moor, and J. Vandewalle, "Computation of the canonical decomposition by means of a simultaneous generalized Schur decompositions," *SIAM J. Matrix Anal. Appl.*, vol. 26, no. 2, pp. 295–327, 2004.
- [19] S. Dégerine and E. Kane, "A comparative study of approximate joint diagonalization algorithms for blind source separation in presence of additive noise," *IEEE Trans. Signal Processing*, vol. 55, no. 6 (part 2), pp. 3022–3031, 2007.
- [20] J. Eriksson and V. Koivunen, "Complex random vectors and ICA models: Identifiability, uniqueness, and separability," *IEEE Trans. Inform. Theory*, vol. 52, no. 3, pp. 1017–1029, 2006.
- [21] E.-M. Fadaïli, N. Thirion-Moreau, and E. Moreau, "Non-orthogonal joint diagonalization/zero-diagonalization for source separation based on time-frequency distributions," *IEEE Trans. Signal Processing*, vol. 55, no. 5, pp. 1673–1687, May 2007.
- [22] R. A. Harshman, "Foundations of the PARAFAC procedure: Model and conditions for an "explanatory" multimode factor analysis," *UCLA Working Papers Phonet.*, vol. 16, pp. 1–84, 1970.
- [23] R. A. Horn and C. R. Johnson, *Matrix Analysis*. Cambridge, U.K.: Cambridge Univ. Press, 1985.
- [24] R. Iferroudjene, K. Abed-Meraim, and A. Belouchrani, "Joint diagonalization of non defective matrices using generalized Jacobi rotations," in *Proc. 10th Int. Conf. Information Science, Signal Processing and Their Applications (ISSPA 2010)*, pp. 345–348.
- [25] M. Kleinstueber and H. Shen, "Uniqueness analysis of non-unitary matrix joint diagonalization," *IEEE Trans. Signal Processing*, vol. 61, no. 7, pp. 1786–1796, Apr. 2013.
- [26] Z. Koldovsky and P. Tichavsky, "Time-domain blind separation of audio sources based on a complete ICA decomposition of an observation space," *IEEE Trans. Audio, Speech Lang. Processing*, vol. 19, no. 2, pp. 406–416, 2011.
- [27] D. Lahat, J. Cardoso, and H. Messer, "Second-order multidimensional ICA: Performance analysis," *IEEE Trans. Signal Processing*, vol. 60, no. 9, pp. 4598–4610, 2012.
- [28] X.-L. Li and X. D. Zhang, "Nonorthogonal joint diagonalization free of degenerate solutions," *IEEE Trans. Signal Processing*, vol. 55, no. 5, pp. 1803–1814, May 2007.
- [29] E. Moreau, "A generalization of joint-diagonalization criteria for source separation," *IEEE Trans. Signal Processing*, vol. 49, no. 3, pp. 530–541, Mar. 2001.
- [30] E. Moreau and N. Thirion-Moreau, "Non symmetrical contrasts for sources separation," *IEEE Trans. Signal Processing*, vol. 47, no. 8, pp. 2241–2252, Aug. 1999.
- [31] D. Nion, "A tensor framework for nonunitary joint block diagonalization," *IEEE Trans. Signal Processing*, vol. 59, no. 10, pp. 4585–4594, 2011.
- [32] E. Ollila and V. Koivunen, "Complex ICA using generalized uncorrelating transform," *Signal Process.*, vol. 89, no. 4, pp. 365–377, 2009.
- [33] L. Parra and P. Sajda, "Blind source separation via generalized eigenvalue decomposition," *J. Mach. Learn. Res.*, vol. 4, nos. 7–8, pp. 1261–1269, 2008.
- [34] D.-T. Pham and Ph. Garat, "Blind separation of mixtures of independent sources through a quasi maximum likelihood approach," *IEEE Trans. Signal Processing*, vol. 45, no. 7, pp. 1712–1725, July 1997.
- [35] D.-T. Pham, "Joint approximate diagonalization of positive definite Hermitian matrices," *SIAM J. Matrix Anal. Appl.*, vol. 22, no. 4, pp. 1136–1152, 2001.
- [36] A. H. Phan, P. Tichavsky, and A. Cichocki, "Low complexity damped Gauss-Newton algorithms for parallel factor analysis," *SIAM J. Linear Algebra Appl.*, vol. 34, no. 1, pp. 126–147, Jan. 2013.
- [37] F. Roemer and M. Haardt, "A semi-algebraic framework for approximate CP decomposition via simultaneous matrix diagonalization (SECSI)," *Signal Process.*, vol. 93, no. 9, pp. 2722–2738, Sept. 2013.
- [38] H. Shen and M. Kleinstueber, "Non-unitary matrix joint diagonalization for complex independent vector analysis," *EURASIP J. Adv. Signal Process.*, vol. 241, pp. 1–10, Nov. 2012.
- [39] H. Shen and M. Kleinstueber, "Complex blind source separation via simultaneous strong uncorrelating transform," in *Proc. 9th Int. Conf. Latent Variable Analysis and Signal Separation*, vol. 6365. Berlin/Heidelberg: Springer-Verlag, 2010, pp. 287–294.
- [40] A. Souloumiac, "Nonorthogonal joint diagonalization by combining givens and hyperbolic rotations," *IEEE Trans. Signal Processing*, vol. 57, no. 6, pp. 2222–2231, 2009.
- [41] F. J. Theis, "A new concept for separability problems in blind source separation," *Neural Computat.*, vol. 16, no. 9, pp. 1827–1850, 2004.
- [42] P. Tichavsky, E. Doron, A. Yeredor, and J. Nielsen, "A computationally affordable implementation of an asymptotically optimal BSS algorithm for AR sources," in *Proc. EUSIPCO 2006*, Florence, Italy, Sept. 2006, pp. 1–5.
- [43] P. Tichavsky and A. Yeredor, "Fast approximate joint diagonalization incorporating weight matrices," *IEEE Trans. Signal Processing*, vol. 57, no. 3, pp. 878–891, Mar. 2009.
- [44] P. Tichavsky and Z. Koldovsky, "Algorithms for nonorthogonal approximate joint block-diagonalization," in *Proc. 20th European Signal Processing Conf. (EUSIPCO)*, Bucharest, Romania, Aug. 27–31, 2012, pp. 2094–2098.
- [45] P. Tichavsky, and Z. Koldovsky, "Weight adjusted tensor method for blind separation of underdetermined mixtures of nonstationary sources," *IEEE Trans. Signal Processing*, vol. 59, no. 3, pp. 1037–1047, Mar. 2011.
- [46] L. Tong, V. C. Soon, Y. Huang, and R. Liu, "AMUSE: A new blind identification algorithm," in *Proc. IEEE Int. Symp. Circuits and Systems (ISCAS)*, New Orleans, LA, 1990, vol. 3, pp. 1784–1787.
- [47] T. Trainini, X.-L. Li, E. Moreau, and T. Adali, "A relative gradient algorithm for joint decompositions of complex matrices," in *Proc. 18th European Signal Processing Conf.*, 2010, pp. 1073–1076.
- [48] R. Vollgraf and K. Obermayer, "Quadratic optimization for simultaneous matrix diagonalization," *IEEE Trans. Signal Processing*, vol. 54, no. 9, pp. 3270–3278, Sept. 2006.
- [49] A. Yeredor, "On using exact joint-diagonalization for non-iterative approximate joint-diagonalization," *IEEE Signal Processing Lett.*, vol. 12, no. 9, pp. 645–648, Sept. 2005.
- [50] A. Yeredor, "Non-orthogonal joint diagonalization in the least square sense with application in blind source separation," *IEEE Trans. Signal Processing*, vol. 50, no. 7, pp. 1545–1553, July 2002.
- [51] A. Yeredor, "Blind separation of Gaussian sources with general covariance structures: Bounds and optimal estimation," *IEEE Trans. Signal Processing*, vol. 58, no. 10, pp. 5057–5068, Oct. 2010.
- [52] A. Yeredor, "Performance analysis of the strong uncorrelating transformation in blind separation of complex-valued sources," *IEEE Trans. Signal Processing*, vol. 60, no. 1, pp. 478–483, Jan. 2012.
- [53] A. Yeredor, "Multiple-snapshots BSS with general covariance structures: A partial maximum likelihood approach involving weighted joint diagonalization," *Signal Process.*, vol. 92, no. 8, pp. 1832–1843, Aug. 2012.
- [54] A. Belouchrani, M. G. Amin, and K. Abed-Meraim, "Direction finding in correlated noise fields based on joint block-diagonalization of spatio-temporal correlation matrices," *IEEE Signal Processing Lett.*, vol. 4, no. 9, pp. 266–268, Sept. 1997.
- [55] A. Ziehe, P. Laskov, G. Nolte, and K.-R. Müller, "A fast algorithm for joint diagonalization with non-orthogonal transformations and its application to blind source separation," *J. Mach. Learn. Res.*, vol. 5, pp. 777–800, July 2004.

[Pierre Comon]

Tensors

[A brief introduction]

Tensor decompositions are at the core of many blind source separation (BSS) algorithms, either explicitly or implicitly. In particular, the canonical polyadic (CP) tensor decomposition plays a central role in the identification of underdetermined mixtures. Despite some similarities, CP and singular value decomposition (SVD) are quite different. More generally, tensors and matrices enjoy different properties, as pointed out in this brief introduction.

MOTIVATION

Originally, BSS exploited mutual statistical independence between sources [20]. Among possible approaches based on the sole hypothesis of source statistical independence, several use cumulants. In fact, when random variables are independent, their cumulant tensor is diagonal [57]. When the source mixture is linear, the decomposition of the data cumulant tensor into a sum of outer products yields the columns of the mixing matrix. This is the first instance of tensor decomposition applied to BSS, even if it is not always explicit. In that case, the tensor is actually symmetric. In the presence of noise, the extraction of sources themselves needs another procedure, based for instance on a spatial matched filter (SMF) [20].

BSS has then been addressed later in different manners. A quite interesting class of approaches consists of exploiting an additional diversity [74]. More precisely, measurements are usually made in two dimensions, generally space and time. But if they are made as a function of three (or more) dimensions, e.g., frequency, polarization, and time repetition, the data are stored in a multiway array. By treating this array as a matrix, information

is lost. Yet, in some real-world applications, it is meaningful to assume a multilinear model for this multiway array, which justifies considering it as a tensor. The decomposition of the latter into a sum of outer products yields not only the columns of the mixture, but also an estimate of the sources. So contrary to the first generation of BSS algorithms, there is no need to resort to an extracting filter. In addition, no statistics are to be estimated, so that the performance is expected to be better for short samples or correlated sources.

Beside numerous books dedicated to applications in physics, there already exist some surveys that can be used in the signal processing field. To begin, some background is presented in [46], i.e., basic engineering tools and a good panel of applications; a more signal processing-oriented tensor overview may be found in [16].

A quite complete digest, more theoretical and oriented toward algebraic geometry, can be found in [49]. This article aims at motivating the signal processing community to dive into the promising world of tensors.

Source Separation and Applications

IMAGE LICENSED BY
INGRAM PUBLISHING

THE WORLD OF TENSORS

Tensors were introduced at the end of the 19th century with the development of the differential calculus. They have then been omnipresent in physics, to express laws independently of coordinate systems. Yet, a tensor is essentially a mapping from a linear space to another, whose coordinates transform multilinearly under a change of bases, as subsequently detailed. For an easier reading, we shall resort to arrays of coordinates, when this indeed eases presentation; interested readers may want to refer to [23] and [49] for a more advanced coordinate-free presentation.

LINEARITY

Linearity expresses the property of a map μ defined on a vector space \mathcal{S} onto another vector space \mathcal{S}' built on the same field \mathbb{K} .

Digital Object Identifier 10.1109/MSP.2014.2298533

Date of publication: 7 April 2014

that: $\mu(\alpha x + \beta y) = \alpha\mu(x) + \beta\mu(y)$, $\forall x, y \in \mathcal{S}, \alpha, \beta \in \mathbb{K}$. (As far as we are concerned, \mathbb{K} will be either the field of real numbers \mathbb{R} or complex numbers \mathbb{C} .) If \mathcal{S} and \mathcal{S}' are of finite dimension, then this map can be represented by a matrix of coordinates, once the bases of \mathcal{S} and \mathcal{S}' have been fixed. We see that every linear map can be associated with a matrix, say A , so that $\mu(x) = Ax$. On the other hand, every matrix does not uniquely define a map. In fact, a matrix A could, e.g., define a bilinear form from $\mathcal{S} \times \mathcal{S}'$ onto \mathbb{K} , i.e., $f(x_1, x_2) = x_1^T Ax_2$. Hence, the correspondence between maps and arrays of coordinates is not one to one.

BILINEARITY

Let's start with a simple example.

EXAMPLE 1

Consider two multidimensional zero-mean random variables \mathbf{z}_1 and \mathbf{z}_2 , and denote the cross-covariance matrix by $\mathcal{G} = \mathbb{E}\{\mathbf{z}_1, \mathbf{z}_2^T\}$. We see that the covariance is linear with respect to \mathbf{z}_1 and \mathbf{z}_2 , which is referred to as *bilinearity*. Now suppose that \mathbf{z}_1 and \mathbf{z}_2 represent two phenomena that are measured in a given coordinate system. \mathcal{G} gives an indication of their correlation. If we change the coordinate system, the covariance matrix changes. More precisely, if $\mathbf{z}'_1 = A\mathbf{z}_1$ and $\mathbf{z}'_2 = B\mathbf{z}_2$, then $\mathcal{G}' = \mathbb{E}\{\mathbf{z}'_1, \mathbf{z}'_2^T\}$ can be written $\mathcal{G}' = A\mathcal{G}B^T$. We see that $\mathcal{G}' \neq \mathcal{G}$, whereas the phenomena remain the same. So we must distinguish between the physical phenomena that are coordinate free, and the arrays of measurements we made. And because of bilinearity, we know how to go from one matrix representation to another. We may say that the covariance object is a tensor of order 2, and can be represented by a matrix in any given coordinate system.

What we just saw in Example 1 can be put in more formal terms. Now assume a linear change of coordinates is made in spaces \mathcal{S} and \mathcal{S}' defined by matrices $\{A, B\}$ so that the new coordinates express as $x'_1 = Ax_1$ and $x'_2 = Bx_2$. A tensor \mathcal{G} represented in the original basis with an array \mathcal{G} will be represented (as in Example 1) in the new basis by the new array \mathcal{G}' whose coordinates are:

$$G'_{ij} = \sum_{p,q} A_{ip} B_{jq} G_{pq}$$

This can be compactly denoted by $\mathcal{G}' = (A, B) \cdot \mathcal{G}$. Another notation, equally acceptable, is sometimes used: $\mathcal{G}' = [\mathcal{G}; A, B]$. This will now be extended to orders higher than 2.

MULTILINEARITY

Now assume \mathcal{S}_d are D vector spaces, $1 \leq d \leq D$, and suppose f is a map from $\mathcal{S}_1 \times \dots \times \mathcal{S}_D$ onto \mathbb{K} . Map f is said to be multilinear if $f(x_1, \dots, x_d)$ is linear with respect to every variable x_d , $1 \leq d \leq D$. In other words, $f(x_1, \dots, \alpha x_d + \beta y_d, \dots, x_D) = \alpha f(x_1, \dots, x_d, \dots, x_D) + \beta f(x_1, \dots, y_d, \dots, x_D)$, $\forall d, \forall \alpha, \beta \in \mathbb{K}$. This map is actually a multilinear form. As in the previous section, map f can be represented by an array of coordinates, once the bases of \mathcal{S}_d have been fixed, $1 \leq d \leq D$, and this array needs D indices.

TENSORS

For the sake of simplicity, let us focus on $D = 3$, which is sufficient to give us an idea. Because of multilinearity, special properties are satisfied. For instance, $f(\alpha x_1, x_2, x_3) = f(x_1, x_2, \alpha x_3)$, so that the two triplets of vectors $(\alpha x_1, x_2, x_3)$ and $(x_1, x_2, \alpha x_3)$ have the same image. When dealing with multilinear forms, it is then relevant to consider the equivalence classes defined by the relation $(x, y, z) \sim (x', y', z')$ if there exist $\alpha, \beta, \gamma \in \mathbb{K}$ such that $(x', y', z') = (\alpha x, \beta y, \gamma z)$, with $\alpha\beta\gamma = 1$. Each class may be regarded as a decomposable tensor (decomposable tensors are also called *pure* or *simple*). The space spanned by these classes is denoted as $\mathcal{S}_1 \otimes \mathcal{S}_2 \otimes \mathcal{S}_3$, where \otimes is called the *tensor product*. An element of this space is called a *tensor of order 3*. (In physics, the word *rank* is also sometimes used, but we shall avoid it because of the possible confusion with the more standard meaning related to *rank* of a linear operator.) In more mathematical words, one would say that $\mathcal{S}_1 \otimes \mathcal{S}_2 \otimes \mathcal{S}_3$ is the quotient space $\mathcal{S}_1 \times \mathcal{S}_2 \times \mathcal{S}_3 / \sim$.

EXAMPLE 2

Let $\mathbf{x}_1 \in \mathcal{S}_1$, $\mathbf{x}_2 \in \mathcal{S}_2$, and $\mathbf{x}_3 \in \mathcal{S}_3$. Tensors $6\mathbf{x}_1 \otimes \mathbf{x}_2 \otimes \mathbf{x}_3$ and $\mathbf{x}_1 \otimes 2\mathbf{x}_2 \otimes 3\mathbf{x}_3$ are the same, but in $\mathcal{S}_1 \times \mathcal{S}_2 \times \mathcal{S}_3$, vectors $(6\mathbf{x}_1, \mathbf{x}_2, \mathbf{x}_3)$ and $(\mathbf{x}_1, 2\mathbf{x}_2, 3\mathbf{x}_3)$ are different.

If a linear change of basis is made in space \mathcal{S}_1 (respectively, \mathcal{S}_2 and \mathcal{S}_3), as $x' = Ax$ (resp. $y' = By$ and $z' = Cz$), then the array \mathcal{T} defining multilinear form f in the new coordinate system expresses as a function of \mathcal{T} . For so-called contravariant tensors, the relationship is

$$T'_{ijk} = \sum_{pqr} A_{ip} B_{jq} C_{kr} T_{pqr} \tag{1}$$

as in Example 1, or in compact form: $\mathcal{T}' = (A, B, C) \cdot \mathcal{T}$. On the other hand, there also exist covariant tensors for which the inverses of the above matrices are instead involved (cf. Example 4), and even mixed tensors that are partly covariant and partly contravariant [23], [71]. However, we shall concentrate only on contravariant tensors in this article, which follow (1) under a multilinear transformation. Note that (1) holds true for contravariant tensors even if the linear transforms (A, B, C) are not invertible; they can even be rectangular matrices. This property is crucial in BSS when mixtures are underdetermined [20], [83].

EXAMPLE 3

Consider three multidimensional random variables \mathbf{x} , \mathbf{y} , and \mathbf{z} . Then the third-order moment tensor \mathcal{M} is represented by the third-order array $M_{ijk} = \mathbb{E}\{x_i y_j z_k\}$. As in the case of second-order moments, it is a contravariant tensor. In fact, if $\mathbf{x}' = A\mathbf{x}$, $\mathbf{y}' = B\mathbf{y}$, and $\mathbf{z}' = C\mathbf{z}$, then $\mathcal{M}' = (A, B, C) \cdot \mathcal{M}$ as in (1). It turns out that cumulants may also be seen as tensors as pointed out in [57]. Because cross-cumulants of independent random variables are null at any order, they have been extensively used in BSS. For instance, the cumulant tensor of order 2 is nothing else but the covariance matrix, and accounts for the correlation at order 2 only; it is not sufficient to account for statistical independence unless variables are Gaussian.

EXAMPLE 4

The derivatives of order D of a multivariate scalar function can be stored in a covariant tensor of order D . For instance at order 2, if $A_{ij} = \partial^2 f / \partial x_i \partial x_j$, $\mathbf{x}' = \mathbf{M}\mathbf{x}$, and $A'_{pq} = \partial^2 f / \partial x'_p \partial x'_q$, then $\mathbf{A}' = \mathbf{N}^T \mathbf{A} \mathbf{N}$, with $\mathbf{N} = \mathbf{M}^{-1}$. From now on and for the sake of simplicity, we shall only consider contravariant tensors in this article.

More generally, a tensor of order D is an element of $\mathcal{S}_1 \otimes \dots \otimes \mathcal{S}_D$, and can be represented by a D -way array \mathcal{T} once bases of spaces \mathcal{S}_d have been fixed. Under multilinear transforms, these arrays of coordinates change similarly to (1).

EXAMPLE 5

In physics, Hooke's law relates the deformation (strain) of a solid under the action of forces (stress). It states that stress \mathcal{F} is related to strain \mathcal{X} by the elasticity tensor as: $\mathcal{F} = \mathcal{C} \bullet \mathcal{X}$, where \bullet is a contraction operator (see the section "Transformations" for a formal definition). Once bases are fixed in the stress and strain spaces, this relationship can be written in terms of arrays of coordinates

$$F_{ij} = \sum_{p,q} C_{ijpq} X_{pq}.$$

The elasticity tensor \mathcal{C} is of order 4. Strain and stress are tensors of order 2, which are represented by matrices.

As illustrated above, it should be kept in mind that an array of coordinates alone does not suffice to define a tensor: spaces and bases need to be defined. Since we are interested mainly in manipulating arrays, and not so much in the map they may represent, arrays will be subsequently associated with multilinear forms, i.e., maps from a product of spaces to their construction field \mathbb{K} . Even if most results can be stated without introducing arrays of coordinates [49], bases are required in engineering applications because calculations are made with arrays of numbers.

NOTATION

In the literature, indices of D -way arrays are sometimes put in superscripts or in subscripts, depending on the covariant or contravariant character of corresponding subspaces; this notation also allows the use the Einstein summation convention. Because we consider essentially fully contravariant tensors in this article, we do not need to make the distinction.

Throughout the article, arrays of numbers will be printed in boldface. More precisely, one- and two-way arrays will be denoted in bold lowercase and bold uppercase, respectively, like, e.g., \mathbf{v} and \mathbf{M} . Arrays with more than two indices will be denoted by bold calligraphic symbols, as \mathcal{A} . Sets and spaces will be noted in script font, like \mathcal{S} , whereas tensors will be printed in calligraphic font, as \mathcal{A} . Entries of arrays \mathbf{v} , \mathbf{M} , and \mathcal{A} will be noted v_i , M_{ij} , and $A_{i,j,k}$, without bold font because they are scalar numbers. In practice, a tensor \mathcal{A} is often assimilated to its array representation \mathcal{A} [16], [21], [46], which is generally not very confusing. Nevertheless, we shall make the distinction in the sequel, to keep the presentation as clear as possible.

TRANSFORMATIONS

The tensor product $\mathcal{A} \otimes \mathcal{B}$ between two tensors $\mathcal{A} \in \mathcal{S}_1 \otimes \mathcal{S}_2$ and $\mathcal{B} \in \mathcal{S}_3 \otimes \mathcal{S}_4$ is a tensor of $\mathcal{S}_1 \otimes \mathcal{S}_2 \otimes \mathcal{S}_3 \otimes \mathcal{S}_4$. The consequence is that the orders add up under tensor product.

EXAMPLE 6

Let \mathcal{A} be represented by a three-way array $\mathcal{A} = [A_{ijk}]$ and \mathcal{B} by a four-way array $\mathcal{B} = [B_{lmnp}]$; then tensor $\mathcal{C} = \mathcal{A} \otimes \mathcal{B}$ is represented by the seven-way array of components $C_{ijklmnp} = A_{ijk} B_{lmnp}$. With some abuse of notation, the tensor product is often applied to arrays of coordinates, so that notation $\mathcal{C} = \mathcal{A} \otimes \mathcal{B}$ may be encountered.

If the tensor product increases the order, the contraction decreases it by two. The contraction consists of a summation over a pair of indices. This operation permits to define the mode- k product between tensors, and can be denoted by \bullet_k , where k indicates which index should be summed.

EXAMPLE 7

If \mathcal{A} and \mathcal{A}' are tensors of order D and D' , the tensor $\mathcal{B} = \mathcal{A} \bullet_k \mathcal{A}'$ is a tensor of order $D + D' - 2$ obtained by summing over the k th index. For instance, if $(D, D', k) = (3, 3, 2)$, this yields $B_{ijpq} = \sum_{\ell} A_{ij\ell} A'_{\ell pq}$. For $(D, D', k) = (2, 2, 1)$, we would have the matrix product $\mathcal{A} \bullet_1 \mathcal{A}' = \mathbf{A}^T \mathbf{A}'$. However, when the product is between a matrix and a tensor of higher order, it has been the usual practice to always sum over the second matrix index. For instance, if \mathbf{M} is a matrix, $\mathcal{A} \bullet_3 \mathbf{M}$ means that the sum is performed on the third tensor index and the second matrix index.

It may be convenient to store D -way arrays in matrices. This transformation is called matrix *unfolding* or *flattening*, and can be performed in different manners, depending on the arbitrarily chosen ordering [27], [46]. Here, the ordering of [46] has been retained, but the choice of [27] would work equally well. In fact, the exact definition is not so important, provided the inverse map is defined consistently. We shall limit ourselves to matrices whose number of rows equals one of the tensor dimensions; this is sometimes referred to as *mode- n unfolding* [46]. Example 8 illustrates how to relate a third-order tensor to its three flattening matrices. But it is also possible to associate a D -way array, $D > 3$, to a multilinear operator of lower order; see, e.g., [9], [29], [64], and [69].

EXAMPLE 8

Let a $2 \times 2 \times 2$ array of coordinates A_{ijk} . Its mode- n unfoldings $\mathbf{A}^{(n)}$ are

$$\begin{aligned} \mathbf{A}^{(1)} &= \begin{bmatrix} A_{111} & A_{121} & A_{112} & A_{122} \\ A_{211} & A_{221} & A_{212} & A_{222} \end{bmatrix} \\ \mathbf{A}^{(2)} &= \begin{bmatrix} A_{111} & A_{211} & A_{112} & A_{212} \\ A_{121} & A_{221} & A_{122} & A_{222} \end{bmatrix} \\ \mathbf{A}^{(3)} &= \begin{bmatrix} A_{111} & A_{211} & A_{121} & A_{221} \\ A_{112} & A_{212} & A_{122} & A_{222} \end{bmatrix}. \end{aligned}$$

Remark that the row number of matrix $\mathbf{A}^{(n)}$ corresponds to the n th index of tensor \mathcal{A} .

The Kronecker product between two matrices \mathbf{A} and \mathbf{B} of size $I \times J$ and $K \times L$, respectively, is the matrix $\mathbf{A} \boxtimes \mathbf{B}$ of size $IK \times JL$ defined blockwise by

$$\mathbf{A} \boxtimes \mathbf{B} = \begin{bmatrix} A_{11}\mathbf{B} & \dots & A_{1J}\mathbf{B} \\ \vdots & & \vdots \\ A_{I1}\mathbf{B} & \dots & A_{IJ}\mathbf{B} \end{bmatrix}.$$

The Kronecker product is used to represent the tensor product when bases are fixed and when tensors are represented by their array of coordinates unfolded into matrices. It should be borne in mind that the Kronecker product usually applies to matrices (although an extended definition has recently been proposed in [63]), whereas the tensor product is more general and coordinate free. Hence they should not be confused.

SPECIAL TENSORS

A particularly important class of tensors is that of *decomposable* tensors, which are tensor products of vectors. As previously stated in the section “Tensors,” they are of the form $\mathcal{D} = \mathbf{u} \otimes \mathbf{v} \otimes \dots \otimes \mathbf{w}$, and span the whole tensor space. The corresponding array of coordinates is $D_{ij..k} = u_i v_j \dots w_k$. One can view these tensors as a discretization of a multivariate function whose variables separate.

EXAMPLE 9

Take a function of two variables with separated variables: $f(x, y) = u(x)v(y)$. Then its discretization takes the form $f(x_i, y_j) = u(x_i)v(y_j)$, and these numbers can be stored in a rank-1 matrix $\mathbf{D} = \mathbf{u}\mathbf{v}^T$.

A tensor is cubical if all its spaces of construction are identical, with the same basis. (The term *homogeneous* is also used in physics.) A cubical tensor \mathcal{A} is symmetric if its array of coordinates is invariant under permutation of its indices: $A_{\sigma(ij..k)} = A_{ij..k}, \forall \sigma$.

EXAMPLE 10

The tensor of moments and the tensor of derivatives, defined in Examples 1, 3, and 4, are symmetric.

The simplest symmetric array is the diagonal one, defined by $\Delta_{ij..k} = 0$ if $(i, j, \dots, k) \neq (i, i, \dots, i)$.

DECOMPOSITIONS AND RANKS

TENSOR RANK

Any tensor \mathcal{T} can be decomposed (nonuniquely) into a linear combination (with coefficients in \mathbb{K}) of decomposable tensors

$$\mathcal{T} = \sum_{r=1}^R \lambda_r \mathcal{D}(r), \tag{2}$$

$\mathcal{D}(r) = \mathbf{a}_r \otimes \mathbf{b}_r \otimes \dots \otimes \mathbf{c}_r$. If tensor spaces are endowed with scalar products, one can impose decomposable tensors $\mathcal{D}(r)$ to be built with unit norm vectors, which permits us to impose $\lambda_r \in \mathbb{R}^+$ if desired. The smallest value R for which (2) holds is called the *tensor rank*. The definition of tensor rank can be traced back to the beginning of the 20th century [38], but it has

been reintroduced in other disciplines under various names [7], [12], [36], [39], [66], [82].

EXAMPLE 11

Let the arrays \mathcal{A} and \mathcal{B} of dimensions $2 \times 2 \times 2$ be defined by their mode-1 unfoldings

$$\mathbf{A}^{(1)} = \begin{bmatrix} 1 & 0 & 1 & 0 \\ 0 & 0 & 0 & 0 \end{bmatrix}$$

$$\mathbf{B}^{(1)} = \begin{bmatrix} 0 & 1 & 1 & 0 \\ 1 & 0 & 0 & 0 \end{bmatrix}$$

Tensor $\mathcal{A} = [1, 0] \otimes [1, 0] \otimes [1, 1]$ has rank 1. Tensor \mathcal{B} is symmetric and has rank 3, as will be seen with \mathcal{T}_0 in Example 18.

Note that, by definition, a tensor is decomposable if and only if it has rank 1. If the order of a tensor \mathcal{T} is ≥ 3 , the rank may depend on the field, in the sense that a real tensor of rank R may have smaller rank if we allow the decomposition (2) to be complex, as demonstrated in Example 12.

EXAMPLE 12

Take a real symmetric array \mathcal{Y} of dimensions $2 \times 2 \times 2$, defined by its mode-1 unfolding

$$\mathbf{Y}^{(1)} = \begin{bmatrix} 2 & 0 & 0 & -2 \\ 0 & -2 & -2 & 0 \end{bmatrix}.$$

Then, we need three decomposable tensors in \mathbb{R} :

$$\mathcal{Y} = 4 \begin{bmatrix} 1 \\ 0 \end{bmatrix}^{\otimes 3} + \begin{bmatrix} -1 \\ -1 \end{bmatrix}^{\otimes 3} + \begin{bmatrix} -1 \\ 1 \end{bmatrix}^{\otimes 3}$$

but only two in \mathbb{C} , setting $j = \sqrt{-1}$:

$$\mathcal{Y} = \begin{bmatrix} 1 \\ j \end{bmatrix}^{\otimes 3} + \begin{bmatrix} 1 \\ -j \end{bmatrix}^{\otimes 3}.$$

Hence its tensor rank in \mathbb{R} is 3 whereas it is 2 in \mathbb{C} .

Other examples may be found in [18], [46], and [48]. Examples 11 and 12 incidentally show that, unlike matrix rank, tensor rank may exceed all dimensions.

TUCKER DECOMPOSITION

At this stage, it is interesting to make a connection with the matrix SVD. Two important features characterize the SVD of a matrix \mathbf{M} :

$$\mathbf{M} = \mathbf{U}\mathbf{\Sigma}\mathbf{V}^T, \tag{3}$$

specifically 1) \mathbf{U} and \mathbf{V} have orthonormal columns, and 2) $\mathbf{\Sigma}$ is diagonal. Consider the decomposition below of a three-way array, introduced by Tucker in the 1960s [85]:

$$\mathcal{T}_{ijk} = \sum_p \sum_q \sum_r A_{ip} B_{jq} C_{kr} G_{pqr}, \tag{4}$$

which we shall compactly denote $\mathcal{T} = (\mathbf{A}, \mathbf{B}, \mathbf{C}) \cdot \mathcal{G}$. It is clear that if the number of free parameters in the right-hand side of (4) is smaller than the number of equations, then there will generally be no solution. This happens to be the case if \mathbf{A} , \mathbf{B} , and \mathbf{C} are

orthonormal and \mathcal{G} is diagonal. In the quest for existence, we have to choose: either \mathcal{G} is diagonal, but we have to relax the orthogonality constraint on factor matrices, which will be allowed to have more columns than rows [this corresponds to decomposition (2)], or we keep the orthonormality constraint, but allow \mathcal{G} to have nonzero extra-diagonal entries as elaborated in the next section.

HOSVD AND MULTILINEAR RANKS

If we impose matrices $\{A, B, C\}$ to have orthogonal and unit-norm columns in the Tucker decomposition (4), then we can make several observations. First, denote by R_n the rank of $T^{(n)}$, the n th unfolding matrix of \mathcal{T} , $1 \leq n \leq D = 3$. Rank R_n is called *mode- n rank* of \mathcal{T} , or n -rank in short. Then the number of columns of A (respectively, B , C) does not need to exceed R_1 (respectively, R_2 , R_3), and the dimension of the core tensor may be imposed to be $R_1 \times R_2 \times R_3$. In addition R_n cannot exceed the tensor rank R defined in (2), nor the n th dimension. This property is not a surprise, if we view decomposition (2) as a decomposition of the n th unfolding matrix into a sum of rank-1 matrices where rows are imposed to have a special structure. The D -uple of n -ranks is the *multilinear rank* of \mathcal{T} . Another property is less immediate to capture: the core array \mathcal{G} can be imposed to be all-orthogonal, which means that all tensor slices of order $D - 1$ are orthogonal to each other in every mode; when $D = 3$ this means:

$$\sum_{j,k} G_{\alpha j k} G_{\beta j k} = \sum_{i,k} G_{i \alpha k} G_{i \beta k} = \sum_{i,j} G_{i j \alpha} G_{i j \beta} = 0$$

if $\alpha \neq \beta$. See [27] and references therein for more details. It is worth noticing the elementary fact that for tensors of order 2 (i.e., matrices), $R_1 = R_2 = R$, and all equal the matrix rank.

EXAMPLE 13

The multilinear rank of array \mathcal{B} defined in Example 11 is $(2, 2, 2)$, whereas that of \mathcal{A} is $(1, 1, 1)$.

CP DECOMPOSITION

On the contrary, if we keep a diagonal form for \mathcal{G} , we end up with the polyadic decomposition [38], also sometimes called CANDECOMP or PARAFAC because of its rediscovery in the 1970s:

$$\mathcal{T}_{ijk} = \sum_{r=1}^R A_{ir} B_{jr} C_{kr} \lambda_r \tag{5}$$

or, in compact form, $\mathcal{T} = (A, B, C) \cdot \mathcal{L}$, where \mathcal{L} is diagonal. If R is not too large, this decomposition can be unique (cf. the section “Exact Decompositions”) and deserves to be called *canonical polyadic* (CP). Following a practice now adopted in applied mathematics and engineering [5], [42], we shall subsequently use the acronym CP, which can also cleverly stand for CANDECOMP/PARAFAC. After inspection, it may be seen that (5) is nothing else but decomposition (2) in array coordinates. In other words, the CP decomposition reveals the tensor rank.

SYMMETRIC RANK

As already pointed out in the section “Special Tensors,” a tensor \mathcal{T} is symmetric if its coordinate array \mathcal{T} is invariant by permutations of indices. If we impose tensors $\mathcal{D}(r)$ in (2) to be themselves symmetric, then we might end up with a larger value of rank, denoted R_s , which is referred to as the *symmetric rank* of \mathcal{T} . It is clear that $R_s \geq R$ for any symmetric tensor \mathcal{T} , since any constraint on decomposable tensors may increase rank; we have already observed this fact with the real constraint in Example 12. It has been conjectured in [19] that rank and symmetric rank are always equal, but this has not yet been proved in the general case.

NONNEGATIVE RANK

When an array is real nonnegative, one may want to impose rank-1 terms in its CP decomposition to be themselves nonnegative. The minimal number of terms is then called the *nonnegative rank* and is generally strictly larger than the rank in \mathbb{R} . This is already the case for matrices ($D = 2$) as shown in Example 14, due to Herbert E. Robbins. The same phenomenon is observed for tensors, although theoretical results are still lacking.

EXAMPLE 14

The following matrix has rank 3 since vector $[1, -1, -1, 1]$ belongs to its kernel. But it can be proved that its nonnegative rank is four

$$\mathbf{M} = \begin{bmatrix} 1 & 1 & 0 & 0 \\ 1 & 0 & 1 & 0 \\ 0 & 1 & 0 & 1 \\ 0 & 0 & 1 & 1 \end{bmatrix}$$

STRUCTURED RANKS

More generally, when matrix factors are imposed to have a special structure, such as banded, van der Monde, Toeplitz, or Hankel, the tensor rank may increase, just as in the nonnegative case. Structure can also have an impact on computational issues [49], [78].

BORDER RANK

A tensor has border rank \underline{R} if it is the limit of tensors of rank R and not the limit of tensors of smaller rank. Rank and border rank always coincide for matrices, but not for tensors of order larger than two, as shown in the next example.

EXAMPLE 15

Let u and v be fixed real or complex numbers, and ϵ a small positive number. Then $(1/\epsilon)[(u + \epsilon v)^3 - u^3] = 3u^2 v + O(\epsilon)$. Now if multiplication is not commutative, we have three distinct terms on the right-hand side; this is what happens for the tensor product, so that $\forall \epsilon > 0$:

$$\mathcal{T}_\epsilon = \frac{1}{\epsilon}[(\mathbf{u} + \epsilon \mathbf{v})^{\otimes 3} - \mathbf{u}^{\otimes 3}] = \mathcal{T}_0 + O(\epsilon),$$

$$\mathcal{T}_0 = \mathbf{u} \otimes \mathbf{u} \otimes \mathbf{v} + \mathbf{u} \otimes \mathbf{v} \otimes \mathbf{u} + \mathbf{v} \otimes \mathbf{u} \otimes \mathbf{u}$$

hold for any vectors \mathbf{u} and \mathbf{v} . If the latter are not collinear, it can be proved that \mathcal{T}_0 is of rank $R = 3$, but is the limit of tensors \mathcal{T}_ϵ , which are all of rank 2. Hence the border rank of \mathcal{T}_0 is $\underline{R} = 2$.



[FIG1] Some contributors to the field of tensors.

The border rank has been defined and utilized by many authors, especially in arithmetic complexity [7], [52], [72], [82]. This concept is crucial in tensor approximation problems, as addressed in the section “Approximate Decompositions.”

RELATION WITH POLYNOMIALS

Homogeneous polynomials are bijectively related to tensors, which allows to transpose existing results of algebraic geometry; see, e.g., [10], [15], [17], [19], [23], [49], [80], and references therein. In fact, one can associate the following polynomial with any array \mathcal{T} :

$$p(x, y, \dots, z) = \sum_{i,j,\dots,k} T_{i,j,\dots,k} x_i y_j \dots z_k.$$

Conversely, any homogeneous polynomial of degree D and partial degree 1 in every variable can be associated with a (nonsymmetric) tensor \mathcal{T} .

Through this bijection, a decomposable tensor of order D is translated into a product of D linear forms, and the CP decomposition can be translated into a linear combination of such terms:

$$p(x, y, \dots, z) = \sum_{r=1}^R \lambda_r (a_r^\top x) (b_r^\top y) \dots (c_r^\top z). \tag{6}$$

In the case of symmetric tensors, $x = y = \dots = z$. More precisely, a symmetric tensor \mathcal{T} of order D can be identified with the homogeneous polynomial of degree D :

$$p(x) = \sum_{i,j,\dots,k} T_{i,j,\dots,k} x_i x_j \dots x_k$$

in the indeterminates x_1, \dots, x_n . It can be easily checked that symmetric tensors of rank 1 are associated with a polynomial of the form $a(x)^D$, where $a(x) = \mathbf{a}^\top x$ is a linear form. In other words, they are exactly the D th powers of a homogeneous linear form. The CP decomposition of \mathcal{T} reduces in this case to

$$p(x) = \sum_{i=1}^{R_s} a_i(x)^D, \tag{7}$$

which has been classically called a Waring decomposition [40]. The minimum number of summands R_s in a Waring decomposition is the symmetric rank of \mathcal{T} , which we defined earlier.

EXAMPLE 16

The polynomials associated with tensors \mathcal{A} and \mathcal{B} of Example 11 are, respectively, $a(x_1, x_2, y_1, y_2, z_1, z_2) = x_1 y_1 (z_1 + z_2)$ and $b(x_1, x_2) = 3x_1^2 x_2$.

EXAMPLE 17

Take the polynomial of degree $D = 3$:

$$2x_1^3 - 6x_1 x_2^2 = (x_1 + jx_2)^3 + (x_1 - jx_2)^3 = 4(x_1)^3 - (x_1 + x_2)^3 - (x_1 - x_2)^3,$$

where $j = \sqrt{-1}$. It has complex symmetric rank equal to two and real symmetric rank equal to three. This polynomial is actually associated with tensor \mathcal{Y} given in Example 12.

EXAMPLE 18

Example 15 can be written in terms of polynomials, and is even easier to understand this way. Take $\mathbf{u} = [1, 0]$ and $\mathbf{v} = [0, 1]$. Then $\mathbf{u}^{\otimes 3}$ and $\mathbf{v}^{\otimes 3}$ are associated with polynomials x_1^3 and x_2^3 respectively, whereas $(\mathbf{u} + \epsilon \mathbf{v})^{\otimes 3}$ is associated with $(x_1 + \epsilon x_2)^3$, which can be expanded as $x_1^3 + 3\epsilon x_1^2 x_2 + o(\epsilon)$. This shows that \mathcal{T}_ϵ is associated with $3x_1^2 x_2 + o(\epsilon)$. Hence \mathcal{T}_ϵ tends to \mathcal{T}_0 , because \mathcal{T}_0 is associated with $3x_1^2 x_2$. Moreover, the rank of \mathcal{T}_0 is three because $3x_1^2 x_2$ cannot be written as a sum of fewer than three cubes.

EXACT DECOMPOSITIONS

Now one can ask whether the CP decomposition defined in (2) and (5) is unique or not. First of all, the D -way array associated with a D th order decomposable tensor \mathcal{D} is not uniquely represented by an outer product of vectors: there remain $D - 1$ scaling factors of unit modulus. So we are rather interested in the uniqueness of coefficients $\lambda_r \in \mathbb{R}^+$ and tensors $\mathcal{D}(r)$, which is more meaningful; this is sometimes called *essential uniqueness*. In this section, we will see two ways of assessing uniqueness: almost surely or deterministically.

EXPECTED RANK

A naive approach is to count the number of degrees of freedom on both sides of (6), which is a rewriting of (2) in terms of polynomials, and say that the number of equations should be at least as large as the number of unknowns. To fix the ideas, take a tensor of order D and dimensions $n_1 \times \dots \times n_D$. It is clear that a necessary condition for uniqueness of the CP decomposition is that

$$R \left(\sum_{i=1}^D n_i - D + 1 \right) \leq N, \tag{8}$$

where $N = \prod_i n_i$. We can proceed similarly for symmetric tensors and count equations and unknowns in (7). This leads to

$$R_s n \leq N_s, \tag{9}$$

where $N_s = \binom{n+D-1}{D}$ corresponds to the number of free parameters in a symmetric tensor. Equations (8) and (9) induce an upper bound on rank, which is called the *expected rank*, and is defined as

$$R \leq R^o = \left\lfloor \frac{N}{1 - D + \sum_i n_i} \right\rfloor \tag{10}$$

$$R_s \leq R_s^o = \left\lfloor \frac{N_s}{n} \right\rfloor. \tag{11}$$

When the fraction above is not an integer, there will always be an infinity of solutions, because of too many free parameters.

When it is an integer, the number of unknowns is equal to the number of equations, and we could expect that there is a finite number of solutions. However, things are not so simple, as pointed out by Clebsch in the 19th century (Figure 1). In fact, there are exceptions [1], [3], [23], [58].

EXAMPLE 19

Consider fourth-order symmetric tensors of dimension three. In that case, $N_s/n = \binom{6}{4}/3 = 5$ is an integer. Our hope is not realized since five forms are generally not sufficient in their decomposition. This exception was first noticed by Clebsch (Figure 1) from the polynomial framework: the “generic rank” of ternary quartics is in fact six [33]. This means that most homogeneous polynomials of degree four in three variables in \mathbb{C} can be written as a sum of six linear forms raised to the fourth power, and not fewer with probability 1.

TYPICAL AND GENERIC RANKS

Generic (resp. typical) ranks are the ranks that we encounter with probability one (resp. nonzero probability), when their entries are drawn independently according to a continuous probability distribution, hence their importance. Contrary to the matrix case, they are not maximal; tables of rank values may be found in [24], as well as simple codes to compute numerically the generic rank of a large panel of tensors. (Codes can be downloaded from [94].)

A striking fact is that only one rank occurs with probability one (the so-called generic rank) in \mathbb{C} , whereas several typical ranks may exist in \mathbb{R} . The generic rank in \mathbb{C} is always equal to the smallest typical rank one would find in \mathbb{R} . This problem was first addressed by Sylvester (Figure 1) in the 19th century. The case of real symmetric tensors of dimension two is now well understood [13], [22], [67]. In fact, all the integers between $\lfloor (D+2)/(2) \rfloor$ and D have been shown to be typical ranks [8]. If the tensor rank is smaller than a bound depending on the generic rank [typically $R^o - 1$ as defined in (10) and (11)], there exist almost surely finitely many CP decompositions. See [23] for a survey of recent results on almost sure uniqueness.

UNIQUENESS RESULTS BASED ON LINEAR ALGEBRA

Instead of associating tensors with polynomials and making use of results borrowed from algebraic geometry, uniqueness conditions can be obtained by considering particular factor matrices. However, these conditions are generally only sufficient [41], and often much more restrictive. The most well known is that published by Kruskal [47] and extended later in [73] and [81]; alternate proofs have been derived in [49] and [68]. It requires the following definition: The Kruskal rank of a matrix is the largest number κ such that any subset of κ columns is full rank. By construction, Kruskal's rank cannot exceed matrix rank.

EXAMPLE 20

The matrix

$$\mathbf{A} = \begin{bmatrix} 1 & 0 & 0 & 0 \\ 0 & 1 & 1 & 0 \\ 0 & 1 & 0 & 1 \end{bmatrix}$$

has rank 3, but its Kruskal rank is $\kappa = 2$.

The CP decomposition is unique if the sufficient condition holds:

$$2R + D - 1 \leq \sum_{d=1}^D \kappa_d, \quad (12)$$

where κ_d denotes the Kruskal rank of the d th factor matrix in the CP decomposition. Further recent deterministic results may be found in [25], [31], and [32]. These results do not need algebraic geometry but advanced linear algebra (i.e., compound matrices formed of minors). They are sometimes much more powerful than Kruskal's bound.

EXACT COMPUTATION

Due to the space restrictions in this article, various existing algorithms will not be described. However, we provide below some guidance to related literature, among many others. In [6], algorithms to compute the symmetric rank of symmetric tensors of small border rank are proposed. When the rank is small, the symmetric CP decomposition can be computed with the help of Sylvester's algorithm [10]; when it is not unique, one CP decomposition can still be delivered. In [60], approaches based on special eigenvector computations are proposed. Direct computation is proposed in [4] for $2 \times n \times n$ arrays.

When one tensor dimension is large compared to its rank and to other dimensions, it is possible to compute the CP decomposition via a joint congruent diagonalization of its matrix slices; this has been first proposed in [50] for two matrix slices. In the presence of errors with more than two slices, such a diagonalization becomes approximate [25] and needs more care (see the next section). In a similar spirit, for low-rank tensors of order larger than three, one can also decrease the order by working jointly on tensor slices of lower orders [29], or by rearranging the original tensor into another of lower order but larger dimensions [64].

APPROXIMATE DECOMPOSITIONS

In practice, measurements are always corrupted by some noise, which almost always has a continuous probability distribution. For this reason, the tensor rank is generic or typical, and the CP decomposition is generally not unique. That's why a best rank- r approximation must be computed [21], [44]. General-purpose optimization algorithms will generally suffice to solve the problem, e.g., [21], [46], [65], [77], and [84]; they are widely used but their convergence toward a minimum is not guaranteed, because the objective function may have only an infimum.

In fact, low-rank approximations are useful and even unavoidable, but unfortunately ill posed in general [37], [75], except for special cases of tensors under constraints, like non-negativity [54]. Most algorithms presently utilized by engineering communities ignore this fact, which may raise serious practical problems in a small fraction of cases.

Ill posedness comes from the fact that the set of tensors of rank at most R is not closed, as pointed out in section “Border Rank.” Some remedies have been proposed in the literature to face or circumvent this difficulty. In practice, this means that another problem is solved, often by imposing constraints in the CP decomposition.

These include:

- Impose orthogonality between columns of factor matrices [20]—in BSS, this takes the form of a spatial prewhitening.
- Impose orthogonality between decomposable tensors [45].
- Prevent divergence by bounding coefficients λ_r [54], [61].
- If the tensor is nonnegative, use a nonnegative CP [54].
- Impose a minimal angle between columns of factor matrices [55].
- Compute an exact CP of another tensor, which has undergone a multilinear compression via truncated HOSVD [11], [21]. It may happen that the problem remains ill posed after this type of compression, because reducing the mode-ranks does not necessarily reduce tensor rank.
- Compute another decomposition where the core tensor is block diagonal instead of diagonal [26], [79].
- Compute a joint approximate diagonalization (JAD) of matrix slices, which may be viewed as another decomposition where the core tensor is not diagonal [2], [14], [20], [30], [51], [56], [62], [69], [86], [87], [89], as depicted in Figure 2. The drawbacks of this family of approaches, which become more and more popular, are threefold. First, rank must be smaller than two dimensions; in [25], the latter constraint is nevertheless relaxed. Second, replacing the core tensor by its diagonal yields an approximate CP decomposition whose optimality is not known. Third, a closed subclass of invertible matrices needs to be (arbitrarily) chosen, and indeed varies from one algorithm to another.
- When one dimension is much larger than the others, the optimality of this kind of approach can be significantly improved by imposing a structure in the diagonalization process [25].

Some codes are freely available on the Internet. See, e.g., the home pages of R. Bro, L. De Lathauwer, T. Kolda, A.H. Phan, and P. Comon [90]–[94]. A good site to find applications and related references is the Three-Mode Company's maintained by P. Kroonenberg [95].

THE CASE OF RANK-1 APPROXIMATE

The rank-1 approximation problem is of interest for at least two reasons: first it is always well posed, and second it shows up in the deflation approach of BSS [20]. In addition, it is much easier to compute than a full CP decomposition [28], [43]. This problem may be seen to be related to tensor eigenvalues [17], [35], [53], [59], [88]. It has been proved recently that the best rank-1 approximation of a symmetric tensor is symmetric [34]; a shorter proof can be found in [35], as well as uniqueness issues. So a question deserves to be raised: can the exact or approximate CP decompositions be computed by successive rank-1 approximations? It is already known that this does not generally work.

In fact, attention should be paid to the fact that subtracting the best rank-1 approximate does not decrease tensor rank in general [80], contrary to the matrix case. Simple examples may be found in [18]; similar examples also exist for nonsymmetric or nonnegative tensors. The consequence is that the rank-1 terms appearing in the best rank- k tensor approximation are not the same for different values of k . Hence, it is not possible

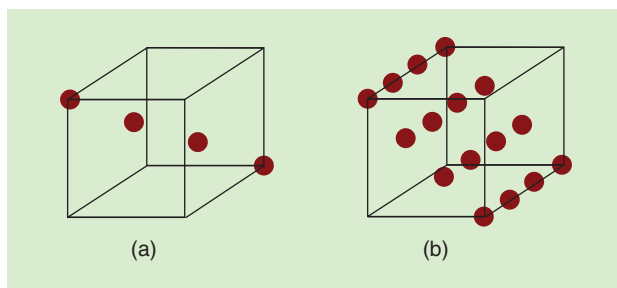


[FIG2] Because the optimization criteria are different in JAD and CP decompositions, one does not attempt to zero the same entries. This figure shows the location of the entries that are (a) not minimized in the core tensor in the CP decomposition of a third-order $4 \times 4 \times 4$ tensor, and (b) during the execution of a JAD algorithm. Note that JAD algorithms deliver two factor matrices; the entries of third one remain in the core tensor.

to compute a full CP decomposition by solving successive best rank-1 approximations, contrary to what has been claimed by some authors. This procedure, called *deflation*, works in BSS for other reasons. In fact, BSS does not only reduce to a low-rank tensor approximation, but also includes a regression stage. However, whether deflation works in special cases (such as structured CP decompositions) is still an open question.

EXAMPLE 21

The tensor defined by its mode-1 unfolding

$$\mathbf{T} = \begin{bmatrix} 1 & 0 & 0 & 1 \\ 0 & 2 & 1 & 0 \end{bmatrix}$$

is of rank 2. Its best rank-1 approximate is [80]:

$$\mathbf{Y} = \begin{bmatrix} 0 & 0 & 0 & 0 \\ 0 & 2 & 0 & 0 \end{bmatrix}.$$

One checks out that the difference

$$\mathbf{T} - \mathbf{Y} = \begin{bmatrix} 1 & 0 & 0 & 1 \\ 0 & 0 & 1 & 0 \end{bmatrix}$$

is of rank 3. In this example, deflation does not permit to decrease tensor rank.

APPLICATIONS

Applications of tensor decompositions (essentially CP) include arithmetic complexity, separation of variables, blind identification of linear mixtures, BSS, data mining, spectroscopy, antenna array processing, and phylogenetics, among others. Tucker and HOSVD have other application fields in which uniqueness is not requested, like data compression. Due to the space constraints of this article, we shall now detail only one application of the CP decomposition, particularly fluorescence spectroscopy [76], for which very few theoretical results can apply, unfortunately. The reader is invited to consult, e.g., [16], [20], and [46] for pointers to other applications.

An optical excitation applied to a solution produces several effects, including Rayleigh and Raman diffusions, and fluorescence. If the latter effect can be isolated, it may allow to accurately measure the relative concentrations of fluorescent solutes. In fact, at low concentrations and in the presence of R

fluorescent solutes, the Beer–Lambert law can be linearized and takes the form

$$\mathcal{T}(x, y, z) = T_o \sum_{\ell=1}^R \gamma_{\ell}(x) \epsilon_{\ell}(y) c_{\ell}(z),$$

where x , y , and z denote the fluorescence emission wavelength, the excitation wavelength, and the sample number, respectively, \mathcal{T} is the fluorescence intensity measured as a function of the latter variables, $\gamma_{\ell}(x)$ denotes fluorescence emission spectrum of the ℓ th solute, $\epsilon_{\ell}(y)$ its absorbance spectrum (sometimes called excitation spectrum), and $c_{\ell}(z)$ its relative concentration. In practice, only a finite number of samples are available, and measurements are made on discrete values within a limited spectral range, so that variables x , y , and z take a finite number of values. In other words, we deal with a CP decomposition of a finite three-way array, often of rather large dimensions (several hundreds). The particularity of this CP decomposition is that \mathcal{T} is real nonnegative, as well as all the terms involved in its CP decomposition. Hence, R is the nonnegative rank of \mathcal{T} . The good news is that 1) the best low-rank approximate always exists [54], and that 2) there are simple efficient numerical algorithms available for its computation [70]. The bad news is that known uniqueness results, which we have reviewed in this article, are not appropriate for nonnegative CP decompositions. For instance, if nonnegative rank is plugged in place of rank in (12), the obtained sufficient condition is more restrictive, and does not even guarantee that factor matrices are nonnegative. This is the subject of ongoing research.

ACKNOWLEDGMENTS

This work has been funded by the European Research Council under the European Community's Seventh Framework Programme FP7/2007–2013 grant agreement number~320594.

AUTHOR

Pierre Comon (p.comon@ieee.org) graduated in 1982 and received the doctorate degree in 1985 both from the University of Grenoble, France. He later received the Habilitation to Lead Research in 1995, from the University of Nice, France. His research interests include high-order statistics (HOS), BSS, statistical signal and array processing, tensor decompositions, multiway factor analysis and data mining, with applications to biomedical end environment. He was an associate editor of *IEEE Transactions on Signal Processing* (1995–1998), the EURASIP journal *Signal Processing* (2006–2011), and a member of the French National Committee of Scientific Research (1995–2000). Between 2001 and 2004, he was an associate editor of *IEEE Transactions on Circuits and Systems I*. He is a member of the editorial board of *SIAM Journal on Matrix Analysis and Applications* since January 2011. He is a Fellow of the IEEE.

REFERENCES

- [1] H. Abo, G. Ottaviani, and C. Peterson, "Induction for secant varieties of Segre varieties," *Trans. Amer. Math. Soc.*, vol. 361, pp. 767–792, 2009.
- [2] L. Albera, A. Ferreol, P. Chevalier, and P. Comon, "ICAR, a tool for blind source separation using fourth order statistics only," *IEEE Trans. Signal Processing*, vol. 53, no. 10, pp. 3633–3643, Oct. 2005.

- [3] J. Alexander and A. Hirschowitz, "Polynomial interpolation in several variables," *J. Algebr. Geom.*, vol. 4, no. 2, pp. 201–222, 1995.
- [4] J. M. F. Ten Berge, "Kruskal's polynomial for $2 \times 2 \times 2$ arrays and a generalization to $2 \times n \times n$ arrays," *Psychometrika*, vol. 56, no. 4, pp. 631–636, 1991.
- [5] J. M. F. Ten Berge, "Simplicity and typical rank of three-way arrays," *J. Chemomet.*, vol. 18, no. 1, pp. 17–21, 2004.
- [6] A. Bernardi, A. Gimigliano, and M. Ida, "Computing symmetric rank for symmetric tensors," *J. Symb. Computat.*, vol. 46, no. 1, pp. 34–53, 2011.
- [7] D. Bini, M. Capovani, F. Romani, and G. Lotti, " $O(n^{2.77})$ complexity for $n \times n$ approximate matrix multiplication," *Inform. Process. Lett.*, vol. 8, no. 5, pp. 234–235, 1979.
- [8] G. Blekherman, "Typical real ranks of binary forms," *Found. Computat. Math.*, to be published. DOI 10.1007/s10208-013-9174-8. arXiv:1205.3257
- [9] M. M. Boizard, G. Ginolhac, F. Pascal, S. Miron, and P. Forster, "Numerical performance of a tensor MUSIC algorithm based on HOSVD," in *Proc. European Signal Processing Conf. (EUSIPCO)*, Marrakech, Morocco, Dec. 13–15, 2013.
- [10] J. Brachat, P. Comon, B. Mourrain, and E. Tsigaridas, "Symmetric tensor decomposition," *Linear Algebr. Applicat.*, vol. 433, nos. 11–12, pp. 1851–1872, Dec. 2010.
- [11] R. Bro and C. A. Andersson, "Improving the speed of multiway algorithms. Part II: Compression," *Chemomet. Intell. Lab. Syst.*, vol. 42, nos. 1–2, pp. 105–113, 1998.
- [12] J. D. Carroll and J. J. Chang, "Analysis of individual differences in multidimensional scaling via n -way generalization of Eckart-Young decomposition," *Psychometrika*, vol. 35, no. 3, pp. 283–319, Sept. 1970.
- [13] A. Causa and R. Re, "On the maximum rank of a real binary form," *Annali di Matematica Pura e Applicata*, vol. 190, no. 1, pp. 55–59, 2011.
- [14] G. Chabriel, M. Kleinstaubler, E. Moreau, H. Shen, P. Tichavsky, and A. Yeredor, "Joint matrices decompositions and blind source separation," *IEEE Signal. Processing Mag.*, vol. 31, no. 3, pp. 34–43, May 2014.
- [15] L. Chiantini and G. Ottaviani, "On generic identifiability of 3-tensors of small rank," *SIAM J. Matrix Anal. Appl.*, vol. 33, no. 3, pp. 1018–1037, 2012.
- [16] A. Cichocki, D. Mandic, A.-H. Phan, C. Caiafa, G. Zhou, Q. Zhao, and L. De Lathauwer, "Tensor decompositions for signal processing applications," *IEEE Signal. Processing Mag.*, to be published.
- [17] P. Comon, "Tensor decompositions, state of the art and applications," in *Mathematics in Signal Processing V*, J. G. McWhirter and I. K. Proudler, Eds. Oxford, U.K.: Clarendon Press, 2002, pp. 1–24.
- [18] P. Comon, "Tensors, usefulness and unexpected properties," in *Proc. 15th IEEE Workshop on Statistical Signal Processing (SSP'09)*, Cardiff, U.K., 31 Aug.–3 Sept., 2009, pp. 781–788.
- [19] P. Comon, G. Golub, L.-H. Lim, and B. Mourrain, "Symmetric tensors and symmetric tensor rank," *SIAM J. Matrix Anal. Appl.*, vol. 30, no. 3, pp. 1254–1279, Sept. 2008.
- [20] P. Comon and C. Jutten, Eds., *Handbook of Blind Source Separation, Independent Component Analysis and Applications*. Oxford U.K.: Academic, 2010.
- [21] P. Comon, X. Luciani, and A. L. F. De Almeida, "Tensor decompositions, alternating least squares and other tales," *J. Chemomet.*, vol. 23, pp. 393–405, Aug. 2009.
- [22] P. Comon and G. Ottaviani, "On the typical rank of real binary forms," *Linear Multilinear Algebr.*, vol. 60, no. 6, pp. 657–667, May 2012.
- [23] P. Comon and G. Ottaviani, "Tensor decompositions, a geometric viewpoint," submitted for publication.
- [24] P. Comon, J. M. F. Ten Berge, L. De Lathauwer, and J. Castaing, "Generic and typical ranks of multi-way arrays," *Linear Algebr. Applicat.*, vol. 430, nos. 11–12, pp. 2997–3007, June 2009.
- [25] L. De Lathauwer, "A link between canonical decomposition in multilinear algebra and simultaneous matrix diagonalization," *SIAM J. Matrix Anal. Appl.*, vol. 28, no. 3, pp. 642–666, 2006.
- [26] L. De Lathauwer, "Blind separation of exponential polynomials and the decomposition of a tensor in rank-($L_x, L_y, 1$) terms," *SIAM J. Matrix Anal. Appl.*, vol. 32, no. 4, pp. 145–1474, 2011.
- [27] L. De Lathauwer, B. De Moor, and J. Vandewalle, "A multilinear singular value decomposition," *SIAM J. Matrix Anal. Appl.*, vol. 21, no. 4, pp. 1253–1278, Apr. 2000.
- [28] L. De Lathauwer, B. De Moor, and J. Vandewalle, "On the best rank-1 and rank-(R_1, R_2, \dots, R_N) approximation of high-order tensors," *SIAM J. Matrix Anal. Appl.*, vol. 21, no. 4, pp. 1324–1342, Apr. 2000.
- [29] L. De Lathauwer, B. De Moor, and J. Vandewalle, "Independent component analysis and (simultaneous) third-order tensor diagonalization," *IEEE Trans. Signal Processing*, vol. 49, no. 10, pp. 2262–2271, Oct. 2001.
- [30] L. De Lathauwer, B. De Moor, and J. Vandewalle, "Computation of the canonical decomposition by means of a simultaneous generalized Schur decomposition," *SIAM J. Matrix Anal. Appl.*, vol. 26, no. 2, pp. 295–327, 2004.
- [31] I. Domanov and L. De Lathauwer, "On the uniqueness of the canonical polyadic decomposition of third-order tensors—Part I: Basic results and uniqueness of one factor matrix," *SIAM J. Matrix Anal. Appl.*, vol. 34, no. 3, pp. 855–875, 2013.
- [32] I. Domanov and L. De Lathauwer, "On the uniqueness of the canonical polyadic decomposition of third-order tensors—Part II: Overall uniqueness," *SIAM J. Matrix Anal. Appl.*, vol. 34, no. 3, pp. 876–903, 2013.

- [33] R. Ehrenborg and G. C. Rota, "Apolarity and canonical forms for homogeneous polynomials," *Eur. J. Combinatorics*, vol. 14, no. 3, pp. 157–181, May 1993.
- [34] S. Friedland, "Best rank one approximation of real symmetric tensors can be chosen symmetric," *Front. Math. China*, vol. 8, no. 1, pp. 19–40, 2013.
- [35] S. Friedland and G. Ottaviani, "The number of singular vector tuples and uniqueness of best rank one approximation of tensors," submitted for publication. arXiv:1210.8316.
- [36] R. A. Harshman, "Foundations of the Parafac procedure: Models and conditions for an explanatory multimodal factor analysis," *UCLA Working Pap. Phonet.*, vol. 16, pp. 1–84, Dec. 1970.
- [37] C. J. Hillar and L.-H. Lim, "Most tensor problems are NP-hard," submitted for publication. arXiv:0911.1393.
- [38] F. L. Hitchcock, "The expression of a tensor or a polyadic as a sum of products," *J. Math. Phys.*, vol. 6, no. 1, pp. 165–189, 1927.
- [39] T. D. Howell, "Global properties of tensor rank," *Linear. Algebr. Applicat.*, vol. 22, pp. 9–23, Dec. 1978.
- [40] A. Iarrobino, "Inverse system of a symbolic power. II. The Waring problem for forms," *J. Algebr.*, vol. 174, no. 3, pp. 1091–1110, June 1995.
- [41] T. Jiang and N. Sidiropoulos, "Kruskal's permutation lemma and the identification of CANDECOMP/PARAFAC and bilinear models," *IEEE Trans. Signal Processing*, vol. 52, no. 9, pp. 2625–2636, Sept. 2004.
- [42] H. A. L. Kiers, "Towards a standardized notation and terminology in multiway analysis," *J. Chemomet.*, vol. 14, no. 3, pp. 105–122, June 2000.
- [43] E. Kofidis and P. Regalia, "One the best rank-1 approximation of higher-order symmetric tensors," *SIAM J. Matrix Anal. Appl.*, vol. 23, no. 3, pp. 863–884, 2002.
- [44] E. Kofidis and P. A. Regalia, "Tensor approximation and signal processing applications," in *Structured Matrices in Mathematics, Computer Science, and Engineering*, V. Olshevsky, Ed. American Math. Soc.: Providence, RI, 2001.
- [45] T. G. Kolda, "Orthogonal tensor decomposition," *SIAM J. Matrix Anal. Appl.*, vol. 23, no. 1, pp. 243–255, 2001.
- [46] T. G. Kolda and B. W. Bader, "Tensor decompositions and applications," *SIAM Rev.*, vol. 51, no. 3, pp. 455–500, Sept. 2009.
- [47] J. B. Kruskal, "Three-way arrays: Rank and uniqueness of trilinear decompositions," *Linear Algebr. Applicat.*, vol. 18, no. 2, pp. 95–138, 1977.
- [48] J. B. Kruskal, "Rank of N-way arrays and the geometry of $2 \times 2 \times 2$ arrays," *Tech. Rep.*, AT&T Bell Labs, Feb. 1985.
- [49] J. M. Landsberg, "Tensors: Geometry and applications," in *Graduate Studies in Mathematics*. American Math. Soc.: Providence, RI, 2012, vol. 128.
- [50] S. Leurgans, R. T. Ross, and R. B. Abel, "A decomposition for three-way arrays," *SIAM J. Matrix Anal. Appl.*, vol. 14, no. 4, pp. 1064–1083, Oct. 1993.
- [51] X. L. Li and X. D. Zhang, "Nonorthogonal joint diagonalization free of degenerate solution," *IEEE Trans. Signal Processing*, vol. 55, no. 5, pp. 1803–1814, 2007.
- [52] T. Lickteig, "Typical tensorial rank," *Linear Algebr. Applicat.*, vol. 69, pp. 95–120, Aug. 1985.
- [53] L.-H. Lim, "Singular values and eigenvalues of tensors: A variational approach," in *Proc. IEEE Int. Workshop on Computational Advances Multi-Sensor Adaptive Processing*, Puerto Vallarta, Mexico, Dec. 13–15, 2005, pp. 129–132.
- [54] L.-H. Lim and P. Comon, "Nonnegative approximations of nonnegative tensors," *J. Chemomet.*, vol. 23, pp. 432–441, Aug. 2009.
- [55] L.-H. Lim and P. Comon, "Blind multilinear identification," *IEEE Trans. Inform. Theory*, vol. 60, no. 2, 2014, pp. 1260–1280.
- [56] X. Luciani and L. Albera, "Semi-algebraic canonical decomposition of multiway arrays and joint eigenvalue decomposition," in *Proc. IEEE Int. Conf. Acoustics, Speech and Signal Processing (ICASSP2011)*, Prague, Mar. 12–15, 2011, pp. 4104–4107.
- [57] P. McCullagh, *Tensor Methods in Statistics*, Monographs on Statistics and Applied Probability. London, U.K.: Chapman & Hall, 1987.
- [58] R. Miranda, "Linear systems of plane curves," *Not. AMS*, vol. 46, no. 2, pp. 192–202, Feb. 1999.
- [59] G. Ni and Y. Wang, "On the best rank-1 approximation to higher-order symmetric tensors," *Math. Comput. Modell.*, vol. 46, no. 9–10, pp. 1345–1352, Nov. 2007.
- [60] L. Oeding and G. Ottaviani, "Eigenvectors of tensors and algorithms for Waring decomposition," *J. Symb. Comput.*, vol. 54, pp. 9–35, July 2013.
- [61] P. Paatero, "Construction and analysis of degenerate Parafac models," *J. Chemomet.*, vol. 14, no. 3, pp. 285–299, May/June 2000.
- [62] D. T. Pham, "Joint approximate diagonalization of positive definite Hermitian matrices," *SIAM J. Matrix Anal. Appl.*, vol. 22, no. 4, pp. 1136–1152, 2001.
- [63] A. H. Phan, A. Cichocki, P. Tichavsky, G. Luta, and A. Brockmeier, "Tensor completion through multiple Kronecker product decomposition," in *Proc. IEEE Int. Conf. Acoustics, Speech and Signal Processing (ICASSP2013)*, Vancouver, Canada, May 26–31, pp. 3233–3237.
- [64] A. H. Phan, P. Tichavsky, and A. Cichocki, "Candecomp/Parafac decomposition of high-order tensors through tensor reshaping," *IEEE Trans. Signal Processing*, vol. 61, pp. 4847–4860, Oct. 2013.
- [65] M. Rajih, P. Comon, and R. Harshman, "Enhanced line search: A novel method to accelerate Parafac," *SIAM J. Matrix Anal. Appl.*, vol. 30, no. 3, pp. 1148–1171, Sept. 2008.
- [66] B. Reznick, "Sums of even powers of real linear forms," *Mem. AMS*, vol. 96, no. 463, pp. 1–155, Mar. 1992.
- [67] B. Reznick, "Laws of inertia in higher degree binary forms," *Proc. Amer. Math. Soc.*, vol. 138, no. 3, pp. 815–826, June 2010.
- [68] J. A. Rhodes, "A concise proof of Kruskal's theorem on tensor decomposition," *Linear Algebr. Applicat.*, vol. 432, no. 7, pp. 1818–1824, Mar. 2010.
- [69] F. Roemer and M. Haardt, "A semi-algebraic framework for approximate CP decompositions via simultaneous matrix diagonalizations (SECSI)," *Signal Process.*, vol. 93, no. 9, pp. 2722–2738, Sept. 2013.
- [70] J.-P. Royer, N. Thirion-Moreau, and P. Comon, "Computing the polyadic decomposition of nonnegative third order tensors," *Signal Process.*, vol. 91, no. 9, pp. 2159–2171, Sept. 2011.
- [71] J. R. Ruiz-Tolosa and E. Castillo, *From Vectors to Tensors*, Universitext. Berlin, Heidelberg: Springer, 2005.
- [72] A. Schönhage, "Partial and total matrix multiplication," *SIAM J. Computat.*, vol. 10, no. 3, pp. 434–455, 1981.
- [73] N. D. Sidiropoulos and R. Bro, "On the uniqueness of multilinear decomposition of N-way arrays," *J. Chemomet.*, vol. 14, no. 3, pp. 229–239, May/June 2000.
- [74] N. D. Sidiropoulos, R. Bro, and G. B. Giannakis, "Parallel factor analysis in sensor array processing," *IEEE Trans. Signal Processing*, vol. 48, no. 8, pp. 2377–2388, Aug. 2000.
- [75] V. De Silva and L.-H. Lim, "Tensor rank and the ill-posedness of the best low-rank approximation problem," *SIAM J. Matrix Anal. Appl.*, vol. 30, no. 3, pp. 1084–1127, 2008.
- [76] A. Smilde, R. Bro, and P. Geladi, *Multi-Way Analysis*. Chichester, U.K.: Wiley, 2004.
- [77] L. Sorber, M. Van Barel, and L. De Lathauwer, "Optimization-based algorithms for tensor decompositions: Canonical polyadic decomposition, decomposition in rank-s terms and a new generalization," *SIAM J. Optim.*, vol. 23, no. 2, pp. 695–720, Apr. 2013.
- [78] M. Sorensen and P. Comon, "Tensor decompositions with banded matrix factors," *Linear Algebr. Applicat.*, vol. 438, no. 1, pp. 919–941, Jan. 2013.
- [79] A. Stegeman and L. De Lathauwer, "A method to avoid diverging components in the Candecomp/Parafac model for generic $I \times J \times 2$ arrays," *SIAM J. Matrix Anal. Appl.*, vol. 30, no. 4, pp. 1614–1638, 2009.
- [80] A. Stegeman and P. Comon, "Subtracting a best rank-1 approximation does not necessarily decrease tensor rank," *Linear Algebr. Applicat.*, vol. 433, no. 7, pp. 1276–1300, Dec. 2010.
- [81] A. Stegeman and N. D. Sidiropoulos, "On Kruskal's uniqueness condition for the Candecomp/Parafac decomposition," *Linear Algebr. Applicat.*, vol. 420, no. 2–3, pp. 540–552, Jan. 2007.
- [82] V. Strassen, "Rank and optimal computation of generic tensors," *Linear Algebr. Applicat.*, vol. 52, pp. 645–685, July 1983.
- [83] P. Tichavsky and Z. Koldovsky, "Weight adjusted tensor method for blind separation of underdetermined mixtures of nonstationary sources," *IEEE Trans. Signal Processing*, vol. 59, no. 3, pp. 1037–1047, Mar. 2011.
- [84] G. Tomasi and R. Bro, "A comparison of algorithms for fitting the Parafac model," *Comp. Stat. Data Anal.*, vol. 50, pp. 1700–1734, 2006.
- [85] L. R. Tucker, "Some mathematical notes for three-mode factor analysis," *Psychometrika*, vol. 31, no. 3, pp. 279–311, Sept. 1966.
- [86] R. Vollgraf and K. Obermayer, "Quadratic optimization for simultaneous matrix diagonalization," *IEEE Trans. Signal Processing*, vol. 54, pp. 3270–3278, Sept. 2006.
- [87] A. Yeredor, "Non-orthogonal joint diagonalization in the LS sense with application in blind source separation," *IEEE Trans. Signal Processing*, vol. 50, no. 7, pp. 1545–1553, 2002.
- [88] X. Zhang, C. Ling, and L. Qi, "The best rank-1 approximation of a symmetric tensor and related spherical optimization problems," *SIAM J. Matrix Anal. Appl.*, vol. 33, no. 3, pp. 806–821, 2012.
- [89] P. Ziehe, G. Nolte, and K. R. Müller, "A fast algorithm for joint diagonalization with non orthogonal transformations and its application to blind source separation," *J. Mach. Learn. Res.*, vol. 5, pp. 777–800, Dec. 2004.
- [90] R. Bro. Home Page. [Online]. Available: <http://www.models.life.ku.dk/users/rasmus>
- [91] L. De Lathauwer. Home Page. [Online]. Available: <http://homes.esat.kuleuven.be/~delathau>
- [92] T. Kolda. Home Page. [Online]. Available: <http://www.sandia.gov/~tgkolda>
- [93] A. H. Phan. Home Page. [Online]. Available: <http://www.bsp.brain.riken.jp/~phan>
- [94] P. Comon. Home Page. [Online]. Available: <http://www.gipsa-lab.grenoble-inp.fr/~pierre.comon>
- [95] P. Kroonenberg. Three-Mode Company. [Online]. Available: <http://www.gipsa-lab.grenoble-inp.fr/~pierre.comon>

[Guoxu Zhou, Andrzej Cichocki, Qibin Zhao, and Shengli Xie]

Nonnegative Matrix and Tensor Factorizations

[An algorithmic perspective]

A common thread in various approaches for model reduction, clustering, feature extraction, classification, and blind source separation (BSS) is to represent the original data by a lower-dimensional approximation obtained via matrix or tensor (multiway array) factorizations or decompositions. The notion of matrix/tensor factorizations arises in a wide range of important applications and each matrix/tensor factorization makes different assumptions regarding component (factor) matrices and their underlying structures. So choosing the appropriate one is critical in each application domain. Approximate low-rank matrix and tensor factorizations play fundamental roles in enhancing the data and extracting latent (hidden) components.

In the nonnegative matrix and tensor factorization approaches, high-dimensional data such as nonnegative time series or images are factorized to find meaningful latent nonnegative components [1]. The motivation behind them is that besides the dimensionality reduction sought in many applications, the underlying data ensemble is nonnegative and can be better modeled and interpreted by means of nonnegative and, preferably, sparse or smooth components to achieve a unique additive parts-based representation (nonsubtractive combinations of nonnegative basis) [2].

Nonnegative matrix factorization (NMF) has been investigated by many researchers, especially Paatero and Tapper [3], for more

than 15 years, but it has gained popularity through the works of Lee and Seung published in *Nature* [2]. Based on the argument that the nonnegative components are important in human brain visual perception, they proposed simple multiplicative update algorithms for finding meaningful parts-based localized additive representations of face images (such as the eyebrows, mouth, and nose). After that, NMF received extensive study and the idea has been extended to multiway models (i.e., multilinear models that perform tensor decompositions) including nonnegative Tucker decompositions (NTDs) and nonnegative polyadic decompositions (NPDs) [1].

In signal processing and data analysis, nonnegative matrix and tensor factorizations are important and pervasive topics due to their unique properties and numerous applications [1]. As the theory and new applications of nonnegative matrix and tensor factorizations are still under development and are subject of extensive research (including uniqueness, performance, and estimation of nonnegative rank), our aim is to present algo-

rithmic and computational frameworks for the analysis and development of reliable, efficient, and robust algorithms for NMF/NPD/NTD for sparse representation of signals, particularly, based on low-rank approximations of high-dimensional data. These topics are key factors for development of many emerging real-life applications, e.g., three-dimensional (3-D) video tensor displays [4], text mining, and classification and clustering [1], [5], [6].

GEOMETRIC INTERPRETATION AND UNIQUENESS OF NMF

In NMF, a given nonnegative matrix $Y \in \mathbb{R}_+^{M \times N}$ is modeled as $Y = AB^T + E$, where $A \in \mathbb{R}_+^{M \times R}$ and $B \in \mathbb{R}_+^{N \times R}$ are called the



Source Separation and Applications

IMAGE LICENSED BY
INGRAM PUBLISHING

Digital Object Identifier 10.1109/MSP.2014.2298891

Date of publication: 7 April 2014

[TABLE 1] NOTATIONS AND DEFINITIONS.

$\mathbf{A}, \mathbf{a}_r, \mathbf{a}_m, [\mathbf{A}]_{mr}$	A MATRIX, THE r th COLUMN, m th ROW, AND THE (m, r) th ENTRY OF MATRIX \mathbf{A} , RESPECTIVELY.
$\mathbf{I}, \mathbf{1}, \mathbf{0}$	THE IDENTITY MATRIX, THE MATRIX WITH ALL OF ITS ELEMENTS BEING ONE, ZERO.
\mathcal{I}_N	THE INDEX SET OF NONZERO INTEGERS NO LARGER THAN N , I.E., $\mathcal{I}_N = \{1, 2, \dots, N\}$. SIMILARLY FOR \mathcal{I}_{R_n} .
$\mathbb{R}_+^{R_1 \times R_2 \times \dots \times R_N}$	SET OF R_1 -BY- R_2 ... BY- R_N NONNEGATIVE TENSORS OR MATRICES.
$\mathbf{A} \geq \mathbf{0}$	NONNEGATIVITY OF \mathbf{A} , I.E., $[\mathbf{A}]_{ij} \geq 0$.
$\mathcal{P}_+(\mathbf{A})$	$[\mathbf{A}]_{ij} = \max([\mathbf{A}]_{ij}, 0), \forall i, j$.
$\mathcal{Y}, \mathcal{Y}_{(n)}$	A TENSOR, THE MODE- n MATRICIZATION OF TENSOR \mathcal{Y} .
\otimes, \oslash	ELEMENT-WISE (HADAMARD) PRODUCT, DIVISION OF MATRICES OR TENSORS.
\otimes, \circ	KRONECKER PRODUCT AND KHATRI-RAO PRODUCT (COLUMN-WISE KRONECKER PRODUCT) OF MATRICES
$Z_{\mathbf{A}}, s_{\mathbf{A}}$	NUMBER OF ZEROS IN $\mathbf{A} \in \mathbb{R}^{M \times N}$, THE SPARSITY DEFINED AS $s_{\mathbf{A}} \triangleq (Z_{\mathbf{A}}/(MN)) \in [0, 1]$.
$\mathbf{A} \sim U(0, 1)$	ELEMENTS OF \mathbf{A} ARE DRAWN FROM INDEPENDENT UNIFORM DISTRIBUTIONS BETWEEN ZERO AND ONE.

basis matrix and the encoding matrix, respectively, and $\mathbf{E} \in \mathbb{R}^{M \times N}$ denotes the noise (See Table 1 for the notations we adopted in this article). The minimum value of R leading to $\mathbf{E} = \mathbf{0}$ is called the nonnegative-rank of \mathbf{Y} . Apparently nonnegative-rank is always no less than the rank of \mathbf{Y} . We assume that $R \ll M \leq N$, as we often can use only a small number of nonnegative components to approximate the original high-dimensional data.

Unfortunately, NMF does not always give correct decomposition into parts [7], which gives rise to the issue of uniqueness. We say that the NMF is (essentially) unique if the factor matrices \mathbf{A} and \mathbf{B} are estimated only up to arbitrary positive scaling and permutation ambiguities of their columns. Uniqueness of NMF is the foundation for NMF to be used as a BSS tool. The first sufficient uniqueness conditions were given by Donoho and Stodden [7] in the context of separable NMF, and later a stronger version was given by Laurbert et al. based on sufficient spread and boundary closeness of factors [8]. New uniqueness results were derived by Gillis and Huang et al. very recently, together with comprehensive reviews and new insights into the uniqueness of NMF (see [9], [10], and references therein). Here we omit the mathematical details but illustrate intuitively when NMF is likely to be unique via a geometric interpretation of NMF. Considering the NMF of $\mathbf{Y} = \mathbf{A}\mathbf{B}^T$ with the given nonnegative-rank R , each column of \mathbf{Y} can be expressed as $\mathbf{y}_n = \sum_{r=1}^R \mathbf{a}_r b_{nr}$ where $b_{nr} \geq 0$, which means that all the points \mathbf{y}_n are enclosed by the conic hull $\text{cone}(\mathbf{A})$ defined by $\{\mathbf{a}_r\}_{r=1}^R$ (see Figure 1 for $M = R = 3$), and these points are either located on the boundary of $\text{cone}(\mathbf{A})$, or inside $\text{cone}(\mathbf{A})$. From the figure, we can observe [11], [5].

SPARSITY

The sparsity of \mathbf{B} are reflected by the points on the boundary of $\text{cone}(\mathbf{A})$ [11]. In Figure 1, the points marked by blue dots are located on the lines collinear with the basis vectors \mathbf{a}_r (i.e., extreme rays), which means $\mathbf{y}_n = \mathbf{a}_r b_{nr}$, and the corresponding

coefficients b_{nr} are 1-sparse (we call a vector k -sparse if it just contains k nonzero elements). The points marked by green ‘o’ are located on the hyperplanes spanned by any two basis vectors and the corresponding b_{nr} are 2-sparse. The red asterisks are located inside $\text{cone}(\mathbf{A})$ and the corresponding $b_{nr} > 0$ are dense.

UNIQUENESS

It is obvious that the NMF is not unique if there exists another conical hull $\text{cone}(\tilde{\mathbf{A}})$ such that $\text{cone}(\mathbf{A}) \subset \text{cone}(\tilde{\mathbf{A}}) \subset \text{cone}(\mathbf{I})$. If $\tilde{\mathbf{A}}$ is chosen as the basis matrix with $\mathbf{Y} = \tilde{\mathbf{A}}\tilde{\mathbf{B}}^T$, $\tilde{\mathbf{B}}$ will be nonnegative but less sparse than \mathbf{B} as all the points are enclosed by $\text{cone}(\tilde{\mathbf{A}})$ and consequently are inside $\text{cone}(\tilde{\mathbf{A}})$. Conversely, suppose that we have an NMF such that $\mathbf{Y} = \tilde{\mathbf{A}}\tilde{\mathbf{B}}^T$ with dense factor $\tilde{\mathbf{B}} > \mathbf{0}$. We can keep shrinking $\text{cone}(\tilde{\mathbf{A}})$ until some points reside on its boundary while the others are inside it, thereby leading to a sparser NMF.

IN SIGNAL PROCESSING AND DATA ANALYSIS, NONNEGATIVE MATRIX AND TENSOR FACTORIZATIONS ARE IMPORTANT AND PERVASIVE TOPICS DUE TO THEIR UNIQUE PROPERTIES AND NUMEROUS APPLICATIONS.

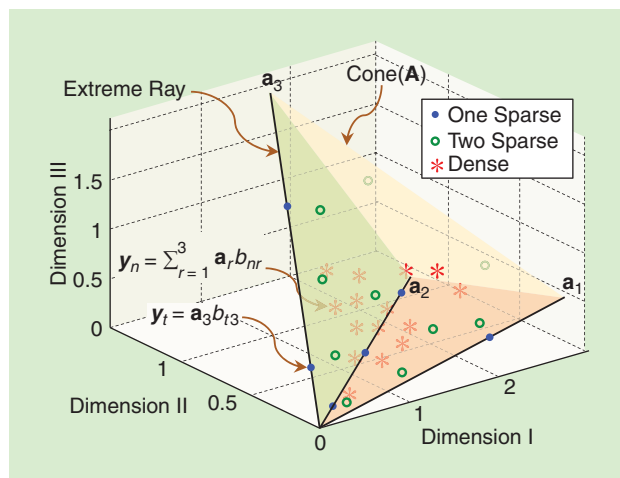


[FIG1] A geometric interpretation of NMF $\mathbf{Y} = \mathbf{A}\mathbf{B}^T$ with $M = R = 3$ in the data space. The columns of \mathbf{A} form a conic hull $\text{cone}(\mathbf{A})$. The sparse points on the boundary (marked by ‘•’ and ‘o’) of $\text{cone}(\mathbf{A})$ govern the sparsity and uniqueness of NMF.

In general the NMF is nonunique. However, intuitively, the NMF with sufficiently sparse nonnegative components of \mathbf{B} , associated with the “smallest” conic hull cone(\mathbf{A}) enclosing all points \mathbf{y}_n , is likely to be unique, and under which NMF can be used as a BSS tool. Particularly, if there exist 1-sparse points on each extreme ray, we call it separable NMF, which restricts the columns of \mathbf{A} to be partial columns of \mathbf{Y} and will be discussed later.

In summary, sparsity not only directly reflects the learning-parts ability of NMF, but also plays a key role in the essential uniqueness analysis of NMF.

SPARSITY NOT ONLY DIRECTLY REFLECTS THE LEARNING-PARTS ABILITY OF NMF, BUT ALSO PLAYS A KEY ROLE IN THE ESSENTIAL UNIQUENESS OF NMF.

ACTIVE-SET METHODS

Kim and Park proposed the efficient block principal pivoting (BPP) method based on the active set method [15], which needs to solve the linear inverse problem $(\partial D_{\text{NLS}}/\partial \mathbf{A}) = \mathbf{0}$ defined over the active set of variables. Different from the standard active set

method, this method exchanges multiple variables between working sets per iteration and effectively exploits the multiple columns feature of variable matrices to achieve high efficiency.

NMF ALGORITHMS BASED ON NONNEGATIVE ALTERNATING LEAST SQUARES

NMF is implemented by minimizing a cost (loss) function $D(\mathbf{Y} \parallel \mathbf{A}\mathbf{B}^T)$ that measures the discrepancy or distance between the factorization $\mathbf{A}\mathbf{B}^T$ and the data matrix \mathbf{Y} . In this article, the Euclidean distance is used because it is the most widely applied in practice. Then NMF can be performed by minimizing the cost function $D_{\text{NMF}} = (1/2)\|\mathbf{Y} - \mathbf{A}\mathbf{B}^T\|_F^2$, where \mathbf{A} and \mathbf{B} are constrained to be nonnegative. As D_{NMF} is not convex, alternating the minimization of D_{NMF} with respect to either \mathbf{A} or \mathbf{B} while fixing the other one has been widely adopted, which is referred to as alternating nonnegative least squares (ANLS) [12]. For example, when \mathbf{B} is fixed, the optimal \mathbf{A} is estimated by solving the following nonnegative least squares (NLS):

$$\min_{\mathbf{A}} D_{\text{NLS}} = \frac{1}{2} \|\mathbf{Y} - \mathbf{A}\mathbf{B}^T\|_F^2, \quad s.t. \mathbf{A} \geq \mathbf{0}. \quad (1)$$

For simplicity, we focus on the update rule of nonnegative matrix \mathbf{A} with fixed \mathbf{B} by solving (1), but keep in mind that by considering $D_{\text{NMF}} = (1/2)\|\mathbf{Y}^T - \mathbf{B}\mathbf{A}^T\|_F^2$, the roles of \mathbf{A} and \mathbf{B} are exchanged and the update rule of \mathbf{B} can be obtained similarly.

Theoretically, second-order methods that exploit both the Hessian matrix and the gradient give more accurate solutions and enjoy a higher rate of convergence than first-order methods. However, the Hessian matrix is huge for large-scale problems. Moreover, the algorithms that need to search step-size involve frequent evaluation of the cost function, which is computationally expensive. Hence we only consider low-complexity algorithms that are free of searching step-size and essentially use the first-order information only, i.e., the gradient $(\partial D_{\text{NLS}}/\partial \mathbf{A}) = -\mathbf{Y}\mathbf{B} + \mathbf{A}\mathbf{B}^T\mathbf{B}$.

MULTIPLICATIVE UPDATE ALGORITHM

In the multiplicative update (MU) method [2], the matrix \mathbf{A} is updated by using $\mathbf{A} \leftarrow \mathbf{A} - \eta_{\mathbf{A}} \odot (\partial D_{\text{NLS}}/\partial \mathbf{A})$ with a smart choice of step-size (learning rate) $\eta_{\mathbf{A}} = \mathbf{A} \oslash (\mathbf{A}\mathbf{B}^T\mathbf{B})$, which leads to the MU rule [2], [13]:

$$\mathbf{A} \leftarrow \mathbf{A} \odot \mathcal{P}_+(\mathbf{Y}\mathbf{B}) \oslash (\mathbf{A}\mathbf{B}^T\mathbf{B}). \quad (2)$$

As such, \mathbf{A} remains nonnegative and D_{NLS} is nonincreasing during iterations (here \mathcal{P}_+ is used to accommodate the case where

\mathbf{Y} occasionally contains some negative entries caused by noise [13]). The MU method converges relatively slowly but it is simple and easy to implement. Hence, based on it many extended versions were proposed [1], [13], [14].

ACCELERATED PROXIMAL GRADIENT METHOD

Taking into account that D_{NLS} is convex and its gradient is Lipschitz continuous, Guan et al. developed the NMF algorithm based on Nesterov’s optimal gradient method (NeNMF) [16], i.e., the accelerated proximal gradient (APG) method to solve (1). In the APG approach, the step-size is selected as the reciprocal of the Lipschitz constant and hence is free of line search [16].

HIERARCHICAL ALTERNATING LEAST SQUARES ALGORITHM

In each iteration, the hierarchical alternating least squares (HALS) [1] algorithm updates only one column of \mathbf{A} (or \mathbf{B}), which leads to the following set of optimization problems:

$$\min_{\mathbf{a}_r \geq \mathbf{0}} \frac{1}{2} \|\mathbf{Y}_r - \mathbf{a}_r \mathbf{b}_r^T\|_F^2, \quad r \in \mathcal{I}_R, \quad (3)$$

where $\mathbf{Y}_r \doteq \mathbf{Y} - \sum_{i \neq r} \mathbf{a}_i \mathbf{b}_i^T$. Equation (3) is strictly convex when $\|\mathbf{b}_r\|_F \neq 0$ and it leads to

$$\mathbf{a}_r \leftarrow \mathcal{P}_+ \left(\mathbf{a}_r + \frac{1}{\mathbf{b}_r^T \mathbf{b}_r} (\mathbf{Y}\mathbf{b}_r - \mathbf{A}\mathbf{B}^T \mathbf{b}_r) \right), \quad r \in \mathcal{I}_R. \quad (4)$$

The NMF algorithms based on the above NLS solvers belong to block coordinate descent methods. This type of method converges if the optimal solution of each subproblem is unique [17]. Note that once the subproblem (1) is strictly convex, its optimal solution will be unique. Hence, these NMF algorithms have the guarantee of local convergence if we can maintain the full column rank of factors during the iterations. In the case where the NMF is not unique, existing NMF algorithms are often blamed for their lack of global convergence. Nevertheless, this drawback does not prevent NMF from performing successfully in many practical applications.

To increase the sparsity of results and/or enforce the uniqueness, we often add penalty or regularization terms to the cost function D_{NMF} , typically l_1 -norm penalty, which leads to $D_{\text{NLS}} = (1/2)\|\mathbf{Y} - \mathbf{A}\mathbf{B}^T\|_F^2 + \lambda \|\mathbf{A}\|_1$ with $\lambda > 0$ in (1). As $\mathbf{A} \geq \mathbf{0}$, we have $\|\mathbf{A}\|_1 = \text{trace}(\mathbf{1}^T \mathbf{A})$ and $(\partial D_{\text{NLS}}/\partial \mathbf{A}) = -\mathbf{Y}\mathbf{B} + \mathbf{A}\mathbf{B}^T\mathbf{B} + \lambda \mathbf{1}$, which allows to apply the aforementioned NLS solvers

straightforwardly. Another popular regularized model is $D_{\text{NLS}} = (1/2)\|Y - AB^T\|_F^2 + (\lambda/2)\|A\|_F^2$, $\lambda > 0$. In this case, D_{NLS} is strictly convex and equivalent to applying the Tikhonov regularization. This model generally results in a denser factor A and consequently a sparser factor B in the ANLS-based NMF. In these methods, how to select the parameter λ is crucial to achieve satisfactory results, and readers are referred to [18] and references therein for an in-depth analysis.

All the NLS solvers we introduced above involve the computation of YB and AB^TB [i.e., the terms of the gradient $(\partial N_{\text{NLS}}/\partial A)$] explicitly or implicitly in each iteration. The time complexity of computing YB is as high as $O(MNR)$. One key factor to achieve fast NMF is to compute YB and Y^TA (used for minimizing $D_{\text{NLS}} = (1/2)\|Y^T - BA^T\|_F^2$ with respect to B) efficiently.

NMF FOR LARGE-SCALE PROBLEMS

NMF BASED ON LOW-RANK APPROXIMATION

In this approach, we consider a two-stage procedure to perform NMF [13] (see Figure 2):

- 1) Obtain the low-rank approximation (LRA) of Y such that $Y \approx \tilde{A}\tilde{B}^T$, where $\tilde{A} \in \mathbb{R}^{M \times R}$ and $\tilde{B} \in \mathbb{R}^{N \times R}$. This can be done by solving the unconstrained optimization problem $\min \|Y - AB^T\|_q$, where $\|\cdot\|_q$ denotes a suitable matrix norm.
- 2) Solve $\min_{A \geq 0, B \geq 0} (1/2)\|\tilde{A}\tilde{B}^T - AB^T\|_F^2$ with fixed \tilde{A} and \tilde{B} , i.e., perform NMF on $\tilde{A}\tilde{B}^T$.

The purposes of LRA in Step 1 are twofold. First, it significantly reduces the subsequent computational complexity of ANLS. After Y is replaced by $\tilde{A}\tilde{B}^T$, the gradient $(\partial D_{\text{NLS}}/\partial A)$ becomes

$$\frac{\partial D_{\text{NLS}}}{\partial A} = -\tilde{A}(\tilde{B}^TB) + A(B^TB), \quad (5)$$

which can be computed in the complexity of $O(NR^2)$ and theoretically is about M/R times faster than the original version, provided that $R \ll M \leq N$ [13].

The second important purpose of applying LRA is to reduce the noise in data matrix Y , which is realized often by choosing a proper matrix norm $\|\cdot\|_q$ in Step 1 according to the distribution of noise. Popular LRA techniques include principal component analysis (PCA) and robust PCA (RPCA) [19] (see, e.g., [13] and references therein). Moreover, if Y contains missing values, one may use matrix completion techniques to complete it by exploiting its intrinsic low-rank structure [19]. Then NMF is applied to the low-rank representation of data. Of course, this two-stage procedure may not give the optimal solution. However, it is easy to

implement and provides an immediate and ad hoc suboptimal solution. Inevitably, the quality of LRA will affect the resulting accuracy of NMF. If the LRA is exact, there is no difference between the direct methods and the two-stage methods. However, if the error caused by LRA is significant, the final accuracy can be poor. In [13], the error bounds of LRA-based NMF has been theoretically investigated for $q = 2$. By exploiting the equivalence of matrix norms, similar results may be obtained easily for other q . Anyway, the LRA procedure should be performed very carefully in practice.

SEPARABLE NMF

The core idea of separable NMF is simple: it assumes that all columns of Y reside in a cone generated by R columns of Y (i.e., there exists at least one 1-sparse point on each extreme ray in Figure 1). Although separable NMF has been widely studied in the context of hyperspectral unmixing [20], [21], only since very recently has separable NMF shown great potential in handling very large-scale data by using linear programs [5], [22], [23]. Separable NMF has many attractive properties: 1) ordinary exact NMF is NP-hard, whereas separable NMF can be solved in polynomial time [22], [23], and can be parallelized and tailored for very large-scale problems; and 2) separable NMF is always essentially unique. Although separability is a strong assumption, unlikely to be satisfied exactly in many practical applications, however, in this case the large-scale data matrix often can be well approximated by separable NMF [22]. So far, separable NMF has been successfully applied to discover topics, find representative objects in a large-scale database, and improve clustering analysis [5], [22], [23]. In BSS, separable NMF corresponds to the pure-source dominance condition, which means that for some sample instants only one source is active or strongly dominant, i.e., assuming source sparsity. Under such an assumption, the non-negative sources can be efficiently separated by using (near) separable NMF, no matter whether they are statistically independent or not. Note that separable NMF also has a close relation with convex NMF [24] and convex hull NMF [6], where Y is approximated as $Y \approx YAB^T$ under nonnegativity constraints on factors. When A is restricted to be R columns of a permutation matrix, convex NMF boils down to separable NMF.

NONNEGATIVE COMMON FEATURE EXTRACTION OF MULTIBLOCK DATA

Very often the data we encounter is a collection of matrices rather than a single matrix, e.g., the electrophysiological signals

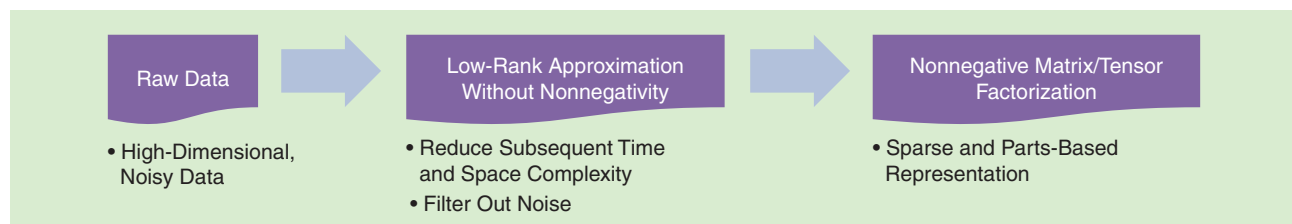


[FIG2] A diagram of the nonnegative matrix/tensor factorizations based on the LRA of high-dimensional noisy data.

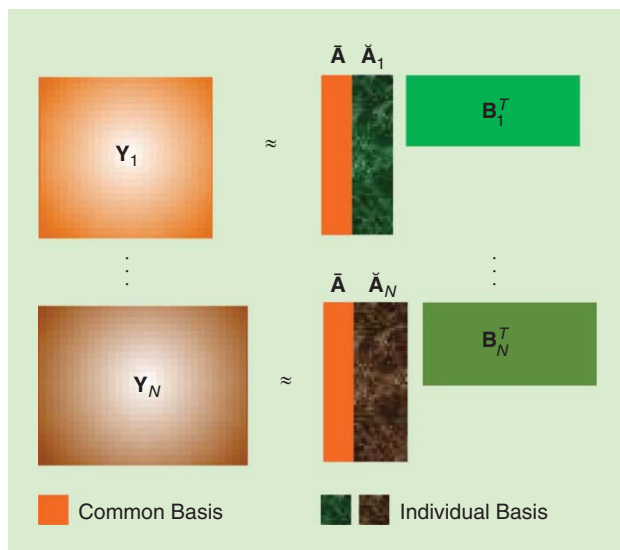


[FIG3] An illustration of nonnegative common and individual feature extraction. Each data matrix is represented as $Y_n \approx [\bar{A} \tilde{A}_n] B_n^T$, where $B_n = [B_n \tilde{B}_n]$, \bar{A} denotes the common components shared by all the matrices and \tilde{A}_n are their individual components.

recorded from different subjects and trials responding to specific stimuli. These multiblock data often share some common features and, at the same time, they have their own individual features, due to the background in which they are measured and collected. It is therefore meaningful to analyze such data blocks in a linked way rather than separately [25], [26]. By assuming that the multiblock data are spanned by a set of common components, group independent component analysis (ICA) and independent vector analysis have been proposed and achieved great success in multiblock functional magnetic resonance imaging data analysis [27], [28]. Besides sharing common components, however, we think the multiblock data also contain their individual components. To model such phenomena, given a set of nonnegative matrices $\mathcal{Y} = \{Y_n \in \mathbb{R}_+^{I \times J_n}, n \in \mathcal{I}_N\}$, we consider a linked NMF model such that (see Figure 3)

$$Y_n \approx \bar{A} \tilde{B}_n^T + \tilde{A}_n \check{B}_n^T, \quad n \in \mathcal{I}_N, \quad (6)$$

where $\bar{A} \in \mathbb{R}_+^{I \times C}$ denotes the common components shared by all data, while $\tilde{A}_n \in \mathbb{R}_+^{I \times (R_n - C)}$ denotes the individual components contained by the data Y_n only, R_n is the positive-rank of Y_n , $0 \leq C \leq R_n$ is the number of common components, and the nonnegative matrices \tilde{B}_n, \check{B}_n are the coefficients. Nonnegativity constraints and permission of existence of both common and individual components distinguish model (6) from existing group ICA methods [27], [28].

To solve (6), a straightforward approach is to minimize $\sum_{n \in \mathcal{N}} (1/2) \|Y_n - \bar{A} \tilde{B}_n^T - \tilde{A}_n \check{B}_n^T\|_F^2$ with respect to $\bar{A}, \tilde{B}_n, \tilde{A}_n, \check{B}_n$ by applying the ANLS method, which is similar to the joint and individual variation explained (JIVE) method [26] but with nonnegativity constraints. However, due to local convergence this approach may fail to extract the common components, especially when the common components are relatively weak.

Another way is to use a two-stage procedure. In the first step, the common and individual subspaces are separated such that $Y_n \approx \bar{U} \bar{R}_n^T + \check{U}_n \check{R}_n^T$, where \bar{U} and \check{U}_n are bases of the common and individual subspaces, respectively, and \bar{R}_n, \check{R}_n are the corresponding coefficients. This step can be done by using the JIVE [26] or common orthogonal basis extraction (COBE) methods [29], where $\bar{U}^T \check{U}_n = 0$ is imposed to achieve a perfect separation of the common and individual subspaces, and this restriction itself will not introduce any additional factorization error [29]. In Step 2, the nonnegative common and individual components are extracted from the respective subspaces. To extract nonnegative common components, we need to solve the following minimization problem:

$$\min_{\bar{A} \geq 0, B_n \geq 0} \sum_n \|\bar{U} \bar{R}_n^T - \bar{A} \tilde{B}_n^T\|_F^2 \quad (7)$$

by applying the ANLS framework for NMF. If we define $\bar{R} = [\bar{R}_1^T \bar{R}_2^T \dots \bar{R}_N^T]^T$ and $\tilde{B} = [\tilde{B}_1^T \tilde{B}_2^T \dots \tilde{B}_N^T]^T$, (7) is equivalent to NMF of $\bar{U} \bar{R}^T$ by applying the LRA and matrix partition techniques, where the latter is a quite useful technique when the matrices are too big to fit into a computer physical memory. Due to the restriction $\bar{U}^T \check{U}_n = 0$, we have $\bar{A}_n^T \tilde{A}_n \approx 0$, which enforces perfect separation of the nonnegative common and individual components, but could lead to larger fitting error (on the contrary, the first approach achieves better fitting while permitting some interactions between the nonnegative common and individual components). Note also that this approach can be viewed as a relaxed version of orthogonal NMF that requires that the nonnegative matrix $A_n = [\bar{A} \tilde{A}_n]$ to be orthogonal [30], if we treat each data Y_n separately. As orthogonal NMF is equivalent to K-means clustering ([30, Th. 1]), the proposed method could be extended to perform linked clustering analysis of multiblock data.

NONNEGATIVE TENSOR DECOMPOSITIONS

In analogy to matrix factorizations, tensor decompositions are developed to analyze high-dimensional tensor data, which have been given increasing importance in recent signal processing and machine-learning applications [1], [31]–[33]. In the past, high-order tensors were reshaped and formatted as matrices such that standard matrix factorization techniques could be applied directly. However, this treatment often causes the loss of useful multiway structure information of data. It is more favorable to analyze these data in their own domain, i.e., tensor domain. In Table 2 we list some basic notations and operations for tensors; readers may refer to [31] for more details.

One of the most widely used model for tensor decompositions is the Tucker model (see [1], [31], and references therein), where a given tensor $\mathcal{Y} \in \mathbb{R}^{I_1 \times I_2 \times \dots \times I_N}$ is decomposed as

$$\mathcal{Y} = \mathcal{G} \times_1 A^{(1)} \times_2 A^{(2)} \dots \times_N A^{(N)} = \mathcal{G} \times_{n \in \mathcal{I}_N} A^{(n)}. \quad (8)$$

$A^{(n)} \in \mathbb{R}^{I_n \times R_n}$ is the mode- n (factor, component) matrix consisting of latent components $a_r^{(n)}$ as its columns, $n \in \mathcal{I}_N, r \in \mathcal{I}_{R_n}$, and $\mathcal{G} \in \mathbb{R}^{R_1 \times R_2 \times \dots \times R_N}$ is the core tensor reflecting interactions

[TABLE 2] NOTATIONS AND PROPERTIES FOR TENSORS.

GIVEN AN n th-ORDER TENSOR $\mathcal{G} \in \mathbb{R}^{R_1 \times R_2 \times \dots \times R_n}$, THE NOTATIONS AND PROPERTIES LISTED BELOW WILL BE USED [31]:

FIBERS: A MODE- n FIBER OF A TENSOR IS A COLUMN VECTOR DEFINED BY FIXING EVERY INDEX EXCEPT FOR n .

MATRICIZATION $\mathbf{G}_{(n)}$: THE MODE- n MATRICIZATION OF \mathcal{G} YIELDS A R_n -BY- $\prod_{p \neq n} R_p$ MATRIX DENOTED BY $\mathbf{G}_{(n)}$, WHOSE COLUMNS CONSIST OF ALL MODE- n FIBERS OF \mathcal{G} .

MODE PRODUCT \times_n : THE MODE- n PRODUCT OF \mathcal{G} AND $\mathbf{A} \in \mathbb{R}^{I_n \times R_n}$ YIELDS A TENSOR $\mathcal{Y} = \mathcal{G} \times_n \mathbf{A} \in \mathbb{R}^{R_1 \times \dots \times R_{n-1} \times I_n \times R_{n+1} \times \dots \times R_n}$ WHOSE ENTRIES ARE DEFINED BY $y_{i_1 \dots i_{n-1} i_{n+1} \dots i_n} = \sum_{j_n=1}^{R_n} g_{i_1 i_2 \dots i_n} a_{j_n i_n}$. NOTE THAT $\mathcal{Y} = \mathcal{G} \times_n \mathbf{A} \Leftrightarrow \mathbf{Y}_{(n)} = \mathbf{A} \mathbf{G}_{(n)}$.

OUTER PRODUCT \circ : THE OUTER PRODUCT OF n VECTORS YIELDS A RANK-1 n th-ORDER TENSOR. FOR EXAMPLE, $\mathbf{a} \circ \mathbf{b} \circ \mathbf{c}$ YIELDS A THIRD-ORDER TENSOR \mathcal{Y} WHOSE ELEMENTS ARE DEFINED AS $y_{ijk} = a_i b_j c_k$, WHERE \mathbf{a} , \mathbf{b} , AND \mathbf{c} ARE COLUMN VECTORS.

LET $\mathcal{K} = \{i_1, i_2, \dots, i_k\}$ BE ANY NONEMPTY SUBSET OF I_N WITH FIXED ORDER OF ELEMENTS, WE SYMBOLICALLY DEFINE

- 1) $\mathcal{G} \times_{k \in \mathcal{K}} \mathbf{A}^{(k)} \triangleq \mathcal{G} \times_{i_1} \mathbf{A}^{(i_1)} \times_{i_2} \mathbf{A}^{(i_2)} \dots \times_{i_k} \mathbf{A}^{(i_k)}$
- 2) $\otimes_{k \in \mathcal{K}} \mathbf{A}^{(k)} \triangleq \mathbf{A}^{(i_k)} \otimes \mathbf{A}^{(i_{k-1})} \dots \otimes \mathbf{A}^{(i_1)}$ (THE INVERSE ORDER OF i_k); SIMILARLY FOR \odot AND \circledast .

between the components in each factor matrix. Generally, $R_n \ll I_n$ to achieve data compression. The Tucker model is quite flexible and it is the foundation of many multiway data analysis tools [34]. However, Tucker decomposition suffers from rotation ambiguity. To achieve essentially unique decomposition with physically meaningful components additional constraints are often essential.

In the special case of (8) where $R_1 = R_2 = \dots = R_N = R$ and the core tensor \mathcal{G} is diagonal, we obtain the polyadic decomposition (PD), also known as parallel factor analysis (PARAFAC) (see [1], [31], and references therein). In PDs, a given tensor \mathcal{Y} is represented as the sum of rank-1 terms

$$\mathcal{Y} = \sum_{r=1}^R \lambda_r \mathbf{a}_r^{(1)} \circ \mathbf{a}_r^{(2)} \dots \circ \mathbf{a}_r^{(N)}. \quad (9)$$

For simplicity, we use $\mathcal{Y} = \llbracket \mathbf{A}^{(1)}, \mathbf{A}^{(2)}, \dots, \mathbf{A}^{(N)} \rrbracket$ as a shorthand notation of (9), where λ_r are absorbed into $\mathbf{A}^{(n)}$. The minimum R making (9) exact is called the rank of the tensor \mathcal{Y} , and in this case (9) is called canonical PD (CANDECOMP or CPD) of \mathcal{Y} . Different from Tucker decompositions, CPD is free of rotation ambiguity and essentially unique under mild conditions [35]. Moreover, the minimum value of R making (9) exact under nonnegativity constraints is called the nonnegative-rank of \mathcal{Y} . Apparently, for any nonnegative tensor the tensor rank is always no greater than the nonnegative rank.

Hereafter we focus on tensor decompositions with nonnegativity constraints imposed on the factors, which is referred to as nonnegative tensor decompositions that not only inherit all the advantages of NMF, but also enjoy additional multilinear structure benefits of multiway data. The general scheme for nonnegative tensor decompositions based on ANLS is illustrated in Figure 4, while details are given in the following sections based on the polyadic and Tucker models.

FAST NTD BASED ON LRA AND SEQUENTIAL NMF

For a given tensor \mathcal{Y} , by NTD we seek a nonnegative tensor $\hat{\mathcal{Y}} = \mathcal{G} \times_{n \in I_N} \mathbf{A}^{(n)}$ that minimizes the cost function $D_{\text{NTD}} =$

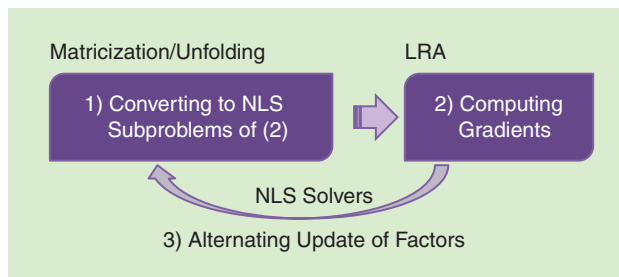


[FIG4] A general ANLS scheme for nonnegative tensor decompositions.

$(1/2) \|\mathcal{Y} - \hat{\mathcal{Y}}\|_F^2$, such that both $\mathbf{A}^{(n)}$ and \mathcal{G} are nonnegative [see (8)]. Considering the mode- n matricizations of \mathcal{Y} and $\hat{\mathcal{Y}}$ in D_{NTD} , i.e., $\mathbf{Y}_{(n)}$ and $\hat{\mathbf{Y}}_{(n)}$, we have

$$D_{\text{NTD}} = \frac{1}{2} \|\mathbf{Y}_{(n)} - \mathbf{A}^{(n)} \mathbf{B}^{(n)T}\|_F^2, \quad (10)$$

where $\mathbf{B}^{(n)} = [\otimes_{p \in I_N \setminus \{n\}} \mathbf{A}^{(p)}] \mathbf{G}_{(n)}^T$ and $\mathbf{G}_{(n)}$ is the mode- n matricization of \mathcal{G} [31]. By vectorizing \mathcal{Y} and $\hat{\mathcal{Y}}$, D_{NTD} can also be written as $D_{\text{NTD}} = (1/2) \|\text{vec}(\mathcal{Y}) - [\otimes_{n \in I_N} \mathbf{A}^{(n)}] \text{vec}(\mathcal{G})\|_F^2$, where $\text{vec}(\cdot)$ is the vectorization operator [31]. These two equivalent forms of D_{NTD} allow us to perform NTD by applying the ANLS straightforwardly with respect to $\mathbf{A}^{(n)}$ and \mathcal{G} . For example, in [36] the multiplicative update rules have been applied to perform NTD. However, computing the matrix $\mathbf{B}^{(n)}$ in each iteration is too expensive, and frequent matricization of tensor \mathcal{Y} is also quite time- and space-consuming for large-scale data.

One efficient approach that allows us to significantly reduce the time and space complexity is to apply the idea of LRA to NTD. Suppose we have achieved a compressed unconstrained Tucker representation of \mathcal{Y} such that $\mathcal{Y} \approx \hat{\mathcal{Y}} = \mathcal{G} \times_{n \in I_N} \hat{\mathbf{A}}^{(n)}$, where $\hat{\mathbf{A}}^{(n)} \in \mathbb{R}^{I_n \times R_n}$ (This can be done, e.g., by using truncated multilinear singular vector decomposition (MLSVD) [37]). Then we minimize $D_{\text{NTD}} = (1/2) \|\hat{\mathcal{Y}} - \mathcal{Y}\|_F^2$, where the gradients can be computed efficiently as

**ONE EFFICIENT APPROACH THAT
 ALLOWS US TO SIGNIFICANTLY
 REDUCE THE TIME AND SPACE
 COMPLEXITY IS TO APPLY
 SUITABLE LOW-RANK
 APPROXIMATION OF DATA.**

One efficient approach that allows us to significantly reduce the time and space complexity is to apply the idea of LRA to NTD. Suppose we have achieved a compressed unconstrained Tucker representation of \mathcal{Y} such that $\mathcal{Y} \approx \hat{\mathcal{Y}} = \mathcal{G} \times_{n \in I_N} \hat{\mathbf{A}}^{(n)}$, where $\hat{\mathbf{A}}^{(n)} \in \mathbb{R}^{I_n \times R_n}$ (This can be done, e.g., by using truncated multilinear singular vector decomposition (MLSVD) [37]). Then we minimize $D_{\text{NTD}} = (1/2) \|\hat{\mathcal{Y}} - \mathcal{Y}\|_F^2$, where the gradients can be computed efficiently as

$$\begin{aligned} \frac{\partial D_{\text{NTD}}}{\partial \mathbf{A}^{(n)}} &= -\tilde{\mathbf{X}}_{(n)} \mathbf{G}_{(n)}^T + \mathbf{X}_{(n)} \mathbf{G}_{(n)}^T, \\ \frac{\partial D_{\text{NTD}}}{\partial \mathcal{G}} &= -\tilde{\mathcal{G}} \times_{n \in \mathcal{I}_N} \tilde{\mathbf{C}}^{(n)} + \mathcal{G} \times_{n \in \mathcal{I}_N} \mathbf{C}^{(n)}, \end{aligned} \quad (11)$$

where $\mathbf{C}^{(n)} = \mathbf{A}^{(n)T} \mathbf{A}^{(n)}$, $\tilde{\mathbf{C}}^{(n)} = \mathbf{A}^{(n)T} \tilde{\mathbf{A}}^{(n)}$, $\tilde{\mathbf{X}}_{(n)}$ and $\mathbf{X}_{(n)}$ are mode- n matricizations of $\tilde{\mathcal{X}}$ and \mathcal{X} , respectively, and

$$\begin{aligned} \tilde{\mathcal{X}} &= \tilde{\mathcal{G}} \times_{p \in \mathcal{I}_N \setminus \{n\}} \tilde{\mathbf{C}}^{(p)} \times_n \tilde{\mathbf{A}}^{(n)}, \\ \mathcal{X} &= \mathcal{G} \times_{p \in \mathcal{I}_N \setminus \{n\}} \mathbf{C}^{(p)} \times_n \mathbf{A}^{(n)}. \end{aligned} \quad (12)$$

Based on (11), any NLS solver can be applied to optimize $\mathbf{A}^{(n)}$ and \mathcal{G} but without directly accessing the large-scale tensor \mathcal{Y} , thereby leading to significantly reduced time and space complexity. We call this method LRNTD.

Another alternative efficient solution is to avoid frequently unfolding operations by applying unique NMF algorithms to extract each non-negative factor sequentially rather than simultaneously, typically by starting with the sparsest factors $\mathbf{A}^{(n)}$

incorporating on it a sparsity penalty. Suppose that the factor $\mathbf{A}^{(n)}$ can be essentially uniquely estimated by running a suitable NMF algorithm on $\mathbf{Y}_{(n)}$. Then \mathcal{Y} is updated as $\mathcal{Y} \leftarrow \mathcal{Y} \times_n \mathbf{A}^{(n)\dagger}$ and we move to the next factor. This method is similar to the multilinear SVD, but orthogonality is replaced by nonnegativity and here is referred to as NTD based on sequential (unique) NMF (NTDSNMF) (see [13]).

FAST NPD BASED ON DIMENSIONALITY AND MODE REDUCTION

Historically, NPD is also referred to as nonnegative tensor factorization in the literature [1], [31], [38], [39]. Quite different from unconstrained PDs, a nonnegative tensor with nonnegative-rank R always has the best nonnegative-rank- r approximations for any $r \leq R$ [38]. Consequently, in the case where the unconstrained PD is not unique or ill posed, NPD may help to extract desired unique components [38], [39]. Moreover, NPD is able to give sparse, parts-based, and physically meaningful representation of high-order tensors. NPD is therefore a very important research topic and has been found many practical applications.

NONNEGATIVE TENSOR DECOMPOSITIONS NOT ONLY INHERIT THE ADVANTAGES OF NMF, BUT ALSO ENJOY ADDITIONAL MULTILINEAR STRUCTURE BENEFITS OF MULTIWAY DATA.

NPD BASED ON LRA

Noticing that unconstrained PD generally converges significantly faster than NPD, we update \mathcal{Y} by its LRA such that $\mathcal{Y} \approx \tilde{\mathcal{Y}} =$

For a given tensor \mathcal{Y} , by NPD we seek a tensor $\hat{\mathcal{Y}} = \llbracket \mathbf{A}^{(1)}, \mathbf{A}^{(2)}, \dots, \mathbf{A}^{(N)} \rrbracket$ minimizing the cost function $D_{\text{NPD}} = (1/2) \|\mathcal{Y} - \hat{\mathcal{Y}}\|_F^2$, where $\mathbf{A}^{(n)} \in \mathbb{R}_+^{I_n \times R}$, $n \in \mathcal{I}_N$. By considering the mode- n matricizations of \mathcal{Y} and $\hat{\mathcal{Y}}$ in D_{NPD} , i.e., $\mathbf{Y}_{(n)}$ and $\hat{\mathbf{Y}}_{(n)}$, we need to solve

$$\min_{\mathbf{A}^{(n)} \geq 0} D_{\text{NPD}} = \frac{1}{2} \|\mathbf{Y}_{(n)} - \mathbf{A}^{(n)} \mathbf{B}^{(n)T}\|_F^2, \quad n \in \mathcal{I}_N, \quad (13)$$

where $\mathbf{B}^{(n)} = \bigcirc_{p \in \mathcal{I}_N \setminus \{n\}} \mathbf{A}^{(p)}$ [31]. Based on (13) we can apply the ANLS with respect to $\mathbf{A}^{(n)}$ to perform NPD [1], [40]. However, direct computations of the gradients $(\partial D_{\text{NPD}} / \partial \mathbf{A}^{(n)}) = -\mathbf{Y}_{(n)} \mathbf{B}^{(n)} + \mathbf{A}^{(n)} \mathbf{B}^{(n)T} \mathbf{B}^{(n)}$ are quite expensive and it is therefore crucial to find more efficient way to compute the gradients [41].

$\llbracket \tilde{\mathbf{A}}^{(1)}, \tilde{\mathbf{A}}^{(2)}, \dots, \tilde{\mathbf{A}}^{(N)} \rrbracket$ in D_{NPD} , thereby leading to $D_{\text{NPD}} = (1/2) \|\tilde{\mathbf{A}}^{(n)} \tilde{\mathbf{B}}^{(n)T} - \mathbf{A}^{(n)} \mathbf{B}^{(n)T}\|_F^2$, where $\tilde{\mathbf{B}}^{(n)} = \bigcirc_{p \in \mathcal{I}_N \setminus \{n\}} \tilde{\mathbf{A}}^{(p)}$, and hence

$$(\partial D_{\text{NPD}} / \partial \mathbf{A}^{(n)}) = -\tilde{\mathbf{A}}^{(n)} [\tilde{\mathbf{B}}^{(n)T} \mathbf{B}^{(n)}] + \mathbf{A}^{(n)} [\mathbf{B}^{(n)T} \mathbf{B}^{(n)}].$$

The key point is that, due to the special structure of $\tilde{\mathbf{B}}^{(n)}$ and $\mathbf{B}^{(n)}$, $\tilde{\mathbf{B}}^{(n)T} \mathbf{B}^{(n)} = \bigoplus_{p \in \mathcal{I}_N \setminus \{n\}} (\tilde{\mathbf{A}}^{(p)T} \mathbf{A}^{(p)})$, similarly for $\mathbf{B}^{(n)T} \mathbf{B}^{(n)}$, both of which can be economically computed during the iterations.

NPD USING MODE REDUCTION

Another key factor affecting the efficiency of NPD is the order of the data tensor N . NPD algorithms that are based on the ANLS framework require to unfold (matricize) the tensor N times in each iteration, which consumes considerable memory and time when $N \gg 3$. To overcome this problem, the mode reduction method [42] can be applied to NPD of high-order tensors. To explain this idea, suppose $\mathcal{Y} = \llbracket \mathbf{A}^{(1)}, \mathbf{A}^{(2)}, \dots, \mathbf{A}^{(N)} \rrbracket$. We can reshape the N th-order tensor \mathcal{Y} properly to yield a third-order tensor $\mathcal{Y}^{(3)}$ by merging (combining) some modes of \mathcal{Y} . It turns out that the components of $\mathcal{Y}^{(3)} = \llbracket \mathbf{H}^{(1)}, \mathbf{H}^{(2)}, \mathbf{H}^{(3)} \rrbracket$ satisfy that

$$\mathbf{H}^{(k)} = \bigcirc_{p \in \mathcal{S}_k} \mathbf{A}^{(p)}, \quad k = 1, 2, 3, \quad (14)$$

where \mathcal{S}_k are pair-wisely disjoint, nonempty subsets of \mathcal{I}_N with $\cup_{k=1,2,3} \mathcal{S}_k = \mathcal{I}_N$. The mode reduced tensor $\mathcal{Y}^{(3)}$ has many interesting properties [42]. Particularly, if \mathcal{Y} satisfies the uniqueness conditions given in [35], there always exists at least one mode reduced tensor $\mathcal{Y}^{(3)}$ whose CPD is also unique. Moreover, the components of $\mathcal{Y}^{(3)}$ are generally of less collinearity than those of \mathcal{Y} (these properties are also true for any $\mathcal{Y}^{(K)}$, $3 \leq K < N$ [42]). Equation (14) allows us to estimate $\mathbf{A}^{(p)}$, $p \in \mathcal{S}_k$, from $\mathbf{H}^{(k)}$ efficiently and uniquely via a Khatri-Rao product approximation [42]. This motivates us to perform NPD on a properly mode-reduced tensor $\mathcal{Y}^{(3)}$ that has unique NPD of $\mathcal{Y}^{(3)} = \llbracket \mathbf{H}^{(1)}, \mathbf{H}^{(2)}, \mathbf{H}^{(3)} \rrbracket$, and

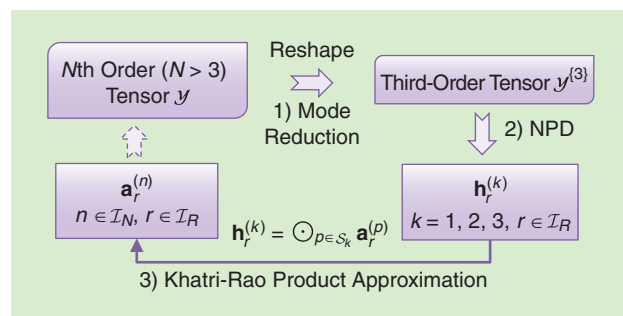


[FIG5] The diagram of NPD based on mode reduction of high-order tensors ($N > 3$).

then to recover the factors $A^{(n)}$ from $H^{(k)}$ ($k = 1, 2, 3$) by exploiting the Khatri–Rao product structure (14); see Figure 5 for the diagram of this method. This method can be much faster than direct NPD of the original high-order tensor, because frequently unfolding to each of the N modes is avoided and the mode-reduced tensors often have well-conditioned factor matrices.

How to merge the modes is crucial to the mode reduction-based method [42]. Theoretically, the two factor matrices having the smallest Kruskal ranks should be merged first to largely maintain the uniqueness property. However, as the Kruskal ranks of factors are unknown before factorization, we often merge the modes whose corresponding matricizations have the smallest ranks first [42].

Next, we briefly discuss how to recover $A^{(n)}$ from $H^{(k)}$ using (14). For simplicity, we let $H \doteq H^{(k)}$, $k = 1, 2, 3$, and consider the following Khatri–Rao product approximation problem

$$\min_{A^{(p)} \geq 0} \|H - \bigcirc_{p \in S_k} A^{(p)}\|_F^2. \quad (15)$$

Let $\mathcal{H}^{(r)}$ be the tensor formed by reshaping the r th column of H according to the dimension of $\mathbf{a}_r^{(p)}$, $p \in S_k$. Then the tensorial power iteration method followed by nonnegative projection can be used to update $\mathbf{a}_r^{(p)}$ [42]

$$\mathbf{a}_r^{(p)} \leftarrow \mathcal{P}_+ \left(\frac{\mathcal{H}^{(r)} \times_{j \in S_k \setminus \{p\}} \mathbf{a}_r^{(j)T}}{\prod_{j \in S_k \setminus \{p\}} \|\mathbf{a}_r^{(j)}\|_2} \right). \quad (16)$$

Repeat (16) for all $p \in S_k$ until convergence, the r th columns of $A^{(p)}$ will be estimated. Then, we repeat the procedure for all $k = 1, 2, 3$, which can be done in a parallel way for all k and r .

FAST NPD BASED ON ESSENTIALLY UNIQUE NMF

Below we discuss the possibility of using $\mathcal{Y}^{(2)} = \llbracket H^{(1)}, H^{(2)} \rrbracket$ in the aforementioned mode-reduction method. Note that $\mathcal{Y}^{(2)}$

IT IS WORTH NOTICING THAT MULTILINEAR STRUCTURES IN NONNEGATIVE TENSOR DECOMPOSITIONS INTRINSICALLY ENFORCE SPARSE REPRESENTATIONS.

is actually a matrix such that $\mathcal{Y}^{(2)} = H^{(1)}H^{(2)T}$ that generalizes the concept of standard matricization of tensors [cf. (13)]. Hence, we may perform NMF on matrix $\mathcal{Y}^{(2)}$ first to obtain factor matrices $H^{(1)}$ and $H^{(2)}$, and then we recover $A^{(n)}$ from $H^{(1)}$ and $H^{(2)}$ by solving (15).

However, this approach works only if the NMF of $\mathcal{Y}^{(2)}$ is essentially unique, e.g., both $H^{(1)}$ and $H^{(2)}$ are sufficiently sparse. Fortunately, in general, the Khatri–Rao products (14) substantially improve the sparsity level.

PROPOSITION 1

Let $\mathbf{a} \in \mathbb{R}^{M \times 1}$ and $\mathbf{b} \in \mathbb{R}^{N \times 1}$. Then $z_{\mathbf{a} \circ \mathbf{b}} = Nz_{\mathbf{a}} + Mz_{\mathbf{b}} - z_{\mathbf{a}}z_{\mathbf{b}}$ and $s_{\mathbf{a} \circ \mathbf{b}} = s_{\mathbf{a}} + s_{\mathbf{b}} - s_{\mathbf{a}}s_{\mathbf{b}}$, which means that $\max(s_{\mathbf{a}}, s_{\mathbf{b}}) \leq s_{\mathbf{a} \circ \mathbf{b}}$.

In other words, both $H^{(1)}$ and $H^{(2)}$ can be very sparse and the NMF of $\mathcal{Y}^{(2)}$ is very likely to be essentially unique, provided that $A^{(n)}$ are sufficiently sparse. In [43], we considered the special case where one specific factor matrix can be essentially uniquely estimated by incorporating suitable a priori information on this factor. Particularly, it can be shown that if one factor matrix satisfies the separable condition, $\mathcal{Y}^{(2)}$ also satisfies the separable condition. In such a case, the NMF of $\mathcal{Y}^{(2)}$ is essentially unique and the above method can be applied.

IMPROVED SPARSITY AND UNIQUENESS OF NONNEGATIVE TENSOR DECOMPOSITIONS

It is worth noticing that multilinear structures in nonnegative tensor decompositions intrinsically enforce sparse representations. By NPD, a tensor \mathcal{Y} can be represented as $Y_{(n)}^T = B^{(n)}A^{(n)T}$ by using the mode- n matricization, where $B^{(n)} = \bigcirc_{p \in I_N \setminus \{n\}} A^{(p)}$. Hence if $B^{(n)}$ is interpreted as the basis matrix, from Proposition 1, it is usually very sparse. This sparsity comes from the sparsity of $A^{(p)}$ ($p \neq n$), and is enhanced by the Khatri–Rao product structure of $B^{(n)}$. We call $B^{(n)}$ a Khatri–Rao product basis. By NTD a tensor \mathcal{Y} can be represented as $Y_{(n)}^T = R^{(n)}G_{(n)}^T A^{(n)T}$ by

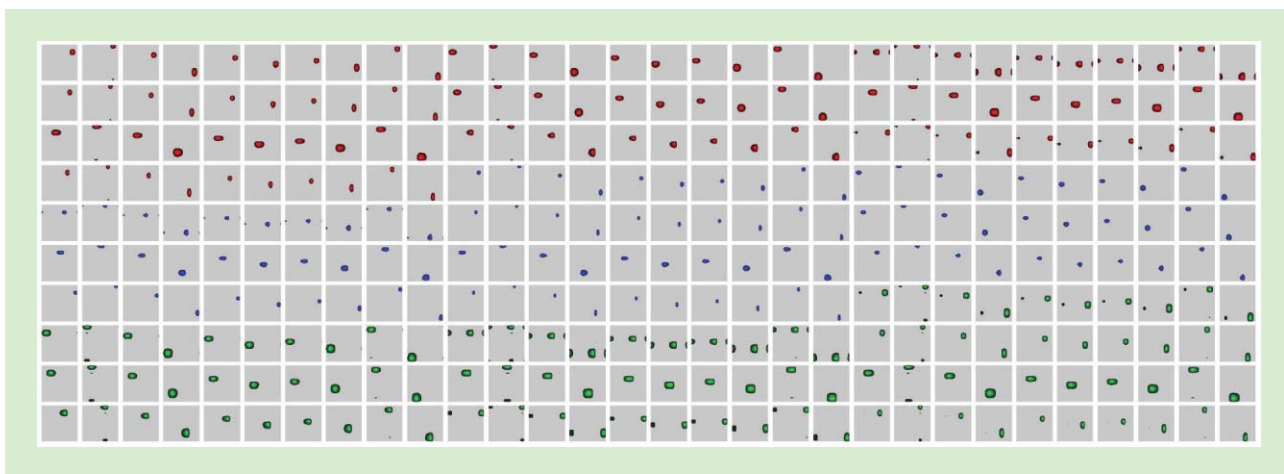


[FIG6] A very sparse and parts-based Kronecker basis (i.e., $\bigotimes_{n \in \{1, 2, 3\}} A^{(n)}$) extracted from the COIL-100 database obtained by the LRNTD based on HALS, which is often used for feature extraction in clustering and classification tasks.

[TABLE 3] THE PERFORMANCE COMPARISON OF THE NMF ALGORITHMS ON SYNTHETIC DATA. THE SIR VALUES AND TIME OF THE PLAIN MODE WERE NOT LISTED AS ALL THE ALGORITHMS FAILED TO RECOVER THE ORIGINAL SOURCES (THE CORRESPONDING SIR VALUES WERE LOWER THAN 10 dB) IN THIS MODE.

ALGORITHMS	PLAIN	FIT (%)			SIR (dB)		TIME (S)	
		RPCA	LRA	LRA	RPCA	LRA	RPCA	LRA
MU	74.3 ± 0.4	93.8 ± 0.0	94.1 ± 0.1	24.5 ± 6.7	24.5 ± 6.8	560.6	170.5	
BPP	74.1 ± 0.4	99.1 ± 0.5	99.1 ± 0.5	28.4 ± 7.1	28.4 ± 7.1	848.1	286.8	
NENMF	74.1 ± 0.4	99.2 ± 0.3	99.4 ± 0.3	29.4 ± 6.1	33.0 ± 5.7	345.0	156.7	
GCD	74.6 ± 0.4	99.4 ± 0.3	99.3 ± 0.3	33.0 ± 5.7	31.8 ± 6.1	325.8	111.1	
HALS	74.2 ± 0.4	99.3 ± 0.3	99.4 ± 0.3	32.8 ± 6.1	33.1 ± 5.7	329.9	57.9	

using the mode- n matricization, where $\mathbf{R}^{(n)} = \otimes_{p \in \mathcal{I}_N \setminus \{n\}} \mathbf{A}^{(p)}$, $n \in \mathcal{I}_N$. If $\mathbf{R}^{(n)}$ is interpreted as the basis matrix, it can also be very sparse due to its Kronecker product structure, and we called it a Kronecker product basis of \mathcal{Y} . In summary, compared with NMF, nonnegative tensor decompositions are able to provide sparser bases, which have multilinear structures. See Figure 6 for a visualization of a very sparse Kronecker product basis of real-world data. Such sparse representation often allows us to perform efficient classification or clustering tasks [1].

As NPD is a special case of unconstrained PD, the uniqueness conditions of PD [35] can be applied to NPD straightforwardly once the nonnegative-rank is equal to the rank. However, the nonnegativity constraints may lead to more relaxed uniqueness conditions. We believe that both NPD and NTD should be essentially unique as long as the latent factors are sufficiently sparse, nevertheless, comprehensive analysis on uniqueness of nonnegative tensor decompositions is still an open issue.

SIMULATIONS

All the simulations were performed in MATLAB 2008a on a PC with i7CPU 3.33 GHz and 24-GB memory running Windows 7.

SYNTHETIC DATA BENCHMARK

We compared the introduced NMF algorithms using synthetic data generated by $\mathbf{Y} = \mathbf{A}\mathbf{B}^T + \mathbf{E}$, where $\mathbf{A}, \mathbf{B} \in \mathbb{R}_+^{10,000 \times 50}$ and $\mathbf{A} \sim U(0, 1)$, $\mathbf{B} \sim U(0, 1)$. Note that all the NMF algorithms using the Euclidean distance are essentially based on the independent and identically distributed Gaussian noise assumption. To investigate their flexibility and robustness to non-Gaussian noise, we added Gaussian noise (with SNR=20 dB) to the only randomly selected 1,000 entries of \mathbf{Y} to be outliers. In other words, the noise term \mathbf{E} contained only 1,000 nonzero entries. The elements of \mathbf{A} and \mathbf{B} , which were less than 0.5, were set to zero to generate sparse factors. The algorithms we compared included the MU algorithm [2], the BPP based on the active-set method [15], the NeNMF using the APG method [16], the greedy coordinate descent (GCD) algorithm [44], and the HALS algorithm [1]. For each NMF algorithm we tested three modes: 1) the plain mode that applied NMF to the noisy data directly; 2) the RPCA mode that applied NMF to the cleaned data preprocessed by using the RPCA [19]; 3) the LRA mode that used the LRAs

(obtained by using truncated SVD) of cleaned data to accelerate each NMF algorithm, in addition to 2). In each run all the algorithms started from the same initial matrices with the maximum iteration number 500. Their performance averaged over ten Monte Carlo runs was shown in Table 3, where the signal-to-interference ratio (SIR) evaluates how well the estimated components match their original ones, and the fit = $(1 - (\|\mathbf{Y} - \mathbf{A}\mathbf{B}^T\|_F / \|\mathbf{Y}\|_F)) \times 100\%$. From the table, we can conclude that

- using suitable LRA techniques to reduce noise prior to NMF is crucial to improve the accuracy. In this case, it is often unnecessary to develop special NMF algorithms for different noise distributions. Instead, we may use suitable LRA methods to substantially reduce noise without considering the nonnegativity constraints prior to applying NMF.
- for cleaned data (i.e., the RPCA mode and the LRA mode), all algorithms with or without LRA achieved almost the same factorization accuracy in terms of fits and SIRs. However, their LRA-based implementations were always much faster than their original ones (the time consumed by RPCA was not counted in both cases). This improvement can be very remarkable for large-scale data.
- as the factors were very sparse (50% entries were zeros) and the number of observations was significantly larger than the number of components, all the true sources were accurately estimated by all NMF algorithms with the RPCA preprocessing. This justifies that NMF may be used a BSS tool when the sources and/or mixing matrix are very sparse and nonnegative.

COIL-100 IMAGES ANALYSIS

In this simulation, we used NTD methods to extract sparse bases of the Columbia Object Image Library (COIL-100, available at <http://www.cs.columbia.edu/CAVE/software/software-lib/coil-100.php>), which is a database of color images of 100 objects, and each object has 72 images. Each image was rescaled as 128×128 . These images formed a big tensor with the size of $128 \times 128 \times 3 \times 7200$. We compared the higher-order NMF (HONMF) algorithm [36], the NTDSNMF algorithm [13], and the new proposed LRANTD based on the MU and the HALS updates, respectively. As our purposes were to illustrate the learning-parts ability of NTD and to compare

the efficiency of NTD algorithms, we simply set the numbers of components as $R_1 = R_2 = 10$, $R_3 = 3$, $R_4 = 100$ for all algorithms (in practical applications, however, we may use the Bayesian information criterion or generalized information criterion [18] to select these parameters) for better visualization, which results in $\otimes_{n \in \{1,2,3\}} \mathbf{A}^{(n)}$ composed of 300 basis images ($128 \times 128 \times 3$) as its columns. We set the maximum iteration numbers to be 100. In the LRANTD, the multilinear SVD [37] was applied to perform LRA. See Table 4 for their performance, where fit is defined similarly as for matrices. Obviously, the NTDSNMF algorithm and the proposed LRANTD algorithms significantly outperformed the standard NTD algorithm HONMF. Figure 6 visualized the Kronecker product basis extracted by LRANTD based on HALS, showing that NTD can provide very sparse bases that are useful in clustering and classification tasks [1].

FACE IMAGES CLUSTERING ANALYSIS

We applied the nonnegative common feature extraction (NCFE) to cluster analysis of human face images. Intuitively, all face images should share some common features as they have common facial characteristics such as cheeks, eyes, and a mouth, whose locations and shapes are similar to some extent. These common features that are presented in all faces are less important for clustering as they do not provide any discriminative information. It is therefore reasonable to remove these common or similar features at first and then use the individual features only to cluster the faces. We validated this idea on the Carnegie Mellon University (CMU) pose, illumination, and expression (PIE) face database (available at <http://vasc.ri.cmu.edu/idb/html/face/>), which is a collection of face images of 68 persons taken under different poses, illumination conditions, and expressions. We used the preprocessed version considered in [45], which consists of 2,856 full frontal face gray-scale images taken at the front pose labeled as c27. Each time we randomly selected K clusters/persons ($K \in \{30, 40, 50, 60, 68\}$). To extract their common features, in each run we permuted the images randomly first and then split them into, for simplicity, K groups to obtain $\mathbf{Y}_{(k)}$, $k \in \mathcal{I}_K$, (each group consisted of face images from unknown different clusters). Then we used the common orthogonal basis extraction [29] to extract the common subspace and then used the NCFE to extract the nonnegative common features. The number of common components was empirically specified as two. After removing the nonnegative common subspace, i.e., the term $\bar{\mathbf{A}}\mathbf{B}_n^T$ in (6), we obtained their individual features. Finally, two components extracted by using the t-distributed stochastic neighbor embedding (tSNE) method [46] from their individual subspace were used to cluster the faces by using the K -means method. As K -means is sensitive to initial centers of clusters, we replicated K -means 20 times in each run. The proposed method was compared with the PCA using 50 principal components, the graph regularized NMF [45], the tSNE, and the improved MinMax Cut method [47].

The mean values and the standard variations of accuracy over 20 Monte Carlo runs were detailed in Figure 7 (the

[TABLE 4] THE PERFORMANCE OF THE NTD ALGORITHMS IN COIL-100 IMAGES DECOMPOSITIONS.

ALGORITHM	HONMF	NTDSNMF	LRANTD_MU	LRANTD_HALS
FIT (%)	63.1	75.3	75.5	75.6
TIME (s)	50,351	232	112	103

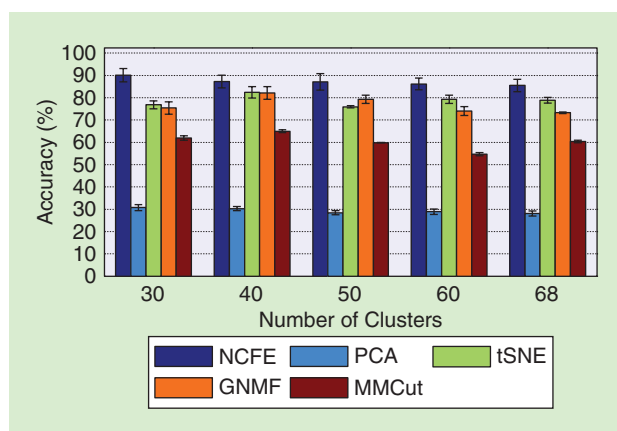


[FIG7] A comparison of clustering performance on the PIE database. In the NCFE-based method, the nonnegative common components were removed first and then the individual components were used for clustering analysis. The NCFE method achieved considerable improvement of performance.

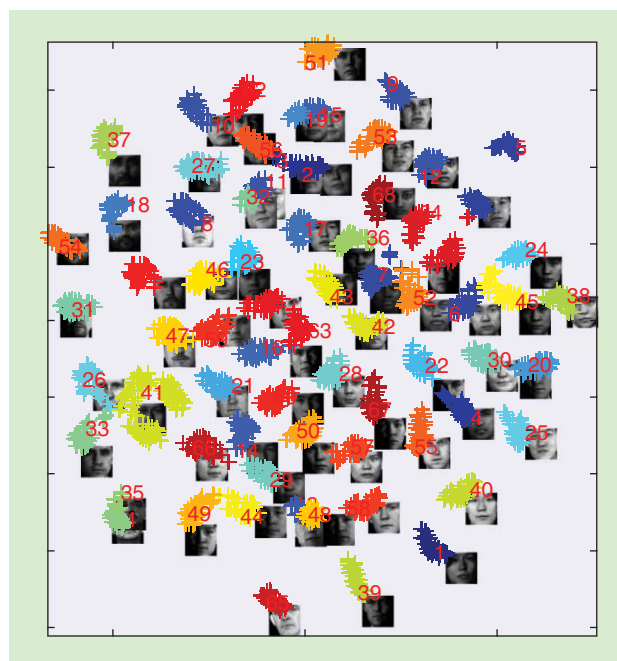


[FIG8] A visualization of clustering results using the two tSNE components of individual information after removing two common nonnegative components from all data. The faces images were from the CMU PIE database (pose c27) and the number of clusters was 68.

performance index accuracy was defined as in [45]), showing that after removing the common features in all faces, the accuracy was significantly improved. Figure 8 visualizes the clusters by using the two tSNE components of the individual subspace of all 68 categories. In fact, all clusters were quite well separated. More details about this method can be found in [29].

CONCLUSIONS

In this article, we reviewed state-of-the-art nonnegative matrix and tensor factorization algorithms, which not only provide faster convergence speed but also can be scaled up for very large-scale problems, particularly by incorporating distributed computing techniques [48]. We discussed how robust, powerful, and efficient LRA techniques (e.g., PCA/truncated SVD, multilinear SVD, RPCA, matrix/tensor completion methods) can be applied to substantially reduce noise and computational complexity in nonnegative matrix and tensor decompositions. Moreover, we introduced several new and promising methods to compute large-scale nonnegative PDs, including the methods that reshape a high-order data tensor to a matrix or a third-order tensor, and in the next step, we estimate nonnegative factor matrices sequentially. We also proposed fast and efficient algorithms for NTDs, which outperform most existing algorithms. Moreover, we discussed how to perform NMF for linked multiblock data and how to extract the nonnegative common and independent components. By representative simulations, we compared performance of state-of-the-art algorithms and illustrated their applications on both synthetic and real-world data.

Supplementary materials containing the pseudocode of selected NPD/NTD algorithms and the MATLAB code are available at <http://bsp.brain.riken.jp/zhougx/tensor.html>.

ACKNOWLEDGMENTS

This work was partially supported by the National Natural Science Foundation of China (grants 61103122, 61202155, 61333013, and U1201253).

AUTHORS

Guoxu Zhou (zhouguoxu@brain.riken.jp) is a research scientist in the Laboratory for Advanced Brain Signal Processing at RIKEN Brain Science Institute, Japan, and a visiting scientist at the School of Automation, Guangdong University of Technology, Guangzhou, China. He received the Ph.D. degree in intelligent signal and information processing from the School of Electronic and Information Engineering, South China University of Technology, Guangzhou, in 2010. His research interests include statistical signal processing, BSS, tensor analysis, intelligent information processing, and machine learning. He has published more than 30 papers in journals and international conferences.

Andrzej Cichocki (a.cichocki@riken.jp) is a senior team leader and head of the Laboratory for Advanced Brain Signal Processing at RIKEN Brain Science Institute, Japan, and a professor at the Systems Research Institute of the Polish Academy of Science, Warsaw. He received the M.S. (honors), Ph.D., and Dr.Sc. (Habilitation) degrees, all in electrical engineering from Warsaw University of Technology. He spent several years at the University Erlangen (Germany) as an Alexander-von-Humboldt research fellow and guest professor. He is the author/coauthor of more than 300 technical journal papers and four monographs in English (two of them translated to Chinese). He is an associate editor of *IEEE Transactions on Signal Processing* and *Journal of Neuroscience Methods*. He was the founding editor-in-chief for the journal *Computational Intelligence and Neuroscience*. Currently, his research focus is on tensor decompositions, electroencephalography hyperscanning, and their practical applications. His publications currently report over 20,000 citations, according to Google Scholar, with an h-index of 62.

Qibin Zhao (qbzhao@brain.riken.jp) is a research scientist in the Laboratory for Advanced Brain Signal Processing at RIKEN Brain Science Institute, Japan, and an

assistant researcher in the Department of Computer Science and Engineering, Shanghai Jiao Tong University, China. He received the Ph.D. degree in computer science from Shanghai Jiao Tong University in 2009. His research interests include machine learning, tensor analysis, Bayesian inference, and brain-computer interface. He has published more than 40 papers in journals and international conferences.

Shengli Xie (shlxie@gdut.edu.cn) is the director of both the Institute of Intelligent Information Processing and the Guangdong Provincial Key Laboratory for Information Technology in Internet of Things and a professor at the School of Automation at Guangdong University of Technology, Guangzhou, China. He received the M.S. degree in mathematics from Central China Normal University, Wuhan, in 1992, and the Ph.D. degree in control theory and applications from the South China University of Technology, Guangzhou, in 1997. He has authored or coauthored more than 100 scientific papers published in journals and conference proceedings and is a holder or joint holder of more than 40 patents. He is an associate editor of *IEEE Transactions on Neural Networks and Learning Systems*.

REFERENCES

- [1] A. Cichocki, R. Zdunek, A. H. Phan, and S.-I. Amari, *Nonnegative Matrix and Tensor Factorizations: Applications to Exploratory Multi-Way Data Analysis and Blind Source Separation*. Chichester, U.K.: Wiley, 2009.
- [2] D. D. Lee and H. S. Seung, "Learning the parts of objects by non-negative matrix factorization," *Nature*, vol. 401, no. 6755, pp. 788–791, Oct. 1999.
- [3] P. Paatero and U. Tapper, "Positive matrix factorization: A non-negative factor model with optimal utilization of error estimates of data values," *Environmetrics*, vol. 5, no. 2, pp. 111–126, 1994.

- [4] G. Wetzstein, D. Lanman, M. Hirsch, and R. Raskar, "Tensor displays: Compressive light field synthesis using multilayer displays with directional backlighting," *ACM Trans. Graph. (Proc. SIGGRAPH)*, vol. 31, no. 4, pp. 1–11, 2012.
- [5] A. Kumar, V. Sindhwani, and P. Kambadur, "Fast conical hull algorithms for near-separable non-negative matrix factorization," in *JMLR W&CP*, ser. 1, S. Dasgupta and D. McAllester, Eds. Atlanta, GA: Microtome, 2013, vol. 28, pp. 231–239.
- [6] C. Thurau, K. Kersting, and C. Bauckhage, "Convex non-negative matrix factorization in the wild," in *Proc. 2009 9th IEEE Int. Conf. Data Mining, ser. ICDM'09*. Washington, D.C.: IEEE Comput. Soc., 2009, pp. 523–532.
- [7] D. Donoho and V. Stodden, "When does non-negative matrix factorization give a correct decomposition into parts?" in *Advances in Neural Information Processing 16 (Proc. NIPS*2003)*, vol. 16. Cambridge, MA: MIT Press, 2004.
- [8] H. Laurberg, M. G. Christensen, M. D. Plumbley, L. K. Hansen, and S. H. Jensen. (2008). Theorems on positive data: On the uniqueness of NMF. *Computat. Intell. Neurosci.* [Online]. Available: <http://www.hindawi.com/journals/cin/2008/764206/>
- [9] N. Gillis, "Sparse and unique nonnegative matrix factorization through data preprocessing," *J. Mach. Learn. Res.*, vol. 13, no. 11, pp. 3349–3386, Nov. 2012.
- [10] K. Huang, N. Sidiropoulos, and A. Swami, "Non-negative matrix factorization revisited: Uniqueness and algorithm for symmetric decomposition," *IEEE Trans. Signal Processing*, vol. 62, no. 1, pp. 211–224, 2014.
- [11] G. Zhou, S. Xie, Z. Yang, J.-M. Yang, and Z. He, "Minimum-volume-constrained nonnegative matrix factorization: Enhanced ability of learning parts," *IEEE Trans. Neural Networks*, vol. 22, no. 10, pp. 1626–1637, Oct. 2011.
- [12] J. Kim, Y. He, and H. Park, "Algorithms for nonnegative matrix and tensor factorizations: A unified view based on block coordinate descent framework," *J. Global Optim.*, vol. 58, no. 2, pp. 1–35, 2013.
- [13] G. Zhou, A. Cichocki, and S. Xie, "Fast nonnegative matrix/tensor factorization based on low-rank approximation," *IEEE Trans. Signal Processing*, vol. 60, no. 6, pp. 2928–2940, June 2012.
- [14] C.-J. Lin, "On the convergence of multiplicative update algorithms for non-negative matrix factorization," *IEEE Trans. Neural Networks*, vol. 18, no. 6, pp. 1589–1596, Nov. 2007.
- [15] J. Kim and H. Park, "Fast nonnegative matrix factorization: An active-set-like method and comparisons," *SIAM J. Sci. Comput.*, vol. 33, no. 6, pp. 3261–3281, 2011.
- [16] N. Guan, D. Tao, Z. Luo, and B. Yuan, "NeNMF: An optimal gradient method for nonnegative matrix factorization," *IEEE Trans. Signal Processing*, vol. 60, no. 6, pp. 2882–2898, 2012.
- [17] D. G. Luenberger, *Linear and Nonlinear Programming*, 2nd ed. Norwell, MA: Kluwer, 2003.
- [18] Y. Zhang, R. Li, and C.-L. Tsai, "Regularization parameter selections via generalized information criterion," *J. Amer. Stat. Assoc.*, vol. 105, no. 489, pp. 312–323, 2010.
- [19] E. J. Candès, X. Li, Y. Ma, and J. Wright, "Robust principal component analysis?," *J. ACM (JACM)*, vol. 58, no. 3, pp. 11:1–11:37, June 2011.
- [20] M. D. Craig, "Minimum-volume transforms for remotely sensed data," *IEEE Trans. Geosci. Remote Sens.*, vol. 32, no. 3, pp. 542–552, 1994.
- [21] J. M. P. Nascimento and J. M. Bioucas-Dias, "Vertex component analysis: A fast algorithm to unmix hyperspectral data," *IEEE Trans. Geosci. Remote Sens.*, vol. 43, no. 4, pp. 898–910, Apr. 2005.
- [22] V. Bittorf, B. Recht, C. Ré, and J. A. Tropp, "Factoring nonnegative matrices with linear programs," in *Proc. Advances in Neural Information Processing Systems (NIPS)*, vol. 25, pp. 1223–1231, 2012.
- [23] N. Gillis and S. A. Vavasis, "Fast and robust recursive algorithms for separable nonnegative matrix factorization," *IEEE Trans. Pattern Anal. Mach. Intell.*, to be published.
- [24] C. Ding, T. Li, and M. Jordan, "Convex and semi-nonnegative matrix factorizations," *IEEE Trans. Pattern Anal. Mach. Intell.*, vol. 32, no. 1, pp. 45–55, Jan. 2010.
- [25] Y.-O. Li, T. Adali, W. Wang, and V. Calhoun, "Joint blind source separation by multitask canonical correlation analysis," *IEEE Trans. Signal Processing*, vol. 57, no. 10, pp. 3918–3929, Oct. 2009.
- [26] E. F. Lock, K. A. Hoadley, J. S. Marron, and A. B. Nobel, "Joint and individual variation explained (JIVE) for integrated analysis of multiple data types," *Ann. Appl. Stat.*, vol. 7, no. 1, pp. 523–542, 2013.
- [27] V. Calhoun, J. Liu, and T. Adali, "A review of group ICA for fMRI data and ICA for joint inference of imaging, genetic, and ERP data," *NeuroImage*, vol. 45, no. 1, pp. 163–172, 2009.
- [28] S. Ma, R. Phlypo, V. D. Calhoun, and T. Adali, "Capturing group variability using IVA: a simulation study and graph-theoretical analysis," in *Proc. IEEE Int. Conf. Acoustics, Speech, and Signal Processing (ICASSP)*, Vancouver, BC, May 2013, pp. 3128–3132.
- [29] G. Zhou, A. Cichocki, and S. Xie. (2013). Common and individual features analysis: Beyond canonical correlation analysis. [Online]. Available: <http://arxiv.org/abs/1212.3913>
- [30] C. Ding, T. Li, W. Peng, and H. Park, "Orthogonal nonnegative matrix tri-factorizations for clustering," in *Proc. 12th ACM SIGKDD Int. Conf. Knowledge Discovery and Data Mining, ser. KDD'06*. New York: ACM, 2006, pp. 126–135.
- [31] T. G. Kolda and B. W. Bader, "Tensor decompositions and applications," *SIAM Rev.*, vol. 51, no. 3, pp. 455–500, 2009.
- [32] A. Cichocki, D. Mandic, A.-H. Phan, C. Caiafa, G. Zhou, Q. Zhao, and L. De Lathauwer, "Tensor decompositions for signal processing application," *IEEE Signal Processing Mag.*, to be published.
- [33] Q. Zhao, G. Zhou, T. Adali, L. Zhang, and A. Cichocki, "Kernelization of tensor-based models for multiway data analysis," *IEEE Signal Processing Mag.*, vol. 30, no. 4, pp. 137–148, 2013.
- [34] R. Bro and C. A. Andersson, "Improving the speed of multiway algorithms: Part II: Compression," *Chemomet. Intell. Lab. Syst.*, vol. 42, no. 1–2, pp. 105–113, 1998.
- [35] N. D. Sidiropoulos and R. Bro, "On the uniqueness of multilinear decomposition of n-way arrays," *J. Chemomet.*, vol. 14, no. 3, pp. 229–239, 2000.
- [36] M. Mørup, L. K. Hansen, and S. M. Arnfred, "Algorithms for sparse nonnegative Tucker decompositions," *Neural Computat.*, vol. 20, no. 8, pp. 2112–2131, Aug. 2008.
- [37] L. De Lathauwer, B. De Moor, and J. Vandewalle, "A multilinear singular value decomposition," *SIAM J. Matrix Anal. Applicat.*, vol. 21, no. 4, pp. 1253–1278, Mar.–May 2000.
- [38] L.-H. Lim and P. Comon, "Nonnegative approximations of nonnegative tensors," *J. Chemomet.*, vol. 23, no. 7–8, pp. 432–441, 2009.
- [39] J.-P. Royer, N. Thirion-Moreau, and P. Comon, "Computing the polyadic decomposition of nonnegative third order tensors," *Signal Process.*, vol. 91, no. 9, pp. 2159–2171, 2011.
- [40] J. Kim and H. Park, "Fast nonnegative tensor factorization with an active-set-like method," in *High-Performance Scientific Computing*, M. W. Berry, K. A. Gallivan, E. Gallopoulos, A. Grama, B. Philippe, Y. Saad, and F. Saied, Eds. London: Springer, 2012, pp. 311–326.
- [41] H. Phan, P. Tichavsky, and A. Cichocki, "Fast alternating LS algorithms for high order CANDECOMP/PARAFAC tensor factorizations," *IEEE Trans. Signal Processing*, vol. 61, no. 19, pp. 4834–4846, 2013.
- [42] G. Zhou, A. Cichocki, and S. Xie, "Accelerated canonical polyadic decomposition by using mode reduction," *IEEE Trans. Neural Networks Learn. Syst.*, vol. 24, no. 12, pp. 2051–2062, Dec. 2013.
- [43] G. Zhou and A. Cichocki, "Canonical polyadic decomposition based on a single mode blind source separation," *IEEE Signal Processing Lett.*, vol. 19, no. 8, pp. 523–526, Aug. 2012.
- [44] C.-J. Hsieh and I. S. Dhillon, "Fast coordinate descent methods with variable selection for non-negative matrix factorization," in *Proc. 17th ACM SIGKDD Int. Conf. Knowledge Discovery and Data Mining, ser. KDD'11*. New York: ACM, 2011, pp. 1064–1072.
- [45] D. Cai, X. He, J. Han, and T. Huang, "Graph regularized nonnegative matrix factorization for data representation," *IEEE Trans. Pattern Anal. Mach. Intell.*, vol. 33, no. 8, pp. 1548–1560, Aug. 2011.
- [46] L. Van Der Maaten and C. Detection, "Visualizing data using t-SNE," *J. Mach. Learn. Res.*, vol. 9, pp. 2579–2605, Nov. 2008.
- [47] F. Nie, C. Ding, D. Luo, and H. Huang, "Improved minmax cut graph clustering with nonnegative relaxation," in *Machine Learning and Knowledge Discovery in Databases (Series Lecture Notes in Computer Science)*. Berlin/Heidelberg: Springer, 2010, vol. 6322, pp. 451–466.
- [48] C. Liu, H.-c. Yang, J. Fan, L.-W. He, and Y.-M. Wang, "Distributed nonnegative matrix factorization for web-scale dyadic data analysis on MapReduce," in *Proc. 19th Int. Conf. World Wide Web*, New York: ACM, 2010, pp. 681–690.

[Paris Smaragdīs, Cédric Févotte, Gautham J. Mysore,
Nasser Mohammadiha, and Matthew Hoffman]

Static and Dynamic Source Separation Using Nonnegative Factorizations

[A unified view]

Source separation models that make use of nonnegativity in their parameters have been gaining increasing popularity in the last few years, spawning a significant number of publications on the topic. Although these techniques are conceptually similar to other matrix decompositions, they are surprisingly more effective in extracting perceptually meaningful sources from complex mixtures. In this article, we will examine the various methodologies and extensions that make up this family of approaches and present them under a unified framework. We will begin with a short description of the basic concepts and in the subsequent sections we will delve in more details and explore some of the latest extensions.

USING NONNEGATIVE FACTORIZATION MODELS FOR SEPARATION

The basic model we will use to get started is a bilinear factorization of a nonnegative input V into two nonnegative matrices W and H , i.e., $V \approx WH$, where both of the two factor matrices can be of lower rank than V . This is known as the *nonnegative matrix factorization (NMF)* [1] model, and it is conceptually similar to other well-known matrix factorizations such as principal component analysis, independent component analysis, sparse linear models, or even vector quantization, which can all be expressed using the same

equation [2]. What makes this model particularly interesting is the constraint that the matrices V , W , and H are all nonnegative. This constraint ensures that the vectors making up the two factor matrices W and H can be interpreted as constructive building blocks of the input. Such an interpretation often does not apply to decompositions that employ negative-valued entries; in such

decompositions, the elements of W and H can cancel each other out, obscuring the

latent components' perceptual meaningfulness [1]. When NMF

is applied to data that was generated by mixing a number of nonnegative sources, the components NMF discovers often correspond remarkably well to those sources, and the decomposition is able to separate out the contributions of each source to the data.

Since NMF can operate even without

any prior information about the nature of the sources in the data, it is particularly well

suitable to unsupervised or blind source separation problems.

Some examples of interpretable components discovered by NMF are presented in Figure 1.

Sometimes it is more natural to represent complex sources using a linear combination of multiple latent components that collectively make up source dictionaries. In this case, we need one more level of hierarchy to group these components in terms of sources. Although in some cases this grouping could be obvious or analytically tractable, it is in principle not easy to compute. One can overcome this problem by using nonnegative factorization models in a supervised manner and explicitly providing cues



Source Separation and Applications

IMAGE LICENSED BY
INGRAM PUBLISHING

Digital Object Identifier 10.1109/MSP.2013.2297715

Date of publication: 7 April 2014

to the nature of the sources. This involves learning a dictionary for each target source by using the above model on clean training data that presents that source in isolation, and then identifying where in a mixture the dictionary elements associated with each source lie. If our data is not nonnegative already, to employ a nonnegative factorization we need to transform our inputs to an additive (or approximately additive) nonnegative representation. For many kinds of time series, such a domain can be a time-frequency localized energy measure computed via a harmonic decomposition such as the Gabor transform, or a wavelet decomposition. Since most natural signals tend to be sparse in the magnitude or power, by using these transforms we can often guarantee with high probability that the transform of the sum of two sources will be equal or approximately equal to the sum of the transforms of the two sources separately, which can satisfy the additivity constraint. As we show later, depending on the exact NMF model and the representation used, the additivity assumption can be one that is either weak or strong.

To demonstrate the separation process with a tangible example, let us look at a hydrophone mixture containing a whale song (target source) and sea clutter (background sources). We

represent this mixture using a magnitude short-time Fourier transform (STFT), which is shown in Figure 2(c). To learn a target source dictionary we use a clean recording of whale songs [Figure 2(a)]. This is done by analyzing the matrix containing the STFT representation using any of the models that we detail in the remainder of this article. A learned dictionary is shown in Figure 2(b), and as one can see its elements represent salient spectral features that comprise the whale song recording. We

can repeat this process for the sea clutter source to get components that describe it too. In practice, a few seconds of training data is usually enough to learn an adequate model of a source, although this can vary depending on the domain and source characteristics we are dealing with. The number of components per dictionary determines how accurately we want to model

the sources, with more components giving us more expressive power but at the cost of making a dictionary so rich that it could describe other sources as well.

Given the approximate additivity assumption and a representative set training data, we can now hypothesize that the mixture recording will be explained by a linear combination of the elements in the source dictionaries, i.e., that $X \approx [W_1, W_2]H$ will

ALTHOUGH THESE TECHNIQUES ARE CONCEPTUALLY SIMILAR TO OTHER MATRIX DECOMPOSITIONS, THEY ARE SURPRISINGLY MORE EFFECTIVE IN EXTRACTING PERCEPTUALLY MEANINGFUL SOURCES FROM COMPLEX MIXTURES.

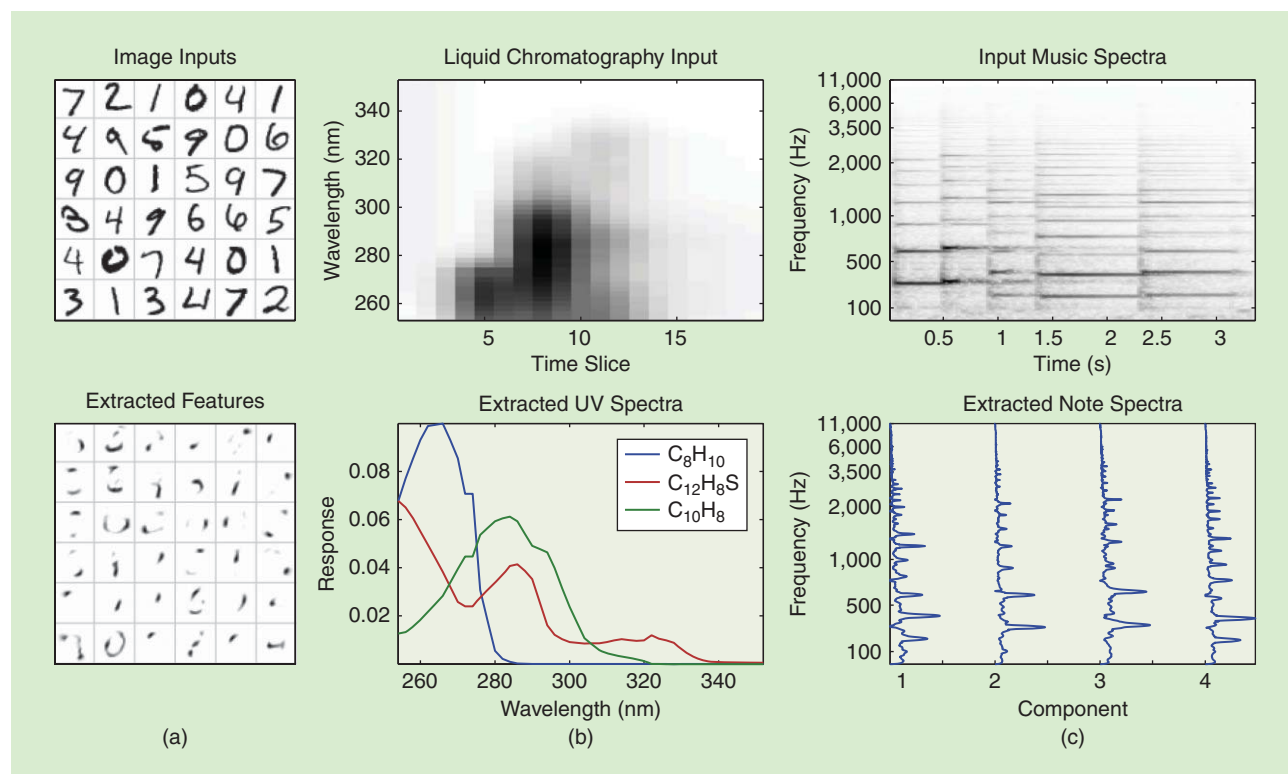


[FIG1] Extracted NMF components from various domains. (a) The analysis of handwritten digital data results in parts of penstrokes, (b) the analysis of chemometric data results in the spectral profiles of the three constituent components (oxylene, naphthalene, dibenzothiophene), and (c) the analysis of music spectrograms results in spectra of musical notes.

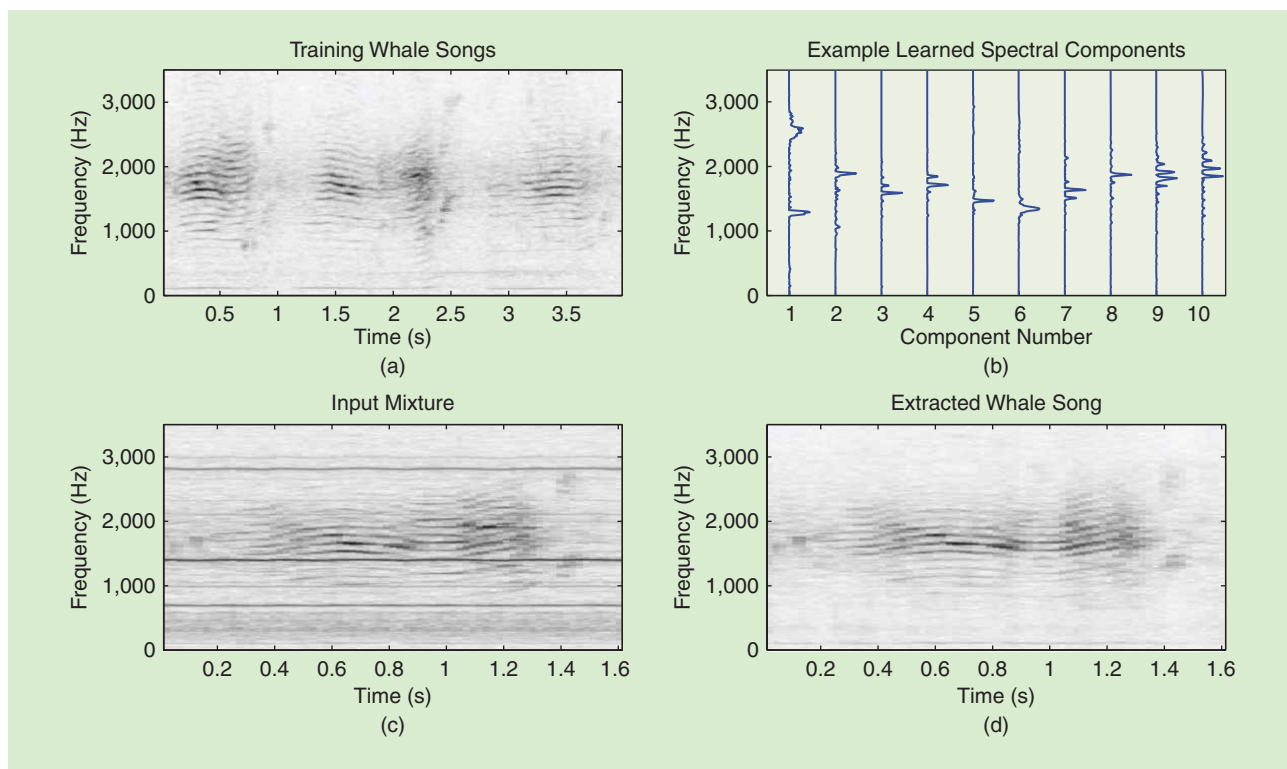


[FIG2] Extracting a target source from a hydrophone ocean mixture using a nonnegative dictionary. The training data in (a) are isolated whale songs used to learn the dictionary shown in (b). Not shown are the equivalent plots for sea clutter sounds. These dictionaries are then used to extract their respective sources from a mixture that includes them, shown in (c). The extracted whale song is shown in (d).

approximately hold, where X contains the magnitude STFT of the mixture and W_1 and W_2 are the learned left factors from the training data of the two sounds. We thus only need to compute the matrix H . Given the ability to compute the full NMF model, the estimation of the H matrix can be easily obtained by fixing $[W_1, W_2]$ and only updating the estimate for H . Once this is computed we can reconstruct the mixture using only the dictionary of one source at a time, which will produce in a time-frequency representation of the two sources separately, which can then be inverted back to the time domain. The only assumption that needs to hold at this point is that the two source dictionaries are sufficiently different from each other so that they do not model the same elements in the mixture. Although there is no easy way of quantifying the required degree of dissimilarity in real-world examples, this is a process that works even in cases where the sources are very similar (e.g., two speakers of the same gender), and by incorporating the ideas in the remainder of this article we can even separate sources that share identical dictionaries by making use of their temporal statistics. In this particular case, the dictionaries that characterize the two sources have minimal similarities and produce a very clean separation. The result of extracting the whale song from the hydrophone mixture is shown in Figure 2. The details of this process and its generalization in the case where we might not have dictionaries for all the sources is described in [3].

This basic approach of supervised separation has spawned much subsequent research using varying approaches and methodologies, often seemingly incompatible with each other. In the following sections we will take a closer look at the details of various formulations of nonnegative factorization models, and will show a unified progression of techniques that spans from the simple static models (such as the ones shown above) to more complex dynamic approaches that incorporate more temporal information and can produce higher-quality results. We will predominantly focus on the statistical interpretation (and variation) within NMF algorithms and then we will show how these can be extended to two kinds of useful temporal models: continuous state and discrete state models, which in turn can take advantage of temporal information to improve the performance of source separation tasks.

STATIC MODELS

A PROBABILISTIC VIEW OF NMF

Traditionally NMF is applied by solving the optimization problem defined by

$$\min_{W,H} D(V|WH) \quad \text{s.t.} \quad W \geq 0, H \geq 0, \quad (1)$$

where V , W , and H are nonnegative matrices of size $F \times T$, $F \times K$, and $K \times T$, respectively. The notation $M \geq 0$ denotes

element-wise nonnegativity of \mathbf{M} (and not semidefinite positivity) and $D(\mathbf{V}|\mathbf{WH})$ is a separable measure of fit such that

$$D(\mathbf{V}|\mathbf{WH}) = \sum_{t=1}^T D(\mathbf{v}_t|\mathbf{Wh}_t). \quad (2)$$

$D(\mathbf{x}|\mathbf{y})$ is a divergence between vectors \mathbf{x} and \mathbf{y} , i.e., a non-negative function of $\mathbf{y} \in \mathbb{R}_+^F$ given $\mathbf{x} \in \mathbb{R}_+^F$, with a single minimum (zero) for $\mathbf{x} = \mathbf{y}$. For convenience we will use the same notation $D(\cdot|\cdot)$ to denote the divergence between vectors or matrices, with the convention that in the matrix case the divergences between columns simply add up as in (2). Common divergences used in NMF include the squared Euclidean distance (see [46]), variants of the Kullback–Leibler (KL) divergence [1], and the Itakura–Saito (IS) divergence [4]. More general families of divergences considered for NMF include alpha-beta [5] and Bregman divergences [6]. A comprehensive review of divergences and algorithms used for NMF can be found in [7].

In many cases divergences are likelihoods in disguise (and are as such sometimes referred to as *pseudolikelihoods*) in the sense that they underlie a probabilistic generative model of the data. The correspondence is such that there exists a probability density function (pdf) $p(\mathbf{V}|\mathbf{W}, \mathbf{H})$ that satisfies

$$-\log p(\mathbf{V}|\mathbf{WH}) = a D(\mathbf{V}|\mathbf{WH}) + b, \quad (3)$$

where a and b are constants with respect to \mathbf{WH} . Some examples of correspondences are given in Table 1. Note that this correspondence does not automatically imply a coherent generative model for nonnegative real-valued data; e.g., although the generalized KL divergence is a valid measure of fit on the whole positive orthant, the corresponding Poisson likelihood is only a true likelihood on the nonnegative integers, and in the large-variance setting the additive Gaussian model could generate negative data. However, these theoretical issues can usually be resolved; see, e.g., [8].

In this article we focus on two probabilistic NMF models that have been widely used in source separation: probabilistic latent component analysis (PLCA), which is closely related to NMF with the KL divergence [9], and the Gaussian composite model (GCM), which is closely related to NMF with the IS divergence [4]. A common feature of these models, shared by the models in Table 1 as well, is that the conditional expectation of \mathbf{V} is \mathbf{WH} (i.e., $\mathbb{E}[\mathbf{V}|\mathbf{WH}] = \mathbf{WH}$), and that the data points are conditionally independent given \mathbf{WH} [i.e., $p(\mathbf{V}|\mathbf{WH}) = \prod_t p(\mathbf{v}_t|\mathbf{Wh}_t)$]. These simple factorization models are “static” in the sense that data points (columns of \mathbf{V}) could be exchanged without any effect on the estimates other than a permutation of \mathbf{H} . Dynamic, nonexchangeable models will be introduced later in the article using temporal priors on \mathbf{H} .

PROBABILISTIC LATENT COMPONENT ANALYSIS

PLCA is an extension of probabilistic latent semantic indexing (PLSI) for signal processing applications [9]. PLSI is a method

for text analysis based on word counts from documents [10]. In PLCA, the input matrix \mathbf{V} is a magnitude spectrogram $v_{nt} = |x_{nt}|$, where x_{nt} is the complex-valued STFT of some time-domain data. PLCA interprets the entries of each column \mathbf{v}_t of \mathbf{V} as a sort of histogram of independent identically distributed (i.i.d.) frequency “quanta” $f \in \{1, \dots, F\}$ in each time frame t . The data distribution in PLCA is therefore

$$\mathbf{v}_t \sim \text{Mult}(\mathbf{v}_t \|\|\mathbf{v}_t\|_1, \hat{\mathbf{v}}_t), \quad (4)$$

where $\|\mathbf{v}\|_1 = \sum_f |v_f|$ is the ℓ_1 norm, $\hat{\mathbf{v}}_t = \mathbf{Wh}_t$, and $\text{Mult}(N, \mathbf{p})$ denotes the multinomial distribution. In PLCA it is imposed that $\|\mathbf{w}_k\|_1 = \|\mathbf{h}_t\|_1 = 1$, which in turn implies that $\|\hat{\mathbf{v}}_t\|_1 = 1$. A draw from $\text{Mult}(N, \mathbf{p})$ returns an integer-valued vector of dimension F whose entries sum to N . The f th entry of this vector corresponds to the number of times event f was sampled in N independent draws from the discrete distribution defined by \mathbf{p} . Although usual inputs in source separation problems are not integer valued, the negative log-likelihood of the data and parameters in PLCA provides

a valid divergence for nonnegative real-valued data. Specifically, under (4) and introducing the normalized data $\tilde{\mathbf{v}}_t = \mathbf{v}_t/\|\mathbf{v}_t\|_1$, the negative log-likelihood is given by

$$-\log p(\mathbf{V}|\hat{\mathbf{V}}) = \sum_t \|\mathbf{v}_t\|_1 D_{\text{KL}}(\tilde{\mathbf{v}}_t|\hat{\mathbf{v}}_t) + \text{cst}, \quad (5)$$

where “cst” denotes terms constant with respect to $\hat{\mathbf{V}}$ and $D_{\text{KL}}(\mathbf{x}|\mathbf{y}) = \sum_f x_f \log(x_f/y_f)$ is the KL divergence between discrete distributions. As such, PLCA essentially minimizes a weighted KL divergence between the normalized input and its factorized approximation, where every data point is given a weight equal to its sum.

IS-NMF AND THE GAUSSIAN COMPOSITE MODEL

Underlying IS-NMF is a multiplicative noise model of the form $v_{nt} = \hat{v}_{nt} \cdot \epsilon_{nt}$, where ϵ_{nt} has a Gamma distribution with

WHEN NMF IS APPLIED TO DATA THAT WAS GENERATED BY MIXING A NUMBER OF NONNEGATIVE SOURCES, THE DISCOVERED COMPONENTS OFTEN CORRESPOND REMARKABLY WELL TO THOSE SOURCES.

[TABLE 1] COMMON DIVERGENCES AND THEIR CORRESPONDING PROBABILISTIC GENERATIVE MODELS. WE DEFINE $\hat{\mathbf{v}}_t = \mathbf{Wh}_t$, WHOSE COEFFICIENTS ARE DENOTED \hat{v}_{ft} . ALL THREE MODELS VERIFY $\mathbb{E}[\mathbf{v}_t|\hat{\mathbf{v}}_t] = \hat{\mathbf{v}}_t$.

DIVERGENCE $D(\mathbf{v}_t \hat{\mathbf{v}}_t)$	LATENT GENERATIVE MODEL $p(\mathbf{v}_t \hat{\mathbf{v}}_t)$
SQUARED EUCLIDEAN DISTANCE $\frac{1}{2\sigma^2} \sum_f (v_{ft} - \hat{v}_{ft})^2$	ADDITIVE GAUSSIAN $\prod_f N(v_{ft} \hat{v}_{ft}, \sigma^2)$
GENERALIZED KL DIVERGENCE $\sum_f (v_{ft} \log \frac{v_{ft}}{\hat{v}_{ft}} - v_{ft} + \hat{v}_{ft})$	POISSON $\prod_f P(v_{ft} \hat{v}_{ft})$
IS DIVERGENCE $\sum_f \left(\frac{v_{ft}}{\hat{v}_{ft}} - \log \frac{v_{ft}}{\hat{v}_{ft}} - 1 \right)$	MULTIPLICATIVE GAMMA $\prod_f G(v_{ft} \alpha, \alpha/\hat{v}_{ft})$

expectation one. The resulting data distribution is given in Table 1 and the negative log-likelihood is such that

$$-\log p(V|\hat{V}) = \alpha D_{IS}(V|\hat{V}) + \text{cst}, \quad (6)$$

where $D_{IS}(\cdot|\cdot)$ is the IS divergence defined in Table 1.

When $\alpha = 1$, i.e., when the multiplicative noise has an exponential distribution, the multiplicative noise model can be related to a generative model of real- or complex-valued data coined *Gaussian composite model (GCM)* [4]. The model is in particular a valid probabilistic model of STFTs. Let $x_{\hat{t}}$ be the complex-valued STFT of some time-domain signal. The GCM is defined by $x_{\hat{t}} = \sum_k c_{\hat{t}k}$ and $c_{\hat{t}k} \sim N_c(0, w_{\hat{t}k} h_{\hat{t}k})$, where $N_c(0, \lambda)$ refers to the circular complex Gaussian distribution with zero mean.

A random variable has distribution $N_c(0, \lambda)$ if its real and imaginary parts are independent centered Gaussian variables with variance $\lambda/2$. In other words, the GCM models the STFT as a sum of uncorrelated centered Gaussian components structured through their variance. The variance of the k th component is characterized by the spectral pattern w_k , amplitude-modulated in time by the coefficients $\{h_{kt}\}_t$. The centered assumption reflects an equivalent assumption in the time domain, which holds for many signals (in particular audio signals). The latent components $c_{\hat{t}k}$ can trivially be marginalized from the generative model, yielding $x_{\hat{t}} \sim N_c(0, \sum_k w_{\hat{t}k} h_{\hat{t}k})$. It follows that the power spectrogram $v_{\hat{t}} = |x_{\hat{t}}|^2$ of $x_{\hat{t}}$ is exponentially distributed with mean $\hat{v}_{\hat{t}} = \sum_k w_{\hat{t}k} h_{\hat{t}k}$, and can thus be written as a special case of the multiplicative Gamma model given in Table 1 with $\alpha = 1$. Under this model, minimum mean squares estimate (MMSE) of the components can be obtained by Wiener filtering and given by $\hat{c}_{\hat{t}k} = [(w_{\hat{t}k} h_{\hat{t}k})/\hat{v}_{\hat{t}}]x_{\hat{t}}$.

A MORE FLEXIBLE APPROACH FOR MODELING TEMPORAL STATISTICS IS TO IMPOSE CONSTRAINTS ON THE MODEL ACTIVATIONS.

WHICH MODEL TO USE?

An important feature of the GCM is that the phase of the original complex-valued data is preserved in the generative model

(though it is modeled in an uninformative way, owing to the circular assumption) rather than discarded, as in PLCA. Additionally, the additivity assumption holds strongly in the original STFT domain. The IS divergence turns out to be a scale-invariant measure, i.e., $d_{IS}(\lambda x|\lambda y) = d_{IS}(x|y)$, where x , y , and λ are positive scalars. This makes it well suited to audio spectrograms and their widely varying ranges of magnitudes; a more detailed discussion is in [4]. In contrast, PLCA will rely more heavily on data vectors with large norms, as can be seen from the divergence expression in (5). Whether this is a desirable property or not depends on the data and specific task. A downside of the IS divergence with respect to the weighted KL divergence of PLCA

is its lack of convexity with respect to its second argument, which leads more often to local solutions in practice, as explained in the next section. PLCA and IS-NMF were benchmarked in [11] for speech separation and audio interpolation tasks. However, a consensus did not

clearly emerge from the experiments as to which method is best, and the conclusions were often data or task dependent.

ESTIMATION

We now discuss estimation in PLCA and IS-NMF, i.e., the optimization of the objective functions (5) and (6) with respect to W and H . Like virtually all NMF algorithms, PLCA and IS-NMF rely on a block-coordinate descent structure that alternates between updating W holding H fixed and updating H holding W fixed. It is easy to see that the updates of W and H are essentially the same by transposition ($V \approx WH \Leftrightarrow V^T \approx H^T W^T$). Each update can be carried out by majorization-minimization (MM) [12]. MM consists in upper bounding the objective function with an auxiliary function that is tight at the current estimate and that can be minimized in closed form. The principle of MM is illustrated in Figure 3. Details of the algorithms can be found in [9] for PLCA and in [13] for IS-NMF. The resulting updates are given in Table 2. Their multiplicative structure automatically ensures the nonnegativity of the updates given positive initialization.

It should be pointed out that in every NMF problem the objective function $D(V|WH)$ is not jointly convex with respect to W and H . When the divergence $D(x|y)$ is convex with respect to its second argument y , like in PLCA, the problem is at least convex with respect to H given W and vice versa. However it is never convex with respect to both. This means that the block-coordinate approach may converge to local solutions that will depend on initialization. Some recent work (e.g., [14] and [15]) has explored alternate estimation algorithms that avoid formulating NMF as a nonconvex optimization and thereby sidestep the local-optima problem. The guarantees associated with these algorithms are dependent on separability and/or sparsity assumptions that may be more appropriate for extremely high-dimensional data like document word counts than for moderately high-dimensional data like audio spectra. However, as shown in [16], separability is not necessary for uniqueness in NMF, and such a

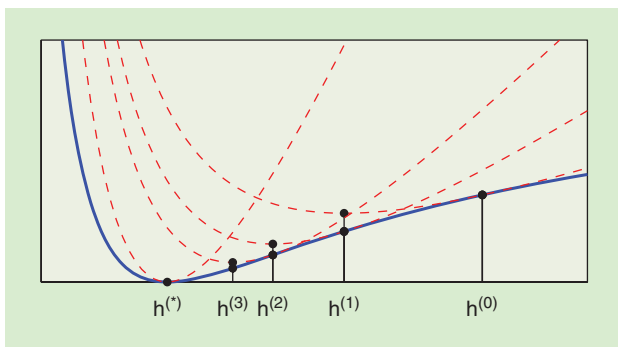


[FIG3] An illustration of the MM principle on a unidimensional problem. Given a current estimate of W , the blue curve acts as the objective function $C(H) = D(V|WH)$ to be minimized with respect to H . The MM approach relies on the iterative minimization of tight upper bounds (dashed red curves). The algorithm is initialized at $H^{(0)}$, at which the first upper bound is minimized during the first iteration to yield $H^{(1)}$, and so on until convergence.

[TABLE 2] PLCA AND IS-NMF FOR THE GCM SUMMARIZED. IN THE UPDATE RULES, \tilde{w}_{fk} AND \tilde{h}_{kt} DENOTE CURRENT PARAMETER VALUES. \tilde{v}_{ft} DENOTES THE CURRENT DATA APPROXIMATION, I.E., $\sum_k w_{fk} \tilde{h}_{kt}$ IN THE UPDATE OF \mathbf{H} AND $\sum_k \tilde{w}_{fk} h_{kt}$ IN THE UPDATE OF \mathbf{W} .

	PLCA	IS-NMF FOR THE GCM
NONNEGATIVE DATA	$\mathbf{V} = \mathbf{X} $	$\mathbf{V} = \mathbf{X} ^2$
OBJECTIVE FUNCTION	$D(\mathbf{V} \mathbf{WH}) = \sum_t \ \mathbf{v}_t\ , D_{KL}(\tilde{\mathbf{v}}_t \hat{\mathbf{v}}_t)$	$D(\mathbf{V} \mathbf{WH}) = D_{IS}(\mathbf{V} \mathbf{WH})$
CONSTRAINTS	$\ \mathbf{w}_k\ _1 = \ \mathbf{h}_t\ _1 = 1$	—
LATENT GENERATIVE MODEL	$p(\mathbf{v}_t \hat{\mathbf{v}}_t) = \text{Mult}(\mathbf{v}_t \ \mathbf{v}_t\ , \hat{\mathbf{v}}_t)$	$p(\mathbf{x}_t \hat{\mathbf{v}}_t) = \prod_f \mathbf{N}_\epsilon(x_{ft} 0, \hat{v}_{ft})$
UPDATES	$h_{kt} = \frac{\tilde{h}_{kt} \sum_f w_{fk} (v_{ft} / \tilde{v}_{ft})}{\sum_k \tilde{h}_{kt} \sum_f w_{fk} (v_{ft} / \tilde{v}_{ft})}$ $w_{fk} = \frac{\tilde{w}_{fk} \sum_t h_{kt} (v_{ft} / \tilde{v}_{ft})}{\sum_f \tilde{w}_{fk} \sum_t h_{kt} (v_{ft} / \tilde{v}_{ft})}$	$h_{kt} = \tilde{h}_{kt} \frac{\sum_f w_{fk} (v_{ft} / \tilde{v}_{ft}^2)}{\sum_f w_{fk} (1 / \tilde{v}_{ft})}$ $w_{fk} = \tilde{w}_{fk} \frac{\sum_t h_{kt} (v_{ft} / \tilde{v}_{ft}^2)}{\sum_n \tilde{h}_{kt} (1 / \tilde{v}_{ft})}$

constraint can be too restrictive when using convex formulations. Regardless, for our purposes, the block-coordinate approach is practical and effective on a wide range of problems, despite its lack of theoretical guarantees.

So far we have presented a basic version of NMF in which the data is approximated as $\mathbf{V} \approx \mathbf{WH}$ without any structural priors (aside from nonnegativity) on either \mathbf{W} or \mathbf{H} . However, in many cases one is expecting the latent factors to have a certain structure, such as smoothness or sparsity. As such, a large part of the NMF literature has concentrated on penalized variants of NMF, in which penalty functions of either \mathbf{W} or \mathbf{H} are added to the divergence $D(\mathbf{V} | \mathbf{WH})$. In our probabilistic setting, this can be viewed as setting prior distributions for the latent factors. In particular, the next section will review temporal priors $p(\mathbf{H})$ that have been used in the literature. In most cases, penalized NMF can be handled with MM, by simply adding the penalty term, or a local majorization of the latter, to the auxiliary function obtained in the static case.

DYNAMIC MODELS

Temporal continuity is one of the most important features of time-series data. Our aim here is to present some of the basic as well as advanced ideas to make use of this information by modeling time dependencies in NMF. These dependencies between consecutive columns of \mathbf{V} can be imposed either on the basis matrix \mathbf{W} or on the activations \mathbf{H} . The former case is known as the convolutive NMF [17]–[19]. In these approaches, the repeating patterns within data are represented with multidimensional bases which are not vectors anymore, but functions that can span an arbitrary number of dimensions (e.g., both frequency and time in examples like the previous one). These models can be seen as a deterministic way to model temporal dependencies. Although they are useful in extracting temporal components, they most often result in very structured representations that do not generalize well enough to be successfully employed for source separation. A more flexible approach for modeling temporal statistics is to impose constraints on the model activations. Such methods are very much in line with traditional dynamic models that have been studied extensively in signal processing, and in this section we will turn our attention to these.

Most models considered in the literature are special cases of the general dynamic model given by

$$\begin{aligned}
 \mathbf{h}_t &\sim p(\mathbf{h}_t | \mathbf{h}_{t-1}, \theta), & (7) \\
 \mathbf{v}_t &\sim p(\mathbf{v}_t | \mathbf{W}\mathbf{h}_t). & (8)
 \end{aligned}$$

We assume that (8) defines a probabilistic NMF observation model such that $\mathbb{E}[\mathbf{V} | \mathbf{WH}] = \mathbf{WH}$. As such, it may refer to any of the static models discussed in the previous section. Equation (7) introduces temporal dynamics by assuming a Markov structure for the activation coefficients. θ denotes the prior parameters. The aim of this section is to describe the general concepts of dynamic NMF and provide references for specific instantiations related to given probabilistic NMF models (PLCA, IS-NMF, generalized KL-NMF, etc.). Two broad classes of models are discussed next, continuous and discrete models.

CONTINUOUS MODELS

SMOOTH NMF

A straightforward approach to use temporal continuity is to apply some constraints that reduce fluctuations in each individual row of \mathbf{H} . This corresponds to assuming that different rows of \mathbf{H} are independent.

In these approaches, the general equation (7) can be written as

$$\mathbf{h}_t \sim \prod_{k=1}^K p(h_{kt} | \mathbf{h}_{k(t-1)}, \theta). \tag{9}$$

A natural choice for $p(h_{kt} | \mathbf{h}_{k(t-1)}, \theta)$ is a pdf that either takes its mode at $h_{k(t-1)}$ or is such that $\mathbb{E}[h_{kt} | \mathbf{h}_{k(t-1)}, \theta] = h_{k(t-1)}$. Various papers have dealt with smooth NMF and they typically differ by the choice of observation models and priors (or in nonprobabilistic settings, penalty term) that is used [4], [20]–[27]. Gaussian priors (or equivalently, squared differences) of the form $p(h_{kt} | \mathbf{h}_{k(t-1)}) = \mathcal{N}(h_{kt} | h_{k(t-1)}, \sigma^2)$ are used in [20], [21], and [26]. Nonnegativity-preserving Gamma or inverse-Gamma Markov chains are considered in [4], [23], [25], and [27]–[30] and Markov random fields in [31].

NONNEGATIVE STATE-SPACE MODELS

Smooth NMF does not capture the full extent of frame-to-frame dependencies in its input. In practice we will observe various temporal correlations between adjacent time frames that will be more nuanced than the continuity that smooth NMF implies. In other words, there is correlation both within (smoothness) and between (transitions) the time frames of the coefficients of \mathbf{H} . For real-valued time series, this type of structure can be handled with the classical linear dynamical system, using dynamics of the form $\mathbf{h}_t = \mathbf{A}\mathbf{h}_{t-1} + \boldsymbol{\epsilon}_t$, where $\boldsymbol{\epsilon}_t$ is a centered Gaussian innovation. This model is not natural in the NMF setting because it may not maintain nonnegativity in the activations. However it is possible to design alternative dynamic models that maintain nonnegativity while preserving

$$\mathbb{E}[\mathbf{h}_t | \mathbf{A}\mathbf{h}_{t-1}] = \mathbf{A}\mathbf{h}_{t-1}. \quad (10)$$

The statistical models considered in the section “Static Models” are good candidates by exchanging \mathbf{v}_t for \mathbf{h}_t and $\hat{\mathbf{v}}_t$ for \mathbf{h}_{t-1} . Following that idea, a nonnegative dynamical system (NDS) with multiplicative Gamma innovations was proposed in [32], in conjunction with multiplicative Gamma noise for the observation (IS-NMF model). Note that in the case of the Gaussian linear dynamical system, integration of the activation coefficients from the joint likelihood $p(\mathbf{V}, \mathbf{H} | \mathbf{W})$ is feasible using the Kalman filter. Such computations are unfortunately intractable with NDS, and a MAP approach based on an MM algorithm is pursued in [32].

Dynamic filtering of the activation coefficients in the PLCA model has also been considered [33], [34], where the proposed algorithms use Kalman-like prediction strategies.

The technique in [34] considers a more general multistep predictor such that $\mathbf{h}_t \approx \sum_j \mathbf{A}_j \mathbf{h}_{t-j}$, and describes an approach for both the smoothing (which relies on both past and future data) and causal filtering (which relies only on the past data) problems.

DISCRETE MODELS

Time-series data often has hidden structure in which each time frame corresponds to a discrete hidden state q_t . Moreover, there is typically a relationship between the hidden states at different time frames, in the form of temporal dynamics. For example, each time frame of a speech signal corresponds to a subunit of speech such as a phoneme, which can be modeled as a distinct state. The subunits evolve over time as governed by temporal dynamics. Hidden Markov models (HMMs) [35] have been used extensively to model such data. They model temporal dynamics with a transition matrix defined by the distribution $p(q_t | q_{t-1})$. There has been a recent thread of literature [36]–[40] that combines these ideas with NMF to model nonnegative data with such structure.

The notion of a state is incorporated in the NMF framework by associating distinct dictionary elements with each state. This is done by allowing each state to determine a different support of

the activations, which we express with the distribution $p(\mathbf{h}_t | q_t)$. This is to say that given a state, the model allows only certain dictionary elements to be active. Some techniques [36], [39] define the support of each state to be a single dictionary element, while other techniques [37], [38], [40], called nonnegative HMMs (N-HMMs), allow the support of each state to be a number of dictionary elements. Since only a subset of the dictionary elements are active at each time frame (as determined by the state at that time frame), we can interpret these models as imposing block sparsity on the dictionary elements [41].

As in (7), there is a dependency between \mathbf{h}_t and \mathbf{h}_{t-1} . However, unlike the continuous models, this dependency is only through the hidden states, which are in turn related through the temporal dynamics. Therefore \mathbf{h}_t is conditionally independent of \mathbf{h}_{t-1} given q_t or q_{t-1} . In the case of discrete models, we can therefore replace (7) with

$$q_t \sim p(q_t | q_{t-1}), \quad (11)$$

$$\mathbf{h}_t \sim p(\mathbf{h}_t | q_t). \quad (12)$$

Since these models incorporate an HMM structure into an NMF framework, one can make use of the vast theory of Markov chains to extend these models in various ways. For example, one can incorporate high-level knowledge of a particular class of signals into the model, use higher-order Markov chains, or use various natural language processing techniques. Language models were recently incorporated in this framework [42] as typically done in the speech recognition literature [35]. Similarly, one can incorporate other types of temporal structure like music theory rules when dealing with music signals.

The above techniques discuss how to model a single source using an HMM structure. However, to perform source separation, we need to model mixtures. This is typically done by combining the individual source models into a factorial HMM [28], [36]–[38], [40], which allows each source to be governed by a distinct pattern of temporal dynamics. One issue with this strategy is that the computational complexity of inference is exponential in the number of sources. This can be circumvented using approximate inference techniques such as variational inference [43], which makes the complexity linear in the number of sources.

THE USE OF DYNAMIC MODELS IN SOURCE SEPARATION

To demonstrate the utility of dynamic models in context, we will once again use a real-world source separation example. This time it will be an acoustic mixture of speech mixed with background noise from a factory (using the TIMIT [47] and NOISEX-92 [48] databases). The mixture is shown using a magnitude STFT representation in Figure 4. This particular case is interesting because of the statistics of speech. We note that human speech

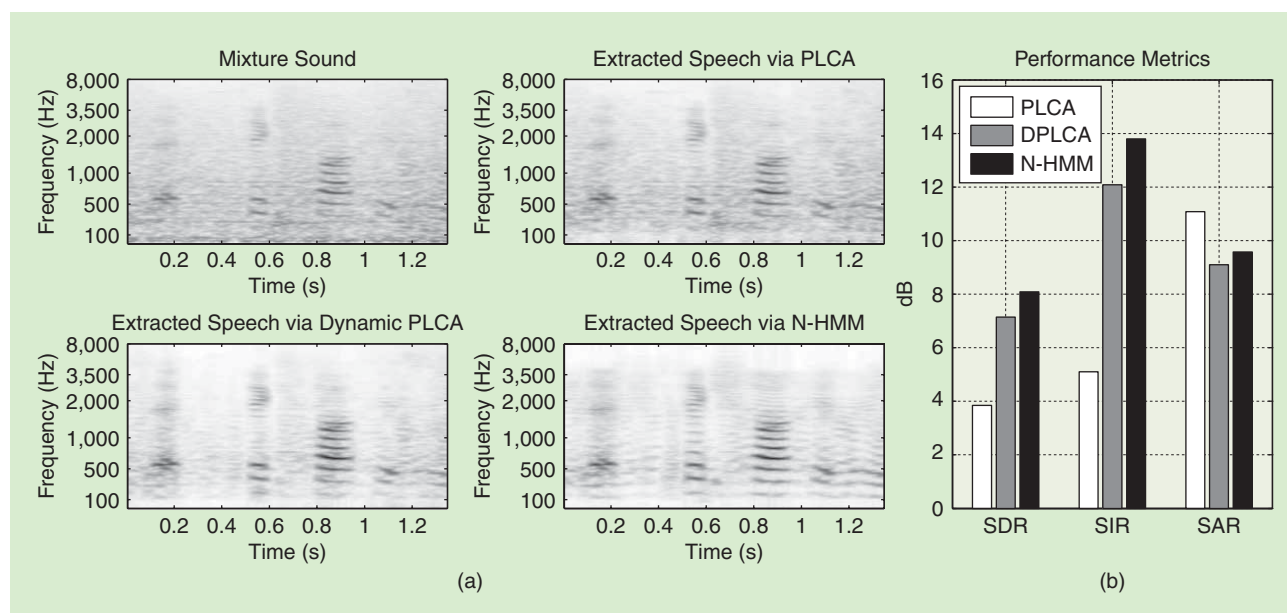


[FIG4] An example of dynamic models for source separation. (a) The four spectrograms show the mixture and the extracted speech for three different approaches. (b) A quantitative evaluation of the separation performance of each approach.

tends to have a smooth acoustic trajectory, which means that there is a strong temporal correlation between adjacent time frames. On the other hand, we also know that speech has a strong discrete hidden structure that is associated with the sequence of spoken phonemes. These properties make this example a good candidate for demonstrating the differences between the methods discussed so far and their effects on source separation.

We performed source separation using the three main approaches that we covered in this article. These include a static PLCA model [44], a dynamic PLCA model [34], and an N-HMM [37]. In all three cases, we trained a model for speech and a model for background noise from training data. The dictionary size for the noise was fixed to 30 elements, whereas the speech model had 60 dictionary elements for PLCA and dynamic PLCA, and 40 states with ten dictionary elements each for the N-HMM. For the dynamic models, we learned the temporal statistics as well. To separate a mixture of test data of the sources, we fixed the learned W matrices for both the speech and noise models and estimated their respective activations H using the context of each model. In Figure 4, we show the reconstruction of speech using each model. We also show a set of objective metrics that evaluate the quality of separation in each case. These include the source-to-distortion ratio (SDR), the source-to-interference ratio (SIR), and the source-to-artifacts ratio (SAR) as defined in [45]. These results are averaged over 20 different speakers to reduce biasing and initialization effects.

WE HOPE THAT BY PRESENTING THIS STREAMLINED FORMULATION WE CAN HELP READERS TO EXPERIMENT WITH THE OTHER MANY POSSIBILITIES IN FORMULATING DYNAMIC SOURCE SEPARATION ALGORITHMS.

For the static PLCA model, we see that there is a detectable amount of visible suppression of the background noise, which amounts to a modest SIR of about 5 dB. The dynamic PLCA model on the other hand, by taking advantage of the temporal statistics of speech, does a much better job resulting in more than double the SIR. Note however that in the process of adhering to the expected statistics, it introduces artifacts, which result in a lower SAR as compared to the static model. The N-HMM results in an even higher SIR and a better SAR than the dynamic PLCA model. This is because the specific signal we are modeling has a temporal structure that is well described by a discrete dynamic model as we transition from phoneme to phoneme. By constraining our model to only use a small dictionary at each discrete state, we obtain a cleaner estimate of the source. An example of that

can be seen when comparing the separation results in Figure 4, where unwanted artifacts between the harmonics of speech in the dynamic PLCA example are not present in the N-HMM example since the dictionary elements within a state cannot produce such complex spectra.

WHICH MODEL TO USE?

Now, in addition to pondering on which divergence function is the most appropriate to employ, we also have a decision to make on which model is best for a source separation approach. As always, the answer depends on the nature of the sources in the mixture. In general, the static model has found success

in a variety of areas but does not take advantage of temporal correlations. In domains where we do not expect a high degree of correlations across time (e.g., short, burstlike sources) this model works well, but in cases where we expect a strong sense of continuity (e.g., a smooth source like a whale song), then a continuous dynamic model would work better. Furthermore, if we know that a source exhibits a behavior of switching through different states, each with its own unique character (e.g., speech), then a model like the N-HMM is more appropriate since it will eliminate the concurrent use of elements that belong at different states and produce a more plausible reconstruction. Of course, by using the generalized formulation we present in this article, there is nothing that limits us from employing different models concurrently. It is entirely plausible to design a source separation system where one source is modeled by a static model and other by a dynamic one, or even have both being described by different kinds of dynamic models. Doing so usually requires a relatively straightforward application of the estimation process that we outlined earlier.

CLOSING THOUGHTS

In this article we presented a unifying look at source separation approaches that employ nonnegative factorizations, and showed how they can be easily extended to temporal models that are either continuous or discrete. Using this methodology one can come up with many more alternative formulations, e.g., factorial HMMs, switching models, etc. and incorporate even more complex priors to better model sources in mixtures. We hope that by presenting this streamlined formulation we can help readers to experiment with the many other possibilities in formulating dynamic source separation algorithms and to help highlight relationships between a family of approaches that can initially seem divergent despite their common roots.

AUTHORS

Paris Smaragdís (paris@illinois.edu) is an assistant professor in the Computer Science Department and the Electrical and Computer Science Department at the University of Illinois at Urbana-Champaign, as well as a senior research scientist at Adobe Research. Prior to that he was a research scientist at Mitsubishi Electric Research Labs, during which time he was selected by *MIT Technology Review* as one of the top 35 young innovators of 2006. His research interests lie in the intersection of machine learning and signal processing. He is a Senior Member of the IEEE.

Cédric Févotte (cfevotte@unice.fr) received his Ph.D. degree from École Centrale de Nantes (2000–2003) and was with the University of Cambridge as a postdoctoral researcher (2003–2006). Previously, he was affiliated with Mist-Technologies (now Audionamix) as a research engineer (2006) and Télécom ParisTech (2007–2013). His research interests generally concern statistical signal processing and machine learning for inverse problems and source separation. He is a CNRS research scientist at the Laboratoire Lagrange (CNRS, Observatoire de la Côte d'Azur and the Université de Nice Sophia Antipolis), France. He is

a member of the IEEE Machine Learning for Signal Processing Technical Committee.

Gautham J. Mysore (gmysore@adobe.com) received the M.A. and Ph.D. degrees from the Center for Computer Research in Music and Acoustics at Stanford University and the M.S. degree in electrical engineering, also from Stanford. He is a senior research scientist at Adobe Research in San Francisco, California, and was previously a visiting researcher at the Gatsby Computational Neuroscience Unit at the University College London. His research interests include various aspects of machine learning and signal processing for audio. He is currently a member of the IEEE Technical Committee on Audio and Acoustic Signal Processing.

Nasser Mohammadiha (nmoh@kth.se) received the M.S. degree in electronics engineering from Sharif University of Technology, Tehran, Iran, in 2006. He worked on digital hardware and software design until 2008. He received his Ph.D. degree from the Communication Theory Laboratory, KTH Royal Institute of Technology, Stockholm, Sweden, in 2013. He received the Best Student Paper Award at the 2013 European Signal Processing Conference. Since November 2013, he has been a postdoctoral researcher at the University of Oldenburg, Germany. His research interests include machine learning for signal processing, statistical signal modeling, speech processing, and image processing. He is a Member of the IEEE.

Matthew Hoffman (mathoffm@adobe.com) is a research scientist in the Creative Technologies Laboratory at Adobe. He was previously a postdoctoral researcher working with Prof. Andrew Gelman in the Statistics Department at Columbia University. He completed his Ph.D. degree at Princeton University in computer science working in the Sound Lab with Prof. Perry Cook and Prof. David Blei. His research interests include developing efficient Bayesian (and pseudo-Bayesian) inference algorithms; hierarchical probabilistic modeling of audio, text, and marketing data; and audio feature extraction, music information retrieval, and the application of music information retrieval and modeling techniques to musical synthesis.

REFERENCES

- [1] D. D. Lee and H. S. Seung, "Learning the parts of objects with nonnegative matrix factorization," *Nature*, vol. 401, pp. 788–791, 1999.
- [2] A. Singh and G. Gordon, "A unified view of matrix factorization models," *Mach. Learn. Knowledge Discovery Databases*, vol. 5212, pp. 358–373, 2008.
- [3] P. Smaragdís, B. Raj, and M. Shashanka, "Supervised and semi-supervised separation of sounds from single-channel mixtures," in *Independent Component Analysis and Signal Separation* (Lecture Notes in Computer Science, vol. 4666). Berlin, Heidelberg, Germany: Springer, 2007, pp. 414–421.
- [4] C. Févotte, N. Bertin, and J.-L. Durrieu, "Nonnegative matrix factorization with the Itakura-Saito divergence. With application to music analysis," *Neural Computat.*, vol. 21, no. 3, pp. 793–830, Mar. 2009.
- [5] A. Cichocki, S. Cruces, and S. Amari, "Generalized Alpha-Beta divergences and their application to robust nonnegative matrix factorization," *Entropy*, vol. 13, pp. 134–170, 2011.
- [6] I. S. Dhillon and S. Sra, "Generalized nonnegative matrix approximations with Bregman divergences," *Adv. Neural Inform. Process. Syst. (NIPS)*, vol. 19, pp. 283–290, 2005.
- [7] A. Cichocki, R. Zdunek, A. H. Phan, and S.-I. Amari, *Nonnegative Matrix and Tensor Factorizations: Applications to Exploratory Multi-Way Data Analysis and Blind Source Separation*. Hoboken, NJ: Wiley, 2009.
- [8] M. D. Hoffman, "Poisson-uniform nonnegative matrix factorization," in *Proc. IEEE Conf. Acoustics, Speech, Signal Processing (ICASSP)*, 2012, pp. 5361–5364.

- [9] P. Smaragdis, B. Raj, and M. V. Shashanka, "A probabilistic latent variable model for acoustic modeling," in *NIPS Workshop on Advances in Models for Acoustic Processing*, 2006.
- [10] T. Hofmann, "Probabilistic latent semantic indexing," in *Proc. 22nd Int. Conf. Research Development Information Retrieval (SIGIR)*, 1999, pp. 50–57.
- [11] B. King, C. Févotte, and P. Smaragdis, "Optimal cost function and magnitude power for NMF-based speech separation and music interpolation," in *Proc. IEEE Int. Workshop Machine Learning Signal Processing (MLSP)*, Santander, Spain, Sep. 2012, pp. 1–6.
- [12] D. R. Hunter and K. Lange, "A tutorial on MM algorithms," *Amer. Statist.*, vol. 58, pp. 30–37, 2004. [Online]. Available: <http://amstat.tandfonline.com/doi/abs/10.1198/0003130042836#tabModule>
- [13] C. Févotte and J. Idier, "Algorithms for nonnegative matrix factorization with the beta-divergence," *Neural Computat.*, vol. 23, no. 9, pp. 2421–2456, Sept. 2011.
- [14] S. Arora, Y. Halpern, D. Mimno, A. Moitra, D. Sontag, Y. Wu, and M. Zhu, "A practical algorithm for topic modeling with provable guarantees," in *Proc. Int. Conf. Machine Learning*, 2013, pp. 280–288.
- [15] A. Anandkumar, D. Hsu, A. Javanmard, and S. Kakade, "Learning latent Bayesian networks and topic models under expansion constraints," submitted for publication. [Online]. Available: <http://arxiv.org/pdf/1209.5350.pdf>
- [16] K. Huang, N. Sidiropoulos, and A. Swami, "Non-negative matrix factorization revisited: Uniqueness and algorithm for symmetric decomposition," *IEEE Trans. Signal Processing*, vol. 62, no. 1, pp. 211–224, 2014.
- [17] P. Smaragdis, "Convolutional speech bases and their application to supervised speech separation," *IEEE Trans. Audio, Speech, Lang. Process.*, vol. 15, no. 1, pp. 1–12, Jan. 2007.
- [18] P. D. O'Grady and B. A. Pearlmutter, "Discovering speech phones using convolutional non-negative matrix factorisation with a sparseness constraint," *Neurocomputat.*, vol. 72, nos. 1–3, pp. 88–101, 2008.
- [19] W. Wang, A. Cichocki, and J. A. Chambers, "A multiplicative algorithm for convolutional non-negative matrix factorization based on squared Euclidean distance," *IEEE Trans. Signal Processing*, vol. 57, no. 7, pp. 2858–2864, July 2009.
- [20] Z. Chen, A. Cichocki, and T. M. Rutkowski, "Constrained non-negative matrix factorization method for EEG analysis in early detection of Alzheimer's disease," in *Proc. IEEE Int. Conf. Acoustics, Speech, Signal Processing (ICASSP)*, Toulouse, France, May 2006.
- [21] T. Virtanen, "Monaural sound source separation by non-negative matrix factorization with temporal continuity and sparseness criteria," *IEEE Trans. Audio, Speech Lang. Process.*, vol. 15, no. 3, pp. 1066–1074, Mar. 2007.
- [22] K. W. Wilson, B. Raj, and P. Smaragdis, "Regularized non-negative matrix factorization with temporal dependencies for speech denoising," in *Proc. Int. Conf. Spoken Language Processing (Interspeech)*, 2008, pp. 411–414.
- [23] T. Virtanen, A. T. Cemgil, and S. Godsill, "Bayesian extensions to non-negative matrix factorisation for audio signal modelling," in *Proc. Int. Conf. Acoustics, Speech, Signal Processing (ICASSP)*, Las Vegas, NV, Apr. 2008, pp. 1825–1828.
- [24] N. Mohammadiha, T. Gerkmann, and A. Leijon, "A new linear MMSE filter for single channel speech enhancement based on nonnegative matrix factorization," in *Proc. IEEE Workshop Applications Signal Processing Audio Acoustics (WASPAA)*, Oct. 2011, pp. 45–48.
- [25] C. Févotte, "Majorization-minimization algorithm for smooth Itakura-Saito nonnegative matrix factorization," in *Proc. IEEE Int. Conf. Acoustics, Speech, Signal Processing (ICASSP)*, May 2011, pp. 1980–1983.
- [26] S. Essid and Févotte, "Smooth nonnegative matrix factorization for unsupervised audiovisual document structuring," *IEEE Trans. Multimedia*, vol. 15, no. 2, pp. 415–425, Feb. 2013.
- [27] N. Mohammadiha, P. Smaragdis, and A. Leijon, "Supervised and unsupervised speech enhancement using NMF," *IEEE Trans. Audio, Speech, Lang. Process.*, vol. 21, no. 10, pp. 2140–2151, Oct. 2013.
- [28] M. Nakano, J. Le Roux, H. Kameoka, T. Nakamura, N. Ono, and S. Sagayama, "Bayesian nonparametric spectrogram modeling based on infinite factorial infinite hidden Markov model," in *Proc. IEEE Workshop Applications Signal Processing Audio Acoustics (WASPAA)*, New Paltz, NY, Oct. 2011, pp. 325–328.
- [29] K. Yoshii and M. Goto, "Infinite composite autoregressive models for music signal analysis," in *Proc. 13th Int. Society Music Information Retrieval Conf. (ISMIR)*, Oct. 2012, pp. 79–84.
- [30] N. Mohammadiha, J. Taghia, and A. Leijon, "Single channel speech enhancement using Bayesian NMF with recursive temporal updates of prior distributions," in *Proc. IEEE Int. Conf. Acoustics, Speech, Signal Processing (ICASSP)*, Mar. 2012, pp. 4561–4564.
- [31] M. Kim and P. Smaragdis, "Single channel source separation using smooth nonnegative matrix factorization with Markov random fields," in *IEEE Workshop Machine Learning Signal Processing (MLSP2013)*, Southampton, U.K., Sept. 2013, pp. 1–6.
- [32] C. Févotte, J. Le Roux, and J. R. Hershey, "Non-negative dynamical system with application to speech and audio," in *Proc. IEEE Int. Conf. Acoustics, Speech, Signal Processing (ICASSP)*, Vancouver, Canada, May 2013, pp. 3158–3162.
- [33] J. Nam, G. Mysore, and P. Smaragdis, "Sound recognition in mixtures," in *Latent Variable Analysis and Signal Separation* (Lecture Notes in Computer Science, vol. 7191). Berlin, Heidelberg, Germany: Springer, 2012, pp. 405–413.
- [34] N. Mohammadiha, P. Smaragdis, and A. Leijon, "Prediction based filtering and smoothing to exploit temporal dependencies in NMF," in *Proc. IEEE Int. Conf. Acoustics, Speech, Signal Processing (ICASSP)*, May 2013, pp. 873–877.
- [35] L. R. Rabiner, "A tutorial on hidden Markov models and selected applications in speech recognition," *Proc. IEEE*, vol. 77, no. 2, pp. 257–286, Feb. 1989.
- [36] A. Ozerov, C. Févotte, and M. Charbit, "Factorial scaled hidden Markov model for polyphonic audio representation and source separation," in *Proc. IEEE Workshop Applications Signal Processing Audio Acoustics (WASPAA)*, Oct. 2009, pp. 121–124.
- [37] G. J. Mysore, P. Smaragdis, and B. Raj, "Non-negative hidden Markov modeling of audio with application to source separation," in *Int. Conf. Latent Variable Analysis and Signal Separation*, 2010, pp. 140–148.
- [38] G. J. Mysore and P. Smaragdis, "A non-negative approach to semi-supervised separation of speech from noise with the use of temporal dynamics," in *Proc. Int. Conf. Acoustics, Speech, Signal Processing (ICASSP)*, May 2011, pp. 17–20.
- [39] M. Nakano, J. Roux, H. Kameoka, Y. Kitano, N. Ono, and S. Sagayama, "Nonnegative matrix factorization with markov-chained bases for modeling time-varying patterns in music spectrograms," in *Latent Variable Analysis and Signal Separation* (Lecture Notes in Computer Science, vol. 6365). Berlin, Heidelberg, Germany: Springer, 2010, pp. 149–156.
- [40] N. Mohammadiha and A. Leijon, "Nonnegative HMM for babble noise derived from speech HMM: Application to speech enhancement," *IEEE Trans. Audio, Speech, Lang. Process.*, vol. 21, no. 5, pp. 998–1011, May 2013.
- [41] G. J. Mysore, "A block sparsity approach to multiple dictionary learning for audio modeling," in *Proc. Int. Conf. Machine Learning (ICML) Workshop Sparsity, Dictionaries, Projections Machine Learning Signal Processing*, June 2012.
- [42] G. Mysore and P. Smaragdis, "A non-negative approach to language informed speech separation," in *Latent Variable Analysis and Signal Separation* (Lecture Notes in Computer Science, vol. 7191). Berlin, Heidelberg, Germany: Springer, 2012, pp. 356–363.
- [43] G. J. Mysore and M. Sahani, "Variational inference in non-negative factorial hidden Markov models for efficient audio source separation," in *Proc. Int. Conf. Machine Learning (ICML)*, June 2012, pp. 1887–1894.
- [44] P. Smaragdis, B. Raj, and M. Shashanka, "Supervised and semi-supervised separation of sounds from single-channel mixtures," in *Independent Component Analysis and Signal Separation* (Lecture Notes in Computer Science, vol. 4666). Berlin, Heidelberg: Springer, 2007, pp. 414–421.
- [45] E. Vincent, R. Gribonval, and C. Févotte, "Performance measurement in blind audio source separation," *IEEE Trans. Audio, Speech, Lang. Process.*, vol. 14, no. 4, pp. 1462–1469, 2006.
- [46] G. Zhou, A. Cichocki, Q. Zhao, and S. Xie, "Nonnegative matrix and tensor factorizations," *IEEE Signal Processing Mag.*, vol. 31, no. 3, pp. 54–65, May 2014.
- [47] J. S. Garofolo, L. F. Lamel, W. M. Fisher, J. G. Fiscus, and D. S. Pallet. (1993). DARPA TIMIT acoustic-phonetic continuous speech corpus CD-ROM. NIST speech disc 1-1.1. NASA STI Tech. Rep. N, 93, 27403.
- [48] A. Varga and H. J. Steeneken, "Assessment for automatic speech recognition: II. NOISEX-92: A database and an experiment to study the effect of additive noise on speech recognition systems," *Speech Commun.*, vol. 12, no. 3, pp. 247–251, 1993.

[Kejun Huang and Nicholas D. Sidiropoulos]

Putting Nonnegative Matrix Factorization to the Test

[A tutorial derivation of pertinent Cramér–Rao bounds and performance benchmarking]

Nonnegative matrix factorization (NMF) is a useful tool in a broad range of applications, from signal separation to computer vision and machine learning. NMF is a hard (NP-hard) computational problem for which various approximate solutions have been developed over the years. Given the widespread interest in NMF and its applications, it is perhaps surprising that the pertinent Cramér–Rao lower bound (CRLB) on the accuracy of the nonnegative latent factor estimates has not been worked out in the literature. In hindsight, one reason may be that the required computations are more subtle than usual: the problem involves constraints and ambiguities that must be dealt with, and the Fisher information matrix is always singular. We provide a concise tutorial derivation of the CRLB for both symmetric NMF and asymmetric NMF, using the latest CRLB tools, which should be of broad interest for analogous derivations in related factor analysis problems. We illustrate the behavior of these bounds with respect to model parameters and put some of the best NMF algorithms to the test against one another and the CRLB. The results help illuminate what can be expected from the current state of art in NMF

algorithms, and they are reassuring in that the gap to optimality is small in relatively sparse and low rank scenarios.

INTRODUCTION

NMF is the problem of (approximately) factoring an element-wise nonnegative matrix $\mathbf{X} \approx \mathbf{W}\mathbf{H}^T$, where \mathbf{W} is $I \times K$, \mathbf{H} is $J \times K$, $K < \min(I, J)$, and $\mathbf{W} \geq 0$, $\mathbf{H} \geq 0$ element-wise [1], [2]. Symmetric NMF is the problem of factoring a square matrix $\mathbf{X} \approx \mathbf{W}\mathbf{W}^T$, where the $I \times K$ matrix $\mathbf{W} \geq 0$ element-wise. Both general (asymmetric) and symmetric NMF have a long history and various applications; they were more recently introduced to the signal processing community, primarily as means to restore identifiability in bilinear matrix factorization/blind source separation (BSS).

The CRLB [3, Ch. 3] is the most widely used estimation benchmark in signal processing. In many cases it is relatively easy to compute, and it is asymptotically achievable by maximum likelihood (ML) estimators in high signal-to-noise ratio (SNR) scenarios [3, pp. 164]. In other cases, there may be technical difficulties in deriving (or complexity issues in computing) the pertinent CRLB; but due to the central role of this bound in signal processing research, work on developing CRLB tools continues [4]–[7], thereby enlarging the set of problems for which the CRLB can be used in practice.



Source Separation and Applications

IMAGE LICENSED BY
INGRAM PUBLISHING

Digital Object Identifier 10.1109/MSP.2013.2296172

Date of publication: 7 April 2014

Interestingly, despite the popularity of NMF, the pertinent CRLB on the latent factors has not been studied, to the best of our knowledge. This is surprising, especially because ML NMF is NP-hard, and it is natural to wonder how far from the best achievable estimation performance existing (suboptimal) NMF algorithms operate, under different scenarios. The missing link can perhaps be explained by the fact that most NMF researchers come from different communities, and, even for someone versed in statistical signal processing, the CRLB computations for NMF are subtle, requiring modern tools, as we will see. The aim of this article is threefold: first, to fill this gap; second, to put some of the leading NMF algorithms to the test using the CRLB as a benchmark; and third, to do so in an easily accessible way that can serve as a starting point for analogous derivations in related constrained matrix and tensor factorization problems.

FUNDAMENTALS

IDENTIFIABILITY

Rank-constrained matrix factorization is highly unidentifiable without additional constraints. For any given factorization $\mathbf{X} = \mathbf{W}\mathbf{H}^T$ and any invertible \mathbf{Q} , $\mathbf{X} = \hat{\mathbf{W}}\hat{\mathbf{H}}^T$ with $\hat{\mathbf{W}} = \mathbf{W}\mathbf{Q}^T$ and $\hat{\mathbf{H}} = \mathbf{H}\mathbf{Q}^{-1}$. For symmetric factorization $\mathbf{X} = \mathbf{W}\mathbf{W}^T$, we need only further require \mathbf{Q} to be unitary. To force the factorization to be unique, one must put additional constraints on the latent factors (the columns of \mathbf{W} and \mathbf{H}), e.g., orthogonality in the case of singular value decomposition (SVD). With $\mathbf{W} := [\mathbf{w}_1, \dots, \mathbf{w}_K]$, $\mathbf{H} := [\mathbf{h}_1, \dots, \mathbf{h}_K]$, $\mathbf{W}\mathbf{H}^T = \mathbf{w}_1\mathbf{h}_1^T + \dots + \mathbf{w}_K\mathbf{h}_K^T$; hence we may permute the rank-one outer products $\{\mathbf{w}_k\mathbf{h}_k^T\}_{k=1}^K$, and/or scale \mathbf{w}_k by $s > 0$ and counterscale \mathbf{h}_k by $1/s$ without changing $\mathbf{W}\mathbf{H}^T$. These ambiguities are inherent to NMF, requiring additional conventions (as opposed to conditions) to resolve, similar to ordering the singular values in the SVD. These inherent ambiguities are often inconsequential in applications, and we will say that a model is essentially identifiable or essentially unique when it can be identified up to these inherently unresolvable ambiguities. Still, these ambiguities are reflected in, and in fact dominate the CRLB, unless they are properly accounted for. In this article, for asymmetric NMF, we assume the columns of \mathbf{W} are scaled to sum up to one, i.e.,

$$\sum_{i=1}^I w_{i1} = \sum_{i=1}^I w_{i2} = \dots = \sum_{i=1}^I w_{iK} = 1 \quad (1)$$

to overcome the scaling ambiguity. Once we get estimates of \mathbf{W} and \mathbf{H} , denoted $\hat{\mathbf{W}}$ and $\hat{\mathbf{H}}$, respectively, using any NMF algorithm, we scale the columns of $\hat{\mathbf{W}}$ to satisfy (1), and counterscale the corresponding columns of $\hat{\mathbf{H}}$. Then least-squares matching of the columns of $\hat{\mathbf{W}}$ to those of \mathbf{W} is equivalent to the so-called linear assignment problem [8], whose solution can be found by the Hungarian algorithm [9], [10]. The MATLAB code is available at <http://www.mathworks.com/matlabcentral/fileexchange/11609-hungarian-algorithm>. In the symmetric case, there is no scaling ambiguity, so we directly use the Hungarian algorithm to find the best column permutation.

Conditions for (essential) uniqueness of NMF (ensuring that \mathbf{Q} can only be a positively scaled permutation matrix in the

asymmetric case, or simply a permutation matrix in the symmetric case) have previously been studied in [11]–[13], and are summarized in [14]. In a nutshell, NMF is not always unique, and pertinent conditions ensuring uniqueness are complicated (e.g., a sufficient condition for uniqueness requires the conic hull of the row vectors of \mathbf{W} to be a superset of a specific second-order cone [14]). The following corollary is a useful rule of thumb: if the sufficient condition given in [14, Th. 4] is satisfied for the symmetric NMF $\mathbf{X} = \mathbf{W}\mathbf{W}^T$, then

- the supports (sets of indices of nonzero entries) of any two columns of \mathbf{W} are not contained in one another.
- each column of \mathbf{W} contains at least $K - 1$ zeros.

The same holds for both \mathbf{W} and \mathbf{H} in the asymmetric case $\mathbf{X} = \mathbf{W}\mathbf{H}^T$. These two properties together are neither sufficient nor necessary for uniqueness; in practice however, as shown empirically in [14, Examples 3 and 4], it is very likely that NMF will give an essentially unique solution if these two conditions are both satisfied. Notice that if we set the zero entries of \mathbf{W} (and \mathbf{H} in the asymmetric case) randomly, with density (number of nonzero entries over the number of entries) less than $(I - K)/I$, then for large I these conditions will be met with high probability.

ALGORITHMS

Owing to the NP-hardness of asymmetric NMF [15], numerous approximation algorithms have been developed (cf. [16] and references therein). On the contrary, there are relatively few algorithms available for symmetric NMF (cf. [17] and references therein and [14]). If a symmetric matrix admits an exact symmetric NMF (not necessarily low rank), it is called *completely positive* (CP) [18]. It was recently proven that checking whether a matrix is CP is also NP-hard [19].

He et al. [17] summarized existing algorithms for symmetric NMF, which turned out being very similar (all based on so-called multiplicative updates). They concluded that those algorithms all belong to two basic kinds of algorithms: α -symmetric NMF and β -symmetric NMF, where α and β are tuning parameters that moderate performance (e.g., the algorithm in [20] belongs to α -symmetric NMF with $\alpha = 1/4$, and the algorithm in [21] belongs to β -symmetric NMF with $\beta = 1/2$). A very different algorithm based on Procrustes rotation was proposed in [14].

The algorithms for asymmetric NMF can be broadly classified as optimization-based and geometry-based. The cost function in optimization-based methods usually measures the quality of factorization, e.g., in terms of Euclidian distance, K-L divergence, etc., and may include regularization terms that capture presumed properties of the sought latent factors, e.g., sparsity, smoothness, etc. None of these formulations is jointly convex in \mathbf{W} and \mathbf{H} ($\mathbf{W}\mathbf{H}^T$ is a bilinear form); but in most cases they are conditionally convex over one factor given the other. Most optimization-based methods therefore adopt an alternating optimization approach—a few algorithms employ all-at-once (joint) parameter updates using gradient or Newton steps, but these require careful parameter tuning to ensure convergence to a local optimum. In the context of alternating optimization algorithms, for the update of one factor, one can take a

gradient direction but with a very conservative step-size such that positivity is always satisfied; this can be reduced to a multiplicative update [22], [23]. Alternatively, a more aggressive step-size can be used, but then a projection back to the nonnegative orthant is required [24]. A less popular way is to take the second-order derivative into account [25].

The most commonly used cost function is Euclidean distance. One reason for this is that when one factor is fixed, and if we ignore the nonnegativity constraint, the problem reduces to linear least squares, in which case we know the solution in closed form. Therefore, a straightforward way is to simply replace the negative entries of the least squares result with zeros in each update [26]—which is, however, suboptimum, and not guaranteed to converge. Taking the nonnegativity constraints back into consideration, the conditional update problem is nonnegative least squares, which is convex but the solution is not in closed form. Existing methods use quadratic programming [27], active set [28], [29], and coordinate descent [30].

Geometry-based methods stem from the geometric interpretation of NMF by Donoho [11]. The basic idea is to find a simplicial cone, with a certain number of extreme rays, that is contained in the nonnegative orthant and contains all the data points. The effectiveness of geometry-based methods is application dependent; in cases where the so-called separability assumption [11] is reasonable, the extreme rays of the simplicial cone can be found by selecting from the data vectors per se [31], [32]. In other cases, nonnegativity is not strictly required for one factor, and the aim is to find the minimum volume simplicial cone that contains the data points [33], [34]. A polytope approximation method [35] seems to be more general compared to the others in this genre.

MODERN CRLB TOOLS

Suppose a set of measurements \mathbf{X} is drawn from a probability density function $p(\mathbf{X}; \theta)$ parameterized by θ , and our goal is to estimate θ given the realizations of \mathbf{X} . If the regularity condition $\mathbb{E}_X\{\nabla_\theta \ln p(\mathbf{X}; \theta)\} = 0$ is satisfied, then we can define the Fisher information matrix (FIM) as $\mathbf{F}_\theta \triangleq \mathbb{E}_X\{[\nabla_\theta \ln p(\mathbf{X}; \theta)][\nabla_\theta \ln p(\mathbf{X}; \theta)]^T\}$, and the CRLB on the covariance matrix of any unbiased estimator of θ on the basis of \mathbf{X} is the inverse of the FIM

[3, Ch. 3], i.e., the difference between the estimator covariance matrix and the inverse of the FIM is positive semidefinite. From this, it follows that $\mathbb{E}_X\{\|\theta - \hat{\theta}\|_2^2\} \geq \text{tr}\{\mathbf{F}_\theta^{-1}\}$, where $\hat{\theta}$ is any unbiased estimator of θ on the basis of \mathbf{X} . More detailed discussion of the CRLB, including conditions under which there exists an estimator that can attain the bound, can be found in classic textbooks on estimation theory, e.g., [3, Ch. 3].

When the FIM is singular, Stoica and Marzetta [6] have shown that we can use the Moore–Penrose pseudoinverse instead (in hindsight, this can be deduced from the Schur complement generalized to singular matrices [36, p. 651]). The pseudoinverse is still a lower bound, albeit it is generally looser, and more difficult to attain. Important references on the CRLB for problems with constraints on the unknown parameters, represented by equalities and inequalities, include [4], [5], and [7]. Their results show that inequality constraints do not affect the CRLB, whereas equality constraints do. (Strictly speaking, inequalities do not affect the CRLB if they are not equivalent to equalities. For example, the two inequality constraints $\theta \geq 0$ and $\theta \leq 0$, are equivalent to $\theta = 0$. See the definition of a regular point in [4] for details.) Suppose the equality constraints are $\mathbf{g}(\theta) = 0$, then we can define \mathbf{U} as an orthonormal matrix whose columns span the null space of $\nabla_\theta \mathbf{g}(\theta)$, the Jacobian matrix of $\mathbf{g}(\theta)$, i.e., $\nabla_\theta \mathbf{g}(\theta)\mathbf{U} = 0$ and $\mathbf{U}^T \mathbf{U} = \mathbf{I}$. Then the constrained CRLB is modified as

$$\mathbb{E}_X\{\|\theta - \hat{\theta}\|_2^2\} \geq \text{tr}\{\mathbf{U}(\mathbf{U}^T \mathbf{F}_\theta \mathbf{U})^\dagger \mathbf{U}^T\},$$

where the superscript “ \dagger ” denotes the pseudoinverse. A simple derivation of the CRLB under affine equality constraints is given in “Cross-Checking the Constrained CRLB.”

CRAMÉR–RAO BOUNDS FOR NMF

In this section, we derive the CRLB for both symmetric and asymmetric NMF, under an additive white Gaussian noise (AWGN) model. Note that at low SNRs, Gaussian noise may generate observations having negative values, albeit the probability that this happens is negligible at higher SNRs. Yet the same is true for any additive noise model that is not one sided. A multiplicative noise model can capture two-sided perturbations with nonnegative noise, but if the signal elements are ≥ 1 , then taking the logarithm one obtains a NMF model with two-sided additive noise in the log domain. Hence the possibility of having negative data is unavoidable. Furthermore, Gaussian noise is implicitly assumed in all NMF applications where least squares is adopted for model fitting—including, e.g., the hierarchical alternating least squares (HALS) algorithm [30]. This is so because the least squares criterion can be interpreted as ML under a Gaussian noise model. Beyond this, it is interesting to note that for general signal models observed in independent and identically distributed (i.i.d.) additive noise, the CRLB under any noise distribution that possesses everywhere continuous first and second derivatives is the same as the corresponding Gaussian CRLB up to a constant multiplicative factor that depends on the noise distribution [37]. Hence, our results are more general than meets the eye.

CROSS-CHECKING THE CONSTRAINED CRLB

It is instructive to check the constrained CRLB for the special case of affine $\mathbf{g}(\theta)$ via the CRLB under transformation [3, Sec. 3.8]. Suppose $\mathbf{g}(\theta) = \mathbf{G}\theta - \mathbf{b} = 0$, and suppose \mathbf{U} satisfies that it is an orthonormal basis of the nullspace of \mathbf{G} . Then any feasible θ can be represented by the unconstrained variable α as $\theta = \mathbf{U}\alpha + \theta_0 \Rightarrow \alpha = \mathbf{U}^T(\theta - \theta_0)$, where θ_0 is one feasible point. Thus,

$$\nabla_\theta \ln p(\mathbf{x}; \theta) = \mathbf{U}^T \nabla_\alpha \ln p(\mathbf{x}; \alpha) \Rightarrow \mathbf{F}_\alpha = \mathbf{U}^T \mathbf{F}_\theta \mathbf{U}.$$

Now α is an unconstrained parameter to estimate, and the CRLB of θ via transformation of α is

$$(\nabla_\theta \alpha) \mathbf{F}_\alpha^\dagger (\nabla_\theta \alpha)^T = \mathbf{U}(\mathbf{U}^T \mathbf{F}_\theta \mathbf{U})^\dagger \mathbf{U}^T.$$

IDENTIFIABILITY, FIM, AND CRLB FOR THE SCALAR CASE

Before we delve into FIM and CRLB computations for NMF, it is instructive to consider the scalar case first, particularly $x = wh + n$, where w and h are nonnegative reals. This is clearly unidentifiable unless, e.g., we fix $w = 1$. Then this is equivalent to the linear estimation problem $x = h + n$, and if n is Gaussian with variance σ^2 , the CRLB is σ^2 . But for now, let us treat it as an estimation problem with two unknown parameters $[wh]^T$, with the constraint $w = 1$. Then the FIM is

$$F_{w,h} = \frac{1}{\sigma^2} \begin{bmatrix} h^2 & wh \\ hw & w^2 \end{bmatrix} = \frac{1}{\sigma^2} \begin{bmatrix} h^2 & h \\ h & 1 \end{bmatrix},$$

while $\mathbf{u} = [01]^T$ spans the null space of the Jacobian of the equality constraint. Therefore, the CRLB is

$$\mathbf{u}(\mathbf{u}^T F_{w,h} \mathbf{u})^{-1} \mathbf{u}^T = \begin{bmatrix} 0 & 0 \\ 0 & \sigma^2 \end{bmatrix},$$

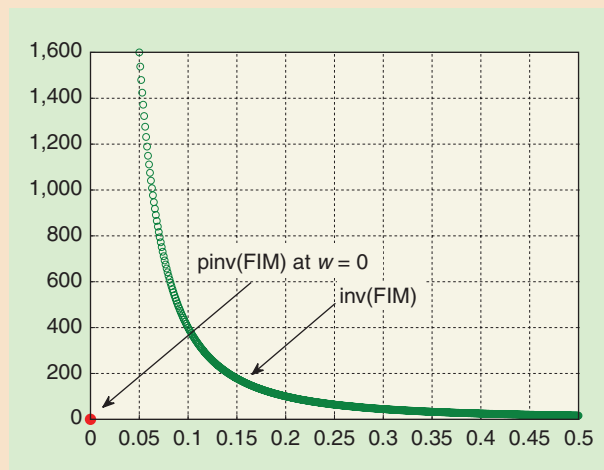
which is consistent with what we get by treating it as a single parameter problem. The symmetric scalar model $x = w^2 + n$ is sign-unidentifiable, but with the nonnegativity constraint $w \geq 0$ it becomes identifiable. For n zero-mean Gaussian with variance σ^2 , it is easy to compute the Fisher information for w , which is

$$F_w = \frac{4}{\sigma^2} w^2.$$

Notice that the Fisher information is zero if $w = 0$, and as a special case of pseudoinverse, $0^\dagger = 0$. Since the parametric constraint is an inequality, the CRLB is unaffected according to [4], so for any unbiased estimator \hat{w} ,

$$E_x\{(w - \hat{w})^2\} \geq \begin{cases} 0 & w = 0, \\ \frac{\sigma^2}{4} w^{-2} & w \neq 0. \end{cases}$$

This is illustrated in Figure S1. Notice that the pseudoinverse of the FIM is a legitimate bound, albeit far from being attainable when $w = 0$. The situation is not as bad in the matrix case—in fact, we will see that existing algorithms come close to attaining the optimistic CRLB obtained from the pseudoinverse, under certain conditions.



[FIGS1] The CRLB for scalar symmetric NMF.

As a warm-up, a derivation of the CRLB for scalar NMF is presented in “Identifiability, FIM, and CRLB for the Scalar Case.”

A CRLB FOR SYMMETRIC NMF

Consider the $I \times I$ symmetric matrix X generated as

$$X = WW^T + N, \tag{2}$$

where W is $I \times K$, $W \geq 0$, and the elements of N are drawn from an i.i.d. Gaussian distribution with zero-mean and variance σ^2 . The $IK \times IK$ Fisher information matrix for W is

$$F_W = \frac{2}{\sigma^2} (W^T W \otimes I_I + (I_K \otimes W) P (I_K \otimes W)^T), \tag{3}$$

where I_I is the identity matrix of size $I \times I$, and likewise for I_K and all the boldface I with a subscript indicating its size in the rest of the article, “ \otimes ” indicates matrix Kronecker product [38, Sec. 10.2.1], and P is a specific permutation matrix; see the supporting supplementary material that accompanies this article in IEEE *Xplore*. Here the constraints are $W \geq 0$, which do not affect the CRLB. In addition, F_W is rank deficient (see the supporting supplementary material), so we need to compute its pseudoinverse to get the CRLB.

In practice, when the size of W is large, we are usually interested in the overall reconstruction error $\|W - \hat{W}\|_F^2$, and the

CRLB implies that $E_x\{\|W - \hat{W}\|_F^2\} \geq \text{tr}\{F_W^\dagger\}$. We also look at the relative error, normalized by $\|W\|_F^2$, so that the scale and the size of W are taken into account. Thus, the normalized aggregate CRLB for symmetric NMF is given by

$$\frac{E_x\{\|W - \hat{W}\|_F^2\}}{\|W\|_F^2} \geq \frac{\text{tr}\{F_W^\dagger\}}{\|W\|_F^2}. \tag{4}$$

For $K = 1$, the symmetric decomposition is unique even without nonnegativity constraints, and the FIM is invertible. The CRLB can be calculated in closed form, as provided in “Identifiability, FIM, and CRLB for the Symmetric Vector Case.”

Figure 1 illustrates how this normalized CRLB changes as a function of the outer dimension I (the number of rows of W), the inner dimension K (the number of columns of W), and the density (the amount of nonzero entries). The pattern of (non)zeros in W were drawn from an i.i.d. Bernoulli distribution, and the nonzero entries of W were drawn from an i.i.d. exponential distribution. In Figure 1(a), the inner dimension is fixed to be ten, while the outer dimension increases from 50 to 150, for different densities; in (b), the outer dimension is fixed at 100, while the inner dimension increases from five to 25, with different densities. In all cases, the SNR

$$\text{SNR} = 10 \log_{10} \frac{\|WW^T\|_F^2}{I^2 \sigma^2}$$

IDENTIFIABILITY, FIM, AND CRLB FOR THE SYMMETRIC VECTOR CASE

Consider the vector case

$$\mathbf{X} = \mathbf{w}\mathbf{w}^T + \mathbf{N}.$$

Obviously, this problem is also identifiable if $\mathbf{N} = 0$, apart from a sign ambiguity. We do not need to impose nonnegativity constraints on all the elements of \mathbf{w} to resolve the ambiguity, but only on one element, e.g., $w_1 \geq 0$. The FIM can be computed as a special case of the formula (3), whose derivation can be found in the supplementary material in IEEE *Xplore*, yielding

$$\mathbf{F}_w = \frac{2}{\sigma^2} (\|\mathbf{w}\|^2 \mathbf{I}_I + \mathbf{w}\mathbf{w}^T),$$

which is nonsingular for $\mathbf{w} \neq \mathbf{0}$, and we can calculate its inverse in closed form, using the matrix inversion lemma [38],

$$\mathbf{F}_w^{-1} = \frac{\sigma^2}{2} \left(\|\mathbf{w}\|^{-2} \mathbf{I}_I - \frac{1}{2} \|\mathbf{w}\|^{-4} \mathbf{w}\mathbf{w}^T \right).$$

Thus,

$$\frac{\mathbf{E}_x \{ \|\mathbf{w} - \hat{\mathbf{w}}\|^2 \}}{\|\mathbf{w}\|^2} \geq \frac{\text{tr}\{\mathbf{F}_w^{-1}\}}{\|\mathbf{w}\|^2} = \frac{\sigma^2}{2} \left(I - \frac{1}{2} \right) \|\mathbf{w}\|^{-4}.$$

Notice here that italic I is the dimension of \mathbf{w} (not to be confused with the identity matrix \mathbf{I}).

is fixed at 10 dB. Each CRLB with the specified size and density is calculated as the average of 100 Monte Carlo draws of \mathbf{W} . Note how the density of \mathbf{W} affects the CRLB—the sparser the latent factors, the lower the CRLB. Not surprisingly, the CRLB increases as the ratio between the outer dimension and the inner dimension decreases.

CRLB FOR ASYMMETRIC NMF

Consider the $I \times J$ asymmetric matrix generated as

$$\mathbf{X} = \mathbf{W}\mathbf{H}^T + \mathbf{N}, \tag{5}$$

where \mathbf{W} is $I \times K$, $\mathbf{W} \geq 0$, \mathbf{H} is $J \times K$, $\mathbf{H} \geq 0$, and the elements of \mathbf{N} are drawn from an i.i.d. Gaussian distribution with zero-mean and variance σ^2 . The $(I+J)K \times (I+J)K$ Fisher information matrix of \mathbf{W} and \mathbf{H} is (cf. supporting supplementary material in IEEE *Xplore*, which also shows that $\mathbf{F}_{\mathbf{W},\mathbf{H}}$ is rank deficient)

$$\mathbf{F}_{\mathbf{W},\mathbf{H}} = \frac{1}{\sigma^2} \begin{bmatrix} \mathbf{H}^T \mathbf{H} \otimes \mathbf{I}_I & (\mathbf{I}_K \otimes \mathbf{W}) \mathbf{P} (\mathbf{I}_K \otimes \mathbf{H})^T \\ (\mathbf{I}_K \otimes \mathbf{H}) \mathbf{P} (\mathbf{I}_K \otimes \mathbf{W})^T & \mathbf{W}^T \mathbf{W} \otimes \mathbf{I}_J \end{bmatrix}. \tag{6}$$

Here, the constraints on the parameters are $\mathbf{W} \geq 0$, $\mathbf{H} \geq 0$, and (1). In calculating the CRLB, we only need to take into account the equality constraints. The Jacobian of the equality constraints over \mathbf{W} is

$$\nabla_{\text{vec}(\mathbf{W})} \begin{bmatrix} \sum_{i=1}^I w_{i1} - 1 \\ \vdots \\ \sum_{i=1}^I w_{iK} - 1 \end{bmatrix} = \mathbf{I}_K \otimes \mathbf{1}^T,$$

where $\mathbf{1}$ is the all 1 vector with dimension I . Upon defining

$$\mathbf{v}_i = \frac{1}{\sqrt{i+i^2}} \left(\sum_{l=1}^i e_l - i e_{i+1} \right), \quad \mathbf{V} = [\mathbf{v}_1 \ \mathbf{v}_2 \ \dots \ \mathbf{v}_{I-1}], \tag{7}$$

we have $\mathbf{V}^T \mathbf{1} = 0$ and $\mathbf{V}^T \mathbf{V} = \mathbf{I}_{I-1}$. Therefore, let

$$\mathbf{U} = \begin{bmatrix} \mathbf{I}_K \otimes \mathbf{V} & \mathbf{0} \\ \mathbf{0} & \mathbf{I}_{JK} \end{bmatrix},$$

satisfying

$$\begin{pmatrix} \nabla_{\text{vec}(\mathbf{W})} \\ \nabla_{\text{vec}(\mathbf{H})} \end{pmatrix} \begin{bmatrix} \sum_{i=1}^I w_{i1} - 1 \\ \vdots \\ \sum_{i=1}^I w_{iK} - 1 \end{bmatrix} \mathbf{U} = \mathbf{0}, \quad \mathbf{U}^T \mathbf{U} = \mathbf{I}_{(I+J-1)K}.$$

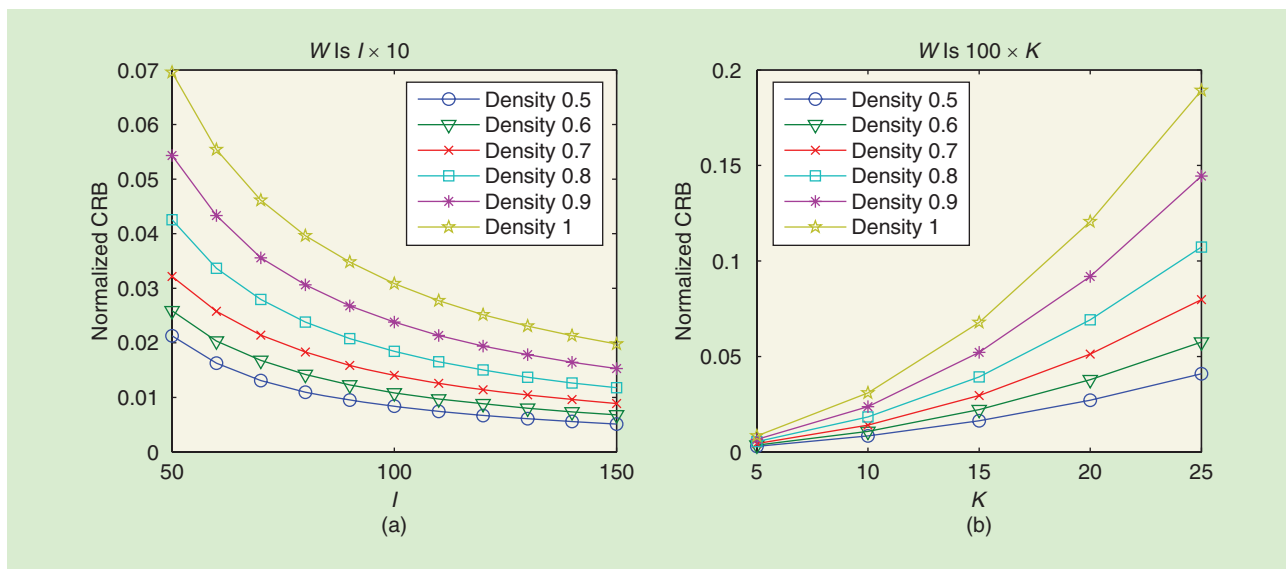


[FIG1] (a) and (b) The symmetric NMF CRLB—how the outer dimension, inner dimension, and density affects the CRLB, for SNR=10 dB.

Using the FIM $\mathbf{F}_{\mathbf{W},\mathbf{H}}$ and the null basis \mathbf{U} above, we obtain the CRLB for \mathbf{W} and \mathbf{H} as $\mathbf{U}(\mathbf{U}^T \mathbf{F}_{\mathbf{W},\mathbf{H}} \mathbf{U})^\dagger \mathbf{U}^T$.

In practice, the reconstruction errors $\|\mathbf{W} - \hat{\mathbf{W}}\|_F^2$ and $\|\mathbf{H} - \hat{\mathbf{H}}\|_F^2$ are usually assessed separately since \mathbf{W} and \mathbf{H} model different entities (e.g., loadings and scores). Partition $(\mathbf{U}^T \mathbf{F}_{\mathbf{W},\mathbf{H}} \mathbf{U})^\dagger$ into blocks

$$(\mathbf{U}^T \mathbf{F}_{\mathbf{W},\mathbf{H}} \mathbf{U})^\dagger = \begin{bmatrix} \Phi_1 & \Phi_2 \\ \Phi_2^T & \Phi_3 \end{bmatrix},$$

where Φ_1 is $IK \times IK$ and Φ_3 is $JK \times JK$. Then

$$\frac{\mathbb{E}_X\{\|\mathbf{W} - \hat{\mathbf{W}}\|_F^2\}}{\|\mathbf{W}\|_F^2} \geq \frac{\text{tr}\{(\mathbf{I}_K \otimes \mathbf{V}) \Phi_1 (\mathbf{I}_K \otimes \mathbf{V})^T\}}{\|\mathbf{W}\|_F^2}, \quad (8a)$$

$$\frac{\mathbb{E}_X\{\|\mathbf{H} - \hat{\mathbf{H}}\|_F^2\}}{\|\mathbf{H}\|_F^2} \geq \frac{\text{tr}\{\Phi_3\}}{\|\mathbf{H}\|_F^2}, \quad (8b)$$

with similar normalization as in the symmetric case.

Similar to the symmetric case, for $K = 1$ the asymmetric decomposition is essentially unique, and the matrix we need to pseudoinvert for calculating the CRLB is actually nonsingular. The closed form CRLB for this case is given in “Identifiability, FIM, and CRLB for the Asymmetric Vector Case.”

Figure 2 plots the CRLB for asymmetric NMF for various sizes and densities. Figure 2(a) and (b) shows the CRLB for \mathbf{W} , which is constrained such that each column sums up to one, while (c) and (d) show the CRLB for \mathbf{H} , which does not have any scaling constraints. Figure 2(a) and (c) shows the CRLB when the size of \mathbf{W} is fixed at 100×10 , and the number of rows in \mathbf{H} increases from 50 to 150, with different densities. Figure 2(b) and (d) shows the CRLB when the number of rows in \mathbf{W} and \mathbf{H} is fixed at 100 and 120, respectively, and the number of columns in \mathbf{W} and \mathbf{H} increases from five to 25, with different densities. As usual, SNR

$$\text{SNR} = 10 \log_{10} \frac{\|\mathbf{W}\mathbf{H}^T\|_F^2}{I J \sigma^2}$$

is fixed at 10 dB. Each CRLB point for a specified size and density is calculated as the average of 100 Monte Carlo draws. Figure 2(c)

may seem curious: it shows the normalized CRLB with respect to \mathbf{H} when we fix \mathbf{W} and gradually increase the number of rows of \mathbf{H} , and we observe that the normalized CRLB does not change very much. It slowly increases as the outer-dimension of \mathbf{H} increases, as opposed to the normalized CRLB for \mathbf{W} , which seems to decrease exponentially. This is because the block in the FIM $\mathbf{F}_{\mathbf{W},\mathbf{H}}$ that corresponds to \mathbf{H} is $\mathbf{W}^T \mathbf{W} \otimes \mathbf{I}_J$, where the dimension of \mathbf{I}_J changes according to the dimension of \mathbf{H} , which contributes the most to the block of the CRLB that corresponds to \mathbf{H} . The $\mathbf{W}^T \mathbf{W}$ part is fixed, and the size of \mathbf{I}_J grows approximately linearly with $\|\mathbf{H}\|_F^2$, which explains intuitively why the normalized CRLB for \mathbf{H} does not change very much. Apart from that, the overall tendency of the CRLB versus the size is similar to the symmetric case: it goes down as one of the outer dimensions increases, and it goes up as the common inner dimension increases, as intuitively expected from “equations versus unknowns” considerations. Note, however, that here as the number of observations increases, so does the number of unknown parameters. For example, if a new column is appended to \mathbf{X} then a new row is appended to \mathbf{H} as well, and the CRLB may worsen, depending on the new entries and other factors [e.g., the way we resolve the scaling ambiguity; see Figure 2(a) and (c)].

What is more, the sparser \mathbf{W} and \mathbf{H} , the lower the CRLB in all cases.

PUTTING NMF ALGORITHMS TO THE TEST

SYMMETRIC NMF

We compared three algorithms for symmetric NMF with the CRLB derived in the section “Cramer–Rao Bounds for NMF.” These are α -symmetric NMF and β -symmetric NMF with $\alpha = \beta = 0.99$ [17], and the algorithm recently proposed in [14]. The true \mathbf{W} is generated such that a certain proportion of its entries are randomly set to zero, and the rest are drawn from an i.i.d. exponential distribution. Using the generative model (2) the

IDENTIFIABILITY, FIM, AND CRLB FOR THE ASYMMETRIC VECTOR CASE

For $K = 1$, i.e., when \mathbf{w} and \mathbf{h} are vectors, asymmetric factorization is identifiable from noiseless (rank-one) data, similar to the symmetric case. There is still a scaling issue, and we can resolve this by fixing the scaling of one factor, e.g., setting $\mathbf{1}^T \mathbf{w} = 1$ as we did in the matrix case. Then, using (6), the FIM is

$$\mathbf{F}_{\mathbf{w},\mathbf{h}} = \frac{1}{\sigma^2} \begin{bmatrix} \|\mathbf{h}\|^2 \mathbf{I}_I & \mathbf{w}\mathbf{h}^T \\ \mathbf{h}\mathbf{w}^T & \|\mathbf{w}\|^2 \mathbf{I}_J \end{bmatrix}.$$

The corresponding \mathbf{U} matrix is

$$\mathbf{U} = \begin{bmatrix} \mathbf{V} & \mathbf{0} \\ \mathbf{0} & \mathbf{I}_J \end{bmatrix}$$

with the same \mathbf{V} as defined in (7). Let us first try to calculate the following inversion

$$(\mathbf{U}^T \mathbf{F}_{\mathbf{w},\mathbf{h}} \mathbf{U})^{-1} = \sigma^2 \begin{bmatrix} \|\mathbf{h}\|^2 \mathbf{I}_{I-1} & \mathbf{V}^T \mathbf{w}\mathbf{h}^T \\ \mathbf{h}\mathbf{w}^T \mathbf{V} & \|\mathbf{w}\|^2 \mathbf{I}_J \end{bmatrix}^{-1} = \begin{bmatrix} \Phi_1 & \Phi_2 \\ \Phi_2^T & \Phi_3 \end{bmatrix}$$

where Φ_1 and Φ_3 are the inverse of the Schur complement [36, p. 650] of $\sigma^{-2} \|\mathbf{h}\|^2 \mathbf{I}_{I-1}$ and $\sigma^{-2} \|\mathbf{w}\|^2 \mathbf{I}_J$, respectively, in $\mathbf{U}^T \mathbf{F}_{\mathbf{w},\mathbf{h}} \mathbf{U}$, i.e.,

$$\Phi_1 = \sigma^2 \left(\|\mathbf{h}\|^2 \mathbf{I}_{I-1} - \frac{\|\mathbf{h}\|^2}{\|\mathbf{w}\|^2} \mathbf{V}^T \mathbf{w}\mathbf{w}^T \mathbf{V} \right)^{-1},$$

$$\Phi_3 = \sigma^2 \left(\|\mathbf{w}\|^2 \mathbf{I}_J - \frac{\|\mathbf{V}^T \mathbf{w}\|^2}{\|\mathbf{h}\|^2} \mathbf{h}\mathbf{h}^T \right)^{-1}.$$

Again, the inverses can be calculated in closed form by using the matrix inversion lemma. Using the Pythagorean theorem $\|\mathbf{w}\|^2 = \|\mathbf{V}^T \mathbf{w}\|^2 + (\mathbf{1}^T \mathbf{w})^2$ (details omitted), we obtain

$$\frac{\mathbb{E}_X\{\|\mathbf{w} - \hat{\mathbf{w}}\|_F^2\}}{\|\mathbf{w}\|^2} \geq \frac{\text{tr}\{\mathbf{V}\Phi_1\mathbf{V}^T\}}{\|\mathbf{w}\|^2} = \sigma^2 \|\mathbf{w}\|^{-2} \|\mathbf{h}\|^{-2} (I - 1 + I(\mathbf{V}^T \mathbf{w})^2),$$

$$\frac{\mathbb{E}_X\{\|\mathbf{h} - \hat{\mathbf{h}}\|_F^2\}}{\|\mathbf{h}\|^2} \geq \frac{\text{tr}\{\Phi_3\}}{\|\mathbf{h}\|^2} = \sigma^2 \|\mathbf{w}\|^{-2} \|\mathbf{h}\|^{-2} (J + I \|\mathbf{V}^T \mathbf{w}\|^2).$$

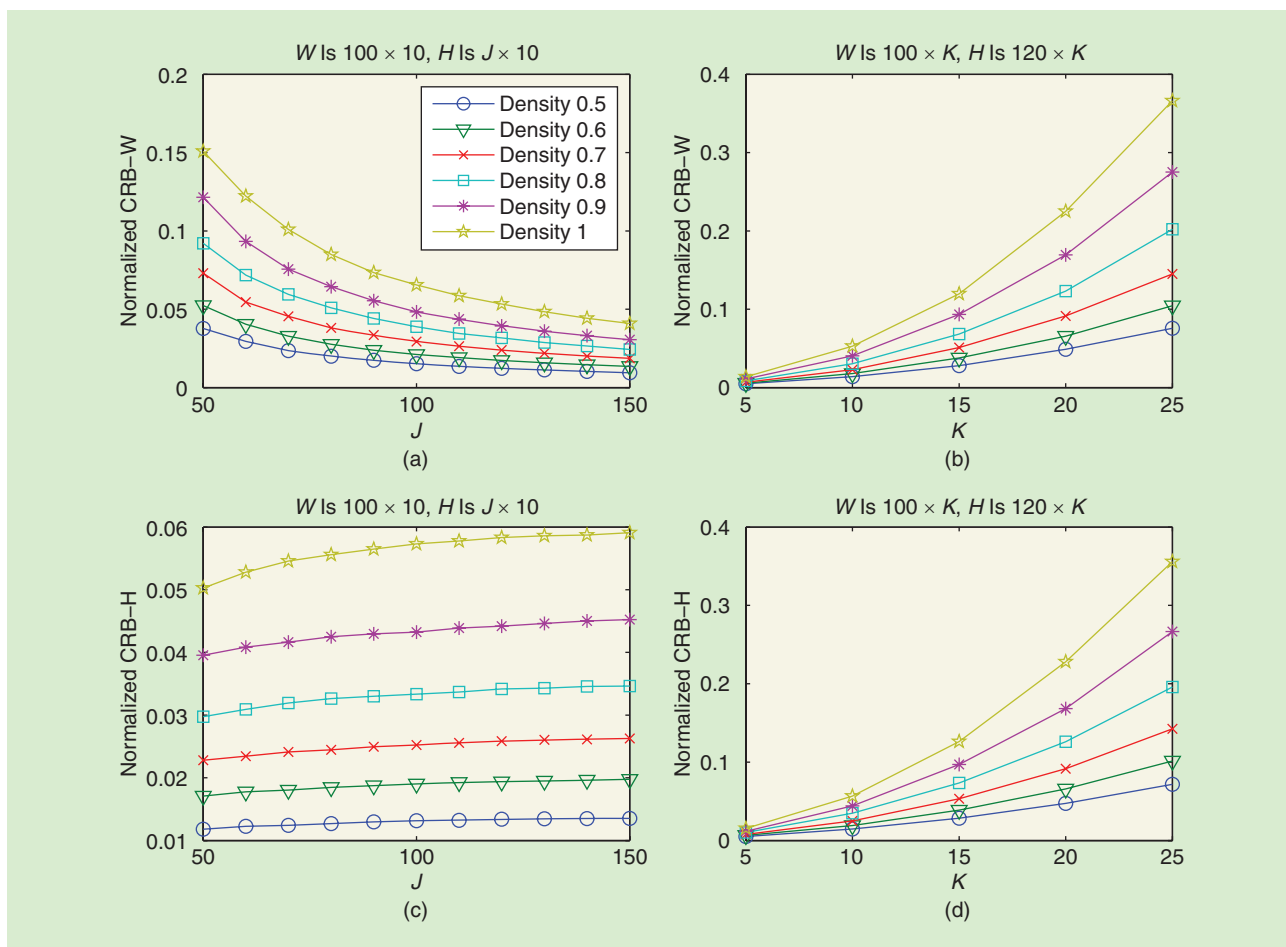


[FIG2] (a)–(d) The asymmetric NMF CRLB—how the outer dimensions, inner dimension, and density affects the CRLB, for SNR=10 dB.

resulting X will not be symmetric, so we use $(1/2)(X + X^T)$, since all algorithms are designed specifically for symmetric nonnegative matrices. Reference [17] did not provide a termination criterion, so both α -symmetric NMF and β -symmetric NMF are left to run for a large number of iterations (10^4), to ensure the best possible results. For the algorithm in [14], we used the termination criterion described in [14, Fig. 4] with the tolerance set to machine precision ϵ . We used a single draw of W for each (size, density) combination reported. Under various SNRs, the normalized squared error $(\| \hat{W} - W_F^2 \|) / (\| W \|_F^2)$ is calculated and averaged over 100 Monte Carlo tests, so that we can get a better approximation to the expected error $E_X \{ (\| \hat{W} - W \|_F^2) / (\| W \|_F^2) \}$.

The results are plotted in Figure 3, where (a) shows the normalized squared error benchmarked by the CRLB, (b) shows the (aggregate) bias for each estimate, defined as

$$\text{bias} = \left\| \frac{1}{T} \sum_{t=1}^T (W - \hat{W}_t) \right\|_F, \quad (9)$$

where T is the number of trials, in this case 100, and (c) shows the model fitting error for each algorithm. The dashed lines in (c) show the total noise power; a good approximation should yield a fitting error close to the noise power. The plots in the left column

show a case where the symmetric NMF problem is relatively “overdetermined,” since the inner dimension (30) is small compared to the outer dimension (200), and the latent factors are quite sparse (density 0.5). The two other columns show more difficult cases—low rank (30 versus 200) but relatively dense latent factors for the middle column, not-so-low rank (50 versus 100) but relatively sparse latent factors for the right column. Recall the discussion in the section “Fundamentals” for the rule of thumb for when identifiability can be expected—the middle and right columns illustrate cases where this requirement is barely satisfied.

In all cases, the aggregate bias is small and goes to zero as SNR increases, indicating that the estimates provided by these algorithms are asymptotically unbiased, and we can use the CRLB to approximately bound the performance. Generally speaking, α/β -symmetric NMF slightly outperform the Procrustes rotation algorithm [14] in the low SNR regime but fail to reach the CRLB in the high SNR regime. The algorithm in [14] exhibits classic threshold behavior—for SNR higher than some threshold, the mean square error (MSE) stays close to the CRLB. The reason is that it employs eigenanalysis to estimate the column space of W as a first step and then applies Procrustes rotations in the estimated subspace. On the other hand, both

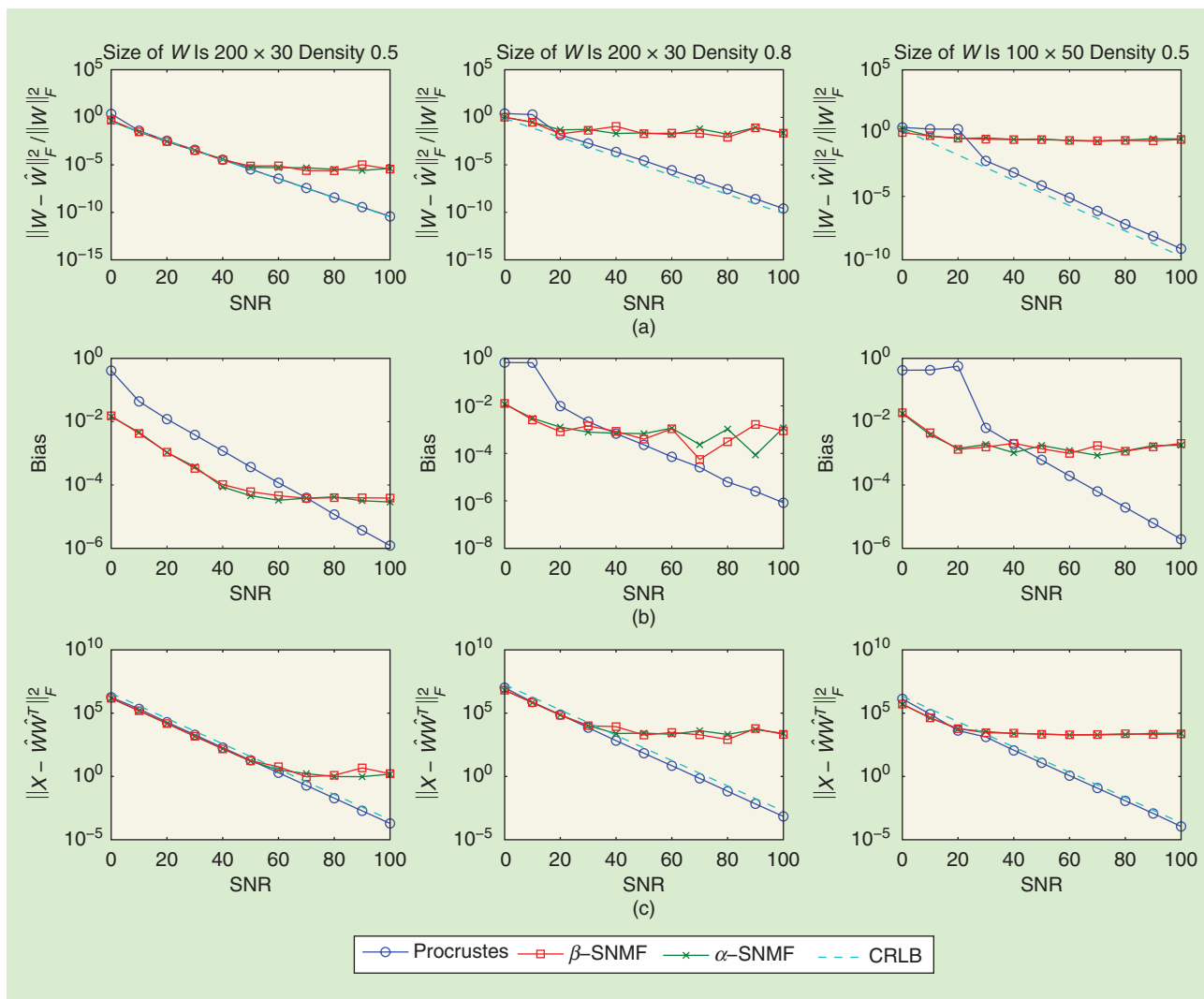


[FIG3] (a) The normalized squared error of three existing symmetric NMF algorithms versus the CRLB; similarly, (b) shows the (aggregate) bias, and (c) shows the fitting error.

symmetric NMF variants are modifications of the multiplicative update algorithm using $\|X - WW^T\|_F^2$ (Gaussian log-likelihood) as the objective, so that it is not surprising that they perform better in the low-SNR regime. We can also see this from Figure 3(b), as the biases of α/β -symmetric NMF are lower than that of the Procrustes method under low SNR.

ASYMMETRIC NMF

In this section, we compare several asymmetric NMF algorithms aiming to minimize the Euclidian distance. Notice that the data we synthetically generated were corrupted by additive i.i.d. Gaussian noise, so using Euclidian distance as the objective actually gives us the ML estimate. This is why algorithms that use other divergence functions as the objective were not considered here. The algorithms tested are:

- multiplicative update (MU) proposed by Lee and Seung [22]
- alternating least squares (ALS) proposed by Berry et al. [26]

- projected gradient (PG) proposed by Lin [24] (the MATLAB code can be downloaded from <http://www.csie.ntu.edu.tw/~cilin/nmf/index.html>)
- fast HALS proposed by Cichocki and Phan [30, Algor. 2]
- block principle pivoting (BPP) alternating nonnegative least squares using BPP proposed by Kim and Park [29] (the MATLAB code can be downloaded from <http://www.cc.gatech.edu/~hpark/nmfsoftware.php>).

For all algorithms, we used the optimality condition in [39] to check for termination, i.e., calculate

$$\left\| \begin{bmatrix} W \circ ((X - WH^T)H) \\ H \circ ((X^T - HW^T)W) \end{bmatrix} \right\|_F$$

in each iteration and terminate when it is smaller than the machine precision ϵ , with a maximum number of iteration set as

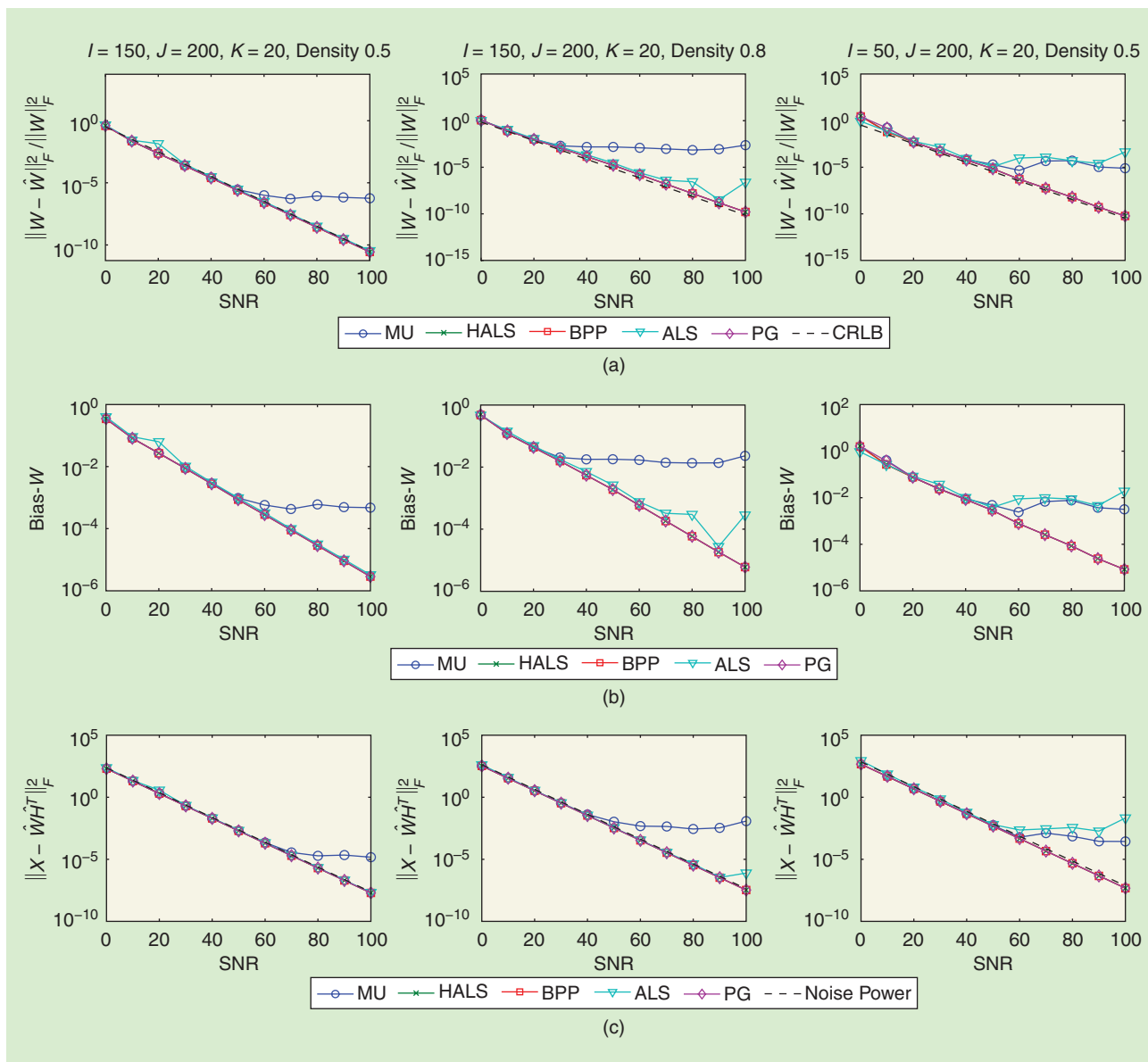


[FIG4] In (a), the normalized squared error for W using various asymmetric NMF algorithms versus the CRLB is shown; similarly, (b) shows the (aggregate) bias for W and (c) the fitting error.

10^4 . In the expression, \odot stands for the Hadamard (element-wise) matrix product. Similar to the symmetric case, the entries of W and H were generated such that a certain proportion of them are randomly set to 0, and the rest are drawn from an i.i.d. exponential distribution. Then the columns of W are scaled to sum up to one.

Three tests were conducted and illustrated in Figures 4 and 5 for W and H , respectively—low-rank and sparse latent factors on the left, low rank but moderately dense in the middle, and an unbalanced case (J much larger than I) where the rank is not small compared to the smaller outer dimension, with density set relatively small to ensure identifiability. Similar to Figure 3, Figures 4(a) and 5(a) show the normalized squared error for each algorithm benchmarked by the CRLB, Figures 4(b) and 5(b) show

the (aggregate) bias of W as defined in (9), and similarly for H , and Figure 4(c) shows the fitting error for each algorithm.

As we can see from Figures 4(b) and 5(b) the biases are generally small and approach zero with increasing SNR, indicating that we can use the CRLB to approximately bound performance. In all three cases, HALS, BPP, and PG were able to provide a good estimate with MSE close to the CRLB, under all SNRs tested. On the other hand, MU and ALS are not guaranteed to work well even under very high SNR. All methods separate the variables into blocks, and HALS, BPP, and PG aim to find the conditionally optimal point before moving to the next block, whereas the updates of MU and ALS cannot guarantee this. Interestingly, in the “well-posed” case shown in the left columns of Figures 4 and 5, ALS

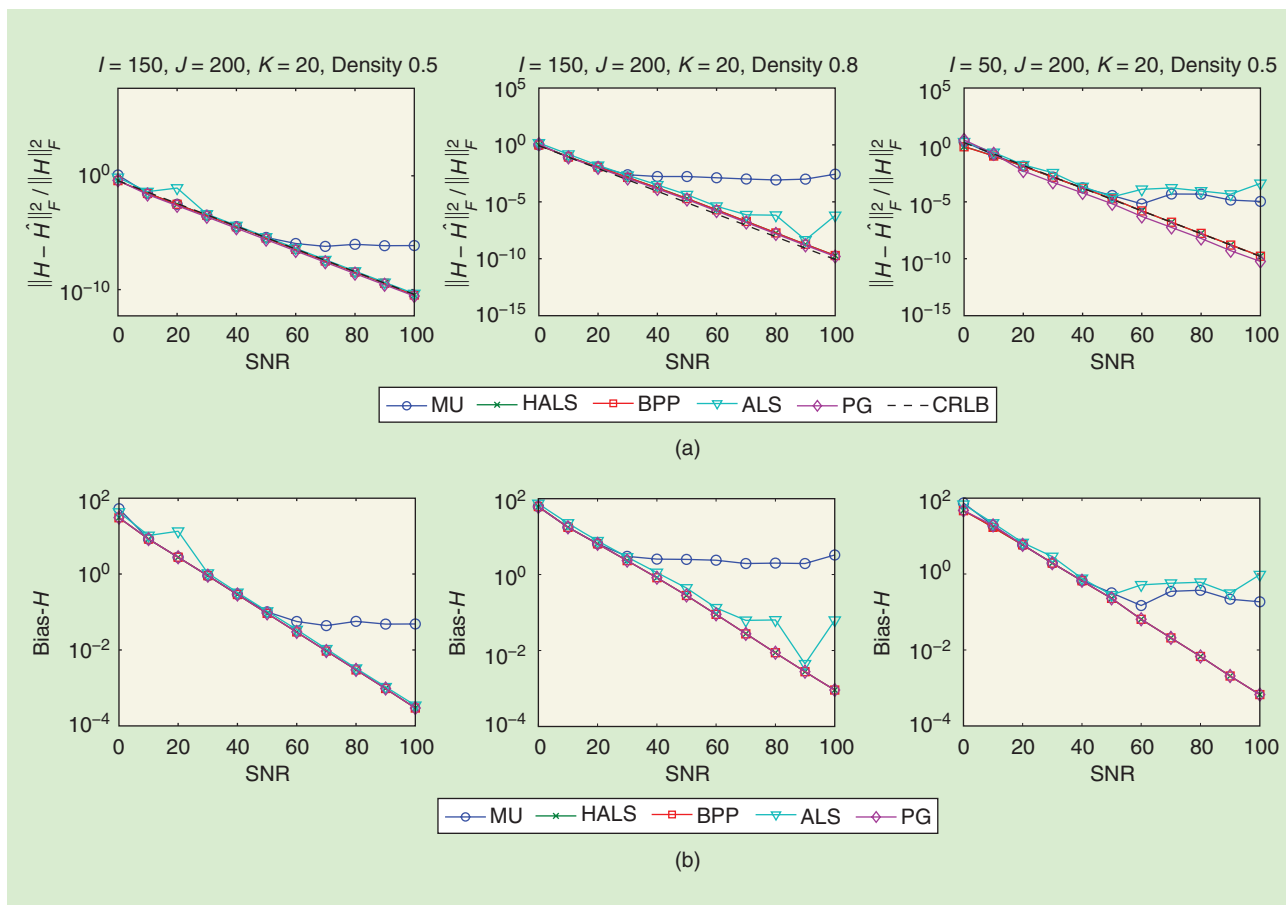


[FIG5] (a) The normalized squared error for H using various asymmetric NMF algorithms versus the CRLB; similarly (b) shows the (aggregate) bias for H.

gave similar results to those three methods, indicating that if we know a priori that the latent factors are both low rank and sparse, it is worth trying ALS, since its updates rules only require linear least-squares followed by simple projection to the nonnegative orthant, which is much simpler than the rest.

RECAP AND TAKE-HOME POINTS

WHAT WE LEARNED

NMF entails a singular FIM as well as constraints and ambiguities that must be dealt with in the computation of the pertinent CRLB. We learned how to tackle those and used the results to benchmark and develop insights on what can be expected from some of the best available algorithms. For symmetric NMF, the CRLB can be approached using the Procrustes rotation algorithm [14] in the high SNR regime, or α/β -symmetric NMF in low SNR cases. For asymmetric NMF, the best-performing algorithms were able to give results with MSE close to the CRLB. In both cases, approaching the CRLB is possible when the signal rank is small and the latent factors are not dense, i.e., when there is a small number of latent components whose loadings contain sufficiently many zeros. This is quite remarkable given that the CRLB with a singular FIM is generally unattainable; see Figure S1.

There may be room for improvement in cases involving moderate SNR and/or moderate rank and/or moderate density.

WHY IT IS IMPORTANT

Beyond NMF, the approach and techniques we learned can be used to facilitate analogous derivations for related factor analysis problems. For example, the FIMs provided here can be applied to more general bilinear matrix factorizations, e.g., using other types of constraints on W. The FIM will remain the same, but the U matrix will be different. Also, we can exploit a basis of the nullspace of the FIM to reduce the complexity of computing its pseudoinverse, and this idea is more broadly applicable to other bilinear matrix factorizations. The results can also be extended toward, e.g., nonnegative tensor factorization.

SUPPLEMENTARY MATERIAL

The supplementary material that is available through IEEE Xplore contains detailed FIM derivations, as well as auxiliary results on FIM rank and efficient numerical computation of its pseudoinverse. These results reduce the complexity of computing the CRLB from $O((IK)^3)$ to $O(IK^5)$ in the symmetric case, and from $O(((I+J)K)^3)$ to $O((I+J)K^5)$ in the asymmetric case (recall $I, J \geq K$, and usually $I, J \gg K$). The supplementary

material also includes streamlined and optimized MATLAB code for computing these CRLBs.

AUTHORS

Kejun Huang (huang663@umn.edu) received the B.Eng. degree in communication engineering from Nanjing University of Information Science and Technology, Nanjing, China, in 2010. He has been working toward his Ph.D. degree in the Department of Electrical and Computer Engineering, University of Minnesota, since 2010. His research interests include signal processing, machine learning, and data analytics. His current research focuses on identifiability, algorithms, and performance analysis for factor analysis of big matrix and tensor data.

Nicholas D. Sidiropoulos (nikos@umn.edu) received the diploma in electrical engineering from the Aristotelian University of Thessaloniki, Greece, and M.S. and Ph.D. degrees in electrical engineering from the University of Maryland, College Park, in 1988, 1990, and 1992, respectively. He was an assistant professor at the University of Virginia (1997–1999); associate professor at the University of Minnesota, Minneapolis (2000–2002); professor at the Technical University of Crete, Greece (2002–2011); and professor at the University of Minnesota, Minneapolis (2011–present). His current research focuses on signal and tensor analytics, with applications in cognitive radio, big data, and preference measurement. He received the National Science Foundation/CAREER Award (1998), the IEEE Signal Processing Society (SPS) Best Paper Award (2001, 2007, 2011), and the IEEE SPS Meritorious Service Award (2010). He has served as an IEEE SPS Distinguished Lecturer (2008–2009) and chair of the IEEE Signal Processing for Communications and Networking Technical Committee (2007–2008). He received the Distinguished Alumni Award of the Department of Electrical and Computer Engineering, University of Maryland, College Park (2013).

REFERENCES

- [1] P. Paatero and U. Tapper, "Positive matrix factorization: A non-negative factor model with optimal utilization of error estimates of data values," *Environmetrics*, vol. 5, no. 2, pp. 111–126, 1994.
- [2] D. D. Lee and H. S. Seung, "Learning the parts of objects by non-negative matrix factorization," *Nature*, vol. 401, no. 6755, pp. 788–791, 1999.
- [3] S. M. Kay, *Fundamentals of Statistical Signal Processing, Volume I: Estimation Theory*. Englewood Cliffs, NJ: Prentice Hall, 1993.
- [4] J. D. Gorman and A. O. Hero, "Lower bounds for parametric estimation with constraints," *IEEE Trans. Inform. Theory*, vol. 36, no. 6, pp. 1285–1301, 1990.
- [5] P. Stoica and B. C. Ng, "On the Cramér–Rao bound under parametric constraints," *IEEE Signal Processing Lett.*, vol. 5, no. 7, pp. 177–179, 1998.
- [6] P. Stoica and T. L. Marzetta, "Parameter estimation problems with singular information matrices," *IEEE Trans. Signal Processing*, vol. 49, no. 1, pp. 87–90, 2001.
- [7] Z. Ben-Haim and Y. C. Eldar, "On the constrained Cramér–Rao bound with a singular Fisher information matrix," *IEEE Signal Processing Lett.*, vol. 16, no. 6, pp. 453–456, 2009.
- [8] P. Tichavský and Z. Koldovský, "Optimal pairing of signal components separated by blind techniques," *IEEE Signal Processing Lett.*, vol. 11, no. 2, pp. 119–122, 2004.
- [9] H. W. Kuhn, "The Hungarian method for the assignment problem," *Naval Res. Logist. Quart.*, vol. 2, no. 1–2, pp. 83–97, 1955.
- [10] R. E. Burkard, M. Dell'Amico, and S. Martello, *Assignment Problems*. Philadelphia, PA: SIAM, 2009.
- [11] D. L. Donoho and V. C. Stodden, "When does non-negative matrix factorization give a correct decomposition into parts?," in *Advances in Neural Information Processing Systems (NIPS)*. Cambridge, MA: MIT Press, 2003, vol. 16, pp. 1141–1148.
- [12] H. Laurberg, M. G. Christensen, M. D. Plumbley, L. K. Hansen, and S. H. Jensen, "Theorems on positive data: On the uniqueness of NMF," *Computat. Intell. Neurosci.*, vol. 2008, Article ID 764206, 9 pages, DOI: 10.1155/2008/764206.
- [13] N. Gillis, "Sparse and unique nonnegative matrix factorization through data preprocessing," *J. Mach. Learn. Res.*, vol. 13, pp. 3349–3386, Nov. 2012.
- [14] K. Huang, N. D. Sidiropoulos, and A. Swami, "Non-negative matrix factorization revisited: Uniqueness and algorithm for symmetric decomposition," *IEEE Trans. Signal Processing*, vol. 62, no. 1, pp. 211–224, Jan. 2014.
- [15] S. A. Vavasis, "On the complexity of nonnegative matrix factorization," *SIAM J. Optim.*, vol. 20, no. 3, pp. 1364–1377, 2009.
- [16] A. Cichocki, R. Zdunek, A. H. Phan, and S. Amari, *Nonnegative Matrix and Tensor Factorizations: Applications to Exploratory Multi-Way Data Analysis and Blind Source Separation*. Hoboken, NJ: Wiley, 2009.
- [17] Z. He, S. Xie, R. Zdunek, G. Zhou, and A. Cichocki, "Symmetric nonnegative matrix factorization: Algorithms and applications to probabilistic clustering," *IEEE Trans. Neural Networks*, vol. 22, no. 12, pp. 2117–2131, 2011.
- [18] A. Berman and N. Shaked-Monderer, *Completely Positive Matrices*. Singapore: World Scientific, 2003.
- [19] P. J. C. Dickinson and L. Gijben, "On the computational complexity of membership problems for the completely positive cone and its dual," *Computat. Optim. Applicat.*, submitted for publication. DOI:10.1007/s10589-013-9594-z
- [20] Z. Yang and E. Oja, "Quadratic nonnegative matrix factorization," *Pattern Recognit.*, vol. 45, no. 4, pp. 1500–1510, 2012.
- [21] C. Ding, X. He, and H. D. Simon, "On the equivalence of nonnegative matrix factorization and spectral clustering," in *Proc. SIAM Int. Conf. Data Mining (SDM'05)*, 2005, vol. 5, pp. 606–610.
- [22] D. D. Lee and H. S. Seung, "Algorithms for non-negative matrix factorization," *Adv. Neural Inform. Process. Syst. (NIPS)*, vol. 13, pp. 556–562, 2001.
- [23] A. Cichocki, S. Amari, R. Zdunek, R. Kompass, G. Hori, and Z. He, "Extended SMART algorithms for non-negative matrix factorization," in *Artificial Intelligence and Soft Computing (ICAISC)*. New York: Springer, 2006, pp. 548–562.
- [24] C.-J. Lin, "Projected gradient methods for nonnegative matrix factorization," *Neural Computat.*, vol. 19, no. 10, pp. 2756–2779, 2007.
- [25] R. Zdunek and A. Cichocki, "Nonnegative matrix factorization with constrained second-order optimization," *Signal Process.*, vol. 87, no. 8, pp. 1904–1916, 2007.
- [26] M. W. Berry, M. Browne, A. N. Langville, V. P. Pauca, and R. J. Plemmons, "Algorithms and applications for approximate nonnegative matrix factorization," *Computat. Stat. Data Anal.*, vol. 52, no. 1, pp. 155–173, 2007.
- [27] M. Heiler and C. Schnörr, "Learning sparse representations by non-negative matrix factorization and sequential cone programming," *J. Mach. Learn. Res.*, vol. 7, pp. 1385–1407, July 2006.
- [28] H. Kim and H. Park, "Nonnegative matrix factorization based on alternating nonnegativity constrained least squares and active set method," *SIAM J. Matrix Anal. Applicat.*, vol. 30, no. 2, pp. 713–730, 2008.
- [29] J. Kim and H. Park, "Fast nonnegative matrix factorization: An active-set-like method and comparisons," *SIAM J. Sci. Comput.*, vol. 33, no. 6, pp. 3261–3281, 2011.
- [30] A. Cichocki and A.-H. Phan, "Fast local algorithms for large scale nonnegative matrix and tensor factorizations," *IEICE Trans. Fundam. Electron., Commun. Comput. Sci.*, vol. 92, no. 3, pp. 708–721, 2009.
- [31] B. Klingenberg, J. Curry, and A. Dougherty, "Non-negative matrix factorization: Ill-posedness and a geometric algorithm," *Pattern Recognit.*, vol. 42, no. 5, pp. 918–928, 2009.
- [32] R. Zdunek, "Initialization of nonnegative matrix factorization with vertices of convex polytope," in *Artificial Intelligence and Soft Computing*. New York: Springer, 2012, pp. 448–455.
- [33] J. Li and J. M. Bioucas-Dias, "Minimum volume simplex analysis: A fast algorithm to unmix hyperspectral data," in *Proc. IEEE Int. Geoscience and Remote Sensing Symp. (IGARSS)*, 2008, vol. 3, pp. 250–253.
- [34] W. S. B. Ouedraogo, A. Souloumiac, M. Jaidane, and C. Jutten, "Simplex cone shrinking algorithm for unmixing nonnegative sources," in *Proc. IEEE Int. Conf. Acoustics, Speech and Signal Processing (ICASSP)* 2012, pp. 2405–2408.
- [35] M. T. Chu and M. M. Lin, "Low-dimensional polytope approximation and its applications to nonnegative matrix factorization," *SIAM J. Sci. Comput.*, vol. 30, no. 3, pp. 1131–1155, 2008.
- [36] S. Boyd and L. Vandenberghe, *Convex Optimization*. Cambridge, UK: Cambridge Univ. Press, 2004.
- [37] A. Swami, "Cramér–Rao bounds for deterministic signals in additive and multiplicative noise," *Signal Process.*, vol. 53, no. 2, pp. 231–244, 1996.
- [38] K. B. Petersen and M. S. Pedersen, *The Matrix Cookbook*. Kongens Lyngby, Denmark: Technical Univ. Denmark, 2006.
- [39] M. Chu, F. Diele, R. Plemmons, and S. Ragni. (2004). Optimality, computation, and interpretation of nonnegative matrix factorizations. [Online]. Available: <http://www4.ncsu.edu/~mtchu/Research/Papers/nmf.pdf>
- [40] C. Hung and T. L. Markham, "The Moore–Penrose inverse of a partitioned matrix $M = \begin{pmatrix} A & D \\ B & C \end{pmatrix}$," *Linear Algebra Appl.*, vol. 11, no. 1, pp. 73–86, 1975.
- [41] C. Hung and T. L. Markham, "The Moore–Penrose inverse of a sum of matrices," *J. Aust. Math. Soc., Ser. A*, vol. 24, no. 4, pp. 385–392, 1977.

Michael B. McCoy, Volkan Cevher, Quoc Tran Dinh,
Afsaneh Asaei, and Luca Baldassarre

Convexity in Source Separation

Models, geometry, and algorithms

Source separation, or demixing, is the process of extracting multiple components entangled within a signal. Contemporary signal processing presents a host of difficult source separation problems, from interference cancellation to background subtraction, blind deconvolution, and even dictionary learning. Despite the recent progress in each of these applications, advances in high-throughput sensor technology place demixing algorithms under pressure to accommodate extremely high-dimensional signals, separate an ever larger number of sources, and cope with more sophisticated signal and mixing models. These difficulties are exacerbated by the need for real-time action in automated decision-making systems.

Recent advances in convex optimization provide a simple framework for efficiently solving numerous difficult demixing problems. This article provides an overview of the emerging field, explains the theory that governs the underlying procedures, and surveys algorithms that solve them efficiently. We aim to equip practitioners with a toolkit for constructing their own demixing algorithms that work, as well as concrete intuition for why they work.

FUNDAMENTALS OF DEMIXING

The most basic model for mixed signals is a superposition model, where we observe a mixed signal $z_0 \in \mathbb{R}^d$ of the form

$$z_0 = x_0 + y_0, \quad (1)$$

and we wish to determine the component signals x_0 and y_0 . This simple model appears in many guises. Sometimes, superimposed signals come from basic laws of nature. The amplitudes of electromagnetic waves, for example, sum together at a receiver, making the superposition model (1) common in wireless communications. Similarly, the additivity of sound waves makes superposition models natural in speech and audio processing.

Other times, a superposition provides a useful, if not literally true, model for more complicated nonlinear phenomena. Many images can be modeled as the sum of constituent features—think of stars and galaxies that sum to create an image of a piece of the night sky [1]. In machine learning, superpositions can describe hidden structure [2], while in statistics, superpositions can model gross corruptions to data [3]. These models also appear in texture repair [4], graph clustering [5], and line-spectral estimation [6].

A conceptual understanding of demixing in all of these applications rests on two key ideas. Natural signals in high dimensions often cluster around low-dimensional structures with few degrees of freedom relative to the ambient dimension [7]. Examples include bandlimited signals, array observations from seismic sources, and natural images. By identifying the convex functions that encourage these low-dimensional structures, we can derive convex programs that disentangle structured components from a signal.

Of course, effective demixing requires more than just structure. To distinguish multiple elements in a signal, the components must look different from one another. We capture this idea by saying that two structured families of signal are incoherent if their constituents appear very different from each other. While demixing is impossible without incoherence, sufficient incoherence



Source Separation and Applications

IMAGE LICENSED BY
INGRAM PUBLISHING

Digital Object Identifier 10.1109/MSP.2013.2296605

Date of publication: 7 April 2014

typically leads to provably correct demixing procedures. The two notions of structure and incoherence above also appear at the core of recent developments in information extraction from incomplete data in compressive sensing and other linear inverse problems [8], [9]. The theory of demixing extends these ideas to a richer class of signal models, and it leads to a more coherent theory of convex methods in signal processing.

While this article primarily focuses on mixed signals drawn from the superposition model (1), recent extensions to nonlinear mixing models arise in blind deconvolution, source separation, and nonnegative matrix factorization [10]–[12]. We will see that the same techniques that let us demix superimposed signals reappear in nonlinear demixing problems.

THE ROLE OF CONVEXITY

Convex optimization provides a unifying theme for all of the demixing problems discussed above. This framework is based on the idea that many structured signals possess corresponding convex functions that encourage this structure [9]. By combining these functions in a sensible way, we can develop convex optimization procedures that demix a given observation. The geometry of these functions lets us understand when it is possible to demix a superimposed observation with incoherent components [13]. The resulting convex optimization procedures usually have both theoretical and practical guarantees of correctness and computational efficiency.

To illustrate these ideas, we consider a classical but surprisingly common demixing problem: separating impulsive signals from sinusoidal signals, called the spikes and sines model. This model appears in many applications, including star–galaxy separation in astronomy, interference cancellation in communications, inpainting and speech enhancement in signal processing [1], [14].

While individual applications feature additional structural assumptions on the signals, a simple low-dimensional signal model effectively captures the main idea present in all of these works: sparsity. A vector $x_0 \in \mathbb{R}^d$ is sparse if most of its entries are equal to zero. Similarly, a vector $y_0 \in \mathbb{R}^d$ is sparse-in-frequency if its discrete cosine transform (DCT) Dy_0 is sparse, where $D \in \mathbb{R}^{d \times d}$ is the matrix that encodes the DCT. Sparse vectors capture impulsive signals like pops in audio, while sparse-in-frequency vectors explain smooth objects like natural images. Clearly, such signals look different from one another. In fact, an arbitrary collection of spikes and sines is linearly independent or incoherent provided that the collection is not too big [14].

Is it possible to demix a superimposition $z_0 = x_0 + y_0$ of spikes and sines into its constituents? One approach is to search for the sparsest possible constituents that generate the observation z_0

$$[\hat{x}, \hat{y}] := \arg \min_{x, y \in \mathbb{R}^d} \{ \|x\|_0 + \lambda \|Dy\|_0 : z_0 = x + y \}, \quad (2)$$

where the ℓ_0 -“norm” measures the sparsity of its input, and $\lambda > 0$ is a regularization parameter that trades the relative sparsity of solutions. Unfortunately, solving (2) involves an intractable computational problem. However, if we replace the ℓ_0 penalty with the convex ℓ_1 -norm, we arrive at a classical sparse approximation program [14]

$$[\hat{x}, \hat{y}] := \arg \min_{x, y \in \mathbb{R}^d} \{ \|x\|_1 + \lambda \|Dy\|_1 : z_0 = x + y \}. \quad (3)$$

This key change to the combinatorial proposal (2) offers numerous benefits. First, the procedure (3) is a convex program, and a number of highly efficient algorithms are available for its solution. Second, this procedure admits provable guarantees of correctness and noise-stability under incoherence. Finally, the demixing procedure (3) often performs admirably in practice.

Figure 1 illustrates the performance of (3) on both a synthetic signal drawn from the spikes-and-sines model above, as well as on a real astronomical image. The resulting performance for the basic model is quite appealing even for real data that mildly violates the modeling assumptions. Last but not least, this strong baseline performance can be obtained in fractions of seconds with simple and efficient algorithms. The combination of efficient algorithms, rigorous theory, and impressive real-world performance are hallmarks of convex demixing methods.

DEMIXING MADE EASY

This section provides a recipe to generate a convex program that accepts a mixed signal $z_0 = x_0 + y_0$ and returns a set of demixed components. The approach requires two ingredients. First, we must identify convex functions that promote the structure we expect in x_0 and y_0 . Second, we combine these functions together into a convex objective. This simple and versatile approach easily extends to multiple signal components and undersampled observations.

STRUCTURE-INDUCING CONVEX FUNCTIONS

We say that a signal has structure when it has fewer degrees of freedom than the ambient space. Familiar examples of structured objects include sparse vectors, sign vectors, and low-rank matrices. It turns out that each of these structured families have an associated convex function, called an atomic gauge, adapted to their specific features [9].

The general principle is simple. Given a set of atoms $\mathcal{A} \subset \mathbb{R}^d$, we say that a signal $x \in \mathbb{R}^d$ is atomic if it is formed by a sum of a small number of scaled atoms. For example, sparse vectors are atomic relative to the set of standard basis vectors because every sparse vector is the sum of just a few standard basis vectors. For a more sophisticated example, recall that the singular value decomposition implies that low-rank matrices are the sum of a few rank-one matrices. Hence, low-rank matrices are atomic relative to the set of all rank-one matrices.

We can define a function that measures the inherent complexity of signals relative to a given set \mathcal{A} . One natural measure is the fewest number of scaled atoms required to write a signal using atoms from \mathcal{A} , but unfortunately, computing this quantity can be computationally intractable. Instead, we define the atomic gauge $\|x\|_{\mathcal{A}}$ of a signal $x \in \mathbb{R}^d$ by

$$\|x\|_{\mathcal{A}} := \inf \{ \lambda > 0 : x \in \lambda \cdot \text{conv}(\mathcal{A}) \},$$

where $\text{conv}(\mathcal{A})$ is the convex hull of \mathcal{A} . In other words, the level sets of the atomic gauge are the scaled versions of the convex hull of all the atoms \mathcal{A} [Figure 2(a)].

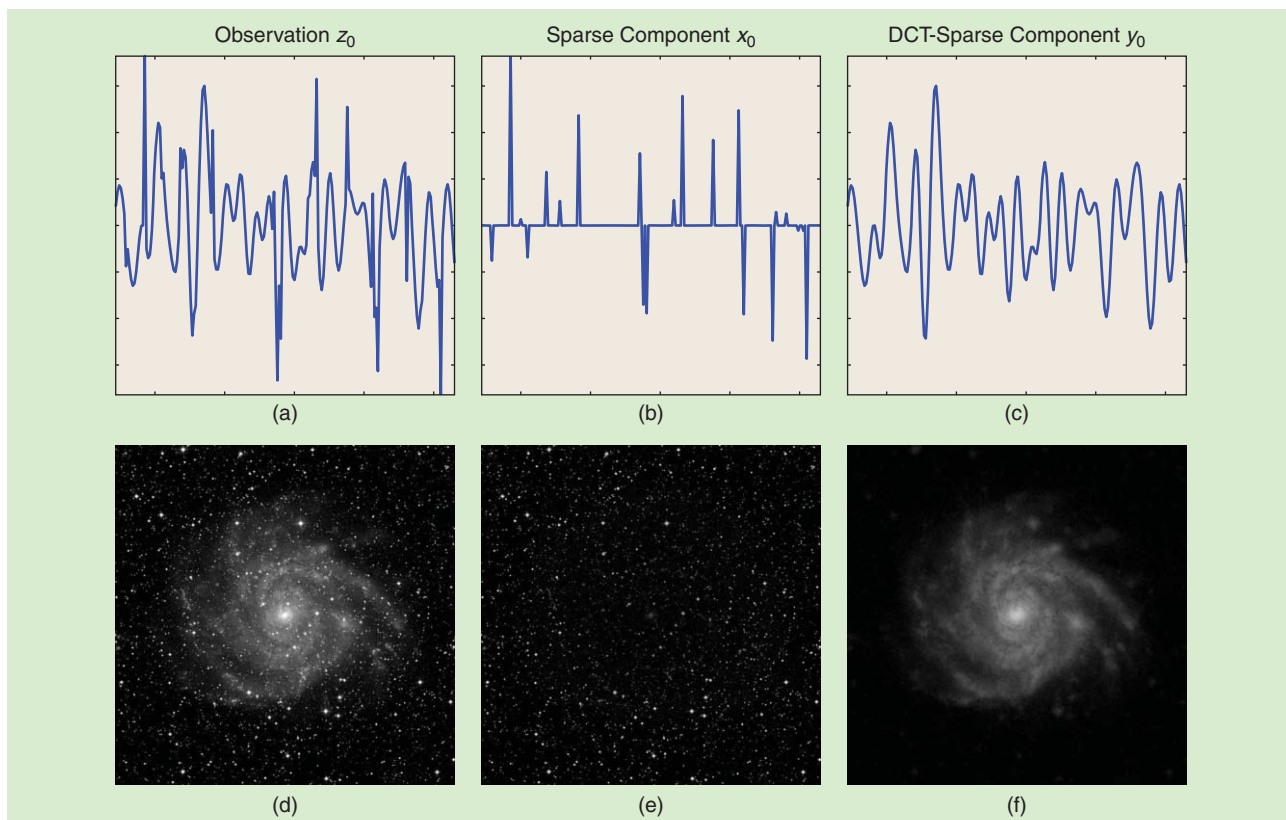


[FIG1] (a)–(c) We obtain perfect separation of spikes from sinusoids by solving (3). The original signal is perfectly separated into (b) its sparse component and (c) its DCT-sparse component. (d)–(f) We also achieve high-quality star-galaxy separation by solving (3) with an astronomical image. (d) The original is separated into (e) a starfield corresponding to a nearly sparse component and (f) a galaxy corresponding to a nearly two-dimensional DCT-sparse component. (Galaxy image courtesy of NASA/JPL-Caltech and used with permission.)

By construction, atomic gauges are “pointy” at atomic vectors. This property means that most deviations away from the atoms result in a rapid increase in the value of the gauge, so that the function tends to penalize deviations away from simple signals [Figure 2(b)]. The pointy geometry plays an important role in the theoretical understanding of demixing, as we will see when we discuss the geometry of demixing below.

A number of common structured families and their associated gauge functions appear in Table 1. More sophisticated examples include gauges for probability measures, cut matrices, and low-rank tensors. We caution, however, that not every atomic gauge is easy to compute, and so we must take care to develop tractable forms of atomic gauges [9], [16]. Surprisingly, it is sometimes easier to compute the value of atomic gauges than it is to compute the (possibly nonunique) decomposition of a vector into its atoms [12]. We will return to the discussion of tractable gauges when we discuss demixing algorithms below.

THE BASIC DEMIXING PROGRAM

Suppose that we know the signal components x_0 and y_0 are atomic with respect to the known atomic sets \mathcal{A}_x and \mathcal{A}_y . In this section, we describe how to use the atomic gauge functions $\|\cdot\|_{\mathcal{A}_x}$ and $\|\cdot\|_{\mathcal{A}_y}$ defined above to help us demix the components x_0 and y_0 from the observation z_0 .

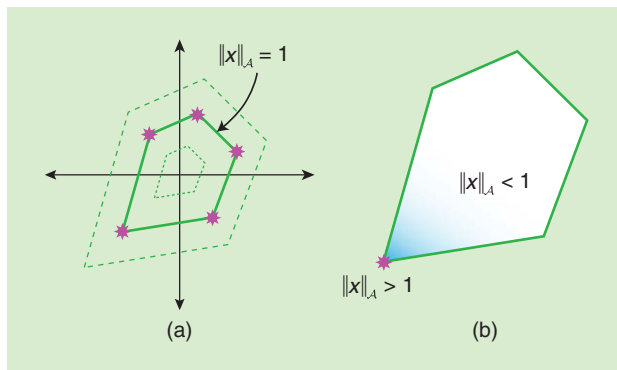


[FIG2] (a) An atomic set \mathcal{A} , consisting of five atoms (stars). The “unit ball” of the atomic gauge $\|\cdot\|_{\mathcal{A}}$ is the closed convex hull of \mathcal{A} (heavy line). Other level sets (dashed lines) of the gauge are dilations of the unit ball. (b) At an atom (star), the unit ball of $\|\cdot\|_{\mathcal{A}}$ tends to have sharp corners. Most perturbations away from this atom increase the value of $\|\cdot\|_{\mathcal{A}}$, so the atomic gauge often penalizes complex signals that are comprised of a large number of atoms.

Our intuition developed above indicates that the values $\|x_0\|_{\mathcal{A}_x}$ and $\|y_0\|_{\mathcal{A}_y}$ are relatively small because the vectors x_0 and y_0 are atomic with respect to the atomic sets \mathcal{A}_x and \mathcal{A}_y . This suggests that we search for constituents that generate the

[TABLE 1] EXAMPLE SIGNAL STRUCTURES AND THEIR ATOMIC GAUGES [9], [15]. THE TOP TWO ROWS CORRESPOND TO VECTORS WHILE THE BOTTOM THREE REFER TO MATRICES. THE VECTOR NORMS EXTEND TO MATRIX NORMS BY TREATING $m \times n$ MATRICES AS LENGTH- mn VECTORS. THE EXPRESSION $\|x\|_p$ DENOTES THE EUCLIDEAN NORM OF THE VECTOR x , WHILE $\sigma_i(\mathbf{X})$ RETURNS THE i TH SINGULAR VALUE OF THE MATRIX \mathbf{X} .

STRUCTURE	ATOMIC SET	ATOMIC GAUGE $\ \cdot\ _{\mathcal{A}}$
SPARSE VECTOR	SIGNED BASIS VECTORS $\{\pm e_i\}$	ℓ_1 NORM $\ x\ _{\ell_1} = \sum_i x_i $
BINARY SIGN VECTOR	SIGN VECTORS $\{\pm 1\}^d$	ℓ_∞ NORM $\ x\ _{\ell_\infty} = \max_i x_i $
LOW-RANK MATRIX	RANK-1 MATRICES $\{uv^T: \ uv^T\ _F = 1\}$	SCHATTEN 1-NORM $\ X\ _{S_1} = \sum_i \sigma_i(\mathbf{X})$
ORTHOGONAL MATRIX	ORTHOGONAL MATRICES $\{O: OO^T = \mathbf{I}\}$	SCHATTEN ∞ -NORM $\ X\ _{S_\infty} = \sigma_1(\mathbf{X})$
ROW-SPARSE MATRIX	MATRICES WITH ONE NONZERO ROW $\{e_i v^T: \ v\ _2 = 1\}$	ROW- ℓ_1 NORM $\ X\ _{\ell_1/2}$

observation and have small atomic gauges. That is, we determine the demixed constituents \hat{x}, \hat{y} by solving

$$[\hat{x}, \hat{y}] := \arg \min_{x,y \in \mathbb{R}^d} \{ \|x\|_{\mathcal{A}_x} + \lambda \|y\|_{\mathcal{A}_y} : x + y = z_0 \}. \quad (4)$$

The parameter $\lambda > 0$ negotiates a tradeoff between the relative importance of the atomic gauges, and the constraint $x + y = z_0$ ensures that our estimates \hat{x} and \hat{y} satisfy the observation model (1). The hope, of course, is that $\hat{x} = x_0$ and $\hat{y} = y_0$, so that the demixing program (4) actually identifies the true components in the observation z_0 .

The demixing program (4) is closely related to linear inverse problems and compressive sampling (CS) [8], [9]. Indeed, the summation map $(x, y) \rightarrow x + y$ is a linear operator, so demixing amounts to inverting an underdetermined linear system using structural assumptions. The main conceptual difference between demixing and standard CS is that demixing treats the components x_0 and y_0 as unrelated structures. Also, unlike conventional CS, demixing does not require exact knowledge of the atomic decomposition, but only the value of the gauge.

The only link between the structures that appears in our recipe comes through the choice of tuning parameter λ in (4), which makes these convex demixing procedures easily adaptable to new problems. In general, determining an optimal value of λ may involve fine-tuning or cross-validation, which can be quite computationally demanding in practice. Some theoretical guidance on explicit choices of the regularization parameter appears in [2], [3], and [17].

EXTENSIONS

There are many extensions of the linear superposition model (1). In some applications, we are confronted with a signal that is only partially observed—compressive demixing. In others, we might consider an observation with additive noise, for instance, or a signal with more than two components. The same ingredients that

we introduced above can be used to demix signals from these more elaborate models.

For example, if we only see $z_0 = \Phi(x_0 + y_0)$, a linear mapping of the superposition, then we simply update the consistency constraint in the usual demixing program (4) and solve instead

$$[\hat{x}, \hat{y}] := \arg \min_{x,y \in \mathbb{R}^d} \{ \|x\|_{\mathcal{A}_x} + \lambda \|y\|_{\mathcal{A}_y} : \Phi(x + y) = z_0 \}. \quad (5)$$

Some applications for this undersampled demixing model appear in image alignment [18], robust statistics [5], and graph clustering [19].

Another straightforward extension involves demixing more than two signals. For example, if we observe $z_0 = x_0 + y_0 + w_0$, the sum of three structured components, we can determine the components by solving

$$[\hat{x}, \hat{y}, \hat{w}] := \arg \min_{x,y,w \in \mathbb{R}^d} \{ \|x\|_{\mathcal{A}_x} + \lambda_1 \|y\|_{\mathcal{A}_y} + \lambda_2 \|w\|_{\mathcal{A}_w} : x + y + w = z_0 \}, \quad (6)$$

where \mathcal{A}_w is an atomic set tuned to w_0 , and as before, the parameters $\lambda_i > 0$ trade off the relative importance of the regularizers. This model appears, for example, in image processing applications where multiple basis representations, such as curvelets, ridgelets, and shearlets, explain different morphological components [1]. Further modifications along the lines above extend the demixing framework to a massive number of problems relevant to modern signal processing.

GEOMETRY OF DEMIXING

A critical question we can ask about a demixing program is “When does it work?” Answers to this question can be found by studying the underlying geometry of convex demixing programs. Surprisingly, we can characterize the success and failure of convex demixing precisely by leveraging a basic randomized model for incoherence. Indeed, the geometric viewpoint reveals a tight characterization of the success and failure of demixing in terms of geometric parameters that act as the “degrees of freedom” of the mixed signal. The consequences for demixing are intuitive: demixing succeeds if and only if the dimensionality of the observation exceeds the total degrees of freedom in the signal.

DESCENT CONES AND THE STATISTICAL DIMENSION

Our study of demixing begins with a basic object that encodes the local geometry of a convex function. The descent cone $\mathcal{D}(\mathcal{A}, x)$ at a point x with respect to an atomic set $\mathcal{A} \subset \mathbb{R}^d$ consists of the directions where the gauge function $\|\cdot\|_{\mathcal{A}}$ does not increase near x . Mathematically, the descent cone is given by

$$\mathcal{D}(\mathcal{A}, x) := \{h : \|x + \tau h\|_{\mathcal{A}} \leq \|x\|_{\mathcal{A}} \text{ for some } \tau > 0\}.$$

The descent cone encodes detailed information about the local behavior of the atomic gauge $\|\cdot\|_{\mathcal{A}}$ near x . Since local optimality implies global optimality in convex optimization, we can characterize when demixing succeeds in terms of a configuration of descent cones. See Figure 3 for a precise description of this optimality condition.

To understand when the geometric optimality condition is likely to hold, we need a measure for the “size” of cones. The most apparent measure of size is perhaps the solid angle, which quantifies the amount of space occupied by a cone. The solid angle, however, proves inadequate for describing the intersection of cones even in the simple case of linear subspaces. Indeed, linear subspaces are cones that take up no space at all, but when their dimensions are large enough, any two subspaces will always intersect along a line. Imagine trying to arrange two flat sheets of paper so that they only touch at their centers: it’s impossible!

We find a much more informative measure of size, called the statistical dimension, when we measure the proportion of space near a cone, rather than the proportion inside the cone.

DEFINITION 1 (STATISTICAL DIMENSION)

Let $C \subset \mathbb{R}^d$ be a closed convex cone, and denote by $\Pi_C(x) := \arg \min_{y \in C} \|x - y\|$ the closest point in C to x . We define the statistical dimension $\delta(C)$ of a convex cone $C \subset \mathbb{R}^d$ by

$$\delta(C) := \mathbb{E} \|\Pi_C(g)\|_2^2, \tag{7}$$

where $g \sim \text{Normal}(0, \mathbf{I})$ is a standard Gaussian random variable and the letter \mathbb{E} denotes the expected value.

The statistical dimension gets its name because it extends many properties of the usual dimension of linear subspaces to convex cones [20], and it is closely related to the Gaussian width used in [9]. Our interest here, however, comes from the interpretation of the statistical dimension as a “size” of a cone. A large statistical dimension $\delta(C) \approx d$ means that $\|\Pi_C(g)\|_2^2$ is usually large, i.e., most points lie near or inside the cone. Conversely, a narrow cone C possesses a small statistical dimension because the nearest point to C is typically close to zero, which drives down the average norm. We will see below that the statistical dimension of descent cones provides the key parameter for understanding the success and failure of demixing procedures.

Of course, a parameter is only useful if we can compute it. Fortunately, the statistical dimension of descent cones is often easy to compute or approximate. Several ready-made statistical dimension formulas and a step-by-step recipe for accurately deriving new formulas appear in [20]. Some useful approximate statistical dimension calculations can also be found in the works [9] and [17]. As an added bonus, recent work indicates that statistical dimension calculations are closely related to the problem of finding optimal regularization parameters [17, Th. 2].

PHASE TRANSITIONS IN CONVEX DEMIXING

The true power of the statistical dimension comes from its ability to predict phase transitions in demixing programs. By phase transition, we mean the peculiar behavior where demixing programs switch from near-certain failure to near-certain success within a narrow range of model parameters. While the optimality condition from Figure 3 characterizes the success and failure of demixing, it is often difficult to certify directly. To understand how demixing operates in typical situations, we need an incoherence model. One proposal to model incoherence assumes that the structured signals are oriented generically relative to one another. This is

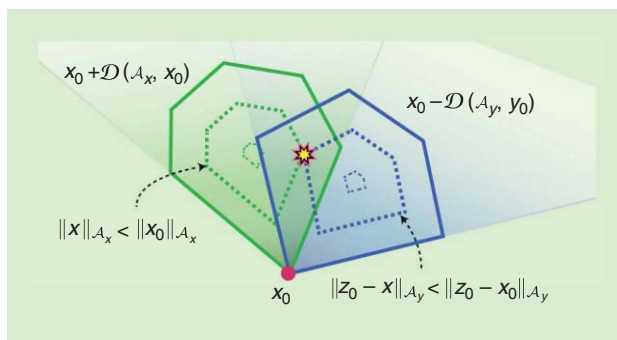


[FIG3] The geometric characterization of demixing. When the descent cones $\mathcal{D}(\mathcal{A}_x, \mathbf{x}_0)$ and $\mathcal{D}(\mathcal{A}_y, \mathbf{y}_0)$ share a line, then there is an optimal point $\hat{\mathbf{x}}$ (star) for the demixing program (4) not equal to \mathbf{x}_0 . Conversely, demixing can succeed for some value of $\lambda > 0$ if the two descent cones touch only at the origin. In other words, demixing can succeed if and only if $\mathcal{D}(\mathcal{A}_x, \mathbf{x}_0) \cap \mathcal{D}(\mathcal{A}_y, \mathbf{y}_0) = \{\mathbf{0}\}$ [13].

achieved, for example, by assuming that the structured components are drawn structured relative to a rotated atomic set $Q\mathcal{A}$, where $Q \in \mathbb{R}^{d \times d}$ is a random orthogonal matrix [13]. Surprisingly, this basic randomized model of incoherence leads to a rich theory with precise guarantees that complement other phase transition characterizations in linear inverse problems [21], [22]. Many works propose alternative incoherence models applicable to specific cases, including [3] and [9], but these specific choices do not possess known phase transitions. Under the random model of [13], however, a very general theory is available. The following result appears in [20, Th. III].

THEOREM 1

Suppose that the atomic set of \mathbf{x}_0 is randomly rotated, i.e., that $\mathcal{A}_x = Q\tilde{\mathcal{A}}_x$ for some random rotation Q and some fixed atomic set $\tilde{\mathcal{A}}_x$. Fix a probability tolerance $\eta \in (0, 1)$, and define the normalized total statistical dimension

$$\Delta := \frac{1}{d} [\delta(\mathcal{D}(\tilde{\mathcal{A}}_x, \mathbf{x}_0)) + \delta(\mathcal{D}(\mathcal{A}_y, \mathbf{y}_0))].$$

Then there is a scalar $C > 0$ that depends only on η such that

$$\begin{aligned} \Delta \leq 1 - C/\sqrt{d} &\Rightarrow \text{demixing can succeed with probability } \geq 1 - \eta \\ \Delta \geq 1 + C/\sqrt{d} &\Rightarrow \text{demixing always fails with probability } \geq 1 - \eta. \end{aligned}$$

In fact, we can take $C := 4\sqrt{\log(4/\eta)}$. By “demixing can succeed,” we mean that there exists a regularization parameter $\lambda > 0$ so that $(\mathbf{x}_0, \mathbf{y}_0)$ is an optimal point of (4). “Demixing always fails” means that $(\mathbf{x}_0, \mathbf{y}_0)$ is not an optimal point of (4) for any parameter $\lambda > 0$.

Theorem 1 indicates that demixing exhibits a phase transition as the normalized statistical dimension Δ increases beyond the one. The first implication above tells us that if Δ is just a little less than one, then we can be confident that demixing will succeed for some tuning parameter $\lambda > 0$. On the other hand, the second implication says that if Δ is slightly larger than one, then demixing is hopeless. See Figure 4 for an example of the accuracy of this

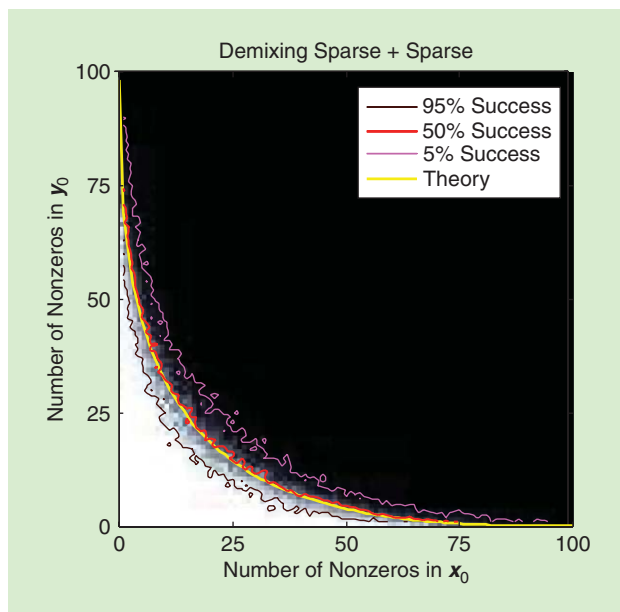


[FIG4] Phase transitions in demixing. Phase transition diagram for demixing two sparse signals using ℓ_1 minimization [20]. This experiment replaces the DCT matrix D in (3) with a random rotation Q . The color map shows the transition from pure success (white) to complete failure (black). The 95%, 50%, and 5% empirical success contours (tortuous curves) appear above the theoretical phase transition curve (yellow), where $\Delta = 1$. See [13] for experimental details. (Figure used with permission from [20].)

theory for the sparse approximation model (3) from the introduction when the DCT matrix D is replaced with a random rotation Q . The agreement between the empirical 50% success line and the curve where $\Delta = 1$ is remarkable.

This theory extends analogously to the compressive and multiple demixing models (5) and (6). Under a similar incoherence model as above, compressive and multiple demixing are likely to succeed if and only if the sum of the statistical dimensions is slightly less than the number of (possibly compressed) measurements [23, Th. A]. This fact lets us interpret the statistical dimension $\delta(\mathcal{A}, x_0)$ as the degrees of freedom of a signal x_0 with respect to the atomic set \mathcal{A} . The message is clear: Incoherent demixing can succeed if and only if the total dimension of the observation exceeds the total degrees of freedom of the constituent signals.

PRACTICAL DEMIXING ALGORITHMS

In theory, many demixing problem instances of the form (4) admit efficient numerical solutions. Indeed, if we can transform these problems into standard linear, cone, or semidefinite formulations, we can apply black-box interior point methods to obtain high-accuracy solutions in polynomial time [24]. In practice, however, the computational burden of interior point methods makes these methods impracticable as the dimension d of the problem grows. Fortunately, a simple and effective iterative algorithm for computing approximate solutions to the demixing program (4) and its extensions can be implemented with just a few lines of high-level code.

SPLITTING THE WORK

The simplest and most popular method for iteratively solving demixing programs goes by the name alternating direction method of multipliers (ADMM). The key object in this algorithm is the augmented Lagrangian function L_ρ defined by

$$L_\rho(x, y, w) := \|x\|_{\mathcal{A}_x} + \lambda \|y\|_{\mathcal{A}_y} + \langle w, x + y - z_0 \rangle + \frac{1}{2\rho} \|x + y - z_0\|^2,$$

where $\langle \cdot, \cdot \rangle$ denotes the usual inner product between two vectors and $\rho > 0$ is a parameter that can be tuned to the problem. Starting with arbitrary points $x^1, y^1, w^1 \in \mathbb{R}^d$, the ADMM method generates a sequence of points iteratively as

$$\begin{cases} x^{k+1} = \arg \min_{x \in \mathbb{R}^d} L_\rho(x, y^k, w^k) \\ y^{k+1} = \arg \min_{y \in \mathbb{R}^d} L_\rho(x^{k+1}, y, w^k) \\ w^{k+1} = w^k + (x^{k+1} + y^{k+1} - z_0)/\rho. \end{cases} \tag{8}$$

In other words, the x - and y -updates iteratively minimize the Lagrangian over just one parameter, leaving all others fixed. The alternating minimization of L_ρ gives the method its name. Despite the simple updates, the sequence (x^k, y^k) of iterates generated in this manner converges to the minimizers (\hat{x}, \hat{y}) of the demixing program (4) under fairly general conditions [25].

The key to the efficiency of ADMM comes from the fact that the updates are often easy to compute. By completing the square, the x - and y -updates above amount to evaluating proximal operators of the form

$$\begin{aligned} x^{k+1} &= \arg \min_{x \in \mathbb{R}^d} \|x\|_{\mathcal{A}_x} + \frac{1}{2\rho} \|u^k - x\|^2 \quad \text{and} \\ y^{k+1} &= \arg \min_{y \in \mathbb{R}^d} \lambda \|y\|_{\mathcal{A}_y} + \frac{1}{2\rho} \|v^k - y\|^2, \end{aligned} \tag{9}$$

where $u^k := z_0 - y^k - \rho w^k$ and $v^k := z_0 - x^{k+1} - \rho w^k$. When solutions to the proximal minimizations (9) are simple to compute, each iteration of ADMM is highly efficient.

Fortunately, proximal operators are easy to compute for many atomic gauges. For example, when the atomic gauge is the ℓ_1 -norm, the proximal operator corresponds to “soft thresholding”

$$\arg \min_{x \in \mathbb{R}^d} \|x\|_{\ell_1} + \frac{1}{2\rho} \|u - x\|^2 = \text{soft}(u, \rho) = \begin{cases} u_i - \rho, & u_i > \rho, \\ 0, & |u_i| \leq \rho, \\ u_i + \rho, & u_i < -\rho. \end{cases}$$

If we replace the ℓ_1 -norm above with the Schatten-1 norm, then the corresponding proximal operator amounts to soft thresholding the singular values. Numerous other explicit examples of proximal operations appear in [25, Sec. 2.6].

Not all atomic gauges, however, have efficient proximal operations. Even sets with finite number of atoms do not necessarily lead to more efficient proximal maps than sets with an infinite number of atoms. For instance, when the atomic set consists of rank-one matrices with unit Frobenius norm, we have an infinite set of atoms and yet the proximal map can be efficiently obtained via singular value thresholding. On the other hand, when the atomic set consists of rank-one matrices with binary ± 1 entries, we have a

finite set of atoms and yet the best-known algorithm for computing the proximal map requires an intractable amount of computation.

There is some hope, however, even for difficult gauges. Recent algebraic techniques for approximating atomic gauges provide computable proximal operators in a relatively efficient manner, which opens the door to additional demixing algorithms for richer signal structures [9], [16].

EXTENSIONS

While the ADMM method is the prime candidate for solving problem (4), it is not usually the best method for the extensions (5) or (6). In the first case, if Φ is a general linear operator, it creates a major computational bottleneck since we need an additional loop to solve the subproblems within the ADMM algorithm. In the latter case, ADMM even loses convergence guarantees [26].

One possible way to handle both (5) and (6) is to use decomposition methods. Roughly speaking, these methods decompose (5) or (6) into smaller components and then solve the convex subproblem corresponding to each term simultaneously. For example, we can use the decomposition method from [27]

$$\begin{cases} v^k &= w^k + \rho(\Phi(x^k + y^k) - z_0) \\ x^{k+1} &= \arg \min_{x \in \mathbb{R}^d} \|x\|_{\mathcal{A}_x} + \langle v^k, \Phi x \rangle + \frac{1}{2\rho} \|x - x^k\|_2^2 \\ y^{k+1} &= \arg \min_{y \in \mathbb{R}^d} \lambda \|y\|_{\mathcal{A}_y} + \langle v^k, \Phi y \rangle + \frac{1}{2\rho} \|y - y^k\|_2^2 \\ w^{k+1} &= w^k + \rho(\Phi(x^{k+1} + y^{k+1}) - z_0). \end{cases} \quad (10)$$

When the parameter ρ is chosen appropriately, the generated sequence $\{(x^k, y^k)\}$ in (10) converges to the solution of (5). Since the second and the third lines of (10) are independent, it is even possible to solve them in parallel. This scheme easily extends to demixing three or more signals (6).

Another practical method appears in [28]. In essence, this approach combines a dual formulation, Nesterov's smoothing technique, and the fast gradient method [24]. This technique works both for (5) and (6), and it possesses a rigorous $\mathcal{O}(1/k)$ convergence rate.

EXAMPLES

The ideas above apply to a large number of examples. Here, we highlight some recent applications of convex demixing in signal processing. The first example, texture inpainting, uses a low-rank and sparse decomposition to discover and repair axis-aligned texture in images. The second example uses the low-rank and diagonal demixing of a sensor array correlation matrix to improve beamforming.

TEXTURE INPAINTING

Many natural and man-made images include highly regular textures. These repeated patterns, when aligned with the image frame, tend to have very low rank. Of course, rarely does a natural image consist solely of a texture. Often, though, a background texture is sparsely occluded by a untextured component. By modeling the occlusion as an additive error, we can use convex demixing to solve for the underlying texture and extract the occlusion [4].

In this model, we treat the observed digital image $Z_0 \in \mathbb{R}^{m \times n}$ as a matrix formed by the sum $Z_0 = X_0 + Y_0$, where the textured component X_0 has low rank and Y_0 is a sparse corruption or occlusion. The natural demixing program in this setting is the rank-sparsity decomposition [2], [3]

$$[\hat{X}, \hat{Y}] = \arg \min_{X, Y \in \mathbb{R}^{m \times n}} \|X\|_{S_1} + \lambda \|Y\|_1 \quad \text{subject to } X + Y = Z_0, \quad (11)$$

This unsupervised texture-repair method exhibits a state-of-the-art performance, exceeding even the quality of a supervised procedure built in to Adobe Photoshop on some images [4]. When applied, e.g., to an image of a chessboard, the method flawlessly recovers the checkerboard from the pieces (Figure 5).

BEAMFORMING

We describe a convex demixing program for signal estimation via beamforming. Beamforming uses an array of n sensors to acquire a source signal from a given direction while suppressing the sources interfering from distinct directions. Denoting the signal of a sensor array with $(S \in \mathbb{C}^{n \times 1})$ where n is the number of snapshots, the desired signal is estimated with $(w^t S)$, where $(w \in \mathbb{C}^{n \times 1})$ is known as the beamforming weights. Assuming that the signal impinges on the array from the direction (d) , the optimal weights for signal prediction are obtained as $(\mu Z_0^{-1} d)$ where $(Z_0 = \mathbb{E}[S S^t])$ is the correlation matrix and (μ) stands for a correction factor to cancel the distortions [29]. When the sources are independent, the joint expected correlation matrix Z_0 of the sensor array signals takes the form $Z_0 = A_0 A_0^t + Y_0$, where the column space of the $n \times r$ matrix A_0 encodes the bearing information from r sources, and Y_0 is the covariance matrix of the noise at the sensors.

When the number of sources r is much smaller than the number of sensors n , the matrix $X_0 := A_0 A_0^t$ is positive semidefinite and has low rank. Moreover, when the sensor noise is uncorrelated, the matrix Y_0 is diagonal. Using the atomic gauge recipe from above, we can demix X_0 and Y_0 from the empirical covariance matrix \hat{Z}_0 by setting

$$\begin{aligned} [\hat{X}, \hat{Y}, \hat{E}] &= \arg \min_{X, Y \in \mathbb{R}^{n \times n}} \|X\|_{S_1^+} + \|Y\|_{\text{diag}} + \lambda \|E\|_{\text{Fro}}^2 \\ &\text{subject to } X + Y + E = \hat{Z}_0, \end{aligned} \quad (12)$$

where E absorbs the deviations in the expectation model due to the finite sample size. Here, $\|\cdot\|_{S_1^+}$ is the atomic gauge generated by positive semidefinite rank-one matrices, which is equal to the trace for positive semidefinite matrices, but returns $+\infty$ when its argument has a negative eigenvalue. Similarly, the gauge $\|\cdot\|_{\text{diag}}$ is the atomic gauge generated by the set of all diagonal matrices, and so it is equal to zero on diagonal matrices but $+\infty$ otherwise. The norm $\|\cdot\|_{\text{Fro}}$ is the usual Frobenius norm on a matrix. The results of [11] relate the success of a similar problem to the geometric problem of ellipsoid fitting, and show that, under some incoherence assumptions, the method (12) succeeds.

In beamforming, the array correlation matrix plays a key role in estimating the optimal weights. For instance, minimum variance distortionless response (MVDR) beamforming exploits

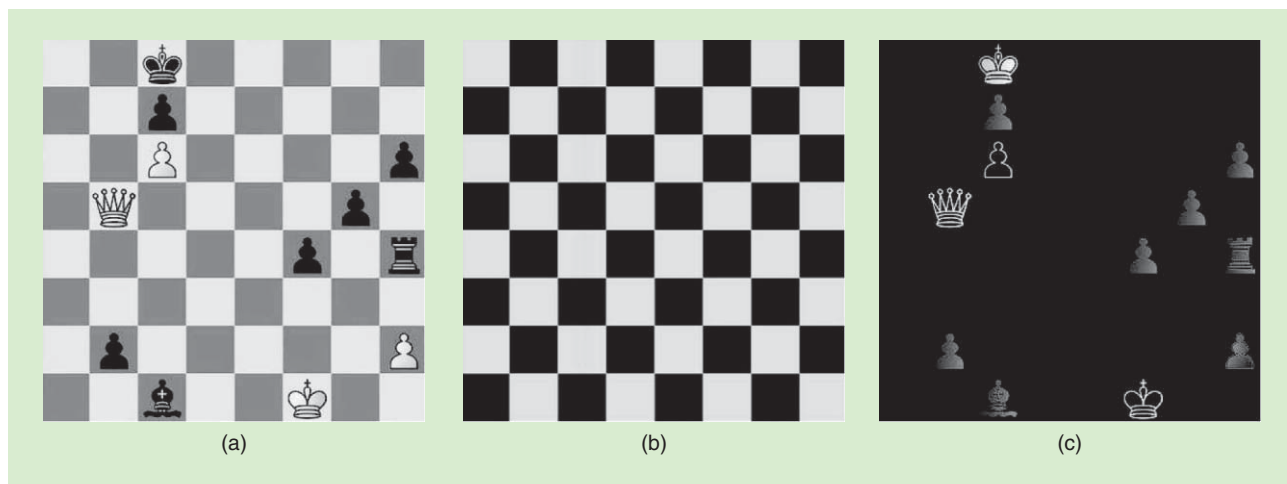


[FIG5] Texture inpainting (white to move, checkmate in two). The rank-sparsity decomposition (11) perfectly separates the chessboard from the pieces. (a) The original image. (b) The low-rank component. (c) The sparse component.

the correlation matrix to estimate the source signals at a given direction. The presence of noise corrupts the empirical correlation matrix estimate, which deteriorates the beamforming performance by MVDR.

The approach in [31] assumes a low-rank correlation matrix and discusses source estimation using atomic regularization. Hence, the demixing results perfectly dovetail with this beamforming approach. To see synergy, we simulate a scenario where three sources impinge on a uniform linear array of ten sensors from far-field in free space. The input source-to-interference ratio (SIR) is -5 dB. In addition, we add isotropic noise to the sensor measurements at -10 dB source-to-noise ratio (SNR).

The results are quite encouraging. The average output SIR of the standard MVDR beamformer using the empirical correlation \hat{Z}_0 turns out to be 5 dB. The beamforming approach [31] with the empirical correlation estimate yields 6.3 dB SIR, while using the demixed estimate \hat{X} of (12) results in an impressive 9.4 dB SIR—with an approximate improvement of 3 dB in interference suppression for source detection.

HORIZONS: NONLINEAR SEPARATION

We conclude our demixing tutorial with some promising directions for the future. In many applications, the constituent signals are tangled together in a nonlinear fashion [10], [12]. While this situation would seem to rule out the linear superposition model considered above, we can leverage the same convex optimization tools to obtain demixing guarantees and often return to a linear model using a technique called semidefinite relaxation.

We describe the basic idea behind this maneuver with a concrete application: blind deconvolution. Convolved signals appear frequently in communications due, e.g., to multipath channel effects. When the channel is known, removing the channel effects is a difficult but well-understood linear inverse problem. With blind deconvolution, however, we see only the convolved signal $z_0 = x_0 * y_0$ from which we must determine both the channel $x_0 \in \mathbb{R}^m$ and the source $y_0 \in \mathbb{R}^d$.

While the convolution $x_0 * y_0$ involves nonlinear interactions between x_0 and y_0 , the convolution is in fact linear in the matrix formed by the outer product $x_0 y_0^t$. In other words, there is a linear operator $C: \mathbb{R}^{m \times d} \rightarrow \mathbb{R}^{m+d}$ such that

$$z_0 = C(X_0) \quad \text{where} \quad X_0 := x_0 y_0^t.$$

The matrix X_0 has rank one by definition, so it is natural use the Schatten 1-norm to search for low-rank matrices that generate the observed signal

$$\hat{X} = \arg \min_{X \in \mathbb{R}^{m \times d}} \|X\|_{s_1} \quad \text{subject to} \quad z_0 = C(X).$$

This is the basic idea behind the convex approach to blind deconvolution of [10].

The implications of the nonlinear demixing example above are far-reaching. There are large classes of signal and mixing models that support efficient, provable, and stable demixing. Viewing different demixing problems within a common framework of convex optimization, we can leverage decades of research in various diverse disciplines from applied mathematics to signal processing, and from theoretical computer science to statistics. We expect that the diversity of convex demixing models and geometric tools will also inspire the development of new kinds of scalable optimization algorithms that handle nonconventional cost functions [30].

AUTHORS

Michael B. McCoy (mccoy@caltech.edu) received the B.S. degree in electrical engineering (honors) in 2007 from the University of Texas at Austin and the Ph.D. degree in applied and computational mathematics in 2013 from the California Institute of Technology (Caltech), Pasadena. His thesis focused on convex methods for signal decompositions and earned a WP Carey & Co. Inc. Prize for an outstanding doctoral dissertation. He is currently a postdoctoral scholar at Caltech, where his research explores the intersections of optimization, signal processing, statistics, and geometry.

Volkan Cevher (volkan.cevher@epfl.ch) received the B.S. (valedictorian) degree in electrical engineering in 1999 from Bilkent University in Ankara, Turkey, and the Ph.D. degree in electrical and computer engineering in 2005 from the Georgia Institute of Technology in Atlanta. He held research scientist positions at the University of Maryland, College Park, from 2006 to 2007 and at Rice University in Houston, Texas, from 2008 to 2009. Currently, he is an assistant professor at the Swiss Federal Institute of Technology Lausanne and a faculty fellow in the Electrical and Computer Engineering Department at Rice University. His research interests include signal processing theory, machine learning, graphical models, and information theory. He received a Best Paper Award at the Signal Processing with Adaptive Sparse Representations Workshop in 2009 and a European Research Council Starting Grant in 2011.

Quoc Tran Dinh (quoc.trandinh@epfl.ch) received the B.S. degree in applied mathematics and informatics and the M.S. degree in computer science, both from Vietnam National University, Hanoi, in 2001 and 2004, respectively, and the Ph.D. degree in electrical engineering from the Department of Electrical Engineering and Optimization in Engineering Center, KU Leuven, Belgium. He is currently a postdoctoral researcher with the Laboratory for Information and Inference Systems, Ecole Polytechnique Federale de Lausanne, Switzerland. His research interests include methods for convex optimization, sequential convex programming, parametric optimization, optimization in machine learning, and methods for variational inequalities and equilibrium problems.

Afsaneh Asaei (afsaneh.asaei@idiap.ch) received the B.S. degree from Amirkabir University of Technology and the M.S. (honors) degree from Sharif University of Technology, in electrical and computer engineering, respectively. She held a research engineer position at Iran Telecommunication Research Center (ITRC) from 2002 to 2008. She then joined Idiap Research Institute in Martigny, Switzerland, and was a Marie Curie fellow on speech communication with adaptive learning training network. She received the Ph.D. degree in 2013 from Ecole Polytechnique Federale de Lausanne. Her thesis focused on model-based sparsity for reverberant speech processing, and its key idea was awarded the IEEE Spoken Language Processing Grant. Currently, she is a research scientist at Idiap Research Institute. Her research interests lie in the areas of signal processing, machine learning, statistics, acoustics, auditory scene analysis and cognition, and sparse signal recovery and acquisition.

Luca Baldassarre (luca.baldassarre@epfl.ch) received the M.S. degree in physics in 2006 and the Ph.D. degree in machine learning in 2010 from the University of Genoa, Italy. He then joined the Computer Science Department of University College London, United Kingdom, to work with Prof. Massimiliano Pontil on structured sparsity models for machine learning and convex optimization. Currently he is with the Laboratory for Information and Inference Systems at the Ecole Polytechnique Federale de Lausanne, Switzerland. His research interests include model-based machine learning and compressive sensing and large-scale optimization.

REFERENCES

- [1] J.-L. Starck, F. Murtagh, and J. M. Fadili, *Sparse Image and Signal Processing*. Cambridge, U.K.: Cambridge Univ. Press, 2010.
- [2] V. Chandrasekaran, S. Sanghavi, P. A. Parrilo, and A. S. Willsky, "Rank-sparsity incoherence for matrix decomposition," *SIAM J. Optim.*, vol. 21, no. 2, pp. 572–596, 2011.
- [3] E. J. Candès, X. Li, Y. Ma, and J. Wright. (2011, May). Robust principal component analysis? *J. Assoc. Comput. Mach.* [Online]. 58(3), pp. 1–37. Available: <http://arxiv.org/pdf/0912.3599>
- [4] X. Liang, X. Ren, Z. Zhang, and Y. Ma, "Repairing sparse low-rank texture," in *Computer Vision—ECCV 2012*. New York: Springer, 2012, pp. 482–495.
- [5] Y. Chen, A. Jalali, S. Sanghavi, and C. Caramanis, "Low-rank matrix recovery from errors and erasures," *IEEE Trans. Inform. Theory*, vol. 59, no. 7, pp. 4324–4337, 2013.
- [6] B. N. Bhaskar, G. Tang, and B. Recht. (2013). Atomic norm denoising with applications to line spectral estimation, preprint. [Online]. Available: <http://arxiv.org/abs/1204.0562>
- [7] R. G. Baraniuk, V. Cevher, and M. B. Wakin, "Low-dimensional models for dimensionality reduction and signal recovery: A geometric perspective," *Proc. IEEE*, vol. 98, no. 6, pp. 959–971, 2010.
- [8] E. J. Candès and M. B. Wakin, "An introduction to compressive sampling," *IEEE Signal Process. Mag.*, vol. 25, no. 2, pp. 21–30, 2008.
- [9] V. Chandrasekaran, B. Recht, P. A. Parrilo, and A. S. Willsky, "The convex geometry of linear inverse problems," *Found. Comput. Math.*, vol. 12, no. 6, pp. 805–849, 2012.
- [10] A. Ahmed, B. Recht, and J. Romberg, "Blind deconvolution using convex programming," preprint. [Online]. Available: <http://arxiv.org/abs/1211.5608>
- [11] J. Saunderson, V. Chandrasekaran, P. A. Parrilo, and A. S. Willsky, "Diagonal and low-rank matrix decompositions, correlation matrices, and ellipsoid fitting," *SIAM J. Matrix Anal. Appl.*, vol. 33, no. 4, pp. 1395–1416, 2012.
- [12] V. Bittorf, C. Ré, B. Recht, and J. A. Tropp, "Factoring nonnegative matrices with linear programs," in *Proc. Advances in Neural Information Processing Systems 25 (NIPS)*, Dec. 2012, pp. 1223–1231.
- [13] M. B. McCoy and J. A. Tropp, "Sharp recovery bounds for convex demixing, with applications," *J. Found. Comput. Math.*, to be published.
- [14] D. L. Donoho and X. Huo, "Uncertainty principles and ideal atomic decomposition," *IEEE Trans. Inform. Theory*, vol. 47, no. 7, pp. 2845–2862, Aug. 2001.
- [15] S. S. Chen, D. L. Donoho, and M. A. Saunders, "Atomic decomposition by basis pursuit," *SIAM J. Sci. Comput.*, vol. 20, no. 1, pp. 33–61, 1998.
- [16] F. Bach, "Structured sparsity-inducing norms through submodular functions," in *Proc. Advances in Neural Information Processing Systems*, 2010, pp. 118–126.
- [17] R. Foygel and L. Mackey. (May, 2013). Corrupted sensing: Novel guarantees for separating structured signals, preprint. [Online]. Available: <http://arxiv.org/abs/1305.2524>
- [18] Y. Peng, A. Ganesh, J. Wright, W. Xu, and Y. Ma, "RASL: Robust alignment by sparse and low-rank decomposition for linearly correlated images," *IEEE Trans. Pattern Anal.*, vol. 34, no. 11, pp. 2233–2246, 2012.
- [19] Y. Chen, A. Jalali, S. Sanghavi, and C. Caramanis, "Clustering partially observed graphs via convex optimization," in *Proc. Int. Symp. Information Theory (ISIT)*, 2011, pp. 1001–1008.
- [20] D. Amelunxen, M. Lotz, M. B. McCoy, and J. A. Tropp, "Living on the edge: A geometric theory of phase transitions in convex optimization," preprint. [Online]. Available <http://arxiv.org/abs/1303.6672>
- [21] D. L. Donoho and J. Tanner, "Precise undersampling theorems," *Proc. IEEE*, vol. 98, no. 6, pp. 913–924, June 2010.
- [22] M. Bayati, M. Lelarge, and A. Montanari, "Universality in polytope phase transitions and message passing algorithms," preprint. [Online]. Available: <http://arxiv.org/abs/1207.7321>
- [23] M. B. McCoy and J. A. Tropp, "The achievable performance of convex demixing," preprint. [Online]. Available: <http://arxiv.org/abs/1309.7478>
- [24] Y. Nesterov, *Introductory Lectures on Convex Optimization: A Basic Course* (Applied Optimization, vol. 87). Norwell, MA: Kluwer, 2004.
- [25] P. L. Combettes and V. R. Wajs, "Signal recovery by proximal forward-backward splitting," *Multiscale Model. Simul.*, vol. 4, no. 4, pp. 1168–1200, 2005.
- [26] C. Chen, B. S. He, Y. Ye, and X. Yuan, "The direct extension of admm for multi-block convex minimization problems is not necessarily convergent," *Optim. Online*, 2013. [Online]. Available: http://www.optimization-online.org/DB_FILE/2013/09/4059.pdf
- [27] G. Chen and M. Teboulle, "A proximal-based decomposition method for convex minimization problems," *Math. Program.*, vol. 64, nos. 1–3, pp. 81–101, Mar. 1994.
- [28] I. Necoara and J. Suykens, "Applications of a smoothing technique to decomposition in convex optimization," *IEEE Trans. Automatic Control*, vol. 53, no. 11, pp. 2674–2679, 2008.
- [29] H. L. V. Trees, *Optimum Array Processing: Part IV of Detection, Estimation, and Modulation Theory*. Hoboken, NJ: Wiley, 2002.
- [30] Q. T. Dinh, A. Kyriillidis, and V. Cevher, "Composite self-concordant minimization," *Lab. Inform. Infér. Sys. (LIONS)*, EPFL, Switzerland, Tech. Rep. 188126, Aug. 2013.
- [31] B. Gözcü, A. Asaei, and V. Cevher, "Manifold sparse beamforming," in *Proc. Int. Workshop on Computational Advances in Multi-Sensor Adaptive Processing (CAMSAP)*, 2013, pp. 113–116.



[Yuanqing Li, Zhu Liang Yu, Ning Bi, Yong Xu, Zhenghui Gu, and Shun-ichi Amari]

Sparse Representation for Brain Signal Processing

[A tutorial on methods and applications]

In many cases, observed brain signals can be assumed as the linear mixtures of unknown brain sources/components. It is the task of blind source separation (BSS) to find the sources. However, the number of brain sources is generally larger than the number of mixtures, which leads to an under-

determined model with infinite solutions.

Under the reasonable assumption that brain sources are sparse within a domain, e.g., in the spatial, time, or time-frequency domain, we may obtain the sources through sparse representation. As explained in this article, several other typical problems, e.g., feature selection in brain signal processing, can also be formulated as the underdetermined linear model and solved by sparse

representation. This article first reviews the probabilistic results of the equivalence between two important sparse solutions—the 0-norm and 1-norm solutions. In sparse representation-based brain component analysis including blind separation of brain sources and electroencephalogram (EEG) inverse imaging, the equivalence is related to the recoverability of the sources. This article also focuses on the applications of sparse representation in brain signal processing, including components extraction, BSS and EEG inverse imaging, feature selection, and classification. Based on functional magnetic resonance imaging (fMRI) and EEG data, the corresponding methods and experimental results are reviewed.

Digital Object Identifier 10.1109/MSP.2013.2296790

Date of publication: 7 April 2014

INTRODUCTION

In recent years, sparse representation has received a great deal of attention in brain signal processing. Many biological findings support sparse representation/coding in the brain. For example,

for simple cells in the primary visual cortex, it was shown that a set of receptive fields learned by maximizing the sparsity

of the output of a neural network model is spatially local-

ized, oriented, and selective to the spatial structure at a specific scale similar to cortical simple cells [1].

Sparsity of the neural response has been observed in neurons and in fMRI [2].

Therefore, sparsity characteristic of brain activities provides a

basis for sparse representation-based

brain data analysis. Many problems in brain

signal processing can be formulated by the sparse

representation models

$$\mathbf{x} = \mathbf{A}\mathbf{s} \quad (\text{noiseless model}), \quad (1)$$

$$\mathbf{x} = \mathbf{A}\mathbf{s} + \mathbf{v} \quad (\text{noisy model}), \quad (2)$$

where $\mathbf{x} \in R^n$ is a given signal vector, $\mathbf{A} \in R^{n \times m}$ ($n < m$) is a basis/dictionary matrix, $\mathbf{s} \in R^m$ is the sparse coefficient vector to be found, and $\mathbf{v} \in R^n$ represents the noise. The basis matrix \mathbf{A} can be randomly generated, or produced, from the union of several known bases such as Fourier and wavelet bases, and it can also be estimated from the data. Equations (1) and (2) can be in a matrix format, in which \mathbf{x} , \mathbf{s} , and \mathbf{v} are replaced by a signal matrix, a coefficient matrix and a noise matrix, respectively.

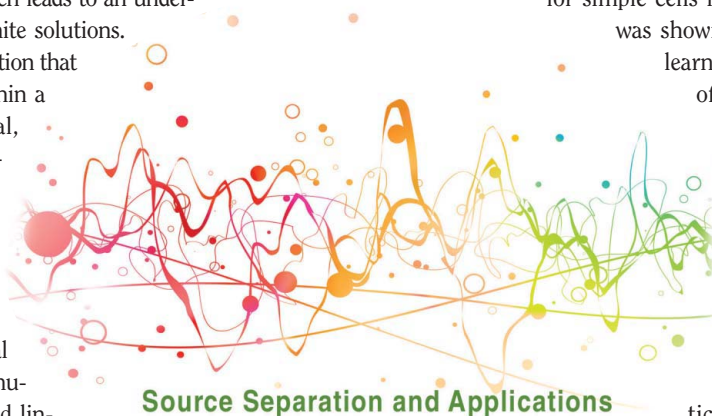
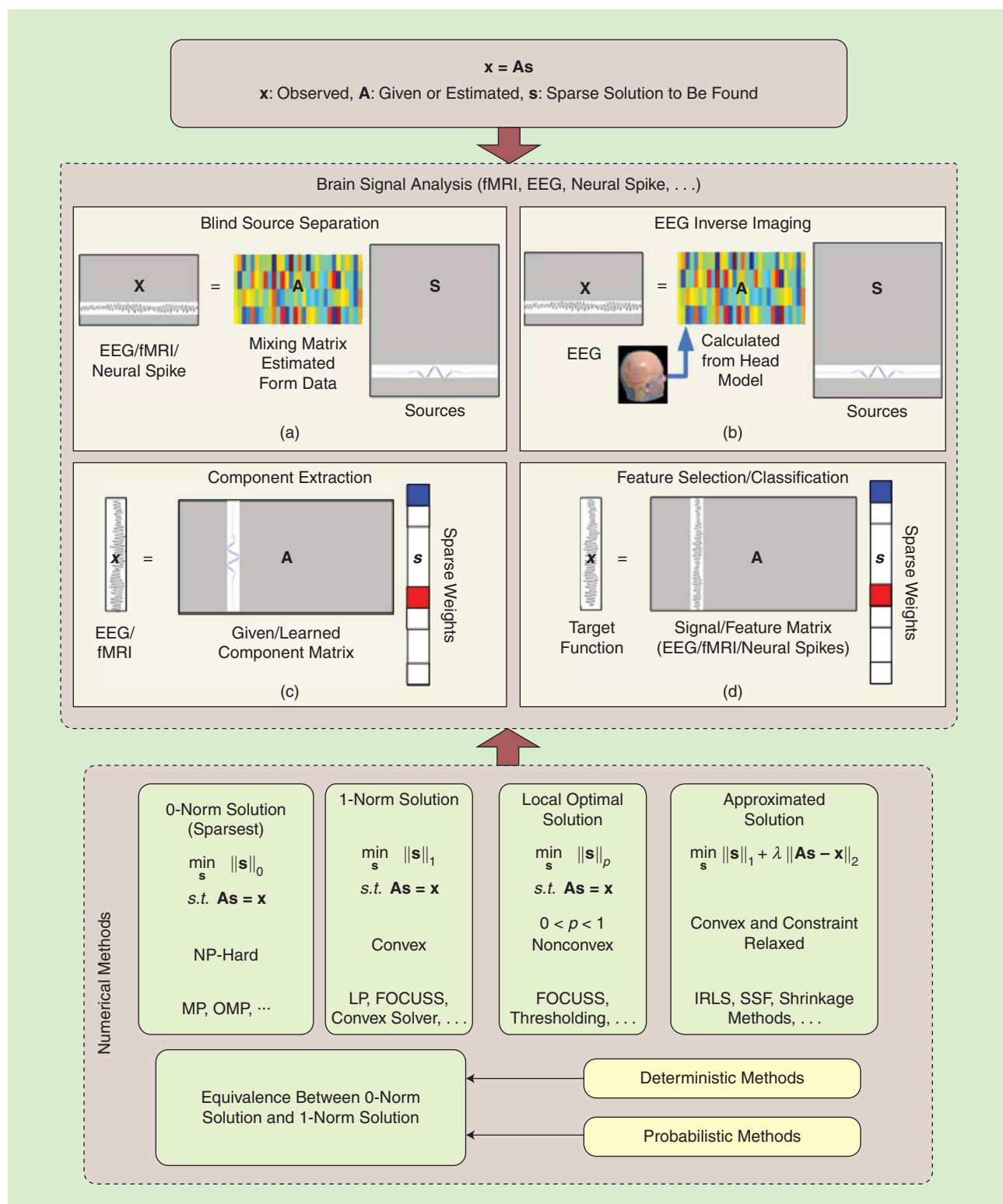


IMAGE LICENSED BY
INGRAM PUBLISHING

For example, we often assume that the observed brain signals are the linear mixtures of brain sources, where both the mixing matrix, i.e., the basis matrix A in (1), and the brain sources are unknown/to be estimated [see Figure 1(a)]. This hypothesis has

been demonstrated for EEG signals [3]. Generally, the number of brain sources is larger than the number of the mixtures. The brain sources can be assumed to be sparse in a domain such as the time domain or the time-frequency domain. Through sparse



[FIG1] The framework for the applications of sparse representation in brain signal analysis.

representation BSS, we can identify the brain sources based on the observed brain signals [4]. The brain sources can also be obtained and localized by sparse representation-based EEG inverse imaging, where the mixing matrix A is first estimated based on a head model, and the brain sources are then separated and localized [see Figure 1(b)]. For component extraction, a channel of brain signal can be treated as a linear mixture of a sparse set of dynamic components, each of which corresponds to a column of the basis matrix A [2] [see Figure 1(c)]. In feature selection, a target function (e.g., a stimulus function in an fMRI experiment) can be linearly regressed using a data/feature matrix A , of which the data for each column are derived from a feature dimension (e.g., a voxel in the fMRI data). In other words, each row of the matrix A is a feature vector [5], as shown in Figure 1(d). The number of features (e.g., the voxels in fMRI data) is generally larger than the number of observations (e.g., the scanning time points for each voxel in the fMRI data). For the classification of brain signals, we may also employ the model shown in Figure 1(d), in which the target function is a test sample/feature vector and each column of the data matrix is a training sample/feature vector of a certain class [6]. These typical problems in brain signal processing can be solved under the framework of sparse representation.

The sparsity of a vector s can be measured by ℓ_p norm $\|s\|_p$, which is defined as $(\sum_{i=1}^m |s_i|^p)^{1/p}$ for $0 < p \leq 1$, and the number of nonzeros of s for $p = 0$. As shown in Figure 1, there are main four classes of algorithms for finding a sparse solution to (1):

- the algorithms for 0-norm minimization, including orthogonal matching pursuit (OMP) and matching pursuit (MP), where the corresponding 0-norm solution, denoted as $s^{(0)}$, is the sparsest among all possible solutions of (1)
- the algorithms for 1-norm minimization, e.g., linear programming (LP) [7], where the corresponding 1-norm solution, denoted as $s^{(1)}$, is also sparse but may not be the sparsest and is relatively easy to obtain
- the algorithms for p -norm minimization ($0 < p < 1$), e.g., focal underdetermined system solver (FOCUSS) and the thresholding algorithm [8], where the p -norm minimization is a nonconvex optimization problem with a global optimal solution that is difficult to be found [9] but is still of interest [10] (some studies have discussed (1/2)-norm minimization [8])
- the algorithms for finding an approximate solution through relaxing the constraints, including least absolute shrinkage and selection operator (LASSO), iterative reweighted least square (IRLS), separable surrogate functionals (SSFs), and the iterative shrinkage and thresholding algorithm (ISTA).

Previous studies have provided detailed reviews on the sparse representation algorithms [9]. These algorithms have been applied in image processing, compressive sensing, and BSS [9]. In

brain signal processing, the choice of an algorithm depends on the specific task. For instance, if BSS/EEG inverse imaging is to be performed, it may be beneficial to use LP algorithms because there have been a lot of corresponding recoverability results and there is no need to set any regularization parameters for the algorithms. For feature selection/classification, all of the above-described sparse representation algorithms may be used, as the objective is generally to improve the classification accuracy, and only part of the relevant features may be required.

Considering both the processing speed and accuracy, if the number of equations is small (e.g., $< 1,000$), greedy algorithms can produce good results with high speed. For a larger number of equations, approximation methods such as ISTA, fast ISTA, and SSF are preferred.

When sparse representation is applied to brain signal processing,

an important objective is to find the sparsest solution, i.e., the 0-norm solution. For instance, under the assumption that the brain sources are sparse, we may obtain the brain sources by finding the 0-norm solution through either sparse representation-based BSS or EEG inverse imaging. Although 0-norm minimization is NP-hard [9], the 0-norm solution can be obtained by 1-norm minimization in many cases. Equivalence between the 0-norm solution and the 1-norm solution thus becomes a key problem (see Figure 1). For sparse representation-based BSS and EEG inverse imaging, the equivalence is related to the recoverability of the brain sources. As shown in Figure 1, this problem can be analyzed using two different types of methods: deterministic methods (see [9] and the references therein) and probabilistic methods (see [4], [7], and [11]–[14]). Compared with the deterministic methods, the conditions under which the two sparse solutions are equivalent with a high probability in the probabilistic methods may be weaker. This is because the conditions obtained by the deterministic methods are sufficient for the equivalence but the probabilistic conditions are not.

RECOVERABILITY RESULTS BASED ON PROBABILISTIC METHODS

In BSS and EEG inverse imaging, it is necessary to consider the recoverability of the brain sources. As stated above, this problem is transformed into the equivalence between the 0-norm solution and the 1-norm solution when sparse representation is applied. Herein, we review several equivalence results obtained by probabilistic methods.

PROBABILISTIC METHODS BASED ON SUFFICIENT CONDITIONS

In references such as [10], [13], and [14], a set of sufficient conditions for the equivalence between the 0- and 1-norm solutions were proposed with respect to the basis matrix and the sparsity of the 0-norm solution. The probability that these sufficient conditions would hold for a random basis matrix was

**THIS ARTICLE FOCUSES
ON THE APPLICATIONS OF
SPARSE REPRESENTATION IN BRAIN
SIGNAL PROCESSING, INCLUDING
COMPONENTS EXTRACTION, BSS
AND EEG INVERSE IMAGING, FEATURE
SELECTION, AND CLASSIFICATION.**

subsequently analyzed. For instance, in [10], it was shown that the proposed sufficient conditions, in particular, the CS conditions, hold for a random basis matrix with an overwhelming probability. In [14], a probability result for the equivalence was obtained based on both an invertibility condition and a magnitude condition, which were imposed on a partial Fourier matrix and a particular polynomial, respectively. To illustrate the probabilistic method, we present several results related to a so-called restricted isometry property (RIP) condition [13], [15].

RIP can be described, as shown in [15], via the following definitions.

DEFINITION 1

For each integer $j = 1, 2, \dots, n$, the matrix $A \in R^{n \times m}$ satisfies the RIP of order j if there exists a $\delta_j \in (0, 1)$ such that

$$(1 - \delta_j) \|s\|_2^2 \leq \|As\|_2^2 \leq (1 + \delta_j) \|s\|_2^2 \quad (3)$$

holds for all j -sparse vectors s . A vector is said to be j -sparse if it has at most j nonzero entries. The isometry constant δ_j of a matrix A is defined as the smallest δ_j satisfying (3).

Recently, it was proven that the equivalence holds if a j -sparse solution exists for (1) and the isometry constant $\delta_j < (1/3)$ [16]. When the matrix A is given randomly, using the Johnson–Lindenstrauss lemma and width theory, R. DeVore et al. provided a probability estimation that (3) holds as below [13].

THEOREM 1

Suppose that for given n, m , and $0 < \delta < 1$, the probability distribution generating the $n \times m$ random matrices A satisfies the concentration inequality, i.e., $\forall v \in (0, 1)$ and $\forall s \in R^m$, there exists a $c_0(\epsilon) > 0$, such that

$$P(|\|As\|_2^2 - \|s\|_2^2| \geq \epsilon \|s\|_2^2) \leq 2e^{-nc_0(\epsilon)}, \quad (4)$$

where the probability is taken over all $n \times m$ matrices A . Then there exist constants $c_1, c_2 > 0$ depending only on δ such that the RIP condition (3) holds for A with the prescribed δ and any $j \leq c_1 n / \log(m/j)$ with a probability $\geq 1 - 2e^{-c_2 n}$ [13].

Remark 1

There are a number of random matrices including random Gaussian and Bernoulli matrices, with distributions satisfying the concentration inequality (4) [13]. Using Theorem 1 and the bound of the isometry constant that guarantees the equivalence, we may obtain a lower bound for the equivalence probability. For example, let $\delta = \delta_j < (1/3)$ and $s^{(0)}$ be j -sparse with $j \leq c_1 n / \log(m/j)$. Following Theorem 1 and Theorem 3.1 in [16], $P(s^{(1)} = s^{(0)}) \geq 1 - 2e^{-c_2 n}$. Because the parameters c_1 and c_2 in Theorem 1 are difficult to explicitly express, the probability (or the lower bound) that the RIP condition holds is difficult to obtain, especially for fixed n and m . In fact, the probability in Theorem 1 shows an overwhelming likelihood with respect to n . The recoverability results based on the RIP condition can be extended to a noisy case (2), as shown in [16].

EQUIVALENCE PROBABILITY ESTIMATION

Different from the above approach, Li et al. proposed an alternative method to directly estimate the probability that the two sparse solutions are equivalent [4], [7], [11], [12]. Several equivalence probability estimates were presented in [11] for a fixed basis matrix and in [12] for a random basis matrix both with a random 0-norm solution. We present several equivalence probability estimations and the corresponding simulation results for a fixed basis matrix with a random 0-norm solution.

THEOREM 2 [12]

Let $A \in R^{n \times m}$, $s^{(0)} \in R^m$, and $s^{(1)}$ be the 1-norm solutions satisfying (1) with $x = As^0$. Then $s^{(0)} = s^{(1)}$, if and only if the optimal value of the following optimization problem is less than 1/2

$$\max \sum_{1 \leq k \leq m} [\text{sign}(s_k^{(0)})z_k]_+ \quad \text{s.t. } Az = 0, \|z\|_1 = 1, \quad (5)$$

where $[y]_+ = \max(y, 0)$ for all $y \in R$.

It is also NP-hard to check the sufficient and necessary condition in Theorem 2 and to precisely specify the set for which the maximum in (5) is computed [11], [12]. However, from Theorem 2, given the basis matrix A the recoverability of the 0-norm solution through 1-norm minimization depends only on the index set and the signs of its nonzero entries, i.e., the sign vector/pattern. The equivalence probability can be obtained by determining how many sign vectors can be recovered through 1-norm minimization, as illustrated in the following three cases [11].

Case 1

The number of nonzero entries for the 0-norm solution $s^{(0)}$ is fixed, e.g., j . In this case, there are a total of $2^j C_m^j$ sign vectors with 0-norm j . Suppose that q_j is the number of sign vectors with 0-norm j which can be recovered by 1-norm minimization. We have

$$p_j = P(s^{(1)} = s^{(0)} | \|s^{(0)}\|_0 = j) = \frac{q_j}{2^j C_m^j}, \quad (6)$$

where q_j can be obtained by checking the equivalence of each sign vector with 0-norm j and its corresponding 1-norm solution. This can be performed either by Theorem 2 or by directly comparing the 0-norm solution with its corresponding 1-norm solution obtained by 1-norm minimization.

Case 2

The number of nonzero entries for $s^{(0)}$ is unknown, but the probability that every entry of $s^{(0)}$ is equal to zero is known and denoted as α . In this case, $P(\|s^{(0)}\|_0 = j) = C_m^j (1 - \alpha)^j \alpha^{m-j}$ and

$$P(s^{(1)} = s^{(0)}) = \sum_{j=0}^m C_m^j (1 - \alpha)^j \alpha^{m-j} p_j. \quad (7)$$

Case 3

All entries for $s^{(0)}$ are drawn from a Laplacian distribution with the probability density function $(\lambda/2) \exp(-\lambda |x|)$. In this case,

$$P(s^{(1)} \approx s^{(0)}) = \sum_{0 \leq j \leq m} C_m^j (1 - \alpha_\lambda)^j \alpha_\lambda^{m-j} p_j, \quad (8)$$

where $\alpha_\lambda = P(|s_k^{(0)}| < \varepsilon_0) = 1 - \exp(-\lambda \varepsilon_0)$ and $\varepsilon_0 > 0$ is a sufficiently small constant.

We review several simulation results [11]. The basis matrix $A \in R^{7 \times 9}$ was arbitrarily given in advance. Figure 2 shows the estimated equivalence probability curves (solid curves with “*”) and the true equivalence probability curves (dash-dotted curves with “o”) for the above three cases. Note that each true probability value was obtained by randomly generating 1,000 corresponding source vectors (0-norm solutions) and counting the number of source vectors recovered by 1-norm minimization. It follows from Figure 2 that the probability estimates from (6)–(8) accurately reflected the true probability that a 0-norm solution was recovered by 1-norm minimization in Cases 1–3, respectively.

Remark 2

Based on the equivalence probability estimates described above, it is still NP-hard to obtain the exact values for a large m . However, approximations can be obtained by applying a sampling method to the set of sign vectors [17]. In addition to the above-described equivalence problem, another important problem in sparse representation is the uniqueness of the 0-norm solution of (1). In [7], it was shown that for model (1), a 0-norm solution with less than n nonzeros is unique with a probability of one if the basis matrix A is randomly given.

In brain signal processing, noise generally can not be neglected. According to the discussion in [7], the 1-norm solution of (1) is robust to noise to some degree. In particular, for a given A , there exists an $M > 0$ such that $\|s_v^{(1)} - s^{(1)}\|_1 < M \|v\|_1$, where $s_v^{(1)}$ is the 1-norm solution of the noisy model (2). Therefore, for a case with low noise, we can determine the 0-norm solution through 1-norm minimization, provided that

the equivalence holds. Furthermore, the above probability estimations on the equivalence have been extended to the noise case in [17]. Simulation results showed that these probability estimations of the equivalence hold at noise levels of approximately 18 dB. However, for brain signals, it is difficult to estimate the noise level, which may be very high. Further studies are needed to demonstrate the effectiveness of the above-described probability estimations and to evaluate the brain sources obtained by sparse representation-based BSS/EEG inverse imaging. Additionally, the above-described probability estimates are based on the sparsity of the 0-norm solution, which is generally difficult to directly determine. It has been shown that the sparsity of sources can be estimated based on the sparsity of the mixtures [17].

FUNCTIONAL MRI DATA ANALYSIS

In this section, we discuss two applications of sparse representation in fMRI data analysis: the modification of a general linear regression model (GLM) with statistical parameter mapping (SPM), and brain decoding.

MODIFIED GLM-SPM APPROACH BASED ON SPARSE REPRESENTATION

An important objective of fMRI data analysis is to detect the weak blood-oxygen-level dependent (BOLD) signal from the noisy data and localize the activated regions in the brain. GLM-SPM is a common method for fMRI data analysis [18] that is based on

$$x_i = G\beta_i + e_i, \quad (9)$$

where $x_i \in R^N$ is a time series of the i th voxel ($i = 1, \dots, M$), $G \in R^{N \times K}$ is a so-called design matrix of which each column corresponds to an explanatory variable related to the specific experimental conditions under which the data were collected, $\beta_i \in R^K$ is an unknown weight vector to be estimated for each voxel, and $e_i \in R^N$ is a noise vector. At the end of the GLM learning process, the statistical parameter map is obtained

based on t - or F -statistics calculated using the regression coefficients, and it can be used to display the activated brain areas and the importance of each voxel.

Several studies have been conducted to improve the GLM-SPM method based on sparse representation. One method for improving GLM is to modify the design matrix to overcome its drawbacks. The design matrix is generally constructed using the canonical hemodynamic response function (HRF). However, this function does not fully reflect the individual and experimental variances that occur during the task period [2]. To overcome this issue, Hu et al. proposed an SPM-ICA framework with a design matrix composed of the components learned by an independent component analysis (ICA) algorithm [19]. In [2], a data-driven sparse GLM method was proposed

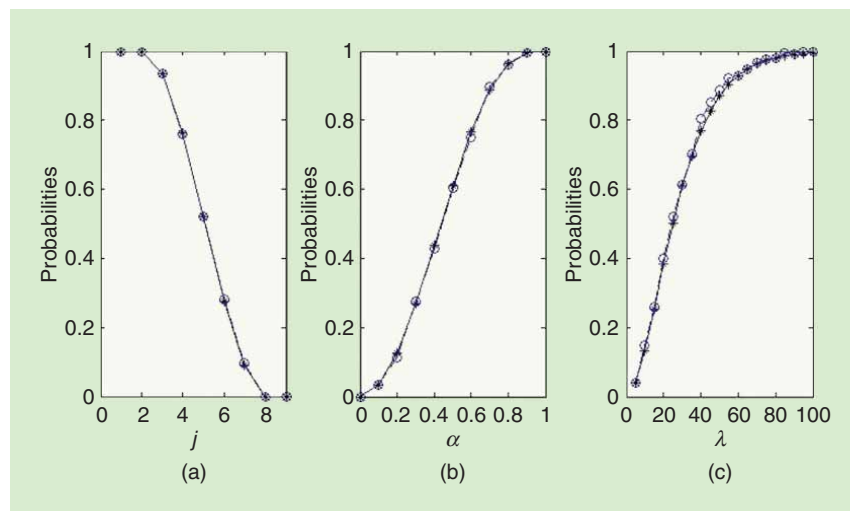


[FIG2] Curves for estimated equivalence probabilities (solid curves with “*”) and true equivalence probabilities (dash-dotted curves with “o”). (a) Case 1, (b) Case 2, and (c) Case 3.

for maximum likelihood (ML) estimation of spatially adaptive design matrices and sparse response signals. In this method, the BOLD signal at a specific voxel can be regarded as a linear combination of a sparse set of dynamic components [see Figure 1(c)]. A K-SVD-based iterative algorithm was used to identify these components and to perform sparse coding at the same time. Based on the learned design matrix and sparse response signals, a statistical test was then used to detect the activated voxels. Using simulated and real fMRI data, this method was demonstrated to adapt to individual variations better than canonical HRF and spatial ICA.

SPARSE REPRESENTATION-BASED MVPA METHODS FOR BRAIN DECODING

Multivariate pattern analysis (MVPA) has recently become a popular approach for analyzing fMRI data. MVPA approaches open the possibility of separating and localizing spatially distributed patterns, which are generally too weak to be detected by univariate methods, such as GLM [20]. By effectively pooling the information available across many fMRI voxels, MVPA methods allow the perceptual, cognitive, and behavioral parameters or features to be decoded. The results of brain decoding can be used to further assess how precisely cognitive information is encoded by the activity of neural populations within the whole brain [21]. Because there are far more voxels (e.g., 30,000) than fMRI volumes/scanning time points for each of the voxels (e.g., 1,000), voxel selection plays an important role in the MVPA-based brain decoding of fMRI data [see Figure 1(d)]. It has been shown that sparse representation is an effective method for voxel selection. The sparseness leads to a simple prediction function useful for avoiding overfitting. For instance, a LASSO regression was used to reconstruct muscle activity from human cortical fMRI data, where the correlated voxels were selected through the learned sparse weights [22]. In the following, we briefly present a sparse representation-based voxel selection algorithm and its two variants/extensions. Specific details for these algorithms can be obtained from [5] and [23].

LINEAR PROGRAMMING-BASED FEATURE SELECTION ALGORITHM

Let $A \in R^{n \times m}$ denote an fMRI data matrix, where each column is the time series of a voxel. Let $x \in R^n$ denote a stimulus/task function convolved with an HRF. A stimulus function can be constructed by setting its value to one when the stimulus is available; otherwise the value is set to zero. The following algorithm is designed to identify the columns of A (i.e., voxels in the fMRI data) that are relevant to x .

Algorithm 1 (LP-Based Feature Selection Algorithm):

Step 1: For $k = 1, \dots, K_0$ (a predefined integer, e.g., 100), perform Steps 1.1 and 1.2.

Step 1.1: Randomly choose L (e.g., $0.3n$) rows from the matrix A to construct an L by m submatrix denoted as A_k , with the corresponding L entries of x forming a column vector denoted by $x_k \in R^L$.

Step 1.2: Solve the optimization problem (denote the optimal solution as $\bar{s}^{(k)}$),

$$\min \|s\|_1, s.t. A_k s = x_k. \quad (10)$$

Step 2: Let

$$s = \frac{1}{K_0} \sum_{k=1}^{K_0} \bar{s}^{(k)}. \quad (11)$$

Step 3: Using the weight vector s , we either select a fixed number (e.g., 100) of voxels with large absolute weights or select voxels with absolute weights higher than a given positive constant θ_0 . The threshold parameter θ_0 can be chosen in various ways, e.g., through the cross-validation method [5].

Because of noise, the weight vector s obtained by a single optimization may not accurately reflect the importance of the features. Thus, we calculate an average weight vector by boosting the 1-norm minimization in Algorithm 1. With the selected voxels, decoding of the stimulus/task parameters can be performed using a classifica-

tion/regression algorithm such as SVM.

OMP-BASED FEATURE SELECTION ALGORITHM

In Step 1.2 of Algorithm 1, we can replace the LP/basis pursuit (BP) algorithm with the OMP algorithm [9] to conduct sparse representation and obtain the OMP-based feature selection algorithm. For fMRI data, we find that the OMP-based algorithm is faster than Algorithm 1 because the number of time samples is generally much smaller than the number of voxels and the OMP algorithm avoids a large-scale LP problem.

SPARSE REPRESENTATION-BASED PATTERN LOCALIZATION ALGORITHM

There are three unsolved problems in Algorithm 1: the abilities to 1) select all informative features, 2) differentiate those selected features according to two stimuli classes/brain states, and 3) remove incorrectly selected features (irrelevant/noisy features). A sparse representation-based pattern localization (SPL) algorithm was used to address these problems [23]. The SPL algorithm contains a K -fold cross-validation procedure. In each fold, a recursive iterative feature elimination method relying on the weights obtained by sparse representation (e.g., Algorithm 1 or the OMP-based feature selection algorithm) is used to identify as many informative features as possible. Each iteration selects those informative features for removal. The next iteration is based on the remaining features. After the selected

MVPA APPROACHES OPEN THE POSSIBILITY OF SEPARATING AND LOCALIZING SPATIALLY DISTRIBUTED PATTERNS, WHICH ARE GENERALLY TOO WEAK TO BE DETECTED BY UNIVARIATE METHODS, SUCH AS GLM.

[TABLE 1] PREDICTION ACCURACIES (PEARSON CORRELATION) FOR FOUR TASK FUNCTIONS (HITS, INSTRUCTIONS, FACES, AND VELOCITY), OBTAINED BY THREE METHODS: GLM-SPM, LP, AND OMP-BASED ALGORITHMS.

TASK	SUBJECT 1			SUBJECT 2			SUBJECT 3		
	GLM-SPM	LP	OMP	GLM-SPM	LP	OMP	GLM-SPM	LP	OMP
HITS	0.18	0.31	0.33	0.35	0.39	0.47	0.25	0.33	0.33
INSTR.	0.51	0.75	0.60	0.63	0.66	0.57	0.32	0.83	0.60
FACES	0.06	0.15	0.12	-0.01	0.31	0.28	0.61	0.65	0.42
VELOCITY	0.25	0.38	0.63	0.38	0.38	0.69	0.16	0.35	0.61

features from all of the iterations are removed, the decoding accuracy based on the remaining features is close to the chance level. According to the signs of the weights, the selected features are divided into two sets corresponding to two stimulus classes/brain states. Next, two probability maps/density functions are constructed using the two classes of features selected across the K folds. Inside each probability map, the probability value of a feature is obtained by counting the number of times that the feature is selected across all folds. Finally, to remove the irrelevant features, the two probability maps are tested with a permutation test either at the individual level or at the group level if group data are available. In this way, two patterns corresponding to the two stimuli classes/brain states are obtained.

EXPERIMENTAL RESULTS

First, we individually applied Algorithm 1 and the OMP-based feature selection algorithm to the fMRI data of PBAIC 2007 for voxel selection. The details for the data can be found at <http://pbc.lrdc.pitt.edu/?q=taxonomy/term/45>. The subject performed several tasks in a virtual reality world during scan acquisition (e.g., Hits: whenever the subject picked up fruits or weapons; Instruction: whenever task instructions were presented; Faces: whenever the subject looked at faces; Velocity: whenever the subject was moving). For each task, a stimulus function was provided by PBAIC 2007. The corresponding task function was computed by convolving this stimulus function with an HRF, which reflected the delay of the hemodynamic responses with respect to the onsets of the stimuli. The data analysis predicted the task functions from the fMRI data.

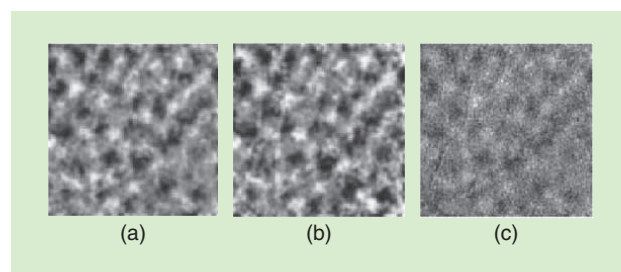


[FIG3] The dark and bright blobs in (a)–(c) are shown for two classes of stimuli, i.e., the horizontal axis-of-motion stimuli and the vertical axis-of-motion stimuli. (a) and (b) The difference maps reconstructed using our BP-based and OMP-based SPL algorithms, respectively. (c) A difference map between the two stimulus conditions.

For each of the three subjects, two runs of data, collected in different time intervals, were analyzed. After data processing, each run of fMRI data corresponded to a matrix with 500 rows (time points) and approximately 32,000 columns (voxels). Based on the BP (Algorithm 1) or OMP-based feature selection algorithm, we performed twofold

cross-validation. In each fold, voxel selection was performed based on the training data (data from Run 1/Run 2) in two steps, i.e., an initial selection based on Pearson correlation coefficients between the time series of voxels and the task function and a second selection based on our algorithm. Using the selected voxels (ranging from two to 100), we predicted the task function of the test data (data from Run 2/Run 1) through ridge regression. The prediction performance was measured as the Pearson correlation between the actual task and the predicted task functions. For the purpose of comparison, we used the GLM-SPM method to replace our method to select the voxels. The average prediction accuracies across all the numbers of the selected voxels are shown in Table 1. The high accuracy values demonstrate the effectiveness of our algorithms. Based on Table 1, our algorithms overperformed GLM-SPM method in the majority of cases, with only two exceptions: the accuracies obtained by the OMP-based method for subject 2 in the instruction task and for subject 3 in the face task. One important reason for this finding is that GLM-SPM is a univariate method, whereas our algorithms are multivariate. Multivariate methods simultaneously consider a set of variables, and their advantages have been shown in numerous studies [20]. For the face task, the results for the three subjects were significantly different, possibly because of the different levels of attention that the subjects paid to this task.

Second, we present results obtained by applying the SPL algorithm to an optical imaging data set that was collected from a macaque monkey. The detailed experimental procedure was described elsewhere [23]. Based on data from 40 horizontal and 40 vertical axis-of-motion trials, we used a leave-one-out method to search the informative pixels and obtained two probability maps. The difference between the two probability maps, which reflects the class information, is shown in Figure 3(a), (based on Algorithm 1) and Figure 3(b) (based on the OMP-based feature selection algorithm). As shown in Figure 3(c), we also obtained a differential map between the two conditions using an established method for optical imaging data analysis (the so-called differential mapping method). The dark and bright blobs in Figure 3(c) represent the two classes of informative features. In Figure 3, a comparison of (a) and (b) to (c) reveals that our algorithms can find all of the informative features and further separate them into two classes corresponding to the two experimental conditions. These results show that the columnar structures in the V1 area of the visual cortex of the monkey can be detected by the SPL algorithm.

EEG DATA ANALYSIS

In this section, we discuss the application of sparse representation in EEG data analysis including component analysis and pattern classification.

EEG COMPONENT ANALYSIS

BLIND SOURCE SEPARATION

EEG signals can be considered as the linear mixtures of unknown sources with an unknown mixing matrix. In this case, the true sources can be obtained through sparse representation-based BSS [see Figure 1(a)]. Under the condition that the sources are sparse within a domain such as the time-frequency domain, the sparse representation-based BSS can be conducted using a two-step method ([7], [11], and the references therein). The mixing matrix is first estimated using, e.g., a clustering algorithm. The sources

are then obtained using a sparse representation algorithm. In the two-step method, it is difficult to estimate the mixing matrix precisely. For sparse representation-based BSS, the number of sources can be larger than the number of the mixtures and the sources can be correlated, provided that the sources are sufficiently sparse. In [4], a wavelet packet transformation was first applied to an EEG data set collected in an experiment with a modified Sternberg memory task for producing sparsity. Specifically, in the experiment, the subjects were instructed to memorize three numbers successively presented at random positions on a computer monitor. The effectiveness of the subjects' memory was evaluated using a "test number" presented 2.5 s later. Next, the ratio matrix was constructed as the mixing matrix using wavelet packet transformation coefficients. Third, the sources were estimated by 1-norm minimization. Furthermore, several pairs of almost uncorrelated sources were obtained, which showed memory-related synchronization and desynchronization.

EEG INVERSE IMAGING

EEG signals are generally considered to be generated from the synchronized activation of cortical pyramidal neurons. Through forward modeling of brain sources and head volume conduction, EEG inverse imaging can identify these sources and their localizations [see Figures 1(b) and 4] [24]. EEG inverse imaging is useful for the study of brain mechanisms and diseases detection. For example, high-resolution EEG inverse imaging can be used to identify the origin and propagation of dynamic epileptic

activity and to provide information for presurgical planning for the patients [24].

The distributed source model for inverse imaging assumes that a large number of unit dipoles are evenly positioned in the brain volume or over the cortical sheet of gray matter, and each dipole represents a candidate source [24]. Under this assumption, the first step of inverse imaging is the forward modeling of the brain sources and head volume conduction to establish a linear source-to-measurement relationship. Specifically, for the model shown in Figure 4, the j th row of X is an observed EEG signal from the j th sensor. The i th column of the matrix A [a lead field matrix (LFM)], corresponding to the i th grid, describes how a unit dipole with a certain location and orientation is related to the EEG measurements [24]. The i th row of S is a brain source associated with the i th grid through the i th column of A . In practice, the number of grids can range from 3,000 to 9,000

depending on several factors, e.g., the data analysis task and whether the grids are evenly distributed in the brain volume or over the cortical sheet of gray matter. Given the configuration of the grids, the placement of the sensors and the head model, the transfer property a_{ji} between the i th grid and the j th sensor can be calculated using either a boundary element model (BEM) or a finite element model (FEM) [24]. Thus, the matrix A is determined. The head model can be constructed from single spherical shell, multiple spherical shells or the structural MRI. The second step is to identify the brain sources from the observed EEG data based on the linear model.

Because the number of electrodes n is much lower than the number of grids m , there are infinite solutions for the linear inverse problem. Various methods have been developed to

**EEG SIGNALS CAN BE
CONSIDERED AS THE LINEAR
MIXTURES OF UNKNOWN SOURCES
WITH AN UNKNOWN MIXING MATRIX.
IN THIS CASE, THE TRUE SOURCES
CAN BE OBTAINED THROUGH SPARSE
REPRESENTATION-BASED BSS.**

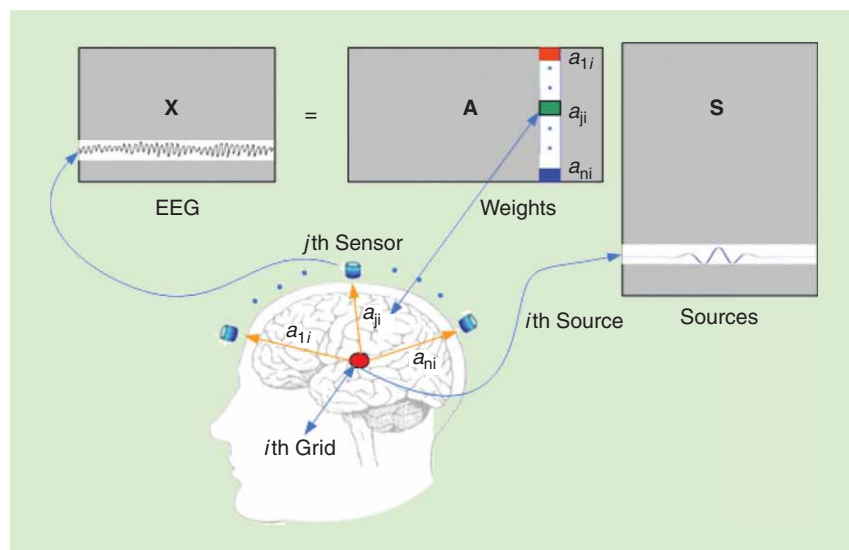


[FIG4] A diagram for EEG inverse imaging.

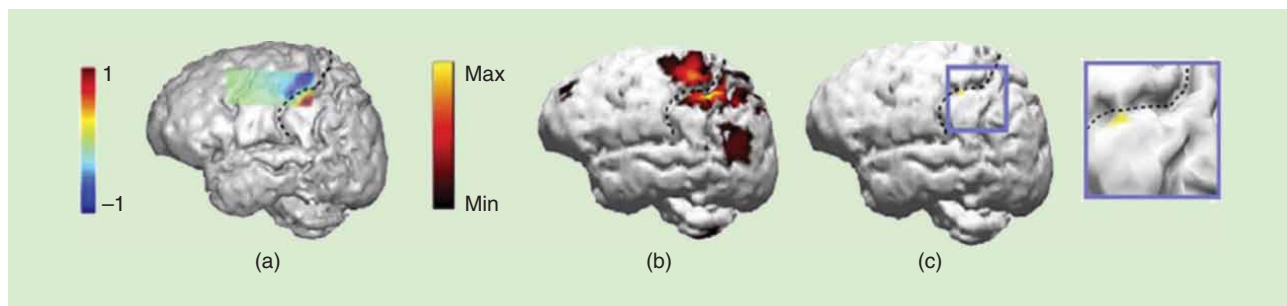


[FIG5] The results for EEG inverse imaging (extracted from Figure 4 in [25] with permission). (a) Direct subdural ECoG recordings, (b) imaging results from LORETA, and (c) imaging results from the sparse method. Dotted lines indicate the central sulcus.

obtain an “optimal” source estimate by introducing biophysical and/or physiological constraints. Under the assumption that the brain sources are sparse, the inverse imaging problem can be solved through sparse representation (1-norm minimization) [25]. Once the sparse brain sources are obtained, they can be localized by the corresponding grids.

Using ECoG mappings as a gold standard for evaluation, it has been shown that the results of the sparse method are comparable to those of other methods, e.g., 2-norm-based low-resolution brain electromagnetic tomography (LORETA) for EEG inverse imaging [25]. We present the partial results from this study in Figure 5. Figure 5(a) shows the direct subdural ECoG recordings, whereas (b) and (c) show the imaging results from the LORETA and sparse methods, respectively. The results are displayed with the threshold set at 70% of the maximum current density (A/mm^2). The hot spots (yellow areas) indicate that the source activities, estimated by the sparse and the LORETA methods, were located on the sensory cortex. However, the hot spot for the sparse method corresponded more closely with the area identified by the subdural ECoG map. This experiment demonstrates that the sparse method provides better specificity than the LORETA method for focal sources. However, for spatial extended sources, multiple distributed source imaging methods have been tested in well-controlled simulations [26]. For sources with large spatial extents ($10\text{ mm}^2 - 40\text{ cm}^2$), the LORETA method could provide effective results. In conclusion, 2-norm-based methods including LORETA are suited to imaging spatially distributed sources, whereas sparse methods are suited to imaging sparse and focal sources. Considering the different advantages of these two classes of methods, several inverse imaging algorithms combining 1-norm and 2-norm have been developed [24].

FEATURE SELECTION AND CLASSIFICATION OF EEG SIGNAL

FEATURE SELECTION

Although the EEG signals are contaminated by noise and artifacts caused by volume conduction effects, EEG patterns still have typical spatial, temporal, and spectral distribution characteristics. For example, the motor imagery of the left/right hand gives rise to contralateral attenuation (or accentuation) in mu

and beta rhythm activities in EEG, known as event-related desynchronization (or synchronization) (ERD/ERS) [27], which can be located in sensorimotor areas. P300 potentials occur approximately 300 ms after the attended stimulation and exist primarily in the parietal area, which means that signals collected from certain electrodes at certain time intervals or frequency bands are easier to discriminate than other signals. Therefore, it is desirable to build a spatial/temporal/spectral filter for feature extraction/selection. Furthermore, dimension reduction based on feature extraction/selection may lead to better generalization performance for the corresponding classifier.

Feature selection from EEG data can be performed by sparse representation, as shown in Figure 1(d). Take the feature extraction for motor imagery-based ERD/ERS as an example. We often use labeled EEG data to train a common spatial pattern (CSP) filter. To distinguish the features of the two classes of data corresponding to the left- and right-hand motor imageries, respectively, the CSP algorithm finds the spatial filters that maximize the variance for one class and at the same time minimize the variance for the other class [27]. Because the CSP method is based on the optimization of signal variance, which is 2-norm, the resultant filter weights are nonsparse, which implies that all of the channels are used in the following classification. However, because the ERD/ERS is located in specific areas (e.g., the sensorimotor area), only nearby channels have good discrimination for the two classes. The other channels need to be removed before classification. In this case, sparse representation is well tailored for channel selection. Selection can be achieved by simply modifying the optimization problem in the CSP method by introducing the 1-norm of the filter weights in the objective function [28]. The lower-weighted channels can be viewed as irrelevant and can thus be removed. This method is called sparse CSP (SCSP). Experiments have shown that the classification accuracy based on SCSP is greater than the accuracy of regular CSP [28]. This outstanding performance can be explained by the fact that sparse representation reduces the number of participating channels, with a concomitant denoising effect.

CLASSIFICATION

Sparse representation-based classification (SRC) can be conducted as shown below [see Figure 1(d)]. Suppose that the basis matrix A is composed of two component submatrices

corresponding to the two classes, i.e., $A = [A_1 | A_2]$. The mutual coherence of the two submatrices is defined by

$$MC(A_1, A_2) = \max\{|\langle \mathbf{a}_{1,i}, \mathbf{a}_{2,j} \rangle| : i=1, \dots, N_1; j=1, \dots, N_2\} \quad (12)$$

where $\mathbf{a}_{1,i}$ is the i th column of A_1 , $\mathbf{a}_{2,j}$ is the j th column of A_2 , and N_1 and N_2 are the numbers of columns in A_1 and A_2 , respectively. The inner product of the two vectors is denoted by $\langle \cdot, \cdot \rangle$. When MC is low, i.e., the basis matrix is incoherent, a test data vector from one

class can be predominantly represented by the columns of the same class in the basis matrix [6]. Thus, the classification based on the sparse coefficients, which can be obtained by sparse representation, is prone to producing the correct label. In ERD/ERS, for example, the CSP features can be used to construct the basis matrix because CSP filtering maximizes the incoherence between the two classes. Using the basis matrix for sparse regression of a test feature vector, a sparse solution is obtained for further classification. Specifically, the class label is determined by computing the energy of the coefficients for each class and assigning the class label of the larger one to the test data. SRC was applied in the data analysis of several motor imagery-based brain-computer interface (BCI) data sets and showed better classification performance than the well-known linear discriminant analysis method [6].

CONCLUDING REMARKS

This article discussed the applications of sparse representation in brain signal processing, including BSS, EEG inverse imaging, feature selection, and classification. Although we mainly focused on fMRI and EEG data, sparse representation can also be applied to other brain signals such as neural spike data [29], magnetoencephalography [30], and MRI [31]. When sparse representation is used to separate sources from brain signals in BSS and EEG inverse imaging, recoverability of the sources is a basic problem. This problem can be transformed to the equivalence between the 0-norm solution and the 1-norm solution. We first reviewed the recoverability/equivalence results obtained by probabilistic methods. Next, we reviewed several fMRI studies to illustrate how to improve the GLM-SPM, a common method in fMRI data analysis, through sparse component analysis, and how to perform feature selection based on LP or OMP methods. For EEG signal processing, we reviewed several sparse representation methods and experimental results for BSS, inverse imaging, feature selection, and classification.

We identified several challenging problems for further study:

- Brain signals are highly dynamic. Several sparse representation methods have been proposed to capture the dynamic properties of the brain signals, e.g., a mixed-norm estimate method based on the structured sparsity of the sources [30]. Because of the high complexity of brain signals, this problem still needs further investigation. It may also be possible to

establish time-varying sparse representation methods in which the basis matrix is time-varying.

- For high-dimensional brain signals, the existing sparse representation algorithms are generally time consuming. For some applications including BCIs, fast/real-time sparse representation algorithms are expected. One option is to reduce the dimensionality by considering the neurophysiological mechanisms of brain activities, e.g., brain functional areas, and develop or choose fast sparse representation algorithms such as fast ISTA.

- Because brain signals are highly noisy, it is challenging to evaluate the obtained brain sources. The existing recoverability results (deterministic/probabilistic) need to be extended to highly noisy cases, and indirect but more effective methods need to be developed to explore the neurophysiological reasonability of the brain sources associated with the corresponding experimental conditions.

ACKNOWLEDGMENTS

This work was supported by 863 Program of China (2012AA011601), the National Foundation of Natural Science of China (91120305, 61105121, and 61175114), and the High-Level Talent Project of Guangdong Province, China.

AUTHORS

Yuanqing Li (auyqli@scut.edu.cn) received the B.S. degree in applied mathematics from Wuhan University, China, in 1988, the M.S. degree in applied mathematics from South China Normal University in 1994, and the Ph.D. degree in control theory and applications from South China University of Technology, China, in 1997. Currently, he is with the South China University of Technology as a full professor. He is the author or coauthor of more than 80 scientific papers in journals and conference proceedings. His research interests include blind signal processing, sparse representation, machine learning, BCIs, EEG, and fMRI data analysis.

Zhu Liang Yu (zlyu@scut.edu.cn) received the B.S.E.E. degree in 1995 and the M.S.E.E. degree in 1998, both in electronic engineering from the Nanjing University of Aeronautics and Astronautics, China. He received his Ph.D. degree in 2006 from Nanyang Technological University, Singapore. He joined the Center for Signal Processing, Nanyang Technological University in 2000, as a research engineer and then as a research fellow. In 2008, he joined the College of Automation Science and Engineering, South China University of Technology, where he was promoted to a full professor in 2009. His research interests include signal processing, pattern recognition, and biomedical applications.

Ning Bi (mcsbn@mail.sysu.edu.cn) received the B.S. and Ph.D. degrees in mathematics from Zhejiang University, China, in 1989 and 2002, respectively. He is currently with the School of Mathematics and Computational Science and Guangdong Province Key

Laboratory of Computational Science, Sun Yat-Sen University, Guangzhou, China. He has published more than 30 papers and coauthored the book *An Introduction to Multiband Wavelets* with Q. Sun and D. Huang. His research interests include multiband wavelets, watermarking, and compressed sensing.

Yong Xu (yxu@scut.edu.cn) received the B.S., M.S., and Ph.D. degrees in mathematics from Nanjing University, Nanjing, China, in 1993, 1996, and 1999, respectively. He was a postdoctoral research fellow in computer science with South China University of Technology, Guangzhou, China, from 1999 to 2001, where he became a faculty member and where he is currently a professor with the School of Computer Science and Engineering. His current research interests include image analysis, image and video recognition, image quality assessment, and object recognition. He is a member of the IEEE Computer Society and the Association of Computing Machinery and a Senior Member of the IEEE.

Zhenghui Gu (zhgu@scut.edu.cn) received the Ph.D. degree from Nanyang Technological University, Singapore, in 2003. From 2002 to 2008, she was with the Institute for Infocomm Research, Singapore. In 2008, she joined the College of Automation Science and Engineering, South China University of Technology, Guangzhou, as an associate professor. Her current research interests include the fields of signal processing and pattern recognition.

Shun-ichi Amari (amari@brain.riken.jp) received the Ph.D. degree in 1963 from the University of Tokyo. He worked as a professor at Kyushu University and then at the University of Tokyo, where he is now professor emeritus. He is an ex director and senior advisor at the RIKEN Brain Science Institute. He has worked on a wide range of mathematical sciences, including information geometry and mathematical neuroscience. He served as president of the International Neural Network Society (INNS). He received the IEEE Emanuel R. Piore Award, the INNS Society Gabor Award, and the Japanese Order of Cultural Merit among many others.

REFERENCES

- [1] B. A. Olshausen and D. J. Field, "Emergence of simple-cell receptive field properties by learning a sparse code for natural images," *Nature*, vol. 381, no. 6583, pp. 607–609, 1996.
- [2] K. Lee, S. Tak, and J. C. Ye, "A data-driven sparse GLM for fMRI analysis using sparse dictionary learning with MDL criterion," *IEEE Trans. Med. Imag.*, vol. 30, no. 5, pp. 1076–1089, 2011.
- [3] J. Sarvas, "Basic mathematical and electromagnetic concepts of the biomagnetic inverse problem," *Phys. Med. Biol.*, vol. 32, no. 1, pp. 11–22, 1987.
- [4] Y. Li, A. Cichocki, and S.-I. Amari, "Blind estimation of channel parameters and source components for EEG signals: A sparse factorization approach," *IEEE Trans. Neural Netw.*, vol. 17, no. 2, pp. 419–431, 2006.
- [5] Y. Li, P. Namburi, Z. Yu, C. Guan, J. Feng, and Z. Gu, "Voxel selection in fMRI data analysis based on sparse representation," *IEEE Trans. Biomed. Eng.*, vol. 56, no. 10, pp. 2439–2451, 2009.
- [6] Y. Shin, S. Lee, J. Lee, and H.-N. Lee, "Sparse representation-based classification scheme for motor imagery-based brain-computer interface systems," *J. Neural Eng.*, vol. 9, no. 5, p. 056002, 2012.
- [7] Y. Li, A. Cichocki, and S.-I. Amari, "Analysis of sparse representation and blind source separation," *Neural Comput.*, vol. 16, no. 6, pp. 1193–1234, 2004.
- [8] Z. Xu, X. Chang, F. Xu, and H. Zhang, " $l_{1/2}$ regularization: A thresholding representation theory and a fast solver," *IEEE Trans. Neural Netw. Learn. Syst.*, vol. 23, no. 7, pp. 1013–1027, 2012.
- [9] A. M. Bruckstein, D. L. Donoho, and M. Elad, "From sparse solutions of systems of equations to sparse modeling of signals and images," *SIAM Rev.*, vol. 51, no. 1, pp. 34–81, 2009.
- [10] D. L. Donoho, "Compressed sensing," *IEEE Trans. Inform. Theory*, vol. 52, no. 4, pp. 1289–1306, 2006.
- [11] Y. Li, S.-I. Amari, A. Cichocki, D. W. C. Ho, and S. Xie, "Underdetermined blind source separation based on sparse representation," *IEEE Trans. Signal Processing*, vol. 54, no. 2, pp. 423–437, 2006.
- [12] Y. Li, S.-I. Amari, A. Cichocki, and C. Guan, "Probability estimation for recoverability analysis of blind source separation based on sparse representation," *IEEE Trans. Inform. Theory*, vol. 52, no. 7, pp. 3139–3152, 2006.
- [13] R. Baraniuk, M. Davenport, R. DeVore, and M. Wakin, "A simple proof of the restricted isometry property for random matrices," *Constr. Approx.*, vol. 28, no. 3, pp. 253–263, 2008.
- [14] E. J. Candès, J. Romberg, and T. Tao, "Robust uncertainty principles: Exact signal reconstruction from highly incomplete frequency information," *IEEE Trans. Inform. Theory*, vol. 52, no. 2, pp. 489–509, 2006.
- [15] E. J. Candès, "The restricted isometry property and its implications for compressed sensing," *C. R. Math.*, vol. 346, no. 9, pp. 589–592, 2008.
- [16] T. Cai and A. Zhang, "Sharp RIP bound for sparse signal and low-rank matrix recovery," *Appl. Comput. Harmon. Anal.*, vol. 35, no. 1, pp. 74–93, 2013.
- [17] Y. Li, A. Cichocki, S.-I. Amari, S. Xie, and C. Guan, "Equivalence probability and sparsity of two sparse solutions in sparse representation," *IEEE Trans. Neural Netw.*, vol. 19, no. 12, pp. 2009–2021, 2008.
- [18] K. J. Friston, A. P. Holmes, K. J. Worsley, J.-P. Poline, C. D. Frith, and R. S. J. Frackowiak, "Statistical parametric maps in functional imaging: A general linear approach," *Hum. Brain Mapp.*, vol. 2, no. 4, pp. 189–210, 1994.
- [19] D. Hu, L. Yan, Y. Liu, Z. Zhou, K. J. Friston, C. Tan, and D. Wu, "Unified SPM-ICA for fMRI analysis," *Neuroimage*, vol. 25, no. 3, pp. 746–755, 2005.
- [20] S. A. Harrison and F. Tong, "Decoding reveals the contents of visual working memory in early visual areas," *Nature*, vol. 458, no. 7238, pp. 632–635, 2009.
- [21] Y. Li, J. Long, B. Huang, T. Yu, W. Wu, Y. Liu, C. Liang, and P. Sun, "Cross-modal integration enhances neural representation of task-relevant features in audiovisual face perception," *Cerebral Cortex*, 2013. [Online]. Available: <http://cercor.oxfordjournals.org/content/early/2013/08/26/cercor.bht228.abstract>
- [22] G. Ganesh, E. Burdet, M. Haruno, and M. Kawato, "Sparse linear regression for reconstructing muscle activity from human cortical fMRI," *Neuroimage*, vol. 42, no. 4, pp. 1463–1472, 2008.
- [23] Y. Li, J. Long, L. He, H. Lu, Z. Gu, and P. Sun, "A sparse representation-based algorithm for pattern localization in brain imaging data analysis," *PLoS ONE*, vol. 7, no. 12, p. e50332, 2012.
- [24] B. He, L. Yang, C. Wilke, and H. Yuan, "Electrophysiological imaging of brain activity and connectivity - challenges and opportunities," *IEEE Trans. Biomed. Eng.*, vol. 58, no. 7, pp. 1918–1931, 2011.
- [25] X. Bai, V. L. Towle, E. J. He, and B. He, "Evaluation of cortical current density imaging methods using intracranial electrocorticograms and functional MRI," *Neuroimage*, vol. 35, no. 2, pp. 598–608, 2007.
- [26] C. Grova, J. Daunizeau, J.-M. Lina, C. G. B. E. nar, H. Benali, and J. Gotman, "Evaluation of EEG localization methods using realistic simulations of interictal spikes," *Neuroimage*, vol. 29, no. 3, pp. 734–753, 2006.
- [27] B. Blankertz, R. Tomioka, S. Lemm, M. Kawanabe, and K.-R. Müller, "Optimizing spatial filters for robust EEG single-trial analysis," *IEEE Signal Process. Mag.*, vol. 25, no. 1, pp. 41–56, 2008.
- [28] M. Arvaneh, C. Guan, K. K. Ang, and C. Quek, "Optimizing the channel selection and classification accuracy in EEG-based BCI," *IEEE Trans. Biomed. Eng.*, vol. 58, no. 6, pp. 1865–1873, 2011.
- [29] K. Oweiss and M. Aghagolzadeh, "Detection and classification of extracellular action potential recordings," in *Statistical Signal Processing for Neuroscience and Neurotechnology*, (Statistical Signal Processing for Neuroscience and Neurotechnology), K. G. Oweiss, Ed. Amsterdam, The Netherlands: Elsevier, 2010.
- [30] A. Gramfort, M. Kowalski, and M. Hämläinen, "Mixed-norm estimates for the M/EEG inverse problem using accelerated gradient methods," *Phys. Med. Biol.*, vol. 57, no. 7, pp. 1937–1961, 2012.
- [31] M. Lustig, D. Donoho, and J. M. Pauly, "Sparse MRI: The application of compressed sensing for rapid MR imaging," *Magn. Reson. Med.*, vol. 58, no. 6, pp. 1182–1195, 2007.

[Emmanuel Vincent, Nancy Bertin, Rémi Gribonval, and Frédéric Bimbot]

From Blind to Guided Audio Source Separation

[How models and side information can improve the separation of sound]

Audio is a domain where signal separation has long been considered as a fascinating objective, potentially offering a wide range of new possibilities and experiences in professional and personal contexts, by better taking advantage of audio material and finely analyzing complex acoustic scenes. It has thus always been a major area for research in signal separation and an exciting challenge for industrial applications.

Starting with blind separation of toy mixtures in the mid-1990s, research has progressed to real-world scenarios today, with applications to speech enhancement and recognition, music editing, three-dimensional sound rendering, and audio information retrieval, among others. This has mostly been made possible by the development of increasingly informed separation techniques incorporating knowledge about the sources and/or the mixtures at hand. For instance, speech source separation for remote conferencing can benefit from prior knowledge of the room geometry and/or the names of the speakers, while music remastering will exploit instrument characteristics and knowledge of sound engineers' mixing habits.

After a brief historical account, we provide an overview of recent and ongoing research in this field, illustrating a variety of

models and techniques designed so as to guide the audio source separation process toward efficient and robust solutions.

AUDIO SOURCE SEPARATION: BASIC CONCEPTS

Initially, audio source separation was formulated as a standard source separation problem, i.e., as a linear system identification and inversion problem. In the following, we assume that the sources do not move, and we denote the number of sources and microphones by J and I , respectively, which are assumed to be known.

We adopt the following notation: scalars are represented by plain letters, vectors by bold lowercase letters, and matrices by bold uppercase letters. The mixture signal $\mathbf{x}(t) = [x_1(t), \dots, x_I(t)]^T$ observed at time t when recording the source signals $\mathbf{s}(t) = [s_1(t), \dots, s_J(t)]^T$ can be modeled by the convolution process

$$\mathbf{x}(t) = (\mathbf{A} * \mathbf{s})(t), \quad (1)$$

where $\mathbf{A}(t) = [\mathbf{a}_1(t), \dots, \mathbf{a}_J(t)]$ is the matrix of room impulse responses or mixing filters associated with sound propagation from each source to each microphone, T denotes matrix transposition, and $*$ is the convolution operator, i.e., $x_i(t) = \sum_{\tau=0}^J a_{ij}(\tau) s_j(t - \tau)$.

SPATIAL IMAGES AND TIME-FREQUENCY PROCESSING

It soon became clear that this formulation had intrinsic limitations, especially with respect to audio specificities. First, the



Source Separation and Applications

IMAGE LICENSED BY
INGRAM PUBLISHING

Digital Object Identifier 10.1109/MSP.2013.2297440

Date of publication: 7 April 2014

modeling of the system as impulse responses between each source location and each microphone location implicitly assumes that each source emits sound from a single point in space, preventing the modeling of spatially diffuse sources [1]. Second, unless extra information is available, the sources may be recovered at best up to indetermined permutation and filtering. Third, the linear system $A(t)$ may be inverted only in determined scenarios involving fewer sources than the number of microphones ($J \leq I$).

In 1998, Cardoso [2] proposed to reformulate the mixing process as

$$\mathbf{x}(t) = \sum_{j=1}^J \mathbf{c}_j(t) \quad (2)$$

so that source separation became the problem of extracting the contribution $\mathbf{c}_j(t) = [c_{j1}(t), \dots, c_{ji}(t)]^T$ of each source to the mixture. The quantity $\mathbf{c}_j(t)$ was later called the *spatial source image* of the j th source [3]. This reformulation circumvented the filtering indeterminacy by joining $\mathbf{a}_j(t)$ and $s_j(t)$ into a single quantity

$$\mathbf{c}_j(t) = (\mathbf{a}_j * s_j)(t) \quad (3)$$

and the general model (2) became applicable to spatially diffuse sources, which cannot be expressed as (3).

At the same time, several researchers proposed switching to the time-frequency domain by means of the complex-valued short-time Fourier transform (STFT). By rewriting the mixing process in each time frame n and each frequency bin f as

$$\mathbf{x}(n, f) = \sum_{j=1}^J \mathbf{c}_j(n, f), \quad (4)$$

source separation was recast as a problem akin to clustering, whereby sound in a given time-frequency bin must be allocated to the one or few active sources in that bin, and separation became achievable in underdetermined scenarios with more sources than microphones ($J > I$) [4]. In the following, \mathbf{x} , \mathbf{s} , \mathbf{A} , \mathbf{c}_j , \mathbf{s}_j , and \mathbf{a}_j refer to time-domain variables when used with the time index t and to their time-frequency domain counterparts when used with the frame and frequency bin indices n and f .

While early source separation techniques relied on spatial diversity, i.e., the assumption that the sources have different directions of arrival, the move to time-frequency domain processing enabled the exploitation of spectral diversity, i.e., the assumption that their short-term spectra follow distinct distributions. This made it possible to handle single-channel mixtures and mixtures of sources sharing the same direction of arrival, such as vocals and drums which are often both mixed to the center in pop music.

LEVELS OF GUIDANCE

Over the past few years, successive breakthroughs have resulted from the development of audio source separation techniques

OVER THE PAST FEW YEARS, SUCCESSIVE BREAKTHROUGHS HAVE RESULTED FROM THE DEVELOPMENT OF AUDIO SOURCE SEPARATION TECHNIQUES INCREASINGLY SUITED TO THE PROPERTIES OF AUDIO SOURCES AND TO THE SPECIFICITIES OF THE ACOUSTIC MIXING CONDITIONS.

increasingly suited to the properties of audio sources and to the specificities of the acoustic mixing conditions: more and more sophisticated models and algorithms have been developed to incorporate available side information (or to estimate it on the fly) about the sources and the mixing environment so as to guide the separation process. Today, some of the most advanced source separation systems integrate a fair number

of spatial and spectral models into a single framework [5], [6]. Figure 1 visually summarizes this evolution.

According to conventional terminology, blind source separation does not exploit any information about the sources nor about the mixing process. Its application domain is essentially restricted to dealing with determined instantaneous mixtures, which practically never arise in audio.

Conversely, various terms such as *semiblind* or *informed* have been used to characterize separation techniques based on some level of informedness. For instance, the use of the adjective *informed* is restricted to separation techniques relying on highly precise side information coded and transmitted along with the audio, e.g., the mixing filters and the short-term power spectra of the sources, which can be seen as a form of audio coding and is not covered hereafter (see [7] for a review). As these terms happen to be used either quite specifically or rather inconsistently, we will use the term *guided source separation* in this article.

In that sense, algorithms employing information about the general behavior of audio sources and/or of the acoustic mixing process in general, e.g., “the sources are sparsely distributed” or “the mixture was recorded outdoors,” can be described as *weakly guided*. By contrast, algorithms taking advantage of specific information about the mixture to be separated, e.g., the source positions, the names of the speakers or the musical score, may be coined as *strongly guided*.

MODELING PARADIGMS

Before we focus on specific types of guidance, let us introduce the common foundations of blind and guided algorithms. It was proved early on that separation is unfeasible if more than one source has a stationary white Gaussian distribution [8]. Separation hence relies on two alternative modeling paradigms: non-Gaussianity or nonstationarity, where nonstationarity may manifest itself over time, over frequency, or over both [8]. These two paradigms are essentially interchangeable: choosing one of them does not restrict the type of information that may be included as guidance or the practical scenarios that can be considered.

SPARSE NONGAUSSIAN MODELING

In the time-frequency domain, the convolutive mixing model (3) may be approximated under a narrowband assumption by complex-valued multiplication in each frequency bin

$$c_j(n, f) = a_j(f)s_j(n, f), \tag{5}$$

where the Fourier transform $a_j(f)$ of $a_j(t)$ is the so-called mixing vector for the j th source or, in matrix form, $x(n, f) = A(f)s(n, f)$, where $A(f) = [a_1(f), \dots, a_J(f)]$ is the so-called mixing matrix.

Assuming that the source STFT coefficients have a stationary non-Gaussian distribution $P(\cdot)$, separation may be achieved in the maximum likelihood (ML) sense as [9]

$$\begin{aligned} \min_{A, s} \sum_{j, n, f} -\log P(s_j(n, f)) \\ \text{subject to } x(n, f) = A(f)s(n, f). \end{aligned} \tag{6}$$

In the absence of specific information over A or s , minimization is typically achieved under a scaling constraint to avoid divergence of A and s to infinitely large or small values. A similar objective may be derived from a deterministic inverse problem perspective [9]

$$\min_{A, s} \frac{1}{2} \sum_{n, f} \|x(n, f) - A(f)s(n, f)\|_2^2 + \lambda \sum_{n, f} \mathcal{P}(s(n, f)), \tag{7}$$

where $\mathcal{P}(\cdot)$ (in calligraphic font) is a penalty term. The choice of the tradeoff parameter λ is not a trivial task. When the constraint $x(n, f) = A(f)s(n, f)$ holds, the minimum of $\sum_{n, f} \mathcal{P}(s(n, f))$ subject to this constraint is obtained in the limit when $\lambda \rightarrow 0$.

For typical STFT window lengths on the order of 50–100 ms [4], the STFT coefficients of audio signals exhibit a sparse

distribution, with a sharp peak at zero and heavy tails compared to a Gaussian. The generalized Gaussian distribution $P(s_j(n, f)) \propto \exp(-\lambda |s_j(n, f)|^p)$ and the associated ℓ_p sparsity inducing norm $\mathcal{P}(s(n, f)) = \|s(n, f)\|_p^p = \sum_{j=1}^J |s_j(n, f)|^p$ with $0 < p < 2$ are popular choices to model this behavior [9], [10].

In the determined case, the objective (6) has been shown to maximize the statistical independence of the sources, hence the name *independent component analysis* (ICA). In the underdetermined case, both objectives are called *sparse component analysis* (SCA), and they are typically addressed by first estimating $A(f)$ and then deriving $s(n, f)$ using greedy algorithms such as matching pursuit, convex optimization algorithms such as iterative soft thresholding, or nonconvex optimization algorithms depending on the chosen distribution $P(\cdot)$ or penalty $\mathcal{P}(\cdot)$.

If the sources are sufficiently sparse, there is a good chance that each time-frequency bin is dominated by a single source, i.e., $x(n, f) \approx a_j(f)s_j(n, f)$ for one source j . This leads to approximate SCA as a clustering problem. The mixing vectors $a_j(f)$ are first estimated by clustering the observations $x(n, f)$ and the sources $s(n, f)$ are derived by grouping the time-frequency bins dominated by the same source, an operation known as *time-frequency masking*. For a more detailed introduction to ICA and SCA, see [11].

SEPARATION HENCE RELIES ON TWO ALTERNATIVE MODELING PARADIGMS: NON-GAUSSIANITY OR NONSTATIONARITY, WHERE NONSTATIONARITY MAY MANIFEST ITSELF OVER TIME, OVER FREQUENCY, OR OVER BOTH.

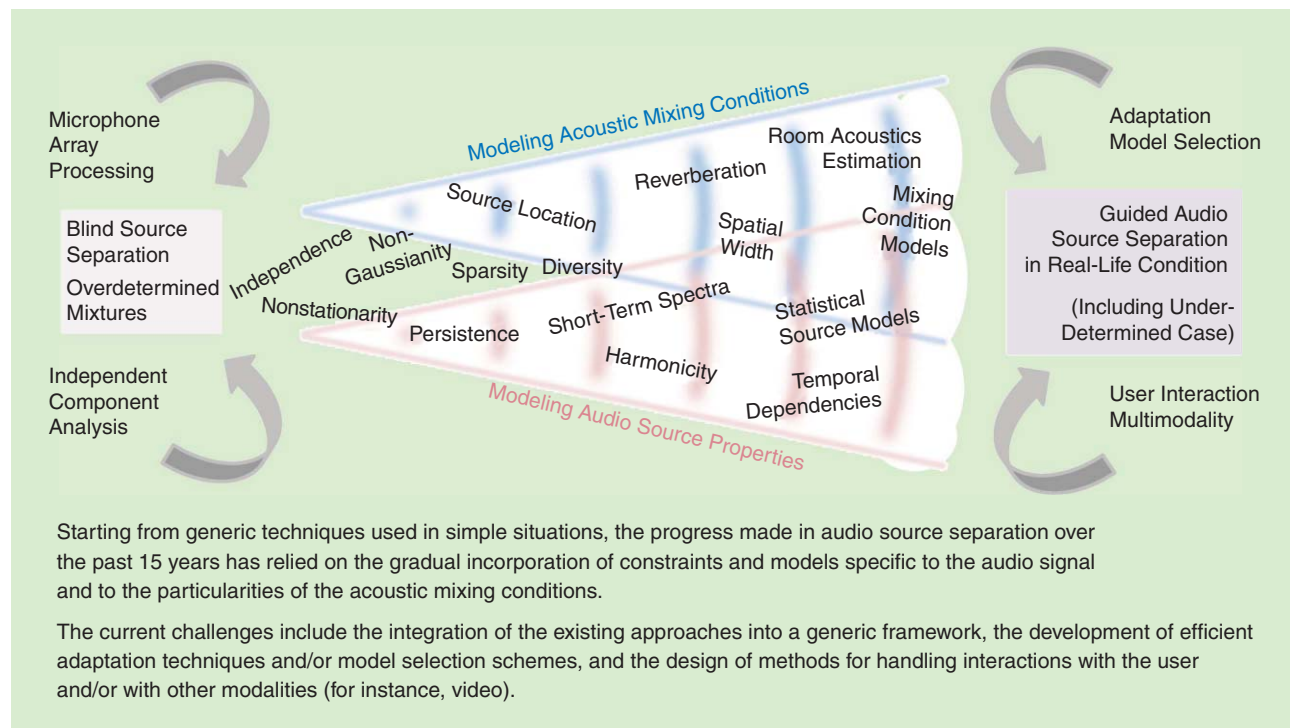


[FIG1] Audio source separation: a general overview of the evolution in the field.

Starting from generic techniques used in simple situations, the progress made in audio source separation over the past 15 years has relied on the gradual incorporation of constraints and models specific to the audio signal and to the particularities of the acoustic mixing conditions.

The current challenges include the integration of the existing approaches into a generic framework, the development of efficient adaptation techniques and/or model selection schemes, and the design of methods for handling interactions with the user and/or with other modalities (for instance, video).

GAUSSIAN NONSTATIONARY MODELING

An alternative paradigm is to assume that the vectors of STFT coefficients of the source spatial images have a zero-mean non-stationary Gaussian distribution

$$P(\mathbf{c}_j(n, f) | \Sigma_{\mathbf{c}_j}(n, f)) = \frac{1}{\det(\pi \Sigma_{\mathbf{c}_j}(n, f))} e^{-\mathbf{c}_j(n, f)^H \Sigma_{\mathbf{c}_j}^{-1}(n, f) \mathbf{c}_j(n, f)}, \quad (8)$$

where H denotes conjugate transposition. The covariance $\Sigma_{\mathbf{c}_j}(n, f)$ depends on time and frequency. It can be factored into the product of a scalar spectrotemporal power $v_j(n, f)$ and a spatial covariance matrix $\mathbf{R}_j(f)$ [1]

$$\Sigma_{\mathbf{c}_j}(n, f) = v_j(n, f) \mathbf{R}_j(f). \quad (9)$$

Separation is typically achieved by estimating the model parameters in the ML sense

$$\min_{\mathbf{R}, v} \sum_{j,n,f} -\log P(\mathbf{c}_j(n, f) | \mathbf{R}, v) \text{ subject to } \mathbf{x}(n, f) = \sum_{j=1}^J \mathbf{c}_j(n, f) \quad (10)$$

using an expectation-maximization (EM) algorithm. Once \mathbf{R} and v have been estimated, $\mathbf{c}_j(n, f)$ can be derived in the minimum mean square error (MMSE) sense by multichannel Wiener filtering

$$\hat{\mathbf{c}}_j(n, f) = \Sigma_{\mathbf{c}_j}(n, f) \left(\sum_{j=1}^J \Sigma_{\mathbf{c}_j}(n, f) \right)^{-1} \mathbf{x}(n, f). \quad (11)$$

For more detailed presentation of this paradigm, see [1].

INTRODUCING INFORMATION ABOUT THE MODEL PARAMETERS

Equations (6), (7), and (10) form the basis for all guided algorithms presented hereafter. Without any further information about \mathbf{A} , \mathbf{s} , \mathbf{R} , or v , the spatial source images $\mathbf{c}_j(n, f)$ may be recovered at best up to arbitrary permutation in each frequency bin f . This so-called permutation problem was historically the first reason to investigate the incorporation of more information

GUIDING SEPARATION DOES NOT ONLY ADDRESS THIS PROBLEM BUT ALSO IMPROVES THE ACCURACY OF THE PARAMETER ESTIMATES, WHICH IN TURN IMPROVES SEPARATION.

into the models. However, guiding separation does not only address this problem but also improves the accuracy of the parameter estimates, which in turn improves separation.

Information may be introduced either in the form of deterministic constraints over \mathbf{A} , \mathbf{s} , \mathbf{R} , or v , which restrict the values that these parameters may take, or in the form of penalty functions or probabilistic priors, which are added to the objective functions in (6), (7), and (10) and used to estimate \mathbf{A} , \mathbf{s} , \mathbf{R} , and v in the maximum a posteriori (MAP) sense. These constraints, penalties, and priors involve their own parameters, which we call *hyperparameters*. The key difference between weakly guided and strongly guided separation is that the values

of the hyperparameters must be estimated from the mixture in the former case, while they are fixed using expert knowledge or training in the latter case.

MODELING AND EXPLOITING SPATIAL INFORMATION

One way to introduce information in audio source separation is to account for the fact that the mixing vectors $\mathbf{a}_j(f)$ and the spatial covariance matrices $\mathbf{R}_j(f)$ are not independent across frequency, but that they are linked by the spatial properties of the source and the recording room. We review a number of increasingly complex properties that may be used in this context, from the spatial location of the source to the full acoustics of the room. Each presented model embeds the information carried by the previous model plus some new information.

SPATIAL LOCATION

In the free field, the mixing vectors $\mathbf{a}_j(f)$ would be collinear with

$$\mathbf{d}_j(f) = \left[\frac{1}{r_{1j}} e^{-2i\pi f r_{1j}/c}, \dots, \frac{1}{r_{ij}} e^{-2i\pi f r_{ij}/c} \right]^T \quad (12)$$

that is the steering vector modeling the sound attenuation and delay from the source to the microphones, with c the sound velocity and r_{ij} the distance from the j th source to the i th microphone. In practical recording conditions, $\mathbf{a}_j(f)$ deviates from

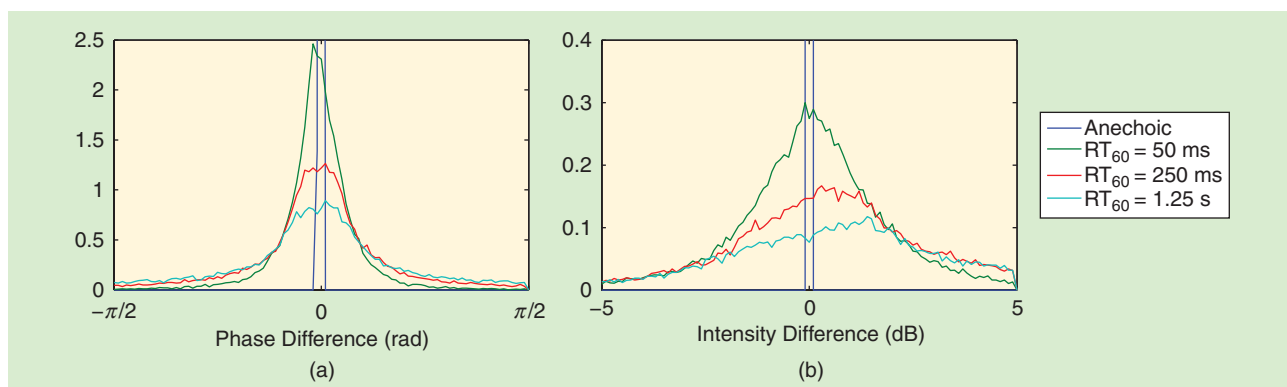


[FIG2] An example distribution over the whole frequency range of the phase and intensity differences between $\mathbf{a}_j(f)$ and $\mathbf{d}_j(f)$ as a function of RT_{60} for two microphones spaced 20-cm apart recording a source at 1-m distance at a sampling frequency of 8 kHz.

$d_j(f)$ due to reflections on the boundaries of the room, which include early echoes and dense late echoes known as *reverberation*. Figure 2 shows the amount of deviation as a function of the reverberation time RT_{60} , i.e., the time taken by late echoes to decay by 60 dB.

Parra and Alvino [12] were the first to exploit the proximity of $a_j(f)$ to $d_j(f)$ by defining a penalty term $\mathcal{P}(A(f))$ over the mixing matrix. Many other penalties and priors were then suggested, including Euclidean distances and Gaussian priors on the inter-channel phase and intensity differences by Yilmaz et al. [4] and Mandel et al. [13]. One of the simplest is the squared Euclidean distance between $a_j(f)$ and $d_j(f)$

$$\mathcal{P}(a_j(f)) = \|a_j(f) - d_j(f)\|_2^2. \quad (13)$$

Sawada et al. [14] showed that minimizing (13) with respect to r_{ij} is equivalent to source localization via the generalized cross-correlation (GCC) technique. This led to a joint iterative approach to source localization and separation where the source signals and the source locations are alternately updated.

SPATIAL WIDTH

Duong et al. [1] later observed that the narrowband approximation (5) is invalid for reverberated and/or spatially diffuse sources: the sound emitted by each source reaches the microphones from many directions at once at each frequency instead of a single apparent direction $a_j(f)$, so that the channels of $c_j(n, f)$ are partly uncorrelated. The spread of the distribution of incoming directions governs the perceived spatial width of the source at that frequency. They introduced the concept of full-rank spatial covariance matrices $\mathbf{R}_j(f)$ which, in comparison with the rank-1 spatial covariance matrices $\mathbf{R}_j(f) = a_j(f)a_j^H(f)$ resulting from (5), account not only for the spatial location of the sources but also for their width.

Assuming that the distances from the sources to the microphones are known but that their absolute location in the room is unknown, the mean of $\mathbf{R}_j(f)$ over these unknown absolute locations is approximately equal to [15]

$$\mu_{\mathbf{R}_j}(f) = d_j(f)d_j^H(f) + \sigma_{\text{ech}}^2 \mathbf{\Omega}(f). \quad (14)$$

The first term accounts for direct sound, as modeled by the steering vector $d_j(f)$ in (12), and the second term for echoes and reverberation, as modeled by the power of echoes and reverberation σ_{ech}^2 and by the covariance matrix of an isotropic sound field $\mathbf{\Omega}(f)$. For omnidirectional microphones, the entries of $\mathbf{\Omega}(f)$ are given by the sinc function

$$\Omega_{ii'}(f) = \frac{\sin(2\pi f d_{ii'}/c)}{2\pi f d_{ii'}/c} \quad (15)$$

with $d_{ii'}$ the distance between microphones i and i' . Theoretical expressions are also available for σ_{ech}^2 depending on the room dimensions and reflection coefficients. Duong et al. [15] exploited this fact to estimate $\mathbf{R}_j(f)$ in the MAP sense under an inverse-Wishart prior $P(\mathbf{R}_j(f))$.

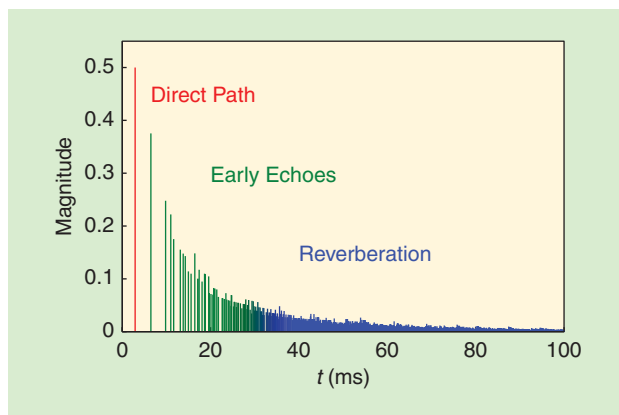


[FIG3] A schematic illustration of the magnitude of a room impulse response between a source and a microphone for a reverberation time $RT_{60} = 250$ ms.

EARLY ECHOES AND REVERBERATION

Although the full-rank model (9) improved upon the narrowband model (5), it remains an approximation of the true mixing process (3). Figure 3 illustrates the shape of a room impulse response $a_{ij}(t)$ over time. In typical reverberation conditions, these responses are several hundred milliseconds long, so that they extend over several time frames. This prompted authors to generalize (9) in the single-channel case as the convolution of $v_j(n, f)$ and a nonnegative exponentially decaying filter $q_j(l, f)$ representing the power of $a_j(t)$ for a delay of l time frames [16]. This model has been used for single-source dereverberation given knowledge of RT_{60} and it is making its way into source separation.

Going one step further, Kowalski et al. [17] argued for a move back to time-domain modeling of the mixing filters, while still exploiting the sparsity of the sources in the time-frequency domain. This was achieved by replacing the narrowband loss term in (7) by the exact wideband loss term

$$\min_{\mathbf{A}, \mathbf{s}} \frac{1}{2} \sum_t \|x(t) - (\mathbf{A} * \mathbf{s})(t)\|_2^2 + \lambda \sum_{n,f} \mathcal{P}(s(n, f)) \quad (16)$$

and by deriving an iterative soft thresholding algorithm that effectively alternates between the time domain and the time-frequency domain at each iteration, assuming that $\mathcal{P}(s(n, f))$ is a convex penalty.

This study was the starting point for subsequent studies aiming to define penalties over the mixing filters in the time domain. Benefiting from the fact that early echoes are sparsely distributed over time, as can be seen from Figure 3, Benichoux et al. [18] exploited an ℓ_p penalty over the filters

$$\mathcal{P}(a_j) = \sum_{i,t} |a_{ij}(t)|^p \quad (17)$$

with $0 < p \leq 2$. The exponential decaying shape of reverberation was later included by time-dependent rescaling of (17). The key difference with previous models is that the deviations of $a_j(f)$ from $d_j(f)$ are not modeled as random anymore, but they must result in sparse early echoes.

FULL ROOM ACOUSTICS

Lately, in a major departure from conventional audio source separation, a number of researchers proposed to stop modeling the room impulse responses between individual sources and microphones but to learn them between all possible pairs of points in the room instead, under the constraint that the source separation system is always to be used in that room. The rationale is that room impulse responses span a manifold (said differently, a small movement in the room results in a small deviation of the impulse response), so that measuring impulse responses for a few points may suffice to predict them for other points. This accounts for all possibly available spatial information, including the direct path, the delays and amplitudes of early echoes, and the shape of reverberation. Asaei et al. [19] consider each point in the room as a source and constrain most sources to be inactive by means of a group sparsity penalty (see below). More recently, Deleforge et al. [20] attempted to learn a smaller-dimensional representation of the manifold by probabilistic local linear embedding. The latter approach achieved impressive source separation results given thousands of room impulse response measurements, and its extension to practical setups with a smaller number of measurements constitutes a great avenue for research.

MODELING AND EXPLOITING SPECTROTEMPORAL INFORMATION

Besides spatial information, the source spectra and their evolution across time are the second main supply of information for audio source separation. We review increasingly complex properties of $s_j(n, f)$ and $v_j(n, f)$ that may be used to guide separation, from local persistence to long-term dependencies.

TIME-FREQUENCY PERSISTENCE

In audio signals, significant STFT coefficients are not randomly distributed in the time-frequency plane but they tend to cluster together. This is illustrated in Figure 4, where vertical and horizontal lines appear, corresponding to transient and tonal parts of

BESIDES SPATIAL INFORMATION, THE SOURCE SPECTRA AND THEIR EVOLUTION ACROSS TIME ARE THE SECOND MAIN SUPPLY OF INFORMATION FOR AUDIO SOURCE SEPARATION.

musical notes, respectively. Similar and more complex structures can be found in speech.

This persistence over time or frequency can be promoted by the use of group sparsity or other structured sparsity penalties on $s_j(n, f)$ [21]. For instance, the $\ell_{1,2}$ norm

$$\mathcal{P}(s_j) = \sum_n \sqrt{\sum_f |s_j(n, f)|^2} \quad (18)$$

imposes sparsity over time but no constraint over frequency. An alternative technique is to set a hidden Markov model (HMM) prior on sequences of STFT coefficients. Févotte et al. [22] showed that the latter approach outperforms unstructured priors in a denoising task.

SHORT-TERM SPECTRA

Beyond frequency persistence, sound sources are characterized by their short-term spectra, i.e., the dependencies between $v_j(n, f)$ over the whole frequency range f . A popular approach is to represent the source short-term spectra $v_j(n, f)$ as the sum of nonnegative basis spectra $w_{jk}(f)$, scaled by nonnegative time-varying activation coefficients $h_{jk}(n)$ [23], [24]

$$v_j(n, f) = \sum_{k=1}^K w_{jk}(f) h_{jk}(n). \quad (19)$$

This model has been indifferently applied to magnitude spectra or to power spectra in the single-channel case, however only the latter easily generalizes to the multichannel case. Each basis spectrum may represent, e.g., part of a speech phoneme or a musical note, as illustrated in Figure 5(a). Due to its equivalent matrix form $\mathbf{V}_j = \mathbf{W}_j \mathbf{H}_j$, this model is better known as *nonnegative matrix factorization* (NMF). Considering the fact that only one speech phoneme or few musical notes may be active at once, sparsity was enforced by reducing the sum to a single component k [25] or by adding penalties such as the ℓ_1 norm $\mathcal{P}(\mathbf{H}_j) = \sum_{k,n} |h_{jk}(n)|$ [23]. Group sparsity penalties and priors were also introduced to favor simultaneous activity of basis spectra associated with the same phoneme or note, or to select the correct speaker or instrument among a collection of basis spectra trained on different speakers or instruments [26].

FINE SPECTRAL STRUCTURE AND SPECTRAL ENVELOPE

Several extensions were brought to NMF to further constrain the basis spectra. A first idea is to decompose the basis spectra themselves by NMF as the sum of narrowband spectral patterns $b_{jkm}(f)$ weighted by spectral envelope coefficients e_{jkm} :

$$w_{jk}(f) = \sum_{m=1}^{M_k} b_{jkm}(f) e_{jkm}. \quad (20)$$

The narrowband spectra may be fixed so as to enforce harmonicity (i.e., spectral peaks at integer multiples of a given fundamental frequency) or smoothness, which are common structures to many sound sources, and to adapt the spectral envelope coefficients to

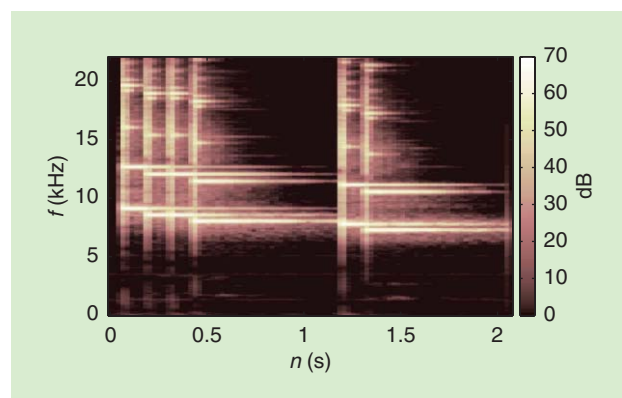


[FIG4] A spectrogram of a xylophone melody.

the mixture, which are specific to each source. These structures are suitable for sustained and transient musical sounds, as shown in Figure 5(b).

Another refinement complying with the physical production of many natural sounds is to decompose the source short-term spectra via the excitation-filter model

$$v_j(n, f) = v_j^{\text{ex}}(n, f)v_j^{\text{ft}}(n, f), \quad (21)$$

where $v_j^{\text{ex}}(n, f)$ and $v_j^{\text{ft}}(n, f)$ represent the excitation signal (e.g., the glottal source) and the response of the filter (e.g., the vocal tract) and they are modeled by NMF [27]. This constraint enforces similar spectra for different fundamental frequencies, in a similar way as the shift-invariance constraint in [28], i.e., the constraint that all basis spectra are spectrally translated versions of a single spectrum.

Ozerov et al. [5] recently proposed a comprehensive multilevel NMF framework integrating (19)–(21) by multiplication of up to eight matrices, each of them capable of embodying specific knowledge or constraints in a flexible way. All these extensions can be compactly formalized as nonnegative tensor factorization (NTF), an extension of NMF to multidimensional arrays.

TEMPORAL EVOLUTION

The aforementioned models do not directly model the temporal evolution of the spectra. At a short time scale, Virtanen [23] enforced the continuity of NMF activation coefficients by adding the penalty $\mathcal{P}(\mathbf{H}_j) = \sum_n |h_{jk}(n+1) - h_{jk}(n)|^2$ while Ozerov et al. [5] modeled them in a similar fashion as (20) as the product of time-localized patterns and sparse temporal envelopes, as depicted in Figure 5(c). Continuous or HMM priors on $h_{jk}(n)$ were also used to this end.

At a medium time scale, Smaragdīs [29] generalized (19) into the convolutive NMF model

$$v_j(n, f) = \sum_{k=1}^K \sum_l w_{jk}(l, f) h_{jk}(n-l), \quad (22)$$

where the basis elements $w_{jk}(l, f)$ are now spectrotemporal patches rather than single-frame spectra, thus explicitly encoding the temporal evolution of sound events at each frequency. Musicological models and spoken language models were also exploited to favor certain note and chord progressions or certain sequences of words using longer-term HMM priors on $h_{jk}(n)$. Mysore and

Sahani [26] provided an efficient algorithm to separate multiple sources, each modeled by an HMM.

In another major departure from conventional audio source separation, several researchers recently proposed to exploit the information encoded by redundancy and repetitive patterns at very long time scales, so as to optimize the use of

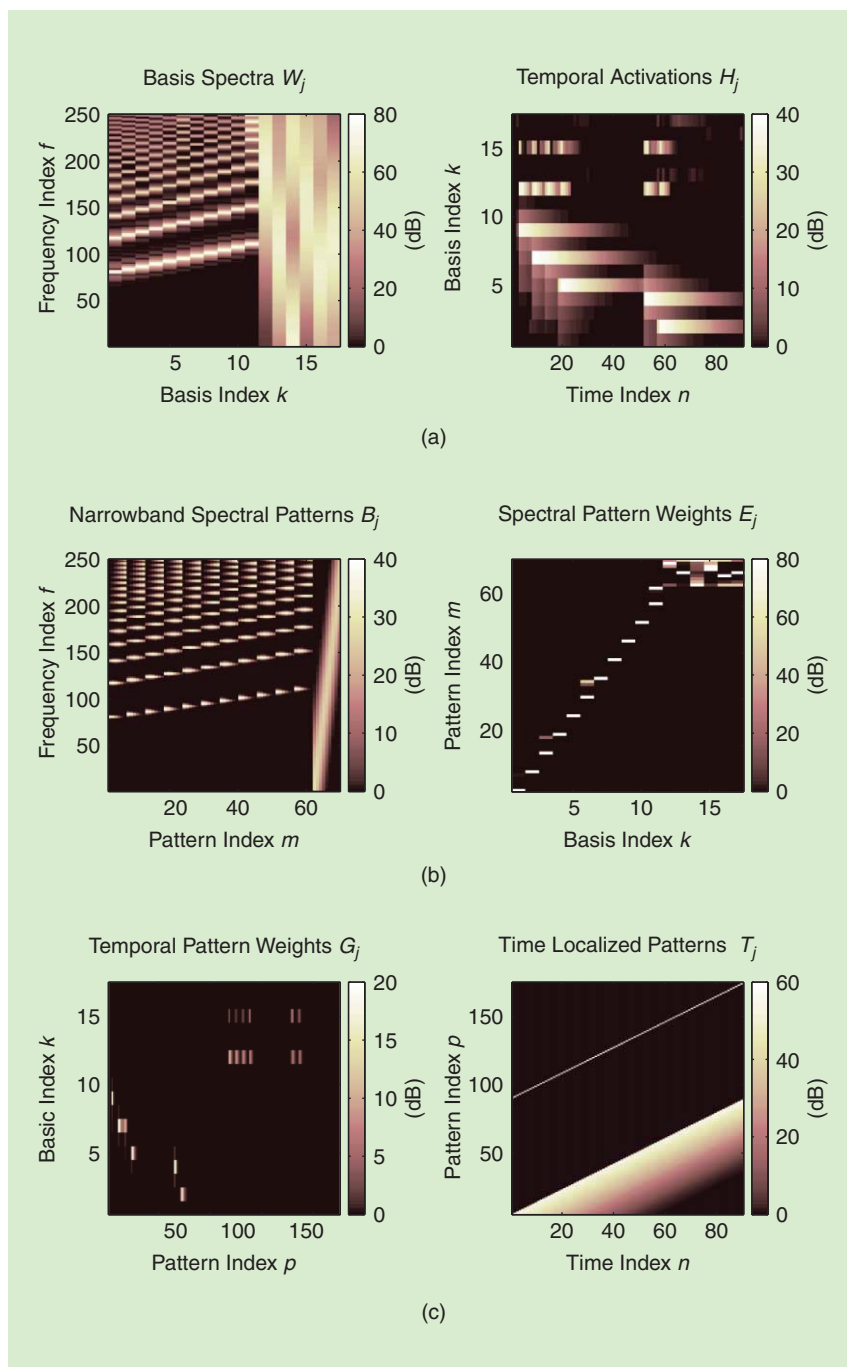


[FIG5] The multilevel NMF decomposition of the spectrogram in Figure 4. (a) The decomposition as the product of basis spectra W_j and temporal activations H_j . (b) The second-level decomposition of W_j as the product of harmonic and noisy narrowband spectral patterns B_j and associated spectral envelopes E_j . (c) The second-level decomposition of H_j as the product of time-localized patterns T_j activated at some time weights G_j .

available information over the whole signal duration. Robust principal component analysis (RPCA), which decomposes an input spectrogram as the sum of a low-rank matrix and a sparse matrix, was used by Huang et al. [30] to separate (sparse) drum and melody sources from a (low-rank) repetitive tonal accompaniment. The search for repeating patterns in music was also exploited by Rafii et al. [31] through the identification of repeating segments (of up to a duration of 40 s), their modeling, and their extraction via time-frequency masking. In the future, such ideas may be applied to automatic learning of fine-grained models from larger and larger amounts of audio data eventually covering the sounds arising in the mixture to be separated.

IMPACT AND PERSPECTIVES

Over the past 15 years, audio source separation has recorded constant progress and today it has reached a level of maturity that enables its integration in real-life application contexts. For instance, multichannel NMF and NTF have improved performance by 3–4 dB signal-to-distortion ratio (SDR) compared to SCA in certain scenarios, and they have made it possible to separate real-world music recordings using weakly guided models for typical instruments (vocals, drums, bass) and for the remaining instruments [3]. Joint spatial and spectral modeling [5], [6] and convolutive NMF have contributed to the reduction of the keyword error rate for small-vocabulary automatic speech recognition (ASR) from 44% down to as little as 8% in a strongly guided real-world domestic scenario involving knowledge of the speaker and his/her spatial position [32]. Finally, weakly guided separation of percussive and harmonic content in music has helped several music information retrieval (MIR) tasks, reducing, e.g., the relative error rate for chord recognition by 28% [33].

These and other results show that improved separation performance in many scenarios can be obtained by modeling and exploiting spatial and spectral properties of sounds, i.e., by designing models and constraints which account for the specificities of audio sources and acoustic mixing conditions. Two trends can be seen: developing complex, hierarchical models with little training so as to adapt to unknown situations with little amounts of data, or training simpler models on huge amounts of data, e.g., thousands of room impulse responses and dozens of hours of speech, so as to benefit from the power of big data and turn parameter estimation into a model selection problem.

In either case, the design of clever, computationally efficient convex relaxations and nonconvex optimization algorithms has given increasing attention to handle the optimization of all model parameters and hyperparameters at once and to escape extra local optima that may hinder the benefit of such models. In certain scenarios, some hyperparameters can be set using expert knowledge

or training on separate data, and only the remaining hyperparameters need to be estimated from the mixture.

With few exceptions [5], [6], most separation systems currently exploit only a limited set of constraints, penalties, or priors. Research is ongoing on the improvement of the above models, as well as on the incorporation of side-information that has little been exploited so far, e.g., visual information about the source movements. Ultimately, the integration of

the variety of developed models and schemes into a complete, fully versatile system constitutes a challenge in itself.

AUTHORS

Emmanuel Vincent (emmanuel.vincent@inria.fr) is a research scientist with Inria (Nancy, France). He received the Ph.D. degree in music signal processing from the Institut de Recherche et Coordination Acoustique/Musique (Paris, France) in 2004 and worked as a research assistant with the Centre for Digital Music at Queen Mary, University of London (United Kingdom), from 2004 to 2006. His research focuses on probabilistic machine learning for speech and audio signal processing, with application to real-world audio source localization and separation, noise-robust speech recognition, and music information retrieval. He is a founder of the series of Signal Separation Evaluation Campaigns and CHiME Speech Separation and Recognition Challenges. He is an associate editor for *IEEE Transactions on Audio, Speech, and Language Processing*. He is a Senior Member of the IEEE.

Nancy Bertin (nancy.bertin@irisa.fr) received the state engineering degree from the École Nationale Supérieure des Télécommunications (ENST), Paris, France, in 2004, the M.S. degree in acoustics, computer science, and signal processing applied to music from the Université Pierre et Marie Curie, Paris, in 2005, and the Ph.D. degree in signal processing from Télécom ParisTech, ENST, in 2009. She joined the French National Center for Scientific Research (CNRS) as a permanent researcher in 2010 and is now part of the Parsimony and New Algorithms for Audio and Signal Modeling Group (IRISA/Inria), where her research focuses on audio source separation and compressed sensing of acoustic fields, with a particular methodological emphasis on sparse and cosparsity representations. She is a Member of the IEEE.

Rémi Gribonval (remi.gribonval@inria.fr) is a senior researcher with Inria (Rennes, France), and the scientific leader of the Parsimony and New Algorithms for Audio and Signal Modeling Group on sparse audio processing. A former student at École Normale Supérieure (Paris, France), he received the Ph.D. degree in applied mathematics from the Université de Paris-IX Dauphine (Paris, France) in 1999, and his habilitation à diriger des recherches in applied mathematics from the Université de Rennes I (Rennes, France) in 2007. His research focuses on mathematical signal processing, machine learning, and

approximation theory and statistics, with an emphasis on sparse approximation, audio source separation, and compressed sensing. He founded SPARS, the series of international workshops on signal processing with adaptive/sparse representations. In 2011, he received the Blaise Pascal Award in applied mathematics and the Scientific Engineering Award from SMAI by the French National Academy of Sciences, and a starting investigator grant from the European Research Council. He is a Fellow of the IEEE.

Frédéric Bimbot (frederic.bimbot@irisa.fr) graduated as a telecommunication engineer from ENST, Paris, France, in 1985, received the B.A. degree in linguistics from Sorbonne Nouvelle University, Paris III, and the Ph.D. degree in signal processing (speech synthesis using temporal decomposition) from ENST in 1988. In 1990, he joined CNRS as a permanent researcher, worked with ENST for seven years, and then moved to IRISA (CNRS and Inria), Rennes, France. He is now a senior researcher with CNRS. His research is focused on speech and audio analysis, speaker recognition, music content modeling, and audio source separation. He is in charge of the coordination of the D5 Department (digital signals and images, robotics) at IRISA.

REFERENCES

- [1] N. Q. K. Duong, E. Vincent, and R. Gribonval, "Under-determined reverberant audio source separation using a full-rank spatial covariance model," *IEEE Trans. Audio, Speech, Lang. Processing*, vol. 18, no. 7, pp. 1830–1840, 2010.
- [2] J.-F. Cardoso, "Multidimensional independent component analysis," in *Proc. IEEE Int. Conf. Acoustics, Speech, Signal Processing*, 1998, vol. 4, pp. 1941–1944.
- [3] E. Vincent, S. Araki, F. J. Theis, G. Nolte, P. Bofill, H. Sawada, A. Ozerov, B. V. Gowreesunker, D. Lutter, and N. Q. K. Duong, "The signal separation evaluation campaign (2007–2010): Achievements and remaining challenges," *Signal Process.*, vol. 92, no. 8, pp. 1928–1936, 2012.
- [4] Ö. Yilmaz and S. T. Rickard, "Blind separation of speech mixtures via time-frequency masking," *IEEE Trans. Signal Processing*, vol. 52, no. 7, pp. 1830–1847, 2004.
- [5] A. Ozerov, E. Vincent, and F. Bimbot, "A general flexible framework for the handling of prior information in audio source separation," *IEEE Trans. Audio, Speech, Lang. Processing*, vol. 20, no. 4, pp. 1118–1133, 2012.
- [6] M. Souden, S. Araki, K. Kinoshita, T. Nakatani, and H. Sawada, "A multichannel MMSE-based framework for speech source separation and noise reduction," *IEEE Trans. Audio, Speech, Lang. Processing*, vol. 21, no. 9, pp. 1913–1928, 2013.
- [7] A. Liutkus, S. Gorlow, N. Sturmel, S. Zhang, L. Girin, R. Badeau, L. Daudet, S. Marchand, and G. Richard, "Informed source separation: A comparative study," in *Proc. 20th European Signal Processing Conf.*, 2012, pp. 2397–2401.
- [8] J.-F. Cardoso, "The three easy routes to independent component analysis; contrasts and geometry," in *Proc. 3rd Int. Conf. Independent Component Analysis and Blind Signal Separation*, 2001, pp. 1–6.
- [9] R. Gribonval and M. Zibulevsky, "Sparse component analysis," in *Handbook of Blind Source Separation, Independent Component Analysis and Applications*. New York: Academic Press, 2010, pp. 367–420.
- [10] E. Vincent, "Complex nonconvex lp norm minimization for underdetermined source separation," in *Proc. 7th Int. Conf. Independent Component Analysis and Signal Separation*, 2007, pp. 430–437.
- [11] P. Comon and C. Jutten, Eds., *Handbook of Blind Source Separation, Independent Component Analysis and Applications*. New York: Academic Press, 2010.
- [12] L. C. Parra and C. V. Alvino, "Geometric source separation: merging convolutive source separation with geometric beamforming," *IEEE Trans. Speech Audio Processing*, vol. 10, no. 6, pp. 352–362, 2002.
- [13] M. I. Mandel, R. J. Weiss, and D. P. W. Ellis, "Model-based expectation maximization source separation and localization," *IEEE Trans. Audio, Speech, Lang. Processing*, vol. 18, no. 2, pp. 382–394, 2010.
- [14] H. Sawada, S. Araki, R. Mukai, and S. Makino, "Grouping separated frequency components by estimating propagation model parameters in frequency-domain blind source separation," *IEEE Trans. Audio, Speech, Lang. Processing*, vol. 15, no. 5, pp. 1592–1604, 2007.
- [15] N. Q. K. Duong, E. Vincent, and R. Gribonval, "Spatial location priors for Gaussian model based reverberant audio source separation," *EURASIP J. Adv. Signal Process.*, vol. 2013, pp. 149, 2013.
- [16] E. A. P. Habets, S. Gannot, and I. Cohen, "Late reverberant spectral variance estimation based on a statistical model," *IEEE Signal Process. Lett.*, vol. 16, no. 9, pp. 770–773, 2009.
- [17] M. Kowalski, E. Vincent, and R. Gribonval, "Beyond the narrowband approximation: Wideband convex methods for under-determined reverberant audio source separation," *IEEE Trans. Audio, Speech, Lang. Processing*, vol. 18, no. 7, pp. 1818–1829, 2010.
- [18] A. Benichou, P. Sudhakar, F. Bimbot, and R. Gribonval, "Well-posedness of the permutation problem in sparse filter estimation with l^p minimization," *Appl. Computat. Harm. Anal.*, vol. 35, no. 3, pp. 394–406, 2013.
- [19] A. Asaei, M. E. Davies, H. Boulard, and V. Cevher, "Computational methods for structured sparse component analysis of convolutive speech mixtures," in *Proc. IEEE Int. Conf. Acoustics, Speech, Signal Processing*, 2012, pp. 2425–2428.
- [20] A. Deleforge, F. Forbes, and R. Horaud, "Variational EM for binaural sound-source separation and localization," in *Proc. IEEE Int. Conf. Acoustics, Speech, Signal Processing*, 2013, pp. 76–80.
- [21] M. Kowalski and B. Torrèsani, "Sparsity and persistence: mixed norms provide simple signal models with dependent coefficients," *Signal, Image, Video Process.*, vol. 3, no. 3, pp. 251–264, 2009.
- [22] C. Févotte, L. Daudet, S. J. Godsill, and B. Torrèsani, "Sparse regression with structured priors: application to audio denoising," in *Proc. IEEE Int. Conf. Acoustics, Speech, Signal Processing*, 2006, vol. 3, pp. 57–60.
- [23] T. Virtanen, "Monaural sound source separation by nonnegative matrix factorization with temporal continuity and sparseness criteria," *IEEE Trans. Audio, Speech, Lang. Processing*, vol. 15, no. 3, pp. 1066–1074, 2007.
- [24] A. Ozerov and C. Févotte, "Multichannel nonnegative matrix factorization in convolutive mixtures for audio source separation," *IEEE Trans. Audio, Speech, Lang. Processing*, vol. 18, no. 3, pp. 550–563, 2010.
- [25] L. Benaroya, F. Bimbot, and R. Gribonval, "Audio source separation with a single sensor," *IEEE Trans. Audio, Speech, Lang. Processing*, vol. 14, no. 1, pp. 191–199, 2006.
- [26] G. Mysore and M. Sahani, "Variational inference in non-negative factorial hidden Markov models for efficient audio source separation," in *Proc. 29th Int. Conf. Machine Learning*, 2012, pp. 1887–1894.
- [27] J.-L. Durrieu, G. Richard, B. David, and C. Févotte, "Source/filter model for unsupervised main melody extraction from polyphonic audio signals," *IEEE Trans. Audio, Speech, Lang. Processing*, vol. 18, no. 3, pp. 564–575, 2010.
- [28] D. FitzGerald, M. Cranitch, and E. Coyle, "Extended nonnegative tensor factorisation models for musical sound source separation," *Comput. Intell. Neurosci.*, vol. 2008, Article ID 872425, May 2008.
- [29] P. Smaragdis, "Convolutive speech bases and their application to supervised speech separation," *IEEE Trans. Audio, Speech, Lang. Processing*, vol. 15, no. 1, pp. 1–12, 2007.
- [30] P. S. Huang, S. D. Chen, P. Smaragdis, and M. Hasegawa-Johnson, "Singing-voice separation from monaural recordings using robust principal component analysis," in *Proc. IEEE Int. Conf. Acoustics, Speech, Signal Processing*, 2012, pp. 57–60.
- [31] Z. Rafii and B. Pardo, "Repeating pattern extraction technique (REPET): A simple method for music/voice separation," *IEEE Trans. Audio, Speech, Lang. Processing*, vol. 21, no. 1, pp. 73–84, 2013.
- [32] J. Barker, E. Vincent, N. Ma, H. Christensen, and P. Green, "The PASCAL CHiME speech separation and recognition challenge," *Comput. Speech Lang.*, vol. 27, no. 3, pp. 621–633, 2013.
- [33] N. Ono, K. Miyamoto, H. Kameoka, J. Le Roux, Y. Uchiyama, E. Tsunoo, T. Nishimoto, and S. Sagayama, "Harmonic and percussive sound separation and its application to MIR-related tasks," in *Advances in Music Information Retrieval*. New York: Springer, 2010.



[Sebastian Ewert, Bryan Pardo, Meinard Müller, and Mark D. Plumbley]

Score-Informed Source Separation for Musical Audio Recordings

[An overview]

In recent years, source separation has been a central research topic in music signal processing, with applications in stereo-to-surround up-mixing, remixing tools for disc jockeys or producers, instrument-wise equalizing, karaoke systems, and preprocessing in music analysis tasks. Musical sound sources, however, are often strongly correlated in time and frequency, and without additional knowledge about the sources, a decomposition of a musical recording is often infeasible. To simplify this complex task, various methods have recently been proposed that exploit the availability of a musical score. The additional instrumentation and note information provided by the score guides the separation process, leading to significant improvements in terms of separation quality and robustness. A major challenge in utilizing this rich source of information is to bridge the gap between high-level musical events specified by the score and their corresponding acoustic realizations in an audio recording. In this article, we review recent developments in score-informed source separation and discuss various strategies for integrating the prior knowledge encoded by the score.

INTRODUCTION

In general, audio source separation methods often rely on assumptions, such as the availability of multiple channels (recorded using

several microphones) or the statistical independence of the source signals, to identify and segregate individual signal components. In music, however, such assumptions are not applicable in many cases. For example, musical sound sources often outnumber the information channels, such as a string quartet recorded in two-channel stereo. Also, sound sources in music are typically highly correlated in time and frequency: instruments follow the same rhythmic patterns and play notes that are harmonically related. Purely statistical methods such as independent component analysis (ICA) or nonnegative matrix factorization (NMF) therefore often fail to completely recover individual sound objects from music mixtures [1].

High-quality source separation for general music remains an open problem. One approach is to exploit known spectrotemporal properties of the sources to facilitate the segregation [1], [2]. For example,

in a time-frequency representation, percussive instruments typically exhibit structures in the frequency direction (short bursts of broadband energy) while harmonic instruments usually lead to structures in the time direction (slowly changing harmonics). Many instruments, however, emit similar energy patterns, and thus they are hard to distinguish based on spectrotemporal characteristics alone. To overcome these problems, various approaches presented in recent years exploit (user-generated) annotations of a recording as additional prior knowledge. For example, to simplify the separation process, one can specify the fundamental frequency of instruments [3], manually assign



Source Separation and Applications

IMAGE LICENSED BY
INGRAM PUBLISHING

Digital Object Identifier 10.1109/MSP.2013.2296076

Date of publication: 7 April 2014

harmonics in a spectrogram to a specific source [4], or provide timing information for instruments [5], [6]. However, while such annotations typically lead to a significant increase in separation performance, their creation can be a laborious task.

In this article, we focus on a natural and particularly valuable source of prior knowledge that exists for many pieces: a musical score. The score contains information about the instruments and notes of the musical piece and can be used to guide and simplify the separation process even if the sources are hard to distinguish based on their spectrotemporal behavior. In particular, information about pitch and timing of note events can be used to locate and isolate corresponding sound events in the audio mixture (Figure 1). For example, note events for a guitar, clarinet, and piano [Figure 1(a)] can be used to direct the extraction of corresponding instrument sounds from a given recording [Figure 1(c)]. Knowledge about the instrumentation can also aid in selecting appropriate source models or training data. For example, the spectrotemporal characteristics of the clarinet [the orange graph in Figure 1(c)] are different from those of the piano and should be modeled accordingly.

The score also gives an intuitive and user-friendly representation for musically experienced users to specify the target sources to be separated. For example, by partitioning the score into groups of note events, one can easily specify that the main melody should be separated from the accompaniment or that all

string instruments should be separated from the wind instruments. This concept led to novel ideas and application scenarios in the context of instrument-wise equalization [8], personal music remixing [9], music information retrieval [10], and intelligent audio editing [7]. Figure 2 gives an example where a user can easily specify the desired audio manipulation within the score simply by editing some of the notes. These manipulations are then automatically transferred to a given audio recording using score-informed audio parametrization techniques [7] (see the demonstration Web site with videos at <http://www.audiolabs-erlangen.de/resources/2013-ACMMM-AudioDe-comp/> for more information). Additionally, applications such as singing voice removal for karaoke [11] or parametric coding of audio objects [12] can significantly benefit from the increase in separation robustness resulting from the integration of score.

While integrating score information bears the potential for a significant gain in separation quality, dealing with real data remains a major issue. In particular, score-informed separation methods often have only been tested on recordings synthesized from the score, such that many practical issues are not reflected in the test data. Some of these issues can be observed on the following demo Web sites, which provide listening examples using nonsynthetic data: <http://www.mpi-inf.mpg.de/resources/MIR/ICASSP2012-ScoreInformedNMF/> [14], <http://www.ece.rochester.edu/~zduan/jtstp2011/examples.html>

A MAJOR CHALLENGE IN UTILIZING THIS RICH SOURCE OF INFORMATION IS TO BRIDGE THE GAP BETWEEN HIGH-LEVEL MUSICAL EVENTS SPECIFIED BY THE SCORE AND THEIR CORRESPONDING ACOUSTIC REALIZATIONS IN AN AUDIO RECORDING.

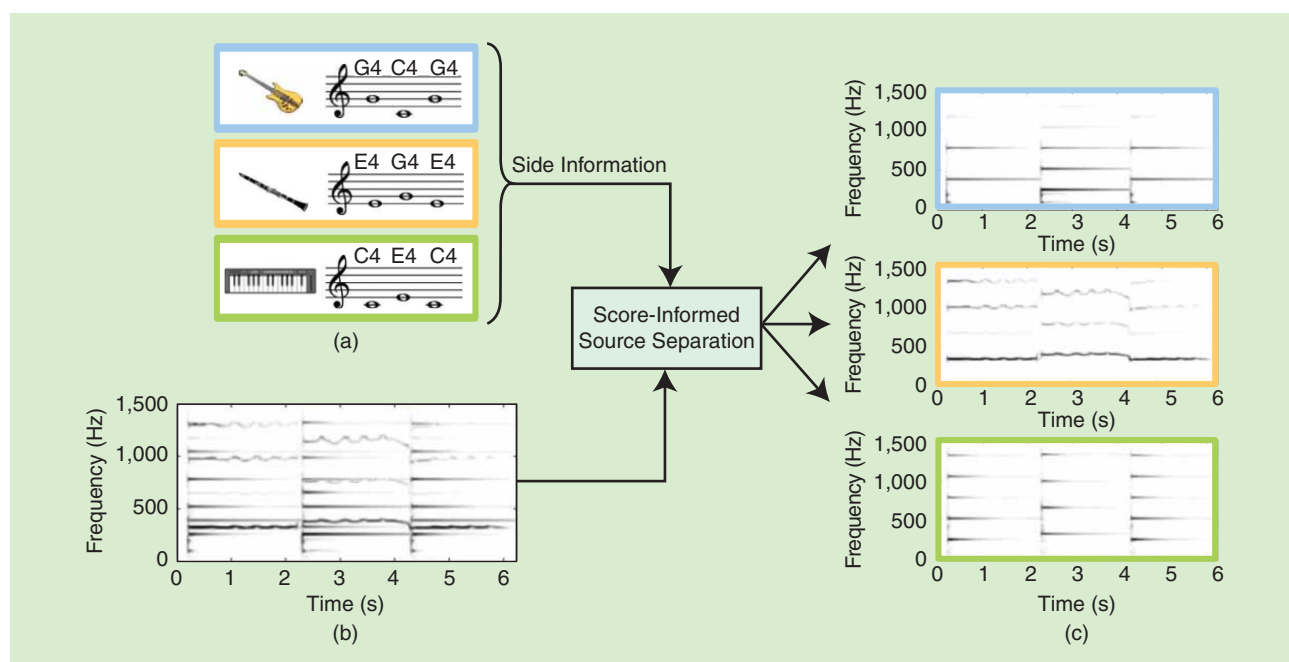


[FIG1] Score-informed source separation: instrument lines as specified by (a) a musical score are employed as prior knowledge for the decomposition of (b) a mixture audio recording into (c) individual instrument sounds. The mixture consists of a guitar (blue), clarinet (orange), and piano (green).

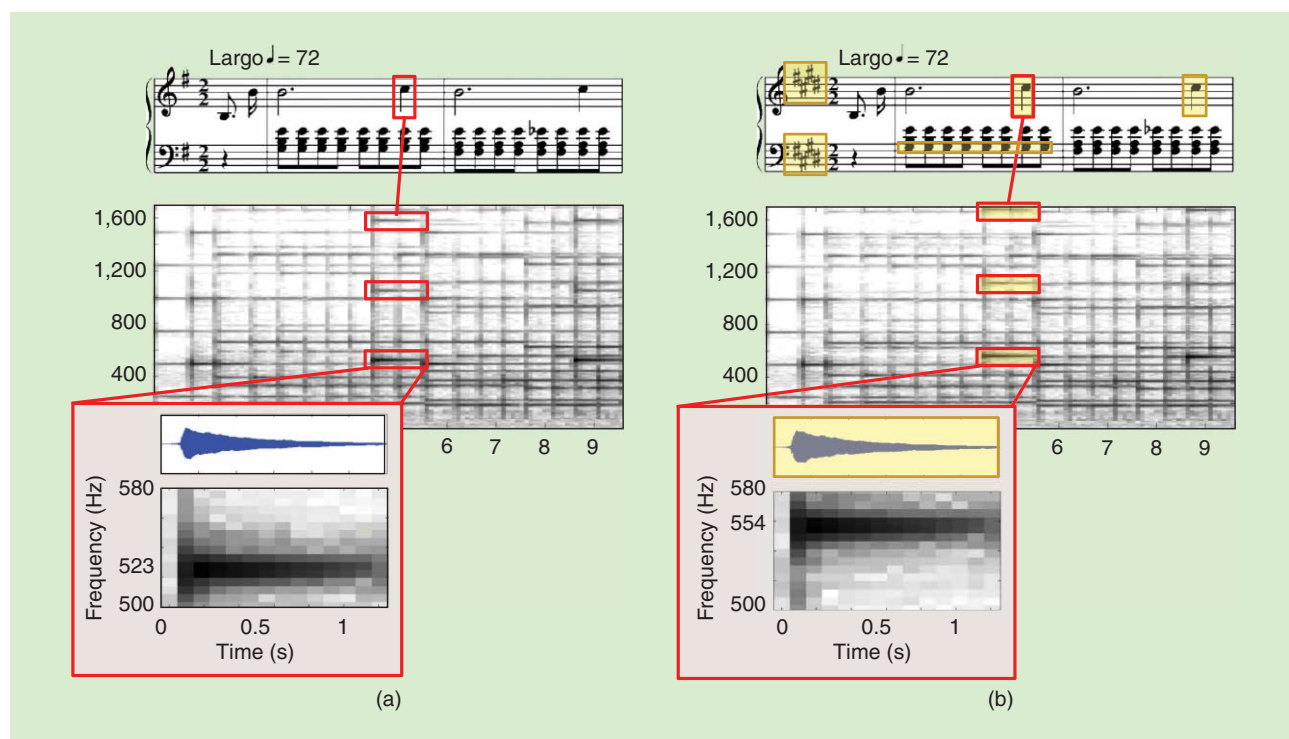


[FIG2] The score-informed audio editing (see [7]). (a) For each note in the score, the corresponding sound is extracted from a recording of Chopin's op. 28, no. 4. (b) By applying pitch-shifting techniques to the individual notes, the piece is changed from minor to major.

[13], and <http://www.eecs.qmul.ac.uk/~jga/eusipco2012.html> [15]. In a real-world scenario, a score specifies relative positions for note events on a musical time and pitch grid using an abstract, high-level language with a lot of leeway for interpretation by a performer. The score specifies neither exact frequencies nor the precise timing and duration of the musical tones. Also, the timbre and the loudness are only specified in terms of coarse instructions such as *forte* meaning *loud*. Additionally, a musician may deviate from the score by adding extra notes (ornaments and grace notes), or there may be playing errors or even structural differences such as skipped sections. Further, while full scores are freely available for many classical pieces as a result of substantial digitization efforts (for example, the International Music Score Library Project, which can be found at <http://imslp.org>), there are often only so-called lead sheets available for pop music, which only specify parts of the score including the melody, lyrics, and harmony. Altogether, such issues and uncertainties lead to significant challenges in score-informed source separation, which current approaches have just started to address.

USING NMF FOR SOURCE SEPARATION

Among the various methods for blind source separation, NMF has been one of the most successful [16]. The method is easy to implement, computationally efficient, and has been successfully applied to various problem areas, ranging from computer vision to text mining and audio processing. Let us see how NMF-based techniques can be used for audio source separation, and how they behave when applied to music.

CLASSIC NMF

Let $Y \in \mathbb{R}_+^{M \times N}$ denote the magnitude spectrogram of a music recording, where $M \in \mathbb{N}$ and $N \in \mathbb{N}$ denote the number of frequency bins and number of time frames, respectively. Given a parameter $K \in \mathbb{N}$, NMF derives two nonnegative matrices $W \in \mathbb{R}_+^{M \times K}$ and $H \in \mathbb{R}_+^{K \times N}$ such that $WH \approx Y$, or more precisely, such that a distance function between Y and WH is minimized. This distance is often a modified Kullback–Leibler divergence [16]. To compute a factorization, the matrices W and H are first initialized with random values and then iteratively updated using multiplicative update rules [16]. After the update process, each column of W (also referred to as *template vector*) corresponds to the prototype spectrum of a certain sound component (e.g., a C4 note played on a piano), and the corresponding row of H (also called *activation*) encodes when that sound was active and its volume. When using NMF to separate musical sound sources, we assume that each pair of template vector and activation describes a sound that was produced by a single instrument, and that this instrument can easily be identified, to allow all the sounds from that instrument to be grouped together.

However, there are various issues with this approach. Consider Figure 3(a) showing a spectrogram of a music recording of a piano and a guitar. The piano plays the notes C4, E4, and C4 and, at the same time, the guitar plays the notes G4, C4, and G4 (see also “Reading a Musical Score”). Figure 3(b) shows an NMF-based decomposition of the spectrogram, with the parameter K manually set to four allowing for one template for each of the two

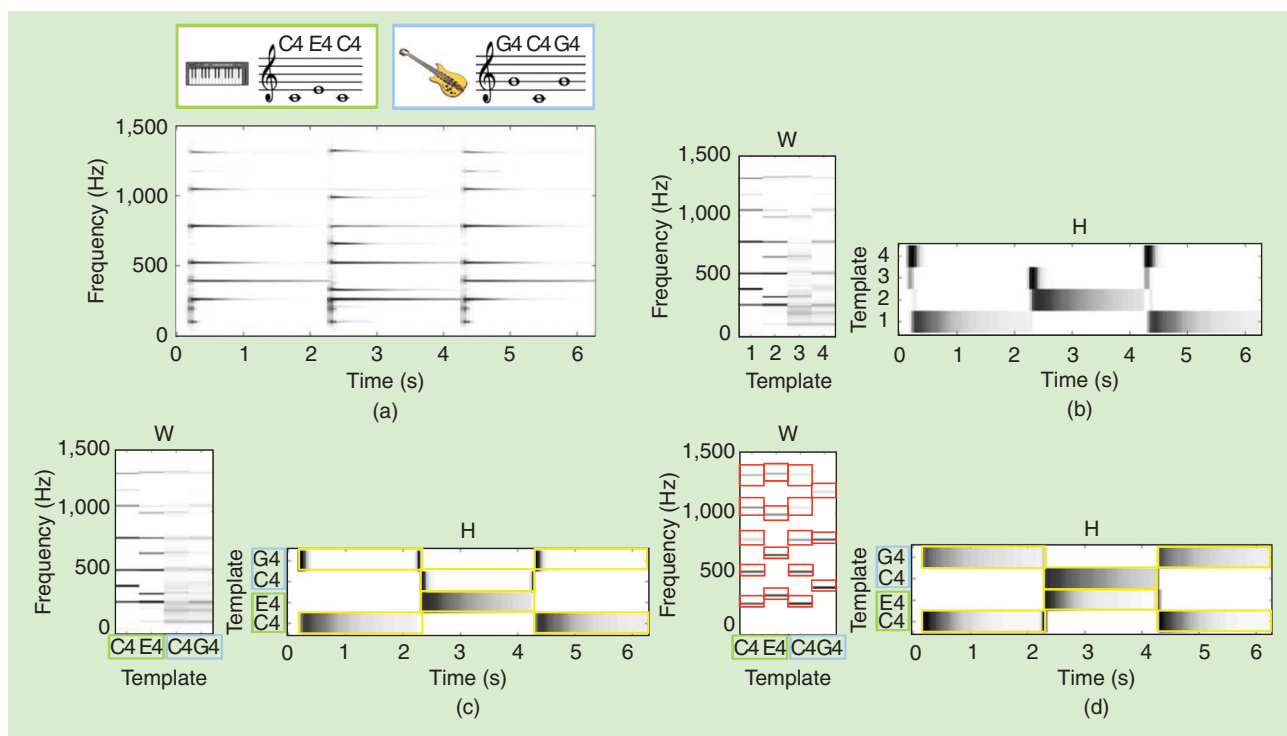


[FIG3] Integrating score information into NMF. (a) A spectrogram of a recording of a piano and a guitar. (b) Factorization into a template matrix W and an activation matrix H resulting from standard NMF. (c) The factorization result after applying constraints to W and H . (d) The factorization result after applying constraints to W and H . The red/yellow boxes indicate areas that were initialized with nonzero values.

different musical pitches used by the two instruments. Looking at the template matrix W and the activation matrix H , some problems become apparent. It is not clear to which sound, pitch, or instrument a given template vector corresponds. Furthermore, the activation patterns in H indicate that the templates correspond to mixtures of notes (and instruments). The first two templates seem to represent the note combinations piano-C4/guitar-G4 and piano-E4/guitar-C4, while the last two templates seem to correspond to short-lived broadband sounds that occur at the beginning of these notes. Based on such a factorization, the two instruments cannot readily be separated.

SCORE-INFORMED CONSTRAINTS

To overcome these issues, most NMF-based musical source separation methods impose certain constraints on W and H . A typical approach is to enforce a harmonic structure in each template in W , and temporal continuity in each activation in H [1], [17]. Further, if the instruments occurring in a recording are known, one can use monophonic training material to learn meaningful templates [17]. While such extensions typically lead to a significant gain in separation quality over classic NMF, they do not fully solve the problem.

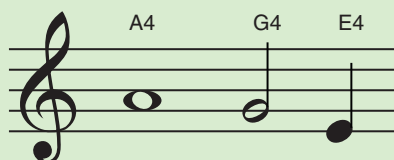
Therefore, if strong prior knowledge is available, it should be exploited to further increase the separation performance. In this context, a musical score is particularly valuable. On a coarse level, we can extract global information from the score, such as which instruments are playing or which and how many pitches occur

over the course of a piece of music. In our example, this information can be used to set the number of templates automatically to $K = 4$ (two instruments each with two different pitches). We can also assign an instrument and pitch attribute to each template [Figure 3(c)]. On a finer level, one may also exploit local information on when notes are actually played. Suppose we could assume that a score prealigned to a corresponding audio recording is available, i.e., that the note events specified by the score are aligned to the time positions where they occur in the audio recording. Using this score information, one can impose constraints on the times that certain templates may become active by initializing those activation entries with zero, where a certain instrument and pitch are known to be inactive. Once an entry in W or H is initialized to zero, it will remain set to zero during the subsequent multiplicative update steps [16]. As an example, consider Figure 3(c), where all entries in H outside the yellow rectangles were initialized with zero values.

In some cases, such an approach will be sufficient to separate many of the notes. However, in our example, the resulting factorization is almost identical to the unconstrained one; compare Figure 3(b) and (c). Since the piano-C4/guitar-G4 and piano-E4/guitar-C4 combinations always occur together, the constraints on the time activations H have no significant effect, and the first two templates still represent these note combinations. Indeed, individual sounds in music recordings often only occur in certain combinations, which limits also for real recordings the benefits of applying constraints on H alone.

READING A MUSICAL SCORE

Modern music notation uses an abstract language to specify musical parameters. Pitch is indicated by the vertical placement of a note on a staff, which consists of five horizontal lines. Each musical pitch is associated with a name, such as A4 (corresponding to the note between the second and the third line from the bottom in Figure S1), and a standard frequency in Hz (440 Hz for the A4). If the standard frequency of a pitch is twice as high compared to another, they are said to differ by an octave. In this case,



[FIGS1] An example of a simple score consisting of three notes.

To overcome this problem, we can apply dual-constraints, where both templates and activations are constrained in parallel [6], [14]. The idea to constrain the templates W is based on the observation that most instruments written in a score produce harmonic sounds and that the templates should reflect this structure. In general, a harmonic sound is one whose energy in a time-frequency representation is concentrated around integer multiples of the so-called fundamental frequency. These energy concentrations are also referred to as *harmonics*. To enforce such a structure in the templates, we can constrain the spectral energy between harmonics to be zero [18]. More precisely, after assigning an instrument and musical pitch to each template vector using the score information, we can use the standard frequency associated with each pitch as an estimate of the fundamental frequency (see “Reading a Musical Score”), and the rough positions for the harmonics can then be derived. As the exact frequencies are not known, a neighborhood around these positions can then be initialized with nonzero values in the templates, while setting the remaining entries to zero; see [14] and [18] for details. Figure 3(d) shows the resulting factorization, with the nonzero neighborhoods around the harmonics indicated by red rectangles in W . All four template vectors in W have now a clearly defined harmonic structure and most disturbing interferences from other sounds have been eliminated, such that the two instruments can finally be separated based on this factorization. Listening examples using full-length piano recordings and publicly available score-data can be found at <http://www.mpi-inf.mpg.de/resources/MIR/ICASSP2012-ScoreInformedNMF/>.

ALIGNING AUDIO AND SCORE DATA

In the previous section, we assumed that we had a temporal alignment between the score’s note events and the physical time position where they actually occur in a given audio recording. While musical scores are available for many songs, they are rarely aligned to a given recording, and aligning them manually is very laborious. To automate this process, there are various methods for

the two pitches share the same letter in their name, also referred to as *chroma*, and only differ in their number (e.g., A3 with 220 Hz is one octave below the A4). In most Western music, a system referred to as *equal temperament* is used that introduces 12 different chromas by the names C, C#, D, ..., B, which subdivide each octave equidistantly on a logarithmic frequency scale. A special symbol at the beginning of a staff, the clef, is used to specify which line corresponds to which pitch (e.g., the first symbol in Figure S1 specifies that the second line from the bottom corresponds to G4). Temporal information is specified in a score using different shapes for the note, which encode the relative duration of a note. For example, a whole note or semibreve (denoted by the symbol \ominus) is played twice as long as a half note or minim (\bullet), which again is played twice as long as a quarter note or crotchet (\blacktriangledown). Additional information on music notation can be found at http://en.wikipedia.org/wiki/Musical_notation.

computing a temporal alignment between score and audio representations, a task also referred to as *score-audio synchronization*.

Rather than giving strict specifications, a score is rather a guide for performing a piece of music, leaving scope for different interpretations (see “Reading a Musical Score”). Reading the instructions in the score, a musician shapes the music by varying the tempo, dynamics, and articulation, thus creating a personal interpretation of the piece. The goal of score-audio synchronization is to automatically match the musical timing as notated in the score to the physical timing used in audio recordings. Automatic methods typically proceed in two steps: feature extraction from both audio and score, followed by temporal alignment [19].

The feature representations should be robust to irrelevant variations yet should capture characteristic information that suffice to accomplish the subsequent synchronization task. Chroma-based music features have turned out to be particularly useful [20]. Capturing the short-time energy distribution of a music representation across the 12 pitch classes (see “Reading a Musical Score”), chroma features closely correlate to the harmonic progression while showing a large degree of robustness to variations in timbre and dynamics. Thanks to this property, chroma features allow for a comparison of score and audio data, where most acoustic properties in the audio that are not reflected in the score are ignored. Figure 4 illustrates chroma feature sequences derived from (a) score data and (b) audio data.

In the second step, the derived feature sequences are brought into temporal correspondence, using an alignment technique such as dynamic time warping (DTW) or hidden Markov models (HMMs) [19]. Intuitively, as indicated by the red bidirectional arrows shown in Figure 4, the alignment can be thought of a structure, which links corresponding positions in the score and the audio and thus annotates the audio recording with available score data.

Various extensions to this basic scheme have been proposed. For example, additional onset cues extracted from the audio can be used to significantly improve on the temporal accuracy

of the alignment [21], [22]. Other approaches address the problem of computing an alignment in real time while the audio is recorded [19], [23]. Furthermore, methods have been proposed for computing an alignment in the presence of structural variations between the score and the audio version, such as the omission of repetitions, the insertion of additional parts (soli, cadenzas), or differences in the number of stanzas [24]. Such advanced score-audio synchronization methods are an active area of current research [21], [23].

DEALING WITH VIBRATO AND FREQUENCY DRIFT

While the approach outlined in the section “Using NMF for Source Separation” yields good results in many cases, it relies on the assumption that the fundamental frequency associated with a musical pitch is approximately constant over time, since the frequency position of harmonics in each template is fixed and cannot move up or down. While this assumption is valid for some instruments such as a piano, it is not true in general. Figure 5 shows an audio recording of a piano and a clarinet. The piano (green) indeed exhibits stable horizontal frequency trajectories, whereas the clarinet produces strong frequency modulations due to the way it is played (“vibrato”). These are clearly visible, for example, between seconds 3 and 4 in a spectral band around 1,200 Hz. Additionally, the clarinet player continuously glides from one note to the next, resulting in smooth transitions between the fundamental frequencies of notes (e.g., between second 4 and 5). As a result, while a single note in the score is associated with a single musical pitch, its realization in the audio can be much more complex, involving a whole range of frequencies.

To deal with such fluctuating fundamental frequencies, parametric signal models have been considered as extensions to NMF [17], [25]. In these approaches, the musical audio signal is modeled using a family of parameters capturing, for example, the fundamental frequency (including its temporal fluctuation), the spectral envelope of instruments or the amplitude progression. Such parameters often have an explicit acoustic or musical interpretation, and it is often straightforward to integrate available score information.

As an example for such a parametric approach, we consider a simplified version of the harmonic temporal structured clustering (HTC) strategy [17], [26]. Variants of this model have been widely employed for score-informed source separation [8]–[10], [27]. In an HTC-based approach, specialized model components replace NMF template vectors and activations. Each HTC template consists of several Gaussians, which represent the partials

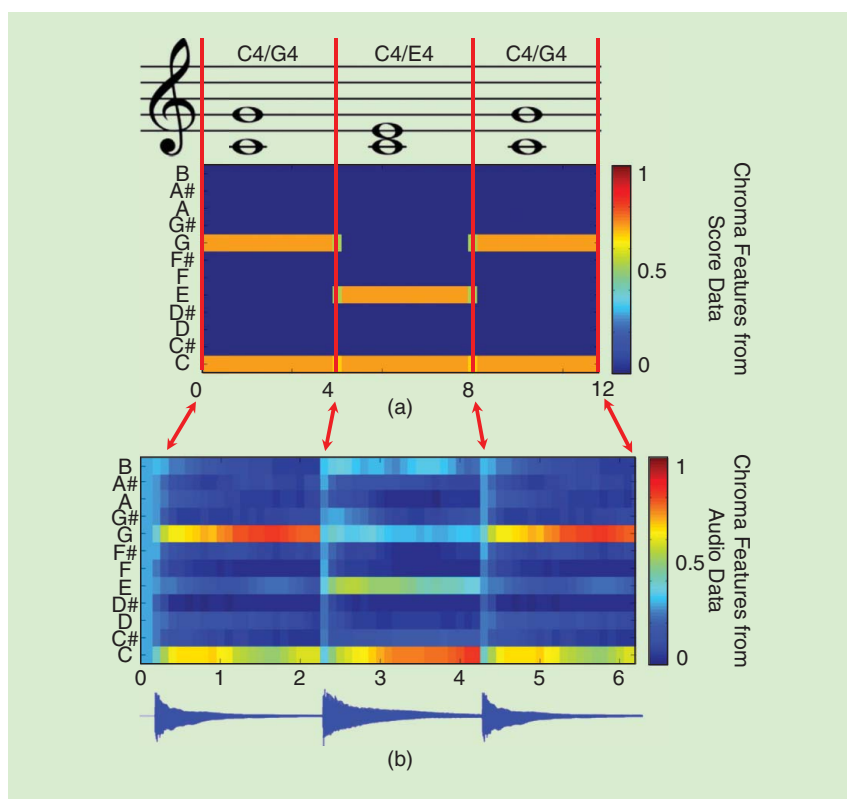


[FIG4] Score-audio synchronization: positions in the (a) score are aligned (red arrows) to positions in the (b) audio recording based on a comparison of chroma features, which were derived from both representations.

of a harmonic sound [Figure 6(a)]. To adapt the model to different instruments and their specific spectral envelopes, the height of each Gaussian in an HTC template can be scaled individually using a set of parameters $\{\gamma_1, \dots, \gamma_5\}$ in Figure 6(a). An additional parameter $f_0^{(n)}$ specifies the fundamental frequency of an HTC template in each time frame n . Assuming a harmonic relationship between the partials, the parameter $f_0^{(n)}$ also controls the exact location of each Gaussian [Figure 6(a)].

HTC activations are also constructed using Gaussians. Their position is typically fixed such that only some height parameters can be adapted [parameters $\alpha_1, \dots, \alpha_7$ in Figure 6(b)]. By choosing suitable values for the variance of these Gaussians, one can enforce a significant overlap between them, which leads to an overall smooth activation progression.

Combining the HTC templates and activations in a way similar to NMF yields a spectrogram model that suppresses both nonharmonic elements in frequency direction and spurious peaks in time direction [Figure 6(c)]; see [17] and [26]. HTC-based approaches model the spectral envelope independently from the fundamental frequency, such that both can be adapted individually. As an illustration, we used a constant fundamental frequency parameter in Figure 6(c) and a fluctuating fundamental frequency in Figure 6(d).

The explicit meaning of most HTC parameters enables a straightforward integration of score information [8]–[10], [27]. For example, after assigning a musical pitch to an HTC template,

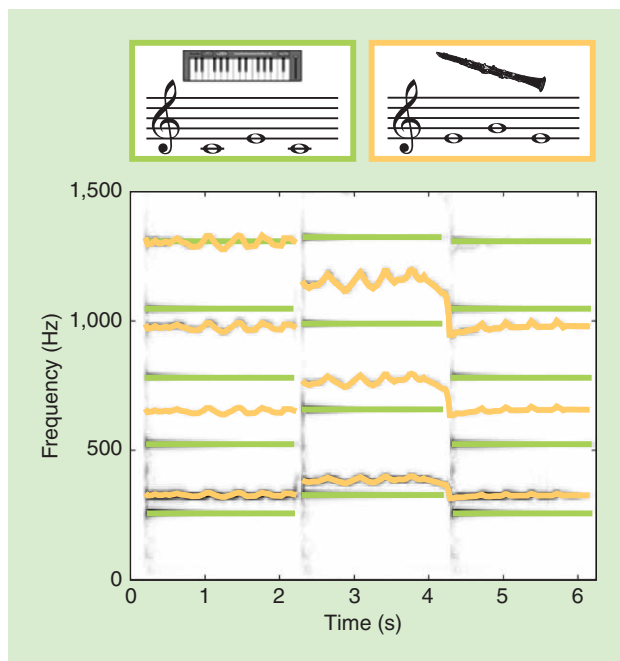


[FIG5] A spectrogram of a recording of a piano and a clarinet. The position of the fundamental frequency and the harmonics is illustrated for the piano (in green) and for the clarinet (in orange).

the fundamental frequency parameter can be constrained to lie in a small interval around the standard frequency of the pitch [9], [10]. Using the score's instrument information, the γ -parameters

can be initialized using sound examples for the specific instrument [8], [27]. Finally, using the position and duration of note events specified by the score, constraints on the activity parameters α can be imposed by setting them to zero whenever the corresponding instrument and pitch are known to be inactive [8], [9].

To model a given recording using the HTC approach, most methods minimize a distance between the spectrogram and the model to find suitable values for the parameters. To this end, most approaches employ minimization methods that are also used in the NMF context: multiplicative updates [9], expectation-minimization [8], [27], or interior points methods [10]. Constraints on the parameters are typically expressed using priors [8], [27] (in probabilistic models) or penalty terms [10] (in deterministic methods).

Many other parametric models are possible. For example, several score-informed source separation methods have used variants of the source/filter (S/F) model as their underlying signal model [25], [28]. In the S/F-model a sound is produced by an excitation source, which is subsequently filtered. When applied in speech processing, the source corresponds to the vocal chords while the filter models the vocal tract. Applied to musical instruments, the source typically corresponds to a vibrating element, e.g., the strings of a violin, and the filter corresponds to the instrument's resonance body. Since the parameters used to model the filter and the excitation source have an explicit meaning, they can often be initialized or constrained based on score information [29], [30].

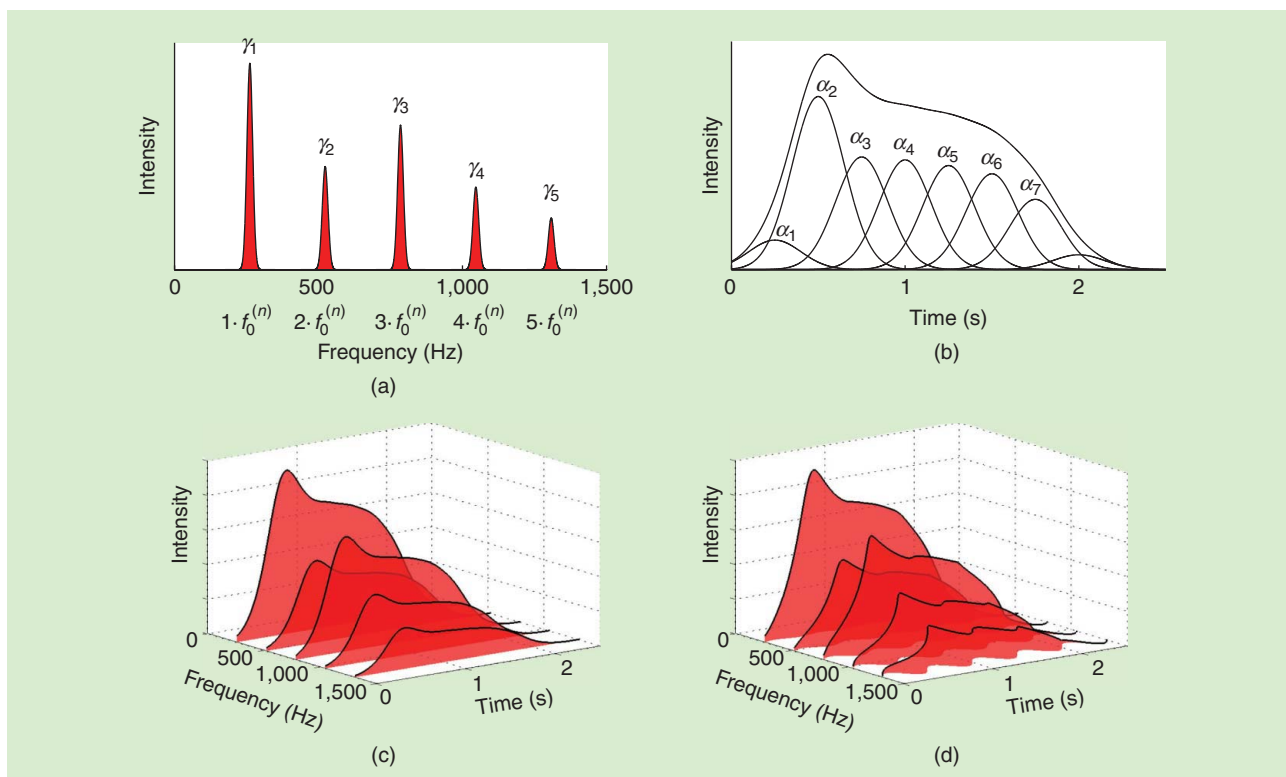


[FIG6] A simplified HTC model. (a) The HTC template with parameters. (b) The HTC activation with parameters. Parts (c) and (d) show illustrations of the full spectrogram model combining the submodels shown in (a) and (b), using a constant and a fluctuating fundamental frequency in (c) and (d), respectively.

EXAMPLE-BASED SOURCE SEPARATION

The approaches discussed in previous sections were based on the assumption that all instruments notated in a score produce purely harmonic sounds. However, this assumption is not perfectly true for many instruments, including the piano or the guitar. Percussive instruments, such as drums or bongos, also exhibit complex broadband spectra instead of a set of harmonics. As an alternative to enforcing a harmonic structure in the signal model, we can use a data-driven approach and guide the separation based on examples for the sound of the segregated sources [5], [15]. Using the score information, we can provide these examples by employing a high-quality synthesizer to render a separate instrument audio track for each instrumental line specified by the score. For each instrument track, an NMF decomposition of the corresponding magnitude spectrogram can be computed, resulting in an instrument template matrix and an instrument activation matrix. Finally, by horizontally stacking the instrument template matrices, one large prior template matrix \tilde{W} can be created. Similarly, a large prior activation matrix \tilde{H} can be built up by vertically stacking all instrument activation matrices. These two prior matrices essentially give an example of how a meaningful factorization of the magnitude spectrogram of the real audio recording could look like. Therefore, the separation of the real recording can be guided by employing the matrices \tilde{W} and \tilde{H} as Bayesian priors for the template matrix W and the activation matrix H within the probabilistic latent component analysis framework, a probabilistic formulation of NMF [3], [31]. This way, the matrices W and H tend to stay close to \tilde{W} and \tilde{H} .

While such an example-based approach to separation enables nonharmonic sounds to be modeled, there are drawbacks if the synthetic examples are not sufficiently similar to the real sounds. For example, if the fundamental frequency of a synthesized harmonic sound is different from the corresponding frequency in the real audio recording, the matrices \tilde{W} and \tilde{H} impose false priors, for the position of the fundamental frequency as well as for the position of the harmonics, such that separation may fail. However, combining example-based source separation with harmonic constraints in the signal model (as discussed in the section “Score-Informed Constraints”) can mitigate these problems, often resulting in a significant increase in separation quality [32], [33].

FURTHER EXTENSIONS AND FUTURE WORK

In this article, we showed how information provided by a musical score can be used to facilitate the separation of musical sound sources, which are typically highly correlated in time and frequency in a music recording. We demonstrated how score and audio data can automatically be aligned and how score information can be integrated into NMF. Further extensions addressed fluctuating fundamental frequencies or enabled the separation of instruments based on example sounds synthesized from the score.

The general idea of score-informed source separation leaves room for many possible extensions. For example, all of the approaches discussed above operate offline, where the audio recording to be processed is available as a whole. For streaming scenarios, the audio stream can only be accessed up to a given position, and

the computational time is also limited to allow the separation result to be returned shortly after the audio data has been streamed.

As a first approach to online score-informed separation, Duan and Pardo [13] combine a real-time score-audio alignment method with an efficient score-informed separation method.

Besides information obtained from a score, various other sources of prior knowledge can be integrated. Examples include spatial information obtained from multichannel recordings [6], [34] or side information describing the mixing process of the sources [35]. A distant goal could be a general framework where various different kinds of prior knowledge can be plugged in as they are available.

Since the prior knowledge provided by a score stabilizes the separation process significantly, one could use this stability to increase the level of detail used to model sound sources. For example, most current signal models typically do not account for the fact that the energy in higher partials of a harmonic sound often decays faster than in lower partials. Also, room acoustics or time-varying effect filters applied to the instruments are often not considered in separation methods. In such cases, score-informed signal models might be stable enough to robustly model even such details.

Further, since it is not always realistic to assume that an entire score is available for a given recording (in particular, for pop music), exploiting partially available score information will be a central challenge. For example, so-called lead sheets often do not encode the entire score but only the main melody and some chords for the accompaniment. Furthermore, the score could be available only for a specific section (e.g., the chorus) and not for the rest of the recording, such that suitable approaches to integrating partial prior knowledge, such as [4], have to be developed. Also, lyrics are often available as pure text without any information about notes or timing. Addressing these scenarios will lead to various novel approaches and interesting extensions of the strategies discussed in this article.

AUTHORS

Sebastian Ewert (sebastian.ewert@eecs.qmul.ac.uk) received the M.Sc./Diplom degree and Ph.D. degree (summa cum laude) in computer science from the University of Bonn, Germany, in 2007 and 2012, respectively. Since 2012, he has been a research fellow at the Centre for Digital Music, Queen Mary University of London, United Kingdom, and program manager for the networking and funding initiative Semantic Media. His research interests include audio signal processing and machine learning with applications to automated music processing, in particular source separation, signal modeling, structured knowledge representation, and informed audio processing.

Bryan Pardo (pardo@northwestern.edu) is the head of the Northwestern University Interactive Audio Lab and an associate professor in the Northwestern University Department of Electrical Engineering and Computer Science. He received an M.Mus. degree in jazz studies in 2001 and a Ph.D. degree in computer science in 2005, both from the University of Michigan. He has authored over 70 peer-reviewed publications. He developed speech

analysis software for the Speech and Hearing Department of The Ohio State University, statistical software for SPSS, and worked as a machine-learning researcher for General Dynamics.

Meinard Müller (meinard.mueller@audiolabs-erlangen.de) received the Diplom degree in mathematics and the Ph.D. degree in computer science from the University of Bonn, Germany. In 2007, he obtained his Habilitation degree publishing a Springer monograph *Information Retrieval for Music and Motion*. Since 2012, he has held a professorship for semantic audio processing at the International Audio Laboratories Erlangen, a joint institution of the Friedrich-Alexander-University Erlangen-Nürnberg and the Fraunhofer-Institut für Integrierte Schaltungen IIS. His recent research interests include content-based multimedia retrieval, audio signal processing, music processing, music information retrieval, and motion processing.

Mark D. Plumbley (mark.plumbley@eecs.qmul.ac.uk) received the B.A. (honors) degree in electrical sciences and the Ph.D. degree in neural networks from the University of Cambridge, United Kingdom, in 1984 and 1991, respectively. From 1991 to 2001, he was a lecturer at King's College London. He moved to Queen Mary University of London in 2002, where he is now an Engineering and Physical Sciences Research Council leadership fellow and director of the Centre for Digital Music. His research focuses on the automatic analysis of music and other audio sounds, including automatic music transcription, beat tracking, and audio source separation, and with interest in the use of techniques such as ICA and sparse representations. He is a past chair of the ICA Steering Committee and is a member of the IEEE Signal Processing Society Technical Committee on Audio and Acoustic Signal Processing. He is a Senior Member of the IEEE.

REFERENCES

- [1] N. Bertin, R. Badeau, and E. Vincent, "Enforcing harmonicity and smoothness in Bayesian non-negative matrix factorization applied to polyphonic music transcription," *IEEE Trans. Audio, Speech, Lang. Processing*, vol. 18, no. 3, pp. 538–549, 2010.
- [2] E. Vincent, M. G. Jafari, S. A. Abdallah, M. D. Plumbley, and M. E. Davies, "Probabilistic modeling paradigms for audio source separation," in *Machine Audition: Principles, Algorithms and Systems*, W. Wang, Ed. Hershey: IGI Global, 2010, pp. 162–185.
- [3] P. Smaragdis and G. J. Mysore, "Separation by humming: User guided sound extraction from monophonic mixtures," in *Proc. IEEE Workshop Application Signal Processing to Audio Acoustics (WASPAA)*, 2009, pp. 69–72.
- [4] A. Lefevre, F. Bach, and C. Févotte, "Semi-supervised NMF with time-frequency annotations for single-channel source separation," in *Proc. Int. Society for Music Information Retrieval Conf. (ISMIR)*, 2012, pp. 115–120.
- [5] U. Simsekli and A. T. Cemgil, "Score guided musical source separation using generalized coupled tensor factorization," in *Proc. European Signal Processing Conf. (EUSIPCO)*, 2012, pp. 2639–2643.
- [6] A. Ozerov, C. Févotte, R. Blouet, and J.-L. Durrieu, "Multichannel nonnegative tensor factorization with structured constraints for user-guided audio source separation," in *Proc. IEEE Int. Conf. Acoustics, Speech, Signal Processing (ICASSP)*, 2011, pp. 257–260.
- [7] J. Driedger, H. Grohgan, T. Prätzlich, S. Ewert, and M. Müller, "Score-informed audio decomposition and applications," in *Proc. ACM Int. Conf. Multimedia (ACM-MM)*, 2013, pp. 541–544.
- [8] K. Itoyama, M. Goto, K. Komatani, T. Ogata, and H. G. Okuno, "Instrument equalizer for query-by-example retrieval: Improving sound source separation based on integrated harmonic and inharmonic models," in *Proc. Int. Conf. Music Information Retrieval (ISMIR)*, 2008, pp. 133–138.
- [9] R. Hennequin, B. David, and R. Badeau, "Score informed audio source separation using a parametric model of non-negative spectrogram," in *Proc. IEEE Int. Conf. Acoustics, Speech, Signal Processing (ICASSP)*, 2011, pp. 45–48.
- [10] S. Ewert and M. Müller, "Estimating note intensities in music recordings," in *Proc. IEEE Int. Conf. Acoustics, Speech, Signal Processing (ICASSP)*, 2011, pp. 385–388.
- [11] P.-S. Huang, S. D. Chen, P. Smaragdis, and M. Hasegawa-Johnson, "Singing-voice separation from monaural recordings using robust principal component analysis," in *Proc. IEEE Int. Conf. Acoustics, Speech Signal Processing (ICASSP)*, 2012, pp. 57–60.
- [12] J. Herre, H. Purnhagen, J. Koppens, O. Hellmuth, J. Engdegård, J. Hilper, L. Villemoes, L. Terentiv, C. Falch, A. Hölzer, M. L. Valero, B. Resch, H. Mundt, and H.-O. Oh, "MPEG spatial audio object coding—The ISO/MPEG standard for efficient coding of interactive audio scenes," *J. Audio Eng. Soc.*, vol. 60, no. 9, pp. 655–673, 2012.
- [13] Z. Duan and B. Pardo, "Soundprism: An online system for score-informed source separation of music audio," *IEEE J. Select. Topics Signal Processing*, vol. 5, no. 6, pp. 1205–1215, 2011.
- [14] S. Ewert and M. Müller, "Using score-informed constraints for NMF-based source separation," in *Proc. IEEE Int. Conf. Acoustics, Speech, Signal Processing (ICASSP)*, 2012, pp. 129–132.
- [15] J. Ganseman, P. Scheunders, G. J. Mysore, and J. S. Abel, "Source separation by score synthesis," in *Proc. Int. Computer Music Conf. (ICMC)*, 2010, pp. 462–465.
- [16] D. D. Lee and H. S. Seung, "Algorithms for non-negative matrix factorization," in *Proc. Neural Information Processing Systems (NIPS)*, 2000, pp. 556–562.
- [17] H. Kameoka, T. Nishimoto, and S. Sagayama, "A multipitch analyzer based on harmonic temporal structured clustering," *IEEE Trans. Audio, Speech Lang. Processing*, vol. 15, no. 3, pp. 982–994, 2007.
- [18] S. A. Raczynski, N. Ono, and S. Sagayama, "Multipitch analysis with harmonic nonnegative matrix approximation," in *Proc. Int. Conf. Music Information Retrieval (ISMIR)*, 2007, pp. 381–386.
- [19] R. B. Dannenberg and C. Raphael, "Music score alignment and computer accompaniment," *ACM Commun.*, vol. 49, no. 8, pp. 38–43, 2006.
- [20] M. A. Bartsch and G. H. Wakefield, "Audio thumbnailing of popular music using chroma-based representations," *IEEE Trans. Multimedia*, vol. 7, no. 1, pp. 96–104, 2005.
- [21] C. Joder, S. Essid, and G. Richard, "A conditional random field framework for robust and scalable audio-to-score matching," *IEEE Trans. Audio, Speech, Lang. Processing*, vol. 19, no. 8, pp. 2385–2397, 2011.
- [22] S. Ewert, M. Müller, and P. Grosche, "High resolution audio synchronization using chroma onset features," in *Proc. IEEE Int. Conf. Acoustics, Speech, Signal Processing (ICASSP)*, 2009, pp. 1869–1872.
- [23] Z. Duan and B. Pardo, "A state space model for online polyphonic audio-score alignment," in *Proc. IEEE Int. Conf. Acoustics, Speech, Signal Processing (ICASSP)*, 2011, pp. 197–200.
- [24] M. Müller and D. Appelt, "Path-constrained partial music synchronization," in *Proc. Int. Conf. Acoustics, Speech Signal Processing (ICASSP)*, 2008, pp. 65–68.
- [25] J.-L. Durrieu, G. Richard, B. David, and C. Févotte, "Source/filter model for unsupervised main melody extraction from polyphonic audio signals," *IEEE Trans. Audio, Speech Lang. Processing*, vol. 18, no. 3, pp. 564–575, 2010.
- [26] M. Goto, "A real-time music-scene-description system: Predominant-F0 estimation for detecting melody and bass lines in real-world audio signals," *Speech Commun. (ISCA J.)*, vol. 43, no. 4, pp. 311–329, 2004.
- [27] Y. Han and C. Raphael, "Informed source separation of orchestra and soloist," in *Proc. Int. Society for Music Information Retrieval Conf. (ISMIR)*, 2010, pp. 315–320.
- [28] T. Heittola, A. P. Klapuri, and T. Virtanen, "Musical instrument recognition in polyphonic audio using source-filter model for sound separation," in *Proc. Int. Society for Music Information Retrieval Conf. (ISMIR)*, 2009, pp. 327–332.
- [29] P. Sprechmann, P. Cancela, and G. Sapiro, "Gaussian mixture models for score-informed instrument separation," in *Proc. IEEE Int. Conf. Acoustics, Speech, Signal Processing (ICASSP)*, 2012, pp. 49–52.
- [30] C. Joder and B. Schuller, "Score-informed leading voice separation from monaural audio," in *Proc. Int. Society for Music Information Retrieval Conf. (ISMIR)*, 2012, pp. 277–282.
- [31] M. Shashanka, B. Raj, and P. Smaragdis, "Probabilistic latent variable models as nonnegative factorizations (Article ID 947438)," *Computat. Intell. Neurosci.*, vol. 2008, p. 9, 2008.
- [32] J. Fritsch and M. D. Plumbley, "Score informed audio source separation using constrained nonnegative matrix factorization and score synthesis," in *Proc. IEEE Int. Conf. Acoustics, Speech, Signal Processing (ICASSP)*, 2013, pp. 888–891.
- [33] J. Fritsch, J. Ganseman, and M. D. Plumbley, "A comparison of two different methods for score-informed source separation," in *Proc. Int. Workshop Machine Learning Music (MLM)*, 2012, p. 2.
- [34] J. Woodruff, B. Pardo, and R. B. Dannenberg, "Remixing stereo music with score-informed source separation," in *Proc. Int. Conf. Music Information Retrieval (ISMIR)*, 2006, pp. 314–319.
- [35] A. Liutkus, S. Gorlow, N. Sturmel, S. Zhang, L. Girin, R. Badeau, L. Daudet, S. Marchand, and G. Richard, "Informed audio source separation: A comparative study," in *Proc. European Signal Processing Conf. (EUSIPCO)*, 2012, pp. 2397–2401.



[Bertrand Rivet, Wenwu Wang, Syed Mohsen Naqvi, and Jonathon A. Chambers]

Audiovisual Speech Source Separation

[An overview of key methodologies]

The separation of speech signals measured at multiple microphones in noisy and reverberant environments using only the audio modality has limitations because there is generally insufficient information to fully discriminate the different sound sources. Humans mitigate this problem by exploiting the visual modality, which is insensitive to background noise and can provide contextual information about the audio scene. This advantage has inspired the creation of the new field of audiovisual (AV) speech source separation that targets exploiting visual modality alongside the microphone measurements in a machine. Success in this emerging field will expand the application of voice-based machine interfaces, such as Siri, the intelligent personal assistant on the iPhone and iPad, to much more realistic settings and thereby provide more natural human-machine interfaces.

INTRODUCTION

The purpose of this article is to provide an overview of the key methodologies in AV speech source separation building from early methods that simply use the visual modality to identify speech activity to sophisticated techniques which synthesise a full AV model. New directions in this exciting area of signal processing are also identified.

Separating speech signals that are only observable as mixtures requires techniques such as blind source separation (BSS). This topic has been investigated extensively in the signal processing community during the past two decades and has had impact upon many applications such as speech enhancement and machine

audition [1]. A well-known example for demonstrating BSS applications is the so-called cocktail-party problem coined by Cherry [2]. His desire was to build a machine to mimic a human's ability in separating target speech sources from a superposition of multiple sound signals including interfering sounds and background noise, often coupled by sound reflections from room surfaces. This problem is usually addressed within the framework of convolutive BSS taking into account room reverberations in the separation model. In this framework, the vector observations $x(t)$ are modeled as a linear convolutive mixture of the vector

sources $s(t)$: $x(t) = H(t) * s(t)$, where $H(t)$

is the matrix of impulse responses between each source and each mixture, and t is the discrete time index. For simplicity, $H(t)$

is assumed to be square so that the number of microphones and sources is equal, but this is not necessary to achieve separation.

The aim is thus to estimate the demixing matrix $W(t)$ so that $\hat{s}(t) = W(t) * x(t)$ contains an estimate of each source $s_i(t)$,

where subscript i is the index of the source. Alternatively, it is solved in a transform

domain by converting the full-band speech mixtures into sub-band components that are then separated either individually or jointly, leading to a computationally more efficient method, e.g., frequency-domain BSS. In this latter case, assuming static sources, the frequency-domain counterparts of mixing and demixing equations are $x(m, f) = H(f)s(m, f)$ and $\hat{s}(m, f) = W(f)x(m, f)$, respectively, where $\cdot(m, f)$ is the short-term discrete-time Fourier transform (STFT) of $\cdot(t)$, $\cdot(f)$ is the Fourier transform of $\cdot(t)$, and m and f are the time frame and frequency bin indices, respectively. This, however, introduces the permutation and scaling ambiguity problems due to the potentially inconsistent orders



Source Separation and Applications

IMAGE LICENSED BY
INGRAM PUBLISHING

Digital Object Identifier 10.1109/MSP.2013.2296173

Date of publication: 7 April 2014

and scales of the separated source components at the individual frequency bands that are inherent to the instantaneous BSS models: in other words, $W(f) = \Lambda(f)P(f)H(f)^{-1}$, where $\Lambda(f)$ is a diagonal matrix (i.e., modeling the scaling indeterminacy) and $P(f)$ is a permutation matrix (i.e., modeling the permutation ambiguity). Many methods have been developed to mitigate these ambiguities before reconstructing the full-band source signals (more details can be found in [1]). A more recent approach is independent vector analysis (IVA), whereby the permutation problem is mitigated via a coupling of the adaptation across all the frequency bands [3].

These convolutive BSS techniques can be broadly attributed to a category of linear filtering-based methods. Another powerful method for separating convolutive mixtures is based on a form of time-varying filtering using time-frequency (T-F) masking where the aim is to form a probabilistic (soft) or binary (hard) mask $\mathcal{M}(m, f)$ for each source, and then applying the mask to the T-F representation of the mixtures for the extraction of that source: $\hat{s}(m, f) = \mathcal{M}(m, f)x(m, f)$. The mask can be estimated by the evaluation of various cues from the mixtures, such as statistical, spatial, temporal and/or spectral cues, using an expectation maximization (EM) algorithm [4] under a maximum likelihood or a Bayesian framework. The T-F masking techniques can often be applied directly on underdetermined mixtures for the extraction of a larger number of sources than the observed signals. Despite these efforts and the promising progress made in this area, the state-of-the-art algorithms commonly suffer in the following two practical situations: highly reverberant and noisy environments, and when multiple moving sources are present. For example, most existing methods of frequency-domain BSS are practically constrained by the data length limitation, i.e., the number of samples available at each frequency bin is not sufficient for learning algorithms to converge [5], while the various cues, such as the spatial cues that are used to calculate the likelihood of the source being present for the T-F mask estimation, become more ambiguous

with the increasing reverberation and background noise. The performance of most existing algorithms degrades substantially in these adverse acoustic environments.

The methods mentioned previously exploit only single modality signals in the audio domain. However, it is now widely accepted that human speech is inherently at least bimodal involving interactions between audio and visual modalities [6]. For example, the uttering activities are often coupled with the visual movements of vocal organs, while reading lip movement can help a human to infer the meaning of a spoken sentence in a noisy environment [7]. The well-known McGurk effect also confirms that visual articulatory information is integrated into the human speech perception process automatically and unconsciously [8]. For example, under certain conditions, a visual /ga/ combined with an auditory /ba/ is often heard as /da/. As also suggested by Cherry [2], fusing the AV information from different sensory measurements would be the best way to address the machine cocktail-party problem. The intrinsic AV coherence has been exploited previously to improve the performance of automatic speech recognition [13] and identification [14]. The term *coherence* is used here to describe the dependency between the audio and visual modalities, to be consistent with the conventional use of the term in previous works in the literature, such as [9]–[12]. As discussed in subsequent sections, the dependency can be modeled as either joint distribution of the AV features or joint AV atoms (i.e., signal components).

In the study in [9], a speech signal corrupted by white noise is enhanced with filters estimated from the video input. The aim is to estimate a time-varying Wiener filter based on a linear regression [linear predictive coding (LPC)] between the audio and visual signals from a regressor trained with a clean database (Figure 1) and therefore is termed an *AV-Wiener filter*. This preliminary study has been shown to be efficient on very simple data (succession of vowels and consonants). For instance, with an input signal-to-noise ratio (SNR) of -18 dB, a simple linear discriminant analysis of the filtered signals leads to a word

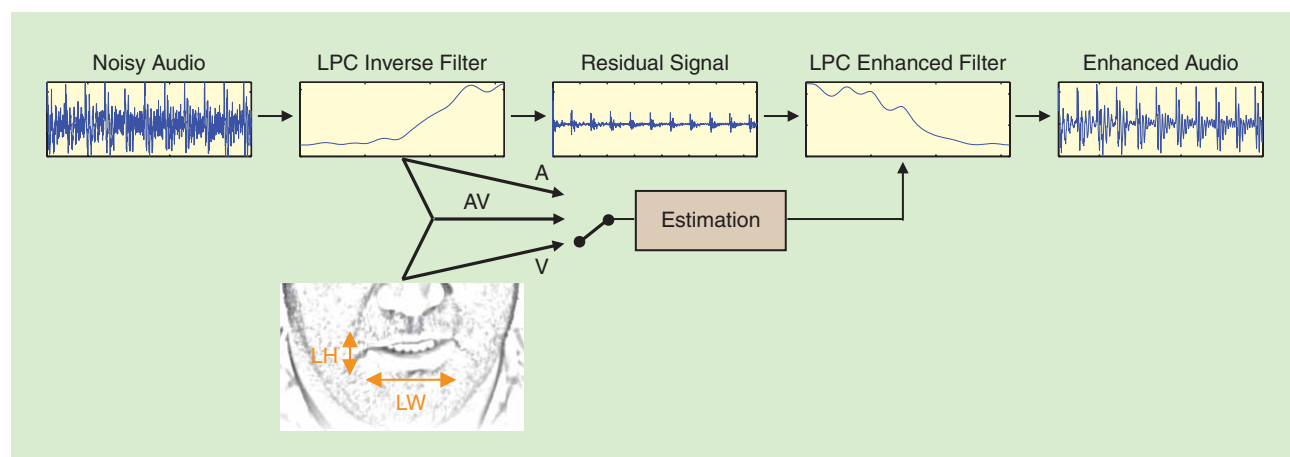


[FIG1] The AV estimation of the Wiener filter from [9]. The LPC method is used to model the noisy speech. The audio feature based on the LPC inverse filtered spectrum is fused with the visual features such as the lip width (LW) and height (LH) for enhancing the LPC spectrum of the noisy speech. The enhanced speech signal can therefore be obtained based on this LPC enhanced filter and the residual signal obtained from the inverse filtering of the noisy speech.

classification accuracy (CA) of 40% after the AV enhancement compared to the CA of 10% with the classical audio enhancement while the unfiltered data leads to a CA of 5%. However, due to the complex relationship between audio and video signals, this simple approach is found to have limitations when applied on more complex signals such as natural speech and other noise sources. Nevertheless, this pioneering approach has shown that it can be extremely beneficial to combine video information when dealing with speech enhancement mirroring the advantage gained in automatic speech recognition systems [13].

During the last decade, integrating visual information into an audio-only speech source separation system has been emerging as an exciting new area in signal processing: AV (i.e., multimodal) speech source separation [10]. The activities in this area include robust modeling of AV coherence [12], [15]; fusing of AV coherence with independent component analysis (ICA) or T-F masking [16]; using AV coherence to resolve ambiguities in BSS [15], [17]; employing visual information for the detection of voice activities [18], [19]; exploiting redundancy within the AV data to design efficient speech separation algorithms based on sparse representations [16], [20];

and more recently, AV scene analysis for addressing the challenging problem of speech separation from moving sources [5], [21] or in environments with long reverberation time [22].

A number of different of approaches have clearly been developed to tackle the speech source separation problem using both audio and visual modalities. To present these in a coherent manner, the remainder of this tutorial is organized according to the increasing sophistication in the way in which video is used to help speech source enhancement as summarized in Table 1. The advantages and disadvantages of the methods are also highlighted in the table, and references are added to papers where the full details can be found of experimental studies that present the performance gains achievable by adding video in the processing.

METHODS BASED ON VISUAL VOICE ACTIVITY

A very simple approach to model the link between audio and video signals is to utilize the voice activity of the time domain speech signal. Indeed, there exist pauses during natural speech: for instance, during breathing or before a plosive (such as /p/). Such silences can importantly be partially predicted by the

[TABLE 1] AN OVERVIEW OF AV METHODS FOR SPEECH ENHANCEMENT/SEPARATION. THE METHODS ARE CLASSIFIED ACCORDING TO THE INCREASING SOPHISTICATION IN THE WAY IN WHICH VIDEO IS USED TO HELP SPEECH SOURCE SEPARATION: FROM A COARSE BINARY INDEX (SECTION II) TO FULL JOINT AV MODEL (SECTION IV) INCLUDING VISUAL SCENE ANALYSIS (SECTION III), AND REFERENCES ARE GIVEN WHICH DETAIL COMPARATIVE PERFORMANCE EVALUATION STUDIES.

DETAIL OF AV REPRESENTATION	BINARY	SECTION:	METHODS	MAIN ADVANTAGES	MAIN DISADVANTAGES	
		SECTION: "METHODS BASED ON VISUAL VOICE ACTIVITY"	SPECTRAL SUBTRACTION [23], [24]	EFFECTIVE IN NOISE REDUCTION; EASY TO IMPLEMENT	INTRODUCES PROCESSING ARTEFACTS; DIFFICULT TO ESTIMATE THE NOISE POWER FOR NONSTATIONARY SIGNALS	
			AV POSTPROCESSING OF AUDIO ICA [17]	LOW COMPUTATIONAL COST; STRENGTH OF ICA FRAMEWORK; CORRECT (ALMOST) ALL PERMUTATIONS	INCREASES DELAY (I.E., LATENCY); POTENTIAL PROCESSING ARTEFACTS	
			EXTRACTION BASED ON TEMPORAL VOICE ACTIVITY [18]	LOW COMPUTATIONAL COST; SIMPLE ASSUMPTIONS	LIMITED TO LOW REVERBERATION	
VISUAL SCENE ANALYSIS		SECTION: "VISUAL SCENE ANALYSIS-BASED METHODS"	AV BEAMFORMING/ ICA/IVA [5], [21], [25]–[27]	POTENTIAL FOR SEPARATING MOVING SOURCES; CORRECT THE PERMUTATIONS; IMPROVE CONVERGENCE OF ICA/IVA ALGORITHMS	DEGRADES WITH HIGH REVERBERATIONS	
			AV T-F MASKING [22]	EXPLOITS TIME-VARYING PROPERTY OF SOURCES; NOT AFFECTED BY THE PERMUTATION PROBLEM	HIGH COMPUTATIONAL COMPLEXITY; CHALLENGING IN RESOLVING SPECTRAL OVERLAPS	
FULL JOINT AV MODEL		SECTION: "INTRODUCTION"	AV-WIENER FILTER [9]	LOW COMPUTATIONAL COST	LIMITED TO SIMPLE SIGNALS; DIFFICULTY IN LEARNING ACCURATE AV MODEL	
			SECTION: "STATISTICAL AV-BASED METHODS"	MAXIMIZATION OF AV LIKELIHOOD [10], [28]	CAN EXTRACT SPEECH SOURCES FROM UNDERDETERMINED MIXTURES	LIMITED TO INSTANTANEOUS MIXTURES; DIFFICULTY IN LEARNING ACCURATE AV MODEL
			AV REGULARIZATION OF ICA [11]	EXPLOITING THE STRENGTH OF THE ICA FRAMEWORK	LIMITED IMPROVEMENT COMPARED TO AUDIO-ONLY ICA IN PARTICULAR FOR CONVOLUTIVE MIXTURES	
			AV POSTPROCESSING OF AUDIO ICA [12]	MODERATE COMPUTATIONAL COST	DIFFICULTY OF LEARNING ACCURATE AV MODEL; INCREASES DELAY (I.E., LATENCY)	
		SECTION: "SPARSE MODELING"	AVDL + T-F MASKING [16]	CAN CAPTURE THE LOCAL INFORMATION WITHIN THE SIGNALS; NOT AFFECTED BY THE PERMUTATION PROBLEM	HIGH COMPUTATIONAL COMPLEXITY; ONLY BIMODALITY INFORMATIVE PARTS OF THE SIGNALS ARE LEARNED	

movements of the lips [19]. Based on this idea, several purely video-based voice activity detectors (V-VADs) have been developed [29]: they are generally based on the velocity of face features, usually motions of the lips. The main advantage of such V-VADs compared to an audio VAD is that they are not corrupted by concurrent audio sources such as environmental noise, or other speakers. It is worth noting that such models do not aim at linking audio and video features, but they try to infer very coarse information on silence [i.e., the probability that speech is present $P(s_i(t) \neq 0 | \zeta_i^v(t))$] or not [i.e., $P(s_i(t) = 0 | \zeta_i^v(m))$] in the audio modality from the video one, where $\zeta_i^v(t)$ is the visual signal associated with the i th source $s_i(t)$. Examples of speech enhancement methods that exploit a V-VAD are discussed next.

SPECTRAL SUBTRACTION

A simple method is to extend classical spectral subtraction by embedding visual features [23], [24]: the spectrum of the enhanced signal is expressed as $|\hat{s}(m, f)|^2 = |x(m, f)|^2 - \alpha |d(m, f)|^2$, where $x(m, f)$ is the STFT of a measured microphone signal $x(t)$, $d(m, f)$ is the estimated interference noise spectrum, and α is a parameter to adjust the subtraction level. The spectrum of the interference noise $d(m, f)$ is estimated from the windows related to the silence of the target source (i.e., the set $\mathcal{T}_i = \{t | P(s_i(t) = 0 | \zeta_i^v(t))\}$). These windows are efficiently detected by a V-VAD, which is thus not corrupted by the interfering audio noise.

AV POSTPROCESSING OF AUDIO ICA

Another use of such high-level information (speech/nonspeech frames) is to embed it into the efficient ICA framework. In this method, the visual information is used as postprocessing after

applying an audio ICA algorithm. Frequency-domain source separation generally suffers from the permutation indeterminacy at each frequency bin: the ICA framework allows the recovery of the sources up to a global permutation (i.e., the order of the estimated sources is arbitrary). As a consequence, to recover the sources, this issue must be solved (i.e., permutation matrices $P(f)$ must be the same for all f). A very intuitive and efficient method is to estimate the permutations in relation to the output power of the sources [17]. Indeed, the V-VAD provides a binary indicator that shows when a specific speaker is silent. Using this information, one can then solve the permutation indeterminacy by simply minimizing the power of the target source during these frames. This method thus exploits the AV dependence, i.e., the joint distribution of AV features, in a very minimal way, but it has been shown to cancel almost all the permutation ambiguities. Compared to purely audio methods, this requires relatively low computational cost to mitigate the permutation ambiguities and allows the extraction of only a specific speech source instead of trying to recover all the sources.

AV EXTRACTION BASED ON TEMPORAL SPEECH ACTIVITY

A more effective use of such high-level information (speech/nonspeech frames) is to directly incorporate it into a separation criterion [18] to extract particular speakers to provide even less computational cost than ICA methods. Indeed, considering a set of time samples \mathcal{D} so that the sources can be split into silent ones ($\forall i \in \mathcal{S}_{\text{silent}}, \forall t \in \mathcal{D}, s_i(t) = 0$) and active ones ($\forall i \in \mathcal{S}_{\text{active}}, \forall t \in \mathcal{D}, s_i(t) \neq 0$), purely audio algebraic methods based on generalized eigendecomposition of two covariance matrices can identify 1) the number of silent speakers (i.e., the cardinality of $\mathcal{S}_{\text{silent}}$), and 2) the associated support subspace (i.e., the subspace spanned

by $\{s_i\}_{i \in \mathcal{S}_{\text{silent}}}$). In other words, considering any time samples including some not in \mathcal{D} (i.e., the sources in $\mathcal{S}_{\text{silent}}$ can become active), the projection of the audio recordings $x(t)$ onto the latter identified subspace cancels all sources in $\mathcal{S}_{\text{active}}$ while sources in $\mathcal{S}_{\text{silent}}$ remain unchanged. However, this method can not identify which source is silent and thus cannot be used to extract a specific speaker. To overcome this, a weighted kernel principal component analysis can be used to improve this approach, where the weights are a mixture between the audio probability of silence (given by the eigenvalues) and the video probability of silence provided by the V-VAD for a particular speaker [18]. This simple property provides a very efficient and elegant AV method to extract speech sources.

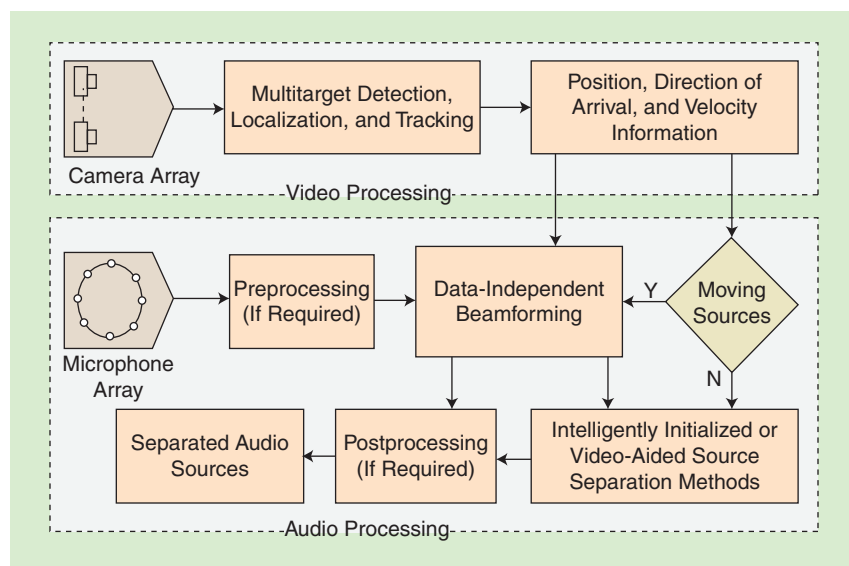


[FIG2] A block diagram of a visual scene analysis-based method for speech enhancement. Video localization is based on face and head detection. A video tracker is implemented for the tracking of multiple humans and based on the MCMC-PF. The output of the video processing is position, direction of arrival, and/or velocity information. On the basis of the visual scene, the preprocessed audio mixtures are separated either by a data-independent beamformer or intelligently initialized video-aided source separation method. Finally, postprocessing is applied to enhance the separated audio sources.

VISUAL SCENE ANALYSIS-BASED METHODS

In the previous section, AV extraction methods use the visual modality in a very

coarse way: simple binary information defining whether or not a specific speaker is silent. In this section, this extra modality is used in a deeper way by visually analyzing the scene for speech enhancement [25], [26]. Such visual scene analysis thereby informs the source separation algorithms of the locations of the speakers, especially when dealing with moving sources, which is a more challenging issue since the mixing filters are now time varying. Thus, the classical ICA framework may be ineffective due to the large number of time samples required to accurately estimate the statistics of the mixtures. These methods are implemented in two stages: mainly video scene analysis (VSA) based on multiple human tracking (MHT) to estimate the position, direction of arrival (DOA), and velocity information of the people in a room or enclosed environment; and audio source separation depending on the scene as illustrated in the schematic diagram in Figure 2.

VIDEO PROCESSING FOR MHT

Video-based face and head detection is applied for multiperson observations from a single image as initialization. Then a Markov chain Monte Carlo-based particle filter (MCMC-PF) is used for MHT in the video. More details of the three important parts of the probabilistic MHT—the state model, the measurement model, and the sampling mechanism—are provided in [5]. Contrary to the V-VAD described in the section “Methods Based on Visual Voice Activity,” it is highlighted that the full-frontal close-up views of the faces of the speakers, which are generally not available in a room or an enclosed environment, are not required for these trackers. The above-mentioned MHT methods provide a very good framework for AV scene modeling for source separation: the output of the video-based tracker is the three-dimensional (3-D) position of each speaker p , the elevation (θ_p), and azimuth (β_p) angles of arrival to the center of the microphone array. The direct-path weight vector $\mathbf{d}_p(f, \theta_p, \beta_p)$ can then be computed for frequency bin f and for source of interest $p = 1, \dots, P$ and the velocity information that can then be used in the AV source separation scheme.

AV SOURCE SEPARATION OF MOVING SOURCES

Speech source separation is a challenging issue when dealing with moving sources [26]. The proposed extraction of a particular speaker in an AV context depends on the velocity of this speaker.

PHYSICALLY MOVING SOURCES

After VSA, if the people are moving, then the challenge of separating respective audio sources is that the mixing filters are time varying; as such, the unmixing filters should also be time varying, but these are difficult to determine from only audio measurements. In [21], a multistage method has been developed for speech separation of moving sources based on VSA. This method consists of several stages including the DOA tracking of speech sources based on video processing, separation of sources based on beamforming with the beampatterns generated by the DOAs, and T-F masking as postprocessing. From the video signal, the direct path parameter vector \mathbf{d}_p can be obtained, as discussed above, which is then used for the design of a robust least squares frequency invariant data independent (RLSFIDI) beamformer to separate the audio sources. The T-F masking is used as postprocessing to further improve the separation quality of the beamformer by reducing the interferences to a much lower level. However, such time-varying filtering techniques may introduce musical noise due to the inaccurate estimate of the mask at some T-F points. To overcome this problem, smoothing techniques such as cepstral smoothing may be used as in [21].

PHYSICALLY STATIONARY SOURCES

After video processing, if the speakers are judged to be physically stationary for at least two seconds, then the direct path parameter vector \mathbf{d}_p with the whitening matrix obtained from the audio mixtures is used to intelligently initialize the learning algorithms, such as FastICA/IVA (many learning algorithms are sensitive to initializations) [3], [5], which solves the inherent permutation problem in ICA or block permutation in IVA algorithms and yields improved convergence [27].

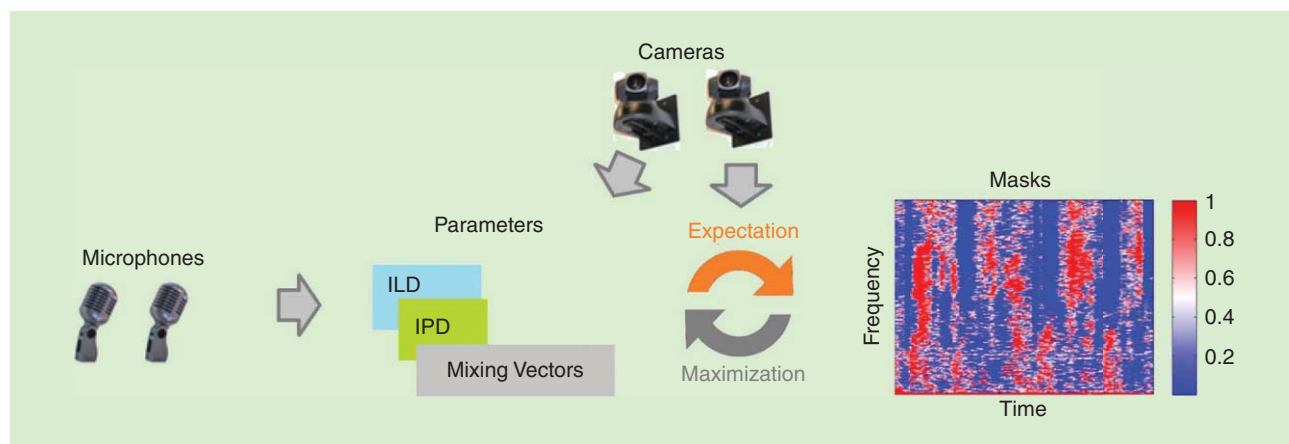


[FIG3] Speech recording is obtained from two microphones. The direct path parameter vector is calculated with the help of video cameras. The ILD, the IPD, and the mixing vectors that utilize the direct path parameter vector are used to estimate the model parameters with the EM algorithm. The final probabilistic mask formed from the resulting probabilistic model is used for source separation.

T-F MASKING BASED ON VSA

More recently, a video-aided model-based source separation technique for underdetermined cases when the reverberation time is significant has been proposed [22]. This probabilistic T-F masking approach is motivated by both computational auditory scene analysis (CASA) and BSS, which relies on the assumption of signal sparseness (Figure 3). The interaural level difference (ILD), the interaural phase difference (IPD), and the mixing vectors are modeled as in [30], and the direct path parameter vector \mathbf{d}_p is used as the mean parameter of the mixing vectors that is obtained from video processing. The parameters are updated iteratively with the EM algorithm. Since the EM algorithm is also sensitive to initialization, we initialize the direction vector parameter with the location information of the speakers obtained from video processing.

To form an AV probabilistic T-F mask $\mathcal{M}_i^{av}(m, f)$ for each static source $s_i(t)$, the IPD and ILD models as well as the model for the mixing vectors that utilize the direct-path weight vector obtained with the aid of video are used. It is a hidden maximum-likelihood parameter estimation problem and thus the EM algorithm can provide the solution. Extensive evaluations can be found in [22], which confirm the advantage of exploiting the visual modality to analyze the scene.

FULL JOINT AV MODELING-BASED METHODS

The most sophisticated approach to use the multimodality is then to build a full AV model of speech rather than the binary modeling of V-VAD (see the section “Methods Based on Visual Voice Activity”) or the VSA (see the section “Visual Scene Analysis-Based Methods”). Two of these models and their uses for speech extraction are presented in this section: 1) AV statistical models, and 2) AV-dictionary-learning (DL)-based sparse representations models. With the statistical modeling approach, the AV coherence is often established explicitly on a feature space, which provides a holistic representation across all the observation frames of the AV signals [10], [11], [28], [31]. On the other hand, with the sparse representation-based methods, the AV coherence is implicitly modeled through the decomposition of an AV signal as a linear combination of a small number of signal components (i.e., atoms) chosen from a dictionary [16], [32]. The sparse model has shown to be effective in capturing the local information, such as temporal dynamic structures of the AV signals, which otherwise may be lost in the statistical modeling methods, but yet could be crucial for speech perception. Note that we distinguish these two models from the perspectives of modeling and optimization algorithms rather than the property of signals since sparsity can be considered as a statistical property of a signal. The two models could be used together if, e.g., the sparse models are built on a feature space described by some statistical models.

STATISTICAL AV-BASED METHODS

AV MODEL

The coherence between audio and visual modalities can be jointly modeled by, e.g., a Gaussian mixture model (GMM)

where the coherence is expressed as a joint AV probability density function (AV-PDF)

$$p_1^{av}(\zeta^a(m), \zeta^v(m)) = \sum_{k=1}^K w_k p_G(\zeta^a(m), \zeta^v(m) | \mu_k^{av}, \Sigma_k^{av}), \quad (1)$$

where the superscripts a and v refer to the audio and visual modalities, respectively, and $\zeta^a(m)$ and $\zeta^v(m)$ are the audio and visual observation vectors at the m th frame, respectively; μ_k^{av} and Σ_k^{av} are the mean vector and the covariance matrix of the k th Gaussian kernel defined by its probability density function (PDF) $p_G(\cdot | \mu, \Sigma)$, w_k is the weight of the related kernel, and k is the number of mixture terms. (For simplicity in development, we will use the same notations to denote the AV feature vectors and AV sequence.) Classically, $\zeta^a(m)$ can be chosen as an audio feature vector, such as the modulus of the Fourier transform or the Mel-frequency cepstrum coefficients [33] of a windowed frame signal with frame index m , while $\zeta^v(m)$ is a visual feature vector, containing some shape parameters, e.g., the width and height of the lips or active appearance-based visual features [34]. When dealing with log scale audio parameters in the frequency domain, a more suitable model is the Log-Rayleigh PDF since this PDF explicitly models the nonsymmetric property of the logarithmic scale. The AV-PDF can thus be expressed as [31]

$$p_2^{av}(\zeta^a(m), \zeta^v(m)) = \sum_{k=1}^K w_k p_{LR}(\zeta^a(m) | \Gamma_k^a) p_G(\zeta^v(m) | \mu_k^v, \Sigma_k^v), \quad (2)$$

where $p_{LR}(\zeta^a(m) | \Gamma)$ is the Log-Rayleigh PDF of localization or power coefficients defined by the diagonal elements of Γ_k^a (see [31] for more details). Such AV-PDFs not only jointly model the two modalities but they can also take into account the ambiguity of speech (i.e., the fact that the same shape of lips can produce several sounds such as /u/ and /y/ in French). The AV-PDF parameters are usually obtained from a clean training AV database using the EM algorithm.

EXTRACTION BY DIRECT AV CRITERIA

One of the first methods for AV source separation [10], [28] was based on the maximization of the AV coherence model described by the joint AV-PDF as in (1)

$$\hat{\mathbf{b}} = \arg \max_{\mathbf{b}} p_1^{av}(\mathbf{b}^T \mathbf{x}(t), \zeta^v(t)), \quad (3)$$

where \mathbf{b} is the extraction vector for a particular speaker in the instantaneous case, and the superscript \cdot^T denotes the transpose operator. Even though such an approach is shown to be efficient when dealing with the simple succession of vowels and consonants [10], this method suffers from two important drawbacks: 1) a relevant AV probabilistic model is quite difficult to obtain for natural speech and 2) a direct maximization of the AV-PDF becomes rapidly computationally inefficient due to the dimensions of the separation filters when considering reverberant environments.

On the other hand, ICA [1] is an extraordinarily effective framework to separate sources from several mixtures. As a

consequence, it is natural to embed AV constraints into a more classical frequency domain ICA criterion $J_{ICA}(\{B(f)\}_t)$ by defining an AV-penalized ICA criterion [11]: $\{\hat{B}(f)\}_t = \arg \min_{\{B(f)\}_t} J_{ICA}(\{B(f)\}_t) + P_{AV}(p_1^w)$, where the constraint term $P_{AV}(\cdot)$ is a function of the AV-PDF as in (1). Note that we intentionally keep $J_{ICA}(\{B(f)\}_t)$ to be general as many frequency-domain ICA criteria defined in the literature, such as in [1], can be used. As one can see, this criterion is a tradeoff between the statistical independence of the estimated sources (first term) based on ICA and the AV coherence of the estimated sources and the video features (second term). This AV constraint only slightly improves the signal-to-interference (SIR) ratio compared to a purely audio criterion [11]: this is mainly due to the difficulty to propose a relevant AV-PDF and appropriate AV constraints.

AV POSTPROCESSING OF AUDIO ICA

One natural way is to estimate the global permutation by maximizing the AV coherence [12] defined by $p_2^{av}(\cdot, \cdot)$ (2). However, even if these algorithms are shown to be effective to solve the permutation ambiguities, they suffer from their computational costs and from the difficulty to train accurately the

statistical parameters that represent all the characteristics of natural speech.

SPARSE MODELING

While the previous methods seem to be quite natural AV extraction methods, the AV coherence used in these methods is often modeled in the feature space from the “global” point of view across all the frames of the AV data. These methods often fail to provide accurate estimation of audio signals due to the difficulty to train a relevant AV statistical model. To address this limitation, an alternative method for capturing the AV coherence has been considered in [16] and [32], using DL-based sparse approximation, which we call *sparse modeling*. As pointed out in [16], this technique can capture the ‘local’ information, i.e., the interconnection between neighboring samples, which is important for speech perception in a noisy environment.

SPARSE CODING OF AV SIGNALS AND DL OF THE AV ATOMS BASED ON A GENERATIVE AV MODEL

To obtain sparse representation of an AV signal, a generative model [16], [32] can be used, where an AV sequence $\zeta = (\zeta^a; \zeta^v)$

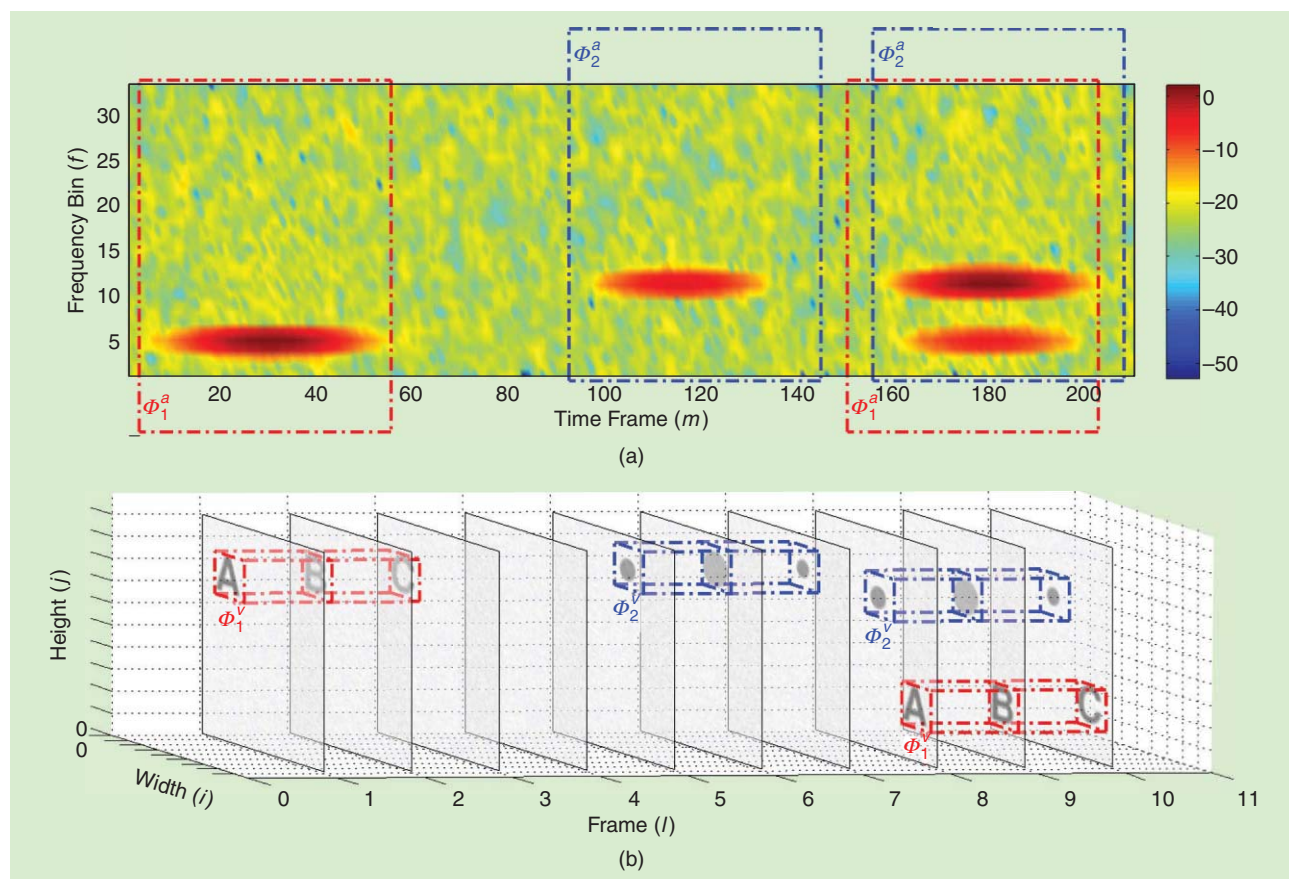


[FIG4] A schematic diagram generated artificially to show the use of a generative model to represent an AV sequence as a linear combination of a small number (two in this case) of atoms. The audio sequence (the spectrogram) is shown in (a) and the video sequence (a series of image frames, depicted as rectangles with solid lines) in (b). The patterns A, B, and C and the dots correspond to the two visual atoms. As highlighted by the rectangles with dot-dashed lines, the AV-coherent part in the sequence is represented by scaling and allocating the atoms at two positions. The audio stream is shown in log scale. The audio atom is a randomly generated spectrogram pattern, rather than a realistic phoneme or word in speech. The figure is modified from [16], where examples of AV sequence and AV atoms from real AV speech data can be found.

is described by a small number of AV atoms $\phi_k = (\phi_k^a, \phi_k^v)$ chosen from an overcomplete dictionary $\mathcal{D} = \{\phi_k\}_{k=1}^K$, where the discrete time index t is omitted here for notational convenience. The audio atoms ϕ_k^a are usually the log-modulus of the STFT of the audio signal component and the video ones ϕ_k^v are the mouth region (i.e. the area in the image frames where the mouth is located) of the video signal. We use a schematic diagram to explain the relationship between the AV sequence and AV atoms as shown in Figure 4, where each audio atom appears in tandem with its corresponding visual atom at a temporal-spatial (TS) position in the related video. In this example, the AV sequence is represented by only two AV atoms with some overlap between the two in a particular TS position.

Given an AV signal and a dictionary \mathcal{D} , the coding processing aims to find the sparse coefficients set that leads to a suitable approximation of the original sequence according to a matching criterion. This can be achieved by many algorithms including the greedy algorithms such as the well known matching pursuit (MP) or orthogonal MP algorithms. In [32], the MP algorithm has been extended to an AV-MP version to obtain the coding coefficients, where the matching criterion is defined as the inner product $\langle \cdot, \cdot \rangle$ between the residue of the AV sequence ($R^n \zeta$) at the n -th iteration and the translated AV atom ϕ_k :

$$J_1^{av}(R^n \zeta, \phi_k) = |\langle R^n \zeta^a, \mathcal{T}_m^a \phi_k^a \rangle| + |\langle R^n \zeta^v, \mathcal{T}_{i,j,l}^v \phi_k^v \rangle|, \quad (4)$$

where \mathcal{T}_m^a is the temporal translation operator of the audio atom (i.e., shifting an audio atom by m time frames) and $\mathcal{T}_{i,j,l}^v$ is the temporal-spatial translation operator of the video atom (i.e., shifting the video atom l time frames along the time axis and (i, j) pixels along the horizontal and vertical axes of the image frames). However, as shown in [16], the latter matching criterion may lead to a monomodal criterion due to the imbalance between the two modalities (due to the scale difference). The following criterion is therefore proposed in [16]:

$$J_2^{av}(R^n \zeta, \phi_k) = |\langle R^n \zeta^a, \mathcal{T}_m^a \phi_k^a \rangle| \times \exp\left\{-\frac{1}{IJL} \|R^n \zeta^v - \mathcal{T}_{i,j,l}^v \phi_k^v\|_1\right\}, \quad (5)$$

where I and J are the number of width and height pixels of the video atom ϕ_k^v , respectively, and L its time duration; $\|\cdot\|_1$ is the ℓ_1 -norm.

The learning process is to adapt the K dictionary atoms $\phi_{k \in \{1, \dots, K\}}$ to fit the training AV sequence. Several well-known DL algorithms can be used for this purpose, such as singular value decomposition (K-SVD) [35]. In [16], the K-SVD and K-means algorithms are used in each iteration for updating the audio and visual atoms respectively, so as to take into account the different sparsity constraints enforced on these two modalities. The sparse coding and DL stages are often performed in an alternating manner until the predefined criterion such as (5) is optimized.

SPARSE AV-DL-BASED AV SPEECH SEPARATION

From the AV-DL methods, T-F masking-based BSS methods are proposed [16], where the audio T-F mask $\mathcal{M}^a(m, f)$ generated by

the purely audio algorithm [36] is fused empirically with a mask $\mathcal{M}^v(m, f)$ defined from the visual modality by the power-law transformation to define an AV T-F mask

$$\mathcal{M}^{av}(m, f) = \mathcal{M}^a(m, f)^{r(\mathcal{M}^v(m, f))}, \quad (6)$$

where the power coefficients r are obtained by applying a nonlinear mapping function to $\mathcal{M}^v(m, f)$ based on how confident the visual information is in determining the source occupation likelihood of each T-F point of the mixtures [16]. There are alternative methods for fusing the audio and visual masks, such as a simple linear combination of these two masks. Such a simple scheme is, however, less effective in taking into account the confidence level of the visual information, as compared with the power-law transformation (more discussions about the motivation of using power-law transformation can be found in [16]). The mask defined from the video can be obtained as

$$\mathcal{M}^v(m, f) = \begin{cases} 1, & \text{if } \hat{\zeta}^a(m, f) > \zeta^a(m, f) \\ \hat{\zeta}^a(m, f) / \zeta^a(m, f), & \text{otherwise.} \end{cases} \quad (7)$$

Here $\hat{\zeta}^a(m, f)$ is the audio signal reconstructed from the speech mixtures by mapping the mixtures (together with the visual sequence) onto the AV dictionary. Note that, even if the latter mask is defined from audio-only sequences $\zeta^a(m, f)$ and $\hat{\zeta}^a(m, f)$, it can be considered as a visually inspired mask since $\hat{\zeta}^a(m, f)$ is taken from $(\hat{\zeta}^a(m, f), \hat{\zeta}^v(y, x, l))$, which represents the AV approximation of the new AV sequence $\zeta = (\zeta^a, \zeta^v)$. In other words, $\hat{\zeta}^a(m, f)$ is the best estimation of the audio signal from the AV sequence ζ obtained from its sparse decomposition on the AV dictionary \mathcal{D} . Finally, the noise-robust AV mask $\mathcal{M}^{av}(m, f)$ can be applied to the T-F spectrum of the mixtures for the target speech separation. Figure 5 shows an example of $\mathcal{M}^v(m, f)$, $\mathcal{M}^a(m, f)$, and AV masks $\mathcal{M}^a(m, f)^{r(\mathcal{M}^v(m, f))}$, as compared with the ideal binary mask (IBM). It can be seen that the fused AV masks improve the quality of the audio mask and the resolution of the visual mask. In [16], it is shown that the power-law transform performs better than the average operation, i.e., $(\mathcal{M}^a + \mathcal{M}^v)/2$.

CONCLUSIONS AND FUTURE DIRECTIONS

Over the past decade, AV speech source separation has emerged as a particularly interesting area of research in signal processing. It aims at improving the classical BSS methods for speech extraction by also using information from video and thereby mimicking the multimodal approach of humans. As shown in this article, the bimodality of speech can be used at different levels of sophistication to help audio source separation: from very coarse binary information through to a complete AV model, or from simple joint lip shape parameters to data-dependent acoustic features represented in an AV dictionary. As a result, the methods using the various level of information show different strength and weakness, as highlighted in Table 1. The main advantage of using the extra information from video is to tackle the problems that cannot be easily solved by audio-only algorithms: handling background noise and interference in strongly

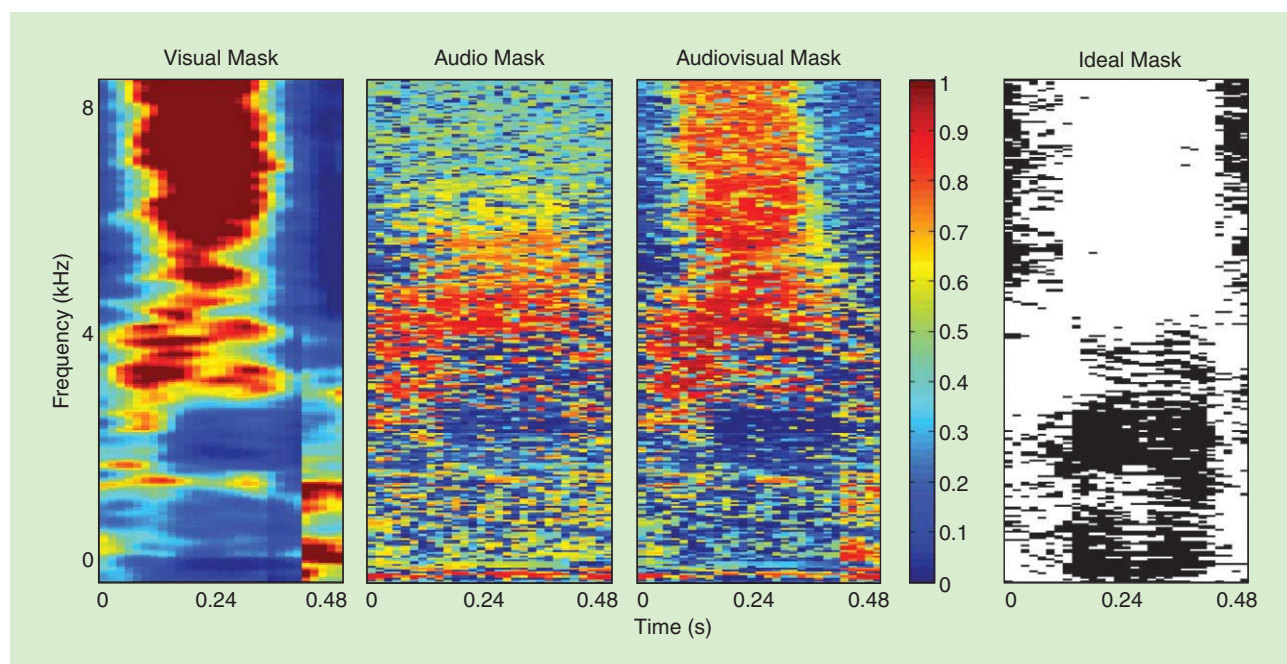


[FIG5] A comparison among the visual mask, audio mask, AV mask (power-law), and IBM that shows improved definition in the AV mask. For the IBM, zero is denoted by black, and one by white. Although the visual mask looks smooth, some detailed audio information is missing. By comparing these masks with the IBM, it can be observed that the AV mask provides the best results. The figure is modified from [16], where more quantitative comparisons and analysis can be found.

reverberant environments, together with multiple, potentially moving sources.

There are many directions for further research. The AV coherence based on statistical methods requires high-quality, low-dimensional features for accurate and computationally efficient modeling, therefore emerging methods from manifold or deep learning could be exploited. The current methods in AV DL that attempt to capture the AV informative structure in the bimodal data are computationally expensive due to the intensive numerical operations required in sparse coding algorithms. Low-complexity and robust algorithms are highly desirable and need to be developed. Moreover, to be embedded in everyday devices such as smartphones, real-time approaches must be proposed to overcome the batch nature of many current algorithms. In the longer term, building richer models exploiting psychoacoustic-visual properties on the basis of the fields of brain-science and psychology can potentially further improve the AV speech separation systems, but this presents a particular challenge for future research in this area.

Finally, as speech source separation is clearly profiting from the bimodality of sources, other fields of source separation/extraction should also be explored using multimodal data, for instance, brain imaging, which can record brain activity by electroencephalography, magnetoencephalography, magnetic resonance imaging, and positron emission tomography. The next generation of intelligent multimodal signal processing techniques will combine such information to provide radically improved performance not achievable with methods based on single-modality data.

ACKNOWLEDGMENTS

The authors thank the guest editors and the anonymous reviewers for their helpful comments to drastically improve the quality of this article. The authors thank Dr. Qingju Liu for regenerating and adapting Figures 4 and 5, which originally appeared in [16]. Part of this work was supported by the Engineering and Physical Sciences Research Council (EPSRC) of the U.K. grant number EP/K014307/1, the U.K. Ministry of Defence University Defence Research Collaboration (MoD UDRC) in Signal Processing, and the European project ERC-2012-AdG-320684-CHESS.

AUTHORS

Bertrand Rivet (berrtrand.rivet@gipsa-lab.grenoble-inp.fr) graduated from the Ecole Normale Supérieure de Cachan, France. He received the Agrégation de Physique Appliquée in 2002, the master's degree from the University of Paris-XI, France, in 2003, and the Ph.D. degree from the Grenoble Institute of Technology (Grenoble-INP, GIT), France, in 2006. He is currently an associate professor of signal processing with Physique, Electronique, Matériaux (PHELMMA) and a member of GIPSA-lab, Grenoble-INP, France. His research concerns biomedical signal processing, audiovisual speech processing, and BSS.

Wenwu Wang (w.wang@surrey.ac.uk) received his Ph.D. degree from Harbin Engineering University, Harbin, China, in 2002. He is a senior lecturer of signal processing and codirector of the Machine Audition Lab within the Centre for Vision Speech and Signal Processing, at the University of Surrey. He is currently a member of the MoD UDRC in Signal Processing

(2009–present) and the BBC Audio Research Partnership (2011–present). His current research interests include blind signal processing, AV signal processing, sparse representation, and DL. He has over 130 publications in these areas.

Syed Mohsen Naqvi (s.m.r.naqvi@lboro.ac.uk) received his Ph.D. degree in signal processing from Loughborough University, Leicestershire, United Kingdom, in 2009, where he is a lecturer in the School of Electronic, Electrical, and Systems Engineering. He was a postdoctoral research associate on the EPSRC U.K.-funded projects from 2009 to 2012. He contributed over 50 research outputs with main focus on multimodal (AV) speech processing and his research interests include nonlinear filtering, data fusion, and multitarget tracking, all for machine learning. He is a Member of the IEEE and the IEEE Signal Processing Society.

Jonathon A. Chambers (j.a.chambers@lboro.ac.uk) received his Ph.D. degree from the Imperial College, London, United Kingdom, in 1990. He is a professor of communications and signal processing and leads the Advanced Signal Processing Group within the School of Electronic, Electrical, and Systems Engineering at Loughborough University. He is also the associate dean (research) for Loughborough University in London. He is a senior area editor of *IEEE Transactions on Signal Processing* and a member of the IEEE Signal Processing Society Conference Board. He is a Fellow of the IEEE and the Royal Academy of Engineering, United Kingdom.

REFERENCES

- [1] P. Comon and C. Jutten, Eds., *Handbook of Blind Source Separation Independent Component Analysis and Applications*. New York: Academic, 2010.
- [2] E. C. Cherry, "Some experiments on the recognition of speech, with one and with two ears," *J. Acoust. Soc. Amer.*, vol. 25, no. 5, pp. 975–979, 1953.
- [3] M. Anderson, G.-S. Fu, R. Phlypo, and T. Adali, "Independent vector analysis: Identification conditions and performance bounds," *IEEE Trans. Signal Processing*, accepted for publication.
- [4] A. P. Dempster, N. M. Laird, and D. B. Rubin, "Maximum-likelihood from incomplete data via the EM algorithm," *J. R. Stat. Soc. Ser. B.*, vol. 39, no. 1, pp. 1–38, 1977.
- [5] S. M. Naqvi, M. Yu, and J. A. Chambers, "A multimodal approach to blind source separation of moving sources," *IEEE J. Select. Topics Signal Processing*, vol. 4, no. 5, pp. 895–910, 2010.
- [6] L. E. Bernstein and C. Benoît, "For speech perception by humans or machines, three senses are better than one," in *Proc. Int. Conf. Spoken Language Processing (ICSLP)*, Philadelphia, PA, 1996, pp. 1477–1480.
- [7] W. Sumbly and I. Pollack, "Visual contribution to speech intelligibility in noise," *J. Acoust. Soc. Amer.*, vol. 26, no. 2, pp. 212–215, 1954.
- [8] A. Liew and S. Wang, Eds., *Visual Speech Recognition: Lip Segmentation and Mapping*. Hershey, PA: IGI Global Press, 2009.
- [9] L. Girin, J.-L. Schwartz, and G. Feng, "Audiovisual enhancement of speech in noise," *J. Acoust. Soc. Amer.*, vol. 109, no. 6, pp. 3007–3020, June 2001.
- [10] D. Sodoyer, J.-L. Schwartz, L. Girin, J. Klinkisch, and C. Jutten, "Separation of audiovisual speech sources: A new approach exploiting the audiovisual coherence of speech stimuli," *EURASIP J. Appl. Signal Processing*, vol. 2002, no. 11, pp. 1165–1173, 2002.
- [11] W. Wang, D. Cosker, Y. Hicks, S. Sanei, and J. A. Chambers, "Video assisted speech source separation," in *Proc. IEEE Int. Conf. Acoustics, Speech, and Signal Processing (ICASSP)*, Philadelphia, PA, March 2005, pp. v/425–v/428.
- [12] B. Rivet, L. Girin, and C. Jutten, "Mixing audiovisual speech processing and blind source separation for the extraction of speech signals from convolutive mixtures," *IEEE Trans. Audio, Speech Lang. Processing*, vol. 15, no. 1, pp. 96–108, 2007.
- [13] G. Potamianos, C. Neti, G. Gravier, A. Garg, and A. W. Senior, "Recent advances in the automatic recognition of audiovisual speech," *Proc. IEEE*, vol. 91, no. 9, pp. 1306–1326, 2003.
- [14] J.-L. Schwartz, F. Berthommier, and C. Savariaux, "Seeing to hear better: Evidence for early audiovisual interactions in speech identification," *Cognition*, vol. 93, no. 2, pp. B69–B78, 2004.
- [15] Q. Liu, W. Wang, and P. Jackson, "Use of bimodal coherence to resolve permutation problem in convolutive BSS," *Signal Processing*, vol. 92, no. 8, pp. 1916–1927, 2012.
- [16] Q. Liu, W. Wang, P. Jackson, M. Barnard, J. Kittler, and J. Chambers, "Source separation of convolutive and noisy mixtures using audiovisual dictionary learning and probabilistic time-frequency masking," *IEEE Trans. Signal Processing*, vol. 61, no. 22, pp. 5520–5535, 2013.
- [17] B. Rivet, L. Girin, C. Servière, D.-T. Pham, and C. Jutten, "Using a visual voice activity detector to regularize the permutations in blind source separation of convolutive speech mixtures," in *Proc. Int. Conf. Digital Signal Processing (DSP)*, Cardiff, Wales, U.K., July 2007, pp. 223–226.
- [18] B. Rivet, L. Girin, and C. Jutten, "Visual voice activity detection as a help for speech source separation from convolutive mixtures," *Speech Commun.*, vol. 49, no. 7–8, pp. 667–677, 2007.
- [19] D. Sodoyer, B. Rivet, L. Girin, C. Savariaux, J.-L. Schwartz, and C. Jutten, "A study of lip movements during spontaneous dialog and its application to voice activity detection," *J. Acoust. Soc. Amer.*, vol. 125, no. 2, pp. 1184–1196, Feb. 2009.
- [20] A. L. Casanovas, G. Monaci, P. Vanderghyest, and R. Gribonval, "Blind audiovisual source separation based on sparse redundant representations," *IEEE Trans. Multimedia*, vol. 12, no. 5, pp. 358–371, 2010.
- [21] S. M. Naqvi, W. Wang, M. S. Khan, M. Barnard, and J. A. Chambers, "Multimodal (audiovisual) source separation exploiting multi-speaker tracking, robust beamforming, and time-frequency masking," *IET Signal Processing*, vol. 6, no. 5, pp. 466–477, 2012.
- [22] M. S. Khan, S. M. Naqvi, A. Rehman, W. Wang, and J. A. Chambers, "Video-aided model-based source separation in real reverberant rooms," *IEEE Trans. Audio, Speech Lang. Processing*, vol. 21, no. 9, pp. 1900–1912, 2013.
- [23] Q. Liu and W. Wang, "Blind source separation and visual voice activity detection for target speech extraction," in *Proc. Int. Conf. Awareness Science and Technology (iCAST)*, 2011, pp. 457–460.
- [24] Q. Liu, A. Aubery, and W. Wang, "Interference reduction in reverberant speech separation with visual voice activity detection," submitted for publication.
- [25] H. K. Maganti, D. Gatica-Perez, and I. McCowan, "Speech enhancement and recognition in meetings with an audiovisual sensor array," *IEEE Trans. Audio, Speech Lang. Processing*, vol. 15, no. 8, pp. 2257–2269, 2007.
- [26] S. T. Shivappa, B. D. Rao, and M. M. Trivedi, "Audiovisual fusion and tracking with multilevel iterative decoding: Framework and experimental evaluation," *IEEE J. Select. Topics Signal Processing*, vol. 4, no. 5, pp. 882–894, Oct. 2010.
- [27] Y. Liang, S. M. Naqvi, and J. A. Chambers, "Audio video based fast fixed-point independent vector analysis for multisource separation in a room environment," *EURASIP J. Adv. Signal Processing*, vol. 2012, no. 1, 2012.
- [28] D. Sodoyer, L. Girin, C. Jutten, and J.-L. Schwartz, "Developing an audiovisual speech source separation algorithm," *Speech Commun.*, vol. 44, no. 1–4, pp. 113–125, Oct. 2004.
- [29] A. J. Aubrey, Y. A. Hicks, and J. A. Chambers, "Visual voice activity detection with optical flow," *IET Image Processing*, vol. 4, no. 6, pp. 463–472, 2010.
- [30] A. Alinaghi, W. Wang, and P. J. B. Jackson, "Integrating binaural cues and blind source separation method for separating reverberant speech mixtures," in *Proc. IEEE Int. Conf. Acoustics, Speech and Signal Processing (ICASSP)*, 2011, pp. 209–212.
- [31] B. Rivet, L. Girin, and C. Jutten, "Log-Rayleigh distribution: A simple and efficient statistical representation of log-spectral coefficients," *IEEE Trans. Audio, Speech Lang. Processing*, vol. 15, no. 3, pp. 796–802, Mar. 2007.
- [32] G. Monaci, P. Vanderghyest, and F. T. Sommer, "Learning bimodal structure in audiovisual data," *IEEE Trans. Neural Networks*, vol. 20, no. 12, pp. 1898–1910, 2009.
- [33] B. Gold, N. Morgan, and D. Ellis, *Speech and Audio Signal Processing—Processing and Perception of Speech and Music*, 2nd ed. Hoboken, NJ: Wiley, 2011.
- [34] T. Cootes, G. Edwards, and C. Taylor, "Active appearance models," *IEEE Trans. Pattern Anal. Mach. Intell.*, vol. 23, no. 6, pp. 681–685, 2001.
- [35] M. Aharon, M. Elad, and A. Bruckstein, "K-SVD: An algorithm for designing overcomplete dictionaries for sparse representation," *IEEE Trans. Signal Processing*, vol. 54, no. 11, pp. 4311–4322, 2006.
- [36] M. I. Mandel, R. J. Weiss, and D. Ellis, "Model-based expectation-maximization source separation and localization," *IEEE Trans. Audio, Speech Lang. Processing*, vol. 18, no. 2, pp. 382–394, 2010.



[Leonardo Tomazeli Duarte, Saïd Moussaoui, and Christian Jutten]

Source Separation in Chemical Analysis

[Recent achievements and perspectives]

Since its origins in the mid-1980s, the field of blind source separation (BSS) has attracted considerable attention within the signal processing community. One of the main reasons for such popularity is the existence of many problems that can be addressed in a BSS framework. Two noteworthy examples of applications can be found in audio and biomedical signal processing, for which a number of efficient solutions are now available. There are relevant BSS problems in other domains but on which less effort has been put.

In this article, we deal with one of these fields, specifically the field of analytical chemistry (AC), whose goal of is to identify or quantify, or both, chemical components present in a given analyte, i.e., the sample under analysis. As recently discussed in [1], several tasks in AC keep some relationship to the broad classes of detection and estimation problems typically found in signal processing.

INTRODUCTION

Source separation is one of the most relevant estimation problems found in chemistry. Indeed, dealing with mixtures is paramount in different kinds of chemical analysis. For instance, there are some cases where the analyte is a chemical mixture of different components, e.g., in the analysis of rocks and heterogeneous materials through spectroscopy. Moreover, a mixing process can also take place even when the components are not chemically mixed. For instance, in the ionic analysis of liquid samples, the ions are not chemically

connected, but, due to the lack of selectivity of the chemical sensors, the acquired responses may be influenced by ions that are not the desired ones. Finally, there are some situations where the pure components cannot be isolated chemically since they appear only in the presence of other components. In this case, BSS may provide these components that cannot be retrieved otherwise.

In AC, there is a trend that advocates acquiring data through sensor arrays or by other instruments that are able to exploit diversity, which is essential in the application of source separation methods. In particular, chemometrics [2], a subfield of AC, aims at extracting the relevant information from the multivariate signals provided by the chemical measurement sensor. Chemometrics is an established domain of research based on different backgrounds (physics, statistics, computer science). Several approaches that are now popular in signal processing arose in chemometrics—a typical example is a problem introduced

in the 1970s known as *multivariate curve resolution (MCR)* [3], which bears strong resemblance to nonnegative matrix factorization (NMF) [4].

Classically, the available methods in chemometrics for dealing with mixtures work in a supervised fashion, thus requiring a set of training samples. The application of supervised methods in this context has been proving successful in tasks such as odor and taste automatic recognition systems (electronic noses and tongues, respectively). However, despite this success, this approach suffers from at least two important practical problems. First, the acquisition of training samples is usually a



Source Separation and Applications

IMAGE LICENSED BY
INGRAM PUBLISHING

Digital Object Identifier 10.1109/MSP.2013.2296099

Date of publication: 7 April 2014

cost- and time-demanding task. Second, due to the drift in the response of chemical sensors, which is usually caused by aging and variation of the acquisition conditions (temperature, pH), the calibration procedure must be performed before each new chemical analysis. Due to these limitations, there is a growing interest in solutions in which the calibration stage may be eliminated or, at least, simplified. This can be achieved by methods, like source separation or multiway data analysis, able to exploit the measurement diversity for discovering latent variables. The goal in considering these approaches is to ultimately have chemical sensing systems that work in a plug-and-measure fashion, which may pave the way for devices operating in more challenging situation, e.g., a calibration-free system would be quite helpful in the context of invasive physiological monitoring by means of miniaturized sensors.

Given the panorama described above, our aim is to shed some light on the use of BSS in chemical analysis. Although dealing with a relatively new field of applications, this article is not an exhaustive survey of source separation methods and algorithms since there are solutions originated in closely related domains (e.g., remote sensing and hyperspectral imaging) that suit well several problems found in chemical analysis. Moreover, we do not discuss the supervised source separation methods, which are basically multivariate regression techniques, that one can find in chemometrics.

SOURCE SEPARATION IN CHEMICAL ANALYSIS

Let us briefly recall the problem of source separation. The observed signals, which are represented by the vector $x(n) = [x_1(n), x_2(n), \dots, x_M(n)]^T$, are given by

$$x(n) = \mathcal{A}(s(n)), \quad (1)$$

where $\mathcal{A}(\cdot)$ represents the operator associated to the mixing process, and the vector $s(n) = [s_1(n), \dots, s_N(n)]^T$ denotes the source signals. The goal in source separation is to provide a good estimation of $s(n)$. In a blind (or unsupervised) context, one has access neither to training points, i.e., a set of pairs $(x_i(n), s_i(n))$, nor to the mixing system $\mathcal{A}(\cdot)$. Therefore, based only on observations $x(n)$, solving (1) for $s(n)$ becomes an ill-posed inverse problem whose handling requires further information [5, Ch. 7, 10, 11, and 13]. For instance, a possible approach is to exploit measurement diversities such as time-frequency representations of nonstationary signals (see, e.g., [5, Ch. 11]).

SOURCE ASSUMPTIONS

Source separation can be solved with independent component analysis (ICA) [6], [7], in which the sources are modeled as mutually independent random variables. Under some mild conditions, including the non-Gaussianity of the sources, the application of ICA ensures a correct retrieval of the sources. It is also

THERE ARE RELEVANT BSS PROBLEMS IN OTHER DOMAINS, SPECIFICALLY THE FIELD OF ANALYTICAL CHEMISTRY, WHOSE GOAL IS TO IDENTIFY OR QUANTIFY (OR BOTH) CHEMICAL COMPONENTS.

possible to achieve source separation by exploiting properties other than statistical independence, e.g., sparsity or nonnegativity [5]. Moreover, one can separate sources that are only mutually uncorrelated provided that additional temporal priors on the source signals hold, e.g., nonstationary or temporally correlated sources. This is very

important in chemical applications since there are some cases in which the source independence assumption fails. For instance, when a chemical reaction takes place, the components exhibit dependency since either they are made of the same chemical elements or their concentrations vary according to stoichiometric coefficients, which stands for the coefficients in a balanced chemical equation.

In chemical analysis, the sources present some features that can be exploited when developing a novel separation method. For instance, in ionic activity analysis (the effective concentration of an ion), the source signals correspond to time-series associated with the activities of each ion within the solution under analysis. Therefore, a first remarkable aspect is that the sources here are always nonnegative, since there is no physical meaning in having a negative concentration. A second prior information is the fact that source signals are smooth, i.e., successive samples are temporally correlated. Indeed, concentrations usually present slow variations of amplitude along time. To illustrate these features, we show in Figure 1(a) an example of sources related to the concentrations of potassium and ammonium ions and acquired in two different experiments. These data are publicly available at the ion-selective electrode array data set [8].

Another category of chemical source signals are those obtained in optical spectroscopy (Raman, infrared). Again, there are some valuable information that can be exploited: 1) the sources are again nonnegative since they correspond to absorption, reflectance, or diffusion spectra, and 2) there exist many libraries containing the spectra of different chemical components. This information can be used to adapt BSS algorithms based on sparse representation over a huge dictionary whose atoms are the pure component spectra. However, it would be difficult to use a reference library since the component spectra may present some variability in actual experiments depending on parameters such as temperature or pH condition. In Figure 1(b), an example of spectral source (infrared reflectance of calcite) is provided.

MIXING MODELS

Much effort was undertaken to develop methods tailored to linear and instantaneous mixing systems in which the number of sources is equal to the number of mixtures ($N = M$). Practically, this assumption implies that the number of sources is known, which is often a tricky issue. In this case, the operator $\mathcal{A}(\cdot)$ is given by a square matrix $A \in \mathbb{R}^{N \times N}$. Moreover, there are many works that

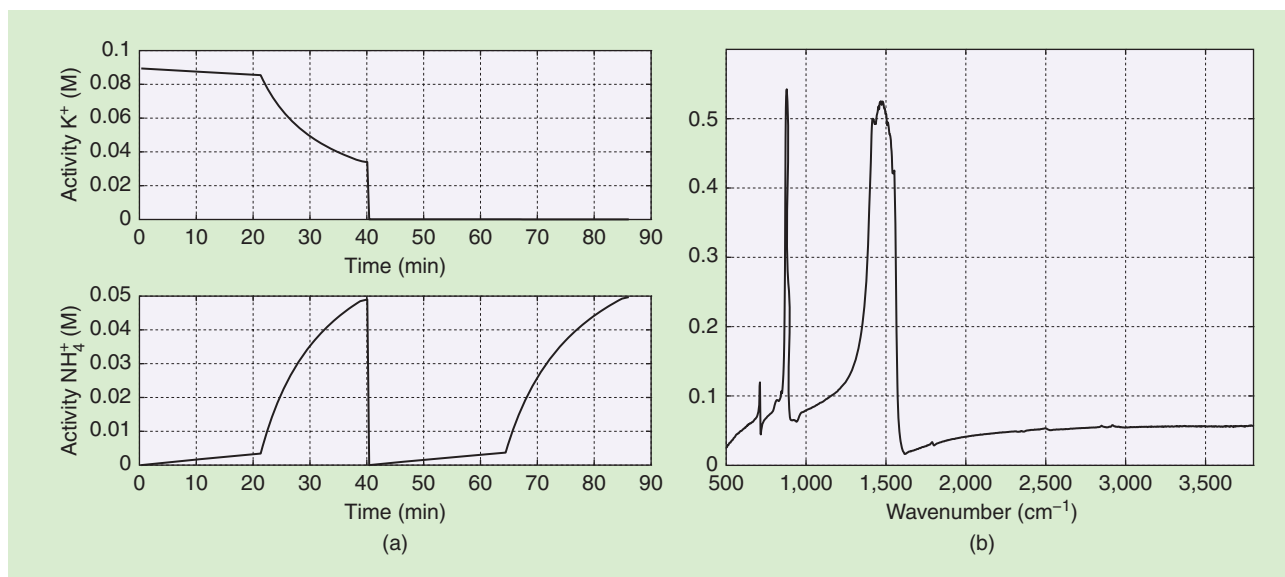


[FIG1] Some examples of sources in chemical analysis. (a) Ionic activities (in molar concentration) of potassium and ammonium. Note that the time scale is in minutes, and the signals were obtained from two different experiments. (b) The infrared reflectance of calcite.

deal with the convolutive case, in which each entry of the mixing matrix corresponds to a linear filter. Finally, there is an important topic in BSS where the aim is to set up separation methods in the case of nonlinear (NL) mixing models. In this context, one must bypass many difficulties that do not arise in the linear case. For instance, ICA does not ensure separation in a general NL context, i.e., retrieving independent components is not enough to reconstruct the actual sources. As a consequence, some researchers have been considering constrained classes of NL model for which ICA is still valid. For instance, ICA-based solutions ensure source separation in an important class of constrained models known as post-nonlinear (PNL) models [5, Ch. 14]. In chemical mixture analysis, one can find in the literature works on both linear and NL mixing models. In the sequel, we provide an (nonexhaustive) overview of source separation problems arising in each situation.

LINEAR MODELS

Measurement techniques such as optical spectroscopy and/or chromatography are frequently used in chemical analysis to extract relevant information related to the chemical composition of an heterogeneous material (identify the components and assess their relative abundance [9]). The data processing corresponds to a source separation problem where the linear instantaneous mixture model holds with relatively small concentrations of the components in absorption spectroscopy, thanks to the Beer-Lambert law [10]. In such model, each measured spectrum $x_i(\lambda)$ is a linear combination of the component spectra $s_j(\lambda)$, and the mixing coefficients a_{ij} are related to the abundances of each component

$$x_i(\lambda) = \sum_{j=1}^N a_{ij}s_j(\lambda). \quad (2)$$

In practice, M spectra [i.e., $i = 1 \dots M$ in (2)] are measured for different chemical conditions and L values of a spectral variable (frequency, wavelength, or wavenumber) λ . Figure 2(b) illustrates three absorption spectra resulting from the linear mixing of two spectral sources, shown in Figure 2(a). By considering a matrix notation for (2) and a noise term, the measured spectra can be stored in the rows of the data matrix $X \in \mathbb{R}^{M \times L}$ that can thus be factorized according to $X = AS + E$. The pure component spectra are identified as the sources (rows of matrix $S \in \mathbb{R}^{N \times L}$) and the abundance fractions of each component are the elements of the mixing matrix $A \in \mathbb{R}^{M \times N}$. The matrix $E \in \mathbb{R}^{M \times L}$ represents measurement errors and any deviation from the linear mixing model. In the chemical analysis community, the problem of estimating S and A knowing only matrix X is termed *MCR*, *spectral mixture analysis*, and *factor analysis* while

TO DEVELOP A LINEAR SPECTRAL MIXTURE SEPARATION METHOD, AN OBJECTIVE FUNCTION MUST BE OBTAINED BY FORMULATING SOME ASSUMPTIONS ON THE SOUGHT COMPONENT SPECTRA AND ON THEIR ABUNDANCES.

in signal and image processing field this problem is called *source separation* and *spectral unmixing*.

To develop a linear spectral mixture separation method, an objective function must be obtained by formulating some assumptions on the sought component spectra (the sources) and on their abundances (the mixing coefficients). Then, one must define a mathematical algorithm to optimize this objective function. The main information in spectral mixture data analysis is the nonnegativity of both the pure component spectra and abundances. However, even with a linear mixing model, only accounting for these constraints does not lead to a unique solution [3].

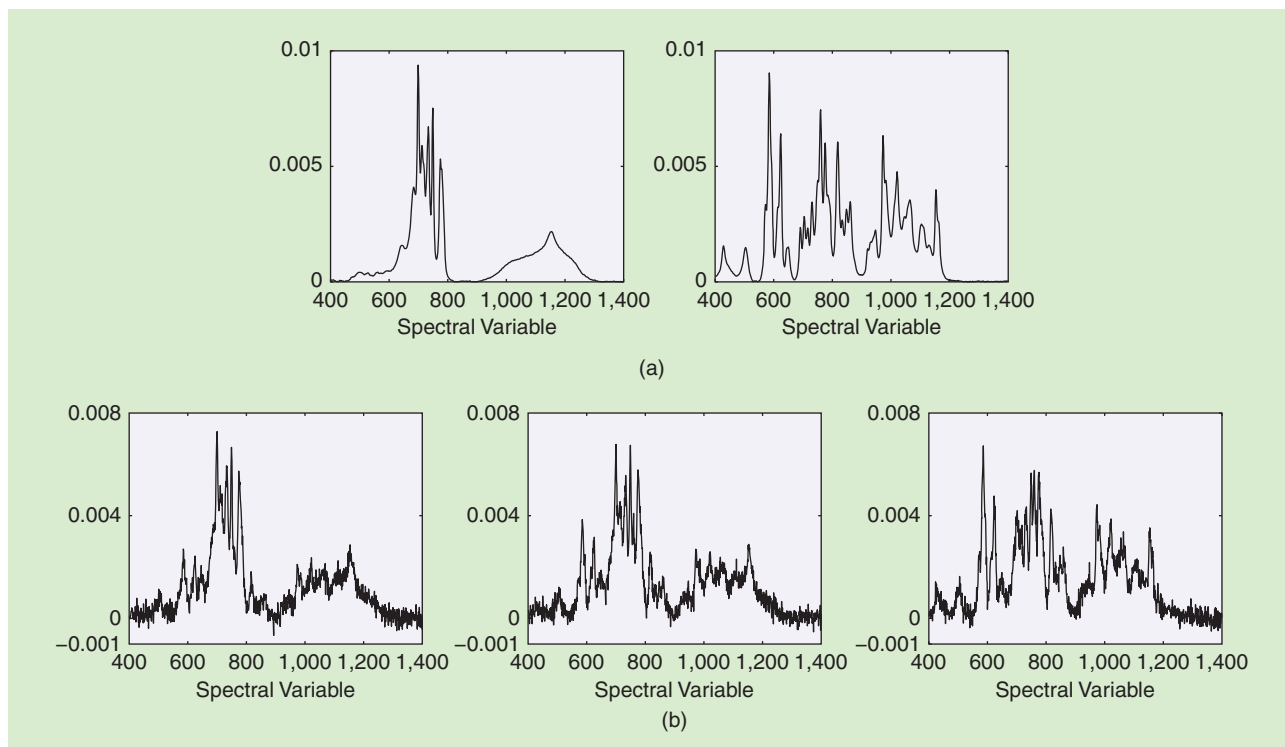


[FIG2] An example of three absorption spectra resulting from the linear mixing of two components with abundance fractions (75%, 25%), (60%, 40%), and (30%, 70%), respectively. (a) Pure component spectra and (b) the mixture spectra.

Additional constraints or assumptions are thus used to select a particular (and meaningful) solution among the feasible ones [11]. The existing methods differ on the way the constraints and the additional assumptions are formulated and how the separation is performed. A short overview of the different approaches is firstly given in this section and an example illustrates the application of one of these techniques to the separation problem.

INDEPENDENT COMPONENT ANALYSIS

As mentioned before, since BSS is an ill-posed inverse problem, prior knowledge and/or additional assumptions should be used to get a unique and correct solution. Principal component analysis (PCA) [12] assumes that the signals to be reconstructed are mutually uncorrelated, but this orthogonality constraint does not ensure the nonnegativity of the solution. A more constraining statistical assumption used for source separation is the mutual independence of the sources, leading to the ICA concept [5], for which many algorithms have been developed (see [5]). If the sought source signals are mutually statistically independent, they can be separated successfully by ICA methods and their nonnegativity will be ensured implicitly (at least, only few negative values appear in the estimates) as reported in [13], where a second-order blind identification algorithm [14] was applied to the analysis of nuclear magnetic resonance (NMR) data. But, when the source signals are not mutually independent or when their mutual independence is not observed due to the finite and small number of samples, the nonnegativity information should be considered. In [15], Plumley showed that it is possible to

incorporate jointly nonnegativity and mutual independence of the sources (see also [5, Ch. 13]). This method yields a correct solution providing the condition of well-grounded sources (i.e., sources having nonvanishing probability distributions around zero) is fulfilled.

MULTIVARIATE CURVE RESOLUTION

This approach, proposed by Lawton and Sylvestre [3], termed *MCR*, first decomposes the data matrix, using PCA, $X = UV$. Then, a linear transformation T is calculated to transform the principal components V and their weight matrix U into nonnegative estimates of pure spectra $S = TV$ and mixing coefficients $A = UT^{-1}$, respectively. Since accounting for nonnegativity alone does not ensure the uniqueness of the solution, this approach leads to several possible values of matrix T that provide the set of admissible (feasible) solutions [3]. To reduce this set, Sasaki et al. [16] suggest adding further constraints, in addition to the nonnegativity, and propose to search a linear transformation T by minimizing a two-term criterion, in which a first part penalizes negative estimates of the pure spectra and mixing coefficients, and the second part uses an entropic cost function to make the estimated spectra smoother and mutually independent. The resulting optimization is given by

$$\min_T \left(\|\min(S, 0)\|_F^2 + \|\min(A, 0)\|_F^2 + \beta \sum_{n=1}^L \sum_{j=1}^N s_j(n) \log s_j(n) \right),$$

where $\|\cdot\|_F$ stands for the Frobenius norm and β is a regularization parameter that allows the adjustment of the tradeoff between

the two parts. The optimization of the whole objective function is performed by using the Nelder–Mead algorithm. However, this method may converge to local or spurious minima since this criterion is nonconvex, and the criterion shape highly depends on the regularization parameters that should be specified manually. This method was revisited in [17] where a simulated annealing optimization algorithm is used. In the signal processing community, the algebraic approach for ICA is very similar to that of Lawton–Sylvestre, but it is based on the statistical independence of the source signals (pure spectra). To get mutually independent signals, the transformation matrix is reduced to a unitary rotation matrix by minimizing a contrast function [5, Ch. 3]. Assuming the independence of the sources leads to a unique solution, but it does not guarantee its nonnegativity.

NONNEGATIVE MATRIX FACTORIZATION

This approach performs a constrained least squares estimation of S and A

$$(\hat{S}, \hat{A}) = \underset{S, A}{\operatorname{argmin}} \|X - AS\|_F^2.$$

This (nonconvex) optimization problem can be solved using alternating least square (ALS) with alternate exact solving [11] or multiplicative [4] alternate update methods. At each iteration k , ALS algorithms minimize alternatively the above criterion with respect to S , keeping A fixed, or to A , keeping S fixed, with nonnegativity constraints [18] on S and A . It leads to solve the following optimization problems

$$\hat{S}^{(k)} = \underset{S}{\operatorname{argmin}} \|X - \hat{A}^{(k-1)}S\|_F^2 \quad \text{s.t. } S \geq 0 \quad (3)$$

$$\hat{A}^{(k)} = \underset{A}{\operatorname{argmin}} \|X - \hat{A}S^{(k)}\|_F^2 \quad \text{s.t. } A \geq 0. \quad (4)$$

Multiplicative methods update iteratively the estimates of the sources and the mixing coefficients using a particular multiplicative learning rule that ensures the nonnegativity [4]. However, since the criterion is nonconvex, NMF algorithms do not lead a unique solution, unless in some particular conditions [19]. Therefore, the NMF results highly depend on the algorithm initialization. Several contributions proposed to initialize the algorithm by the results obtained with an unconstrained decomposition method such as PCA, factor analysis algorithms, or using pure variable detection methods such as simple-to-use interactive self modeling mixture analysis (SIMPLISMA) [20] and orthogonal projection approach (OPA) [21]. In [13], for NMR spectroscopy, it has been shown that ICA methods can be used successfully for the initialization of the ALS approach. However, each initialization leads to a local minimum of the criterion and none of these methods has proven to outperform the others since the result of each method highly depends on the data at hand.

Similarly to the case of curve resolution methods, additional constraints such as sum-to-one (also called *closure* or *full additivity*) and unimodality (i.e., presence of only one maximum in each column of matrix A) may be added to

reduce the set of admissible solutions [22]. The sum-to-one constraint corresponds to assuming that the sum of the elements of each row of matrix A is equal to one (or to a known constant). This is the case for instance in reaction-based systems, where a mass balance equation is obeyed by the concentration profiles of the species present in the system; see, for instance, [23]. However, adding this constraint can alter the separation performance if the number of sources is not correctly selected or if the mixture data are subject to attenuation and variability. A discussion on this point can be found in [24]. Another constraint that reduces the set of admissible solution is the local rank or selectivity [22], which refers to the fact that for certain rows or columns of the data matrix, some mixing coefficients are known to be nonzero while other coefficients are known to have zero values.

There are other constraints that can be taken into account through a penalized least squares estimation approach. This idea is used in positive matrix factorization (PMF) [25] (this work was historically the first one dealing with spectral mixture analysis as a matrix factorization problem under positivity constraints) where the criterion to minimize is

$$\min_{S, A} \left(\|X - AS\|_F^2 + \alpha \|A\|_F^2 + \beta \|S\|_F^2 - \gamma \sum_{n=1}^L \sum_{j=1}^N \log s_j(n) - \delta \sum_{i=1}^M \sum_{j=1}^N \log a_{ij} \right). \quad (5)$$

The hyperparameters γ and δ control the strength of the logarithmic barrier function that prevents negative values of the source samples and mixing coefficients. Hyperparameters α and β allows to adjust the weight of the quadratic regularization criteria. Contrarily to the constrained least squares methods, the PMF approach leads to an unconstrained optimization problem.

It is also possible to consider the sparsity constraint through a penalized least squares approach. Such an idea gives rise to nonnegative sparse coding (NNSC) [26], which searches for minimizing the following cost function

$$\min_{S, A} (\|X - AS\|_F^2 + \beta \|S\|_1) \quad \text{s.t. } A \geq 0 \text{ and } S \geq 0. \quad (6)$$

This approach was applied by [27] for the analysis of magnetic resonance chemical shift imaging data. There are other alternative approaches for reducing the set of admissible solutions; see, for instance, [28] and [29].

BAYESIAN APPROACHES

The formulation of source separation using Bayesian estimation theory is reported in [5, Ch. 12]. Its first application to the separation of spectral mixture data has been proposed in [30]. The spectral mixture separation in a Bayesian framework consist in describing the statistical properties of the measurement noise and assigning parametric a priori distributions $p(S|\theta)$ and $p(A|\theta)$ on the pure component spectra and abundances, respectively. These distribution are defined with some hyperparameters represented by θ . A multivariate Gaussian distribution

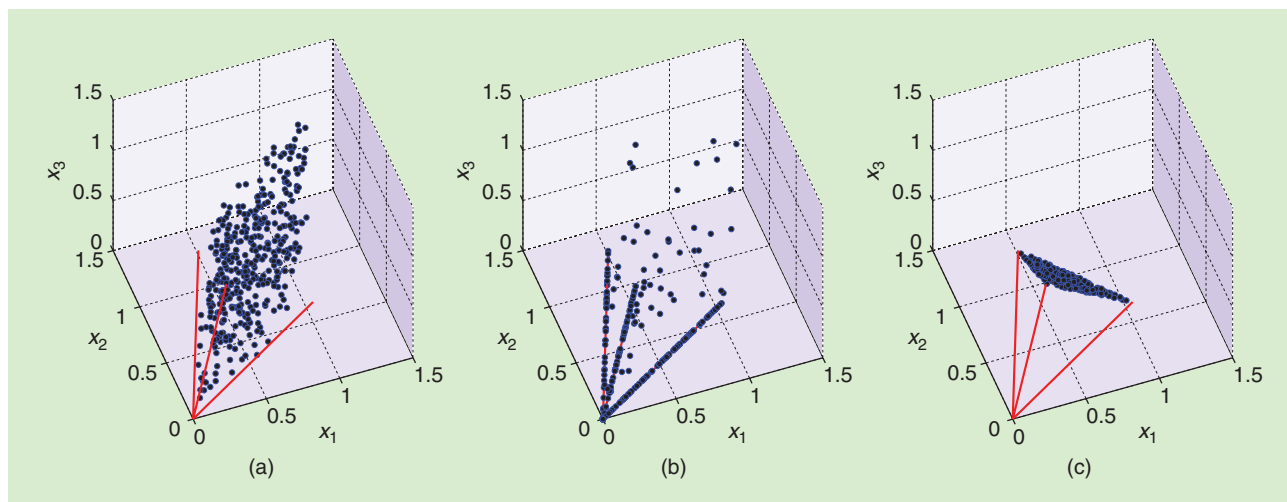


[FIG3] An illustration of the simplicial cone and the empirical distribution of the mixture data for three types of nonnegative sources: (a) uniform well-grounded sources, (b) sparse sources, and (c) uniform sources with sum-to-one mixing constraint.

is generally used to model the noise statistics, which yields the likelihood

$$p(X|A, S, \Sigma) = \mathcal{N}(X - AS; \Sigma),$$

where $\mathcal{N}(\mu, \Sigma)$ stands for the Gaussian distribution with mean μ and covariance matrix Σ . This matrix reduces to $\sigma^2 I_L$ when the noise samples are assumed to be independent and identically distributed. To account for the nonnegativity and the sparsity of the component spectra, a Gamma distribution model was used in [30], while a truncated Gaussian distribution or a Dirichlet distribution can be used to encode the sum-to-one constraint on the mixing coefficients [31].

The key point of the Bayesian approach is to apply Bayes' theorem to express the a posteriori density

$$p(S, A | X, \theta, \Sigma) = p(X | A, S, \theta, \Sigma) p(A | \theta) p(S | \theta, \Sigma) / p(X), \quad (7)$$

from which a statistical inference is conducted to perform the separation. This distribution combines explicitly the available assumptions on the pure component spectra and their abundances with the information coming from the measured data. The inference of the unknown quantities can be conducted by minimizing $J(S, A) = -\log p(S, A | X, \theta)$ or calculating empirical posterior means of S and A after drawing samples from $p(S, A | X, \theta)$ using Monte Carlo Markov chain (MCMC) methods (see [30] and [31] for details). The first approach is equivalent to minimizing a criterion similar to (6) with regularization criteria $\mathcal{R}(A)$ and $\mathcal{R}(S)$ linked to the prior distributions according to $\mathcal{R}(A) = -\log p(A | \theta)$ and $\mathcal{R}(S) = -\log p(S | \theta)$, while the second approach allows to infer all the weighting parameters at the price of a significant increase of the computation time. The Bayesian method was successfully applied for the analysis of hyperspectral data in [32] and chemical reaction monitoring [33].

GEOMETRICAL METHODS

Geometrical methods are based on the empirical distribution (geometrically speaking, the scatter plot) of the mixture data.

Since these data result from a nonnegative mixing of nonnegative data, the scatter plot of the mixed data is contained in the simplicial cone generated by the columns of the mixing matrix [19]. Figure 3 illustrates three examples of mixture data distribution for different types of sources. It can be noted that in the case of sparse sources, each row of S has a dominant peak at some location (column number) where other rows have zero elements, then the problem of finding the columns of the mixing matrix A reduces to the identification of the edges of a simplicial cone, edges where the data are concentrated in Figure 3(b). In the case of sum-to-one mixing, the mixture data will be distributed on a simplex whose vertices correspond to mixture data containing only one component. Thus, each vertex is associated with a column of the mixing matrix A . In [34], efficient algorithms are designed for data where the sources are not well grounded and the mixing matrix does not satisfy the sum-to-one or the pure pixel assumptions. This method can also handle noisy data and was applied to positron emission tomography (PET) imaging and mass spectroscopy.

In chemical imaging spectrometry and remote sensing by hyperspectral imaging [35], [36], the spectral mixture analysis is often handled using a two-step procedure: the pure spectra estimation and the abundance fraction assessment, respectively. In the first step, the pure components of the mixture are identified by using an endmember extraction algorithm (EEA). See, for instance, [37] for a recent performance comparison and discussion on EEAs. The most popular EEA is the N-FINDR algorithm. N-FINDR estimates the pure component spectra by identifying the largest simplex whose vertices are taken from the convex hull of the data. Another popular and faster alternative is the vertex component analysis (VCA) method, which has been proposed in [38]. It works by iteratively estimating the vertices of the simplex without calculating the convex hull. A common assumption in VCA and N-FINDR is the existence of pure pixels (pixels composed of a single component) in the observed data. Alternatively, the minimum volume transform (MVT) finds the smallest simplex that contains all the pixels [39], [40]. The second step of the

spectral unmixing can use various strategies such as those based on constrained least squares estimation [24], [41].

TENSORIAL METHODS

Most of the methods mentioned earlier simply exploit one type of diversity: it leads to a two-way array of data, easily represented by a matrix. The previous examples consider two-way arrays based on space and time (mixtures of signals) or space and frequency (spectral mixtures) dimensions. But in many chemical experiments, one or more additional diversities can be considered, leading to a three-way (or, more generally, a multi-way) array of data, which can be represented by a tensor. As an example, in fluorescence spectroscopy, the (measured) fluorescence intensity depends on three variables: the fluorescence emission spectrum, the absorbance spectrum, and the relative concentration of the components. Of course, tensorial decomposition is not restricted to fluorescence, and other applications include time resolved spectroscopy [42], multidimensional NMR [43], or polarized Raman spectroscopy [44].

Historically, parallel factor analysis, or canonical polyadic decomposition (CPD), inspired from early works on factor analysis in psychometrics, has been intensively studied in chemometrics since the 1990s and was popularized by Bro [18]. Currently, many theoretical contributions and applications are addressing the CPD decomposition of three-way arrays. More details and references of tensorial methods [45] and an application in fluorescence spectroscopy [46] are provided in accompanying articles also found in this issue of *IEEE Signal Processing Magazine*.

APPLICATION EXAMPLE

Calcium carbonate is a chemical material used for a large variety of applications such as filler for plastics or paper. Depending on operating conditions, calcium carbonate crystallizes as calcite, aragonite, or vaterite. The formation of calcium carbonate by mixing two solutions containing, respectively, calcium and carbonate ions takes place in two steps. The first is the precipitation step, which is very fast and provides a mixture of calcium carbonate polymorphs. The second step (a slow process) represents the phase transformation from the unstable polymorphs to the stable one (calcite). The physical properties of the crystallized product depend largely on the polymorphic composition, so it is necessary to quantify these polymorphs when they are mixed. The main purpose of this application is to study the relation of polymorphs and temperature and to explore favorable conditions for calcite formation.

Calcium chloride and sodium carbonate separately dissolved in sodium chloride solutions of the same concentration were rapidly mixed to precipitate calcium carbonate. A sample was collected two minutes after the beginning of the experiment to determine the polymorphic composition at the end of the precipitation step. Raman spectra of this sample have been measured for various temperatures ranging between 20 to 70°C to determine the influence of temperature on the polymorphs precipitation. Moreover for each temperature, Raman spectra were collected at regular time intervals for monitoring the phase transformation.

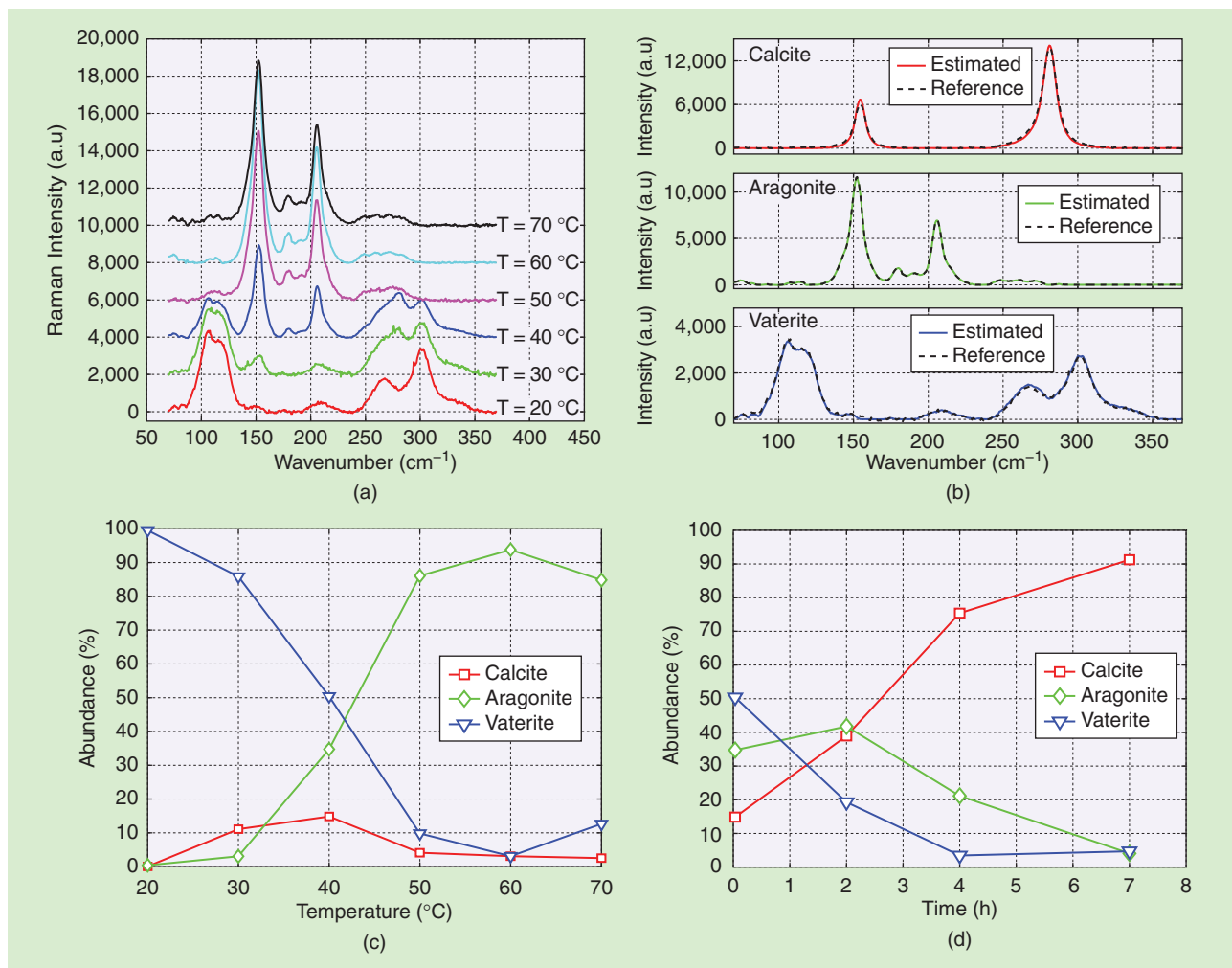
Finally, a total of $M = 37$ spectra (each one obtained for a given temperature and phase transformation time) of $L = 477$ wavelengths are obtained. Details on the experiment can be found in [33]. Figure 4(a) shows six spectra measured at the beginning the phase transformation step.

Figure 4(b) shows the estimated sources using a Bayesian separation approach with a Gamma distribution prior on the sources and a Dirichlet distribution as prior on the mixing coefficients [30], [31]. From the spectroscopic point of view and according to the locations of the vibrational peaks, the identification of the three components is easy. The evolution of the concentration profile versus the temperature is shown in Figure 4(c). It can be deduced that pure vaterite is observed at 20°C and a quite pure aragonite is obtained at 60°C. However, between 20 to 60°C, ternary mixtures are observed. The abundance of calcite is maximal at 40°C, which is in agreement with results reported in the literature. Let us now consider the phase transformation evolution at this temperature value. The concentration profile versus precipitation time at 40°C is shown in Figure 4(d). At the beginning of the phase transformation (two minutes), the ternary mixture is composed of 50% vaterite, 35% aragonite, and 15% calcite. Then, after two hours, the vaterite is transformed to aragonite and calcite. Finally, after seven hours, vaterite and aragonite are almost totally transformed to calcite. So, aging time promotes the formation of calcite.

NONLINEAR MODELS

Although linear mixing models provide a satisfactory first-order approximation of the measurement process in several applications, there are some cases in which an NL model is mandatory. Indeed, exploiting the physical theory behind the measurement transducer allows the increase of the amount of information that can be extracted from the data. For example, the sensitive membrane of potentiometric sensors such as ion-selective electrodes (ISEs) or ion-selective field effect transistors (ISFETs) can be described by the classical Nernst equation [47], which establishes a logarithmic relation between ionic activity and the membrane potential. In this section, we shall discuss how source separation methods can be set to deal with NL mixing models, paying special attention to the illustrative example of ISE arrays. Afterward, some considerations on other types of sensors are made.

ISEs, which are the most used chemical sensors in industry, are simple devices for measuring ionic activity. A well-known example of ISE is the glass electrode, which is used for measuring the pH of a given solution. Besides, one can find ISEs tailored to different ions such as ammonium, potassium, and sodium. These devices have been intensively used, for instance, in food and soil inspection, clinical analysis, and water quality monitoring. One of the reasons that explains the success of ISEs in such applications is the simplicity of this approach. Indeed, ISE-based analyses do not require sophisticated laboratory equipment and procedures and, thus, can be carried out in the field if necessary. Although attractive, potential electrodes such as ISEs and ISFETs suffer from an important drawback: they are not selective, i.e., the generated potential depends on a given target ion but also on other undesirable ions, which are called



[FIG4] The separation of Raman spectra of calcium carbonate: mixture data and separation results. (a) The collected mixture spectra at 2 min after the beginning of the phase transformation for different temperature values. (b) A comparison between the estimated sources (continuous) and the reference spectra (dashed) of the three components. (c) Abundances of the three components at the beginning of the phase transformation for different temperature values. (d) The temporal evolution of the three component abundances at T = 40 °C.

interfering ions [47]. There are some situations in which this interfering process is so weak that it can be neglected. However, this phenomenon may become important when the target ion and the interfering ones have similar physical and/or chemical properties. A possible solution to eliminate this interference effect is to consider the diversity provided by an ISE array using a source separation approach.

The interference in ISE can be modeled through an empirical extension of the Nernst equation called the Nicolsky–Eisenman (NE) equation [47]. According to this model, the response of the i th sensor (dedicated to measure the i th ion) within the array is given by

$$x_i(n) = e_i + d_i \log \left(s_i(n) + \sum_{j, j \neq i} a_{ij} s_j(n)^{z_i/z_j} \right), \quad (8)$$

where d_i and e_i are constants that depend on some physical parameters, z_i and $s_i(n)$ denote the valence and the activity of the i th ion, respectively. The nonnegative parameters a_{ij} , the

selectivity coefficients, explain the influence (interference) of the j th ion on the i th sensor; and n stands for the temporal index.

There are some pairs of ions for which high values of selectivity coefficients are observed. When the valences of the ions are different, the model (8) becomes difficult to deal with because a nonlinearity (power term) appears inside the logarithm term [48]. However, when the valences are equal, which is the most common situation, (8) becomes a special NL model known as the PNL model [49]. Indeed, in PNL systems, there is a linear mixing stage followed by a set of component-wise NL function, which in the case of ISE arrays correspond to logarithms. As mentioned before, an interesting property of PNL models is that, under conditions that are close to those required in the linear case [5], the application of ICA leads to source separation.

NONLINEAR INDEPENDENT COMPONENT ANALYSIS

For equal valences, when the number of mixtures and sources is the same, the mixing process described in (8) can be

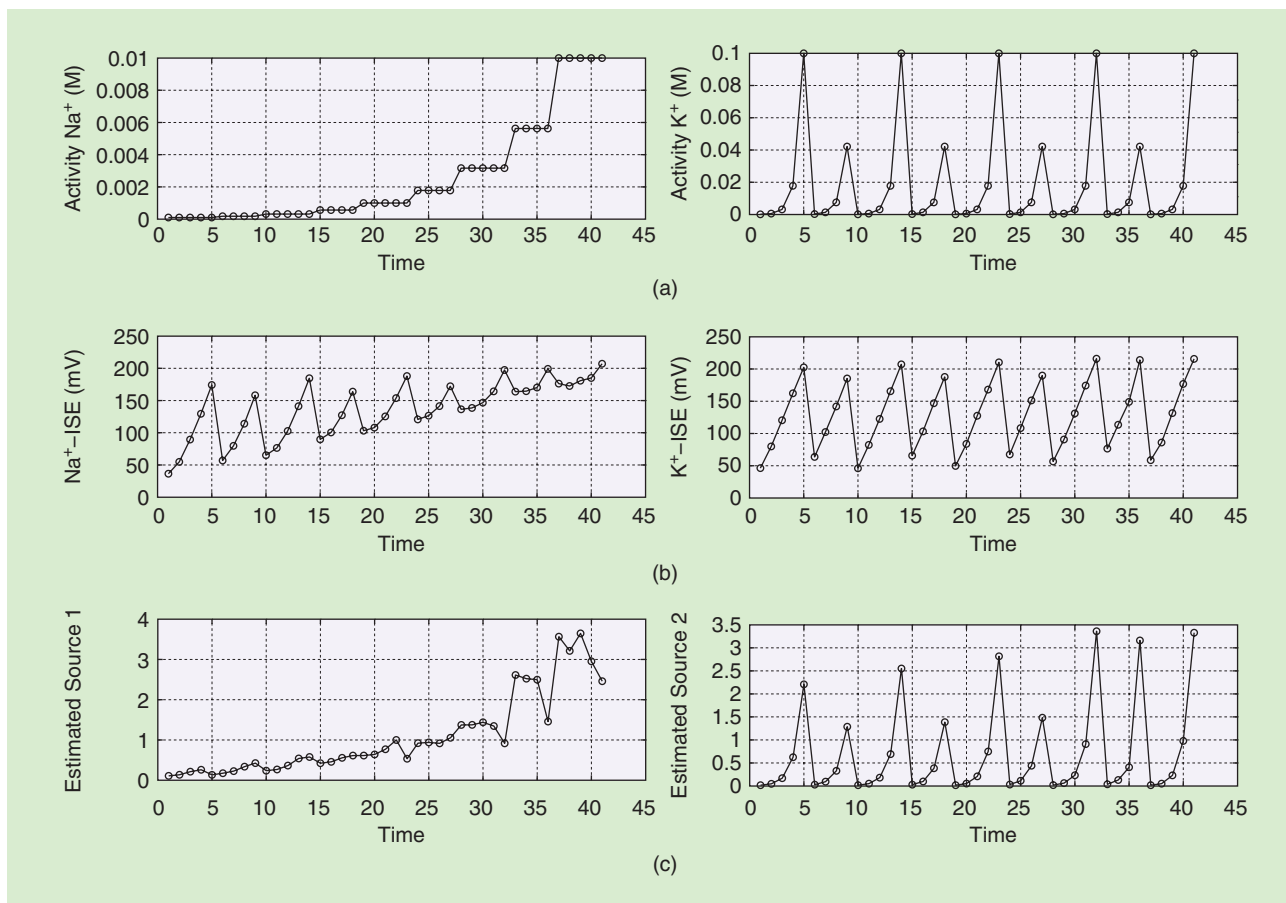


[FIG5] An experiment with data acquired by an array composed of a sodium and a potassium ISE. Sources: (a) activities of sodium and potassium, (b) array response, and (c) retrieved sources.

counterbalanced by a separating system in which each estimated source is given by

$$y_k(n) = \sum_{i=1}^M w_{ki} \exp(f_i + h_i x_i(n)), \text{ for } k = 1, \dots, N, \quad (9)$$

where w_{ki} , f_i , and h_i are unknown parameters that must be adjusted and M the number of sensors and N the number of target ions—actually, the parameters f_i only introduce a scale ambiguity, which is usual in BSS, and, therefore, can be fixed a priori to a given value.

As in the linear case, the adjustment of PNL separating models can be performed by means of ICA, but some care must be taken while developing the separation algorithm. For instance, one must resort to stronger independence measures such as the mutual information. The adjustment of the separating system is thus carried out by the following optimization problem

$$\min_{w_{ki}, h_i} \mathcal{I}(y_1(n), \dots, y_N(n)), \quad (10)$$

where $\mathcal{I}(y_1, \dots, y_N)$ denotes the mutual information between the estimated signals $y(n)$. There are several algorithms for solving (10), where main difficulties are related to the

estimation of the mutual information and to the existence of spurious local minima in this cost function. In [50], for instance, the optimization problem expressed in (10) was tackled by a bioinspired optimization method that is robust to convergence to local minima and does not require the calculation of the derivatives of (10). Moreover, [50] adopts a mutual information estimator based on order statistics.

To illustrate the application to a real situation of the ICA method [50], we considered an experiment where the data was acquired by an array composed of a sodium and a potassium ISE (two mixtures). Therefore, there are two mixtures and two sources (the activities of potassium and sodium). Data acquisition was achieved via a flow-injection analysis system, which usually increases the stability and the sensitivity of the array. In Figure 5(a), the actual sources are depicted. As a result of the low selectivity of each sensor within the array, the acquired signals correspond to NL mixtures of the sources, which is illustrated in Figure 5(b). After solving the problem (10), the retrieved sources are shown in Figure 5(c). Despite the reduced number of samples (41 points), the ICA technique was able to provide signals that are good approximations of the original sources. A more detailed description of this experiment is provided in [51].

BAYESIAN APPROACH

Bayesian source separation can also be applied in the context of ISE arrays. Actually, differing from ICA, whose basis lies in the independence assumption, the Bayesian approach does not introduce a measure of independence but it searches a solution allowing to jointly explain the data according to the mixing model and fulfill some prior knowledge. Similarly to the linear case [see (7)], the posterior distribution in the NL case is given by

$$p(s, A, g | x) = p(x | A, s, g)p(A)p(s)p(g)/p(x), \quad (11)$$

where the vector g includes the parameters associated with the logarithmic functions [see (8)]. As in the linear case, the inference step can be done based on a set of samples drawn from the posterior distribution via MCMC methods. The main difficulty when dealing with NL models using MCMC methods is the need to draw samples from distributions for which a classical sampling method may be inefficient. In [49], by relying on lognormal prior distributions on $p(s)$, limited support Gaussian densities on $p(g)$, we showed the relevance of accounting for the nonnegativity constraint and introducing auxiliary variables to handle the sampling difficulties.

EXPLOITING OTHER PRIOR INFORMATION

In addition to the nonnegativity of the sources, other prior information can be considered when developing NL source separation methods. For example, in [52], a method exploiting the assumption that the sources are bandlimited is proposed to compensate the NL stage of PNL systems. The advantage brought by this approach is that, once the NL component-wise functions are counterbalanced, the resulting separation problem becomes linear and, therefore, can be dealt with by means of linear BSS methods. In the context of ISE arrays, assuming bandlimited sources is realistic since the signals of interest have a spectral content concentrated on low-frequency bands. The approach proposed in [52] was applied in the analysis of the ions ammonium and potassium, leading to a good estimation of the sensors' nonlinearities.

Other prior information that can be considered is the existence of silent periods of a given ion, i.e., time windows in which the concentration of a given ion is approximately zero. Interestingly, this scenario is close to that of found in speech separation and can be interpreted as a sparsity-based approach. In [48], a method that uses this information was proposed to estimate the parameters d_i of (8) in the case where the valences of the ions are different. In this situation, as can be noted in (8), the mixing model is much more complex than PNL model, and, thus, estimating the nonlinearities at first usually simplifies the problem.

LINEAR-QUADRATIC MIXING MODEL

In addition to the complex model (8) considered in the context of ISE arrays for analyzing ions with different valences,

there is another relevant class of models that arises in chemical analysis: the linear-quadratic (LQ) model ([5, Ch. 14]). An interesting aspect of the LQ mixture is that it can be seen as a linear mixture of dependent sources. Such a feature simplifies the derivation of separation algorithms in this case. According to the Clifford–Touma equation [53], the mixing process that takes place in the analysis of two gases by using a tin oxide gas sensor can be described by an LQ model.

Moreover, LQ models also arise in the context of hyperspectral imaging, especially when there are multiple reflexions caused by the presence of buildings or trees [36]. This is an interesting problem since hyperspectral imaging is closely related to the above-mentioned problems of separating spectra. Such a model is also considered in fluorescence spectroscopy of highly concentrated solution, involving a screen effect, and a possible method for solving this problem is proposed in [54].

CONCLUSIONS AND FURTHER CHALLENGES

In this article, we presented an overview on how source separation methods can be applied in chemical analysis. We briefly discussed some kinds of chemical data and presented several approaches that can be applied. A typical characteristic of chemical data is the existence of prior information on the sources and the mixing process. These priors have motivated researchers working on the subject to consider alternatives to the framework of ICA, thus showing that, besides being an exciting field of application to classical BSS methods, chemical analysis may also be inspiring environment for novel BSS paradigms. Another interesting aspect of this relatively new field of applications is related to the challenges that are found when developing separation methods, e.g., NL mixtures and dependent sources.

Despite the current advances achieved in source separation for chemical data, there are still many issues that must be tackled.

MIXING MODELS

A first important point concerns the mixing models that should be adopted. Indeed, transducer physics gives realistic mixing models whose processing in a raw version or even after some simplifications will provide very challenging signal processing problems. Moreover, most of the models give a static description, i.e., we assume that the mixtures follow an instantaneous model. Therefore, if a dynamical mixing model were available, it would be possible to take advantage of the sensor's dynamics to obtain better separation results. This could be achieved by considering convolutive models.

NOISE AND MEASUREMENT PROCESS MODELING

Another difficult aspect that must be handled in chemical analysis is the existence of noise and other complex

phenomena. In ISEs, for instance, since there are NL elements in the transducer stage, there may be a strong noise amplification during the separation process—one can show that a separation method based on inversion leads to a multiplicative noise model [49]. Moreover, in the context of spectral unmixing, finding realistic noise models for nonnegative sources is still an open issue. Finally, when dealing with chemical sensors one may find hysteresis, which is an NL and dynamical phenomenon that is very difficult to model.

SOURCE NUMBER

Assessing how many sources are present in a mixture data is one of the oldest questions in signal analysis and remains of huge interest for the application of source separation methods to real applications. In the linear mixing model, additive noise and mutually uncorrelated sources, it is generally addressed by a subspace analysis approach. However, the theory behind such analysis breaks down when dealing with either NL mixing models or nonnegative sources. For instance, by considering nonnegativity in the linear mixing model the source number corresponds to the nonnegative rank, which is different from the classical matrix rank. Fortunately, when dealing with mixture data obtained from some chemical reaction monitoring, the number of sources can be known in advance, thanks to the chemical theory.

ENHANCING THE DATA ACQUISITION SETUP

The performances of any signal processing method will highly depend on how much the data fulfill the method hypotheses. For instance, the application of NMF will be more efficient when the sources are well grounded, when there is some pure pixels in the spectral image, and, more generally, when the uniqueness conditions are respected. It would be therefore useful to pay attention on how to design the measurement setup in such a way to meet, at best, these conditions or how to introduce additional measurement modalities to make the mixture analysis problem more tractable. In that respect, chemists play a fundamental role here especially in data acquisition. There is a great number of different acquisition techniques, even for the same kind of analysis, and many properties, such as temperature, pH, pressure, and humidity, that when correctly controlled by a chemist, may lead to a good diversity within the acquired data. Therefore, to further advance in the application of source separation in chemistry, the collaboration between researchers in the fields of AC and signal processing should be reinforced, even more than before.

ACKNOWLEDGMENTS

This work has been partially funded by the European project ERC-2012-AdG-320684-CHESS. Leonardo T. Duarte would like to thank FAPESP (São Paulo, Brazil) for funding his research.

TO FURTHER ADVANCE IN THE APPLICATION OF SOURCE SEPARATION IN CHEMISTRY, THE COLLABORATION BETWEEN RESEARCHERS IN THE FIELDS OF AC AND SIGNAL PROCESSING SHOULD BE REINFORCED, EVEN MORE THAN BEFORE.

AUTHORS

Leonardo Tomazeli Duarte (leonardo.duarte@fca.unicamp.br) received the B.S. and M.Sc. degrees in electrical engineering from Campinas University (Brazil) in 2004 and 2006, respectively, and the Ph.D. degree from the Grenoble Institute of Technology (Grenoble INP), France, in 2009. He is currently an assistant professor at the School of

Applied Sciences at Campinas University. His research interests are mainly associated with the theory of unsupervised signal processing and include signal separation, independent component analysis, Bayesian methods, and applications in chemical sensors and seismic signal processing. He is a Member of the IEEE.

Saïd Moussaoui (Saïd.Moussaoui@ircsyn.ec-nantes.fr) received the state engineering degree from Ecole Nationale Polytechnique, Algiers, Algeria, in 2001, and the Ph.D. degree in automatic control and signal processing from the Université Henri Poincaré, Nancy, France, in 2005. He is currently an associate professor at Ecole Centrale de Nantes, Nantes, France. Since 2006, he has been with the Institut de Recherche en Communications et Cyberétique de Nantes (IRCCYN, UMR CNRS 6597). His research interests are in the development of advanced methods for statistical signal and image processing including source separation, Bayesian estimation, numerical optimization, and their applications in spectrometry and hyperspectral imaging.

Christian Jutten (Christian.Jutten@gipsa-lab.grenoble-inp.fr) received the Ph.D. degree in signal processing from the Grenoble Institute of Technology (1981) and docteur ès sciences degree in physics from the University of Grenoble (1987). He has been a full professor at the University Joseph Fourier of Grenoble since 1989. He was visiting professor at EPFL (Lausanne, Switzerland) in 1989 and Campinas University (Brazil) in 2010. His research interests are statistical signal processing and especially source separation including theoretical aspects and applications (brain imaging, hyperspectral imaging, chemical sensing). He is a coauthor of more than 75 papers in international journals, four books, 25 invited plenary talks, and 170 communications in international conferences. He is a member of the Institut Universitaire de France (2008–present) and obtained an ERC Advanced grant in 2012.

REFERENCES

- [1] L. Duval, L. T. Duarte, and C. Jutten, "An overview of signal processing issues in chemical sensing," in *Proc. IEEE Int. Conf. Acoustics, Speech and Signal Processing (ICASSP)*, 2013, pp. 8742–8746.
- [2] J. N. Miller and J. C. Miller, *Statistics and Chemometrics for Analytical Chemistry*. Englewood Cliffs, NJ: Prentice Hall, 2005.
- [3] W. H. Lawton and E. Sylvestre, "Self-modeling curve resolution," *Technometrics*, vol. 13, no. 3, pp. 617–633, 1971.
- [4] D. Lee and H. Seung, "Learning the parts of objects by non-negative matrix factorization," *Nature*, vol. 401, no. 6755, pp. 788–791, 1999.
- [5] P. Comon and C. Jutten, Eds., *Handbook of Blind Source Separation: Independent Component Analysis and Applications*. New York: Academic, 2010.
- [6] C. Jutten and J. Héroult, "Blind separation of sources, part I: An adaptive algorithm based on neuromimetic architecture," *Signal Process.*, vol. 24, no. 1, pp. 1–10, 1991.

- [7] P. Comon, "Independent component analysis: A new concept?" *Signal Process.*, vol. 36, no. 3, pp. 287–314, 1994.
- [8] L. Duarte, C. Jutten, P. Temple-Boyer, A. Benyahia, and J. Launay, "A dataset for the design of smart ion-selective electrode arrays for quantitative analysis," *IEEE Sensors J.*, vol. 10, no. 12, pp. 1891–1892, 2010.
- [9] E. Malinowski, *Factor Analysis in Chemistry*, 3rd ed. New York: Wiley, 2000.
- [10] H. Pfeiffer and H. Liebhafsky, "The origins of Beer's law," *J. Chem. Educ.*, vol. 28, no. 3, p. 123, 1951.
- [11] R. Tauler, A. Izquierdo-Ridora, and E. Casassas, "Simultaneous analysis of several spectroscopic titrations with self-modelling curve resolution," *Chemometrics Intell. Lab. Syst.*, vol. 18, no. 3, pp. 293–300, 1993.
- [12] H. Hotelling, "Analysis of a complex of statistical variables into principal components," *J. Educ. Psychol.*, vol. 24, no. 6, pp. 417–441, 1933.
- [13] D. Nuzillard and J.-M. Nuzillard, "Application of blind source separation to 1-D and 2-D nuclear magnetic resonance spectroscopy," *IEEE Signal Processing Lett.*, vol. 5, no. 8, pp. 209–211, 1998.
- [14] A. Belouchrani, K. Abed-Meraim, J.-F. Cardoso, and E. Moulines, "A blind source separation technique using second-order statistics," *IEEE Trans. Signal Processing*, vol. 45, no. 2, pp. 434–444, Feb. 1997.
- [15] M. Plumbley, "Algorithms for non-negative independent component analysis," *IEEE Trans. Neural Networks*, vol. 14, no. 3, pp. 534–543, 2003.
- [16] K. Sasaki, S. Kawata, and S. Minami, "Constrained nonlinear method for estimating component spectra from multicomponent mixtures," *Appl. Opt.*, vol. 22, no. 22, pp. 3599–3606, 1983.
- [17] E. Widjaja and M. Garland, "Pure component spectral reconstruction from mixture data using SVD, global entropy minimization, and simulated annealing. numerical investigations of admissible objective functions using a synthetic 7-species data set," *J. Computat. Chem.*, vol. 23, no. 9, pp. 911–919, 2003.
- [18] R. Bro, "PARAFAC, tutorial and applications," *Chemometrics Intell. Lab. Syst.*, vol. 38, no. 2, pp. 149–171, 1997.
- [19] D. Donoho and V. Stodden, "When does non-negative matrix factorization give a correct decomposition into parts?" in *Proc. Advances in Neural Information Processing Systems (NIPS)*, Cambridge, MA, 2003, pp. 1141–1148.
- [20] W. Windig and J. Guilment, "Interactive self-modeling mixture analysis," *Anal. Chem.*, vol. 63, no. 14, pp. 1425–1432, 1991.
- [21] F. C. Sanchez, J. Toft, B. van den Bogaert, and D. L. Massart, "Orthogonal projection approach applied to peak purity assessment," *Anal. Chem.*, vol. 68, no. 1, pp. 79–85, 1996.
- [22] R. Tauler, "Calculation of maximum and minimum band boundaries of feasible solutions for species profiles obtained by multivariate curve resolution," *J. Chemometrics*, vol. 15, no. 8, pp. 627–646, 2001.
- [23] A. de Juan, Y. V. Heyden, R. Tauler, and D. Massart, "Assessment of new constraints applied to the alternating least squares method," *Anal. Chim. Acta*, vol. 346, no. 3, pp. 307–318, 1997.
- [24] E. Chouzenoux, M. Legendre, S. Moussaoui, and J. Idier, "Fast constrained least squares spectral unmixing using primal-dual interior-point optimization," *IEEE J. Select. Topics Appl. Earth Observ. Remote Sensing*, vol. 7, no. 1, pp. 59–69, Jan. 2014.
- [25] P. Paatero and U. Tapper, "Positive matrix factorization: A nonnegative factor model with optimal utilization of error estimates of data values," *Environmetrics*, vol. 5, no. 2, pp. 111–126, 1994.
- [26] P. O. Hoyer, "Non-negative matrix factorization with sparseness constraints," *J. Mach. Learn. Res.*, vol. 5, pp. 1457–1469, Nov. 2004.
- [27] P. Sajda, S. Du, T. Brown, R. Stoyanova, D. Shungu, X. Mao, and L. Parra, "Non-negative matrix factorization for rapid recovery of constituent spectra in magnetic resonance chemical shift imaging of the brain," *IEEE Trans. Medical Imaging*, vol. 23, no. 12, pp. 1453–1465, 2004.
- [28] A. de Juan, S. Navea, J. Diewok, and R. Tauler, "Local rank exploratory analysis of evolving rank-deficient systems," *Chemometrics Intell. Lab. Syst.*, vol. 70, no. 1, pp. 11–21, 2004.
- [29] L. Miao and H. Qi, "Endmember extraction from highly mixed data using minimum volume constrained nonnegative matrix factorization," *IEEE Trans. Geosci. Remote Sensing*, vol. 45, no. 3, pp. 765–777, 2007.
- [30] S. Moussaoui, D. Brie, A. Mohammad-Djafari, and C. Carteret, "Separation of non-negative mixture of non-negative sources using a Bayesian approach and MCMC sampling," *IEEE Trans. Signal Processing*, vol. 54, no. 11, pp. 4133–4145, 2006.
- [31] N. Dobigeon, J.-Y. Tourneret, and C.-I. Chang, "Semi-supervised linear spectral unmixing using a hierarchical Bayesian model for hyperspectral imagery," *IEEE Trans. Signal Processing*, vol. 56, no. 7, pp. 2684–2695, 2008.
- [32] S. Moussaoui, H. Hauksdóttir, F. Schmidt, C. Jutten, J. Chanussot, D. Brie, S. Douté, and J. Benediktsson, "On the decomposition of Mars hyperspectral data by ICA and Bayesian positive source separation," *Neurocomputing*, vol. 71, no. 10–12, pp. 2194–2208, June 2008.
- [33] C. Carteret, A. Dandeu, S. Moussaoui, H. Muhr, B. Humbert, and E. Plasari, "Polymorphism studied by lattice phonon Raman spectroscopy and statistical mixture analysis method," *Cryst. Growth Des.*, vol. 9, no. 2, pp. 807–812, 2009.
- [34] W. S. B. Ouedraogo, A. Soulloumiac, M. Jaidane, and C. Jutten, "Simplicial cone shrinking algorithm for unmixing nonnegative sources," in *Proc. Int. Conf. Acoustics, Speech and Signal Processing (ICASSP)*, 2012, pp. 2405–2408.
- [35] C.-I. Chang, *Hyperspectral Data Exploitation*. New York: Wiley Interscience, 2007.
- [36] J. M. Bioucas-Dias, A. Plaza, N. Dobigeon, M. Parente, D. Qian, P. Gader, and J. Chanussot, "Hyperspectral unmixing overview: Geometrical, statistical, and sparse regression-based approaches," *IEEE J. Select. Topics Appl. Earth Observ. Remote Sensing*, vol. 5, no. 2, pp. 354–379, Apr. 2012.
- [37] A. Plaza, P. Martínez, R. Perez, and J. Plaza, "A quantitative and comparative analysis of endmember extraction algorithms from hyperspectral data," *IEEE Trans. Geosci. Remote Sensing*, vol. 42, no. 3, pp. 650–663, Mar. 2004.
- [38] J. M. P. Nascimento and J. M. Bioucas-Dias, "Vertex component analysis: A fast algorithm to unmix hyperspectral data," *IEEE Trans. Geosci. Remote Sensing*, vol. 43, no. 4, pp. 898–910, Apr. 2005.
- [39] M. D. Craig, "Minimum-volume transforms for remotely sensed data," *IEEE Trans. Geosci. Remote Sensing*, vol. 32, no. 3, pp. 542–552, May 1994.
- [40] L. Miao and H. Qi, "Endmember extraction from highly mixed data using minimum volume constrained nonnegative matrix factorization," *IEEE Trans. Geosci. Remote Sensing*, vol. 45, no. 3, pp. 765–777, Mar. 2007.
- [41] S. Moussaoui, E. Chouzenoux, and J. Idier, "Primal-dual interior point optimization for penalized least squares estimation of abundance maps in hyperspectral imaging," in *Proc. IEEE Workshop Hyperspectral Image and Signal Processing: Evolution in Remote Sensing (WHISPERS'12)*, Shanghai, China, June 2012.
- [42] A. Niazi, J. Ghasemi, and A. Yazdanipour, "PARAFAC decomposition of three-way kinetic-spectrophotometric spectral matrices based on phosphomolybdenum blue complex chemistry for nitrite determination in water and meat samples," *Anal. Lett.*, vol. 38, no. 14, pp. 2377–2392, 2005.
- [43] M. Nilsson, A. Botana, and G. Morris, "T1-diffusion-ordered spectroscopy: Nuclear magnetic resonance mixture analysis using parallel factor analysis," *Anal. Chem.*, vol. 81, no. 19, pp. 8119–8125, 2009.
- [44] S. Miron, M. Dossot, C. Carteret, S. Margueron, and D. Brie, "Joint processing of the parallel and crossed polarized Raman spectra and uniqueness in blind nonnegative source separation," *Chemometrics Intell. Lab. Syst.*, vol. 105, no. 1, pp. 7–18, 2011.
- [45] G. Zhou, A. Cichocki, Q. Zhao, and S. Xie, "Nonnegative matrix and tensor factorizations," *IEEE Signal Processing Mag.*, vol. 31, no. 3, pp. 54–65, May 2013.
- [46] P. Comon, "Tensors," *IEEE Signal Processing Mag.*, vol. 31, no. 3, pp. 44–53, May 2013.
- [47] P. Gründler, *Chemical Sensors: An Introduction for Scientists and Engineers*. New York: Springer, 2007.
- [48] L. T. Duarte and C. Jutten, "A nonlinear source separation approach to the Nicksolsky-Eisenman model," in *Proc. 16th European Signal Processing Conf., EU-SIPCO 2008*.
- [49] L. T. Duarte, C. Jutten, and S. Moussaoui, "A Bayesian nonlinear source separation method for smart ion-selective electrode arrays," *IEEE Sensors J.*, vol. 9, no. 12, pp. 1763–1771, 2009.
- [50] L. T. Duarte, R. Suyama, R. R. F. Attux, F. J. V. Zuben, and J. M. T. Romano, "Blind source separation of post-nonlinear mixtures using evolutionary computation and order statistics," in *Independent Component Analysis and Blind Signal Separation* (ser. Lecture Notes in Computer Science). Berlin: Springer, 2006, vol. 3889, pp. 66–73.
- [51] L. T. Duarte, J. M. T. Romano, C. Jutten, K. Y. Chumbimuni-Torres, and L. T. Kubota, "Application of blind source separation methods to ion-selective electrode arrays in flow-injection analysis," submitted for publication.
- [52] L. T. Duarte, R. Suyama, B. Rivet, R. Attux, J. M. T. Romano, and C. Jutten, "Blind compensation of nonlinear distortions: Application to source separation of post-nonlinear mixtures," *IEEE Trans. Signal Processing*, vol. 60, no. 11, pp. 5832–5844, 2012.
- [53] N. Yamazoe and K. Shimano, "Theory of power laws for semiconductor gas sensors," *Sens. Actuators B*, vol. 128, no. 2, pp. 566–573, 2008.
- [54] X. Luciani, S. Mounier, R. Redon, and A. Bois, "A simple correction method of inner filter effects affecting FEEM and its application to the PARAFAC decomposition," *Chemometrics Intell. Lab. Syst.*, vol. 96, no. 2, pp. 227–238, 2009.

[Rafael F. Schaefer and Holger Boche]



IMAGE PUBLISHED BY INGRAM PUBLISHING

Physical Layer Service Integration in Wireless Networks

[Signal processing challenges]

It is becoming more important that next-generation wireless networks wisely integrate multiple services at the physical layer to increase spectral efficiency. In this article, physical layer service integration in wireless networks is considered, where senders not only transmit individual data to certain receivers but also integrate additional multicast or confidential services that have to be kept secret from nonlegitimate receivers. In this context, physical layer security techniques are becoming a promising complement to cryptographic techniques since they establish security using only the physical properties of the wireless channel. State-of-the-art solutions for certain important communication scenarios are discussed, and signal processing challenges and promising research directions are identified.

Digital Object Identifier 10.1109/MSP.2013.2271190

Date of publication: 7 April 2014

MOTIVATION

Significant progress has recently been made in improving the performance of current third-generation/fourth-generation cellular networks. Techniques such as high-speed downlink packet access/high-speed uplink packet access; multiuser multiple input, multiple output (MIMO); channel adaptive scheduling; cooperative multipoint transmission; and relaying can increase spectral efficiency.

An additional research area that is gaining importance is the efficient implementation of services at the physical layer. For example, in current cellular systems, operators offer not only traditional services such as (bidirectional) voice communication but also multicast services and/or confidential services that are subject to certain secrecy constraints. Today, the integration of multiple services is realized by higher-layer policies that allocate different services on different logical channels. The security issue is usually addressed by applying cryptographic techniques at higher levels. In general, this is quite inefficient, and there is a trend to merge multiple coexisting services efficiently so that they work on the same wireless resources. This is

referred to as *physical layer service integration* and has the potential to significantly increase the spectral efficiency for next-generation wireless networks and, especially, fifth-generation cellular networks. These networks will not only be designed to realize traditional communication but will also be applied to machine-to-machine communication or sensor networks, which have strict requirements on security and robustness. This is being intensively discussed by the Third Generation Partnership Project (3GPP) Long-Term Evolution Advanced (LTE-Advanced) group [1].

Multicast services can efficiently be realized by common messages. For example, the Multimedia Broadcast Multicast Service, as specified by the 3GPP organization [2], [3], or the Multicast and Broadcast Service in Worldwide Interoperability for Microwave Access, commonly known as WiMax [4], benefit from such studies. This substantiates the concern of merging such services efficiently on the physical layer so that the broadcast nature of the wireless medium is advantageously exploited.

If such services are not required to be kept secret from nonlegitimate receivers, they are classified as *public services*. Accordingly, services that have this additional secrecy requirement are classified as *confidential services*. Currently, secrecy techniques on higher layers such as cryptographic-based techniques have a wide variety of uses and usually rely on the assumption of the unproven hardness of certain problems or on the insufficient computational capabilities of nonlegitimate receivers. Because of increasing computational power, recent advances in number theory, and improved algorithms, there is also interest in identifying alternative approaches for establishing security.

The security of confidential information becomes even more important in wireless networks since such systems are inherently vulnerable to eavesdropping due to the open nature of the wireless medium. On the other hand, the physical properties of the wireless channel make the communication easily accessible to external wiretappers, but they also offer possibilities for establishing security by approaches other than cryptographic techniques.

In this context, the concept of physical layer security is becoming more attractive since it solely uses the physical properties of the wireless channel to establish security [5]–[8]. So regardless of what transformation is applied to the signals that are received by nonlegitimate receivers, the original message

cannot be reproduced. Therefore, such approaches provide so-called unconditional security and, not surprisingly, are identified by operators and national agencies as promising and important tasks for next-generation mobile networks [9], [10]. Since the wireless channel has a huge impact on the performance of wireless systems, the analysis of information theoretic security for different models of channel uncertainty is an impor-

tant research field and, thus, indispensable for bringing this concept into practice. Thereby, uncertainty models that take both kinds of effects into account are needed: those that are based on the nature of the wireless medium and those that are due to implementational issues.

There are currently many research activities that analyze the efficient integration of different services at the physical layer, but most of them tackle this problem from an information theoretic point of view. This means that their main goal is to derive capacity results or to characterize coding strategies that result in certain rate regions. Along with this comes the unsatisfying fact that most activities end when a certain characterization of a rate region is obtained. Unfortunately, for the practically relevant case of multiple transmit and receive antennas, such descriptions are usually given by a union over all possible transmit covariance matrices satisfying certain power constraints.

For further implementational developments, it is also important to treat physical layer service integration from a signal processing point of view and analyze such capacity descriptions in more detail. In particular, spatial MIMO techniques as well as optimal or complexity-efficient transmit strategies have to be characterized. Such strategies are usually given by optimization problems. For the simultaneous integration of multiple services and, especially, of confidential services, such optimization problems turn out to be generally nonconvex.

To pave the way for practical implementation, there is the need to intensify the efforts analyzing physical layer service integration from a signal processing point of view. Therefore,

OPERATORS OFFER NOT ONLY TRADITIONAL SERVICES SUCH AS (BIDIRECTIONAL) VOICE COMMUNICATION BUT ALSO MULTICAST SERVICES AND/OR CONFIDENTIAL SERVICES THAT ARE SUBJECT TO CERTAIN SECRECY CONSTRAINTS.

the main objective of this article is to review the state-of-the-art solutions and to point out where further studies are needed and those that are promising.

PRINCIPLES OF PHYSICAL LAYER SERVICE INTEGRATION

We restrict the discussion to small networks to focus on the key ideas of how to efficiently integrate different services at the physical layer. To highlight the key ideas and insights, we usually consider the simplest possible scenario. However, the results are also relevant for larger networks since they provide valuable insights into how strategies or heuristics for service integration in larger networks should be designed. This is most obviously the case for multicast services, where ideas presented for two receivers naturally extend to more than two receivers. But general insights regarding the optimal processing structure, such as superimposing different data streams or rate splitting techniques obtained for simple scenarios, are also valuable for larger networks.

Unless otherwise noted, we consider a simple three-node network with one transmitter and two receivers, as shown in Figure 1. In the most general setup, the aim of the transmitter is to provide individual, multicast, and confidential services simultaneously and as efficiently as possible. Since spatial MIMO techniques can improve the performance significantly [11], we especially concentrate on the case where the transmitter and receivers are equipped with multiple antennas. Therefore, let N_T be the number of transmit antennas and N_i be the number of antennas at receiver i , $i = 1, 2$. The discrete-time, real-valued, input–output relation between the transmitter and receiver i can then be modeled as

$$y_i = H_i x + n_i, \tag{1}$$

where $y_i \in \mathbb{R}^{N_i \times 1}$ denotes the output at receiver i , $H_i \in \mathbb{R}^{N_i \times N_T}$ the multiplicative channel matrix, $x \in \mathbb{R}^{N_T \times 1}$ the input at the transmitter, and $n_i \in \mathbb{R}^{N_i \times 1}$ the independent additive noise according to a Gaussian distribution $\mathcal{N}(0, I_{N_i})$ with zero mean and identity covariance matrix. We consider an average transmit power constraint $\text{tr}(Q) \leq P$, where $Q = \mathbb{E}\{xx^T\}$ denotes the transmit covariance matrix.

Individual and multicast services belong to the class of public services, which means that they are not required to be kept secret from nonlegitimate receivers, and the only task is to integrate them as efficiently as possible to allow for high data rates. On the other hand, services with such a security requirement belong to the class of confidential services. Here, we are confronted with two different intentions: these services should be integrated as efficiently as possible, but more importantly, they have to be secure from nonlegitimate receivers.

To guarantee the confidentiality of the transmitted message, we require that

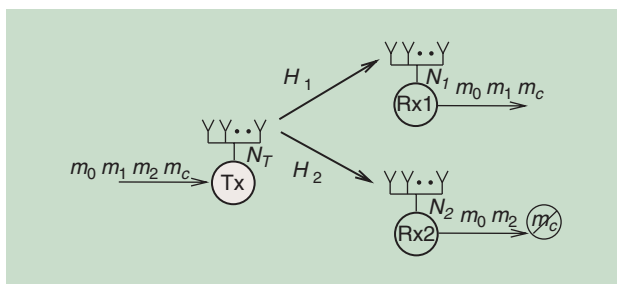


[FIG1] The general scenario of physical layer service integration in a three-node network. The transmitter provides private, common, and confidential services.

$$I(M_c; Y_2^n) \underset{n \rightarrow \infty}{\rightarrow} 0, \tag{2}$$

where n denotes the code block length. Thus, the mutual information between the confidential message M_c and the output Y_2^n at the nonlegitimate receiver has to be small [5], [8], [12]. This is known as physical layer, or information theoretic, strong secrecy and ensures that even if the nonlegitimate receiver has its channel output Y_2^n , it still has no knowledge

about the transmitted confidential message M_c . Recently, it has been shown that the strong secrecy criterion has the following operational meaning: no matter how the nonlegitimate receiver tries to decode the confidential message, the average probability of error tends exponentially fast to one, cf., for example, [13]–[16]. This paves

the way for operators to provide confidential services with guaranteed, i.e., provable, secrecy.

There exists a weaker notion of secrecy where the mutual information term is additionally normalized by the block length n , i.e., we require $(1/n)I(M_c; Y_2^n) \rightarrow 0$ as $n \rightarrow \infty$. This criterion is known as *weak secrecy* and has the drawback that no operational meaning has been given to it yet. However, this secrecy criterion is widely assumed and was first analyzed by Wyner and subsequently by Csiszár and Körner in their landmark articles [17] and [18].

PUBLIC SERVICES

We start with the scenario where there are only public services to be integrated at the physical layer. The aim is to do it in such a way that the data rates are maximized to allow for high spectral efficiency.

UNICAST SERVICES

The broadcast channel (BC), which corresponds to the downlink scenario in a cellular network, serves as a starting point. Here, the base station wants to transmit individual messages to several receivers, where each receiver is only interested in its own message. The BC with individual messages is well understood, and the optimal processing for multiple antennas

can be found in [19]. The capacity region C_{BC} of the two-user MIMO Gaussian BC is given by

$$C_{BC} = \text{co}(\mathcal{R}_{12} \cup \mathcal{R}_{21}),$$

where \mathcal{R}_{12} is given by all rate pairs $(R_1, R_2) \in \mathbb{R}_+^2$ that satisfy

$$R_1 \leq \frac{1}{2} \log \left| \frac{I_{N_1} + H_1 Q_1 H_1^T + H_1 Q_2 H_1^T}{I_{N_1} + H_1 Q_2 H_1^T} \right| \quad (3a)$$

$$R_2 \leq \frac{1}{2} \log |I_{N_2} + H_2 Q_2 H_2^T| \quad (3b)$$

for some $Q_1, Q_2 \geq 0$ with $\text{tr}(Q_1 + Q_2) \leq P$. Region \mathcal{R}_{21} is obtained by exchanging the indices 1 and 2 in (3).

The downlink scenario is well studied from a signal processing point of view as well. It is shown that capacity can be achieved by dirty paper coding (DPC), where the regions \mathcal{R}_{12} and \mathcal{R}_{21} describe the different (dirty paper) encoding orders, cf., for example, [11], [20]. There is also a duality theory between the MIMO Gaussian BC and multiple-access channel (MAC), which allows the transfer of optimal processing strategies from the MAC to the corresponding BC [21]–[23]. Beamforming with individual signal-to-interference-plus-noise ratio constraints is discussed in [24].

MULTICAST SERVICES

Besides individual messages, operators of cellular systems also offer multicast services such as common video streams or common signaling data.

Multicast communication can efficiently be realized by common messages. Thus, the aim of the transmitter is to transmit a common message in such a way that all receivers can decode it. Obviously, with the input–output relation given in (1), the maximal multicast rate $R_0 \in \mathbb{R}_+$ is characterized by the following optimization problem:

$$R_0 = \max_{\text{tr}(Q) \leq P} \min_{i \in \{1, 2\}} \left\{ \frac{1}{2} \log |I_{N_i} + H_i Q H_i^T| \right\}. \quad (4)$$

Such problems are known as max–min fair optimization problems since the overall aim is to maximize the smallest (single-user) rate over the receivers subject to the transmit power.

If the processing at the transmitter is restricted to beamforming, i.e., the transmit covariance matrix has to be rank one, we know the problem has been well studied in literature, cf., for example, [25]–[28] and the references therein. Unfortunately, even for beamforming, the problem in (4) is shown to be non-deterministic polynomial-time hard or NP-hard [25], which makes it difficult to characterize the optimal transmit covariance matrix in detail. Thus, convex relaxations of this problem have been considered [25], [28]. The feasible signal-to-noise ratio (SNR) region for multicast beamforming is analyzed in [26] and [27].

The problem of multicasting can also be interpreted from a channel state information (CSI) point of view. Instead of

transmitting one common message to several receivers, the scenario can also be interpreted as a point-to-point transmission with one receiver, where the channel is not exactly known to the users. It is only known that the actual channel realization belongs to a set of prespecified channels. In this case, the transmission rate has to be chosen such that it works for all channels simultaneously. This corresponds to the model of compound channels [29]–[31]. Thus, the optimization problem in (4) can also be interpreted as a robust optimization problem for a point-to-point link with channel uncertainty, cf., for example, [32] and [33].

While the transmission of a single multicast message to several receivers is somewhat understood, the integration of multicast and individual services is much more involved and less understood. The capacity region for the MIMO Gaussian BC with common and individual messages can be found in [34] and [35]. The achievability of this region was proposed in [34] and recently established as capacity region in [35] by showing its optimality. Although the efficient integration of multicast and individual services is known in terms of transmission rates, the optimal or complexity-efficient transmit strategies are still unknown and have to be analyzed.

CONFIDENTIAL SERVICES

Next, we discuss the efficient integration of confidential services. We concentrate on the simplest model incorporating secrecy, which is the so-called wiretap channel. Here, a sender wants to transmit a confidential message to a legitimate receiver while keeping this message completely secret from a nonlegitimate eavesdropper. Since the wireless channel has a huge impact on the communication, it is important to study information theoretic security for different models of CSI.

PERFECT CSI

The wiretap channel [17], [36]–[44] can be regarded as the basic scenario of the efficient implementation of a secure point-to-point transmission in the presence of an external eavesdropper. With the secrecy criterion (2), the secrecy capacity $R_S \in \mathbb{R}_+$ of the MIMO Gaussian wiretap channel is given by

$$R_S = \max_{\text{tr}(Q) \leq P} \left(\frac{1}{2} \log |I_{N_1} + H_1 Q H_1^T| - \frac{1}{2} \log |I_{N_2} + H_2 Q H_2^T| \right), \quad (5)$$

where H_1 is the channel to the legitimate receiver, and H_2 is the channel to the nonlegitimate eavesdropper.

This specifies the maximal transmission rate for the MIMO Gaussian wiretap channel. Note that the optimal input is Gaussian distributed with zero mean, but unfortunately, it does not directly characterize in detail the optimal signal processing, since the capacity-achieving transmit covariance matrix is given by an optimization over all matrices that satisfy the power constraint. In addition, the optimization problem in (5) is nonconvex in general, and the optimal transmit covariance matrix is only known for some special cases.

For the multiple-input, single-output (MISO) scenario, where the transmitter has multiple antennas and the legitimate receiver

and eavesdropper have only a single antenna, the optimal transmit strategy is known in closed form, cf. [38], [39], [43]–[45]. Denoting the channel vectors by $\mathbf{h}_1 \in \mathbb{R}^{N_T \times 1}$ and $\mathbf{h}_2 \in \mathbb{R}^{N_T \times 1}$, the optimization problem reduces to

$$R_S = \max_{\text{tr}(Q) \leq P} \frac{1}{2} \log \frac{1 + \mathbf{h}_1^T Q \mathbf{h}_1}{1 + \mathbf{h}_2^T Q \mathbf{h}_2},$$

and the solution is given by

$$R_S = \frac{1}{2} \log(\lambda_{\max}(\mathbf{I}_{N_T} + P \mathbf{h}_1 \mathbf{h}_1^T, \mathbf{I}_{N_T} + P \mathbf{h}_2 \mathbf{h}_2^T)),$$

where λ_{\max} is the largest generalized eigenvalue of the two matrices $\mathbf{I}_{N_T} + P \mathbf{h}_1 \mathbf{h}_1^T$ and $\mathbf{I}_{N_T} + P \mathbf{h}_2 \mathbf{h}_2^T$. In addition, the secrecy capacity is achieved by beamforming, i.e., the optimal transmit covariance matrix is of rank one, in the direction of the generalized eigenvector of λ_{\max} [39], [43]. Subsequently, closed-form solutions of the optimal beamforming vector and the corresponding secrecy capacity have been established in [38] and [44].

For the general MIMO case, the problem becomes much more intricate. For a general matrix power constraint, the optimal transmit strategy is derived in [42] using the relation between mutual information and minimum mean square error (I-MMSE relation). The high SNR regime has been studied in [40]. But the general MIMO case is still an open problem, and only partial results are available [38], [45]–[47]. In particular, only properties of the optimal transmit covariance matrix are available. For example, a necessary condition for an optimal transmit strategy is to transmit in the positive directions of $\mathbf{H}_1^T \mathbf{H}_1 - \mathbf{H}_2^T \mathbf{H}_2$, i.e., the directions where the channel to the legitimate receiver is stronger than the one to the eavesdropper [44], [45].

PARTIAL CSI

The assumption of perfect CSI at all nodes is quite unrealistic in practical wireless systems due to the nature of the wireless medium but also due to implementational issues such as imperfect or quantized channel estimation or limited feedback schemes. Moreover, CSI of the eavesdropper channel is especially questionable since a nonlegitimate receiver will not report its channel conditions to the transmitter.

To model channel uncertainty, the concept of compound channels [29]–[31] is designated because it not only perfectly captures the phenomena of the wireless medium but also includes these implementational issues of practical systems. Moreover, the concept of compound channels ensures the reliability and secrecy for all possible channel realizations in the set. Thus, it provides a certain guaranteed performance. This is desirable, especially for the transmission of confidential information, since the information must be kept secret under all circumstances. The usual

procedure is to first study the compound scenario for a finite set of channels and then extend these results to arbitrary, possibly nonfinite, sets of channels. In general, this can be done as in [29]–[31] by approximation arguments.

The corresponding compound wiretap channel is studied in [13], [14], [48], where the exact channels to the legitimate receiver and the eavesdropper are not known; rather, it is only known that they belong to the set of channels \mathcal{S} and \mathcal{T} . Such sets can be given in an abstract way by letting them contain a, possibly infinite, number of channel realizations. But there are also other more concrete uncertainty sets possible that fall in the framework of compound channels. For example, motivated by the fact that the true channel realization will always be in a certain area around its rough channel estimation, the channel uncertainty of the eavesdropper channel can be modeled by a (spherical) set

$$\mathcal{T} := \{\mathbf{H}_{2,s} : \|\mathbf{H}_{2,s} - \hat{\mathbf{H}}_2\|_F \leq \epsilon_2\} \quad (6)$$

with $\|\cdot\|_F$ the Frobenius norm. Here, $\hat{\mathbf{H}}_2$ is the channel estimation, and ϵ_2 is the corresponding estimation error bound. Another valid model for the channel uncertainty of the eavesdropper would be

to assume that his received channel gain is bounded by a spectral norm constraint as

$$\mathcal{T} := \{\mathbf{H}_{2,s} : \|\mathbf{H}_{2,s}\|_2 = \max_{|\mathbf{x}|=1} |\mathbf{H}_{2,s} \mathbf{x}| \leq \epsilon_2\}$$

with $\|\cdot\|_2$ the spectral norm. Here, $|\mathbf{H}_{2,s} \mathbf{x}|$ represents the channel gain in transmit direction \mathbf{x} and, hence, $\|\mathbf{H}_{2,s}\|_2$ corresponds to the largest channel gain. This characterizes the scenario where the eavesdropper cannot approach the transmitter beyond a minimum protection distance. All these examples fall in the concept of compound channels, where the transmitter has to ensure that reliability and secrecy is guaranteed for the whole (uncertainty) set of channels.

The secrecy capacity of the degraded MIMO Gaussian compound wiretap channel for the weak secrecy criterion with arbitrary finite uncertainty sets \mathcal{S} and \mathcal{T} is established in [48] and is given by

$$R_S = \max_{\text{tr}(Q) \leq P} \left(\min_{s \in \mathcal{S}} \frac{1}{2} \log |I_{N_1} + \mathbf{H}_{1,s} Q \mathbf{H}_{1,s}^T| - \max_{t \in \mathcal{T}} \frac{1}{2} \log |I_{N_2} + \mathbf{H}_{2,t} Q \mathbf{H}_{2,t}^T| \right).$$

The compound wiretap channel under the strong secrecy criterion is analyzed in [13] and [14], where an achievable secrecy rate is given for discrete memoryless channels as

$$\max_X \left(\min_{s \in \mathcal{S}} I(X; Y_{1,s}) - \max_{t \in \mathcal{T}} I(X; Y_{2,t}) \right),$$

where $I(X; Y_{1,s})$ denotes the mutual information between the transmitter and the legitimate receiver for channel realization

ALTHOUGH SECURE COMMUNICATION IS OFTEN UNDERSTOOD FROM THE CODING POINT OF VIEW, IT IS RARELY STUDIED FROM A SIGNAL PROCESSING POINT OF VIEW.

$s \in \mathcal{S}$, and $I(X; Y_{2,t})$ denotes the mutual information between the transmitter and the eavesdropper for realization $t \in \mathcal{T}$.

The analysis reveals the characteristic structure of the secure communication. The secrecy rate is limited by the worst channel to the legitimate receiver and the best channel to the eavesdropper. This agrees with the intuition that one has to prepare for the worst to ensure reliable and secure communication. Further, this shows that the communication experiences a degradation in performance, but in principle, secure communication is possible under channel uncertainty.

Although secure communication is often understood from the coding point of view, it is rarely studied from a signal processing point of view. The next important step is to analyze optimal and complexity-efficient transmit strategies. To obtain such transmit covariance matrices, an optimization problem has to be solved, which is, in general, nonconvex. There are connections to multicast scenarios, as the channel uncertainty to the legitimate receiver can be interpreted as transmitting to a whole group of legitimate receivers and, similarly, the uncertainty to the wiretapper can be interpreted as keeping a whole group of nonlegitimate receivers ignorant.

At any rate, some preliminary studies have been done. The MISO wiretap channel under channel uncertainty is studied in [49], which tackles the nonconvex optimization problem by a semidefinite programming approach. The special case of spherical uncertainty, cf. (6), is studied in [50], where an explicit solution of the worst-case secrecy rate is derived. In [51], the worst-case secrecy rate is optimized by transferring the nonconvex optimization problem into a quasi-convex problem that can be efficiently solved. Some further work on the MIMO Gaussian compound wiretap channel can be found in [52]. The secrecy capacity in the high SNR regime is studied from a secrecy degree of freedom point of view in [48] and [53]. Robust beamforming in MIMO Gaussian wiretap channels under channel uncertainty is considered in [54]. The secrecy capacity for the MIMO Gaussian wiretap channel with eavesdropper channel uncertainty based on the spectral norm constraint is derived in [81].

ACTIVE EAVESDROPPERS

So far, we have only considered passive eavesdroppers, which are nonlegitimate receivers eavesdropping on the transmission to solely capture the confidential information. We want to briefly mention that one can also think of active eavesdroppers, or jammers, who have the ability to influence the channel conditions of the legitimate users.

The case where the eavesdropper is able to control his channel state is discussed in [55]–[57] for various scenarios. In [58]–[60], both channels—the one to the legitimate receiver and the one to the eavesdropper—may vary in an arbitrary and unknown manner. This can be interpreted as a scenario where

the eavesdropper is able to control both channels. Thus, if he is not able to intercept the confidential information, he can try to disturb the communication between the transmitter and the legitimate receiver. Interestingly, in such scenarios, new phenomena of superactivation appear in the sense that two orthogonal arbitrarily varying wiretap channels, each with zero secrecy capacity, i.e., useless for secure transmission, can be superactivated to a useful channel allowing for secure communication at nonzero secrecy rates [61], [82].

Another scenario of active or more powerful wiretappers is the case where the nonlegitimate receiver has some certain prior knowledge, or side information, about the transmitted message avail-

able. This is studied in [62]–[64], and it is shown that side information at the nonlegitimate receiver does not decrease the secrecy capacity of the wiretap channel. Again, there are only some preliminary results available, and there is a need to study it in detail from a signal processing point of view.

NETWORK STRUCTURE

We have discussed the basic principles of physical layer service integration. Next, we want to tackle more complicated networks and show how the existing network structure can be efficiently exploited to further increase the spectral efficiency. In particular, side information, which is available at transmitters or receivers due to a certain network structure, can be exploited efficiently to increase data rates and security.

INTERACTION OF PUBLIC AND CONFIDENTIAL SERVICES

We want to go one step further and address the efficient integration of public and confidential services within the same network. This is much more involved than the basic wiretap channel. Here, we are confronted with two different intentions: on the one hand, the services should be integrated as efficiently as possible to allow for high data rates; on the other hand, some services have to be secure from nonlegitimate receivers. Because of the security issue, the interaction of security-achieving coding strategies with appropriate signal processing schemes becomes very important.

OPTIMAL INTEGRATION

The efficient integration of multicast services and confidential services was first considered in [18]. This is the first time that a strategy for efficient service integration of public and confidential services is presented. In more detail, let us go back to our scenario with one transmitter and two receivers. The transmitter has a common message intended for both receivers and a confidential message for one legitimate receiver, which has to be kept secret from the other nonlegitimate receiver, cf. (2). The secrecy capacity region of the corresponding MIMO Gaussian BC with common

BECAUSE OF THE SECURITY ISSUE, THE INTERACTION OF SECURITY-ACHIEVING CODING STRATEGIES WITH APPROPRIATE SIGNAL PROCESSING SCHEMES BECOMES VERY IMPORTANT.

and confidential messages is studied in [65] and is given by all rate pairs $(R_0, R_c) \in \mathbb{R}_+^2$ that satisfy

$$R_c \leq \frac{1}{2} \log |I_{N_1} + H_1 Q_c H_1^T| - \frac{1}{2} \log |I_{N_2} + H_2 Q_c H_2^T| \quad (7a)$$

$$R_0 \leq \min_{i \in \{1,2\}} \left\{ \frac{1}{2} \log \left| \frac{I_{N_i} + H_i (Q_c + Q_0) H_i^T}{I_{N_i} + H_i Q_c H_i^T} \right| \right\} \quad (7b)$$

for some $Q_c, Q_0 \geq 0$ with $\text{tr}(Q_c + Q_0) \leq P$. Interestingly, it is shown that for multiantenna systems, this strategy is given by a superposition of efficient processing for the public communication, i.e., Q_0 , and for the confidential communication, i.e., Q_c . Although the general structure is known, the optimal transmit strategies still need to be analyzed and characterized in detail.

There is also some work on the compound BC with confidential messages [66], where an achievable secrecy rate region is given by all rate pairs $(R_0, R_c) \in \mathbb{R}_+^2$ that satisfy

$$R_c \leq \min_s I(X; Y_{1,s} | U) - \max_t I(X; Y_{2,t} | U)$$

$$R_0 \leq \min_{s,t} \{I(U; Y_{1,s}), I(U; Y_{2,t})\}$$

for random variables $U - X - (Y_{1,s}, Y_{2,t})$. Again, this indicates that integration of public and confidential services at the physical layer is also possible under channel uncertainty.

Furthermore, this gives valuable insights for further studies, as in the case with more than one confidential message, such as the MIMO Gaussian BC with a common message and two confidential messages [67], [68].

COMPUTATION OF OPTIMAL TRANSMIT COVARIANCE MATRICES

As argued above, the optimal transmit covariance matrices Q_c and Q_0 in (2) are determined by nonconvex optimization problems, as are the weighted rate sum optimal rate pairs. Hence, obtaining the optimal transmit covariance matrices and the boundary of the capacity region is, in general, nontrivial.

In the following, for the MISO scenario, we present one way the optimization problem can be reformulated such that it becomes convex and therewith tractable. Denoting the channel vectors by h_1 and h_2 , the region in (2) can be rewritten as

$$R_c \leq \frac{1}{2} \log(1 + h_1^T Q_c h_1) - \frac{1}{2} \log(1 + h_2^T Q_c h_2) \quad (8)$$

$$R_0 \leq \min_{i \in \{1,2\}} \left\{ \frac{1}{2} \log \left(\frac{1 + h_i^T (Q_c + Q_0) h_i}{1 + h_i^T Q_c h_i} \right) \right\}. \quad (9)$$

As in [65], one can follow the framework in [69] and consider a reparameterization of the rates as

$$R_c = \log(1 + \alpha \gamma_c)$$

$$R_0 = \log(1 + \alpha \gamma_0),$$

where α is an auxiliary parameter, and γ_c and γ_0 can be interpreted as received SNR “weights.” Combining this one obtains a set of linear constraints

$$h_1^T Q_c h_1 - h_2^T Q_c h_2 \geq \alpha \gamma_c (1 + h_2^T Q_c h_2) \quad (10a)$$

$$h_i^T Q_0 h_i \geq \alpha \gamma_0 (1 + h_i^T Q_c h_i), i = 1, 2 \quad (10b)$$

$$\text{tr}(Q_c + Q_0) \leq P \quad (10c)$$

$$Q_c \geq 0, Q_0 \geq 0. \quad (10d)$$

Instead of using (7) to check if a rate pair is in the capacity region, one can alternatively look for positive semidefinite matrices Q_c and Q_0 that satisfy the conditions above. Since all of these conditions are linear in Q_c and Q_0 , this problem belongs to the class of convex optimization problems that can be solved efficiently.

Obviously, all rates increase as the auxiliary parameter α increases. Thus, one obtains the weighted rate sum optimal rate pair on the boundary of the capacity region for fixed weights γ_c and γ_0 by finding the maximum α such that (10) provides at least one feasible solution [65]. Finally, running through all weight vectors with $\gamma_c + \gamma_0 = 1$ yields all weighted rate sum optimal rate pairs and characterizes the boundary of the capacity region.

This approach is based on the framework in [69] and has been applied to several communication scenarios to obtain optimal transmit strategies for the MISO case. In [65], it was applied to the MIMO Gaussian BC with common and confidential messages and in [34] to the MIMO Gaussian BC with common and multiple individual messages. In [70] and [71], it was used in the context of bidirectional relaying.

BIDIRECTIONAL RELAYING

We consider the scenario where two users within the same cell want to communicate with each other with the help of the base station. Here, the efficiency of the downlink phase can be significantly increased by exploiting available side information at the receivers. Both users transmit the messages they want to exchange in the initial uplink phase to the base station. In the succeeding downlink phase, both receivers can use their own message from the previous phase as side information for decoding, as shown in Figure 2. This is known as bidirectional relaying, or two-way relaying, and it leads to significant gains [72]–[74], showing that individual services can be much more efficiently integrated if available side information is exploited. If

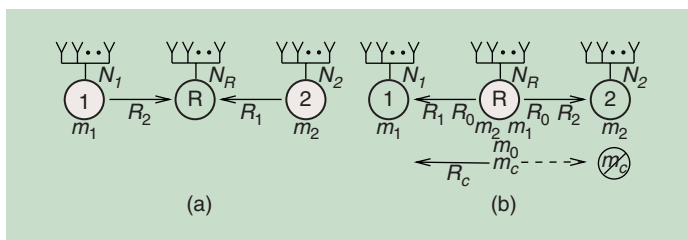


[FIG2] The physical layer service integration in decode-and-forward bidirectional relaying. In the initial MAC phase, nodes 1 and 2 transmit their messages m_1 and m_2 with rates R_2 and R_1 to the relay node. Then, in the bidirectional broadcast phase, the relay forwards the messages m_1 and m_2 as a common message m_0 with rate R_0 to the communication, and further, a confidential message m_c for node 1 with rate R_c , which should be kept secret from node 2. (a) The MAC phase and (b) the bidirectional broadcast phase.

the relay only establishes the bidirectional communication, the individual rates are given by

$$R_1 \leq \frac{1}{2} \log |I_{N_1} + H_1 Q H_1^T|$$

$$R_2 \leq \frac{1}{2} \log |I_{N_2} + H_2 Q H_2^T|$$

for some $Q \geq 0$ with $\text{tr}(Q) \leq P$. This shows that the exploitation of the available side information at the receiving nodes leads to significant gains in transmission rates compared to (3), which does not utilize available side information at the receivers. Optimal transmit strategies are further analyzed for the broadcast phase in [73] and [74], where it is shown that beamforming is always optimal for the MISO scenario.

This extends to multicast services [75] and confidential services [16], [71], [76] as follows. Besides establishing the bidirectional communication, the relay integrates an additional common message for both nodes and a confidential message for one node, which has to be kept secret from the other nonlegitimate node. For an additional common message, the capacity region is given by all rate triples $(R_0, R_1, R_2) \in \mathbb{R}_+^3$ that satisfy

$$R_0 + R_i \leq \frac{1}{2} \log |I_{N_i} + H_i Q H_i^T|, \quad i = 1, 2,$$

for some $Q \geq 0$ with $\text{tr}(Q) \leq P$. Again, the available side information leads to significant gains compared to [34], which considers the corresponding scenario without side information at the receivers. Interestingly, the available side information at the receivers results in a shift in optimal processing. While in [34] there is a superposition coding-based approach applied, the side information at the receivers allows us to use a rate splitting approach. The result is that only one transmit covariance matrix has to be optimized. Moreover, it is shown that optimal transmit strategies for bidirectional relaying with and without a common message are closely related so that the

optimal signal processing from one scenario carries over to the other one [75].

For the integration of additional confidential services, we obtain

$$R_c \leq \frac{1}{2} \log |I_{N_1} + H_1 Q_c H_1^T| - \frac{1}{2} \log |I_{N_2} + H_2 Q_c H_2^T|$$

$$R_i \leq \frac{1}{2} \log \left| \frac{I_{N_i} + H_i(Q_c + Q_p)H_i^T}{I_{N_i} + H_i Q_c H_i^T} \right|, \quad i = 1, 2,$$

for some $Q_c, Q_p \geq 0$ with $\text{tr}(Q_c + Q_p) \leq P$. For the MISO case, the optimal transmit covariance matrices can be obtained using the same approach as discussed in the “Interaction of Public and Confidential Services” section, cf. [70], [71].

THE CONCEPT OF PHYSICAL LAYER SERVICE INTEGRATION HAS THE POTENTIAL TO SIGNIFICANTLY INCREASE THE SPECTRAL EFFICIENCY OF WIRELESS NETWORKS.

BASE STATION COOPERATION

Another example is the cooperation between different base stations, where they coordinate their transmission to the user terminals—also known as coordinated multipoint (CoMP) transmission. This can be

modeled by a MAC with conferencing encoders [77]–[79], as shown in Figure 3. The capacity region for the single antenna case is given by all rate pairs $(R_1, R_2) \in \mathbb{R}_+^2$ that satisfy

$$R_1 \leq \frac{1}{2} \log(1 + \beta_1 P_1) + C_{12}$$

$$R_2 \leq \frac{1}{2} \log(1 + \beta_2 P_2) + C_{21}$$

$$R_1 + R_2 \leq \frac{1}{2} \log(1 + \beta_1 P_1 + \beta_2 P_2) + C_{12} + C_{21}$$

$$R_1 + R_2 \leq \frac{1}{2} \log(1 + P_1 + P_2 + 2\sqrt{P_1 P_2 \beta_1 \beta_2})$$

for all $0 \leq \beta_1, \beta_2 \leq 1$ with $\bar{\beta}_i = 1 - \beta_i$. The striking observation is that the capacities of the cooperation links lead directly to gains in the air.

The ability of cooperation between the transmitters leads to significant gains in capacity. Not surprisingly, this can also be exploited to enable secure communication, as discussed in [80].

Again, this is mostly treated from a coding point of view, and there is a great demand for developing optimal transmit strategies from a signal processing point of view that takes the cooperation capability into account.

CONCLUSIONS

Because of recent research activities, there has been significant progress in the efficient integration of different services on the physical layer. To date, most of this work has been done only from an information theoretic point of view. This means that, for certain scenarios, capacity results are derived, or coding strategies and corresponding rate regions are characterized. Thereby, it is shown that the concept of physical layer service integration has the potential to significantly increase the spectral efficiency of wireless networks. To bring this concept into practice, it is

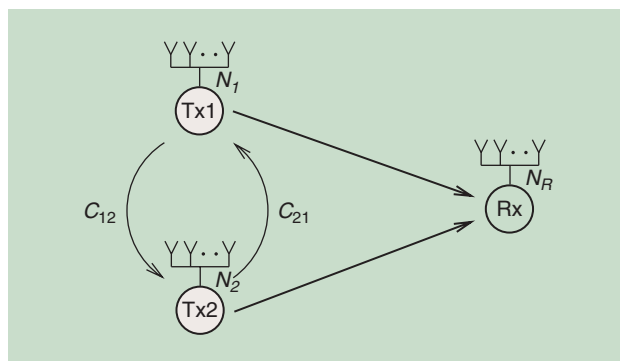


[FIG3] A CoMP transmission, where two senders can use their exchange pipes with capacities C_{12} and C_{21} to coordinate their transmission.

important to treat physical layer service integration from a signal processing point of view as well. Thus, building on these (capacity) results, the next step must be to analyze spatial MIMO techniques and to characterize optimal or complexity-efficient transmit strategies to make these results practically more relevant.

ACKNOWLEDGMENTS

The work of Rafael F. Schaefer was supported by the German Research Foundation under grant WY 151/2-1. The work of Holger Boche was supported in part by the German Ministry of Education and Research under grant 01BQ1050 and by the German Research Foundation under grant BO 1734/25-1.

AUTHORS

Rafael F. Schaefer (rafaelfs@princeton.edu) received his Dipl.-Ing. degree in electrical engineering and computer science in 2007 from the Technische Universität Berlin, Germany, and his Dr.-Ing. degree in electrical engineering in 2012 from the Technische Universität München, Germany. He worked as a research and teaching assistant at the Heinrich-Hertz-Lehrstuhl für Mobilkommunikation at the Technische Universität Berlin from 2007 to 2010 and at the Lehrstuhl für Theoretische Informationstechnik at the Technische Universität München from 2010 to 2013. He is currently a postdoctoral research fellow with the Department of Electrical Engineering at Princeton University. He is a Member of the IEEE.

Holger Boche (boche@tum.de) received his Dipl.-Ing. and Dr.-Ing. degrees in electrical engineering from the Technische Universität Dresden, Germany, in 1990 and 1994, respectively. He graduated in mathematics from the Technische Universität Dresden in 1992. From 1994 to 1997, he did postgraduate studies in mathematics at the Friedrich-Schiller Universität Jena, Germany. He received his Dr.rer.nat. degree in pure mathematics from the Technische Universität Berlin, Germany, in 1998. He is a member of the IEEE Signal Processing Society SPCOM and SPTM Technical Committee. He was elected a member of the German Academy of Sciences (Leopoldina) in 2008 and of the Berlin Brandenburg Academy of Sciences and Humanities in 2009. He was a coreipient of the 2006 IEEE Signal Processing Society Best Paper Award and recipient of the 2007 IEEE Signal Processing Society Best Paper Award. He is a Fellow of the IEEE.

REFERENCES

- [1] 3rd Generation Partnership Project. [Online]. Available: www.3gpp.org/
- [2] 3GPP, "E-UTRAN, overall description stage 2," TS 36.300 V9.0.0 Rel. 9, 2009.
- [3] 3GPP, "Multimedia broadcast/multicast service (MBMS); Architecture and functional description," TS 23.246 V9.1.0 Rel. 9, 2009.
- [4] K. Etemad and L. Wang, "Multicast and broadcast multimedia services in mobile WiMAX networks," *IEEE Commun. Mag.*, vol. 47, no. 10, pp. 84–91, Oct. 2009.
- [5] Y. Liang, H. V. Poor, and S. Shamai (Shitz), "Information theoretic security," *Found. Trends Commun. Inform. Theory*, vol. 5, no. 4–5, pp. 355–580, 2009.
- [6] E. A. Jorswieck, A. Wolf, and S. Gerbracht. (2010). Secrecy on the physical layer in wireless networks. *Trends in Telecommunications Technologies*. C. J. Bouras, Ed. [Online]. Available: <http://www.intechopen.com/books/trends-in-telecommunications-technologies/secrecy-on-the-physical-layer-in-wireless-networks>
- [7] R. Liu and W. Trappe, Eds., *Securing Wireless Communications at the Physical Layer*. New York: Springer, 2010.
- [8] M. Bloch and J. Barros, *Physical-Layer Security: From Information Theory to Security Engineering*. Cambridge, U.K.: Cambridge Univ. Press, 2011.
- [9] Deutsche Telekom AG Laboratories. (2010). Next generation mobile networks: (R)evolution in mobile communications. Technology Radar Edition III/2010, Feature Paper. [Online]. Available: www.lti.ei.tum.de/index.php?id=boche
- [10] U. Helmbrecht and R. Plaga, "New challenges for IT-security research in ICT," in *Proc. World Federation of Scientists Int. Seminars on Planetary Emergencies*, Erice, Italy, Aug. 2008, pp. 1–6.
- [11] E. Biglieri, R. Calderbank, A. Constantinides, A. Goldsmith, A. Paulraj, and H. V. Poor, *MIMO Wireless Communications*. Cambridge, U.K.: Cambridge Univ. Press, 2007.
- [12] U. M. Maurer and S. Wolf, "Information-theoretic key agreement: From weak to strong secrecy for free," in *EUROCRYPT 2000 (Lecture Notes in Computer Science)*. New York: Springer-Verlag, May 2000, vol. 1807, pp. 351–368.
- [13] I. Bjelaković, H. Boche, and J. Sommerfeld, "Capacity results for compound wiretap channels," in *Proc. IEEE Information Theory Workshop*, Paraty, Brazil, Oct. 2011, pp. 60–64.
- [14] I. Bjelaković, H. Boche, and J. Sommerfeld, "Secrecy results for compound wiretap channels," *Probl. Inf. Transmiss.*, vol. 49, no. 1, pp. 73–98, Mar. 2013.
- [15] R. F. Wyrembelski, M. Wiese, and H. Boche, "Strong secrecy in bidirectional relay networks," in *Proc. Asilomar Conf. Signals, Systems, Computers*, Pacific Grove, CA, Nov. 2011, pp. 217–221.
- [16] R. F. Wyrembelski, M. Wiese, and H. Boche, "Strong secrecy in bidirectional broadcast channels with confidential messages," *IEEE Trans. Inform. Forensics Sec.*, vol. 8, no. 2, pp. 324–334, Feb. 2012.
- [17] A. D. Wyner, "The wire-tap channel," *Bell Syst. Tech. J.*, vol. 54, pp. 1355–1387, Oct. 1975.
- [18] I. Csiszár and J. Körner, "Broadcast channels with confidential messages," *IEEE Trans. Inform. Theory*, vol. 24, no. 3, pp. 339–348, May 1978.
- [19] H. Weingarten, Y. Steinberg, and S. Shamai (Shitz), "The capacity region of the Gaussian multiple-input multiple-output broadcast channel," *IEEE Trans. Inform. Theory*, vol. 52, no. 9, pp. 3936–3964, Sept. 2006.
- [20] A. El Gamal and Y.-H. Kim, *Network Information Theory*. Cambridge, U.K.: Cambridge Univ. Press, 2011.
- [21] G. Caire and S. Shamai (Shitz), "On the achievable throughput of a multi-antenna Gaussian broadcast channel," *IEEE Trans. Inform. Theory*, vol. 49, no. 7, pp. 1691–1706, July 2003.
- [22] P. Viswanath and D. N. C. Tse, "Sum capacity of the vector Gaussian broadcast channel and uplink–downlink duality," *IEEE Trans. Inform. Theory*, vol. 49, no. 8, pp. 1912–1921, Aug. 2003.
- [23] S. Vishwanath, N. Jindal, and A. Goldsmith, "Duality, achievable rates, and sum-rate capacity of Gaussian MIMO broadcast channels," *IEEE Trans. Inform. Theory*, vol. 49, no. 10, pp. 2658–2668, Oct. 2003.
- [24] M. Schubert and H. Boche, "Solution of the multiuser downlink beamforming problem with individual SINR constraints," *IEEE Trans. Veh. Technol.*, vol. 53, no. 1, pp. 18–28, Jan. 2004.
- [25] N. D. Sidiropoulos, T. N. Davidson, and Z.-Q. T. Luo, "Transmit beamforming for physical-layer multicasting," *IEEE Trans. Signal Processing*, vol. 54, no. 6, pp. 2239–2251, June 2006.
- [26] D. Tomecki and S. Stańczak, "On feasible SNR region for multicast downlink channel: Two user case," in *Proc. IEEE Int. Conf. Acoustics, Speech, Signal Processing*, Dallas, TX, Mar. 2010, pp. 3474–3477.
- [27] R. Mochaourab and E. A. Jorswieck, "Optimal beamforming in interference networks with perfect local channel information," *IEEE Trans. Signal Processing*, vol. 59, no. 3, pp. 1128–1141, Mar. 2011.
- [28] J. Li and A. P. Petropulu, "On transmit beamforming for physical-layer multicasting," in *Proc. IEEE Global Commun. Conf.*, Houston, TX, Dec. 2011, pp. 1–5.
- [29] D. Blackwell, L. Breiman, and A. J. Thomasian, "The capacity of a class of channels," *Ann. Math. Stat.*, vol. 30, no. 4, pp. 1229–1241, Dec. 1959.
- [30] J. Wolfowitz, "Simultaneous channels," *Arch. Ration. Mech. Anal.*, vol. 4, no. 4, pp. 371–386, 1960.
- [31] W. L. Root and P. P. Varaiya, "Capacity of classes of Gaussian channels," *SIAM J. Appl. Math.*, vol. 16, no. 6, pp. 1350–1393, 1968.
- [32] S. A. Vorobyov, A. B. Gershman, and Z.-Q. Luo, "Robust adaptive beamforming using worst-case performance optimization: A solution to the signal mismatch problem," *IEEE Trans. Signal Processing*, vol. 51, no. 2, pp. 313–324, Feb. 2003.
- [33] S. A. Vorobyov, H. Chen, and A. B. Gershman, "On the relationship between robust minimum variance beamformers with probabilistic and worst-case distortionless response constraints," *IEEE Trans. Signal Processing*, vol. 56, no. 11, pp. 5719–5724, Nov. 2008.
- [34] H. Weingarten, Y. Steinberg, and S. Shamai (Shitz), "On the capacity region of the multi-antenna broadcast channel with common messages," in *Proc. IEEE Int. Symp. Information Theory*, Seattle, WA, July 2006, pp. 2195–2199.

- [35] Y. Geng and C. Nair. (2012, Feb.). The capacity region of the two-receiver vector Gaussian broadcast channel with private and common messages. [Online]. Available: <http://arxiv.org/abs/1202.0097>
- [36] S. K. Leung-Yan-Cheong and M. E. Hellman, "The Gaussian wire-tap channel," *IEEE Trans. Inform. Theory*, vol. 24, no. 4, pp. 451–456, July 1978.
- [37] T. Liu and S. Shamai (Shitz), "A note on the secrecy capacity of the multiple-antenna wiretap channel," *IEEE Trans. Inform. Theory*, vol. 55, no. 6, pp. 2547–2553, June 2009.
- [38] J. Li and A. Petropulu, "Optimal input covariance for achieving secrecy capacity in Gaussian MIMO wiretap channels," in *Proc. IEEE Int. Conf. Acoustics, Speech, Signal Processing*, Dallas, TX, Mar. 2010, pp. 3362–3365.
- [39] A. Khisti and G. W. Wornell, "Secure transmission with multiple antennas—Part I: The MISOME wiretap channel," *IEEE Trans. Inform. Theory*, vol. 56, no. 7, pp. 3088–3104, July 2010.
- [40] A. Khisti and G. W. Wornell, "Secure transmission with multiple antennas—Part II: The MIMOME wiretap channel," *IEEE Trans. Inform. Theory*, vol. 56, no. 11, pp. 5515–5532, Nov. 2010.
- [41] F. Oggier and B. Hassibi, "The secrecy capacity of the MIMO wiretap channel," *IEEE Trans. Inform. Theory*, vol. 57, no. 8, pp. 4961–4972, Aug. 2011.
- [42] R. Bustin, R. Liu, H. V. Poor, and S. Shamai (Shitz), "An MMSE approach to the secrecy capacity of the MIMO Gaussian wiretap channel," in *Proc. IEEE Int. Symp. Information Theory*, Seoul, Korea, June 2009, pp. 2602–2606.
- [43] Z. Li, W. Trappe, and R. Yates, "Secret communication via multi-antenna transmission," in *Proc. Conf. Information Sciences and Systems*, Baltimore, MD, Mar. 2007, pp. 905–910.
- [44] J. Li and A. Petropulu. (2009, Sept.). Transmitter optimization for achieving secrecy capacity in Gaussian MIMO wiretap channels [Online]. Available: <http://arxiv.org/abs/0909.2622v1>
- [45] S. Loyka and C. D. Charalambous, "On optimal signaling over secure MIMO channels," in *Proc. IEEE Int. Symp. Information Theory*, Cambridge, MA, July 2012, pp. 443–447.
- [46] S. Shafiee, N. Liu, and S. Ulukus, "Towards the secrecy capacity of the Gaussian MIMO wire-tap channel: The 2-2-1 channel," *IEEE Trans. Inform. Theory*, vol. 55, no. 9, pp. 4033–4039, Sept. 2009.
- [47] S. Loyka and C. D. Charalambous, "Further results on optimal signaling over secure MIMO channels," in *Proc. IEEE Int. Symp. Information Theory*, Istanbul, Turkey, July 2013, pp. 2019–2023.
- [48] Y. Liang, G. Kramer, H. V. Poor, and S. Shamai (Shitz), "Compound wiretap channels," *EURASIP J. Wireless Commun. Network.*, vol. 2009, Article ID 142374, 12 pp.
- [49] Q. Li and W.-K. Ma, "Optimal and robust transmit designs for MISO channel secrecy by semidefinite programming," *IEEE Trans. Signal Processing*, vol. 59, no. 8, pp. 3799–3812, Aug. 2011.
- [50] J. Li and A. P. Petropulu, "Explicit solution of worst-case secrecy rate for MISO wiretap channels with spherical uncertainty," *IEEE Trans. Signal Processing*, vol. 60, no. 7, pp. 3892–3895, July 2012.
- [51] J. Huang and A. L. Swindlehurst, "Robust secure transmission in MISO channels based on worst-case optimization," *IEEE Trans. Signal Processing*, vol. 60, no. 4, pp. 1696–1707, Apr. 2012.
- [52] E. Ekrem and S. Ulukus, "On Gaussian MIMO compound wiretap channels," in *Proc. Conf. Information Sciences and Systems*, Baltimore, MD, Mar. 2010, pp. 1–6.
- [53] A. Khisti, "Interference alignment for the multiantenna compound wiretap channel," *IEEE Trans. Inform. Theory*, vol. 57, no. 5, pp. 2976–2993, May 2011.
- [54] A. Mukherjee and A. L. Swindlehurst, "Robust beamforming for security in MIMO wiretap channels with imperfect CSI," *IEEE Trans. Signal Processing*, vol. 59, no. 1, pp. 351–361, Jan. 2011.
- [55] X. He and A. Yener, "Secrecy when the eavesdropper controls its channel states," in *Proc. IEEE Int. Symp. Information Theory*, Saint Petersburg, Russia, July 2011, pp. 618–622.
- [56] X. He, A. Khisti, and A. Yener, "MIMO broadcast channel with arbitrarily varying eavesdropper channel: Secrecy degrees of freedom," in *Proc. IEEE Global Communication Conf.*, Houston, TX, Dec. 2011, pp. 1–5.
- [57] X. He and A. Yener, "Gaussian two-way wiretap channel with an arbitrarily varying eavesdropper," in *Proc. IEEE Global Communication Conf. Workshops*, Houston, TX, Dec. 2011, pp. 854–858.
- [58] I. Bjelaković, H. Boche, and J. Sommerfeld, "Strong secrecy in arbitrarily varying wiretap channels," in *Proc. IEEE Information Theory Workshop*, Lausanne, Switzerland, Sept. 2012, pp. 617–621.
- [59] I. Bjelaković, H. Boche, and J. Sommerfeld, "Capacity results for arbitrarily varying wiretap channels," in *Information Theory, Combinatorics, and Search Theory*, H. Aydinian, F. Cicalese, and C. Deppe, Eds. Berlin, Germany: Springer, 2013, pp. 123–144.
- [60] H. Boche and R. F. Wyrembelski, "Comparison of different attack classes in arbitrarily varying wiretap channels," in *Proc. IEEE Int. Workshop Information Forensics and Security*, Tenerife, Spain, Dec. 2012, pp. 270–275.
- [61] H. Boche and R. F. Schaefer, "Capacity results, coordination resources, and super-activation in wiretap channels," in *Proc. IEEE Int. Symp. Information Theory*, Istanbul, Turkey, July 2013, pp. 1342–1346.
- [62] H. Boche and R. F. Schaefer, "On the strong secrecy capacity of wiretap channels with side information," in *Proc. IEEE Int. Conf. Communication*, Budapest, Hungary, June 2013, pp. 3408–3412.
- [63] H. Boche and R. F. Schaefer, "Optimal transceiver design for wiretap channels with side information," in *Proc. IEEE Int. Conf. Acoustics, Speech, Signal Processing*, Vancouver, Canada, May 2013, pp. 2891–2895.
- [64] H. Boche and R. F. Schaefer, "Wiretap channels with side information—Strong secrecy capacity and optimal transceiver design," *IEEE Trans. Inform. Forensics Security*, vol. 8, no. 8, pp. 1397–1408, Aug. 2013.
- [65] H. D. Ly, T. Liu, and Y. Liang, "Multiple-input multiple-output Gaussian broadcast channels with common and confidential messages," *IEEE Trans. Inform. Theory*, vol. 56, no. 11, pp. 5477–5487, Nov. 2010.
- [66] R. F. Wyrembelski and H. Boche, "Strong secrecy in compound broadcast channels with confidential messages," in *Proc. IEEE Int. Symp. Information Theory*, Cambridge, MA, July 2012, pp. 76–80.
- [67] R. Liu, T. Liu, H. V. Poor, and S. Shamai (Shitz), "MIMO Gaussian broadcast channels with confidential and common messages," in *Proc. IEEE Int. Symp. Information Theory*, Austin, TX, June 2010, pp. 2578–2582.
- [68] E. Ekrem and S. Ulukus, "Gaussian MIMO broadcast channels with common and confidential messages," in *Proc. IEEE Int. Symp. Information Theory*, Austin, TX, June 2010, pp. 2583–2587.
- [69] A. Wiesel, Y. C. Eldar, and S. Shamai (Shitz), "Linear precoding via conic optimization for fixed MIMO receivers," *IEEE Trans. Signal Processing*, vol. 54, no. 1, pp. 161–176, Jan. 2006.
- [70] R. F. Wyrembelski and H. Boche, "Service integration in multiantenna bidirectional relay networks: Public and confidential services," in *Proc. IEEE Global Communication Conf. Workshops*, Houston, TX, Dec. 2011, pp. 884–888.
- [71] R. F. Wyrembelski and H. Boche, "Physical layer integration of private, common, and confidential messages in bidirectional relay networks," *IEEE Trans. Wireless Commun.*, vol. 11, no. 9, pp. 3170–3179, Sept. 2012.
- [72] R. F. Wyrembelski, T. J. Oechtering, I. Bjelaković, C. Schnurr, and H. Boche, "Capacity of Gaussian MIMO bidirectional broadcast channels," in *Proc. IEEE Int. Symp. Information Theory*, Toronto, Canada, July 2008, pp. 584–588.
- [73] T. J. Oechtering, R. F. Wyrembelski, and H. Boche, "Multiantenna bidirectional broadcast channels—Optimal transmit strategies," *IEEE Trans. Signal Processing*, vol. 57, no. 5, pp. 1948–1958, May 2009.
- [74] T. J. Oechtering, E. A. Jorswieck, R. F. Wyrembelski, and H. Boche, "On the optimal transmit strategy for the MIMO bidirectional broadcast channel," *IEEE Trans. Commun.*, vol. 57, no. 12, pp. 3817–3826, Dec. 2009.
- [75] R. F. Wyrembelski, T. J. Oechtering, and H. Boche, "MIMO Gaussian bidirectional broadcast channels with common messages," *IEEE Trans. Wireless Commun.*, vol. 10, no. 9, pp. 2950–2959, Sept. 2011.
- [76] R. F. Wyrembelski and H. Boche, "Privacy in bidirectional relay networks," *IEEE Trans. Commun.*, vol. 60, no. 6, pp. 1659–1668, June 2012.
- [77] F. M. J. Willems, "The discrete memoryless multiple access channel with partially cooperating encoders," *IEEE Trans. Inform. Theory*, vol. 29, no. 3, pp. 441–445, Nov. 1983.
- [78] S. I. Bross, A. Lapidoth, and M. A. Wigger, "The Gaussian MAC with conferring encoders," in *Proc. IEEE Int. Symp. Information Theory*, Toronto, Canada, July 2008, pp. 2702–2706.
- [79] M. Wiese, H. Boche, I. Bjelaković, and V. Jungnickel, "The compound multiple access channel with partially cooperating encoders," *IEEE Trans. Inform. Theory*, vol. 57, no. 5, pp. 3045–3066, May 2011.
- [80] M. Wiese and H. Boche, "An achievable region for the wiretap multiple-access channel with common message," in *Proc. IEEE Int. Symp. Information Theory*, Cambridge, MA, July 2012, pp. 249–253.
- [81] R. F. Schaefer and S. Loyka, "The secrecy capacity of a compound MIMO Gaussian channel," in *Proc. IEEE Information Theory Workshop*, Seville, Spain, Sept. 2013, pp. 104–108.
- [82] H. Boche and R. F. Schaefer, "Capacity results and super-activation for wiretap channels with active wiretappers," *IEEE Trans. Inform. Forensics and Security*, vol. 8, no. 9, pp. 1482–1496, Sept. 2013.

William Rowe, Petre Stoica,
and Jian Li

Spectrally Constrained Waveform Design

In active sensing, transmitters emit probing waveforms into the environment. The probing waveforms interact with scatters that reflect distorted copies of the waveforms. Receivers then measure the distorted copies to infer information about the environment. The choice of the probing waveform is important because it affects slant range resolution, Doppler tolerance, clutter, and electronic countermeasures. A traditional performance metric for the probing waveform is the ambiguity function, which describes the correlation between the waveform and a delayed and (narrow-band) Doppler shifted copy of the same waveform [1]. The direct synthesis of a waveform given a desired ambiguity function is exceedingly difficult [2]. Often designers focus on optimizing only the waveform's autocorrelation function (which is the zero Doppler cut of the ambiguity function). Any method that optimizes the autocorrelation function is implicitly performing spectral shaping by trying to flatten the passband of the waveform's spectrum [1], [2].

INTRODUCTION

For most practical applications, the waveform design problem is exacerbated by a constant amplitude constraint on the waveform that significantly increases the problem's complexity. The reason for this constraint is that transmitters operate more efficiently when using a high-power amplifier in the saturation region rather than in the linear region. With the amplitude of the probing waveform fixed, the only degree of freedom is the phase. Waveforms that utilize discrete phase shifts are referred to as phase-coded

waveforms. Common examples of phase codes are Barker codes, maximum length sequences, Frank codes, Golomb codes, and pseudonoise codes [1].

Research into spectrally shaped waveforms has increased over the past decade due to the desire for wideband applications. In these applications the waveform was required to have nulls in specific bands (which we call *notches* in this column) to prevent interference with systems operating in those bands. The existing methods focused on placing notches in the spectrum while maintaining good autocorrelation properties. However, the existing methods fall short because they are either limited by notch depth, notch width, or the number of notches. They also do not allow for arbitrary spectral shape, hence they may not be able to meet all the spectral requirements. Furthermore, most methods are based on linear frequency modulation (LFM) waveforms, which might not be ideal for all applications. See [2]–[4] for previous work in this area.

In this article we present the SHAPE algorithm, a computationally efficient method of designing sequences with desired spectrum shapes. The algorithm uses alternating fast Fourier transforms (FFTs), element-wise comparison, and element-wise arithmetic such that it can easily be implemented using parallel computing methods. SHAPE solves the problem of finding a sequence with an arbitrary time-domain complex envelope and an arbitrarily shaped spectrum. The ubiquitous constant amplitude sequence design problem is a special case that SHAPE can solve. MATLAB scripts for SHAPE as well as further images and examples are available on the supplementary material Web site, www.sal.ufl.edu/shape.

In this article we shall denote a vector with boldface lowercase letter (\mathbf{x}) and we denote the elements of the vector as $\mathbf{x} = [x_1, x_2, \dots, x_N]^T$. Similarly a matrix is denoted by a boldface uppercase letter (\mathbf{X}). Here $(\cdot)^T$ represents the transpose operation and the conjugate transpose operation is denoted by $(\cdot)^H$. The operator $\|\cdot\|_2^2$ represents the euclidean norm of a vector squared. A superscript on a variable such as \mathbf{x}^k represents an iteration counter and not a power operation. A hat symbol on a variable ($\hat{\mathbf{x}}$) represents the solution to a minimization problem. Finally, we denote a column vector of ones of size N as $\mathbf{1}_N$.

SHAPE ALGORITHM

A least-squares fitting approach for the spectral shaping problem can be formulated as

$$\begin{aligned} & \underset{\mathbf{x}, \theta}{\text{minimize}} \quad \|\mathbf{F}^H \mathbf{x} - \mathbf{y} \odot e^{j\theta}\|_2^2 \\ & \text{subject to} \quad |x_i|^2 = h_i, \quad \text{for } i = 1, 2, \dots, N, \end{aligned} \quad (1)$$

where \odot represents the element-wise product operation, $\mathbf{x} \in \mathbb{C}^{N \times 1}$ is our sequence we seek to design, $\mathbf{y} \in \mathbb{R}_0^{+N \times 1}$ is the desired spectrum magnitude, $\mathbf{F} \in \mathbb{C}^{N \times N}$ is a unitary Fourier matrix, and the phase variable $\theta \in \mathbb{R}^{N \times 1}$ is an auxiliary variable. The envelope constraint on the time-domain sequence is represented by $\mathbf{h} = [h_1, h_2, \dots, h_N]^T$. In general, we allow \mathbf{h} to have any value, but it commonly only takes on values relating to window functions (e.g., box, Hamming, Taylor, or Tukey) [5]. This problem is well known and is easy to solve in an iterative manner since the matrix \mathbf{F} is unitary (see [2])

$$\begin{aligned} \text{Given } \mathbf{x}: \hat{\theta} &= \arg\{\mathbf{F}^H \mathbf{x}\} \\ \text{Given } \theta: \hat{\mathbf{x}} &= \sqrt{\mathbf{h}} \odot e^{j \arg\{\mathbf{F}(\mathbf{y} \odot e^{j\theta})\}}. \end{aligned}$$

Digital Object Identifier 10.1109/MSP.2014.2301792
Date of publication: 7 April 2014

SP TIPS&TRICKS continued

Here the $\sqrt{\cdot}$ represents an element-wise square root operation. Using this approach for arbitrary spectrum shapes and arbitrary envelope functions may result in convergence of the cost function in (1) to significant nonzero values, which implies that the spectral requirements will not be met. Even when the convergence is to a value near zero, the resulting spectrum may oscillate around the desired spectrum shape, y , which may not meet strict spectrum requirements either.

We overcome the problems of the direct fitting approach by using a relaxation on the desired spectrum shape to introduce more degrees of freedom. Instead of fitting to a specific y as in (1), we search for any sequence with a spectrum contained within some upper and lower bounds, $f(\omega)$ and $g(\omega)$, respectively. We denote the vectors $f = [f_1, f_2, \dots, f_N]^T$ and $g = [g_1, g_2, \dots, g_N]^T$ as the bounding functions sampled on our frequency grid points. Then we can search instead for some spectrum z with modulus contained within the bounds. We also introduce a scalar factor α to account for any possible energy mismatch and/or constant phase offset between the sequence x and the spectrum z . This results in the following minimization problem:

$$\begin{aligned} & \underset{x, z, \alpha}{\text{minimize}} \quad \|F^H x - \alpha z\|_2^2 \\ & \text{subject to} \quad |x_i|^2 = h_i, \text{ for } i = 1, 2, \dots, N \\ & \quad |z_i| \leq f_i \text{ for } i = 1, 2, \dots, N \\ & \quad |z_i| \geq g_i \text{ for } i = 1, 2, \dots, N. \end{aligned} \quad (2)$$

The SHAPE algorithm minimizes (2) using an iterative approach.

There are three main steps to solve in each iteration of the SHAPE algorithm: 1) given (α, x) minimize with respect to (w.r.t.) z such that z satisfies the constraints, 2) given (x, z) minimize w.r.t. α , and 3) given (α, z) minimize w.r.t. x such that x satisfies the constraints. We start by examining the first minimization subproblem that finds a satisfactory spectrum vector z given some time-domain sequence x and energy scalar α :

$$\begin{aligned} & \underset{z}{\text{minimize}} \quad \|F^H x - \alpha z\|_2^2 \\ & \text{subject to} \quad |z_i| \leq f_i \text{ for } i = 1, 2, \dots, N \\ & \quad |z_i| \geq g_i \text{ for } i = 1, 2, \dots, N. \end{aligned} \quad (3)$$

If there were no constraints on z , the answer is simply $z_{\text{opt}} = \tilde{x}/\alpha$ or $(z_i)_{\text{opt}} = (|\tilde{x}_i|/|\alpha|)e^{j(\phi_{\tilde{x}_i} - \phi_\alpha)}$ where $\tilde{x} = F^H x$. The constrained problem posed in (3) has a solution similar to the unconstrained problem. Let $c_1(z)$ be the cost function from (3)

$$\begin{aligned} c_1(z) &= (F^H x - \alpha z)^H (F^H x - \alpha z) \\ &= x^H F F^H x + |\alpha|^2 z^H z \\ &\quad - 2\Re\{e^{j(\phi_{\tilde{x}_i} - \phi_\alpha)} \alpha^H z^H F^H x\}, \end{aligned} \quad (4)$$

which we rewrite as

$$\begin{aligned} c_1(|z_1|, \phi_{z_1}, \dots, |z_N|, \phi_{z_N}) \\ &= \sum_{i=1}^N (|\tilde{x}_i|^2 + |\alpha|^2 |z_i|^2 \\ &\quad - 2|\alpha||z_i||\tilde{x}_i| \Re\{e^{j(\phi_{\tilde{x}_i} - \phi_\alpha - \phi_{z_i})}\}). \end{aligned}$$

Since $|\tilde{x}_i|, |\alpha|, |z_i| \geq 0$ and $-1 \leq \Re\{e^{j(\phi_{\tilde{x}_i} - \phi_\alpha - \phi_{z_i})}\} \leq 1$, the minimum of $c_1(z)$ will occur at $\Re\{e^{j(\phi_{\tilde{x}_i} - \phi_\alpha - \phi_{z_i})}\} = 1$. This results in the same phase as the unconstrained optimal answer $\phi_{z_i} = \phi_{\tilde{x}_i} - \phi_\alpha$. Using the optimal phase in $c_1(\cdot)$ results in a quadratic function for each $|z_i|$

$$\begin{aligned} & \sum_{i=1}^N (|\tilde{x}_i|^2 + |\alpha|^2 |z_i|^2 - 2|\alpha||z_i||\tilde{x}_i|) \\ &= \sum_{i=1}^N (|\tilde{x}_i| - |\alpha||z_i|)^2. \end{aligned}$$

For each $|z_i|$ the zero cost value is achieved at $|\tilde{x}_i|/|\alpha|$, but this point may not be in the feasible set $[g_i, f_i]$. If $|\tilde{x}_i|/|\alpha| < g_i$ then the minimum value of the cost function occurs at $|z_i| = g_i$. Similarly, if $|\tilde{x}_i|/|\alpha| > f_i$ then the minimum value of the cost function occurs at $|z_i| = f_i$. Then the solution to (3) is given by

$$\hat{z}_i = \begin{cases} f_i e^{j(\phi_{\tilde{x}_i} - \phi_\alpha)} & : |\tilde{x}_i|/|\alpha| > f_i, \\ g_i e^{j(\phi_{\tilde{x}_i} - \phi_\alpha)} & : |\tilde{x}_i|/|\alpha| < g_i, \\ \frac{\tilde{x}_i}{\alpha} & : \text{otherwise.} \end{cases} \text{ for } i = 1, 2, \dots, N.$$

The second step in SHAPE is to minimize w.r.t α given x and z . The problem is written as

$$\underset{\alpha}{\text{minimize}} \quad \|F^H x - \alpha z\|_2^2. \quad (5)$$

Since α has no constraints, the solution to (5) is simply

$$\hat{\alpha} = \frac{z^H F^H x}{\|z\|_2^2}.$$

The third step in SHAPE is to minimize w.r.t. x given z and α such that x has the desired envelope shape. The cost function is written as

$$\begin{aligned} & \underset{x}{\text{minimize}} \quad \|x - \alpha F z\|_2^2 \\ & \text{subject to} \quad |x_i|^2 = h_i, \text{ for } i = 1, 2, \dots, N, \end{aligned} \quad (6)$$

where we utilize the fact that F is unitary and a matrix norm is invariant to a unitary transformation. Then following an approach similar to the expansion in (4), the phase minimizer of the cost function is $\phi_{x_i} = \phi_{\tilde{x}_i} + \phi_\alpha$, where $\tilde{z} = Fz$. The amplitude of x_i is fixed by the constraints so then the resulting minimizer is given by

$$\hat{x}_i = \sqrt{h_i} e^{j(\phi_{\tilde{x}_i} + \phi_\alpha)}, \text{ for } i = 1, 2, \dots, N. \quad (7)$$

The SHAPE algorithm is presented on the next page in a step-by-step guide. The supplementary material, which can be found at www.sal.ufl.edu/shape, also contains a MATLAB function for SHAPE and scripts to demonstrate the implementation. SHAPE is computationally efficient since it utilizes only FFTs, inner products, and element-wise operations (magnitude, scalar division, scalar multiplication, and scalar comparisons). All of the for loops in the algorithm can be unrolled and implemented using parallel processing further increasing the speed.

PRACTICAL ISSUES

To successfully utilize the SHAPE algorithm for a specific application, several practical issues need to be addressed. The first problem is the selection of the bounding functions $f(\omega)$ and $g(\omega)$ and how they affect the convergence of SHAPE. The second problem is that, in any real system, the sequence will be quantized, which distorts the spectrum. The third problem deals with sampling in the frequency domain. Finally, the initialization of the SHAPE algorithm is also a critical consideration.

CONVERGENCE

A priori there is no guarantee that a solution exists for a given spectral shape and

The SHAPE Algorithm.

initialize:

- 1) Set $\alpha^0 = 1$
 - 2) Choose \mathbf{x}^0 such that $|x_i|^2 = h_i$, for $i = 1, 2, \dots, N$
 - 3) Set the iteration index $k = 1$ and set max iteration K
 - 4) Initialize temp variable $\mathbf{u} = \mathbf{F}^H \mathbf{x}^0 / \alpha^0$
repeat
 - 1) Calculate \mathbf{z}^k given α^{k-1} , \mathbf{x}^{k-1}
using \mathbf{u}
for $i = 1$ to N do
if $|u_i| > f_i$ then
 $z_i^k = f_i u_i / |u_i|$
else if $|u_i| < g_i$ then
 $z_i^k = g_i u_i / |u_i|$
else
 $z_i^k = u_i$
end if
end for
 - 2) Calculate α^k given \mathbf{x}^{k-1} and \mathbf{z}^k
as $\alpha = \mathbf{z}^H \mathbf{F}^H \mathbf{x} / \|\mathbf{z}\|_2^2$
 - 3) Calculate \mathbf{x}^k given α^k and \mathbf{z}^k
using $\mathbf{v} = \alpha \mathbf{F} \mathbf{z}$
for $i = 1$ to N do
if $|v_i|^2 \neq h_i$ then
 $x_i^k = \sqrt{h_i} v_i / |v_i|$
else
 $x_i^k = v_i$
end if
end for
 - 4) $\mathbf{u} = \mathbf{F}^H \mathbf{x}^k / \alpha^k$
 - 5) $k = k + 1$
- until $g_i \leq u_i \leq f_i$ for $i = 1, 2, \dots, N$
or $k > K$
-

time-domain window. When SHAPE encounters scenarios where a solution does not exist, it will converge to a nonzero value of the cost function. However, we have found that we greatly increase our chances of finding a sequence \mathbf{x} that satisfy the constraints by allowing some bands (Ω) to be unrestricted ($f(\Omega) = \infty$ and $g(\Omega) = 0$). How to choose Ω is dependent upon the restrictions that are placed on the spectrum shape. There is no formula or method for an optimal selection of Ω , but a designer can typically find a solution by choosing Ω to be small transition bands near sharp spectral jumps. A demonstration using a notched random phase

**THE SHAPE ALGORITHM
PROVIDES AN ANSWER
TO THE QUESTION OF
HOW TO FIND SEQUENCES
THAT STRICTLY SATISFY
SPECTRAL REQUIREMENTS
AND HAVE A DESIRED
ENVELOPE.**

sequence is available on the supplementary material Web site.

Another factor that helps improve the convergence of SHAPE to zero cost is the use of an offset for the spectral shapes. Suppose that we have the desired spectral shaping functions $f(\omega)$ and $g(\omega)$. When SHAPE solves the minimization step it uses a least squares criteria fitting solution to fit to these bounds. This means that the answer may tend to oscillate around $f(\omega)$ and $g(\omega)$. This problem is especially prevalent in the notches, but it is easily accounted for by using a small offset δ . Note the subtle difference that the desired bounds are still \mathbf{f} and \mathbf{g} , but we fit to offset bounds $\tilde{\mathbf{f}} = \mathbf{f} - \delta \mathbf{1}_N$ and $\tilde{\mathbf{g}} = \mathbf{g} + \delta \mathbf{1}_N$. This modification forces the fit to a slightly more restrictive constraint. This allows for ripples to be contained within the desired values, which helps strictly meet the spectrum requirements.

QUANTIZATION

The SHAPE algorithm assumes that we have access to infinite precision numbers, which is not true in any actual signal processing application. The use of double precision (64-bit) numbers is more than adequate for finding sequences using SHAPE, but the problem is in truncation to lower-precision integer sequences. The spectral shape is determined by the phase and amplitude of the complex sequence, and bit truncation may distort the spectral shape. Similarly, the complex envelope may become distorted, which will introduce amplitude fluctuations from the desired envelope.

The quantization problem is relevant because digital-to-analog converters (DACs) of modest bandwidth will typically have bit precision fewer than 32

bits and utilize fixed-point representations. The use of the fixed-point values results in a discrete set of phase values. Hence the reduced precision of the DAC is going to quantize our phase sequence and distort our spectrum. From our empirical results, the quantization by itself does not have a serious impact on the resulting spectrum until approximately 8–10 bits are used to represent each number. Some figures and scripts to explore the quantization behaviour are available for the readers examination on the supplementary material Web site.

FREQUENCY SAMPLING

If we consider nonperiodic waveforms, then the spectra will be continuous [5]. SHAPE would have to approximate such a spectrum by using the DFT (FFT in SHAPE). Still there would hardly be any guarantee that spectral compliance could be met at every point in the frequency domain. On the other hand, if we consider periodic waveforms, then the resulting spectra are actually discrete and can be matched perfectly by SHAPE.

For example, consider an active sensing system that utilizes a pulsed mode of operation. We can consider this to be a periodic waveform design by accounting for the listening time between transmissions. That is, we design our sequence according to the appropriate amount of zeros needed during the listening time. Using this approach results in a discrete spectrum, which can match the designed spectrum and be in full spectral compliance.

INITIALIZATION

SHAPE is dependent on the initial signal \mathbf{x}^0 . Recall that SHAPE searches for a pair (\mathbf{z}, \mathbf{x}) that satisfies the time domain and spectral constraints and there is an unknown number of pairs that actually satisfies the constraints. Then different initializations can lead to different outputs from the SHAPE algorithm. How to choose an initial signal is dependent upon a system's requirements, but when the initial signal's spectrum has features similar to the desired spectrum, SHAPE seems to converge faster to zero cost value. Further discussion, images, and

sp TIPS&TRICKS continued

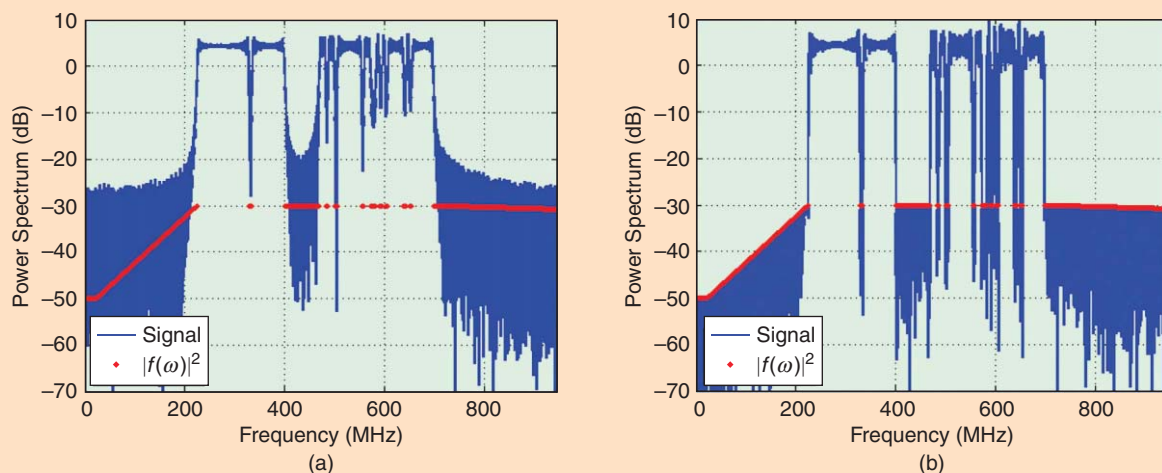


[FIG1] The wideband radar waveform design example. (a) Initialization (gapped LFM waveform) and (b) SHAPE output.

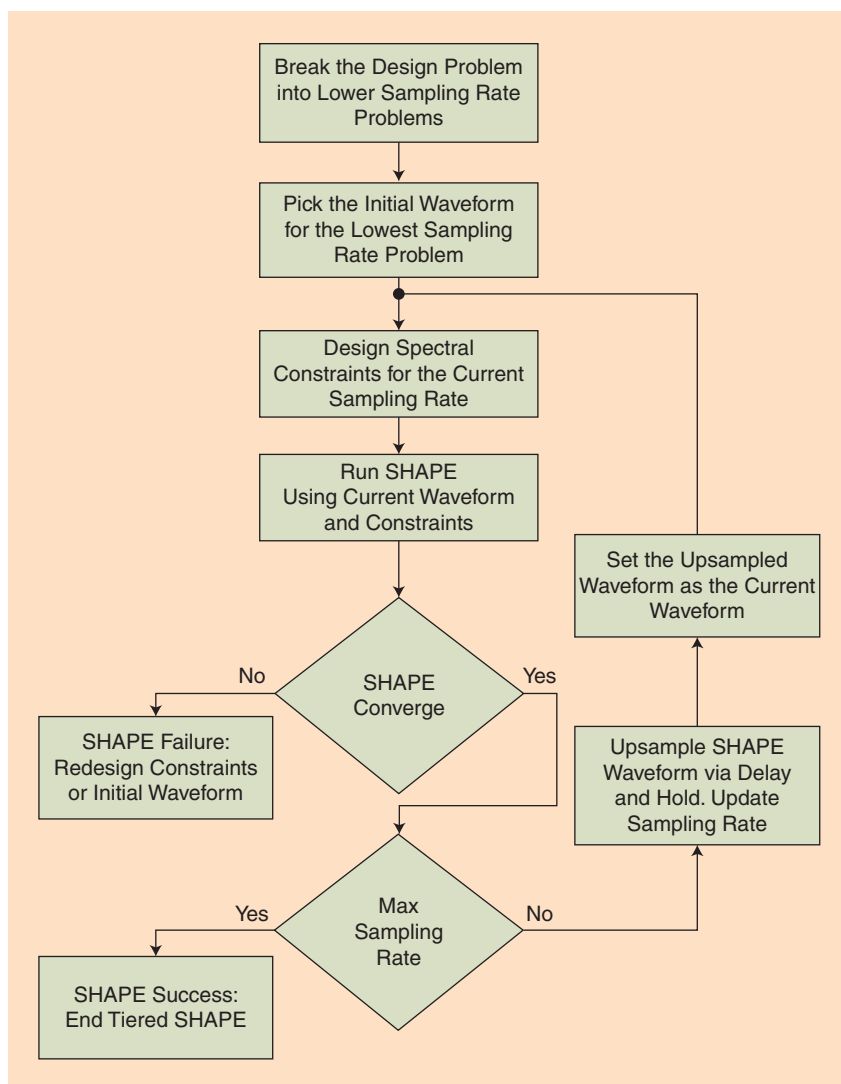


[FIG2] A flowchart of the tiered approach to SHAPE.

an example script are available on the supplementary material Web site.

SHAPE waveforms can be used as good initial waveforms in scenarios where the spectrum constraints are very strict and a good initial waveform is not readily available. Here we design a lower sampling rate waveform using SHAPE that has desired spectral properties. This waveform is then upsampled to the desired sampling rate and used as the initial waveform for SHAPE again. This concept will be explained in greater detail in the random phase sonar example.

EXAMPLES OF WAVEFORM DESIGN FOR SPECTRAL COMPLIANCE

WIDEBAND RADAR

We demonstrate the utility of the SHAPE algorithm by considering a practical sequence design example for wideband radar imaging. We assume that we have access to the 225–328.6 MHz and 335–400.15 MHz bands allocated for the U.S. Federal Government. The bands are quite limited for high-resolution imaging; therefore, we seek to utilize the nearby white space in the unused portions of the spectrum allocated for licensed television broadcasts that occur from 470 to 698 MHz. Each television station is allocated 6 MHz of bandwidth that we must not interfere with and ten stations are licensed for operation in

Alachua County, Florida. We then wish to exploit the 473 MHz of available space by placing notches in the bands (MHz): (328.6–335), (400.15–470), (482–486), (500–506), (554–560), (572–578), (590–596), (602–608), (638–644), (650–656), (674–680), and (680–686). For the radar waveform, we also shape the spectrum roll-off factor according to the National Telecommunications and Information Administration (NTIA) standards for group C radar [6]. Finally, in radar it is particularly important to have a constant amplitude sequence and hence $h_i = 1$ for $i = 1, 2, \dots, N$.

SHAPE is initialized with a gapped LFM waveform that does not meet the spectral shaping requirements $f(\omega)$ as shown in Figure 1(a). In this example, $g(\omega) = 0$ since the LFM waveform has a fairly flat passband already and the

ANOTHER FACTOR THAT HELPS IMPROVE THE CONVERGENCE OF SHAPE TO ZERO COST IS THE USE OF AN OFFSET FOR THE SPECTRAL SHAPES.

notch requirements are numerous and deep. The LFM pulse width is $25 \mu/s$ with a total bandwidth of 473 MHz. The sampling frequency is set to be exactly twice the total bandwidth in this example resulting in a length 23,645 phase-coded waveform. The FFT size used was 65,536 (2^{16}). The SHAPE waveform shown in Figure 1(b) strictly meets the spectral requirements. The script used to generate this waveform is available on the supplementary material Web site.

RANDOM PHASE SONAR WAVEFORM

The application of SHAPE using a tiered approach will be demonstrated using a sonar example with very strict spectral requirements. The script used to generate these results is available on the supplementary material Web site. The time-domain sequence in this particular example is a 1-s signal windowed with a Tukey window with parameter 0.1. The window shape allows for rise and fade times in the complex envelope. The spectrum passband is given as 1,050–1,950 Hz; then the power spectrum must decrease by 100 dB at $\pm 5,000$ Hz, and finally the spectrum must linearly decrease to -150 dB at ± 50 kHz. There are sequences that can meet this spectral requirement, but they typically resemble LFM waveforms. An adversary would

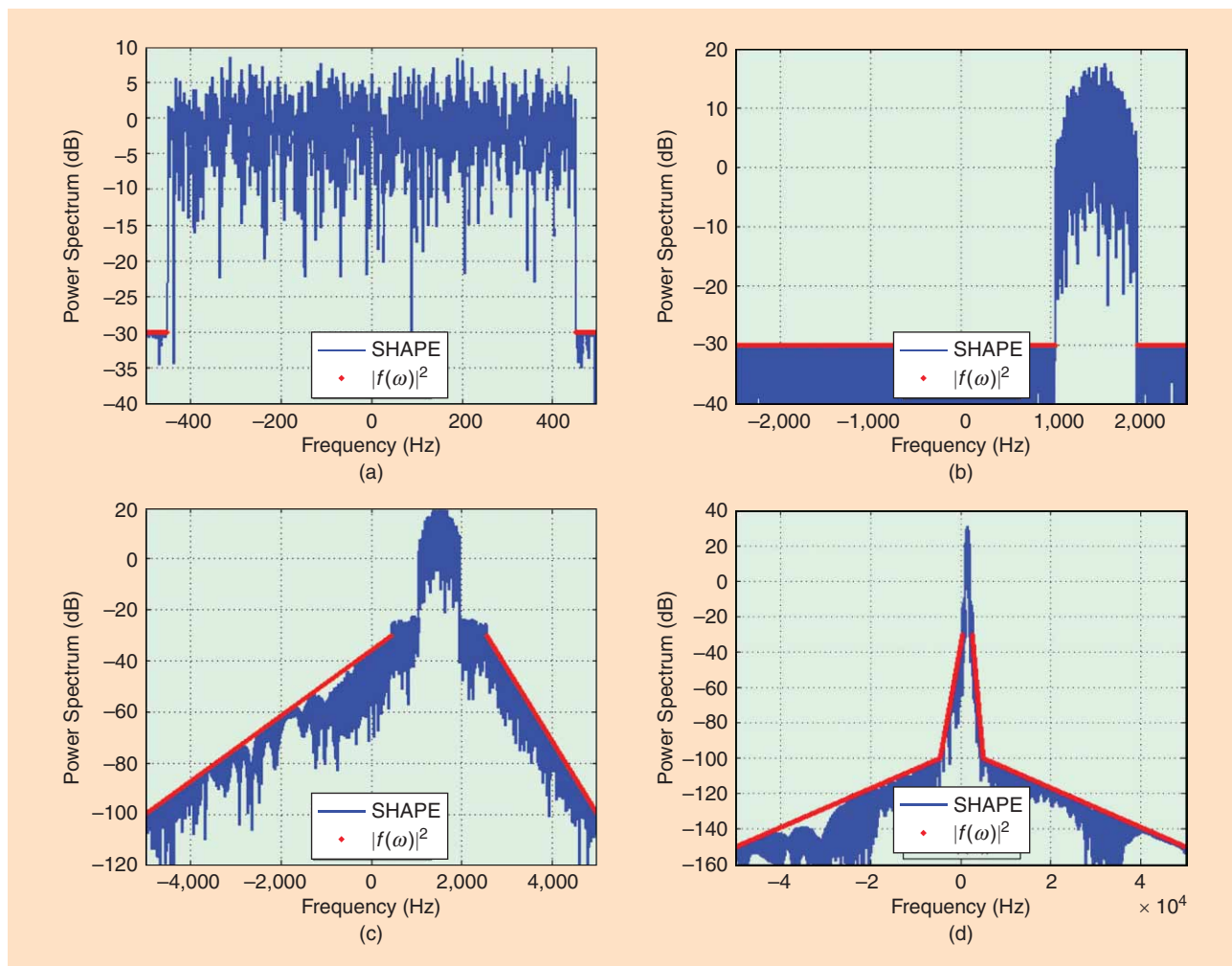


[FIG3] The tiered SHAPE waveforms. (a) Stage 1 output, (b) stage 2 output, (c) stage 3 output, and (d) stage 4 output.

likely recognize one of these sequences as a sonar waveform. Since a primary goal in sonar is also to be covert, we would like our sequence to be similar to a random phase sequence to prevent recognition by an adversary.

The design of this SHAPE waveform with a random phase signal initialization is difficult due to the small passband and the steep spectral roll-off requirements. We overcome this by using a tiered approach to SHAPE. The tiered approach breaks the waveform design problem down into smaller subproblems. For example, in this problem we will start by designing a 900-Hz passband (complex) waveform at a sampling rate of 1,000 Hz using SHAPE. The output from SHAPE is upsampled using a simple delay and hold approach to a sampling rate of 5,000 Hz. The upsampled waveform's spectrum is the original spectrum repeated five times and modulated by a sinc function. The upsampled waveform's spectrum is a good initializer since the majority of the energy we are interested in is already placed in our passband. We then design a new set of spectral constraints for our new sampling rate of 5,000 Hz that moves us closer toward our final spectral constraints that exist from ± 50 kHz. This design and upsample process is repeated until we meet our final sampling rate requirements. For simplicity, we call each usage of SHAPE and upsampling a *stage*. A basic block diagram showing layout of the tiered approach to SHAPE is shown in Figure 2 and a more technical explanation is available on the supplementary material Web site.

We utilize sampling rates of 1, 5, 10, and 100 kHz in stages 1–4. For stage 1, we have to first shape the spectrum to satisfy the 900-Hz passband. We initialize SHAPE with a random phase waveform and get the stage 1 output waveform shown in Figure 3(a). Notice that we have made our random phase waveform satisfy the 900-Hz passband requirement.

For the second stage, we upsample the stage 1 output by a factor of five

SHAPE WAVEFORMS CAN BE USED AS GOOD INITIAL WAVEFORMS IN SCENARIOS WHERE THE SPECTRUM CONSTRAINTS ARE VERY STRICT AND A GOOD INITIAL WAVEFORM IS NOT READILY AVAILABLE.

using a sample and hold approach. We then shift the waveform to the carrier frequency of 1,500 Hz. We do not have a required spectral constraint until 5,000 Hz so we simply restrict the stopband to -30 dB, and the stage 2 output is shown in Figure 3(b). For stage 3, the stage 2 output is upsampled by a factor of two using the sample and hold approach again. Now we enforce a linear suppression of -30 dB to -100 dB from 2,550 Hz to 5,000 Hz and 450 to $-5,000$ Hz. Notice that between 1,950 to 2,550 Hz and 450 to 1,050 Hz there are no restrictions. This gives SHAPE some freedom when shaping the spectrum (see the discussion on the cost function's convergence to zero). The stage 3 output waveform is shown in Figure 3(c).

For the final stage, we utilize an upsampling factor of ten using the sample and hold method again. We then introduce the final and complete spectral requirements. The spectrum of the upsampled waveform is peaky, but the majority of the energy lies in the passband. SHAPE is able to move the energy into the passband and unrestricted regions such that the spectral restrictions can be met. Figure 3(d) is the SHAPE waveform output. A discussion of the output waveform's properties is available on the supplementary material Web site.

CONCLUSIONS

The RF spectrum is overcrowded, and static spectral management is not going to be able to efficiently use this limited

natural resource. Dynamic spectrum management will allow for more systems to share the spectrum for higher bandwidth applications. Many questions remain for how to implement such a standard across multiple systems, but the SHAPE algorithm provides an answer to the question of how to find sequences that strictly satisfy spectral requirements and have a desired envelope.

ACKNOWLEDGMENTS

This work was supported in part by the Office of Naval Research (ONR) under grant number N00014-12-1-0381, the Swedish Research Council (VR), the European Research Council, and the SMART fellowship program. The views and conclusions contained herein are those of the authors and should not be interpreted as necessarily representing the official policies or endorsements, either expressed or implied, of the U.S. Government.

AUTHORS

William Rowe (wrowe001@ufl.edu) is an electrical engineering Ph.D. candidate at the University of Florida.

Petre Stoica (peter.stoica@it.uu.se) is a professor in the Department of Information Technology at Uppsala University.

Jian Li (li@dsp.ufl.edu) is a professor in the Department of Electrical and Computer Engineering at the University of Florida.

REFERENCES

- [1] N. Levanon and E. Mozeson, *Radar Signals*. Hoboken, NJ: Wiley, 2004.
- [2] H. He, J. Li, and P. Stoica, *Waveform Design for Active Sensing Systems: A Computational Approach*. Cambridge, U.K.: Cambridge Univ. Press, 2012.
- [3] M. Lindenfeld, "Sparse frequency transmit and receive waveform design," *IEEE Trans. Aerospace Electron. Syst.*, vol. 40, pp. 851–861, 2004.
- [4] C. Nunn and L. Moyer, "Spectrally-compliant waveforms for wideband radar," *IEEE Aerospace Electron. Syst. Mag.*, vol. 27, pp. 11–15, Aug. 2012.
- [5] P. Stoica and R. L. Moses, *Spectral Analysis of Signals*. Upper Saddle River, NJ: Prentice Hall, 2005.
- [6] *Manual of Regulations and Procedures for Federal Radio Frequency Management*, National Telecommunications and Information Agency, Washington D.C., 2012, ch. 5.

Ljubiša Stanković, Srdjan Stanković,
and Miloš Daković

From the STFT to the Wigner Distribution

The analysis, processing, and parameters estimation of signals whose spectral content changes in time are of crucial interest in many applications, including radar, acoustics, biomedicine, communications, multimedia, seismic, and the car industry [1]– [11]. Various signal representations have been introduced to deal with this kind of signals within the area known as time-frequency (TF) signal analysis. The oldest analysis tool in this area is the short-time Fourier transform (STFT), as a direct extension of the classical Fourier analysis. The other key tool is the Wigner distribution (WD), introduced in signal analysis from quantum mechanics. The aim of this lecture note is to present and relate these two of the most important tools in the TF signal analysis, the STFT and the WD (introduced by two Nobel prize winners, D. Gabor and E. Wigner, respectively). This relation is a basis for the S-method (SM), an efficient and simple TF signal analysis tool providing a gradual transition between these two representations.

RELEVANCE

TF analysis is of great importance to researchers, students, and engineers dealing, in their work or research, with processing of signals with time-varying spectra. Two main approaches are used in the TF signal analysis. One of them is based on the STFT and its variations and parameter optimizations. The other is based on the WD, including its cross-terms reduced forms, defined through a general Cohen class of distributions. Since most of

the classical TF analysis tools are based on the STFT calculation, an approach that can simply and efficiently upgrade the existing STFT based systems toward higher concentrated WD forms is of great practical and theoretical significance.

PREREQUISITES

This article assumes a basic knowledge of linear algebra and the Fourier transforms (FTs), including the discrete FT (DFT).

PROBLEM STATEMENT

The goal of this lecture note is to present a direct relation between the STFT and the WD. Using this relation, a gradual transition from the STFT toward the WD is implemented. A TF representation, combining good properties of the cross-terms-free STFT and the highly concentrated WD, is obtained.

SHORT-TIME FOURIER TRANSFORM

The basic idea behind the STFT, as the initial and the simplest TF representation, is to apply the FT to a localized (truncated) signal $x(t)$, obtained by using a sliding window function $w(t)$. It is defined by

$$S(t, \Omega) = \int_{-\infty}^{\infty} x(t + \tau)w(\tau)e^{-j\Omega\tau} d\tau. \quad (1)$$

It is clear that the STFT satisfies properties inherited from the FT.

In the discrete TF domain, the STFT, at an instant n and frequency k , reads

$$S_N(n, k) = \sum_{m=-\frac{N}{2}}^{\frac{N}{2}-1} x(n+m)w(m)e^{-j\frac{2\pi}{N}mk}.$$

The STFT $S_N(n, k)$ is calculated using signal samples within the window

$[n - N/2, n + N/2 - 1]$ for $-N/2 \leq k \leq N/2 - 1$, corresponding to an even number of N discrete frequencies from $-\pi$ to π . For an odd N , the summation limits are $\pm(N-1)/2$. A wide window includes signal samples over a wide time interval, losing the possibility to detect fast changes in time, but achieving high-frequency resolution. A narrow window in the STFT will track time changes, but with a low resolution in frequency. Two extreme cases are $N=1$ when $S_1(n, k) = x(n)$ and $N=M$ when $S_M(n, k) = X(k)$, where M is the number of all available signal samples and $X(k) = \text{DFT}\{x(n)\}$.

Constant or, in general, varying window widths N_i could be used for different time instants n_i . Assuming a rectangular window we can write,

$$S_{N_i}(n_i, k) = \sum_{m=-\frac{N_i}{2}}^{\frac{N_i}{2}-1} x(n_i+m)e^{-j\frac{2\pi}{N_i}mk}$$

$$S_{N_i}(n_i) = W_{N_i}x_{N_i}(n_i), \quad (2)$$

where $S_{N_i}(n_i)$ and $x_{N_i}(n_i)$ are column vectors with elements $S_{N_i}(n_i, k)$, $k = -N_i/2, \dots, N_i/2 - 1$ and $x(n_i+m)$, $m = -N_i/2, \dots, N_i/2 - 1$, respectively. Matrix W_{N_i} is an $N_i \times N_i$ DFT matrix with elements $\exp(-j2\pi mk/N_i)$, where m is the column index and k is the row index of the matrix. The STFT value $S_{N_i}(n_i, k)$ is presented as a block in the TF plane of the width N_i in the time direction, covering all time instants $[n_i - N_i/2, n_i + N_i/2 - 1]$ used in its calculation. The frequency axis can be labeled with the DFT indices $p = -M/2, \dots, M/2 - 1$ corresponding to the DFT frequencies $2\pi p/M$ [the blue dots in Figure 1(a) and (b)]. With respect to this axis labeling, the

lecture NOTES continued

block $S_{N_i}(n_i, k)$ will be positioned at the frequency $2\pi k/N_i = 2\pi(kM/N_i)/M$, i.e., at $p = kM/N_i$. The block width in frequency is M/N_i DFT samples. Therefore the block area in time and DFT frequency is always equal to the number of all available signal samples M as shown in Figure 1, where $M = 16$.

When N_i changes with n_i we have the case of a time-varying window. In a nonoverlapping STFT, covering all signal samples $\mathbf{x} = [x(0), x(1), \dots, x(M-1)]^T$ with $S_{N_i}(n_i)$, the STFT should be calculated at $n_0 = N_0/2, n_1 = N_0 + N_1/2, n_2 = N_0 + N_1 + N_2/2, \dots, n_K = M - N_K/2$. A matrix form for all STFT values is

$$\mathbf{S} = \begin{bmatrix} \mathbf{W}_{N_0} & \mathbf{0} & \dots & \mathbf{0} \\ \mathbf{0} & \mathbf{W}_{N_1} & \dots & \mathbf{0} \\ \vdots & \vdots & \ddots & \vdots \\ \mathbf{0} & \mathbf{0} & \dots & \mathbf{W}_{N_K} \end{bmatrix} \mathbf{x},$$

$$\mathbf{S} = \bar{\mathbf{W}}\mathbf{x} = \bar{\mathbf{W}}\mathbf{W}_M^{-1}\mathbf{X}, \quad (3)$$

where \mathbf{S} is a column vector containing all STFT vectors $S_{N_i}(n_i), i = 0, 1, \dots, K, \mathbf{X} = \mathbf{W}_M\mathbf{x}$ is a DFT of the whole signal $x(n)$, while $\bar{\mathbf{W}}$ is a block matrix ($M \times M$) formed from the smaller DFT matrices $\mathbf{W}_{N_0}, \mathbf{W}_{N_1}, \dots, \mathbf{W}_{N_K}$, as in (2). Since the time-varying nonoverlapping STFT corresponds to a decimation-in-time DFT scheme, its calculation is more

efficient than the DFT calculation of the whole signal. An illustration of time-varying window STFTs is shown in Figure 1(a) and (b). For a signal with M samples, there is a large number $F(M) = 2^{M-1}$ of possible nonoverlapping STFTs with a time-varying window $N_i \in \{1, 2, 3, \dots, M\}$ [11]. A simple way to compare various STFTs from the concentration point of view is described in "Example 1."

In general, for a nonrectangular window, (2) is slightly modified as $S_{N_i}(n_i) = \mathbf{W}_{N_i}\mathbf{H}_{N_i}\mathbf{x}_{N_i}(n_i)$, where \mathbf{H}_{N_i} is a diagonal $N_i \times N_i$ matrix with the window values on the diagonal, $H_i(m, m) = w_i(m), m = -N_i/2, \dots, N_i/2 - 1$. In a full

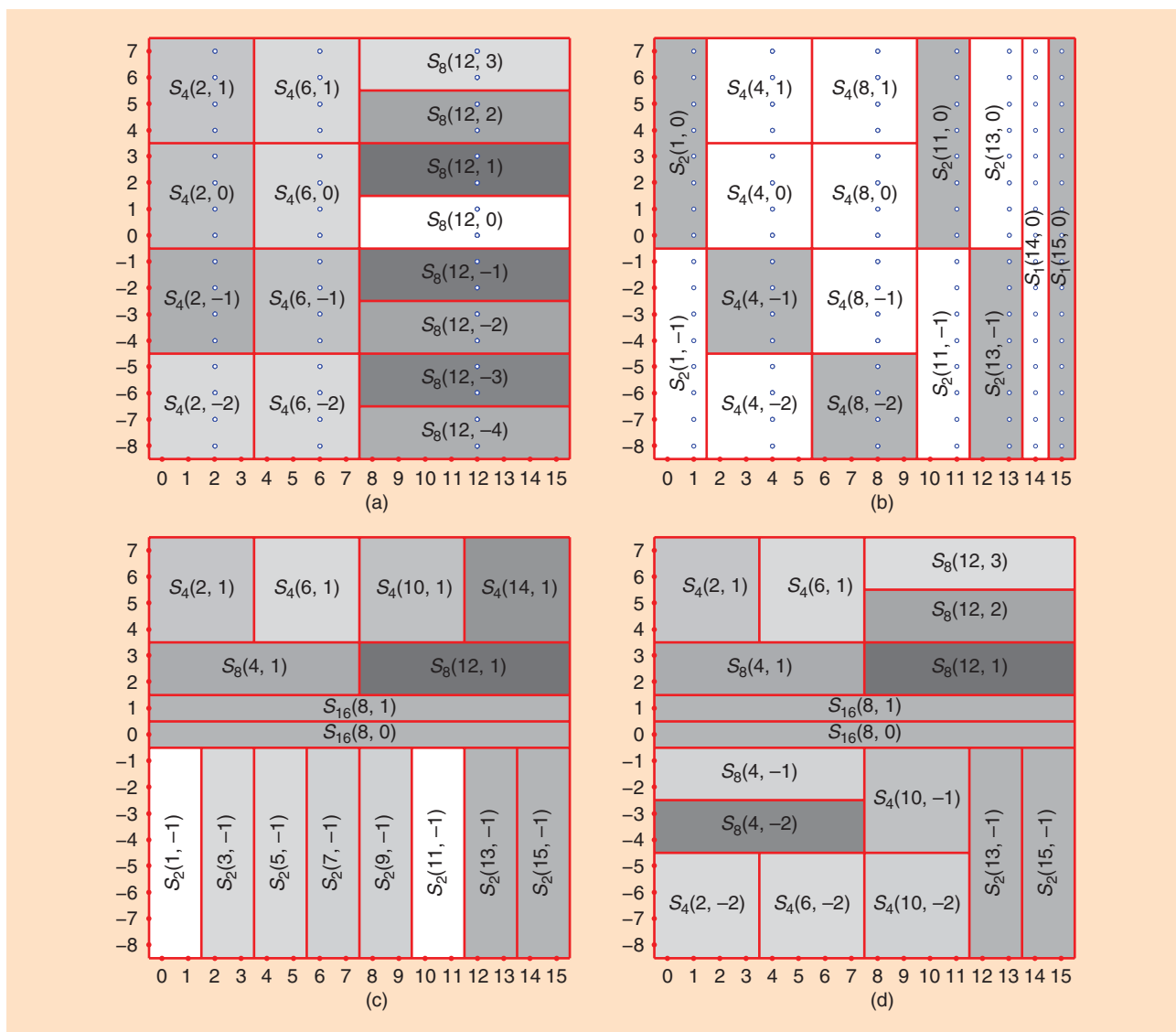


[FIG1] The STFTs with (a), (b) a time-varying window, (c) frequency-varying window, and (d) time-frequency-varying window. The time index is presented on the horizontal axis, while the DFT frequency index is shown on the vertical axis.

EXAMPLE 1

Consider a signal $x(n)$ with $M = 16$ samples, whose values are $\mathbf{x} = [0.5, 0.5, -0.25, j0.25, 0.25, -j0.25, -0.25, 0.25, -0.25, 0.25, 0.5, 0.5, -j0.5, j0.5, 0, -1]$. Some of its nonoverlapping STFTs are calculated according to (2) and shown in Figure 1. Different representations can be compared based on the concentration measures, e.g.,

$$\mu[S_N(n, k)] = \sum_n \sum_k |S_N(n, k)| = \|\mathbf{S}\|_1.$$

The best STFT representation, in this sense, would be the one with the smallest $\mu[S_N(n, k)]$ [8]. For the considered

signal and its four representations shown in Figure 1, the best representation, according to this criterion, is the one shown in Figure 1(b). If we know the best concentrated STFT representation of signal, we may use it to define an efficient filter form using TF mask $B(n, k) = 1$ for the TF part of plane with significant signal values and $B(n, k) = 0$ for noise-only parts. When the measure is used for concentration comparison of different representations, it is recommended to use their normalized values.

matrix notation, for nonoverlapping case, we get

$$\mathbf{S} = \tilde{\mathbf{W}}\tilde{\mathbf{H}}\mathbf{x}, \quad (4)$$

where $\tilde{\mathbf{W}}$ and $\tilde{\mathbf{H}}$ are $M \times M$ matrices formed from smaller $N_i \times N_i$ matrices \mathbf{W}_{N_i} and \mathbf{H}_{N_i} , respectively, as in (3). Another way of composing STFTs calculated with a rectangular window into a STFT with, e.g., the Hann(ing), Hamming, or Blackman window, is presented in "Example 2."

The STFT may use a frequency-varying window as well. For a given DFT frequency p_i , the window width in time is constant [Figure 1(c)]. Combining time-varying and frequency-varying windows, we get hybrid TF-varying windows with $S_{N_i(n_i, k_i)}$ [Figure 1(d)]. They are efficiently used for

adaptive estimation and filtering. For a graphical representation of the STFT with varying windows, the corresponding STFT value should be assigned to each instant $n = 0, 1, \dots, M-1$ and each DFT frequency $p = -M/2, -M/2 + 1, \dots, M/2 - 1$ within a block. In the case of a hybrid TF-varying window, the matrix form is obtained from the definition for each STFT value. For example, for the STFT calculated as in Figure 1(d), for each STFT value $S_4(2, -2), S_4(6, -2), S_4(10, -2), S_2(13, -1), \dots$, and $S_8(12, 3)$, an expression based on (2) should be written. Then the resulting matrix $\mathbf{S} = \tilde{\mathbf{W}}\mathbf{x}$ can be formed.

Nonoverlapping cases are important and easy for analysis. They also keep the number of the STFT coefficients equal to the number of the signal

samples. However, there are several reasons for introducing overlapped STFT representations. Rectangular windows have poor localization in the frequency domain. The study of the well-localized window forms in the TF domain has been an important topic since the STFT concept was introduced. In the case of nonrectangular windows, some of the signal samples are weighted in such a way that their contribution to the final representation is small. Then we want to use at least one more STFT with a window centered at these samples. Also, in the parameters estimation and detection the task is to achieve the best possible estimation or detection for each time instant instead of using interpolations for the skipped instants. Commonly, the

EXAMPLE 2

A nonoverlapping STFT is presented in Figure 1(a). Calculation instants are $n_i \in \{2, 6, 12\} = \mathbf{N}_c$. If we want to use only this STFT for a TF representation of a signal, then the STFT values calculated at $n_i \in \mathbf{N}_c$ should be used for signal parameters estimation at instants $n_i \in \{0, 1, 3, 4, 5, 7, 8, 9, 10, 11, 13, 14, 15\}$. This could be too rough for many applications. Then, instead of using the STFTs calculated for $n_i \in \mathbf{N}_c$ we would like to calculate STFT for some or all $n_i \notin \mathbf{N}_c$. For example, we may also want to calculate STFTs at $n_i \in \{1, 4, 8, 11, 13, 14, 15\}$, with respective window widths $N_i = 2, 4, 4, 2, 2, 1, 1$ [Figure 1(b)]. The overlapped STFT, calculated at $n_i \in \{1, 2, 4, 6, 8, 11, 12, 13, 14, 15\}$, can be written in a matrix form (4) by using appropriate matrices \mathbf{W}_{N_i} and \mathbf{H}_{N_i} with overlapping in rows, corresponding to the signal overlapping in time. In this case, there are $2M$ STFT values calculated for a signal with M samples. These STFT values are not independent. The dimension of the transformation matrix $\tilde{\mathbf{W}}$ in (4) is now $2M \times M$. Another possible way of writing an overlapping STFT is in splitting it into nonoverlapping STFTs (as in the STFTs presented in Figure 1(a) and (b) and denoted by \mathbf{S}^a and \mathbf{S}^b , respectively, using the corresponding figure labels as a super-

script). The full STFT set \mathbf{S} , with overlapping \mathbf{S}^a , and \mathbf{S}^b , is calculated based on (3) as

$$\begin{bmatrix} \mathbf{S}^a \\ \mathbf{S}^b \end{bmatrix} = \begin{bmatrix} \tilde{\mathbf{W}}^a \\ \tilde{\mathbf{W}}^b \end{bmatrix} \mathbf{x}.$$

For the analysis of signal inversion, by using the overlap and add method, we can write $\mathbf{S}^a + \mathbf{S}^b = (\tilde{\mathbf{W}}^a + \tilde{\mathbf{W}}^b) \mathbf{x}$.

For instants $n = 0, 3, 5, 7, 9, 10$, we can use one of the existing STFTs that include these instants in calculation or calculate new STFTs, introducing the third, fourth, etc. overlapping layer.

A special case of overlapping STFT with a constant rectangular window and step 1, $n_i = n_{i-1} + 1$ can be calculated from (2) in a recursive way

$$S_N(n, k) = e^{j2\pi k/N} \{S_N(n-1, k) + (-1)^k [x(n + \frac{N}{2} - 1) - x(n - \frac{N}{2} - 1)]\}.$$

For the Hann(ing) window, the STFT is related to the STFT calculated with a rectangular window as $S_N^h(n, k) = (1/2) S_N(n, k) + (1/4) S_N(n, k-1) + (1/4) S_N(n, k+1)$. Similar relations may be written for the Hamming and the Blackman window.

lecture NOTES continued

overlapped STFTs are calculated using, e.g., rectangular, Hann(ing), Hamming, Bartlett, Kaiser, or Blackman window of a constant window width N with steps $N/2, N/4,$ and $N/8, \dots$ in time. Computational cost is increased in the overlapped STFTs. An analysis of overlapping cases may be considered as

a superposition of the nonoverlapping cases (see "Example 2").

The dimensions of the STFT blocks (resolutions) are determined by the window width. The best STFT for a signal would be the one whose window form fits the best to the signal's TF content. Consider, e.g., an important and simple signal

such as a linear frequency modulated (LFM) chirp. For simplicity of analysis, assume that its instantaneous frequency (IF) coincides with the TF plane diagonal. It is obvious that, due to symmetry, both time and frequency resolution are equally important. Therefore, the best STFT would be the one calculated by using a

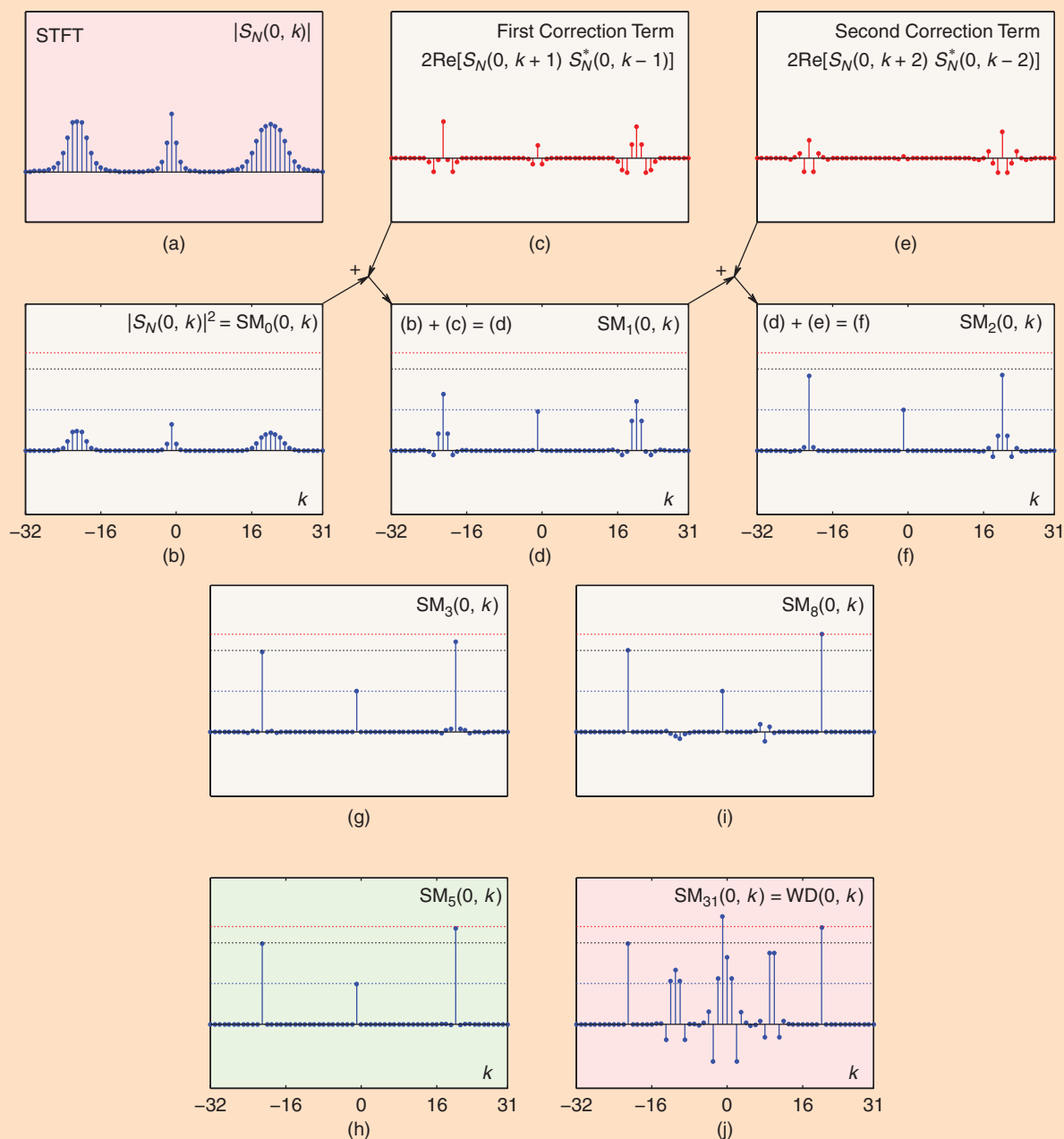


[FIG2] The analysis of a signal consisting of three LFM components (at the instant $n = 0$). (a) The STFT with a cosine window of the width $N = 64$. (b) The spectrogram. (c) The first correction term. (d) The SM with one correction term. (e) The second correction term. (f) The SM with two correction terms. (g) The SM with three correction terms. (h) The SM with five correction terms. (i) The SM with eight correction terms. (j) The WD (the SM with $L = 31$ correction term).

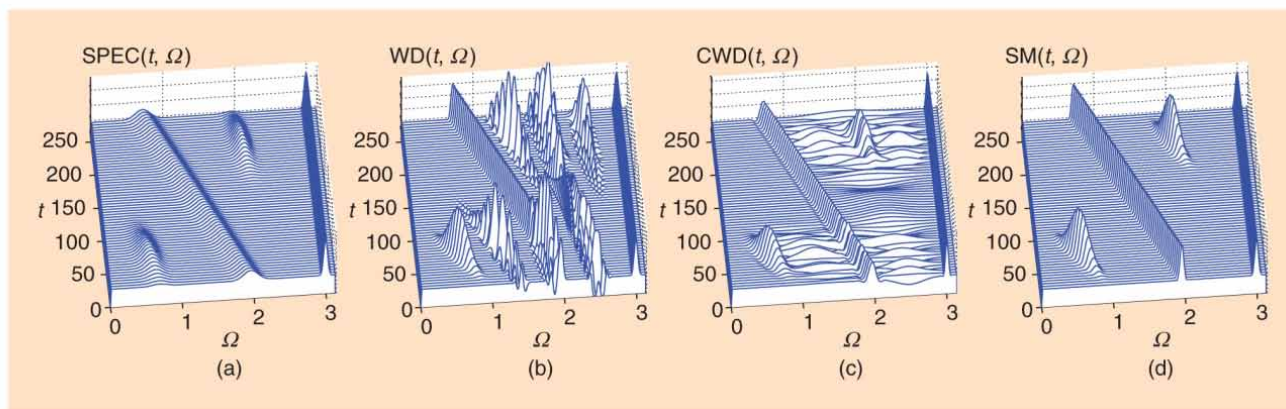


[FIG3] The time-frequency representation of a four component signal: (a) the spectrogram, (b) WD, (c) Choi-Williams distribution, and (d) S-method.

constant window whose block has an equal number of samples in time and DFT frequency, $N_i = M/N_i$ [4], [11]. For this LFM signal, e.g., with $M = 256$ samples in total, the best choice would be the STFT with $N_i = \sqrt{M} = 16$. With such a window, both resolutions will be the same and equal to 16. These resolutions could be unacceptably low for many applications. It means that the STFT, including all of its possible time and/or frequency-varying window forms, would be unacceptable as a TF representation of this signal. The overlapping STFT could be used for better signal tracking, without any effect on the resolution. A way to improve TF representation of this signal is in transforming the signal into a sinusoid whose constant frequency is equal to the IF value of the LFM signal at the considered instant. Then, a wide window can be used, with a high-frequency resolution. The obtained result is valid for the considered instant only and the signal transformation procedure should be repeated for each instant of interest.

WIGNER DISTRIBUTION

Quadratic TF representations are introduced to improve TF concentration of signals with time-varying spectral content and to satisfy some other important properties, e.g., time and frequency marginal properties [2]–[11]. The most important member of quadratic representations is the WD. It was defined in the quantum mechanics literature and later reintroduced in signal analysis by Ville.

A simple way to introduce this distribution is presented. Consider an LFM signal, $x(t) = A \exp(j\phi(t)) = A \exp(j(at^2/2 + bt + c))$. Its IF changes in time as $\Omega_i(t) = d\phi(t)/dt = at + b$. One of the goals of TF analysis is to obtain a function that will fully concentrate the signal power along its IF. In this case an ideal representation would be $2\pi A^2 \delta(\Omega - \Omega_i(t))$. For a quadratic function $\phi(t)$, it is known that

$$\begin{aligned} \tau \frac{d\phi(t)}{dt} &= \phi\left(t + \frac{\tau}{2}\right) - \phi\left(t - \frac{\tau}{2}\right) \\ &= \tau(at + b) = \tau\Omega_i(t). \end{aligned}$$

This property can easily be converted into an ideal TF representation for an LFM signal by using

$$\begin{aligned} \text{FT}_\tau\{x(t + \tau/2)x^*(t - \tau/2)\} &= \\ \text{FT}_\tau\{A^2 e^{j\Omega_i(t)\tau}\} &= 2\pi A^2 \delta(\Omega - \Omega_i(t)). \end{aligned}$$

The FT of $x(t + \tau/2)x^*(t - \tau/2)$ over τ , for a given t , is the WD. Its definition, in a pseudoform (including window), is

$$\begin{aligned} WD(t, \Omega) &= \int_{-\infty}^{\infty} x\left(t + \frac{\tau}{2}\right)x^*\left(t - \frac{\tau}{2}\right) \\ &\quad \times w\left(\frac{\tau}{2}\right)w\left(-\frac{\tau}{2}\right)e^{-j\Omega\tau} d\tau. \end{aligned} \quad (5)$$

Soon after it was introduced in signal processing it has been concluded that, due to its quadratic nature, this distribution has very emphatic cross-terms, limiting its applications. The cross-terms correspond to the product of one signal component in a multicomponent signal $x(t + \tau/2)$ with

the other component in $x^*(t - \tau/2)$. The main research direction for decades was to attenuate the cross-terms once the WD or its two-dimensional FT [well-known ambiguity function (AF)] is calculated. Various forms of two-dimensional smoothing of the WD are proposed, using the property that the cross-terms are oscillatory in the TF domain; see Figures 2(j) and 3(b). After the WD or the AF is calculated, two-dimensional low-pass kernels are used to suppress the cross-terms (such as the Choi-Williams, Butterworth, Sinc, optimal Gaussian, Zao-Atlas-Marks kernels [2]–[6]). Keeping the values of the AF along the axes unchanged, the marginal properties are preserved. The reason for introducing so many distributions lies in the fact that the cross-terms reduction and high concentration of autoterms are two contradictory requirements.

FROM THE STFT TO THE WD

A simple way to get a highly concentrated representation, while preventing the cross-terms appearance, is based on the relation between the STFT and the WD. It is established via the SM, [11],

$$\begin{aligned} SM(t, \Omega) &= \\ \frac{1}{\pi} \int_{-\infty}^{\infty} P(\theta)S(t, \Omega + \theta)S^*(t, \Omega - \theta) d\theta. \end{aligned}$$

This relation easily follows from (5), replacing $x(t + \tau/2)w(\tau/2)$ by its inverse transform $\int_{-\infty}^{\infty} S(t, \theta) \exp(j\theta\tau/2) d\theta / (2\pi)$ from (1). The special cases of the SM are the WD for $P(\theta) = 1$ and the spectrogram (the STFT squared modulus) for

EXAMPLE 3

A signal consisting of three LFM components, $x(n) = \sum_{i=1}^3 A_i \exp(ja_i \pi n/32 + jb_i \pi n^2/1024)$, with $(a_1, a_2, a_3) = (-21, -1, 20)$ and $(b_1, b_2, b_3) = (2, -0.75, -2.8)$, is considered at the instant $n = 0$. The IFs of the signal components are $k_i = a_i$, while the normalized squared amplitudes of the components are indicated by dotted lines in Figure 2. An ideal TF representation of this signal, at $n = 0$, would be $I(0, k) = A_1^2 \delta(k - k_1) + A_2^2 \delta(k - k_2) + A_3^2 \delta(k - k_3)$. The starting STFT, with the corresponding spectrogram, obtained by using the cosine window of the width $N = 64$ is shown in Figure 2(a) and (b). The first correction term is presented in Figure 2(c). The result of summing the spectrogram with the first correction term is the SM with $L = 1$ [Figure 2(d)]. The second correction term [Figure 2(e)] when added to

$SM_1(0, k)$, produces the SM with $L = 2$ [Figure 2(f)]. The SMs for $L = 3, 5$, and 8 , ending with the WD ($L = 31$) are presented in Figure 2(g)–(j). Just a few correction terms are sufficient in this case to achieve a high concentration. The cross-terms start appearing at $L = 8$ and increase as L increases toward the WD. They make the WD almost useless, since they cover a great part of the frequency range, including some signal components [Figure 2(j) and “Example 4”].

The optimal number of correction terms L is the one that produces the best SM concentration (sparsity), using the norm-one of the spectrogram and the SM (corresponding to the norm-one of the STFT) as in “Example 1” [8]. In this case, the best concentrated SM is detected for $L = 5$.

$P(\theta) = \pi \delta(\theta)$. By increasing the width of $P(\theta)$ from the spectrogram case, we get a gradual transition toward the highly concentrated WD. The best choice of the width of $P(\theta)$ is the one which enables complete integration over the auto-terms, without the cross-terms. Then, the SM produces a sum of the WDs of signal components.

A discrete form of the SM reads

$$SM_L(n, k) = \sum_{i=-L}^L S_N(n, k+i) S_N^*(n, k-i)$$

for $P(i) = 1$, $-L \leq i \leq L$ (a weighted form $P(i) = 1/(2L+1)$ could be used). A recursive relation for the SM calculation is

$$\begin{aligned} SM_L(n, k) &= SM_{L-1}(n, k) \\ &+ 2 \operatorname{Re} [S_N(n, k+L) S_N^*(n, k-L)], \end{aligned}$$

The spectrogram is the initial distribution $SM_0(n, k) = |S_N(n, k)|^2$ and $2 \operatorname{Re} [S_N(n, k+i) S_N^*(n, k-i)]$, $i = 1, 2, \dots, L$ are the correction terms. Considering the parameter L as a frame index, we can make a video of the transition from the spectrogram to the WD.

There are two ways to implement summation in the SM. The first one is with a constant L . Theoretically, to get the WD for each individual component, the number of correcting terms L should be such that $2L$ is equal to the width of the widest autoterm. This will guarantee cross-terms free distribution for all components that are at least $2L$ frequency samples apart. The optimal number of correction terms can be found by measuring the SM concentration (sparsity), as a function of L , using the norm-one of the STFT or

norm-one-half of the spectrogram and the SM, as in [8] (see “Example 3”).

The second way to implement the SM is with a TF dependent $L = L(n, k)$. The summation, for each point (n, k) , is performed as long as the absolute values of $S_N(n, k+i)$ and $S_N^*(n, k-i)$ for that (n, k) are above an assumed reference level (established, for example, as a few percents of the STFT maximal value). Here, we start with the spectrogram, $L = 0$. Consider the correction term $S_N(n, k+i) S_N^*(n, k-i)$ with $i = 1$. If the STFT values are above the reference level then it is included in summation. The next term, with $i = 2$ is considered in the same way, and so on. The summation is stopped when a STFT in a correcting

(continued on page 174)

EXAMPLE 4

A four-component real-valued signal with $M = 384$ samples is considered. Its STFT is calculated with a Hann(ing) window of the width $N = 128$ with a step of four samples. The spectrogram ($L = 0$) is shown in Figure 3(a). The alias-free WD ($L = N/2$) is presented in Figure 3(b). The Choi–Williams distribution of an analytic signal is shown in Figure 3(c). Its cross-terms are smoothed by the kernel that also spreads the autoterm of the LFM signal and chirps. The SM with $L = 10$ is shown in Figure 3(d). For graphical presentation, the distributions are interpolated by a factor of two. In all cases, the pure sinusoidal signal is well concentrated. In the WD and the SM the same concentration is achieved for the LFM signal.

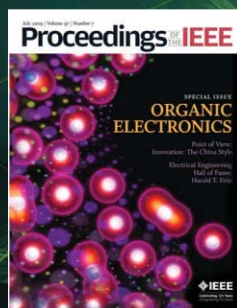
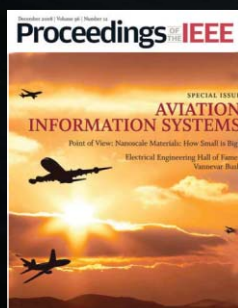
If the STFT matrix is rewritten as $\mathbf{S} = [\mathbf{S}_N(n_0), \dots, \mathbf{S}_N(n_k)]$, with rows corresponding to frequency and columns to time, then the SM, for a given L , can be implemented as a MATLAB function

```
function SM=SM_calc(S,L)
N=size(S,1);
SM=abs(S).^2;
for k=1:L;
    SM(1+k:N-k,:) = SM(1+k:N-k,:) + ...
        2*real(S(1:N-2*k,:).*...
            conj(S(1+2*k:N,:)));
end
```

All programs for the presented examples, including multimedia files, can be downloaded from <http://www.tfsa.ac.me/LN>. A simple SM calculation form, through the STFT corrections, along with the recursive STFT realization (“Example 2”) is a basis for online SM realization.

Think you know about the latest technology? You haven't even scratched the surface.

See all the layers of technology with *Proceedings of the IEEE*. Every issue brings comprehensive, in-depth coverage on technology breakthroughs. From outlining new uses for existing technology to detailing cutting-edge innovations in a variety of disciplines, you'll find the breadth of content and depth of knowledge that only IEEE can provide.



Go beyond the surface—subscribe today.
www.ieee.org/proceedings



Ultra-High-Definition Television (Rec. ITU-R BT.2020): A Generational Leap in the Evolution of Television

The International Telecommunication Union Radiocommunication Sector (ITU-R) published Recommendation (Rec.) BT.2020 “Parameter Values for Ultra-High-Definition Television Systems for Production and International Programme Exchange” [1] in August 2012. The parameters for television (TV) systems are roughly equivalent to the image format, including pixel count, frame frequency, and colorimetry. These basic system parameters determine what kind of visual experiences the system can provide to the viewers in terms of possible field of view (FOV) size, quality of motion portrayal, and accuracy of color reproduction.

Technologies progress in generations, and the duration of a generation for TV technology is longer than in many other areas such as information technology (IT). Major changes have happened only twice since the advent of black and white standard-definition TV (SDTV). These were the advent of color TV and the spread of high-definition TV (HDTV). The reason for the relatively slow changes in TV systems is due to the special characteristics of the TV system or service: to reduce the overall system cost, a TV broadcast system consists of a few expensive transmission parts and many inexpensive reception parts. The system also requires strict standards to support exchange of programs over as wide an area as possible. Currently, HDTV is being spread worldwide over various phases. The interest for the next generation after HDTV is increasing among early-adopting countries and broadcasters. This new TV format is called ultra-HDTV (UHDTV), also known

as 4K or 8K according to its approximated pixel counts in a horizontal direction. Rec. BT.2020 specifies the system parameters for such TVs. This article provides an introduction to UHDTV as defined in Rec. BT.2020, with emphasis on the background of how the major parameter values were determined.

BACKGROUND

One of the main objectives of the activities of ITU-R is to provide the environments for effective usage of the limited resource of radio spectrum by ensuring the required performance and quality for the operation of radiocommunication systems. This is the reason why the ITU-R, whose main scope is radiocommunications,

UNTIL NOW, THERE HAS BEEN NO PERFECT WORLD-UNIFIED STANDARD FOR TV SYSTEMS, ALTHOUGH IT IS DESIRABLE TO FACILITATE SMOOTH PROGRAM EXCHANGE AND LOW-PRICED EQUIPMENT.

deals with the standardization of TV image formats. Broadcasting services in particular require optimizing the system over the end-to-end chain from the program origination at the broadcasters to the program presentation at the end users. They also require international program exchange. In the analog age, the TV image format was directly connected to the required bandwidth of radio wave and modulation methods. Now the broadcast chain has been digitalized, and the image format is mainly driven by the

effort to improve the quality of end users' visual experience.

Until now, there has been no perfect world-unified standard for TV systems, although it is desirable to facilitate smooth program exchange and low-priced equipment. For example, three color TV systems were standardized in ITU-R Rec. BT.470 [2] in 1970, and they evolved to what we call SDTV [3] now. Those standards specify the 625/50 and 525/60 systems with frame (or field) frequencies of 50 and 60 Hz, respectively, where 625 or 525 describe the number of scan lines and 50 or 60 describe frame (or field) frequencies. There were various reasons why a single format was not standardized. Regarding the frame frequency, the fact that the power line frequencies in Europe and the United States were 50 and 60 Hz, respectively, is supposed to have had a great influence on the decision because adopting the same value was advantageous for the technologies in that age.

A Japanese proposal in 1972 was the start of the study on HDTV in ITU-R [4]. The standardization of HDTV focused mainly on the increase of scan lines (pixel count) and frame frequencies, although other parameters such as colorimetry were studied. The process took a long time due to a conflict of opinions regarding the backward compatibility with SDTV. The first version of Rec. ITU-R BT.709 [5] was created in 1990. However, it specified only aspect ratio and colorimetry, while scan lines and frame frequencies remained under study. Finally, the fourth version was published in 2000 to realize the world-unified HDTV system parameters, except for frame frequencies. This has simplified the program exchange between 50 and 60 Hz regions with the format conversion in which frame frequency is the only element.

STANDARDIZATION PROCESS

The study on TV systems beyond HDTV began in ITU-R in 1993, soon after the HDTV standard Rec. BT.709 was established. It was called extremely high-resolution imagery at that time. It was intended to standardize the approach to video systems of very high resolution for both broadcasting and nonbroadcasting use. The study results were reflected in ITU-R Rec. BT.1201 [6]. One of the recommendations of the standard is as follows:

Television system image spatial resolution of the electronic devices for acquisition and display should be related to 1,920 pixels in the horizontal and 1,080 pixels in the vertical directions based on Recommendation ITU-R BT.709 by simple integer ratios.

The next study on beyond-HDTV systems conducted in ITU-R was called large-screen digital imagery (LSDI). LSDI was defined as a family of digital imagery systems applicable to programs such as dramas, plays, sporting events, concerts, and cultural events from capture to large-screen presentation in high-resolution quality in appropriately equipped theatres, halls, and other venues. The extended version of LSDI was studied and Rec. ITU-R BT.1769 was created. It specifies $7,680 \times 4,320$ and $3,840 \times 2,160$ systems. The parameter values other than pixel count are the same as those specified in Rec. BT.709 or Rec. BT.1361 [7].

While the applications that use image formats beyond HDTV were under study, HDTV has been steadily spreading worldwide, and some pioneering countries and broadcasters have begun to consider the next-generation TV system and its standardization. In light of these developments, ITU-R started the study of UHDTV according to a proposal made at the ITU-R's Study Group (SG) 6 meeting in 2008. The framework of the study was decided and a Rapporteur Group was established (a Rapporteur Group is a scheme to accelerate the study by conducting the work during the period between SG6 meetings held twice a year). The efforts of four years' study led to the establishment of Rec. BT.2020 in August 2012.

The detailed study results are compiled in ITU-R Rep. BT.2246 [8].

KEY FEATURES

The major parameters and their values specified in Rec. BT.2020 are listed in Table 1. While the evolution from SDTV to HDTV changed the pixel count only, the evolution from HDTV to UHDTV involves an additional frame frequency and new colorimetry. In this regard, Rec. BT.2020 will

THE EVOLUTION FROM HDTV TO UHDTV INVOLVES AN ADDITIONAL FRAME FREQUENCY AND NEW COLORIMETRY.

bring important changes to this field that only happen once in a few decades. The conceptual basis for the study is described in Rep. BT.2246 as follows:

UHDTV is a television application that will provide viewers with a better visual experience primarily by offering a wide FOV which virtually covers all of

the human visual field, while maintaining other features of HDTV or improving them. UHDTV could therefore be characterized as a TV system having a wide field of view supported by enhanced spatial resolution.

PIXEL COUNT

The primary aim of UHDTV is to expand the FOV. The pixel count is the main consideration when determining system parameters because it fulfills the primary aim of expanding the FOV while maintaining the picture quality, which is predominantly influenced by the angular resolution. Subjective and objective experiments were conducted to determine the required pixel count for UHDTV. These experiments focused on the relationship between the FOV and the sensation of reality (the sense of "being there"). The results show that sensation of reality goes up as the FOV increases to around 100° [9].

Another use-case can be assumed where the higher pixel count serves to increase not only the FOV but also the angular resolution. Higher pixel count leads to an increase in angular resolution for the same screen size and absolute

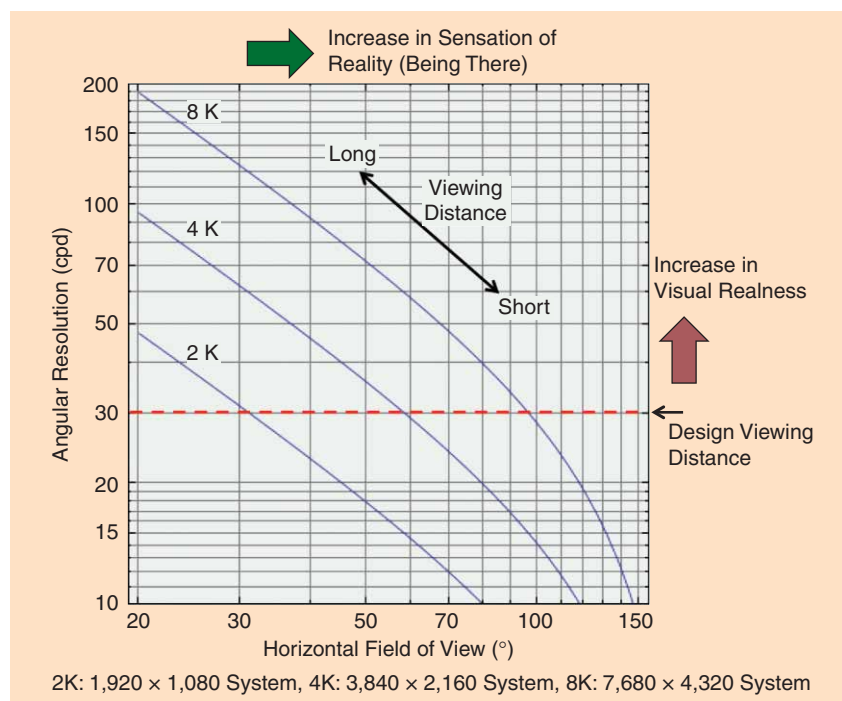


[FIG1] The FOV and angular resolution offered by HDTV and UHDTV systems.

standards **IN A NUTSHELL** continued

viewing distance. In conventional TV, the design viewing distance where the angular resolution is 30 cycles/degree (cpd) represents the condition where the picture quality is rated “five” on a five-grade quality scale [10]. This was generally regarded as the “optimal” viewing distance. However, experimental results show that discrimination ability (visual acuity measured with natural images) and increase perceived “realness” (subjective visual fidelity of reproduced images) were observed when the angular resolution exceeds 30 cpd [11].

Figure 1 plots the horizontal FOV and angular resolution that three systems with different pixel counts provide. The optimal viewing distance for the 1,920 × 1,080 (full HDTV or 2K) system provides an angular resolution of 30 cpd at an FOV of 30°. The 3,840 × 2,160 (4K) and 7,680 × 4,320 (8K) systems can increase the FOV up to 60 and 100°, respectively while maintaining angular resolution. This leads to the stronger sensation of reality as mentioned earlier. When the higher pixel count is used for increasing the angular resolution, it leads to improved realness. Some experimental results on the subjective effects

of increased pixel counts are described in ITU-R documents [8], [12].

Meanwhile, according to Rec. BT.1201, it is desirable that systems beyond HDTV have an integer multiple of the number of pixels in HDTV. The number of pixels in UHD TV was chosen to be exactly two or four times that of HDTV both in a horizontal and vertical direction.

FRAME FREQUENCY

Progressive scanning was the only scanning method under consideration because UHD TV is only likely to be used in digital systems. Up to 60 Hz, the frame frequencies are the same as for HDTV. Additionally, 120 Hz is also included in UHD TV. The need for this was asserted and observed from the results of an investigation of flicker and motion blur. These two characteristics for a particular frequency conflict in terms of the duty ratio, i.e., the ratio of the lighting period of the display to the whole frame duration. Flicker becomes more visible and motion blur decreases as the duty ratio decreases, and vice versa. Although many studies on flicker had been reported, a new experiment was conducted under varying conditions

such as FOV, screen luminance, and duty ratios appropriate for current display technologies and UHD TV. The result shows that the wider FOV requires a higher frame frequency to suppress flicker perception [13]. The frame frequency of 60 Hz (the frequency of HDTV) almost satisfies the critical fusion frequency (CFF) limit at an FOV of 30°, i.e., at the design viewing distance of HDTV. However, 8K UHD TV requires a frame frequency higher than 80 Hz to satisfy the CFF limit at an FOV of 100°.

Motion blur is one of the main artifacts caused by temporal sampling and finite temporal aperture. Conventional TV systems have been designed on the basis of an acquisition with 100% temporal aperture and impulse-type displays. This means that motion blur is attributed to the acquisition side. However, the technology shift from cathode ray tube (CRT) to non-CRT has brought motion blur to the display side. Subjective test results show that a simulated motion blur of 6~11 pixels/frame is an acceptable limit. This corresponds to the temporal aperture duration of 1/320th of a second for an object moving at 32%/s, which is near the limits of the tracking

[TABLE 1] THE COMPARISON OF UHD TV AND HDTV PARAMETERS.

PARAMETERS	UHDTV (BT.2020)		HDTV (BT.709 PART 2)	
PIXEL COUNT	7,680 X 4,320, 3,840 X 2,160		1,920 X 1,080	
FRAME FREQUENCY	120, 60, 60/1.001, 50, 30, 30/1.001, 25, 24, 24/1.001		60, 60/1.001, 50, 30, 30/1.001, 25, 24, 24/1.001	
SCANNING	PROGRESSIVE		PROGRESSIVE/INTERLACED	
COLORIMETRY	x	y	x	y
R	0.708	0.292	0.640	0.330
G	0.170	0.797	0.300	0.600
B	0.131	0.046	0.150	0.060
W	0.3127	0.3290	0.3127	0.3290
NONLINEAR TRANSFER FUNCTION	$E' = \begin{cases} 4.5E, & 0 \leq E < \beta \\ \alpha E^{0.45} - (\alpha - 1), & \beta \leq E \leq 1 \end{cases}$		SAME AS ON THE LEFT	
COLOR EQUATIONS	$Y'_c = (0.2627R + 0.6780G + 0.0593B)'$	$Y' = 0.2627R' + 0.6780G' + 0.0593B'$	$Y' = 0.2126R' + 0.7152G' + 0.0722B'$	
	$C'_{bc} = \begin{cases} \frac{B' - Y'_c}{1.9404}, & -0.9702 \leq B' - Y'_c \leq 0 \\ \frac{B' - Y'_c}{1.5816}, & 0 < B' - Y'_c \leq 0.7908 \end{cases}$	$C'_b = \frac{B' - Y'}{1.8814}$ $C'_r = \frac{R' - Y'}{1.4746}$	$C'_b = \frac{B' - Y'}{1.8556}$ $C'_r = \frac{R' - Y'}{1.5748}$	
	$C'_{rc} = \begin{cases} \frac{R' - Y'_c}{1.7184}, & -0.8592 \leq R' - Y'_c \leq 0 \\ \frac{R' - Y'_c}{0.9936}, & 0 < R' - Y'_c \leq 0.4968 \end{cases}$			
CHROMA SUBSAMPLING	4:4:4, 4:2:2, 4:2:0		4:2:2	
BIT DEPTH	12, 10		10, 8	

ability of human eyes and object speeds in TV programs. This can be realized by reducing the duty ratio or increasing the frame frequency. A minimal increase in frame frequency is desirable from the bandwidth viewpoint. It is therefore reasonable to take the following approach. First, the frame frequency should be increased up to the point where no flicker is perceptible at any duty ratio. Accordingly, motion blur can be reduced by shortening the duty ratio at the camera and/or display side. These are also reported in Rep. BT.2246, together with the overall motion picture quality evaluation results. Harmonization with the existing HDTV system is also desirable. Consequently, the additional frame frequency of 120 Hz is specified in Rec. BT.2020.

COLORIMETRY

The system colorimetry of conventional TV—both SDTV and HDTV—was limited by the type of display device. In short, the chromaticity coordinates of the red (R), green (G), blue (B) (RGB) primaries were determined on the basis of the properties of CRT phosphors. However, CRT technology is unlikely to be used for UHDTV displays. Moreover, it is difficult to imagine a particular display technology that will be predominant in the future. Under such circumstances, the following three requirements were taken into account for the system colorimetry of UHDTV:

- 1) Wide-gamut TV colorimetry should handle all the colors covered by existing TV systems and other related nonbroadcasting systems.
- 2) The color-coding efficiency of wide-gamut TV should be comparable to that in the currently used broadcasting systems.
- 3) Every color used in wide-gamut content should be displayable on a reference monitor so that broadcasters can monitor and control the image quality.

Consequently, it was agreed upon to use real physical colors for the three primary colors, resulting in the values shown in Table 1 and Figure 2. These values correspond to the monochromatic colors at wavelengths of 467 nm,

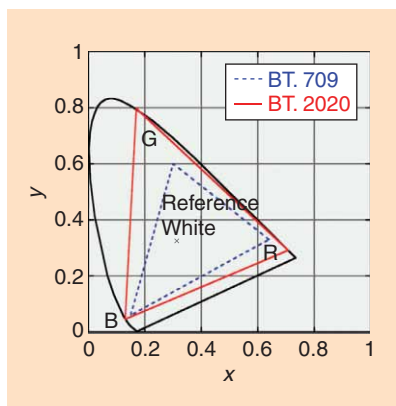


[FIG2] The chromaticity coordinate of RGB primaries and reference white for HDTV and UHDTV systems.

532 nm, and 630 nm for the blue, green, and red primaries, respectively.

In HDTV and earlier standards, the luminance (Y) signal was not a true representation of luminance (nonconstant luminance). This is due to the order of gamma-correction and Y signal calculation. In current systems, R, G, B signals are gamma-corrected before the Y signal, also called “luma,” is calculated. This deviates slightly from the true luminance, which can be derived by computing Y followed by gamma-correction. Although this only had a small effect on subjective picture quality, the issue was common knowledge among TV engineers, most of whom considered that a constant luminance system should be introduced sooner or later. On the other hand, the little-known benefits of the current nonconstant luminance approach (for example, the fact that signal processing operations, such as adding two images, can be done in gamma-corrected luma and color-difference space because they are linear combination of gamma-corrected RGB signals) became clear through the ITU-R activities. Considering the benefits and drawbacks of the constant and nonconstant method, the BT.2020 was formulated to contain both methods alongside each other.

With regard to chroma subsampling, the 4:2:0 and 4:4:4 ratios were added due to their applicability to progressive scanning; with regard to bit depth, the 8-bit depth was dropped and a 12-bit depth was added, to better match the contrast sensitivity of the human visual system (HVS).

CONCLUSIONS

UHDTV is a generational change in TV and will provide viewers with a much better audiovisual experience. New technologies are needed for implementing UHDTV systems effectively and efficiently to facilitate such an experience. Also, the receivers and the content have to be provided to the users at a reasonable cost.

We believe that the specifications of Rec. BT.2020 meet these requirements with regard to video. Their performance matches well with the HVS, since the parameter values were determined by carefully considering HVS characteristics. At the same time, recent prototypes of 4K- and 8K-resolution TV systems as well as digital cinema systems have proven their feasibility with current or near-term technologies.

The determination of system parameters is the first step in the development of TV systems. The agreed upon set of system parameters and its international standardization will accelerate the development of technologies and equipment aiming at the start of the UHDTV broadcasting services.

RESOURCES

The ITU home page (www.itu.int) has links to all ITU-R publications. ITU members can access the contribution documents for the study on UHDTV.

ACKNOWLEDGMENTS

The authors would like to thank the contributors to WP6C for their excellent work that has led to the establishment of Rec. BT.2020.

AUTHORS

Masayuki Sugawara (sugawara.m-fq@nhk.or.jp) is the head of the Advanced Television Systems Research Division at NHK Science & Technology Research Laboratories, Japan. He has been an active contributor to ITU-R SG6 since 2004.

Seo-Young Choi (seoyoung228@gmail.com) is an R&D staff member at Samsung Advanced Institute of Technology, Samsung Electronics Co., LTD., South Korea. She has been actively involved in the ITU-R standardization of the UHDTV baseband image format.

standards **IN A NUTSHELL** continued

David Wood (wood@ebu.ch) is a consultant, technology and innovation at the headquarters of the European Broadcasting Union in Geneva, Switzerland. He chairs the World Broadcasting Union's Technical Committee, ITU-R Working Group 6P, and DVB groups on 3DTV and UHDTV.

REFERENCES

- [1] "Parameter values for ultra-high definition television systems for production and international programme exchange," Recommendation ITU-R BT.2020, Aug. 2012.
- [2] "Conventional analogue television systems," Recommendation ITU-R BT.470-7, Feb. 2005.

[3] "Studio encoding parameters of digital television for standard 4:3 and wide screen 16:9 aspect ratios," Recommendation ITU-R BT.601-7, Mar. 2011.

[4] M. I. Krivocheev and S. N. Baron, "The first twenty years of HDTV: 1972-1992," *SMPTE Motion Imaging J.*, vol. 102, no. 10, pp. 913-930, Oct. 1993.

[5] "Parameter values for the HDTV standards for production and international programme exchange," Recommendation ITU-R BT.709-5, Apr. 2002.

[6] "Extremely high resolution imagery," Recommendation ITU-R BT.1201-1, Mar. 2004.

[7] "Worldwide unified colorimetry and related characteristics of future television and imaging systems," Recommendation ITU-R BT.1361, Feb. 1998.

[8] "The present state of ultra-high definition television," Report ITU-R BT.2246, 2012.


[9] M. Sugawara, K. Masaoka, M. Emoto, Y. Matsuo, and Y. Nojiri, "Research on human factors in ultra-high-definition television to determine its specifications," *SMPTE Motion Imaging J.*, vol. 117, no. 3, pp. 23-29, Apr. 2008.

[10] "Relative quality requirements of television broadcast systems," Recommendation ITU-R BT.1127, July 1994.

[11] K. Masaoka, Y. Nishida, M. Sugawara, E. Nakasu, and Y. Nojiri, "Sensation of realness from high-resolution images of real objects," *IEEE Trans. Broadcast.*, vol. 59, no. 1, pp. 72-83, Jan. 2013.

[12] "Parameter values for an expanded hierarchy of LSDI image formats for production and international programme exchange," Recommendation ITU-R BT.1769, July 2006.

[13] M. Emoto and M. Sugawara, "Critical fusion frequency for bright and wide field-of-view image display," *J. Display Technol.*, vol. 8, no. 7, pp. 424-429, July 2012.

[14] M. Sugawara, M. Emoto, K. Masaoka, Y. Nishida, and Y. Shishikui, "SUPER Hi-VISION for the next generation television: Determination of system parameters," *ITE Trans. MTA*, vol. 1, no. 1, pp. 27-33, Jan. 2013. 

lecture **NOTES** (continued from page 168)

term is below the reference level. This procedure will guarantee cross-terms-free distribution for components that do not overlap in the STFT.

Note that the SM calculation is alias free for any L (including the alias-free WD), with the same signal sampling rate as in the STFT (see "Example 3" and Figure 2 and "Example 4" and Figure 3).

GENERALIZATIONS

The smoothed spectrogram is composed of two STFTs $S_N(n, k+i)S_N^*(n, k+i)$ for several values of $i = 0, \pm 1, \dots$ in the same direction of index i . This kind of composition results in the distribution spread, in contrast to the SM, where two STFTs are composed in a counter-direction, $S_N(n, k+i)S_N^*(n, k-i)$. These two forms of composing the STFTs were used as a basis for classification of all discrete time-varying processes estimators in [7].

The SM as a concept of composing two transforms in a counter-direction has been generalized and used in the realization of cross-terms-free higher-order FT

representations (e.g., the polynomial Wigner-Ville, the L-Wigner, or the complex-time distributions). The same concept of composition has been used in the time-direction, two-dimensional TF domain, fractional domain, local polynomial FT domain, and on the affine forms, [3], [11].

CONCLUSIONS

The STFT as a time- and frequency-localized version of the FT is presented. It has been shown that this representation can be gradually transformed into better concentrated WD. From this transition process, we can learn about the autoterms concentration improvement, cross-terms appearance, how to control them, and how to obtain a representation combining good properties of the cross-terms-free STFT and highly concentrated WD.


AUTHORS

Ljubisa Stanković (ljubisa@ac.me) is a professor with the University of Montenegro.

Srdjan Stanković (srdjan@ac.me) is a professor with the University of Montenegro.

Miloš Daković (milos@ac.me) is an associate professor with the University of Montenegro.

REFERENCES

- [1] M. G. Amin, *Through-the-Wall Radar Imaging*. Boca Raton, FL: CRC Press, 2010.
- [2] F. Auger and F. Hlawatsch, Eds., *Time-Frequency Analysis: Concepts and Methods*. Hoboken, NJ: Wiley, 2008.
- [3] B. Boashash, Ed., *Time-Frequency Signal Analysis and Processing*. Amsterdam, The Netherlands: Elsevier, 2003.
- [4] L. Cohen, *Time-Frequency Analysis*. Englewood Cliffs, NJ: Prentice Hall, 1995.
- [5] P. Flandrin, *Temps-fréquence*. Paris: Hermes, 1993.
- [6] A. Papandreou-Suppappola, Ed., *Applications in Time-Frequency Signal Processing*. Boca Raton, FL: CRC Press, 2010.
- [7] L. L. Scharf and B. Friedlander, "Toeplitz and Hankel kernels for estimating time-varying spectra of discrete-time random processes," *IEEE Trans. Signal Processing*, vol. 49, no. 1, pp. 179-189, 2001.
- [8] L. Stanković, "A measure of some time-frequency distributions concentration," *Signal Process.*, vol. 81, no. 3, pp. 621-631, 2001.
- [9] S. Stanković, I. Orović, and E. Sejdić, *Multimedia Signals and Systems*. New York: Springer, 2012.
- [10] M. Vetterli and J. Kovačević, *Wavelets and Subband Coding*. Englewood Cliffs, NJ: Prentice Hall, 1994.
- [11] L. Stanković, M. Daković, and T. Thayaparan, *Time-Frequency Signal Analysis with Applications*. Norwood, MA: Artech House, 2013. 

[dates **AHEAD**]

Please send calendar submissions to:
Dates Ahead, c/o Jessica Barragué
IEEE Signal Processing Magazine
445 Hoes Lane
Piscataway, NJ 08855 USA
e-mail: j.barrague@ieee.org
(Colored reference title indicates
SP-sponsored conference.)

2014**[APRIL]**

IEEE International Symposium on Biomedical Imaging (ISBI)
28 April–2 May, Beijing, China.
General Chairs: Ge Wang and Bin He
URL: <http://biomedicalimaging.org/2014/>

[MAY]

IEEE International Conference on Acoustics, Speech, and Signal Processing (ICASSP)
4–9 May, Florence, Italy.
General Cochairs: Fulvio Gini and Marco Luise
URL: <http://www.icassp2014.org/>

IEEE Radar Conference (RadarCon)

19–23 May, Cincinnati, Ohio.
General Chair: Brian Rigling
URL: <http://www.radarcon2014.org/>

6th International Symposium on Communications, Control, and Signal Processing (ISCCSP)

21–23 May, Athens, Greece.
Honorary Chair: Anastasios Venetsanopoulos
General Cochairs: Sanjit K. Mitra and Thanos Stouraitis
URL: <http://isccsp2014.upatras.gr/>

Digital Object Identifier 10.1109/MSP.2014.2300739
Date of publication: 7 April 2014

[JUNE]

IEEE Sensor Array and Multichannel Signal Processing Workshop (SAM)
22–25 June, A Caruña, Spain.
URL: <http://www.gtec.udc.es/sam2014/>

IEEE Statistical Signal Processing Workshop (SSP)

29 June–2 July, Gold Coast, Australia.
General Cochairs: Rob Evans and Abd-Krim Seghouane
URL: <http://www.ee.unimelb.edu.au/SSP2014/index.html>

[JULY]

2nd IEEE China Summit and International Conference on Signal and Information Processing (ChinaSIP)
9–13 July, Xi'an, China.
General Chairs: Mingyi He and Kung Yao
URL: <http://www.chinasip2014.org/CfP.htm>

IEEE International Conference on Multimedia and Expo (ICME)

14–18 July, Chengdu, China.
General Cochairs: Touradj Ebrahimi, Shipeng Li, Houjun Wang, and Jie Yang
URL: <http://www.icme2014.org/>

[AUGUST]

11th IEEE International Conference on Advanced Video and Signal-Based Surveillance (AVSS)
26–29 August, Seoul, South Korea.
General Chair: Hanseok Ko
General Cochair: Jin Young Choi
URL: <http://www.avss2014.org/>

[SEPTEMBER]

24th IEEE International Workshop on Machine Learning for Signal Processing (MLSP)
21–24 September, Reims, France.
General Chair: Mamadou Mboup
URL: <http://mlsp2014.conwiz.dk/home.htm>

16th IEEE International Workshop on Multimedia Signal Processing (MMSP)

22–24 September, Jakarta, Indonesia.
General Chairs: Susanto Rahardja and Zhengyou Zhang
URL: <http://mmsp2014.ilearning.me/call-for-paper/>

[OCTOBER]

IEEE Workshop on Signal Processing Systems (SIPS)
20–23 October, Belfast, Ireland.

[DECEMBER]

IEEE Global Conference on Signal and Information Processing (GlobalSIP)
3–5 December, Atlanta, Georgia.
General Chairs: Geoffrey Li and Fred Juang
URL: <http://renyi.ece.iastate.edu/globalsip2014/>

IEEE Spoken Language Technology Workshop (SLT)

6–9 December, South Lake Tahoe, California.
General Chairs: Murat Akbacak and John Hansen

2015**[APRIL]**

IEEE International Conference on Acoustics, Speech, and Signal Processing (ICASSP)
19–24 April, Brisbane, Australia.
General Cochairs: Vaughan Clarkson and Jonathan Manton
URL: <http://icassp2015.org/>

[SEPTEMBER]

IEEE International Conference on Image Processing (ICIP)
28 September–1 October, Quebec City, Quebec, Canada.

advertisers **INDEX**

The Advertisers Index contained in this issue is compiled as a service to our readers and advertisers: the publisher is not liable for errors or omissions although every effort is made to ensure its accuracy. Be sure to let our advertisers know you found them through *IEEE Signal Processing Magazine*.

ADVERTISER	PAGE	URL	PHONE
Cambridge University Press	9	www.journals.cambridge.org/sip	
CRC Press/Taylor & Francis	13	www.crcpress.com	
IEEE GlobalSIP 2014	11	www.ieeeglobalsip.org	
IEEE Marketing Department	7	www.ieee.org/digitalsubscriptions	
IEEE MDL/Marketing	3	www.ieee.org/go/trymdl	
Mathworks	CVR 4	www.mathworks.com/accelerate	+1 508 647 7040
Mini-Circuits	CVR 2, 5, CVR 3	www.minicircuits.com	+1 718 934 4500

advertising **SALES OFFICES**

James A. Vick

Sr. Director, Advertising

Phone: +1 212 419 7767;

Fax: +1 212 419 7589

jv.ieeemedia@ieee.org

Marion Delaney

Advertising Sales Director

Phone: +1 415 863 4717;

Fax: +1 415 863 4717

md.ieeemedia@ieee.org

Susan E. Schneiderman

Business Development Manager

Phone: +1 732 562 3946;

Fax: +1 732 981 1855

ss.ieeemedia@ieee.org

Product Advertising

MIDATLANTIC

Lisa Rinaldo

Phone: +1 732 772 0160;

Fax: +1 732 772 0164

lr.ieeemedia@ieee.org

NY, NJ, PA, DE, MD, DC, KY, WV

**NEW ENGLAND/SOUTH CENTRAL/
EASTERN CANADA**

Jody Estabrook

Phone: +1 774 283 4528;

Fax: +1 774 283 4527

je.ieeemedia@ieee.org

ME, VT, NH, MA, RI, CT, AR, LA, OK, TX

Canada: Quebec, Nova Scotia,

Newfoundland, Prince Edward Island,

New Brunswick

SOUTHEAST

Thomas Flynn

Phone: +1 770 645 2944;

Fax: +1 770 993 4423

tf.ieeemedia@ieee.org

VA, NC, SC, GA, FL, AL, MS, TN

MIDWEST/CENTRAL CANADA

Dave Jones

Phone: +1 708 442 5633;

Fax: +1 708 442 7620

dj.ieeemedia@ieee.org

IL, IA, KS, MN, MO, NE, ND,

SD, WI, OH

Canada: Manitoba,

Saskatchewan, Alberta

**MIDWEST/ ONTARIO,
CANADA**

Will Hamilton

Phone: +1 269 381 2156;

Fax: +1 269 381 2556

wh.ieeemedia@ieee.org

IN, MI. Canada: Ontario

**WEST COAST/MOUNTAIN STATES/
WESTERN CANADA**

Marshall Rubin

Phone: +1 818 888 2407;

Fax: +1 818 888 4907

mr.ieeemedia@ieee.org

AZ, CO, HI, NM, NV, UT, AK, ID, MT,

WY, OR, WA, CA. Canada: British

Columbia

**EUROPE/AFRICA/MIDDLE EAST
ASIA/FAR EAST/PACIFIC RIM**

Louise Smith

Phone: +44 1875 825 700;

Fax: +44 1875 825 701

les.ieeemedia@ieee.org

Europe, Africa, Middle East

Asia, Far East, Pacific Rim, Australia,

New Zealand

Recruitment Advertising

MIDATLANTIC

Lisa Rinaldo

Phone: +1 732 772 0160;

Fax: +1 732 772 0164

lr.ieeemedia@ieee.org

NY, NJ, CT, PA, DE, MD, DC, KY, WV

NEW ENGLAND/EASTERN CANADA

Liza Reich

Phone: +1 212 419 7578;

Fax: +1 212 419 7589

e.reich@ieee.org

ME, VT, NH, MA, RI. Canada: Quebec,

Nova Scotia, Prince Edward Island,

Newfoundland, New Brunswick

SOUTHEAST

Cathy Flynn

Phone: +1 770 645 2944;

Fax: +1 770 993 4423

cf.ieeemedia@ieee.org

VA, NC, SC, GA, FL, AL, MS, TN

**MIDWEST/SOUTH CENTRAL/
CENTRAL CANADA**

Darcy Giovino

Phone: +224 616 3034;

Fax: +1 847 729 4269

dg.ieeemedia@ieee.org;

AR, IL, IN, IA, KS, LA, MI, MN, MO, NE,

ND, SD, OH, OK, TX, WI. Canada:

Ontario, Manitoba, Saskatchewan, Alberta

**WEST COAST/SOUTHWEST/
MOUNTAIN STATES/ASIA**

Tim Matteson

Phone: +1 310 836 4064;

Fax: +1 310 836 4067

tm.ieeemedia@ieee.org

AZ, CO, HI, NV, NM, UT, CA, AK, ID, MT,

WY, OR, WA. Canada: British Columbia

EUROPE/AFRICA/MIDDLE EAST

Louise Smith

Phone: +44 1875 825 700;

Fax: +44 1875 825 701

les.ieeemedia@ieee.org

Europe, Africa, Middle East

Digital Object Identifier 10.1109/MSP.2013.2290961

FILTER SOLUTIONS

DC to 15 GHz



Over 300 Models **IN STOCK** ... Immediate Delivery! from **\$199** ea. 10-49

Different needs demand different technologies, and the Mini-Circuits RF/microwave filter lineup delivers. Over 300 proven solutions, from DC to 15 GHz, are standing by, ready to ship. High-pass or low-pass, band-pass or band-stop, in coaxial, surface-mount, or plug-in packages. Across the board, our filters achieve low insertion loss and low VSWR in the passband and high attenuation in the rejection band. Just go to minicircuits.com for more information. If you need a specific performance and want to search our entire model database, including engineering models, click on Yoni2, our

exclusive search engine.

In Yoni2, you can enter the response type, connection option, frequency, insertion loss, or any other specifications you have. If a model cannot be found, we understand the sense of urgency. So contact us, and our engineers will find a quick, cost-effective, custom solution and deliver simulation results within a few days.

Yoni2™ The Design Engineers Search Engine...
U.S. Patent 7739260, 7761442 finds the model you need, instantly.



www.minicircuits.com P.O. Box 350166, Brooklyn, NY 11235-0003 (718) 934-4500 sales@minicircuits.com

484 Rev D



Find it at
mathworks.com/accelerate
datasheet
video example
trial request

GENERATE HDL CODE AUTOMATICALLY

from

MATLAB and Simulink



HDL CODER™ automatically converts Simulink models and MATLAB algorithms directly into Verilog and VHDL code for FPGAs or ASIC designs. The code is bit-true, cycle-accurate and synthesizable.

MATLAB®
& SIMULINK®

IEEE SIGNAL PROCESSING SOCIETY

CONTENT GAZETTE

[ISSN 2167-5023]



MAY 2014



IEEE GlobalSIP

December 3-5, 2014
Georgia Tech Hotel
and Conference Center
Atlanta, GA USA

General Chairs

Geoffrey Li
Georgia Tech

Fred Juang
Georgia Tech

Technical Program Chairs

Douglas Williams
Georgia Tech

Timothy Davidson
McMaster University

Ghassan AlRegib
Georgia Tech

Finance Chair

David V. Anderson
Georgia Tech

Local Arrangement Chair

Xiaoli Ma
Georgia Tech

Publications/Publicity Chair

Zhengdao Wang
Iowa State University

Industrial Liaison Chairs

Ahsan Aziz
National Instruments

Mashhour Solh
Texas Instruments

The 2nd IEEE Global Conference on Signal and Information Processing (GlobalSIP 2014)

The IEEE Global Conference on Signal and Information Processing (GlobalSIP) is a recently launched flagship conference of the IEEE Signal Processing Society. It is made up of a series of symposia and workshops. GlobalSIP 2014 will focus broadly on signal and information processing with an emphasis on up-and-coming signal processing themes. For details and paper submission, please go to <http://www.ieeeglobalsip.org>.

List of Symposia

1. Information Processing for Big Data
2. Perception Inspired Multimedia Signal Processing Techniques
3. Machine Learning Applications in Speech Processing
4. Data Flow Algorithms and Architecture for Signal Processing Systems
5. Advances in Mixed-Signal and Optical Sensing: Hardware to Algorithms
6. Signal Processing Applications Related to Animal Environments
7. Signal Processing for Next Generation Semiconductor Integrated Circuits
8. Energy Exchange and Intelligent Trading
9. Signal Processing for Cognitive Radios and Networks
10. Energy Efficiency and Energy Harvesting Related Signal Processing and Communications
11. Game Theory for Signal Processing and Communications
12. Signal Processing Challenges and Architectures for High Throughput Satellite Communications
13. Massive MIMO Communications
14. Network Theory

Workshops

1. Workshop on Information Forensics and Security (WIFS)
 - Privacy Preserving Technologies
 - Information Forensics and Watermarking
 - Biometrics, Authentication and Secure Multiparty Computation
 - Secure Communication and Networking
2. Workshop on Genomic Signal Processing and Statistics (GENSIPS)
 - Signal Processing of Genomic Sequencing Data
 - Modeling and Integration of Multi-Modality Omics Data
 - Dynamics and Control of Regulatory and Signaling Networks

Paper Submission

Paper submission instructions are available through the GlobalSIP 2014 website at <http://www.ieeeglobalsip.org>.

Contacts

Zhengdao Wang
Email: zhengdao@iastate.edu
for website and EDAS-related questions

Important Dates

May 16, 2014
June 27, 2014
September 5, 2014

Paper submission deadline (regular and invited)
Review results announced
Camera-ready regular and invited papers due



IEEE TRANSACTIONS ON SIGNAL PROCESSING

A PUBLICATION OF THE IEEE SIGNAL PROCESSING SOCIETY



www.signalprocessingsociety.org

Indexed in PubMed® and MEDLINE®, products of the United States National Library of Medicine



MARCH 15, 2014

VOLUME 62

NUMBER 6

ITPRED

(ISSN 1053-587X)

REGULAR PAPERS

Robust MIMO Equalization for Non-Parametric Channel Model Uncertainty http://dx.doi.org/10.1109/TSP.2014.2298378	<i>G. O. Corrêa</i>	1335
Asymptotic and Non-Asymptotic Analysis of Uplink Sum Rate for Relay-Assisted MIMO Cellular Systems http://dx.doi.org/10.1109/TSP.2013.2274642	<i>H. Wu, L. Wang, X. Wang, and X. You</i>	1348
On the Unique Identification of Continuous-Time Autoregressive Models From Sampled Data http://dx.doi.org/10.1109/TSP.2013.2296879 ..	<i>H. Kirshner, M. Unser, and J. P. Ward</i>	1361
Single Receiver Emitter Geolocation Based on Signal Periodicity With Oscillator Instability http://dx.doi.org/10.1109/TSP.2014.2298831 ..	<i>E. Tzoreff, B. Z. Bobrovsky, and A. J. Weiss</i>	1377
Distributed Sparse Recursive Least-Squares Over Networks http://dx.doi.org/10.1109/TSP.2014.2302731	<i>Z. Liu, Y. Liu, and C. Li</i>	1386

IEEE TRANSACTIONS ON SIGNAL PROCESSING (ISSN 1053-587X) is published semimonthly by the Institute of Electrical and Electronics Engineers, Inc. Responsibility for the contents rests upon the authors and not upon the IEEE, the Society/Council, or its members. **IEEE Corporate Office:** 3 Park Avenue, 17th Floor, New York, NY 10016-5997. **IEEE Operations Center:** 445 Hoes Lane, Piscataway, NJ 08854-4141. **NJ Telephone:** +1 732 981 0060. **Price/Publication Information:** Individual copies: IEEE Members \$20.00 (first copy only), nonmembers \$569.00 per copy. (Note: Postage and handling charge not included.) Member and nonmember subscription prices available upon request. **Copyright and Reprint Permissions:** Abstracting is permitted with credit to the source. Libraries are permitted to photocopy for private use of patrons, provided the per-copy fee of \$31.00 is paid through the Copyright Clearance Center, 222 Rosewood Drive, Danvers, MA 01923. For all other copying, reprint, or republication permission, write to Copyrights and Permissions Department, IEEE Publications Administration, 445 Hoes Lane, Piscataway, NJ 08854-4141. Copyright © 2014 by the Institute of Electrical and Electronics Engineers, Inc. All rights reserved. Periodicals Postage Paid at New York, NY and at additional mailing offices. **Postmaster:** Send address changes to IEEE TRANSACTIONS ON SIGNAL PROCESSING, IEEE, 445 Hoes Lane, Piscataway, NJ 08854-4141. GST Registration No. 125634188. CPC Sales Agreement #40013087. Return undeliverable Canada addresses to: Pitney Bowes IMEX, P.O. Box 4332, Stanton Rd., Toronto, ON M5W 3J4, Canada. IEEE prohibits discrimination, harassment and bullying. For more information visit <http://www.ieee.org/nondiscrimination>. Printed in U.S.A.



Detection of Spatially Correlated Time Series From a Network of Sensor Arrays http://dx.doi.org/10.1109/TSP.2014.2298833	1396
..... <i>N. Klausner, M. R. Azimi-Sadjadi, and L. L. Scharf</i>	
Feasibility Conditions for Interference Neutralization in Relay-Aided Interference Channel http://dx.doi.org/10.1109/TSP.2014.2301971 ...	1408
..... <i>D. Wu, C. Yang, T. Liu, and Z. Xiong</i>	
Distributed Maximum Likelihood Sensor Network Localization http://dx.doi.org/10.1109/TSP.2014.2302746	1424
..... <i>A. Simonetto and G. Leus</i>	
An Algebraic Translation of Cayley-Dickson Linear Systems and Its Applications to Online Learning	1438
http://dx.doi.org/10.1109/TSP.2013.2296881	
..... <i>T. Mizoguchi and I. Yamada</i>	
Stochastic MIMO Detector Based on the Markov Chain Monte Carlo Algorithm http://dx.doi.org/10.1109/TSP.2014.2301131	1454
..... <i>J. Chen, J. Hu, and G. E. Sobelman</i>	
l_q Sparsity Penalized Linear Regression With Cyclic Descent http://dx.doi.org/10.1109/TSP.2014.2302740	1464
..... <i>G. Marjanovic and V. Solo</i>	
Optimal Cooperative Beamforming Design for MIMO Decode-and-Forward Relay Channels http://dx.doi.org/10.1109/TSP.2014.2298380 ..	1476
..... <i>K. Xiong, P. Fan, Z. Xu, H.-C. Yang, and K. B. Letaief</i>	
Efficient Transmit Beamspace Design for Search-Free Based DOA Estimation in MIMO Radar	1490
http://dx.doi.org/10.1109/TSP.2014.2299513	
..... <i>A. Khabbazibasmenj, A. Hassanien, S. A. Vorobyov, and M. W. Morency</i>	
Sum-Rate Maximization in the Multicell MIMO Broadcast Channel With Interference Coordination	1501
http://dx.doi.org/10.1109/TSP.2014.2299512	
..... <i>D. H. N. Nguyen and T. Le-Ngoc</i>	
Series Expansion Approximations of Brownian Motion for Non-Linear Kalman Filtering of Diffusion Processes	1514
http://dx.doi.org/10.1109/TSP.2014.2303430	
..... <i>S. M. J. Lyons, S. Särkkä, and A. J. Storkey</i>	
Estimation for the Linear Model With Uncertain Covariance Matrices http://dx.doi.org/10.1109/TSP.2014.2301973	1525
..... <i>D. Zachariah, N. Shariati, M. Bengtsson, M. Jansson, and S. Chatterjee</i>	
On Kronecker and Linearly Structured Covariance Matrix Estimation http://dx.doi.org/10.1109/TSP.2014.2298834	1536
..... <i>P. Wirfält and M. Jansson</i>	
Real-Valued MUSIC for Efficient Direction Estimation With Arbitrary Array Geometries http://dx.doi.org/10.1109/TSP.2014.2298384	1548
..... <i>F.-G. Yan, M. Jin, S. Liu, and X.-L. Qiao</i>	
Spatial-Frequency Signal Alignment for Opportunistic Transmission http://dx.doi.org/10.1109/TSP.2014.2301975	1561
..... <i>L. Lu, G. Y. Li, and A. Maaref</i>	
A Factor Graph Approach to Joint OFDM Channel Estimation and Decoding in Impulsive Noise Environments	1576
http://dx.doi.org/10.1109/TSP.2013.2295063	
..... <i>M. Nassar, P. Schniter, and B. L. Evans</i>	
New Efficient 2-D Lattice Structures for General Autoregressive Modeling of Random Fields http://dx.doi.org/10.1109/TSP.2014.2301142 ..	1590
..... <i>A. H. Kayran and E. Camcioglu</i>	
Generation of Antipodal Random Vectors With Prescribed Non-Stationary 2-nd Order Statistics	1603
http://dx.doi.org/10.1109/TSP.2014.2302737	
..... <i>A. Caprara, F. Furini, A. Lodi, M. Mangia, R. Rovatti, and G. Setti</i>	

IEEE TRANSACTIONS ON SIGNAL PROCESSING

A PUBLICATION OF THE IEEE SIGNAL PROCESSING SOCIETY



www.signalprocessingsociety.org

Indexed in PubMed® and MEDLINE®, products of the United States National Library of Medicine



MARCH 15, 2014

VOLUME 62

NUMBER 6

ITPRED

(ISSN 1053-587X)

REGULAR PAPERS

Adaptive Signal Processing

Distributed Sparse Recursive Least-Squares Over Networks <http://dx.doi.org/ves> Z. Liu, Y. Liu, and C. Li 1386

An Algebraic Translation of Cayley-Dickson Linear Systems and Its Applications to Online Learning
<http://dx.doi.org/10.1109/TSP.2013.2296881> T. Mizoguchi and I. Yamada 1438

Digital and Multirate Signal Processing

On the Unique Identification of Continuous-Time Autoregressive Models From Sampled Data <http://dx.doi.org/10.1109/TSP.2013.2296879> ..
..... H. Kirshner, M. Unser, and J. P. Ward 1361

Multidimensional Signal Processing

Series Expansion Approximations of Brownian Motion for Non-Linear Kalman Filtering of Diffusion Processes
<http://dx.doi.org/10.1109/TSP.2014.2303430> S. M. J. Lyons, S. Särkkä, and A. J. Storkey 1514

New Efficient 2-D Lattice Structures for General Autoregressive Modeling of Random Fields <http://dx.doi.org/10.1109/TSP.2014.2301142> ..
..... A. H. Kayran and E. Camcioglu 1590

IEEE TRANSACTIONS ON SIGNAL PROCESSING (ISSN 1053-587X) is published semimonthly by the Institute of Electrical and Electronics Engineers, Inc. Responsibility for the contents rests upon the authors and not upon the IEEE, the Society/Council, or its members. **IEEE Corporate Office:** 3 Park Avenue, 17th Floor, New York, NY 10016-5997. **IEEE Operations Center:** 445 Hoes Lane, Piscataway, NJ 08854-4141. **NJ Telephone:** +1 732 981 0060. **Price/Publication Information:** Individual copies: IEEE Members \$20.00 (first copy only), nonmembers \$569.00 per copy. (Note: Postage and handling charge not included.) Member and nonmember subscription prices available upon request. **Copyright and Reprint Permissions:** Abstracting is permitted with credit to the source. Libraries are permitted to photocopy for private use of patrons, provided the per-copy fee of \$31.00 is paid through the Copyright Clearance Center, 222 Rosewood Drive, Danvers, MA 01923. For all other copying, reprint, or republication permission, write to Copyrights and Permissions Department, IEEE Publications Administration, 445 Hoes Lane, Piscataway, NJ 08854-4141. Copyright © 2014 by the Institute of Electrical and Electronics Engineers, Inc. All rights reserved. Periodicals Postage Paid at New York, NY and at additional mailing offices. **Postmaster:** Send address changes to IEEE TRANSACTIONS ON SIGNAL PROCESSING, IEEE, 445 Hoes Lane, Piscataway, NJ 08854-4141. GST Registration No. 125634188. CPC Sales Agreement #40013087. Return undeliverable Canada addresses to: Pitney Bowes IMEX, P.O. Box 4332, Stanton Rd., Toronto, ON M5W 3J4, Canada. IEEE prohibits discrimination, harassment and bullying. For more information visit <http://www.ieee.org/nondiscrimination>. Printed in U.S.A.



<i>Machine Learning</i>	
A Factor Graph Approach to Joint OFDM Channel Estimation and Decoding in Impulsive Noise Environments http://dx.doi.org/none	M. Nassar, P. Schniter, and B. L. Evans 1576
<i>MIMO Communications & Signal Processing</i>	
Sum-Rate Maximization in the Multicell MIMO Broadcast Channel With Interference Coordination http://dx.doi.org/10.1109/TSP.2014.2299512	D. H. N. Nguyen and T. Le-Ngoc 1501
Asymptotic and Non-Asymptotic Analysis of Uplink Sum Rate for Relay-Assisted MIMO Cellular Systems http://dx.doi.org/10.1109/TSP.2013.2274642	H. Wu, L. Wang, X. Wang, and X. You 1348
Feasibility Conditions for Interference Neutralization in Relay-Aided Interference Channel http://dx.doi.org/10.1109/TSP.2014.2298378 D. Wu, C. Yang, T. Liu, and Z. Xiong 1408
Robust MIMO Equalization for Non-Parametric Channel Model Uncertainty http://dx.doi.org/10.1109/TSP.2014.2298380	G. O. Corrêa 1335
Optimal Cooperative Beamforming Design for MIMO Decode-and-Forward Relay Channels http://dx.doi.org/10.1109/TSP.2014.2302740 K. Xiong, P. Fan, Z. Xu, H.-C. Yang, and K. B. Letaief 1476
<i>Optimization Methods for Signal Processing</i>	
Generation of Antipodal Random Vectors With Prescribed Non-Stationary 2-nd Order Statistics http://dx.doi.org/10.1109/TSP.2014.2298833	A. Caprara, F. Furini, A. Lodi, M. Mangia, R. Rovatti, and G. Setti 1603
l_q Sparsity Penalized Linear Regression With Cyclic Descent http://dx.doi.org/10.1109/TSP.2014.2298831	G. Marjanovic and V. Solo 1464
<i>Sensor Array and Multichannel Processing</i>	
Detection of Spatially Correlated Time Series From a Network of Sensor Arrays http://dx.doi.org/10.1109/TSP.2014.2299513 N. Klausner, M. R. Azimi-Sadjadi, and L. L. Scharf 1396
Single Receiver Emitter Geolocation Based on Signal Periodicity With Oscillator Instability http://dx.doi.org/10.1109/TSP.2014.2298384 E. Tzoref, B. Z. Bobrovsky, and A. J. Weiss 1377
Efficient Transmit Beamspace Design for Search-Free Based DOA Estimation in MIMO Radar http://dx.doi.org/10.1109/TSP.2014.2302746	A. Khabbazi, A. Hassani, S. A. Vorobyov, and M. W. Morency 1490
Real-Valued MUSIC for Efficient Direction Estimation With Arbitrary Array Geometries http://dx.doi.org/10.1109/TSP.2014.2301975 F.-G. Yan, M. Jin, S. Liu, and X.-L. Qiao 1548
<i>Signal Processing for Sensor Networks</i>	
Distributed Maximum Likelihood Sensor Network Localization http://dx.doi.org/10.1109/TSP.2014.2301973	A. Simonetto and G. Leus 1424
<i>Signal Processing for Communications</i>	
Spatial-Frequency Signal Alignment for Opportunistic Transmission http://dx.doi.org/10.1109/TSP.2014.2298834	L. Lu, G. Y. Li, and A. Maaref 1561
<i>Statistical Signal Processing</i>	
Estimation for the Linear Model With Uncertain Covariance Matrices http://dx.doi.org/10.1109/TSP.2014.2301131	D. Zachariah, N. Shariati, M. Bengtsson, M. Jansson, and S. Chatterjee 1525
On Kronecker and Linearly Structured Covariance Matrix Estimation http://dx.doi.org/	P. Wirfält and M. Jansson 1536
<i>Signal Processing for Wireless Networks</i>	
Stochastic MIMO Detector Based on the Markov Chain Monte Carlo Algorithm http://dx.doi.org/	J. Chen, J. Hu, and G. E. Sobelman 1454

IEEE TRANSACTIONS ON SIGNAL PROCESSING

A PUBLICATION OF THE IEEE SIGNAL PROCESSING SOCIETY



www.signalprocessingsociety.org

Indexed in PubMed® and MEDLINE®, products of the United States National Library of Medicine



APRIL 1, 2014

VOLUME 62

NUMBER 7

ITPRED

(ISSN 1053-587X)

REGULAR PAPERS

Two-Way Range Estimation Utilizing Uplink and Downlink Channels Dependency http://dx.doi.org/10.1109/TSP.2014.2301976	<i>O. Bialer, D. Raphaeli, and A. J. Weiss</i>	1619
Dependence of the Stability of the Least Mean Fourth Algorithm on Target Weights Non-Stationarity http://dx.doi.org/10.1109/TSP.2014.2303426	<i>E. Eweda</i>	1634
On l_q Optimization and Sparse Inverse Covariance Selection http://dx.doi.org/10.1109/TSP.2014.2303429	<i>G. Marjanovic and V. Solo</i>	1644
Modal Analysis With Compressive Measurements http://dx.doi.org/10.1109/TSP.2014.2302736	<i>J. Y. Park, M. B. Wakin, and A. C. Gilbert</i>	1655
Decomposition Approach for Low-Rank Matrix Completion and Its Applications http://dx.doi.org/10.1109/TSP.2014.2301139	<i>R. Ma, N. Barzigar, A. Roozgard, and S. Cheng</i>	1671

IEEE TRANSACTIONS ON SIGNAL PROCESSING (ISSN 1053-587X) is published semimonthly by the Institute of Electrical and Electronics Engineers, Inc. Responsibility for the contents rests upon the authors and not upon the IEEE, the Society/Council, or its members. **IEEE Corporate Office:** 3 Park Avenue, 17th Floor, New York, NY 10016-5997. **IEEE Operations Center:** 445 Hoes Lane, Piscataway, NJ 08854-4141. **NJ Telephone:** +1 732 981 0060. **Price/Publication Information:** Individual copies: IEEE Members \$20.00 (first copy only), nonmembers \$569.00 per copy. (Note: Postage and handling charge not included.) Member and nonmember subscription prices available upon request. **Copyright and Reprint Permissions:** Abstracting is permitted with credit to the source. Libraries are permitted to photocopy for private use of patrons, provided the per-copy fee of \$31.00 is paid through the Copyright Clearance Center, 222 Rosewood Drive, Danvers, MA 01923. For all other copying, reprint, or republication permission, write to Copyrights and Permissions Department, IEEE Publications Administration, 445 Hoes Lane, Piscataway, NJ 08854-4141. Copyright © 2014 by the Institute of Electrical and Electronics Engineers, Inc. All rights reserved. Periodicals Postage Paid at New York, NY and at additional mailing offices. **Postmaster:** Send address changes to IEEE TRANSACTIONS ON SIGNAL PROCESSING, IEEE, 445 Hoes Lane, Piscataway, NJ 08854-4141. GST Registration No. 125634188. CPC Sales Agreement #40013087. Return undeliverable Canada addresses to: Pitney Bowes IMEX, P.O. Box 4332, Stanton Rd., Toronto, ON M5W 3J4, Canada. IEEE prohibits discrimination, harassment and bullying. For more information visit <http://www.ieee.org/nondiscrimination>. Printed in U.S.A.



Hierarchical Radio Resource Optimization for Heterogeneous Networks With Enhanced Inter-Cell Interference Coordination (eICIC) http://dx.doi.org/10.1109/TSP.2014.2302748	<i>A. Liu, V. K. N. Lau, L. Ruan, J. Chen, and D. Xiao</i>	1684
Greedy Algorithms for Joint Sparse Recovery http://dx.doi.org/10.1109/TSP.2014.2301980	<i>J. D. Blanchard, M. Cermak, D. Hanle, and Y. Jing</i>	1694
A Committee Machine Approach for Compressed Sensing Signal Reconstruction http://dx.doi.org/10.1109/TSP.2014.2303941	<i>S. K. Ambat, S. Chatterjee, and K. V. S. Hari</i>	1705
Single-Site Localization via Maximum Discrimination Multipath Fingerprinting http://dx.doi.org/10.1109/TSP.2014.2304923	<i>A. Jaffe and M. Wax</i>	1718
Design of IIR Digital Differentiators Using Constrained Optimization http://dx.doi.org/10.1109/TSP.2014.2302733	<i>R. C. Nongpiur, D. J. Shpak, and A. Antoniou</i>	1729
Deterministic Blind Identification of IIR Systems With Output-Switching Operations http://dx.doi.org/10.1109/TSP.2014.2300061	<i>C. Yu, L. Xie, and C. Zhang</i>	1740
On the Linear Convergence of the ADMM in Decentralized Consensus Optimization http://dx.doi.org/10.1109/TSP.2014.2304432	<i>W. Shi, Q. Ling, K. Yuan, G. Wu, and W. Yin</i>	1750
Smoothing and Decomposition for Analysis Sparse Recovery http://dx.doi.org/10.1109/TSP.2014.2304932	<i>Z. Tan, Y. C. Eldar, A. Beck, and A. Nehorai</i>	1762
Decentralized Data Reduction With Quantization Constraints http://dx.doi.org/10.1109/TSP.2014.2303432	<i>G. Xu, S. Zhu, and B. Chen</i>	1775
Performance Analysis and Optimization for Interference Alignment Over MIMO Interference Channels With Limited Feedback http://dx.doi.org/10.1109/TSP.2014.2304926	<i>X. Chen and C. Yuen</i>	1785
Sub-Nyquist Radar via Doppler Focusing http://dx.doi.org/10.1109/TSP.2014.2304917	<i>O. Bar-Ilan and Y. C. Eldar</i>	1796
On the Pilot Carrier Placement in Multicarrier-Based Systems http://dx.doi.org/10.1109/TSP.2014.2306179	<i>H. Steendam</i>	1812
Linear-Quadratic Blind Source Separation Using NMF to Unmix Urban Hyperspectral Images http://dx.doi.org/10.1109/TSP.2014.2306181	<i>I. Meganem, Y. Deville, S. Hosseini, P. Déliot, and X. Briottet</i>	1822
Robust Beamforming by Linear Programming http://dx.doi.org/10.1109/TSP.2014.2304438	<i>X. Jiang, W.-J. Zeng, A. Yasotharan, H. C. So, and T. Kirubarajan</i>	1834
Secrecy Wireless Information and Power Transfer With MISO Beamforming http://dx.doi.org/10.1109/TSP.2014.2303422	<i>L. Liu, R. Zhang, and K.-C. Chua</i>	1850
Bayesian Tracking in Underwater Wireless Sensor Networks With Port-Starboard Ambiguity http://dx.doi.org/10.1109/TSP.2014.2305640 ..	<i>P. Braca, P. Willett, K. LePage, S. Marano, and V. Matta</i>	1864
Minimum Dispersion Beamforming for Non-Gaussian Signals http://dx.doi.org/10.1109/TSP.2014.2305639	<i>X. Jiang, W.-J. Zeng, A. Yasotharan, H. C. So, and T. Kirubarajan</i>	1879

IEEE TRANSACTIONS ON SIGNAL PROCESSING

A PUBLICATION OF THE IEEE SIGNAL PROCESSING SOCIETY



www.signalprocessingsociety.org

Indexed in PubMed® and MEDLINE®, products of the United States National Library of Medicine



APRIL 1, 2014

VOLUME 62

NUMBER 7

ITPRED

(ISSN 1053-587X)

REGULAR PAPERS

Adaptive Signal Processing

Dependence of the Stability of the Least Mean Fourth Algorithm on Target Weights Non-Stationarity
<http://dx.doi.org/10.1109/TSP.2014.2303426> E. Eweda 1634

Digital and Multirate Signal Processing

Modal Analysis With Compressive Measurements <http://dx.doi.org/10.1109/TSP.2014.2302736> J. Y. Park, M. B. Wakin, and A. C. Gilbert 1655

Greedy Algorithms for Joint Sparse Recovery <http://dx.doi.org/10.1109/TSP.2014.2301980> J. D. Blanchard, M. Cermak, D. Hanle, and Y. Jing 1694

Decomposition Approach for Low-Rank Matrix Completion and Its Applications <http://dx.doi.org/10.1109/TSP.2014.2301139> R. Ma, N. Barzigar, A. Roozgard, and S. Cheng 1671

Design of IIR Digital Differentiators Using Constrained Optimization <http://dx.doi.org/10.1109/TSP.2014.2302733> R. C. Nongpiur, D. J. Shpak, and A. Antoniou 1729

Sub-Nyquist Radar via Doppler Focusing <http://dx.doi.org/10.1109/TSP.2014.2304917> O. Bar-Ilan and Y. C. Eldar 1796

A Committee Machine Approach for Compressed Sensing Signal Reconstruction <http://dx.doi.org/10.1109/TSP.2014.2303941> S. K. Ambat, S. Chatterjee, and K. V. S. Hari 1705

IEEE TRANSACTIONS ON SIGNAL PROCESSING (ISSN 1053-587X) is published semimonthly by the Institute of Electrical and Electronics Engineers, Inc. Responsibility for the contents rests upon the authors and not upon the IEEE, the Society/Council, or its members. **IEEE Corporate Office:** 3 Park Avenue, 17th Floor, New York, NY 10016-5997. **IEEE Operations Center:** 445 Hoes Lane, Piscataway, NJ 08854-4141. **NJ Telephone:** +1 732 981 0060. **Price/Publication Information:** Individual copies: IEEE Members \$20.00 (first copy only), nonmembers \$569.00 per copy. (Note: Postage and handling charge not included.) Member and nonmember subscription prices available upon request. **Copyright and Reprint Permissions:** Abstracting is permitted with credit to the source. Libraries are permitted to photocopy for private use of patrons, provided the per-copy fee of \$31.00 is paid through the Copyright Clearance Center, 222 Rosewood Drive, Danvers, MA 01923. For all other copying, reprint, or republication permission, write to Copyrights and Permissions Department, IEEE Publications Administration, 445 Hoes Lane, Piscataway, NJ 08854-4141. Copyright © 2014 by the Institute of Electrical and Electronics Engineers, Inc. All rights reserved. Periodicals Postage Paid at New York, NY and at additional mailing offices. **Postmaster:** Send address changes to IEEE TRANSACTIONS ON SIGNAL PROCESSING, IEEE, 445 Hoes Lane, Piscataway, NJ 08854-4141. GST Registration No. 125634188. CPC Sales Agreement #40013087. Return undeliverable Canada addresses to: Pitney Bowes IMEX, P.O. Box 4332, Stanton Rd., Toronto, ON M5W 3J4, Canada. IEEE prohibits discrimination, harassment and bullying. For more information visit <http://www.ieee.org/nondiscrimination>. Printed in U.S.A.



<i>Machine Learning</i>	
Linear-Quadratic Blind Source Separation Using NMF to Unmix Urban Hyperspectral Images http://dx.doi.org/10.1109/TSP.2014.2306181	I. Meganem, Y. Deville, S. Hosseini, P. Déliot, and X. Briottet 1822
<i>Optimization Methods for Signal Processing</i>	
Smoothing and Decomposition for Analysis Sparse Recovery http://dx.doi.org/10.1109/TSP.2014.2304932	Z. Tan, Y. C. Eldar, A. Beck, and A. Nehorai 1762
Secrecy Wireless Information and Power Transfer With MISO Beamforming http://dx.doi.org/10.1109/TSP.2014.2303422	L. Liu, R. Zhang, and K.-C. Chua 1850
On the Linear Convergence of the ADMM in Decentralized Consensus Optimization http://dx.doi.org/10.1109/TSP.2014.2304432	W. Shi, Q. Ling, K. Yuan, G. Wu, and W. Yin 1750
<i>Sensor Array and Multichannel Processing</i>	
Robust Beamforming by Linear Programming http://dx.doi.org/10.1109/TSP.2014.2304438	X. Jiang, W.-J. Zeng, A. Yasotharan, H. C. So, and T. Kirubarajan 1834
Minimum Dispersion Beamforming for Non-Gaussian Signals http://dx.doi.org/10.1109/TSP.2014.2305639	X. Jiang, W.-J. Zeng, A. Yasotharan, H. C. So, and T. Kirubarajan 1879
Two-Way Range Estimation Utilizing Uplink and Downlink Channels Dependency http://dx.doi.org/10.1109/TSP.2014.2301976	O. Bialer, D. Raphaeli, and A. J. Weiss 1619
Single-Site Localization via Maximum Discrimination Multipath Fingerprinting http://dx.doi.org/10.1109/TSP.2014.2304923	A. Jaffe and M. Wax 1718
Bayesian Tracking in Underwater Wireless Sensor Networks With Port-Starboard Ambiguity http://dx.doi.org/10.1109/TSP.2014.2305640 ..	P. Braca, P. Willett, K. LePage, S. Marano, and V. Matta 1864
<i>Signal Processing for Communications</i>	
On the Pilot Carrier Placement in Multicarrier-Based Systems http://dx.doi.org/10.1109/TSP.2014.2306179	H. Steendam 1812
Performance Analysis and Optimization for Interference Alignment Over MIMO Interference Channels With Limited Feedback http://dx.doi.org/10.1109/TSP.2014.2304926	X. Chen and C. Yuen 1785
<i>Statistical Signal Processing</i>	
Deterministic Blind Identification of IIR Systems With Output-Switching Operations http://dx.doi.org/10.1109/TSP.2014.2300061	C. Yu, L. Xie, and C. Zhang 1740
On l_q Optimization and Sparse Inverse Covariance Selection http://dx.doi.org/10.1109/TSP.2014.2303429	G. Marjanovic and V. Solo 1644
<i>Signal Processing for Sensor Networks</i>	
Decentralized Data Reduction With Quantization Constraints http://dx.doi.org/10.1109/TSP.2014.2303432	G. Xu, S. Zhu, and B. Chen 1775
<i>Signal Processing for Wireless Networks</i>	
Hierarchical Radio Resource Optimization for Heterogeneous Networks With Enhanced Inter-Cell Interference Coordination (eICIC) http://dx.doi.org/10.1109/TSP.2014.2302748	A. Liu, V. K. N. Lau, L. Ruan, J. Chen, and D. Xiao 1684

IEEE/ACM TRANSACTIONS ON AUDIO, SPEECH, AND LANGUAGE PROCESSING

A PUBLICATION OF THE IEEE SIGNAL PROCESSING SOCIETY



www.signalprocessingsociety.org

Indexed in PubMed® and MEDLINE®, products of the United States National Library of Medicine



MARCH 2014

VOLUME 22

NUMBER 3

ITASFA

(ISSN 2329-9290)

REGULAR PAPERS

Synthesis of Spontaneous Speech With Syllable Contraction Using State-Based Context-Dependent Voice Transformation http://dx.doi.org/10.1109/TASLP.2013.2297018	<i>C.-H. Wu, Y.-C. Huang, C.-H. Lee, and J.-C. Guo</i>	585
Quasi Closed Phase Glottal Inverse Filtering Analysis With Weighted Linear Prediction http://dx.doi.org/10.1109/TASLP.2013.2294585	<i>M. Airaksinen, T. Raitio, B. Story, and P. Alku</i>	596
Online Speech Dereverberation Algorithm Based on Adaptive Multichannel Linear Prediction http://dx.doi.org/10.1109/TASLP.2013.2294578	<i>J.-M. Yang and H.-G. Kang</i>	608

IEEE TRANSACTIONS ON AUDIO, SPEECH, AND LANGUAGE PROCESSING (ISSN 2329-9290) is published bimonthly in print and monthly online by the Institute of Electrical and Electronics Engineers, Inc. Responsibility for the contents rests upon the authors and not upon the IEEE, the Society/Council, or its members. **IEEE Corporate Office:** 3 Park Avenue, 17th Floor, New York, NY 10016-5997. **IEEE Operations Center:** 445 Hoes Lane, Piscataway, NJ 08854-4141. **NJ Telephone:** +1 732 981 0060. **Price/Publication Information:** Individual copies: IEEE Members \$20.00 (first copy only), nonmembers \$307.00 per copy. (Note: Postage and handling charge not included.) Member and nonmember subscription prices available upon request. **Copyright and Reprint Permissions:** Abstracting is permitted with credit to the source. Libraries are permitted to photocopy for private use of patrons, provided the per-copy fee of \$31.00 is paid through the Copyright Clearance Center, 222 Rosewood Drive, Danvers, MA 01923. For all other copying, reprint, or republication permission, write to Copyrights and Permissions Department, IEEE Publications Administration, 445 Hoes Lane, Piscataway, NJ 08854-4141. Copyright © 2013 by the Institute of Electrical and Electronics Engineers, Inc. All rights reserved. Periodicals Postage Paid at New York, NY and at additional mailing offices. **Postmaster:** Send address changes to IEEE TRANSACTIONS ON AUDIO, SPEECH, AND LANGUAGE PROCESSING, IEEE, 445 Hoes Lane, Piscataway, NJ 08854-4141. GST Registration No. 125634188. CPC Sales Agreement #40013087. Return undeliverable Canada addresses to: Pitney Bowes IMEX, P.O. Box 4332, Stanton Rd., Toronto, ON M5W 3J4, Canada. IEEE prohibits discrimination, harassment and bullying. For more information visit <http://www.ieee.org/nondiscrimination>. Printed in U.S.A.



(Contents Continued from Page 581)

Structured Sparsity Models for Reverberant Speech Separation http://dx.doi.org/10.1109/TASLP.2013.2297012	620
..... <i>A. Asaei, M. Golbabaee, H. Bourlard, and V. Cevher</i>	
Multichannel Equalization in the KLT and Frequency Domains With Application to Speech Dereverberation http://dx.doi.org/10.1109/TASLP.2013.2297013	634
..... <i>R. S. Rashobh, A. W. H. Khong, and D. Liu</i>	
Wavefield Analysis Over Large Areas Using Distributed Higher Order Microphones http://dx.doi.org/10.1109/TASLP.2014.2300341	647
..... <i>P. Samarasinghe, T. Abhayapala, and M. Poletti</i>	
Exploiting Psychological Factors for Interaction Style Recognition in Spoken Conversation http://dx.doi.org/10.1109/TASLP.2014.2300339 ..	659
..... <i>W.-L. Wei, C.-H. Wu, J.-C. Lin, and H. Li</i>	
Genre-Based Music Language Modeling with Latent Hierarchical Pitman-Yor Process Allocation http://dx.doi.org/10.1109/TASLP.2014.2300344	672
..... <i>S. A. Raczynski and E. Vincent</i>	
The Theory of Compressive Sensing Matching Pursuit Considering Time-domain Noise with Application to Speech Enhancement http://dx.doi.org/10.1109/TASLP.2014.2300336	682
..... <i>D. Wu, W.-P. Zhu, and M. N. S. Swamy</i>	
Cascaded Long Term Prediction for Enhanced Compression of Polyphonic Audio Signals http://dx.doi.org/10.1109/TASLP.2014.2303292 ...	697
..... <i>T. Nanjundaswamy and K. Rose</i>	
Theoretical Analysis of Diversity in an Ensemble of Automatic Speech Recognition Systems http://dx.doi.org/10.1109/TASLP.2014.2303295	711
..... <i>K. Audhkhasi, A. M. Zavou, P. G. Georgiou, and S. S. Narayanan</i>	
Direction of Arrival Based Spatial Covariance Model for Blind Sound Source Separation http://dx.doi.org/10.1109/TASLP.2014.2303576	727
..... <i>J. Nikunen and T. Virtanen</i>	

IEEE/ACM TRANSACTIONS ON AUDIO, SPEECH, AND LANGUAGE PROCESSING

A PUBLICATION OF THE IEEE SIGNAL PROCESSING SOCIETY



www.signalprocessingsociety.org

Indexed in PubMed® and MEDLINE®, products of the United States National Library of Medicine



MARCH 2014

VOLUME 22

NUMBER 3

ITASFA

(ISSN 2329-9290)

REGULAR PAPERS

Room Acoustics and Acoustic System Modeling

Multichannel Equalization in the KLT and Frequency Domains With Application to Speech Dereverberation
<http://dx.doi.org/10.1109/TASLP.2013.2297013> R. S. Rashobh, A. W. H. Khong, and D. Liu 634

Loudspeaker and Microphone Array Signal Processing

Wavefield Analysis Over Large Areas Using Distributed Higher Order Microphones <http://dx.doi.org/10.1109/TASLP.2014.2300341>
 P. Samarasinghe, T. Abhayapala, and M. Poletti 647

IEEE TRANSACTIONS ON AUDIO, SPEECH, AND LANGUAGE PROCESSING (ISSN 2329-9290) is published bimonthly in print and monthly online by the Institute of Electrical and Electronics Engineers, Inc. Responsibility for the contents rests upon the authors and not upon the IEEE, the Society/Council, or its members. **IEEE Corporate Office:** 3 Park Avenue, 17th Floor, New York, NY 10016-5997. **IEEE Operations Center:** 445 Hoes Lane, Piscataway, NJ 08854-4141. **NJ Telephone:** +1 732 981 0060. **Price/Publication Information:** Individual copies: IEEE Members \$20.00 (first copy only), nonmembers \$307.00 per copy. (Note: Postage and handling charge not included.) Member and nonmember subscription prices available upon request. **Copyright and Reprint Permissions:** Abstracting is permitted with credit to the source. Libraries are permitted to photocopy for private use of patrons, provided the per-copy fee of \$31.00 is paid through the Copyright Clearance Center, 222 Rosewood Drive, Danvers, MA 01923. For all other copying, reprint, or republication permission, write to Copyrights and Permissions Department, IEEE Publications Administration, 445 Hoes Lane, Piscataway, NJ 08854-4141. Copyright © 2013 by the Institute of Electrical and Electronics Engineers, Inc. All rights reserved. Periodicals Postage Paid at New York, NY and at additional mailing offices. **Postmaster:** Send address changes to IEEE TRANSACTIONS ON AUDIO, SPEECH, AND LANGUAGE PROCESSING, IEEE, 445 Hoes Lane, Piscataway, NJ 08854-4141. GST Registration No. 125634188. CPC Sales Agreement #40013087. Return undeliverable Canada addresses to: Pitney Bowes IMEX, P.O. Box 4332, Stanton Rd., Toronto, ON M5W 3J4, Canada. IEEE prohibits discrimination, harassment and bullying. For more information visit <http://www.ieee.org/nondiscrimination>. Printed in U.S.A.



<i>Audio Source Separation and Enhancement</i>	
Structured Sparsity Models for Reverberant Speech Separation http://dx.doi.org/10.1109/TASLP.2013.2297012	620
..... A. Asaei, M. Golbabaee, H. Boulard, and V. Cevher	
Direction of Arrival Based Spatial Covariance Model for Blind Sound Source Separation http://dx.doi.org/10.1109/TASLP.2014.2303576	727
..... J. Nikunen and T. Virtanen	
<i>Audio Coding</i>	
Cascaded Long Term Prediction for Enhanced Compression of Polyphonic Audio Signals http://dx.doi.org/10.1109/TASLP.2014.2303292 ...	697
..... T. Nanjundaswamy and K. Rose	
<i>Content-Based Music Processing</i>	
Genre-Based Music Language Modeling with Latent Hierarchical Pitman-Yor Process Allocation http://dx.doi.org/10.1109/TASLP.2014.2300344	672
..... S. A. Raczynski and E. Vincent	
<i>Speech Analysis</i>	
Quasi Closed Phase Glottal Inverse Filtering Analysis With Weighted Linear Prediction http://dx.doi.org/10.1109/TASLP.2013.2294585	596
..... M. Airaksinen, T. Raitio, B. Story, and P. Alku	
<i>Speech Synthesis and Generation</i>	
Synthesis of Spontaneous Speech With Syllable Contraction Using State-Based Context-Dependent Voice Transformation http://dx.doi.org/10.1109/TASLP.2013.2297018	585
..... C.-H. Wu, Y.-C. Huang, C.-H. Lee, and J.-C. Guo	
<i>General Topics in Speech Recognition</i>	
Theoretical Analysis of Diversity in an Ensemble of Automatic Speech Recognition Systems http://dx.doi.org/10.1109/TASLP.2014.2303295	711
..... K. Audhkhasi, A. M. Zavou, P. G. Georgiou, and S. S. Narayanan	
<i>Speech Enhancement</i>	
Online Speech Dereverberation Algorithm Based on Adaptive Multichannel Linear Prediction http://dx.doi.org/10.1109/TASLP.2013.2294578	608
..... J.-M. Yang and H.-G. Kang	
The Theory of Compressive Sensing Matching Pursuit Considering Time-domain Noise with Application to Speech Enhancement http://dx.doi.org/10.1109/TASLP.2014.2300336	682
..... D. Wu, W.-P. Zhu, and M. N. S. Swamy	
<i>Spoken Language Understanding</i>	
Exploiting Psychological Factors for Interaction Style Recognition in Spoken Conversation http://dx.doi.org/10.1109/TASLP.2014.2300339 ..	659
..... W.-L. Wei, C.-H. Wu, J.-C. Lin, and H. Li	

IEEE TRANSACTIONS ON IMAGE PROCESSING

A PUBLICATION OF THE IEEE SIGNAL PROCESSING SOCIETY



www.signalprocessingsociety.org

Indexed in PubMed® and MEDLINE®, products of the United States National Library of Medicine



MARCH 2014

VOLUME 23

NUMBER 3

IIPRE4

(ISSN 1057-7149)

PAPERS

- A Novel Joint Data-Hiding and Compression Scheme Based on SMVQ and Image Inpainting <http://dx.doi.org/10.1109/TIP.2014.2260760> ..
..... *C. Qin, C.-C. Chang, and Y.-P. Chiu* 969
- Kernel-Based Learning from Both Qualitative and Quantitative Labels: Application to Prostate Cancer Diagnosis Based
on Multiparametric MR Imaging <http://dx.doi.org/10.1109/TIP.2014.2295759> ..
..... *É. Niaf, R. Flamary, O. Rouvière, C. Lartizien, and S. Canu* 979
- Efficient Circular Thresholding <http://dx.doi.org/10.1109/TIP.2014.2297014> ..
..... *Y.-K. Lai and P. L. Rosin* 992
- Sparse Label-Indicator Optimization Methods for Image Classification <http://dx.doi.org/10.1109/TIP.2014.2294546> ..
..... *L. Jing and M. K. Ng* 1002
- LineCast: Line-Based Distributed Coding and Transmission for Broadcasting Satellite Images <http://dx.doi.org/10.1109/TIP.2014.2298972> ..
..... *F. Wu, X. Peng, and J. Xu* 1015
- Multi-Label Image Categorization With Sparse Factor Representation <http://dx.doi.org/10.1109/TIP.2014.2298978> ..
..... *F. Sun, J. Tang, H. Li, G.-J. Qi, and T. S. Huang* 1028
- A New Iterative Triclass Thresholding Technique in Image Segmentation <http://dx.doi.org/10.1109/TIP.2014.2298981> ..
..... *H. Cai, Z. Yang, X. Cao, W. Xia, and X. Xu* 1038
- Learning and Recognition of On-Premise Signs from Weakly Labeled Street View Images <http://dx.doi.org/10.1109/TIP.2014.2298982> ..
..... *T.-H. Tsai, W.-H. Cheng, C.-W. You, M.-C. Hu, A. W. Tsui, and H.-Y. Chi* 1047
- Insights Into Analysis Operator Learning: From Patch-Based Sparse Models to Higher Order MRFs
<http://dx.doi.org/10.1109/TIP.2014.2299065> ..
..... *Y. Chen, R. Ranftl, and T. Pock* 1060
- An Automatic Graph-Based Approach for Artery/Vein Classification in Retinal Images <http://dx.doi.org/10.1109/TIP.2014.2263809> ..
..... *B. Dashtbozorg, A. M. Mendonça, and A. Campilho* 1073
- Image Interpolation via Graph-Based Bayesian Label Propagation <http://dx.doi.org/10.1109/TIP.2014.2294543> ..
..... *X. Liu, D. Zhao, J. Zhou, W. Gao, and H. Sun* 1084
- A Rain Pixel Recovery Algorithm for Videos With Highly Dynamic Scenes <http://dx.doi.org/10.1109/TIP.2014.2290595> ..
..... *J. Chen and L.-P. Chau* 1097



Robust Face Recognition from Multi-View Videos http://dx.doi.org/10.1109/TIP.2014.2300812	<i>M. Du, A. C. Sankaranarayanan, and R. Chellappa</i>	1105
Angular Pattern and Binary Angular Pattern for Shape Retrieval http://dx.doi.org/10.1109/TIP.2014.2286330	<i>R.-X. Hu, W. Jia, H. Ling, Y. Zhao, and J. Gui</i>	1118
Cartoon-Texture Image Decomposition Using Blockwise Low-Rank Texture Characterization http://dx.doi.org/10.1109/TIP.2014.2299067 ..	<i>S. Ono, T. Miyata, and I. Yamada</i>	1128
Convex-Relaxed Kernel Mapping for Image Segmentation http://dx.doi.org/10.1109/TIP.2014.2297019	<i>M. B. Salah, I. B. Ayed, J. Yuan, and H. Zhang</i>	1143
Joint Non-Gaussian Denoising and Superresolving of Raw High Frame Rate Videos http://dx.doi.org/10.1109/TIP.2014.2298976	<i>J. Suo, Y. Deng, L. Bian, and Q. Dai</i>	1154
Does Deblurring Improve Geometrical Hyperspectral Unmixing? http://dx.doi.org/10.1109/TIP.2014.2300822	<i>S. Henrot, C. Soussen, M. Dossot, and D. Brie</i>	1169
Super-Resolution for Computed Tomography Based on Discrete Tomography http://dx.doi.org/10.1109/TIP.2014.2297025	<i>W. van Aarle, K. J. Batenburg, G. V. Gompel, E. V. de Castele, and J. Sijbers</i>	1181
Evaluating Combinational Illumination Estimation Methods on Real-World Images http://dx.doi.org/10.1109/TIP.2014.2277943	<i>B. Li, W. Xiong, W. Hu, and B. Funt</i>	1194
An Unsupervised Feature Selection Dynamic Mixture Model for Motion Segmentation http://dx.doi.org/10.1109/TIP.2014.2300811	<i>T. M. Nguyen and Q. J. Wu</i>	1210
Quadtree Structured Image Approximation for Denoising and Interpolation http://dx.doi.org/10.1109/TIP.2014.2300817	<i>A. Scholefield and P. L. Dragotti</i>	1226
Robust Automatic Line Scratch Detection in Films http://dx.doi.org/10.1109/TIP.2014.2300824	<i>A. Newson, A. Almansa, Y. Gousseau, and P. Pérez</i>	1240
An Unbiased Risk Estimator for Image Denoising in the Presence of Mixed Poisson-Gaussian Noise http://dx.doi.org/10.1109/TIP.2014.2300821	<i>Y. L. Montagner, E. D. Angelini, and J.-C. Olivo-Marin</i>	1255
Improved Block Truncation Coding Using Optimized Dot Diffusion http://dx.doi.org/10.1109/TIP.2014.2257812	<i>J.-M. Guo and Y.-F. Liu</i>	1269
Group-Invariant Colour Morphology Based on Frames http://dx.doi.org/10.1109/TIP.2014.2300816	<i>J. J. van de Gronde and J. B. T. M. Roerdink</i>	1276
On Averaging Multiview Relations for 3D Scan Registration http://dx.doi.org/10.1109/TIP.2014.2246517	<i>V. M. Govindu and P. A.</i>	1289
Transparent Composite Model for DCT Coefficients: Design and Analysis http://dx.doi.org/10.1109/TIP.2014.2300818	<i>E.-H. Yang, X. Yu, J. Meng, and C. Sun</i>	1303
A Compressive Sensing based Secure Watermark Detection and Privacy Preserving Storage Framework http://dx.doi.org/10.1109/TIP.2014.2298980	<i>Q. Wang, W. Zeng, and J. Tian</i>	1317
Noise Parameter Estimation for Poisson Corrupted Images Using Variance Stabilization Transforms http://dx.doi.org/10.1109/TIP.2014.2300813	<i>X. Jin, Z. Xu, and K. Hirakawa</i>	1329
A Complete System for Automatic Extraction of Left Ventricular Myocardium From CT Images Using Shape Segmentation and Contour Evolution http://dx.doi.org/10.1109/TIP.2014.2300751	<i>L. Zhu, Y. Gao, V. Appia, A. Yezzi, C. Arepalli, T. Faber, A. Stillman, and A. Tannenbaum</i>	1340
Blind Prediction of Natural Video Quality http://dx.doi.org/10.1109/TIP.2014.2299154	<i>M. A. Saad, A. C. Bovik, and C. Charrier</i>	1352
Color-Image Quality Assessment: From Prediction to Optimization http://dx.doi.org/10.1109/TIP.2014.2302684	<i>J. Preiss, F. Fernandes, and P. Urban</i>	1366
Accelerated Nonlinear Multichannel Ultrasonic Tomographic Imaging Using Target Sparseness http://dx.doi.org/10.1109/TIP.2014.2302679	<i>C. Dong, Y. Jin, and E. Lu</i>	1379
Robust Estimation of Motion Blur Kernel Using a Piecewise-Linear Model http://dx.doi.org/10.1109/TIP.2014.2303637	<i>S. Oh and G. Kim</i>	1394
Common Visual Pattern Discovery via Directed Graph http://dx.doi.org/10.1109/TIP.2014.2298973	<i>C. Wang and K.-K. Ma</i>	1408
Fusion of Multichannel Local and Global Structural Cues for Photo Aesthetics Evaluation http://dx.doi.org/10.1109/TIP.2014.2303650	<i>L. Zhang, Y. Gao, R. Zimmermann, Q. Tian, and X. Li</i>	1419
Multilabel Image Classification via High-Order Label Correlation Driven Active Learning http://dx.doi.org/10.1109/TIP.2014.2302675	<i>B. Zhang, Y. Wang, and F. Chen</i>	1430

IEEE TRANSACTIONS ON IMAGE PROCESSING

A PUBLICATION OF THE IEEE SIGNAL PROCESSING SOCIETY



www.signalprocessingsociety.org

Indexed in PubMed® and MEDLINE®, products of the United States National Library of Medicine



MARCH 2014

VOLUME 23

NUMBER 3

IIPRE4

(ISSN 1057-7149)

PAPERS

Statistical-Model Based Methods

- Cartoon-Texture Image Decomposition Using Blockwise Low-Rank Texture Characterization <http://dx.doi.org/10.1109/TIP.2014.2299067> ... *S. Ono, T. Miyata, and I. Yamada* 1128
- Blind Prediction of Natural Video Quality <http://dx.doi.org/10.1109/TIP.2014.2299154> *M. A. Saad, A. C. Bovik, and C. Charrier* 1352
- Transparent Composite Model for DCT Coefficients: Design and Analysis <http://dx.doi.org/10.1109/TIP.2014.2300818> *E.-H. Yang, X. Yu, J. Meng, and C. Sun* 1303
- An Unsupervised Feature Selection Dynamic Mixture Model for Motion Segmentation <http://dx.doi.org/10.1109/TIP.2014.2300811> *T. M. Nguyen and Q. J. Wu* 1210

Image and Video Representation

- Insights Into Analysis Operator Learning: From Patch-Based Sparse Models to Higher Order MRFs <http://dx.doi.org/10.1109/TIP.2014.2299065> *Y. Chen, R. Ranftl, and T. Pock* 1060

Perception and Quality Models for Images and Video

- Color-Image Quality Assessment: From Prediction to Optimization <http://dx.doi.org/10.1109/TIP.2014.2302684> *J. Preiss, F. Fernandes, and P. Urban* 1366

Linear and Nonlinear Filtering of Images and Video

- Group-Invariant Colour Morphology Based on Frames <http://dx.doi.org/10.1109/TIP.2014.2300816> *J. J. van de Gronde and J. B. T. M. Roerdink* 1276

Partial Differential Equation Based Processing of Images and Video

- A Complete System for Automatic Extraction of Left Ventricular Myocardium From CT Images Using Shape Segmentation and Contour Evolution <http://dx.doi.org/10.1109/TIP.2014.2300751> *L. Zhu, Y. Gao, V. Appia, A. Yezzi, C. Arepalli, T. Faber, A. Stillman, and A. Tannenbaum* 1340



<i>Restoration and Enhancement</i>	
Quadtree Structured Image Approximation for Denoising and Interpolation http://dx.doi.org/10.1109/TIP.2014.2300817	1226
..... A. Scholefield and P. L. Dragotti	
Robust Automatic Line Scratch Detection in Films http://dx.doi.org/10.1109/TIP.2014.2300824	1240
..... A. Newson, A. Almansa, Y. Gousseau, and P. Pérez	
A Rain Pixel Recovery Algorithm for Videos With Highly Dynamic Scenes http://dx.doi.org/10.1109/TIP.2014.2290595	1097
..... J. Chen and L.-P. Chau	
Joint Non-Gaussian Denoising and Superresolving of Raw High Frame Rate Videos http://dx.doi.org/10.1109/TIP.2014.2298976	1154
..... J. Suo, Y. Deng, L. Bian, and Q. Dai	
Noise Parameter Estimation for Poisson Corrupted Images Using Variance Stabilization Transforms http://dx.doi.org/10.1109/TIP.2014.2300813	1329
..... X. Jin, Z. Xu, and K. Hirakawa	
An Unbiased Risk Estimator for Image Denoising in the Presence of Mixed Poisson-Gaussian Noise http://dx.doi.org/10.1109/TIP.2014.2300821	1255
..... Y. L. Montagner, E. D. Angelini, and J.-C. Olivo-Marin	
Image Interpolation via Graph-Based Bayesian Label Propagation http://dx.doi.org/10.1109/TIP.2014.2294543	1084
..... X. Liu, D. Zhao, J. Zhou, W. Gao, and H. Sun	
Does Deblurring Improve Geometrical Hyperspectral Unmixing? http://dx.doi.org/10.1109/TIP.2014.2300822	1169
..... S. Henrot, C. Soussen, M. Dossot, and D. Brie	
Robust Estimation of Motion Blur Kernel Using a Piecewise-Linear Model http://dx.doi.org/10.1109/TIP.2014.2303637	1394
..... S. Oh and G. Kim	
<i>Biomedical and Biological Image Processing</i>	
An Automatic Graph-Based Approach for Artery/Vein Classification in Retinal Images http://dx.doi.org/10.1109/TIP.2014.2263809	1073
..... B. Dashtbozorg, A. M. Mendonça, and A. Campilho	
<i>Lossy Coding of Images and Video</i>	
Improved Block Truncation Coding Using Optimized Dot Diffusion http://dx.doi.org/10.1109/TIP.2014.2257812	1269
..... J.-M. Guo and Y.-F. Liu	
<i>Error Resilience and Channel Coding for Image and Video Systems</i>	
LineCast: Line-Based Distributed Coding and Transmission for Broadcasting Satellite Images http://dx.doi.org/10.1109/TIP.2014.2298972 ..	1015
..... F. Wu, X. Peng, and J. Xu	
<i>Imaging and Video Networks</i>	
A Novel Joint Data-Hiding and Compression Scheme Based on SMVQ and Image Inpainting http://dx.doi.org/10.1109/TIP.2014.2260760 ..	969
..... C. Qin, C.-C. Chang, and Y.-P. Chiu	
<i>Image and Video Processing for Watermarking and Security</i>	
A Compressive Sensing based Secure Watermark Detection and Privacy Preserving Storage Framework http://dx.doi.org/10.1109/TIP.2014.2298980	1317
..... Q. Wang, W. Zeng, and J. Tian	
<i>Color and Multispectral Imaging</i>	
Evaluating Combinational Illumination Estimation Methods on Real-World Images http://dx.doi.org/10.1109/TIP.2014.2277943	1194
..... B. Li, W. Xiong, W. Hu, and B. Funt	
<i>Acoustic and Ultrasound Imaging</i>	
Accelerated Nonlinear Multichannel Ultrasonic Tomographic Imaging Using Target Sparseness http://dx.doi.org/10.1109/TIP.2014.2302679	1379
..... C. Dong, Y. Jin, and E. Lu	
<i>Microscopic Imaging</i>	
A New Iterative Triclass Thresholding Technique in Image Segmentation http://dx.doi.org/10.1109/TIP.2014.2298981	1038
..... H. Cai, Z. Yang, X. Cao, W. Xia, and X. Xu	
<i>Tomographic Imaging</i>	
Super-Resolution for Computed Tomography Based on Discrete Tomography http://dx.doi.org/10.1109/TIP.2014.2297025	1181
..... W. van Aarle, K. J. Batenburg, G. V. Gompel, E. V. de Castele, and J. Sijbers	

Magnetic Resonance Imaging

Kernel-Based Learning from Both Qualitative and Quantitative Labels: Application to Prostate Cancer Diagnosis Based on Multiparametric MR Imaging <http://dx.doi.org/10.1109/TIP.2014.2295759> *É. Niaf, R. Flamary, O. Rouvière, C. Lartizien, and S. Canu* 979

Region, Boundary, and Shape Analysis

Angular Pattern and Binary Angular Pattern for Shape Retrieval <http://dx.doi.org/10.1109/TIP.2014.2286330> *R.-X. Hu, W. Jia, H. Ling, Y. Zhao, and J. Gui* 1118

Image and Video Mid Level Analysis

Efficient Circular Thresholding <http://dx.doi.org/10.1109/TIP.2014.2297014> *Y.-K. Lai and P. L. Rosin* 992

On Averaging Multiview Relations for 3D Scan Registration <http://dx.doi.org/10.1109/TIP.2014.2246517> *V. M. Govindu and P. A.* 1289

Common Visual Pattern Discovery via Directed Graph <http://dx.doi.org/10.1109/TIP.2014.2298973> *C. Wang and K.-K. Ma* 1408

Image and Video Interpretation and Understanding

Convex-Relaxed Kernel Mapping for Image Segmentation <http://dx.doi.org/10.1109/TIP.2014.2297019> *M. B. Salah, I. B. Ayed, J. Yuan, and H. Zhang* 1143

Multilabel Image Classification via High-Order Label Correlation Driven Active Learning <http://dx.doi.org/10.1109/TIP.2014.2302675> *B. Zhang, Y. Wang, and F. Chen* 1430

Learning and Recognition of On-Premise Signs from Weakly Labeled Street View Images <http://dx.doi.org/10.1109/TIP.2014.2298982> *T.-H. Tsai, W.-H. Cheng, C.-W. You, M.-C. Hu, A. W. Tsui, and H.-Y. Chi* 1047

Multi-Label Image Categorization With Sparse Factor Representation <http://dx.doi.org/10.1109/TIP.2014.2298978> *F. Sun, J. Tang, H. Li, G.-J. Qi, and T. S. Huang* 1028

Image and Video Biometric Analysis

Robust Face Recognition from Multi-View Videos <http://dx.doi.org/10.1109/TIP.2014.2300812> *M. Du, A. C. Sankaranarayanan, and R. Chellappa* 1105

Image and Video Storage and Retrieval

Sparse Label-Indicator Optimization Methods for Image Classification <http://dx.doi.org/10.1109/TIP.2014.2294546> *L. Jing and M. K. Ng* 1002

Fusion of Multichannel Local and Global Structural Cues for Photo Aesthetics Evaluation <http://dx.doi.org/10.1109/TIP.2014.2303650> *L. Zhang, Y. Gao, R. Zimmermann, Q. Tian, and X. Li* 1419

IEEE TRANSACTIONS ON IMAGE PROCESSING

A PUBLICATION OF THE IEEE SIGNAL PROCESSING SOCIETY



www.signalprocessingsociety.org

Indexed in PubMed® and MEDLINE®, products of the United States National Library of Medicine



APRIL 2014

VOLUME 23

NUMBER 4

IIPRE4

(ISSN 1057-7149)

PAPERS

Lazy Random Walks for Superpixel Segmentation http://dx.doi.org/10.1109/TIP.2014.2302892	<i>J. Shen, Y. Du, W. Wang, and X. Li</i>	1451
A Unified Data Embedding and Scrambling Method http://dx.doi.org/10.1109/TIP.2014.2302681	<i>R. M. Rad, K. Wong, and J.-M. Guo</i>	1463
Saliency Prediction on Stereoscopic Videos http://dx.doi.org/10.1109/TIP.2014.2303640	<i>H. Kim, S. Lee, and A. C. Bovik</i>	1476
Progressive Image Denoising Through Hybrid Graph Laplacian Regularization: A Unified Framework http://dx.doi.org/10.1109/TIP.2014.2303638	<i>X. Liu, D. Zhai, D. Zhao, G. Zhai, and W. Gao</i>	1491
Analyzing Training Information from Random Forests for Improved Image Segmentation http://dx.doi.org/10.1109/TIP.2014.2305073	<i>D. Mahapatra</i>	1504
Image Classification Using Multiscale Information Fusion Based on Saliency Driven Nonlinear Diffusion Filtering http://dx.doi.org/10.1109/TIP.2014.2303639	<i>W. Hu, R. Hu, N. Xie, H. Ling, and S. Maybank</i>	1513
Quality Assessment of Stereoscopic 3D Image Compression by Binocular Integration Behaviors http://dx.doi.org/10.1109/TIP.2014.2302686	<i>Y.-H. Lin and J.-L. Wu</i>	1527
Parsimonious Path Openings and Closings http://dx.doi.org/10.1109/TIP.2014.2303647	<i>V. Morard, P. Dokládal, and E. Decencière</i>	1543
Data-Driven Spatially-Adaptive Metric Adjustment for Visual Tracking http://dx.doi.org/10.1109/TIP.2014.2303656	<i>N. Jiang and W. Liu</i>	1556
Evaluation of Color Spatio-Temporal Interest Points for Human Action Recognition http://dx.doi.org/10.1109/TIP.2014.2302677	<i>I. Everts, J. C. van Gemert, and T. Gevers</i>	1569
Analysis and Exploitation of Multipath Ghosts in Radar Target Image Classification http://dx.doi.org/10.1109/TIP.2014.2302683	<i>G. E. Smith and B. G. Mobasseri</i>	1581
Manifold Learning for Object Tracking With Multiple Nonlinear Models http://dx.doi.org/10.1109/TIP.2014.2303652	<i>J. C. Nascimento, J. G. Silva, J. S. Marques, and J. M. Lemos</i>	1593
Contextual Hashing for Large-Scale Image Search http://dx.doi.org/10.1109/TIP.2014.2305072	<i>Z. Liu, H. Li, W. Zhou, R. Zhao, and Q. Tian</i>	1606
Spatiotemporal Grid Flow for Video Retargeting http://dx.doi.org/10.1109/TIP.2014.2305843	<i>B. Li, L.-Y. Duan, J. Wang, R. Ji, C.-W. Lin, and W. Gao</i>	1615
Clustering-Based Discriminant Analysis for Eye Detection http://dx.doi.org/10.1109/TIP.2014.2294548	<i>S. Chen and C. Liu</i>	1629



Robust Superpixel Tracking http://dx.doi.org/10.1109/TIP.2014.2300823	<i>F. Yang, H. Lu, and M.-H. Yang</i>	1639
Lossy Cutset Coding of Bilevel Images Based on Markov Random Fields http://dx.doi.org/10.1109/TIP.2014.2302678	<i>M. G. Reyes, D. L. Neuhoff, and T. N. Pappas</i>	1652
Characterness: An Indicator of Text in the Wild http://dx.doi.org/10.1109/TIP.2014.2302896	<i>Y. Li, W. Jia, C. Shen, and A. van den Hengel</i>	1666
Tensor-Based Formulation and Nuclear Norm Regularization for Multienergy Computed Tomography http://dx.doi.org/10.1109/TIP.2014.2305840	<i>O. Semerci, N. Hao, M. E. Kilmer, and E. L. Miller</i>	1678
Optimal Transport for Secure Spread-Spectrum Watermarking of Still Images http://dx.doi.org/10.1109/TIP.2014.2305873	<i>B. Mathon, F. Cayre, P. Bas, and B. Macq</i>	1694
Robust Point Matching via Vector Field Consensus http://dx.doi.org/10.1109/TIP.2014.2307478	<i>J. Ma, J. Zhao, J. Tian, A. L. Yuille, and Z. Tu</i>	1706
Augmented Multiple Instance Regression for Inferring Object Contours in Bounding Boxes http://dx.doi.org/10.1109/TIP.2014.2307436	<i>K.-J. Hsu, Y.-Y. Lin, and Y.-Y. Chuang</i>	1722
LGE-KSVD: Robust Sparse Representation Classification http://dx.doi.org/10.1109/TIP.2014.2303648	<i>R. Ptucha and A. E. Savakis</i>	1737
Analysis, Evaluation, and Comparison of Polarimetric SAR Speckle Filtering Techniques http://dx.doi.org/10.1109/TIP.2014.2307437	<i>S. Foucher and C. López-Martnez</i>	1751
Data-Driven Hierarchical Structure Kernel for Multiscale Part-Based Object Recognition http://dx.doi.org/10.1109/TIP.2014.2307480	<i>B. Wang, H. Xiong, X. Jiang, and Y. F. Zheng</i>	1765
Local-Prediction-Based Difference Expansion Reversible Watermarking http://dx.doi.org/10.1109/TIP.2014.2307482	<i>I.-C. Dragoi and D. Coltuc</i>	1779
Double-Layer Video Transmission Over Decode-and-Forward Wireless Relay Networks Using Hierarchical Modulation http://dx.doi.org/10.1109/TIP.2014.2308428	<i>T. V. Nguyen, P. C. Cosman, and L. B. Milstein</i>	1791
Maximum-Likelihood Based Synthesis of Volumetric Textures from a 2D Sample http://dx.doi.org/10.1109/TIP.2014.2307477	<i>R.-D. Urs, J.-P. Da Costa, and C. Germain</i>	1820
Context-Aware Discovery of Visual Co-Occurrence Patterns http://dx.doi.org/10.1109/TIP.2014.2308416	<i>H. Wang, J. Yuan, and Y. Wu</i>	1805
Speckle Reduction via Higher Order Total Variation Approach http://dx.doi.org/10.1109/TIP.2014.2308432	<i>W. Feng, H. Lei, and Y. Gao</i>	1831
A Novel Multiple Hypothesis Based Particle Tracking Method for Clathrin Mediated Endocytosis Analysis Using Fluorescence Microscopy http://dx.doi.org/10.1109/TIP.2014.2303633	<i>L. Liang, H. Shen, P. De Camilli, and J. S. Duncan</i>	1844
Learning Cascaded Shared-Boost Classifiers for Part-Based Object Detection http://dx.doi.org/10.1109/TIP.2014.2307432	<i>Y. Li, S. Wang, Q. Tian, and X. Ding</i>	1858
Visual Tracking via Discriminative Sparse Similarity Map http://dx.doi.org/10.1109/TIP.2014.2308414	<i>B. Zhuang, H. Lu, Z. Xiao, and D. Wang</i>	1872
Novel Example-Based Method for Super-Resolution and Denoising of Medical Images http://dx.doi.org/10.1109/TIP.2014.2308422	<i>D.-H. Trinh, M. Luong, F. Dibos, J.-M. Rocchisani, C.-D. Pham, and T. Q. Nguyen</i>	1882
Colored Coded Aperture Design by Concentration of Measure in Compressive Spectral Imaging http://dx.doi.org/10.1109/TIP.2014.2310125	<i>H. Arguello and G. R. Arce</i>	1896
Regularized Tree Partitioning and Its Application to Unsupervised Image Segmentation http://dx.doi.org/10.1109/TIP.2014.2307479	<i>J. Wang, H. Jiang, Y. Jia, X.-S. Hua, C. Zhang, and L. Qian</i>	1909
CORRESPONDENCE		
<i>Printing and Halftoning</i>		
Inverse Halftoning With Context Driven Prediction http://dx.doi.org/10.1109/TIP.2014.2305102	<i>J.-M. Guo, Y.-F. Liu, J.-H. Chen, and J.-D. Lee</i>	1923
EDICS—Editor's Information Classification Scheme http://dx.doi.org/10.1109/TIP.2014.2312879		1925
Information for Authors http://dx.doi.org/10.1109/TIP.2014.2312880		1926

IEEE TRANSACTIONS ON IMAGE PROCESSING

A PUBLICATION OF THE IEEE SIGNAL PROCESSING SOCIETY



www.signalprocessingsociety.org

Indexed in PubMed® and MEDLINE®, products of the United States National Library of Medicine



APRIL 2014

VOLUME 23

NUMBER 4

IIPRE4

(ISSN 1057-7149)

PAPERS

Statistical-Model Based Methods

- Robust Superpixel Tracking <http://dx.doi.org/10.1109/TIP.2014.2300823> F. Yang, H. Lu, and M.-H. Yang 1639
- Clustering-Based Discriminant Analysis for Eye Detection <http://dx.doi.org/10.1109/TIP.2014.2294548> S. Chen and C. Liu 1629
- Manifold Learning for Object Tracking With Multiple Nonlinear Models <http://dx.doi.org/10.1109/TIP.2014.2303652> J. C. Nascimento, J. G. Silva, J. S. Marques, and J. M. Lemos 1593

Structural-Model Based Methods

- Robust Point Matching via Vector Field Consensus <http://dx.doi.org/10.1109/TIP.2014.2307478> J. Ma, J. Zhao, J. Tian, A. L. Yuille, and Z. Tu 1706

Perception and Quality Models for Images and Video

- Quality Assessment of Stereoscopic 3D Image Compression by Binocular Integration Behaviors <http://dx.doi.org/10.1109/TIP.2014.2302686> Y.-H. Lin and J.-L. Wu 1527
- Saliency Prediction on Stereoscopic Videos <http://dx.doi.org/10.1109/TIP.2014.2303640> H. Kim, S. Lee, and A. C. Bovik 1476

Linear and Nonlinear Filtering of Images and Video

- Evaluation of Color Spatio-Temporal Interest Points for Human Action Recognition <http://dx.doi.org/10.1109/TIP.2014.2302677> I. Everts, J. C. van Gemert, and T. Gevers 1569
- Parsimonious Path Openings and Closings <http://dx.doi.org/10.1109/TIP.2014.2303647> V. Morard, P. Dokládál, and E. Decenciére 1543
- Image Classification Using Multiscale Information Fusion Based on Saliency Driven Nonlinear Diffusion Filtering <http://dx.doi.org/10.1109/TIP.2014.2303639> W. Hu, R. Hu, N. Xie, H. Ling, and S. Maybank 1513

Restoration and Enhancement

- Speckle Reduction via Higher Order Total Variation Approach <http://dx.doi.org/10.1109/TIP.2014.2308432> W. Feng, H. Lei, and Y. Gao 1831
- Progressive Image Denoising Through Hybrid Graph Laplacian Regularization: A Unified Framework <http://dx.doi.org/10.1109/TIP.2014.2303638> X. Liu, D. Zhai, D. Zhao, G. Zhai, and W. Gao 1491



Regularized Tree Partitioning and Its Application to Unsupervised Image Segmentation http://dx.doi.org/10.1109/TIP.2014.2307479	1909
..... J. Wang, H. Jiang, Y. Jia, X.-S. Hua, C. Zhang, and L. Quan	
<i>Biomedical and Biological Image Processing</i>	
Analyzing Training Information from Random Forests for Improved Image Segmentation http://dx.doi.org/10.1109/TIP.2014.2305073	1504
..... D. Mahapatra	
Novel Example-Based Method for Super-Resolution and Denoising of Medical Images http://dx.doi.org/10.1109/TIP.2014.2308422	1882
..... D.-H. Trinh, M. Luong, F. Dibos, J.-M. Rocchisani, C.-D. Pham, and T. Q. Nguyen	
<i>Lossy Coding of Images and Video</i>	
Lossy Cutset Coding of Bilevel Images Based on Markov Random Fields http://dx.doi.org/10.1109/TIP.2014.2302678	1652
..... M. G. Reyes, D. L. Neuhoff, and T. N. Pappas	
<i>Image and Video Processing for Watermarking and Security</i>	
Local-Prediction-Based Difference Expansion Reversible Watermarking http://dx.doi.org/10.1109/TIP.2014.2307482	1779
..... I.-C. Dragoi and D. Coltuc	
Optimal Transport for Secure Spread-Spectrum Watermarking of Still Images http://dx.doi.org/10.1109/TIP.2014.2305873	1694
..... B. Mathon, F. Cayre, P. Bas, and B. Macq	
A Unified Data Embedding and Scrambling Method http://dx.doi.org/10.1109/TIP.2014.2302681	1463
..... R. M. Rad, K. Wong, and J.-M. Guo	
<i>Image and Video Multimedia Communications</i>	
Double-Layer Video Transmission Over Decode-and-Forward Wireless Relay Networks Using Hierarchical Modulation http://dx.doi.org/10.1109/TIP.2014.2308428	1791
..... T. V. Nguyen, P. C. Cosman, and L. B. Milstein	
<i>Color and Multispectral Imaging</i>	
Colored Coded Aperture Design by Concentration of Measure in Compressive Spectral Imaging http://dx.doi.org/10.1109/TIP.2014.2310125	1896
..... H. Arguello and G. R. Arce	
<i>Microscopic Imaging</i>	
A Novel Multiple Hypothesis Based Particle Tracking Method for Clathrin Mediated Endocytosis Analysis Using Fluorescence Microscopy http://dx.doi.org/10.1109/TIP.2014.2303633	1844
..... L. Liang, H. Shen, P. De Camilli, and J. S. Duncan	
<i>Tomographic Imaging</i>	
Tensor-Based Formulation and Nuclear Norm Regularization for Multienergy Computed Tomography http://dx.doi.org/10.1109/TIP.2014.2305840	1678
..... O. Semerci, N. Hao, M. E. Kilmer, and E. L. Miller	
<i>Radar Imaging, Remote Sensing, and Geophysical Imaging</i>	
Analysis, Evaluation, and Comparison of Polarimetric SAR Speckle Filtering Techniques http://dx.doi.org/10.1109/TIP.2014.2307437	1751
..... S. Foucher and C. López-Martnez	
Analysis and Exploitation of Multipath Ghosts in Radar Target Image Classification http://dx.doi.org/10.1109/TIP.2014.2302683	1581
..... G. E. Smith and B. G. Mobasseri	
<i>Region, Boundary, and Shape Analysis</i>	
Augmented Multiple Instance Regression for Inferring Object Contours in Bounding Boxes http://dx.doi.org/10.1109/TIP.2014.2307436	1722
..... K.-J. Hsu, Y.-Y. Lin, and Y.-Y. Chuang	
Lazy Random Walks for Superpixel Segmentation http://dx.doi.org/10.1109/TIP.2014.2302892	1451
..... J. Shen, Y. Du, W. Wang, and X. Li	
<i>Image and Video Mid Level Analysis</i>	
Data-Driven Hierarchical Structure Kernel for Multiscale Part-Based Object Recognition http://dx.doi.org/10.1109/TIP.2014.2307480	1765
..... B. Wang, H. Xiong, X. Jiang, and Y. F. Zheng	
Characterness: An Indicator of Text in the Wild http://dx.doi.org/10.1109/TIP.2014.2302896	1666
..... Y. Li, W. Jia, C. Shen, and A. van den Hengel	
Data-Driven Spatially-Adaptive Metric Adjustment for Visual Tracking http://dx.doi.org/10.1109/TIP.2014.2303656	1556
..... N. Jiang and W. Liu	
<i>Image and Video Interpretation and Understanding</i>	
Context-Aware Discovery of Visual Co-Occurrence Patterns http://dx.doi.org/10.1109/TIP.2014.2308416	1805
..... H. Wang, J. Yuan, and Y. Wu	
LGE-KSVD: Robust Sparse Representation Classification http://dx.doi.org/10.1109/TIP.2014.2303648	1737
..... R. Ptucha and A. E. Savakis	
Learning Cascaded Shared-Boost Classifiers for Part-Based Object Detection http://dx.doi.org/10.1109/TIP.2014.2307432	1858
..... Y. Li, S. Wang, Q. Tian, and X. Ding	

Visual Tracking via Discriminative Sparse Similarity Map http://dx.doi.org/10.1109/TIP.2014.2308414	1872
<i>Image and Video Storage and Retrieval</i>	
Spatiotemporal Grid Flow for Video Retargeting http://dx.doi.org/10.1109/TIP.2014.2305843	1615
<i>Image and Video Synthesis, Rendering, and Visualization</i>	
Contextual Hashing for Large-Scale Image Search http://dx.doi.org/10.1109/TIP.2014.2305072	1606
<i>Image and Video Synthesis, Rendering, and Visualization</i>	
Maximum-Likelihood Based Synthesis of Volumetric Textures from a 2D Sample http://dx.doi.org/10.1109/TIP.2014.2307477	1820
<hr/>	
CORRESPONDENCE	
<i>Printing and Halftoning</i>	
Inverse Halftoning With Context Driven Prediction http://dx.doi.org/10.1109/TIP.2014.2305102	1923
<hr/>	
EDICS —Editor's Information Classification Scheme http://dx.doi.org/10.1109/TIP.2014.2312879	1925
Information for Authors http://dx.doi.org/10.1109/TIP.2014.2312880	1926
<hr/>	

IEEE TRANSACTIONS ON INFORMATION FORENSICS AND SECURITY

A PUBLICATION OF THE IEEE SIGNAL PROCESSING SOCIETY



www.signalprocessingsociety.org

MARCH 2014

VOLUME 9

NUMBER 3

ITIFA6

(ISSN 1556-6013)

Editorial <http://dx.doi.org/10.1109/TIFS.2014.2300292> C.-C. J. Kuo 337

PAPERS

Modeling the Vulnerability of Feedback-Control Based Internet Services to Low-Rate DoS Attacks http://dx.doi.org/10.1109/TIFS.2014.2291970 Y. Tang, X. Luo, Q. Hui, and R. K. C. Chang	339
Non-Invasive Recognition of Poorly Resolved Integrated Circuit Elements http://dx.doi.org/10.1109/TIFS.2014.2297518 E. Matlin, M. Agrawal, and D. Stoker	354
Faved! Biometrics: Tell Me Which Image You Like and I'll Tell You Who You Are http://dx.doi.org/10.1109/TIFS.2014.2298370 P. Lovato, M. Bicego, C. Segalin, A. Perina, N. Sebe, and M. Cristani	364
Optimal Probabilistic Encryption for Secure Detection in Wireless Sensor Networks http://dx.doi.org/10.1109/TIFS.2014.2298813 R. Soosahabi, M. Naraghi-Pour, D. Perkins, and M. A. Bayoumi	375
Tradeoff Between Reliability and Security in Multiple Access Relay Networks Under Falsified Data Injection Attack http://dx.doi.org/10.1109/TIFS.2014.2299401 T. A. Khalaf, S. W. Kim, and A. E. Abdel-Hakim	386
Robust Lossless Watermarking of Relational Databases Based on Circular Histogram Modulation http://dx.doi.org/10.1109/TIFS.2014.2294240 J. Franco-Contreras, G. Coatrieux, F. Cuppens, N. Cuppens-Bouahia, and C. Roux	397
A Phase-Based Audio Watermarking System Robust to Acoustic Path Propagation http://dx.doi.org/10.1109/TIFS.2014.2293952 M. Arnold, X.-M. Chen, P. Baum, U. Gries, and G. Doërr	411
Nonparametric Density Estimation, Hypotheses Testing, and Sensor Classification in Centralized Detection http://dx.doi.org/10.1109/TIFS.2014.2300939 E. Soltanmohammadi and M. Naraghi-Pour	426
Toward Incentivizing Anti-Spoofing Deployment http://dx.doi.org/10.1109/TIFS.2014.2296437 B. Liu, J. Bi, and A. V. Vasilakos	436
Integrated Security Analysis on Cascading Failure in Complex Networks http://dx.doi.org/10.1109/TIFS.2014.2299404 J. Yan, H. He, and Y. Sun	451
Soft Biometrics and Their Application in Person Recognition at a Distance http://dx.doi.org/10.1109/TIFS.2014.2299975 P. Tome, J. Fierrez, R. Vera-Rodriguez, and M. S. Nixon	464
Secret Key Generation in the Two-Way Relay Channel With Active Attackers http://dx.doi.org/10.1109/TIFS.2014.2301233 H. Zhou, L. M. Huie, and L. Lai	476
Identification of Electronic Disguised Voices http://dx.doi.org/10.1109/TIFS.2014.2301912 H. Wu, Y. Wang, and J. Huang	489
Matching NIR Face to VIS Face Using Transduction http://dx.doi.org/10.1109/TIFS.2014.2299977 J.-Y. Zhu, W.-S. Zheng, J.-H. Lai, and S. Z. Li	501
Contrast Enhancement-Based Forensics in Digital Images http://dx.doi.org/10.1109/TIFS.2014.2300937 G. Cao, Y. Zhao, R. Ni, and X. Li	515
Offline Text-Independent Writer Identification Based on Scale Invariant Feature Transform http://dx.doi.org/10.1109/TIFS.2014.2301274 ... X. Wu, Y. Tang, and W. Bu	526



IEEE TRANSACTIONS ON INFORMATION FORENSICS AND SECURITY

A PUBLICATION OF THE IEEE SIGNAL PROCESSING SOCIETY



www.signalprocessingsociety.org

MARCH 2014

VOLUME 9

NUMBER 3

ITIFA6

(ISSN 1556-6013)

Editorial <http://dx.doi.org/10.1109/TIFS.2014.2300292> C.-C. J. Kuo 337

PAPERS

Biometrics

- Faved! Biometrics: Tell Me Which Image You Like and I'll Tell You Who You Are <http://dx.doi.org/10.1109/TIFS.2014.2298370> P. Lovato, M. Bicego, C. Segalin, A. Perina, N. Sebe, and M. Cristani 364
- Matching NIR Face to VIS Face Using Transduction <http://dx.doi.org/10.1109/TIFS.2014.2299977> J.-Y. Zhu, W.-S. Zheng, J.-H. Lai, and S. Z. Li 501
- Offline Text-Independent Writer Identification Based on Scale Invariant Feature Transform <http://dx.doi.org/10.1109/TIFS.2014.2301274> .. X. Wu, Y. Tang, and W. Bu 526

Communication and Physical-Layer Security

- Modeling the Vulnerability of Feedback-Control Based Internet Services to Low-Rate DoS Attacks <http://dx.doi.org/10.1109/TIFS.2014.2291970> Y. Tang, X. Luo, Q. Hui, and R. K. C. Chang 339
- Optimal Probabilistic Encryption for Secure Detection in Wireless Sensor Networks <http://dx.doi.org/10.1109/TIFS.2014.2298813> R. Soosahabi, M. Naraghi-Pour, D. Perkins, and M. A. Bayoumi 375
- Tradeoff Between Reliability and Security in Multiple Access Relay Networks Under Falsified Data Injection Attack <http://dx.doi.org/10.1109/TIFS.2014.2299401> T. A. Khalaf, S. W. Kim, and A. E. Abdel-Hakim 386
- Secret Key Generation in the Two-Way Relay Channel With Active Attackers <http://dx.doi.org/10.1109/TIFS.2014.2301233> H. Zhou, L. M. Huie, and L. Lai 476

Forensics Analysis

- Nonparametric Density Estimation, Hypotheses Testing, and Sensor Classification in Centralized Detection <http://dx.doi.org/10.1109/TIFS.2014.2300939> E. Soltanmohammadi and M. Naraghi-Pour 426
- Identification of Electronic Disguised Voices <http://dx.doi.org/10.1109/TIFS.2014.2301912> H. Wu, Y. Wang, and J. Huang 489

Hardware Security

- Non-Invasive Recognition of Poorly Resolved Integrated Circuit Elements <http://dx.doi.org/10.1109/TIFS.2014.2297518> E. Matlin, M. Agrawal, and D. Stoker 354
-



<i>Multimedia Content Hash</i>	
Contrast Enhancement-Based Forensics in Digital Images http://dx.doi.org/10.1109/TIFS.2014.2300937	515
..... <i>G. Cao, Y. Zhao, R. Ni, and X. Li</i>	
<i>Network Security</i>	
Toward Incentivizing Anti-Spoofing Deployment http://dx.doi.org/10.1109/TIFS.2014.2296437	436
..... <i>B. Liu, J. Bi, and A. V. Vasilakos</i>	
<i>Security of Large Networked Systems</i>	
Integrated Security Analysis on Cascading Failure in Complex Networks http://dx.doi.org/10.1109/TIFS.2014.2299404	451
..... <i>J. Yan, H. He, and Y. Sun</i>	
<i>Surveillance</i>	
Soft Biometrics and Their Application in Person Recognition at a Distance http://dx.doi.org/10.1109/TIFS.2014.2299975	464
..... <i>P. Tome, J. Fierrez, R. Vera-Rodriguez, and M. S. Nixon</i>	
<i>Watermarking and Data Hiding</i>	
Robust Lossless Watermarking of Relational Databases Based on Circular Histogram Modulation http://dx.doi.org/10.1109/TIFS.2014.2294240	397
..... <i>J. Franco-Contreras, G. Coatrieux, F. Cuppens, N. Cuppens-Boulahia, and C. Roux</i>	
A Phase-Based Audio Watermarking System Robust to Acoustic Path Propagation http://dx.doi.org/10.1109/TIFS.2014.2293952	411
..... <i>M. Arnold, X.-M. Chen, P. Baum, U. Gries, and G. Doërr</i>	

CALL FOR PAPERS
IEEE TRANSACTIONS ON INFORMATION FORENSICS AND SECURITY
Special Issue on Biometric Spoofing and Countermeasures

Guest Editors

<i>Nicholas Evans</i>	EURECOM, France (evans@eurecom.fr)
<i>Sébastien Marcel</i>	Idiap Research Institute, Switzerland (marcel@idiap.ch)
<i>Arun Ross</i>	Michigan State University, USA (rossarun@cse.msu.edu)
<i>Stan Z. Li</i>	Chinese Academy of Sciences, China (szli@nlpr.ia.ac.cn)

While biometrics technology has revolutionized approaches to person authentication and has evolved to play a critical role in personal, national and global security, the potential for the technology to be fooled or ‘spoofed’ is widely acknowledged. Efforts to study such threats and to develop countermeasures are now well underway resulting in some promising solutions. While progress with respect to each biometric modality has attained varying degrees of maturity, there are some notable shortcomings in research methodologies. Current spoofing studies focus on specific, known attacks. Existing countermeasures designed to detect and deflect such attacks are often based on unrealistic *a priori* knowledge and typically learned using training data produced using exactly the same spoofing method that is to be detected. Current countermeasures thus have questionable application in practical scenarios where the nature of the attack can never be known. This special issue will focus on the latest research on the topic of biometric spoofing and countermeasures, with a particular emphasis on novel methodologies and generalized spoofing countermeasures that have the potential to protect biometric systems against varying or previously unseen attacks. The aim is to further the state-of-the-art in this field, to stimulate interactions between the biometrics and information forensic communities, to encourage the development of reliable methodologies in spoofing and countermeasure assessment and solutions, and to promote the development of generalized countermeasures. Papers on biometric obfuscation (e.g., fingerprint or face alteration) and relevant countermeasures will also be considered in the special issue. Novel contributions related to both traditional biometric modalities such as face, iris, fingerprint, and voice, and other modalities such as vasculature and electrophysiological signals will be considered. The focus includes, but is not limited to, the following topics related to spoofing and anti-spoofing countermeasures in biometrics:

- vulnerability analysis with an emphasis on previously unconsidered spoofing attacks;
- theoretical models for attack vectors;
- advanced machine learning and pattern recognition algorithms for anti-spoofing;
- information theoretic approaches to quantify spoofing vulnerability;
- spoofing and anti-spoofing in mobile devices;
- generalized countermeasures;
- challenge-response countermeasures;
- sensor-based solutions to spoof attacks;
- biometric obfuscation schemes;
- information forensic approaches to spoofing detection;
- new evaluation protocols, datasets, and performance metrics;
- reproducible research (public databases, open source software and experimental setups).

Submission Procedure: Manuscripts are to be submitted according to the Information for Authors at <http://www.signalprocessingsociety.org/publications/periodicals/forensics/forensics-authors-info/> using the IEEE online manuscript system, Manuscript Central. Papers must not have appeared or be under review elsewhere. Manuscripts by the guest editors submitted to this SI will be handled by the EIC of IEEE-TIFS.

Schedule:

Submission deadline: 1st June 2014
First Review: 15th September 2014
Revisions Due: 1st November 2014
Final Decision: 15th December 2014
Final manuscript due: 15th January 2015
Tentative publication date: 1st April 2015

WIFS'14 IEEE Workshop on Information Forensics and Security at IEEE GlobalSIP

Atlanta, Georgia, USA, December 3-5, 2014



Preliminary Call For Papers

The IEEE International Workshop on Information Forensics and Security (WIFS) is the primary annual event organized by the IEEE SPS Information Forensics and Security Technical Committee. The objective of WIFS is to provide the most prominent venue for researchers to exchange ideas and identify potential areas of collaboration. WIFS'14 will feature keynotes, tutorials, special sessions, and lecture & poster sessions. For the first time ever, WIFS is being organized with IEEE GlobalSIP, giving WIFS attendees a rich selection of research symposia in addition to WIFS.

Topics of interest: Topics include, but are not limited to:

- Anonymity & Privacy
- Applied Cryptography
- Biometrics
- Communication & Physical-Layer Security
- Forensics Analysis
- Hardware Security
- Information-Theoretic Security
- Multimedia Content Hash
- Security of Large Networked Systems
- Steganography
- Surveillance
- Usability & Human Factors
- Watermarking & Data Hiding
- Covert Communication & Side Channel Attacks

Submission of Papers: Prospective authors are invited to submit full-length, 6-page papers, formatted according to IEEE guidelines, including figures and references, to the WIFS Technical Program Committee. Papers will be accepted only by electronic submission through the GlobalSIP 2014 conference web site. Accepted papers may be scheduled in the lectures track or in the poster session. Prospective authors are expected to present their papers at the conference.

Important Dates:

Paper submission deadline	May 16, 2014
Announcement of review results	June 27, 2014
Due date for camera-ready papers	September 5, 2014

Upcoming:

More details about WIFS'14 Technical Programs, Special Topics, Best Paper Awards will be available soon at the GlobalSIP'14 website: <http://renyi.ece.iastate.edu/globalsip2014>.

IEEE TRANSACTIONS ON **MULTIMEDIA**

A PUBLICATION OF
THE IEEE CIRCUITS AND SYSTEMS SOCIETY
THE IEEE SIGNAL PROCESSING SOCIETY
THE IEEE COMMUNICATIONS SOCIETY
THE IEEE COMPUTER SOCIETY



<http://www.signalprocessingsociety.org/tmm/>

APRIL 2014

VOLUME 16

NUMBER 3

ITMUF8

(ISSN 1520-9210)

SPECIAL SECTION ON SOCIO-MOBILE MEDIA ANALYSIS AND RETRIEVAL

Message from the Editor-in-Chief <http://dx.doi.org/10.1109/TMM.2014.2309998> C. W. Chen 585

GUEST EDITORIAL

Guest Editorial: Special Section on Socio-Mobile Media Analysis and Retrieval <http://dx.doi.org/10.1109/TMM.2014.2304314>
..... A. D. Bimbo, Candan, Y.-G. , J. Luo, T. Mei, N. Sebe, H. T. Shen, C. G. M. Snoek, and R. Yan 586

SPECIAL SECTION PAPERS

Personalized Geo-Specific Tag Recommendation for Photos on Social Websites <http://dx.doi.org/10.1109/TMM.2014.2302732>
..... J. Liu, Z. Li, J. Tang, Y. Jiang, and H. Lu 588

Towards Codebook-Free: Scalable Cascaded Hashing for Mobile Image Search <http://dx.doi.org/10.1109/TMM.2014.2301979>
..... W. Zhou, M. Yang, H. Li, X. Wang, Y. Lin, and Q. Tian 601

Discriminative Soft Bag-of-Visual Phrase for Mobile Landmark Recognition <http://dx.doi.org/10.1109/TMM.2014.2301978>
..... T. Chen, K.-H. Yap, and D. Zhang 612

Mobile Landmark Search with 3D Models <http://dx.doi.org/10.1109/TMM.2014.2302744> W. Min, C. Xu, M. Xu, X. Xiao, and B.-K. Bao 623

REGULAR ISSUE PAPERS

Audio/Video Analysis and Synthesis

Illumination Robust Video Foreground Prediction Based on Color Recovering <http://dx.doi.org/10.1109/TMM.2014.2299515>
..... Y. Wan, Z. Miao, X.-P. Zhang, Z. Tang, and Z. Wang 637



Atmospheric Perspective Effect Enhancement of Landscape Photographs Through Depth-Aware Contrast Manipulation http://dx.doi.org/10.1109/TMM.2014.2299511	<i>X. Zhang, K. L. Chan, and M. Constable</i>	653
Glottal and Vocal Tract Characteristics of Voice Impersonators http://dx.doi.org/10.1109/TMM.2014.2300071	<i>T. B. Amin, P. Marziliano, and J. S. German</i>	668
Trace Transform Based Method for Color Image Domain Identification http://dx.doi.org/10.1109/TMM.2014.2300843	<i>I. G. Olaizola, M. Quartulli, J. Flórez, and B. Sierra</i>	679
Classification of Cinematographic Shots Using Lie Algebra and its Application to Complex Event Recognition http://dx.doi.org/10.1109/TMM.2014.2300833	<i>S. Bhattacharya, R. Mehran, R. Sukthankar, and M. Shah</i>	686
<i>Compression and Coding</i>		
Layered Wireless Video Relying on Minimum-Distortion Inter-Layer FEC Coding http://dx.doi.org/10.1109/TMM.2014.2300449	<i>Y. Huo, M. El-Hajjar, R. G. Maunder, and L. Hanzo</i>	697
<i>3-D Audio/Video Processing</i>		
Loss-Resilient Coding of Texture and Depth for Free-Viewpoint Video Conferencing http://dx.doi.org/10.1109/TMM.2014.2299768	<i>B. Macchiavello, C. Dorea, E. M. Hung, G. Cheung, and W.-T. Tan</i>	711
An Efficient Multi-View Generation Method From a Single-View Video Based on Affine Geometry Information http://dx.doi.org/10.1109/TMM.2014.2299771	<i>H. Lim and H. Park</i>	726
<i>Quality Assessment and User Experience</i>		
Acceptability-Based QoE Models for Mobile Video http://dx.doi.org/10.1109/TMM.2014.2298217	<i>W. Song and D. W. Tjondronegoro</i>	738
<i>Content Understanding and Knowledge Modeling</i>		
Similarity Assessment Model for Chinese Sign Language Videos http://dx.doi.org/10.1109/TMM.2014.2298382	<i>L.-C. Wang, R. Wang, D.-H. Kong, and B.-C. Yin</i>	751
<i>Content Description and Annotation</i>		
Concurrent Single-Label Image Classification and Annotation via Efficient Multi-Layer Group Sparse Coding http://dx.doi.org/10.1109/TMM.2014.2299516	<i>S. Gao, L.-T. Chia, I. W.-H. Tsang, and Z. Ren</i>	762
<i>Multimedia Search and Retrieval</i>		
Texture Modeling Using Contourlets and Finite Mixtures of Generalized Gaussian Distributions and Applications http://dx.doi.org/10.1109/TMM.2014.2298832	<i>M. S. Allili, N. Baaziz, and M. Mejri</i>	772
Weakly Supervised Multi-Graph Learning for Robust Image Reranking http://dx.doi.org/10.1109/TMM.2014.2298841	<i>C. Deng, R. Ji, D. Tao, X. Gao, and X. Li</i>	785
<i>Social and Web Multimedia</i>		
Topic-Sensitive Influencer Mining in Interest-Based Social Media Networks via Hypergraph Learning http://dx.doi.org/10.1109/TMM.2014.2298216	<i>Q. Fang, J. Sang, C. Xu, and Y. Rui</i>	796
<i>Multimedia Streaming and Transport</i>		
Analysis of Buffer Starvation With Application to Objective QoE Optimization of Streaming Services http://dx.doi.org/10.1109/TMM.2014.2300041	<i>Y. Xu, E. Altman, R. El-Azouzi, M. Haddad, S. Elayoubi, and T. Jimenez</i>	813
<i>Wireless/Mobile Multimedia</i>		
Channel Time Allocation PSO for Gigabit Multimedia Wireless Networks http://dx.doi.org/10.1109/TMM.2014.2298211	<i>S. Scott-Hayward and E. Garcia-Palacios</i>	828
An Advanced Moving Object Detection Algorithm for Automatic Traffic Monitoring in Real-World Limited Bandwidth Networks http://dx.doi.org/10.1109/TMM.2014.2298377	<i>B.-H. Chen and S.-C. Huang</i>	837
Distortion-Fair Cross-Layer Resource Allocation for Scalable Video Transmission in OFDMA Wireless Networks http://dx.doi.org/10.1109/TMM.2014.2300442	<i>S. Cicalò and V. Tralli</i>	848
<i>Multimedia Algorithms, Systems, and Interfaces</i>		
Robust Multi-Speaker Tracking via Dictionary Learning and Identity Modeling http://dx.doi.org/10.1109/TMM.2014.2301977	<i>M. Barnard, P. Koniusz, W. Wang, J. Kittler, S. M. Naqvi, and J. Chambers</i>	864
<hr/>		
EDICS—Editors Classification Scheme http://dx.doi.org/10.1109/TMM.2014.2310698		881
Information for Authors http://dx.doi.org/10.1109/TMM.2014.2310699		882

IEEE JOURNAL OF SELECTED TOPICS IN SIGNAL PROCESSING



www.ieee.org/sp/index.html

APRIL 2014

VOLUME 8

NUMBER 2

IJSTGY

(ISSN 1932-4553)

EDITORIAL

Introduction to the Issue on Statistical Parametric Speech Synthesis http://dx.doi.org/10.1109/IJSTSP.2014.2309416	170
..... <i>J. Tao, K. Hirose, K. Tokuda, A. W. Black, and S. King</i>	

PAPERS

Statistical Parametric Speech Synthesis Based on Gaussian Process Regression http://dx.doi.org/10.1109/IJSTSP.2013.2283461	173
..... <i>T. Koriyama, T. Nose, and T. Kobayashi</i>	
Harmonics Plus Noise Model Based Vocoder for Statistical Parametric Speech Synthesis http://dx.doi.org/10.1109/IJSTSP.2013.2283471	184
..... <i>D. Erro, I. Sainz, E. Navas, and I. Hernaez</i>	
Glottal Spectral Separation for Speech Synthesis http://dx.doi.org/10.1109/IJSTSP.2014.2307274	195
..... <i>J. P. Cabral, K. Richmond, J. Yamagishi, and S. Renals</i>	
Modeling Irregular Voice in Statistical Parametric Speech Synthesis With Residual Codebook Based Excitation http://dx.doi.org/10.1109/IJSTSP.2013.2292037	209
..... <i>T. G. Csapó and G. Németh</i>	
A Parameter Generation Algorithm Using Local Variance for HMM-Based Speech Synthesis http://dx.doi.org/10.1109/IJSTSP.2013.2283459	221
..... <i>T. Nose, V. Chunwijitra, and T. Kobayashi</i>	
Contextual Additive Structure for HMM-Based Speech Synthesis http://dx.doi.org/10.1109/IJSTSP.2014.2305919	229
..... <i>S. Takaki, Y. Nankaku, and K. Tokuda</i>	
Parameter Generation Methods With Rich Context Models for High-Quality and Flexible Text-To-Speech Synthesis http://dx.doi.org/10.1109/IJSTSP.2013.2288599	239
..... <i>S. Takamichi, T. Toda, Y. Shiga, S. Sakti, G. Neubig, and S. Nakamura</i>	
Factored Maximum Penalized Likelihood Kernel Regression for HMM-Based Style-Adaptive Speech Synthesis http://dx.doi.org/10.1109/IJSTSP.2014.2305131	251
..... <i>J. S. Sung, D. H. Hong, and N. S. Kim</i>	
Combining Vocal Tract Length Normalization With Hierarchical Linear Transformations http://dx.doi.org/10.1109/IJSTSP.2013.2295554	262
..... <i>L. Saheer, J. Yamagishi, P. N. Garner, and J. Dines</i>	
Arousal-Driven Synthesis of Laughter http://dx.doi.org/10.1109/IJSTSP.2014.2309435	273
..... <i>J. Urbain, H. Çakmak, A. Charlier, M. Dentí, T. Dutoit, and S. Dupont</i>	
Noise in HMM-Based Speech Synthesis Adaptation: Analysis, Evaluation Methods and Experiments http://dx.doi.org/10.1109/IJSTSP.2013.2278492	285
..... <i>R. Karhila, U. Remes, and M. Kurimo</i>	
Building HMM-TTS Voices on Diverse Data http://dx.doi.org/10.1109/IJSTSP.2013.2295058	296
..... <i>V. Wan, J. Latorre, K. Yanagisawa, N. Braunschweiler, L. Chen, M. J. F. Gales, and M. Akamine</i>	
Automatic Variation of the Degree of Articulation in New HMM-Based Voices http://dx.doi.org/10.1109/IJSTSP.2014.2302742	307
..... <i>B. Picart, T. Drugman, and T. Dutoit</i>	
Integrated Expression Prediction and Speech Synthesis From Text http://dx.doi.org/10.1109/IJSTSP.2013.2294938	323
..... <i>L. Chen, M. J. F. Gales, N. Braunschweiler, M. Akamine, and K. Knill</i>	
Joint Audiovisual Hidden Semi-Markov Model-Based Speech Synthesis http://dx.doi.org/10.1109/IJSTSP.2013.2281036	336
..... <i>D. Schabus, M. Pucher, and G. Hofer</i>	
Information for Authors http://dx.doi.org/10.1109/IJSTSP.2014.2310414	348



IEEE

SIGNAL PROCESSING LETTERS

A PUBLICATION OF THE IEEE SIGNAL PROCESSING SOCIETY


www.ieee.org/sp/index.html

MARCH 2014

VOLUME 21

NUMBER 3

ISPLEM

(ISSN 1070-9908)

LETTERS

Scalable and Compact Representation for Motion Capture Data Using Tensor Decomposition http://dx.doi.org/10.1109/LSP.2014.2299284 ..	255
..... <i>J. Hou, L.-P. Chau, N. Magnenat-Thalmann, and Y. He</i>	
Strong Impossibility Results for Sparse Signal Processing http://dx.doi.org/10.1109/LSP.2014.2298499	260
..... <i>V. Y. F. Tan and G. K. Atia</i>	
Adaptive Widely Linear Reduced-Rank Beamforming Based on Joint Iterative Optimization http://dx.doi.org/10.1109/LSP.2013.2295943 ..	265
..... <i>N. Song, W. U. Alokozai, R. C. de Lamare, and M. Haardt</i>	
Adaptive Compressed Sensing via Minimizing Cramer–Rao Bound http://dx.doi.org/10.1109/LSP.2014.2299814	270
..... <i>T. Huang, Y. Liu, H. Meng, and X. Wang</i>	
Revealing the Traces of Median Filtering Using High-Order Local Ternary Patterns http://dx.doi.org/10.1109/LSP.2013.2295858	275
..... <i>Y. Zhang, S. Li, S. Wang, and Y. Q. Shi</i>	
Efficient Sparse Banded Acoustic Models for Speech Recognition http://dx.doi.org/10.1109/LSP.2013.2292920	280
..... <i>W. Zhang and P. Fung</i>	
On Even-Period Binary Z-Complementary Pairs with Large ZCZs http://dx.doi.org/10.1109/LSP.2014.2300163	284
..... <i>Z. Liu, U. Parampalli, and Y. L. Guan</i>	
Hierarchical Data Association Framework with Occlusion Handling for Multiple Targets Tracking http://dx.doi.org/10.1109/LSP.2014.2300497	288
..... <i>Y. Yi and H. Xu</i>	
Modified Large Margin Nearest Neighbor Metric Learning for Regression http://dx.doi.org/10.1109/LSP.2014.2301037	292
..... <i>K. C. Assi, H. Labelle, and F. Cheriet</i>	
A Bayesian Framework for Sparse Representation-Based 3-D Human Pose Estimation http://dx.doi.org/10.1109/LSP.2014.2301726	297
..... <i>B. Babagholami-Mohamadabadi, A. Jourabloo, A. Zarghami, and S. Kasaei</i>	
Optimizing a High-Order Graphic Equalizer for Audio Processing http://dx.doi.org/10.1109/LSP.2014.2301557	301
..... <i>J. Rämö and V. Välimäki</i>	
An Efficient Multichannel Linear Prediction-Based Blind Equalization Algorithm in Near Common Zeros Condition http://dx.doi.org/10.1109/LSP.2014.2301831	306
..... <i>J.-M. Yang and H.-G. Kang</i>	

IEEE SIGNAL PROCESSING LETTERS (ISSN 1070-9908) is published quarterly in print and monthly online by the Institute of Electrical and Electronics Engineers, Inc. Responsibility for the contents rests upon the authors and not upon the IEEE, the Society/Council, or its members. **IEEE Corporate Office:** 3 Park Avenue, 17th Floor, New York, NY 10016-5997. **IEEE Operations Center:** 445 Hoes Lane, Piscataway, NJ 08854-4141. **NJ Telephone:** +1 732 981 0060. **Price/Publication Information:** Individual copies: IEEE Members \$20.00 (first copy only), nonmembers \$304.00 per copy. (Note: Postage and handling charge not included.) Member and nonmember subscription prices available upon request. Available in microfiche and microfilm. **Copyright and Reprint Permissions:** Abstracting is permitted with credit to the source. Libraries are permitted to photocopy for private use of patrons, provided the per-copy fee indicated in the code at the bottom of the first page is paid through the Copyright Clearance Center, 222 Rosewood Drive, Danvers, MA 01923. For all other copying, reprint, or republication permission, write to Copyrights and Permissions Department, IEEE Publications Administration, 445 Hoes Lane, Piscataway, NJ 08854-4141. Copyright © 2014 by the Institute of Electrical and Electronics Engineers, Inc. All rights reserved. Periodicals Postage at New York, NY and at additional mailing offices. **Postmaster:** Send address changes to IEEE SIGNAL PROCESSING LETTERS, IEEE, 445 Hoes Lane, Piscataway, NJ 08854-4141. GST Registration No. 125634188. CPC Sales Agreement #40013087. Return undeliverable Canada addresses to: Pitney Bowes IMEX, P.O. Box 4332, Stanton Rd., Toronto, ON M5W 3J4, Canada. IEEE prohibits discrimination, harassment and bullying. For more information visit <http://www.ieee.org/nondiscrimination>. Printed in U.S.A.

Large Vocabulary Continuous Speech Recognition With Reservoir-Based Acoustic Models http://dx.doi.org/10.1109/LSP.2014.2302080 ...	311
..... <i>F. Triefenbach, K. Demuynck, and J.-P. Martens</i>	
Stereophonic Acoustic Echo Suppression Incorporating Spectro-Temporal Correlations http://dx.doi.org/10.1109/LSP.2014.2302438	316
..... <i>C. M. Lee, J. W. Shin, and N. S. Kim</i>	
Scale and Rotation Invariant Texture Classification Using Covariate Shift Methodology http://dx.doi.org/10.1109/LSP.2014.2302576	321
..... <i>A. Hassan, F. Riaz, and A. Shaikat</i>	
An Adaptive Detector with Range Estimation Capabilities for Partially Homogeneous Environment http://dx.doi.org/10.1109/LSP.2014.2301763	325
..... <i>A. D. Maio, C. Hao, and D. Orlando</i>	
On the Randomized Kaczmarz Algorithm http://dx.doi.org/10.1109/LSP.2013.2294376	330
..... <i>L. Dai, M. Soltanian, and K. Pelckmans</i>	
Decentralized Robust Beamforming for Coordinated Multi-Cell MISO Networks http://dx.doi.org/10.1109/LSP.2014.2302387	334
..... <i>H. Pennanen, A. Tölli, and M. Latva-aho</i>	
SLD: A Novel Robust Descriptor for Image Matching http://dx.doi.org/10.1109/LSP.2013.2294458	339
..... <i>W. Zhou, C. Wang, B. Xiao, and Z. Zhang</i>	
Exact ML Criterion Based on Semidefinite Relaxation for MIMO Systems http://dx.doi.org/10.1109/LSP.2013.2297407	343
..... <i>M. Kim, J. Park, K. Kim, and J. Kim</i>	
K-SVD Meets Transform Learning: Transform K-SVD http://dx.doi.org/10.1109/LSP.2014.2303076	347
..... <i>E. M. Eksioglu and O. Bayir</i>	
Spectro-Temporal Filtering for Multichannel Speech Enhancement in Short-Time Fourier Transform Domain http://dx.doi.org/10.1109/LSP.2014.2302897	352
..... <i>Y. G. Jin, J. W. Shin, and N. S. Kim</i>	
Subspace Clustering Through Parametric Representation and Sparse Optimization http://dx.doi.org/10.1109/LSP.2014.2303122 ...	356
..... <i>L. Bako</i>	
Conditional Cramér–Rao Lower Bounds for DOA Estimation and Array Calibration http://dx.doi.org/10.1109/LSP.2013.2281972	361
..... <i>Z.-M. Liu</i>	
Feedback Cancellation With Probe Shaping Compensation http://dx.doi.org/10.1109/LSP.2014.2301832	365
..... <i>C. R. C. Nakagawa, S. Nordholm, and W.-Y. Yan</i>	
<hr/>	
Information for Authors http://dx.doi.org/10.1109/LSP.2014.2305346	370
EDICS—Editors' Information Classification Scheme http://dx.doi.org/10.1109/LSP.2014.2305348	372

IEEE

SIGNAL PROCESSING LETTERS

A PUBLICATION OF THE IEEE SIGNAL PROCESSING SOCIETY


www.ieee.org/sp/index.html

MARCH 2014

VOLUME 21

NUMBER 3

ISPLEM

(ISSN 1070-9908)

LETTERS

Audio and Acoustic Signal Processing

- Optimizing a High-Order Graphic Equalizer for Audio Processing <http://dx.doi.org/10.1109/LSP.2014.2301557> *J. Rämö and V. Välimäki* 301
- An Efficient Multichannel Linear Prediction-Based Blind Equalization Algorithm in Near Common Zeros Condition
<http://dx.doi.org/10.1109/LSP.2014.2301831> *J.-M. Yang and H.-G. Kang* 306
- Stereophonic Acoustic Echo Suppression Incorporating Spectro-Temporal Correlations <http://dx.doi.org/10.1109/LSP.2014.2302438>
..... *C. M. Lee, J. W. Shin, and N. S. Kim* 316
- Feedback Cancellation With Probe Shaping Compensation <http://dx.doi.org/10.1109/LSP.2014.2301832>
..... *C. R. C. Nakagawa, S. Nordholm, and W.-Y. Yan* 365

Image and Multidimensional Signal Processing

- Scalable and Compact Representation for Motion Capture Data Using Tensor Decomposition <http://dx.doi.org/10.1109/LSP.2014.2299284> ..
..... *J. Hou, L.-P. Chau, N. Magnenat-Thalmann, and Y. He* 255
- Hierarchical Data Association Framework with Occlusion Handling for Multiple Targets Tracking
<http://dx.doi.org/10.1109/LSP.2014.2300497> *Y. Yi and H. Xu* 288
- SLD: A Novel Robust Descriptor for Image Matching <http://dx.doi.org/10.1109/LSP.2013.2294458>
..... *W. Zhou, C. Wang, B. Xiao, and Z. Zhang* 339

Machine Learning and Statistical Signal Processing

- Strong Impossibility Results for Sparse Signal Processing <http://dx.doi.org/10.1109/LSP.2014.2298499> *V. Y. F. Tan and G. K. Atia* 260
- A Bayesian Framework for Sparse Representation-Based 3-D Human Pose Estimation <http://dx.doi.org/10.1109/LSP.2014.2301726>
..... *B. Babagholami-Mohamadabadi, A. Jourabloo, A. Zarghami, and S. Kasaei* 297
- Scale and Rotation Invariant Texture Classification Using Covariate Shift Methodology <http://dx.doi.org/10.1109/LSP.2014.2302576>
..... *A. Hassan, F. Riaz, and A. Shaukat* 321
- K-SVD Meets Transform Learning: Transform K-SVD <http://dx.doi.org/10.1109/LSP.2014.2303076> *E. M. Eksioğlu and O. Bayir* 347
- Subspace Clustering Through Parametric Representation and Sparse Optimization <http://dx.doi.org/10.1109/LSP.2014.2303122> ... *L. Bako* 356

IEEE SIGNAL PROCESSING LETTERS (ISSN 1070-9908) is published quarterly in print and monthly online by the Institute of Electrical and Electronics Engineers, Inc. Responsibility for the contents rests upon the authors and not upon the IEEE, the Society/Council, or its members. **IEEE Corporate Office:** 3 Park Avenue, 17th Floor, New York, NY 10016-5997. **IEEE Operations Center:** 445 Hoes Lane, Piscataway, NJ 08854-4141. **NJ Telephone:** +1 732 981 0060. **Price/Publication Information:** Individual copies: IEEE Members \$20.00 (first copy only), nonmembers \$304.00 per copy. (Note: Postage and handling charge not included.) Member and nonmember subscription prices available upon request. Available in microfiche and microfilm. **Copyright and Reprint Permissions:** Abstracting is permitted with credit to the source. Libraries are permitted to photocopy for private use of patrons, provided the per-copy fee indicated in the code at the bottom of the first page is paid through the Copyright Clearance Center, 222 Rosewood Drive, Danvers, MA 01923. For all other copying, reprint, or republication permission, write to Copyrights and Permissions Department, IEEE Publications Administration, 445 Hoes Lane, Piscataway, NJ 08854-4141. Copyright © 2014 by the Institute of Electrical and Electronics Engineers, Inc. All rights reserved. Periodicals Postage at New York, NY and at additional mailing offices. **Postmaster:** Send address changes to IEEE SIGNAL PROCESSING LETTERS, IEEE, 445 Hoes Lane, Piscataway, NJ 08854-4141. GST Registration No. 125634188. CPC Sales Agreement #40013087. Return undeliverable Canada addresses to: Pitney Bowes IMEX, P.O. Box 4332, Stanton Rd., Toronto, ON M5W 3J4, Canada. IEEE prohibits discrimination, harassment and bullying. For more information visit <http://www.ieee.org/nondiscrimination>. Printed in U.S.A.

Multimedia Signal Processing

Revealing the Traces of Median Filtering Using High-Order Local Ternary Patterns <http://dx.doi.org/10.1109/LSP.2013.2295858> Y. Zhang, S. Li, S. Wang, and Y. Q. Shi 275

Sensor Array and Multichannel Signal Processing

Adaptive Widely Linear Reduced-Rank Beamforming Based on Joint Iterative Optimization <http://dx.doi.org/10.1109/LSP.2013.2295943> ... N. Song, W. U. Alokozai, R. C. de Lamare, and M. Haardt 265

Conditional Cramér–Rao Lower Bounds for DOA Estimation and Array Calibration <http://dx.doi.org/10.1109/LSP.2013.2281972> Z.-M. Liu 361

Signal Processing for Communications

On Even-Period Binary Z-Complementary Pairs with Large ZCZs <http://dx.doi.org/10.1109/LSP.2014.2300163> Z. Liu, U. Parampalli, and Y. L. Guan 284

Decentralized Robust Beamforming for Coordinated Multi-Cell MISO Networks <http://dx.doi.org/10.1109/LSP.2014.2302387> H. Pennanen, A. Tölli, and M. Latva-aho 334

Exact ML Criterion Based on Semidefinite Relaxation for MIMO Systems <http://dx.doi.org/10.1109/LSP.2013.2297407> M. Kim, J. Park, K. Kim, and J. Kim 343

Speech Processing

Efficient Sparse Banded Acoustic Models for Speech Recognition <http://dx.doi.org/10.1109/LSP.2013.2292920> W. Zhang and P. Fung 280

Large Vocabulary Continuous Speech Recognition With Reservoir-Based Acoustic Models <http://dx.doi.org/10.1109/LSP.2014.2302080> ... F. Triefenbach, K. Demuynck, and J.-P. Martens 311

Spectro-Temporal Filtering for Multichannel Speech Enhancement in Short-Time Fourier Transform Domain <http://dx.doi.org/10.1109/LSP.2014.2302897> Y. G. Jin, J. W. Shin, and N. S. Kim 352

Statistical and Adaptive Signal Processing

Adaptive Compressed Sensing via Minimizing Cramer–Rao Bound <http://dx.doi.org/10.1109/LSP.2014.2299814> T. Huang, Y. Liu, H. Meng, and X. Wang 270

Modified Large Margin Nearest Neighbor Metric Learning for Regression <http://dx.doi.org/10.1109/LSP.2014.2301037> K. C. Assi, H. Labelle, and F. Cherié 292

An Adaptive Detector with Range Estimation Capabilities for Partially Homogeneous Environment <http://dx.doi.org/10.1109/LSP.2014.2301763> A. D. Maio, C. Hao, and D. Orlando 325

On the Randomized Kaczmarz Algorithm <http://dx.doi.org/10.1109/LSP.2013.2294376> L. Dai, M. Soltanian, and K. Pelckmans 330

Information for Authors <http://dx.doi.org/10.1109/LSP.2014.2305346> 370

EDICS—Editors’ Information Classification Scheme <http://dx.doi.org/10.1109/LSP.2014.2305348> 372

IEEE

SIGNAL PROCESSING LETTERS

A PUBLICATION OF THE IEEE SIGNAL PROCESSING SOCIETY


www.ieee.org/sp/index.html

APRIL 2014

VOLUME 21

NUMBER 4

ISPLEM

(ISSN 1070-9908)

LETTERS

Efficient One-Pass Decoding with NNLM for Speech Recognition http://dx.doi.org/10.1109/LSP.2014.2303136	<i>Y. Shi, W.-Q. Zhang, M. Cai, and J. Liu</i>	377
Image Contrast Enhancement Using Color and Depth Histograms http://dx.doi.org/10.1109/LSP.2014.2303157	<i>S.-W. Jung</i>	382
A TR-MISI Serial Prefilter for Robustness to ISI and Noise in Indoor Wireless Communication System http://dx.doi.org/10.1109/LSP.2014.2303814	<i>M. Yoon and C. Lee</i>	386
Coherent Versus Non-Coherent Reconfigurable Antenna Aided Virtual MIMO Systems http://dx.doi.org/10.1109/LSP.2014.2303471	<i>S. Sugiura</i>	390
Source Identification Using Signal Characteristics in Controller Area Networks http://dx.doi.org/10.1109/LSP.2014.2304139	<i>P.-S. Murvay and B. Groza</i>	395
A Robust SIFT Descriptor for Multispectral Images http://dx.doi.org/10.1109/LSP.2014.2304073	<i>S. Saleem and R. Sablatnik</i>	400
Reverberant Audio Source Separation via Sparse and Low-Rank Modeling http://dx.doi.org/10.1109/LSP.2014.2303135	<i>S. Arberet and P. Vanderghyest</i>	404
An Improved Frequency Offset Estimation Based on Companion Matrix in Multi-User Uplink Interleaved OFDMA Systems http://dx.doi.org/10.1109/LSP.2014.2303138	<i>S.-W. Keum, D.-H. Kim, and H.-M. Kim</i>	409
An Efficient Decoding Algorithm of Matrix Partition Codes http://dx.doi.org/10.1109/LSP.2014.2303421	<i>F. Chen and S. Cheng</i>	414
Successive Projection Method for Well-Conditioned Matrix Approximation Problems http://dx.doi.org/10.1109/LSP.2014.2303153	<i>M. Tanaka and K. Nakata</i>	418
Depth-Assisted Frame Rate Up-Conversion for Stereoscopic Video http://dx.doi.org/10.1109/LSP.2014.2304975	<i>X. Yang, J. Liu, J. Sun, Y. Lee, and T. Q. Nguyen</i>	423
Compressive Circulant Matrix Based Analog to Information Conversion http://dx.doi.org/10.1109/LSP.2013.2285444	<i>J. Zhang, N. Fu, and X. Peng</i>	428
Sensor Noise Modeling by Stacking Pseudo-Periodic Grid Images Affected by Vibrations http://dx.doi.org/10.1109/LSP.2014.2304570	<i>F. Sur and M. Grédiac</i>	432
Image Quality Assessment with Degradation on Spatial Structure http://dx.doi.org/10.1109/LSP.2014.2304714	<i>J. Wu, W. Lin, and G. Shi</i>	437
Block-Based In-Loop View Synthesis for 3-D Video Coding http://dx.doi.org/10.1109/LSP.2013.2283251	<i>Y. Zhang, Y. Zhao, and L. Yu</i>	441
Spatially Adaptive Kernel Regression Using Risk Estimation http://dx.doi.org/10.1109/LSP.2014.2305176	<i>S. R. Krishnan, C. S. Seelamantula, and P. Chakravarti</i>	445

IEEE SIGNAL PROCESSING LETTERS (ISSN 1070-9908) is published quarterly in print and monthly online by the Institute of Electrical and Electronics Engineers, Inc. Responsibility for the contents rests upon the authors and not upon the IEEE, the Society/Council, or its members. **IEEE Corporate Office:** 3 Park Avenue, 17th Floor, New York, NY 10016-5997. **IEEE Operations Center:** 445 Hoes Lane, Piscataway, NJ 08854-4141. **NJ Telephone:** +1 732 981 0060. **Price/Publication Information:** Individual copies: IEEE Members \$20.00 (first copy only), nonmembers \$304.00 per copy. (Note: Postage and handling charge not included.) Member and nonmember subscription prices available upon request. Available in microfiche and microfilm. **Copyright and Reprint Permissions:** Abstracting is permitted with credit to the source. Libraries are permitted to photocopy for private use of patrons, provided the per-copy fee indicated in the code at the bottom of the first page is paid through the Copyright Clearance Center, 222 Rosewood Drive, Danvers, MA 01923. For all other copying, reprint, or republication permission, write to Copyrights and Permissions Department, IEEE Publications Administration, 445 Hoes Lane, Piscataway, NJ 08854-4141. Copyright © 2014 by the Institute of Electrical and Electronics Engineers, Inc. All rights reserved. Periodicals Postage at New York, NY and at additional mailing offices. **Postmaster:** Send address changes to IEEE SIGNAL PROCESSING LETTERS, IEEE, 445 Hoes Lane, Piscataway, NJ 08854-4141. GST Registration No. 125634188. CPC Sales Agreement #40013087. Return undeliverable Canada addresses to: Pitney Bowes IMEX, P.O. Box 4332, Stanton Rd., Toronto, ON M5W 3J4, Canada. IEEE prohibits discrimination, harassment and bullying. For more information visit <http://www.ieee.org/nondiscrimination>. Printed in U.S.A.

Track-to-Track Association for Biased Data Based on the Reference Topology Feature http://dx.doi.org/10.1109/LSP.2014.2305305	449
..... <i>W. Tian, Y. Wang, X. Shan, and J. Yang</i>	
Relay Beamforming for Amplify-and-Forward Multi-Antenna Relay Networks with Energy Harvesting Constraint http://dx.doi.org/10.1109/LSP.2014.2305737	454
..... <i>J. Huang, Q. Li, Q. Zhang, G. Zhang, and J. Qin</i>	
Persistent Homology of Delay Embeddings and its Application to Wheeze Detection http://dx.doi.org/10.1109/LSP.2014.2305700	459
..... <i>S. Emrani, T. Gentimis, and H. Krim</i>	
The Marginal Enumeration Bayesian Cramér–Rao Bound for Jump Markov Systems http://dx.doi.org/10.1109/LSP.2014.2305115	464
..... <i>C. Fritsche, U. Orguner, L. Svensson, and F. Gustafsson</i>	
Computing Jacobian and Hessian of Estimators and Their Application to Risk Approximation http://dx.doi.org/10.1109/LSP.2014.2304693 ..	469
..... <i>S. Uhlich</i>	
Identifiability Analysis for Array Shape Self-Calibration Based on Hybrid Cramér-Rao Bound http://dx.doi.org/10.1109/LSP.2014.2306326	473
..... <i>S. Wan, J. Tang, W. Zhu, and N. Zhang</i>	
A Hybrid Descent Method for Optimal Sigmoid Filter Design http://dx.doi.org/10.1109/LSP.2014.2303498	478
..... <i>K. Y. Chan, S. Nordholm, S. Y. Low, P. C. Yong, and K. F. C. Yiu</i>	
Novel Tridiagonal Commuting Matrices for Types I, IV, V, VIII DCT and DST Matrices http://dx.doi.org/10.1109/LSP.2014.2306996	483
..... <i>D. Wei and Y. Li</i>	
Extended Grouping of RFID Tags Based on Resolvable Transversal Designs http://dx.doi.org/10.1109/LSP.2014.2306264	488
..... <i>Y.-S. Su</i>	
Improved Bases Selection in Acoustic Model Interpolation for Fast On-Line Adaptation http://dx.doi.org/10.1109/LSP.2014.2306451	493
..... <i>S. Shahnawazuddin and R. Sinha</i>	
Sparse Recovery by Means of Nonnegative Least Squares http://dx.doi.org/10.1109/LSP.2014.2307064	498
..... <i>S. Foucart and D. Koslicki</i>	
Cepstrum-Based Bandwidth Extension for Super-Wideband Coders http://dx.doi.org/10.1109/LSP.2014.2307074	503
..... <i>K. Cho, S. Jeong, and M. Hahn</i>	

IEEE

SIGNAL PROCESSING LETTERS

A PUBLICATION OF THE IEEE SIGNAL PROCESSING SOCIETY


www.ieee.org/sp/index.html

APRIL 2014

VOLUME 21

NUMBER 4

ISPLEM

(ISSN 1070-9908)

LETTERS

Audio and Acoustic Signal Processing

A Hybrid Descent Method for Optimal Sigmoid Filter Design <http://dx.doi.org/10.1109/LSP.2014.2303498> *K. Y. Chan, S. Nordholm, S. Y. Low, P. C. Yong, and K. F. C. Yiu* 478

Digital and Multirate Signal Processing

Persistent Homology of Delay Embeddings and its Application to Wheeze Detection <http://dx.doi.org/10.1109/LSP.2014.2305700> *S. Emrani, T. Gentimis, and H. Krim* 459

Novel Tridiagonal Commuting Matrices for Types I, IV, V, VIII DCT and DST Matrices <http://dx.doi.org/10.1109/LSP.2014.2306996> *D. Wei and Y. Li* 483

Design and Implementation of Signal Processing Systems

Compressive Circulant Matrix Based Analog to Information Conversion <http://dx.doi.org/10.1109/LSP.2013.2285444> *J. Zhang, N. Fu, and X. Peng* 428

Emerging Signal Processing Applications

Extended Grouping of RFID Tags Based on Resolvable Transversal Designs <http://dx.doi.org/10.1109/LSP.2014.2306264> *Y.-S. Su* 488

Image and Multidimensional Signal Processing

Image Contrast Enhancement Using Color and Depth Histograms <http://dx.doi.org/10.1109/LSP.2014.2303157> *S.-W. Jung* 382

A Robust SIFT Descriptor for Multispectral Images <http://dx.doi.org/10.1109/LSP.2014.2304073> *S. Saleem and R. Sablatnig* 400

Sensor Noise Modeling by Stacking Pseudo-Periodic Grid Images Affected by Vibrations <http://dx.doi.org/10.1109/LSP.2014.2304570> *F. Sur and M. Grédiac* 432

Image Quality Assessment with Degradation on Spatial Structure <http://dx.doi.org/10.1109/LSP.2014.2304714> *J. Wu, W. Lin, and G. Shi* 437

Block-Based In-Loop View Synthesis for 3-D Video Coding <http://dx.doi.org/10.1109/LSP.2013.2283251> *Y. Zhang, Y. Zhao, and L. Yu* 441

IEEE SIGNAL PROCESSING LETTERS (ISSN 1070-9908) is published quarterly in print and monthly online by the Institute of Electrical and Electronics Engineers, Inc. Responsibility for the contents rests upon the authors and not upon the IEEE, the Society/Council, or its members. **IEEE Corporate Office:** 3 Park Avenue, 17th Floor, New York, NY 10016-5997. **IEEE Operations Center:** 445 Hoes Lane, Piscataway, NJ 08854-4141. **NJ Telephone:** +1 732 981 0060. **Price/Publication Information:** Individual copies: IEEE Members \$20.00 (first copy only), nonmembers \$304.00 per copy. (Note: Postage and handling charge not included.) Member and nonmember subscription prices available upon request. Available in microfiche and microfilm. **Copyright and Reprint Permissions:** Abstracting is permitted with credit to the source. Libraries are permitted to photocopy for private use of patrons, provided the per-copy fee indicated in the code at the bottom of the first page is paid through the Copyright Clearance Center, 222 Rosewood Drive, Danvers, MA 01923. For all other copying, reprint, or republication permission, write to Copyrights and Permissions Department, IEEE Publications Administration, 445 Hoes Lane, Piscataway, NJ 08854-4141. Copyright © 2014 by the Institute of Electrical and Electronics Engineers, Inc. All rights reserved. Periodicals Postage at New York, NY and at additional mailing offices. **Postmaster:** Send address changes to IEEE SIGNAL PROCESSING LETTERS, IEEE, 445 Hoes Lane, Piscataway, NJ 08854-4141. GST Registration No. 125634188. CPC Sales Agreement #40013087. Return undeliverable Canada addresses to: Pitney Bowes IMEX, P.O. Box 4332, Stanton Rd., Toronto, ON M5W 3J4, Canada. IEEE prohibits discrimination, harassment and bullying. For more information visit <http://www.ieee.org/nondiscrimination>. Printed in U.S.A.

<i>Machine Learning and Statistical Signal Processing</i>	
Sparse Recovery by Means of Nonnegative Least Squares http://dx.doi.org/10.1109/LSP.2014.2307064	S. Foucart and D. Koslicki 498
<i>Multimedia Signal Processing</i>	
Depth-Assisted Frame Rate Up-Conversion for Stereoscopic Video http://dx.doi.org/10.1109/LSP.2014.2304975	X. Yang, J. Liu, J. Sun, Y. Lee, and T. Q. Nguyen 423
<i>Sensor Array and Multichannel Signal Processing</i>	
Identifiability Analysis for Array Shape Self-Calibration Based on Hybrid Cramér-Rao Bound http://dx.doi.org/10.1109/LSP.2014.2306326	S. Wan, J. Tang, W. Zhu, and N. Zhang 473
<i>Signal Processing for Communications</i>	
A TR-MISI Serial Prefilter for Robustness to ISI and Noise in Indoor Wireless Communication System http://dx.doi.org/10.1109/LSP.2014.2303814	M. Yoon and C. Lee 386
Coherent Versus Non-Coherent Reconfigurable Antenna Aided Virtual MIMO Systems http://dx.doi.org/10.1109/LSP.2014.2303471	S. Sugiura 390
Source Identification Using Signal Characteristics in Controller Area Networks http://dx.doi.org/10.1109/LSP.2014.2304139	P.-S. Murvay and B. Groza 395
An Improved Frequency Offset Estimation Based on Companion Matrix in Multi-User Uplink Interleaved OFDMA Systems http://dx.doi.org/10.1109/LSP.2014.2303138	S.-W. Keum, D.-H. Kim, and H.-M. Kim 409
An Efficient Decoding Algorithm of Matrix Partition Codes http://dx.doi.org/10.1109/LSP.2014.2303421	F. Chen and S. Cheng 414
Relay Beamforming for Amplify-and-Forward Multi-Antenna Relay Networks with Energy Harvesting Constraint http://dx.doi.org/10.1109/LSP.2014.2305737	J. Huang, Q. Li, Q. Zhang, G. Zhang, and J. Qin 454
<i>Speech Processing</i>	
Efficient One-Pass Decoding with NNLM for Speech Recognition http://dx.doi.org/10.1109/LSP.2014.2303136	Y. Shi, W.-Q. Zhang, M. Cai, and J. Liu 377
Improved Bases Selection in Acoustic Model Interpolation for Fast On-Line Adaptation http://dx.doi.org/10.1109/LSP.2014.2306451	S. Shahnawazuddin and R. Sinha 493
Cepstrum-Based Bandwidth Extension for Super-Wideband Coders http://dx.doi.org/10.1109/LSP.2014.2307074	K. Cho, S. Jeong, and M. Hahn 503
<i>Statistical and Adaptive Signal Processing</i>	
Reverberant Audio Source Separation via Sparse and Low-Rank Modeling http://dx.doi.org/10.1109/LSP.2014.2303135	S. Arberet and P. Vanderghyest 404
Successive Projection Method for Well-Conditioned Matrix Approximation Problems http://dx.doi.org/10.1109/LSP.2014.2303153	M. Tanaka and K. Nakata 418
Spatially Adaptive Kernel Regression Using Risk Estimation http://dx.doi.org/10.1109/LSP.2014.2305176	S. R. Krishnan, C. S. Seelamantula, and P. Chakravarti 445
Track-to-Track Association for Biased Data Based on the Reference Topology Feature http://dx.doi.org/10.1109/LSP.2014.2305305	W. Tian, Y. Wang, X. Shan, and J. Yang 449
The Marginal Enumeration Bayesian Cramér-Rao Bound for Jump Markov Systems http://dx.doi.org/10.1109/LSP.2014.2305115	C. Fritsche, U. Orguner, L. Svensson, and F. Gustafsson 464
Computing Jacobian and Hessian of Estimators and Their Application to Risk Approximation http://dx.doi.org/10.1109/LSP.2014.2304693 ..	S. Uhlich 469

IEEE SignalProcessing

MAGAZINE

[VOLUME 31 NUMBER 3 MAY 2014]



SOURCE SEPARATION AND APPLICATIONS

RECENT ADVANCES



PHYSICAL LAYER SERVICE INTEGRATION
IN WIRELESS NETWORKS

SPECTRALLY CONSTRAINED WAVEFORM DESIGN

UHDTV: THE EVOLUTION OF TELEVISION

THE PHOTOGRAPHIC AND IMAGING REVOLUTION

IEEE
Signal Processing Society

IEEE

CONTENTS

[VOLUME 31 NUMBER 3]

SPECIAL SECTION—SOURCE SEPARATION AND APPLICATIONS

16 FROM THE GUEST EDITORS

Tülay Adalı, Christian Jutten, Arie Yeredor, Andrzej Cichocki, and Eric Moreau

18 DIVERSITY IN INDEPENDENT COMPONENT AND VECTOR ANALYSES

Tülay Adalı, Matthew Anderson, and Geng-Shen Fu

34 JOINT MATRICES DECOMPOSITIONS AND BLIND SOURCE SEPARATION

Gilles Chabriel, Martin Kleinstueber, Eric Moreau, Hao Shen, Petr Tichavsky, and Arie Yeredor

44 TENSORS

Pierre Comon

54 NONNEGATIVE MATRIX AND TENSOR FACTORIZATIONS

Guoxu Zhou, Andrzej Cichocki, Qibin Zhao, and Shengli Xie

66 STATIC AND DYNAMIC SOURCE SEPARATION USING NONNEGATIVE FACTORIZATIONS

Paris Smaragdīs, Cédric Févotte, Gautham J. Mysore, Nasser Mohammadiha, and Matthew Hoffman

76 PUTTING NONNEGATIVE MATRIX FACTORIZATION TO THE TEST

Kejun Huang and Nicholas D. Sidiropoulos

87 CONVEXITY IN SOURCE SEPARATION

Michael B. McCoy, Volkan Cevher, Quoc Tran Dinh, Afsaneh Asaei, and Luca Baldassarre

96 SPARSE REPRESENTATION FOR BRAIN SIGNAL PROCESSING

Yuanqing Li, Zhu Liang Yu, Ning Bi, Yong Xu, Zhenghui Gu, and Shun-ichi Amari

107 FROM BLIND TO GUIDED AUDIO SOURCE SEPARATION

Emmanuel Vincent, Nancy Bertin, Rémi Gribonval, and Frédéric Bimbot

116 SCORE-INFORMED SOURCE SEPARATION FOR MUSICAL AUDIO RECORDINGS

Sebastian Ewert, Bryan Pardo, Meinard Müller, and Mark D. Plumbley

125 AUDIOVISUAL SPEECH SOURCE SEPARATION

Bertrand Rivet, Wenwu Wang, Syed Mohsen Naqvi, and Jonathon A. Chambers

135 SOURCE SEPARATION IN CHEMICAL ANALYSIS

Leonardo Tomazeli Duarte, Saïd Moussaoui, and Christian Jutten

FEATURE

147 PHYSICAL LAYER SERVICE INTEGRATION IN WIRELESS NETWORKS

Rafael F. Schaefer and Holger Boche

COLUMNS

4 FROM THE EDITOR

Journals and Magazine Reviews: A Quality Control Mechanism
Abdelhak Zoubir

6 PRESIDENT'S MESSAGE

GlobalSIP and ChinaSIP: New Conferences Developed by the IEEE Signal Processing Society
Alex Acero

10 SPECIAL REPORTS

Signal Processing Leads a Photographic and Imaging Revolution
John Edwards

157 SP TIPS & TRICKS

Spectrally Constrained Waveform Design
William Rowe, Petre Stoica, and Jian Li

163 LECTURE NOTES

From the STFT to the Wigner Distribution
Ljubiša Stanković, Srdjan Stanković, and Miloš Daković

170 STANDARDS IN A NUTSHELL

Ultra-High-Definition Television (Rec. ITU-R BT.2020): A Generational Leap in the Evolution of Television
Masayuki Sugawara, Seo-Young Choi, and David Wood

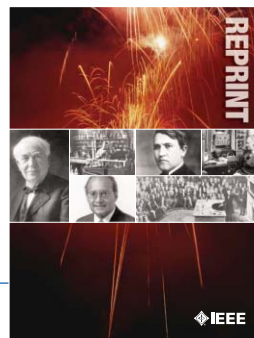
DEPARTMENTS

8 SOCIETY NEWS

SPS Members Recognized with Awards

175 DATES AHEAD

Digital Object Identifier 10.1109/MSP.2014.2300737



IEEE ORDER FORM FOR REPRINTS

Purchasing IEEE Papers in Print is easy, cost-effective and quick.

Complete this form, tear it out, and either fax it (24 hours a day) to 732-981-8062 or mail it back to us.

PLEASE FILL OUT THE FOLLOWING

Author: _____

Publication Title: _____

Paper Title: _____

RETURN THIS FORM TO:

IEEE Publishing Services
445 Hoes Lane
Box 1331

Piscataway, NJ 08855-1331

**Call Reprint Department at (732) 562-3941
for questions regarding this form
(732) 981-8062 - FAX**

PLEASE SEND ME

50 100 200 300 400 500 or _____ (in multiples of 50) reprints.

YES NO Self-covering/title page required. COVER PRICE: \$74 per 100, \$39 per 50.

\$58.00 Air Freight must be added for all orders being shipped outside the U.S.

\$18.50 must be added for all USA shipments to cover the cost of UPS shipping and handling.

PAYMENT

Check enclosed. Payable on a bank in the USA.

Charge my: Visa Mastercard Amex Diners Club

Account # _____ Exp. date _____

Cardholder's Name (please print): _____

Bill me (you must attach a purchase order) Purchase Order Number _____

Send Reprints to:	Bill to address, if different:
_____	_____
_____	_____
_____	_____

Because information and papers are gathered from various sources, there may be a delay in receiving your reprint request. This is especially true with postconference publications. Please provide us with contact information if you would like notification of a delay of more than 12 weeks.

Telephone: _____ Fax: _____ Email Address: _____

2011 REPRINT PRICES (without covers)

Number of Text Pages

	1-4	5-8	9-12	13-16	17-20	21-24	25-28	29-32	33-36	37-40	41-44	45-48
50	\$126	\$211	\$243	\$245	\$285	\$340	\$371	\$408	\$440	\$477	\$510	\$543
100	\$242	\$423	\$476	\$492	\$570	\$680	\$742	\$817	\$885	\$953	\$1021	\$1088

Larger quantities can be ordered. Email reprints@ieee.org with specific details.

Tax Applies on shipments of regular reprints to CA, DC, FL, MI, NJ, NY, OH and Canada (GST Registration no. 12534188).

Prices are based on black & white printing. Please call us for full color price quote, if applicable.

Authorized Signature: _____ Date: _____

2014 IEEE MEMBERSHIP APPLICATION

(students and graduate students must apply online)

Start your membership immediately: Join online www.ieee.org/join

Please complete both sides of this form, typing or **printing in capital letters**. Use only English characters and abbreviate only if more than 40 characters and spaces per line. We regret that incomplete applications cannot be processed.

1 Name & Contact Information

Please PRINT your name as you want it to appear on your membership card and IEEE correspondence. As a key identifier for the IEEE database, circle your last/surname.

Male Female Date of birth (Day/Month/Year) ____/____/____

Title First/Given Name Middle Last/Family Surname

▼ **Primary Address** Home Business (All IEEE mail sent here)

Street Address

City State/Province

Postal Code Country

Primary Phone

Primary E-mail

▼ **Secondary Address** Home Business

Company Name Department/Division

Street Address City State/Province

Postal Code Country

Secondary Phone

Secondary E-mail

To better serve our members and supplement member dues, your postal mailing address is made available to carefully selected organizations to provide you with information on technical services, continuing education, and conferences. Your e-mail address is not rented by IEEE. Please check box only if you do not want to receive these postal mailings to the selected address. □

2 Attestation

I have graduated from a three- to five-year academic program with a university-level degree.

Yes No

This program is in one of the following fields of study:

- Engineering
- Computer Sciences and Information Technologies
- Physical Sciences
- Biological and Medical Sciences
- Mathematics
- Technical Communications, Education, Management, Law and Policy
- Other (please specify): _____

This academic institution or program is accredited in the country where the institution is located. Yes No Do not know

I have _____ years of professional experience in teaching, creating, developing, practicing, or managing within the following field:

- Engineering
- Computer Sciences and Information Technologies
- Physical Sciences
- Biological and Medical Sciences
- Mathematics
- Technical Communications, Education, Management, Law and Policy
- Other (please specify): _____



3 Please Tell Us About Yourself

Select the numbered option that best describes yourself. This information is used by IEEE magazines to verify their annual circulation. Please enter numbered selections in the boxes provided.

A. Primary line of business _____ →

1. Computers
2. Computer peripheral equipment
3. Software
4. Office and business machines
5. Test, measurement and instrumentation equipment
6. Communications systems and equipment
7. Navigation and guidance systems and equipment
8. Consumer electronics/appliances
9. Industrial equipment, controls and systems
10. ICs and microprocessors
11. Semiconductors, components, sub-assemblies, materials and supplies
12. Aircraft, missiles, space and ground support equipment
13. Oceanography and support equipment
14. Medical electronic equipment
15. OEM incorporating electronics in their end product (not elsewhere classified)
16. Independent and university research, test and design laboratories and consultants (not connected with a mfg. co.)
17. Government agencies and armed forces
18. Companies using and/or incorporating any electronic products in their manufacturing, processing, research or development activities
19. Telecommunications services, telephone (including cellular)
20. Broadcast services (TV, cable, radio)
21. Transportation services (airline, railroad, etc.)
22. Computer and communications and data processing services
23. Power production, generation, transmission and distribution
24. Other commercial users of electrical, electronic equipment and services (not elsewhere classified)
25. Distributor (reseller, wholesaler, retailer)
26. University, college/other educational institutions, libraries
27. Retired
28. Other _____

B. Principal job function _____ →

- | | |
|--|--|
| 1. General and corporate management | 9. Design/development engineering—digital |
| 2. Engineering management | 10. Hardware engineering |
| 3. Project engineering management | 11. Software design/development management |
| 4. Research and development management | 12. Computer science |
| 5. Design engineering management—analogue | 13. Science/physics/mathematics specified |
| 6. Design engineering management—digital | 14. Engineering (not elsewhere specified) |
| 7. Research and development engineering | 15. Marketing/sales/purchasing |
| 8. Design/development engineering—analogue | 16. Consulting |
| | 17. Education/teaching |
| | 18. Retired |
| | 19. Other _____ |

C. Principal responsibility _____ →

- | | |
|--|-----------------------|
| 1. Engineering and scientific management | 6. Education/teaching |
| 2. Management other than engineering | 7. Consulting |
| 3. Engineering design | 8. Retired |
| 4. Engineering | 9. Other _____ |
| 5. Software: science/mngmnt/engineering | |

D. Title _____ →

- | | |
|--|--------------------------------|
| 1. Chairman of the Board/President/CEO | 10. Design Engineering Manager |
| 2. Owner/Partner | 11. Design Engineer |
| 3. General Manager | 12. Hardware Engineer |
| 4. VP Operations | 13. Software Engineer |
| 5. VP Engineering/Dir. Engineering | 14. Computer Scientist |
| 6. Chief Engineer/Chief Scientist | 15. Dean/Professor/Instructor |
| 7. Engineering Management | 16. Consultant |
| 8. Scientific Management | 17. Retired |
| 9. Member of Technical Staff | 18. Other _____ |

Are you now or were you ever a member of IEEE?

Yes No If yes, provide, if known:

Membership Number _____ Grade _____ Year Expired _____

4 Please Sign Your Application

I hereby apply for IEEE membership and agree to be governed by the IEEE Constitution, Bylaws, and Code of Ethics. I understand that IEEE will communicate with me regarding my individual membership and all related benefits. **Application must be signed.**

Signature _____ Date _____ *Over Please*

Information for Authors

(Updated March 2012)

The IEEE TRANSACTIONS are published monthly covering advances in the theory and application of signal processing. The scope is reflected in the EDICS: the Editor's Information and Classification Scheme. Please consider the journal with the most appropriate scope for your submission.

Authors are encouraged to submit manuscripts of Regular papers (papers which provide a complete disclosure of a technical premise), or Correspondences (brief items that describe a use for or magnify the meaning of a single technical point, or provide comment on a paper previously published in the TRANSACTIONS). Submissions/resubmissions must be previously unpublished and may not be under consideration elsewhere.

Every manuscript must (a) provide a clearly defined statement of the problem being addressed, (b) state why it is important to solve the problem, and (c) give an indication as to how the current solution fits into the history of the problem.

By submission/resubmission of your manuscript to this TRANSACTIONS, you are acknowledging that you accept the rules established for publication of manuscripts, including agreement to pay all overlength page charges, color charges, and any other charges and fees associated with publication of the manuscript. Such charges are not negotiable and cannot be suspended.

New and revised manuscripts should be prepared following the "New Manuscript Submission" guidelines below, and submitted to the online manuscript system ScholarOne Manuscripts. After acceptance, finalized manuscripts should be prepared following the "Final Manuscript Submission Guidelines" below. Do not send original submissions or revisions directly to the Editor-in-Chief or Associate Editors; they will access your manuscript electronically via the ScholarOne Manuscripts system.

New Manuscript Submission. Please follow the next steps.

1. **Account in ScholarOne Manuscripts.** If necessary, create an account in the on-line submission system ScholarOne Manuscripts. Please check first if you already have an existing account which is based on your e-mail address and may have been created for you when you reviewed or authored a previous paper.
2. **Electronic Manuscript.** Prepare a PDF file containing your manuscript in double-spaced format (one full blank line between lines of type) using a font size of 11 points or larger, having a margin of at least 1 inch on all sides. For a regular paper, the manuscript may not exceed 30 double-spaced pages, including title; names of authors and their complete contact information; abstract; text; all images, figures and tables; and all references. Upload your manuscript as a PDF file "manuscript.pdf" to the ScholarOne Manuscripts site, then proofread your submission, confirming that all figures and equations are visible in your document before you "SUBMIT" your manuscript. Proofreading is critical; once you submit your manuscript, the manuscript cannot be changed in any way. You may also submit your manuscript as a PostScript or MS Word file. The system has the capability of converting your files to PDF, however it is your responsibility to confirm that the conversion is correct and there are no font or graphics issues prior to completing the submission process.
3. **Double-Column Version of the Manuscript.** You are required to also submit a roughly formatted version of the manuscript in single-spaced, double column IEEE format (10 points for a regular submission or 9 points for a Correspondence) using the IEEE style files (it is allowed to let long equations stick out). *If accepted for publication*, over length page charges are levied beginning with the 11th published page of your manuscript. You are, therefore, advised to be conservative in your submission. This double-column version submitted will serve as a confirmation of the approximate publication length of the manuscript and gives an additional confirmation of your understanding that over length page charges will be paid when billed upon publication. Upload this version of the manuscript as a PDF file "double.pdf" to the ScholarOneManuscripts site.
4. **Additional Material for Review.** Please upload pdf versions of all items in the reference list which are not publicly available, such as unpublished (submitted) papers. Other materials for review such as supplementary tables and figures, audio fragments and QuickTime movies may be uploaded as well. Reviewers will be able to view these files only if they have the appropriate software on their computers. Use short filenames without spaces or special characters. When the upload of each file is completed, you will be asked to provide a description of that file.
5. **Submission.** After uploading all files and proofreading them, submit your manuscript by clicking "Submit." A confirmation of the successful submission will open on screen containing the manuscript tracking number and will be followed with an e-mail confirmation to the corresponding and all contributing authors. Once you click "Submit," your manuscript cannot be changed in any way.

6. **Copyright Form and Consent Form.** By policy, IEEE owns the copyright to the technical contributions it publishes on behalf of the interests of the IEEE, its authors, and their employers; and to facilitate the appropriate reuse of this material by others. To comply with the IEEE copyright policies, authors are required to sign and submit a completed "IEEE Copyright and Consent Form" prior to publication by the IEEE.

The IEEE recommends authors to use an effective electronic copyright form (eCF) tool within the ScholarOne Manuscripts system. You will be redirected to the "IEEE Electronic Copyright Form" wizard at the end of your original submission; please simply sign the eCF by typing your name at the proper location and click on the "Submit" button.

Correspondence Items. Correspondence items are short disclosures with a reduced scope or significance that typically describe a use for or magnify the meaning of a single technical point, or provide brief comments on material previously published in the TRANSACTIONS. These items may not exceed 12 pages in double-spaced format (3 pages for Comments), using 11 point type, with margins of 1 inch minimum on all sides, and including: title, names and contact information for authors, abstract, text, references, and an appropriate number of illustrations and/or tables. Correspondence items are submitted in the same way as regular manuscripts (see "New Manuscript Submission" above for instructions).

Manuscript Length. Papers published on or after 1 January 2007 can now be up to 10 pages, and any paper in excess of 10 pages will be subject to over length page charges. The IEEE Signal Processing Society has determined that the standard manuscript length shall be no more than 10 published pages (double-column format, 10 point type) for a regular submission, or 6 published pages (9 point type) for a Correspondence item, respectively. Manuscripts that exceed these limits will incur mandatory over length page charges, as discussed below. Since changes recommended as a result of peer review may require additions to the manuscript, it is strongly recommended that you practice economy in preparing original submissions.

Exceptions to the 30-page (regular paper) or 12-page (Correspondences) manuscript length may, under extraordinary circumstances, be granted by the Editor-in-Chief. However, such exception does not obviate your requirement to pay any and all over length or additional charges that attach to the manuscript.

Resubmission of Previously Rejected Manuscripts. Authors of rejected manuscripts are allowed to resubmit their manuscripts only once. The Signal Processing Society strongly discourages resubmission of rejected manuscripts more than once. At the time of submission, you will be asked whether you consider your manuscript to be a new submission or a resubmission of an earlier rejected manuscript. If you choose to submit a new version of your manuscript, you will be asked to submit supporting documents detailing how your new version addresses all of the reviewers' comments.

Full details of the resubmission process can be found in the Signal Processing Society "Policy and Procedures Manual" at <http://www.signalprocessingsociety.org/about/governance/policy-procedure/>. Also, please refer to the decision letter and your Author Center on the on-line submission system.

Author Misconduct.

Author Misconduct Policy: Plagiarism includes copying someone else's work without appropriate credit, using someone else's work without clear delineation of citation, and the uncited reuse of an authors previously published work that also involves other authors. Plagiarism is unacceptable.

Self-plagiarism involves the verbatim copying or reuse of an authors own prior work without appropriate citation; it is also unacceptable. Self-plagiarism includes duplicate submission of a single journal manuscript to two different journals, and submission of two different journal manuscripts which overlap substantially in language or technical contribution.

Authors may only submit original work that has not appeared elsewhere in a journal publication, nor is under review for another journal publication. Limited overlap with prior journal publications with a common author is allowed only if it is necessary for the readability of the paper. If authors have used their own previously published work as a basis for a new submission, they are required to cite the previous work and very briefly indicate how the new submission offers substantively novel contributions beyond those of the previously published work.

It is acceptable for conference papers to be used as the basis for a more fully developed journal submission. Still, authors are required to cite related prior work; the papers cannot be identical; and the journal publication must include novel aspects.

Author Misconduct Procedures: The procedures that will be used by the Signal Processing Society in the investigation of author misconduct allegations are described in the IEEE SPS Policies and Procedures Manual.

Author Misconduct Sanctions: The IEEE Signal Processing Society will apply the following sanctions in any case of plagiarism, or in cases of self-plagiarism that involve an overlap of more than 25% with another journal manuscript:

- 1) immediate rejection of the manuscript in question;
- 2) immediate withdrawal of all other submitted manuscripts by any of the authors, submitted to any of the Society's publications (journals, conferences, workshops), except for manuscripts that also involve innocent co-authors; immediate withdrawal of all other submitted manuscripts by any of the authors, submitted to any of the Society's publications (journals, conferences, workshops), except for manuscripts that also involve innocent co-authors;
- 3) prohibition against each of the authors for any new submissions, either individually, in combination with the authors of the plagiarizing manuscript, or in combination with new co-authors, to all of the Society's publications (journals, conferences, workshops). The prohibition shall continue for one year from notice of suspension.

Further, plagiarism and self-plagiarism may also be actionable by the IEEE under the rules of Member Conduct.

Submission Format.

Authors are encouraged to prepare manuscripts employing the on-line style files developed by IEEE. All manuscripts accepted for publication will require the authors to make final submission employing these style files. The style files are available on the web at http://www.ieee.org/publications_standards/publications/authors/authors_journals.html#sect2 under "Template for all Transactions." (LaTeX and MS Word).

Authors using LaTeX: the two PDF versions of the manuscript needed for submission can both be produced by the IEEEtran.cls style file. A double-spaced document is generated by including `\documentclass[11pt,draftcls,onecolumn]{IEEEtran}` as the first line of the manuscript source file, and a single-spaced double-column document for estimating the publication page charges via `\documentclass[10pt,twocolumn,twoside]{IEEEtran}` for a regular submission, or `\documentclass[9pt,twocolumn,twoside]{IEEEtran}` for a Correspondence item.

- **Title page and abstract:** The first page of the manuscript shall contain the title, names and contact information for all authors (full mailing address, institutional affiliations, phone, fax, and e-mail), the abstract, and the EDICS. An asterisk * should be placed next to the name of the Corresponding Author who will serve as the main point of contact for the manuscript during the review and publication processes.

An abstract should have not more than 200 words for a regular paper, or 50 words for a Correspondence item. The abstract should indicate the scope of the paper or Correspondence, and summarize the author's conclusions. This will make the abstract, by itself, a useful tool for information retrieval.

- **EDICS:** All submissions must be classified by the author with an EDICS (Editors' Information Classification Scheme) selected from the list of EDICS published online at <http://www.signalprocessingsociety.org/publications/periodicals/tsp/TSP-EDICS/>
- **NOTE:** EDICS are necessary to begin the peer review process. Upon submission of a new manuscript, please choose the EDICS categories that best suit your manuscript. Failure to do so will likely result in a delay of the peer review process.
- The EDICS category should appear on the first page—i.e., the title and abstract page—of the manuscript.
- **Illustrations and tables:** Each figure and table should have a caption that is intelligible without requiring reference to the text. Illustrations/tables may be worked into the text of a newly-submitted manuscript, or placed at the end of the manuscript. (However, for the final submission, illustrations/tables must be submitted separately and not interwoven with the text.)

Illustrations in color may be used but, unless the final publishing will be in color, the author is responsible that the corresponding grayscale figure is understandable.

In preparing your illustrations, note that in the printing process, most illustrations are reduced to single-column width to conserve space. This may result in as much as a 4:1 reduction from the original. Therefore, make sure that all words are in a type size that will reduce to a minimum of 9 points or 3/16 inch high in the printed version. Only the major grid lines on graphs should be indicated.

- **Abbreviations:** This TRANSACTIONS follows the practices of the IEEE on units and abbreviations, as outlined in the Institute's published standards. See http://www.ieee.org/portal/cms_docs_iportals/iportals/publications/authors/transjnl/auinfo07.pdf for details.
- **Mathematics:** All mathematical expressions must be legible. Do not give derivations that are easily found in the literature; merely cite the reference.

Final Manuscript Submission Guidelines.

Upon formal acceptance of a manuscript for publication, instructions for providing the final materials required for publication will be sent to the Corresponding Author. Finalized manuscripts should be prepared in LaTeX or MS Word, and are required to use the style files established by IEEE, available at http://www.ieee.org/publications_standards/publications/authors/authors_journals.html#sect2.

Instructions for preparing files for electronic submission are as follows:

- Files must be self-contained; that is, there can be no pointers to your system setup.
- Include a header to identify the name of the TRANSACTIONS, the name of the author, and the software used to format the manuscript.
- Do not import graphics files into the text file of your finalized manuscript (although this is acceptable for your initial submission). If submitting on disk, use a separate disk for graphics files.
- Do not create special macros.
- Do not send PostScript files of the text.
- File names should be lower case.
- Graphics files should be separate from the text, and not contain the caption text, but include callouts like "(a)," "(b)."
- Graphics file names should be lower case and named fig1.eps, fig2.tif, etc.
- Supported graphics types are EPS, PS, TIFF, or graphics created using Word, Powerpoint, Excel or PDF. Not acceptable is GIF, JPEG, WMF, PNG, BMP or any other format (JPEG is accepted for author photographs only). The provided resolution needs to be at least 600 dpi (400 dpi for color).
- Please indicate explicitly if certain illustrations should be printed in color; note that this will be at the expense of the author. Without other indications, color graphics will appear in color in the online version, but will be converted to grayscale in the print version.

Additional instructions for preparing, verifying the quality, and submitting graphics are available via http://www.ieee.org/publications_standards/publications/authors/authors_journals.html.

Multimedia Materials.

IEEE Xplore can publish multimedia files and Matlab code along with your paper. Alternatively, you can provide the links to such files in a README file that appears on Xplore along with your paper. For details, please see http://www.ieee.org/publications_standards/publications/authors/authors_journals.html#sect6 under "Multimedia." To make your work reproducible by others, the TRANSACTIONS encourages you to submit all files that can recreate the figures in your paper.

Page Charges.

Voluntary Page Charges. Upon acceptance of a manuscript for publication, the author(s) or his/her/their company or institution will be asked to pay a charge of \$110 per page to cover part of the cost of publication of the first ten pages that comprise the standard length (six pages, in the case of Correspondences).

Mandatory Page Charges. The author(s) or his/her/their company or institution will be billed \$220 per each page in excess of the first ten published pages for regular papers and six published pages for correspondence items. These are mandatory page charges and the author(s) will be held responsible for them. They are not negotiable or voluntary. The author(s) signifies his willingness to pay these charges simply by submitting his/her/their manuscript to the TRANSACTIONS. The Publisher holds the right to withhold publication under any circumstance, as well as publication of the current or future submissions of authors who have outstanding mandatory page charge debt.

Color Charges. Color figures which appear in color only in the electronic (Xplore) version can be used free of charge. In this case, the figure will be printed in the hardcopy version in grayscale, and the author is responsible that the corresponding grayscale figure is intelligible. Color reproduction in print is expensive, and all charges for color are the responsibility of the author. The estimated costs are as follows. There will be a charge of \$62.50 for each figure; this charge may be subject to change without notification. In addition, there are printing preparation charges which may be estimated as follows: color reproductions on four or fewer pages of the manuscript: a total of approximately \$1045; color reproductions on five pages through eight pages: a total of approximately \$2090; color reproductions on nine through 12 pages: a total of approximately \$3135, and so on. Payment of fees on color reproduction is not negotiable or voluntary, and the author's agreement to publish the manuscript in the TRANSACTIONS is considered acceptance of this requirement.

To find the Information for Authors for IEEE Signal Processing Letters, the IEEE Journal of Selected Topics in Signal Processing or the IEEE Signal Processing Magazine, please refer to the IEEE Signal Processing website at www.signalprocessingsociety.org.

2014 IEEE SIGNAL PROCESSING SOCIETY MEMBERSHIP APPLICATION

(Current and reinstating IEEE members joining SPS complete areas 1, 2, 8, 9.)

Mail to: IEEE OPERATIONS CENTER, ATTN: Louis Curcio, Member and Geographic Activities, 445 Hoes Lane, Piscataway, New Jersey 08854 USA
or Fax to (732) 981-0225 (credit card payments only.)

For info call (732) 981-0060 or 1 (800) 678-IEEE or E-mail: new.membership@ieee.org



1. PERSONAL INFORMATION

NAME AS IT SHOULD APPEAR ON IEEE MAILINGS: SEND MAIL TO: Home Address OR Business/School Address

If not indicated, mail will be sent to home address. Note: Enter your name as you wish it to appear on membership card and all correspondence.

PLEASE PRINT Do not exceed 40 characters or spaces per line. Abbreviate as needed. Please circle your last/surname as a key identifier for the IEEE database.

TITLE	FIRST OR GIVEN NAME	MIDDLE NAME	SURNAME/LAST NAME
HOME ADDRESS			
CITY		STATE/PROVINCE	POSTAL CODE
COUNTRY			

2. Are you now or were you ever a member of IEEE? Yes No
If yes, please provide, if known:

MEMBERSHIP NUMBER _____

Grade _____ Year Membership Expired: _____

3. BUSINESS/PROFESSIONAL INFORMATION

Company Name _____

Department/Division _____

Title/Position _____ Years in Current Position _____

Years in the Profession Since Graduation _____ PE State/Province _____

Street Address _____

City _____ State/Province _____ Postal Code _____ Country _____

4. EDUCATION A baccalaureate degree from an IEEE recognized educational program assures assignment of "Member" grade. For others, additional information and references may be necessary for grade assignment.

A. Baccalaureate Degree Received _____ Program/Course of Study _____

College/University _____ Campus _____

State/Province _____ Country _____ Mo./Yr. Degree Received _____

B. Highest Technical Degree Received _____ Program/Course of Study _____

College/University _____ Campus _____

State/Province _____ Country _____ Mo./Yr. Degree Received _____

5. Full signature of applicant _____

6. DEMOGRAPHIC INFORMATION – ALL APPLICANTS -

Date Of Birth _____ Male Female

Day Month Year

7. CONTACT INFORMATION

Office Phone/Office Fax _____ Home Phone/Home Fax _____

Office E-Mail _____ Home E-Mail _____

8. 2014 IEEE MEMBER RATES

IEEE DUES	16 Aug-28 Feb 14 Pay Full Year	1 Mar-15 Aug 14 Pay Half Year**
Residence		
United States	\$187.00 <input type="checkbox"/>	\$93.50 <input type="checkbox"/>
Canada (incl. GST)	\$168.10 <input type="checkbox"/>	\$84.05 <input type="checkbox"/>
Canada (incl. HST for NB, NF and ON)	\$179.46 <input type="checkbox"/>	\$89.73 <input type="checkbox"/>
Canada (incl. HST for Nova Scotia)	\$182.30 <input type="checkbox"/>	\$91.15 <input type="checkbox"/>
Canada (incl. HST for PEI)	\$180.88 <input type="checkbox"/>	\$90.44 <input type="checkbox"/>
Africa, Europe, Middle East	\$155.00 <input type="checkbox"/>	\$77.50 <input type="checkbox"/>
Latin America	\$146.00 <input type="checkbox"/>	\$73.00 <input type="checkbox"/>
Asia, Pacific	\$147.00 <input type="checkbox"/>	\$73.50 <input type="checkbox"/>

Canadian Taxes (GST/HST): All supplies, which include dues, Society membership fees, online products and publications (except CD-ROM and DVD media), shipped to locations within Canada are subject to the GST of 5% or the HST of 13%, 14% or 15%, depending on the Province to which the materials are shipped. GST and HST do not apply to Regional Assessments. (IEEE Canadian Business Number 12563 4188 RT0001)

Value Added Tax (VAT) in the European Union: In accordance with the European Union Council Directives 2002/38/EC and 77/388/EEC amended by Council Regulation (EC)/92/2002, IEEE is required to charge and collect VAT on electronic/digitized products sold to private consumers that reside in the European Union. The VAT rate applied is the EU member country standard rate where the consumer is resident. (IEEE's VAT registration number is EU82600081)

U.S. Sales Taxes: Please add applicable state and local sales and use tax on orders shipped to Alabama, Arizona, California, Colorado, District of Columbia, Florida, Georgia, Illinois, Indiana, Kentucky, Massachusetts, Maryland, Michigan, Minnesota, Missouri, New Jersey, New Mexico, New York, North Carolina, Ohio, Oklahoma, West Virginia, Wisconsin. Customers claiming a tax exemption must include an appropriate and properly completed tax-exemption certificate with their first order.



2014 SPS MEMBER RATES

	16 Aug-28 Feb Pay Full Year	1 Mar-15 Aug Pay Half Year
Signal Processing Society Membership Fee*	\$ 20.00 <input type="checkbox"/>	\$ 10.00 <input type="checkbox"/>
Fee includes: IEEE Signal Processing Magazine (electronic and digital), Inside Signal Processing eNewsletter (electronic) and IEEE Signal Processing Society Content Gazette (electronic).		
Add \$15 to enhance SPS Membership and also receive:	\$ 15.00 <input type="checkbox"/>	\$ 7.50 <input type="checkbox"/>
IEEE Signal Processing Magazine (print) and SPS Digital Library: online access to Signal Processing Magazine, Signal Processing Letters, Journal of Selected Topics in Signal Processing, Trans. on Audio, Speech, and Language Processing, Trans. on Image Processing, Trans. on Information Forensics and Security and Trans. on Signal Processing.		
<i>Publications available only with SPS membership:</i>		
Signal Processing, IEEE Transactions on:	Print	\$190.00 <input type="checkbox"/> \$95.00 <input type="checkbox"/>
Audio, Speech, and Language Proc., IEEE/ACM Trans. on:	Print	\$145.00 <input type="checkbox"/> \$72.50 <input type="checkbox"/>
Image Processing, IEEE Transactions on:	Print	\$188.00 <input type="checkbox"/> \$94.00 <input type="checkbox"/>
Information Forensics and Security, IEEE Trans. on:	Print	\$163.00 <input type="checkbox"/> \$81.50 <input type="checkbox"/>
IEEE Journal of Selected Topics in Signal Processing:	Print	\$160.00 <input type="checkbox"/> \$80.00 <input type="checkbox"/>
Affective Computing, IEEE Transactions on:	Electronic	\$ 33.00 <input type="checkbox"/> \$ 16.50 <input type="checkbox"/>
Biomedical and Health Informatics, IEEE Journal of:	Print	\$ 55.00 <input type="checkbox"/> \$ 27.50 <input type="checkbox"/>
	Electronic	\$ 40.00 <input type="checkbox"/> \$ 20.00 <input type="checkbox"/>
	Print & Electronic	\$ 65.00 <input type="checkbox"/> \$ 32.50 <input type="checkbox"/>
IEEE Cloud Computing	Electronic and Digital	\$ 39.00 <input type="checkbox"/> \$ 19.50 <input type="checkbox"/>
Computing in Science & Engineering:	Electronic and Digital	\$ 45.00 <input type="checkbox"/> \$ 22.50 <input type="checkbox"/>
	Print & Electronic	\$ 49.00 <input type="checkbox"/> \$ 24.50 <input type="checkbox"/>
Medical Imaging, IEEE Transactions on:	Print	\$ 74.00 <input type="checkbox"/> \$ 37.00 <input type="checkbox"/>
	Electronic	\$ 53.00 <input type="checkbox"/> \$ 26.50 <input type="checkbox"/>
	Print & Electronic	\$ 89.00 <input type="checkbox"/> \$ 44.50 <input type="checkbox"/>
Mobile Computing, IEEE Trans. on:	ELE/Print Abstract/CD-ROM	\$ 36.00 <input type="checkbox"/> \$ 18.00 <input type="checkbox"/>
Multimedia, IEEE Transactions on:	Electronic	\$ 42.00 <input type="checkbox"/> \$ 21.00 <input type="checkbox"/>
IEEE MultiMedia Magazine:	Electronic and Digital	\$ 45.00 <input type="checkbox"/> \$ 22.50 <input type="checkbox"/>
	Print & Electronic	\$ 49.00 <input type="checkbox"/> \$ 24.50 <input type="checkbox"/>
Network Science and Engrg, IEEE Trans. on:	Electronic	\$ 32.00 <input type="checkbox"/> \$ 16.00 <input type="checkbox"/>
IEEE Reviews in Biomedical Engineering:	Print	\$ 25.00 <input type="checkbox"/> \$ 12.50 <input type="checkbox"/>
	Electronic	\$ 25.00 <input type="checkbox"/> \$ 12.50 <input type="checkbox"/>
	Print & Electronic	\$ 40.00 <input type="checkbox"/> \$ 20.00 <input type="checkbox"/>
IEEE Security and Privacy Magazine:	Electronic and Digital	\$ 45.00 <input type="checkbox"/> \$ 22.50 <input type="checkbox"/>
	Print and Electronic	\$ 49.00 <input type="checkbox"/> \$ 24.50 <input type="checkbox"/>
IEEE Biometrics Compendium	Online	\$ 30.00 <input type="checkbox"/> \$ 15.00 <input type="checkbox"/>
IEEE Sensors Journal:	Print	\$150.00 <input type="checkbox"/> \$ 75.00 <input type="checkbox"/>
	Electronic	\$ 50.00 <input type="checkbox"/> \$ 25.00 <input type="checkbox"/>
	Print & Electronic	\$190.00 <input type="checkbox"/> \$ 95.00 <input type="checkbox"/>
Smart Grid, IEEE Transactions on:	Print	\$100.00 <input type="checkbox"/> \$ 50.00 <input type="checkbox"/>
	Electronic	\$ 40.00 <input type="checkbox"/> \$ 20.00 <input type="checkbox"/>
	Print & Electronic	\$120.00 <input type="checkbox"/> \$ 60.00 <input type="checkbox"/>
IEEE Transactions on Engineering Management:	Print & Electronic	\$ 39.00 <input type="checkbox"/> \$ 19.50 <input type="checkbox"/>
IEEE Engineering Management Review:	Print & Electronic	\$ 29.00 <input type="checkbox"/> \$ 14.50 <input type="checkbox"/>
IEEE Technology Management Package:	Print & Electronic	\$ 60.00 <input type="checkbox"/> \$ 30.00 <input type="checkbox"/>
Wireless Communications, IEEE Transactions on:	Print	\$ 87.00 <input type="checkbox"/> \$ 43.50 <input type="checkbox"/>
	Electronic	\$ 42.00 <input type="checkbox"/> \$ 21.00 <input type="checkbox"/>
	Print & Electronic	\$ 87.00 <input type="checkbox"/> \$ 43.50 <input type="checkbox"/>
IEEE Wireless Communications Letters:	Print	\$ 80.00 <input type="checkbox"/> \$ 40.00 <input type="checkbox"/>
	Electronic	\$ 18.00 <input type="checkbox"/> \$ 9.00 <input type="checkbox"/>
	Print & Electronic	\$ 95.00 <input type="checkbox"/> \$ 47.50 <input type="checkbox"/>

*IEEE membership required or requested
Affiliate application to join SP Society only. Amount Paid \$ _____

9. IEEE Membership Dues (See pricing in Section 8) \$ _____

Signal Processing Society Fees \$ _____

Canadian residents pay 5% GST or 13% HST
Reg. No. 125634188 on Society payment(s) & pubs only Tax \$ _____

AMOUNT PAID WITH APPLICATION TOTAL \$ _____

Prices subject to change without notice.

Check or money order enclosed Payable to IEEE on a U.S. Bank

American Express VISA MasterCard

Diners Club

Exp. Date	Mo./Yr.								
-----------	---------	--	--	--	--	--	--	--	--

Cardholder 5 Digit Zip Code Billing									
-------------------------------------	--	--	--	--	--	--	--	--	--

Statement Address/USA Only									
----------------------------	--	--	--	--	--	--	--	--	--

10. WERE YOU REFERRED?

Yes No If yes, please provide the follow information:

Member Recruiter Name: _____

IEEE Recruiter's Member Number (Required): _____

Full signature of applicant using credit card _____ Date _____

